INTERNATIONAL DOCTORAL
SCHOOL OF THE USC

Tomás
Lama Díaz

PhD Thesis

Impact of Pif1 translational mechanism on genetic interactions with *YEN1*^{ON} and other DNA repair enzymes

Santiago de Compostela, 2023

Doctoral Programme in Molecular Medicine

USC
UNIVERSIDADE
DE SANTIAGO
DE COMPOSTELA

DOCTORAL THESIS

IMPACT OF *PIF1* TRANSLATIONAL MECHANISM ON GENETIC INTERACTIONS WITH *YEN1*^{ON} AND OTHER DNA REPAIR ENZYMES

Tomás Lama Díaz

INTERNATIONAL PHD SCHOOL OF THE UNIVERSITY OF SANTIAGO DE COMPOSTELA

PHD PROGRAMMA IN MOLECULAR MEDICINE

SANTIAGO DE COMPOSTELA

AÑO 2023

USC
UNIVERSIDADE
DE SANTIAGO
DE COMPOSTELA

DECLARACIÓN DEL AUTOR/A DE LA TESIS

D./Dña. **Tomás Lama Díaz**

Título de la tesis: **Impact of Pif1 translational mechanism on genetic interactions with YEN1-ON and other DNA repair enzymes**

Presento mi tesis, siguiendo el procedimiento adecuado al Reglamento y declaro que:

1) La tesis abarca los resultados de la elaboración de mi trabajo.
2) De ser el caso, en la tesis se hace referencia a las colaboraciones que tuvo este trabajo.
3) Confirmo que la tesis no incurre en ningún tipo de plagio de otros autores ni de trabajos presentados por mí para la obtención de otros títulos.
4) La tesis es la versión definitiva presentada para su defensa y coincide la versión impresa con la presentada en formato electrónico.

Y me comprometo a presentar el Compromiso Documental de Supervisión en el caso que el original no esté depositado en la Escuela.

En **Santiago de Compostela**, **23 diciembre 2022**.

USC
UNIVERSIDADE
DE SANTIAGO
DE COMPOSTELA

AUTORIZACIÓN DEL DIRECTOR/TUTOR DE LA TESIS

D./Dña. **Miguel González Blanco**

En condición de: **Tutor/a y director/a**

Título de la tesis: **Impact of Pif1 translational mechanism on genetic interactions with YEN1-ON and other DNA repair enzymes**

INFORMA:

Que la presente tesis, se corresponde con el trabajo realizado por D/Dña **Tomás Lama Díaz**, bajo mi dirección/tutorización, y autorizo su presentación, considerando que reúne los requisitos exigidos en el Reglamento de Estudios de Doctorado de la USC, y que como director/tutor de esta no incurre en las causas de abstención establecidas en la Ley 40/2015.

En **Santiago de Compostela**, **23 de diciembre de 2022**

USC
UNIVERSIDADE
DE SANTIAGO
DE COMPOSTELA

DECLARACIÓN DE CONFLICTO DE INTERESES Y AUTORÍA DE DATOS PRESENTADOS

Yo, Tomás Lama Díaz, con DNI 50487181-L:

Declaro no tener ningún tipo de conflicto de intereses, ni ninguna relación económica, personal, política, interés financiero o académico que pueda influir en este trabajo.

Así mismo, declaro la completa autoría de todas las imágenes y figuras que se muestran en la tesis.

USC
UNIVERSIDADE
DE SANTIAGO
DE COMPOSTELA

A mis padres

USC
UNIVERSIDADE
DE SANTIAGO
DE COMPOSTELA

USC
UNIVERSIDADE
DE SANTIAGO
DE COMPOSTELA

AGRADECIMIENTOS

A mi director de tesis, el Dr. Miguel González Blanco, por brindarme la oportunidad de formar parte de su grupo de investigación. Durante estos años, gracias a tu supervisión, he aprendido a desarrollar proyectos de investigación de la manera más rigurosa posible. Además, me has inculcado unos estándares para este trabajo que, allá donde esté y con independencia de a qué me dedique, me acompañarán toda la vida. Has puesto todo de tu parte, con tu tiempo, paciencia y esfuerzo, para formarme de la mejor manera posible en todos los ámbitos. Lo mejor de este lustro han sido las incontables discusiones científicas, sazonadas de humor, sobre experimentos y proyectos potenciales; las celebraciones conjuntas en las victorias, y la ayuda para levantarme en los fracasos. Por último, agradecerte la libertad con la que me has dejado explorar mis ideas, felicitando los aciertos, y sin reprochar los errores. Con la perspectiva que dan los años y la experiencia, termino con el convencimiento absoluto de que has sido, para mí, el mejor director posible. Gracias.

Al codirector espiritual de esta tesis, el Dr. Francisco Boán, que, además, se sitúa en la base de mi árbol genealógico científico, ese que lleva por lema: *tu experimento es tan bueno como el más débil de tus controles*. Estaré siempre en deuda contigo por descubrirme una vocación, por la fe que siempre has tenido en mí, por tu apoyo incondicional y por motivarme a esforzarme al máximo desde que entré por la puerta del Blanco Amor. Gracias por abrirme este camino, y ayudarme a recorrerlo.

A todos mis compañeros de laboratorio, pasados y presentes. A Paula, sin la que no hubiese llegado a comenzar esta tesis, por su contribución a este trabajo durante el primer año. A María, por su inestimable ayuda en el tramo final. A Eva, por su apoyo dentro y fuera del laboratorio, y por su estupenda labor como técnico, que tanto nos facilita el trabajo día a día. A Javi, por las risas compartidas cada vez que la ciencia nos soltaba un amable sopapo, su ayuda siempre que la he necesitado, y las conversaciones variopintas sobre cualquier tema, incluyendo, cómo no, el baloncesto.

Al Dr. Rodrigo Bermejo, y la Dra. Grazzia Pellicano, por su excelente trato y ayuda durante mi estancia en su laboratorio, en el Centro de Investigaciones Biológicas Margarita Salas.

I would also like to thank Prof. Joao Matos, and all the members of his laboratory, for the fantastic three months I spent during my research stay at the Matos lab. Especially, to Rahel, Philipp, Adrian and Rokas.

A todas las personas del centro nos ayudan cada día, incluidos los técnicos (Pili, Lucía, y Jose) y Xestión. Con un agradecimiento especial a Carmen, por su ayuda y apoyo logístico, y a Juan, con quien tantas veces he arreglado el mundo al final del día.

USC
UNIVERSIDADE DE SANTIAGO DE COMPOSTELA

A mis amigos madrileños de toda la vida: Miguel, Gabri, y Juan. A Moncho, y cómo no, a mi compañero de mil batallas, Dani. A mis amigas galegas: Andrea, Laura, Raquel y Maca. A los que se han ido sumando durante esta tesis, tanto al principio (Yara, Adriana), como al final (Álex, Joan, Damián). A las personas que, durante todos estos años en Santiago, han formado mi otra familia, y que habéis llenado estos años de buenos momentos, risas y apoyo: Lucas, Rubas, Rubén y Vera. A Alberto, el mejor amigo que puede uno tener, y que me ha influenciado de manera tan positiva en tantos aspectos, como el hermano mayor que *de facto* ha sido para mí.

A la familia González-Fariñas, por darme todo su apoyo cuando más lo necesitaba.

A la familia Eiroa-Pereira, por todos estos años cuidando de mí.

A mi familia. A mi abuela Alejandra. A miña avoa Concha. Y cómo no, a las dos personas más importantes de mi vida, mis padres Justino y Bea, que me han dado todo lo importante, y a los que tanto quiero. *Pater*, desta vez cumprín.

During the development of this doctoral thesis, the PhD student was recipient of a predoctoral fellowship from Xunta de Galicia (Axudas de apoio á etapa predoutoral (modalidade A) nas universidades do SUG, nos organismos públicos de investigación de Galicia e noutras entidades so Sistema galego de I+D+i, cofinanciadas parcialmente polo programa operativo FSE Galicia 2014-2020 [ED481A-2018/042] Xunta de Galicia).

The Blanco lab was supported by MCIN / AEI / 10.13039/ 501100011033 [PID2020-115472GB-I00]; MCIN/ AEI / 10.13039/ 501100011033 / FEDER 'Una manera de hacer Europa' [BFU2016- 78121-P]; Xunta de Galicia / FEDER 'Una manera de hacer Europa' [ED431F-2016/ 019, ED431B-2016/ 016 and ED431C 2019/ 013]; CIMUS receives financial support from the Xunta de Galicia / FEDER [ED431G 2019/ 02, Centro Singular de Investigación de Galicia, accreditation 2019–2022].

USC
UNIVERSIDADE DE SANTIAGO DE COMPOSTELA

USC
UNIVERSIDADE
DE SANTIAGO
DE COMPOSTELA

INDEX

AGRADECIMIENTOS **13**

INDEX **16**

ABBREVIATIONS **20**

EXTENDED SUMMARY EN GALICIAN **22**

SUMMARY **28**

INTRODUCTION **29**

1. GENOME INTEGRITY AND DNA REPAIR 29

1.1 DNA damage response *31*

1.1.1 Direct reversal of DNA damage 31

1.1.2 Base excision repair 31

1.1.3 Nucleotide excision repair 33

1.1.4 Mismatch repair 35

1.1.5 DSB repair: NHEJ, HR and alternative pathways 37

1.1.5.1 NHEJ 37

1.1.5.2 Homologous recombination 39

1.1.5.3 Homology-mediated repair: MMEJ and SSA 41

1.1.6 Replication stress: DDT and fork reversal 43

1.1.6.1 DDT pathways: DNA damage bypass at the fork and behind the fork. 44

1.1.6.2 Fork reversal 48

1.2 Coordination of DNA repair by DNA damage checkpoint and cell cycle kinases *50*

1.2.1 DNA damage checkpoint 50

1.2.2 DNA repair throughout the cell cycle 54

2. HOMOLOGOUS RECOMBINATION AND ITS CELL-CYCLE REGULATION 55

2.1 DSB end resection and pathway choice *55*

2.2 Nucleofilament assembly, strand invasion and D-loop formation *60*

2.3 Extended D-loop disruption: BIR and SDSA *64*

2.4 Second-end capture: Dissolution and Resolution of dHJs *68*

2.4.1 Dissolution of dHJs 70

2.4.2 Resolution of dHJs 72

2.4.3 Crossover regulation 76

2.5 Modulation of SSE activity outside the NCO/CO balance *81*

3. PIF1 FAMILY OF HELICASES 87

3.1 Structural motifs and protein isoforms of Pif1-family helicases *88*

3.2 Pif1-helicases in DNA replication through physical barriers *91*

3.2.1 G-quadruplex structures 91

3.2.2 Highly transcribed genes and protein barriers 92

3.3 Pif1-helicases in Okazaki fragment maturation *93*

USC DE COMPOSTELA

3.4 Pif1-helicases in fork convergence during replication termination *94*

3.5 Pif1-helicases in telomere length homeostasis *94*

3.6 Pif1-helicases in DSB repair *95*

3.7 Pif1-helicases in mtDNA maintenance *96*

CHAPTER 1: ANALYSIS OF YEN1 PREMATURE ACTIVATION 98

1. OBJECTIVES 100

2. RESULTS 101

2.1 Overexpression of YEN1 deregulated alleles results in lethality, cell cycle arrest and Rad53 phosphorylation *101*

2.2 The lethality at strain overexpressing deregulated YEN1 is not dependent on checkpoint activation or homologous recombination, ... *104*

2.3 Expression of Yen1^{ON} at endogenous levels displays genetic interactions with HR helicases *105*

2.4 Cells deficient in nuclear Pif1 become hypersensitive to HU upon expression of Yen1^{ON} *109*

3. DISCUSSION 113

3.1 Cell-cycle regulation of Yen1 prevents genome instability. *113*

3.2 Upon genotoxic stress, nuclear Pif1 may prevent the accumulation of DNA secondary structures that Yen1^{ON} could hydrolyse. *114*

3.3 Future plans *115*

CHAPTER 2: PIF1 TRANSLATIONAL MECHANISM 118

1. OBJECTIVES 121

2. RESULTS 122

2.1 The pif1-m2 allele does not fully recapitulate the phenotypes derived from loss of Pif1 nuclear functions in pif1Δ mutants. *122*

2.2 A novel, fast-migrating isoform of Pif1 produced by alternative translation initiation *125*

2.3 Pif1 isoforms are produced through ribosomal leaky scanning *128*

2.4 Pif1$^{107-859}$ is catalytically active and retains partial functionality in the nucleus. *133*

2.5 Identification of the nuclear localization signal in Pif1 ..... *137*

2.6 Generation of an improved nuclear-null PIF1 allele *143*

2.7 Residual mitochondrial activity is present in pif1-m1 mutants *146*

3. DISCUSSION 152

3.1 Variable phenotypic impact of the residual nuclear Pif1 activity in pif1-m2 mutants *152*

3.2 Pervasive ribosomal leaky scanning of PIF1 mRNA facilitates ATI from AUG^{1}, AUG^{40} and AUG^{107} *153*

3.3 The intrinsic ATI mechanism operating on PIF1 mRNA constrains the efficiency of pif1-m1 and pif1-m2 as separation-of-function alleles. *153*

3.4 On the novel Pif1 isoform and the functionality of the N-terminal domain *156*

3.5 pif1^{nuc} and pif1^{mit} as valuable tools for the DNA repair field. *158*

3.6 Extensibility of our model to other genes *158*

CONCLUSIONS 166

MATERIALS 168

USC DE SANTIAGO DE COMPOSTELA

1. BACTERIAL STRAINS 168
2. YEAST STRAINS 168
3. PLASMIDS 173
4. OLIGONUCLEOTIDES 178
5. ANTIBODIES 185
6. MEDIA 185
7. REAGENTS 187
METHODS 192
1. MICROBIOLOGY 192
1.1 Bacterial methods 192
1.1.1 Bacterial inoculation and stocks 192
1.1.2 Preparation and transformation of competent cells 192
1.2 Yeast methods 193
1.2.1 Yeast cultures and stocks 193
1.2.2 Yeast mating, sporulation and tetrad dissection 193
1.2.3 Yeast transformation 193
2. MOLECULAR BIOLOGY 194
2.1 Isolation of plasmid DNA from bacteria 194
2.1.1 Isolation of plasmid DNA by alkaline lysis 194
2.1.2 Isolation of plasmid DNA by non-ionic detergent (NID) boiling. 195
2.2 Isolation of yeast genomic DNA 195
2.3 Polymerase chain reaction (PCR) 196
2.4 DNA purifications 196
2.4.1 PCR cassettes 196
2.4.2 Gel extraction 196
2.4.3 Ethanol precipitation 196
2.5 DNA sequencing 197
2.6 Cloning and mutagenesis of DNA fragments 197
2.6.1 Cloning with restriction enzymes 197
2.6.2 Gateway cloning 198
2.6.3 Mutagenesis by inverse PCR 198
2.6.4 Gene editing of *S. cerevisiae* 198
2.6.4.1 Integration of plasmids in the host chromosomes 198
2.6.4.2 Knockouts, promoter replacement and epitope tagging. 199
2.7 Determination of telomere length by Southern Blot. 199
2.8 Purification of synthetic DNA substrates 201
2.8.1 Purification of unlabelled and fluorescently labelled oligos 201
2.8.2 Hybridization of oligonucleotides and purification of fluorescentlylabeled substrates 203
3. BIOCHEMICAL TECHNIQUES 205
3.1 Preparation and analysis of protein extracts 205
3.1.1 Preparation of denatured protein extracts with trichloroacetic acid (TCA) 205

3.1.2 Total Protein detection by direct staining 206
3.1.2.1 Ponceau staining 206
3.1.2.2 Coomassie staining 206
3.1.2.3 Total protein staining 206
3.1.3 Protein detection by Western blot 206
3.2 Protein purifications *207*
3.2.1 Purification of scPif1 in *E. coli* 207
3.2.1.1 Optimization of induction conditions and solubility tests 208
3.2.1.2 Purification of Pif1 209
3.2.2 Purification of Yen1 210
3.3 Biochemical assays *213*
3.3.1 ATPase assays 213
3.3.2 DNA unwinding assays 214
4. CELL BIOLOGY TECHNIQUES 215
4.1 Fluorescence microscopy *215*
4.2 Flow cytometry *216*
4.3 Genotoxicity assays *217*
5. *IN SILICO* ANALYSES 218
BIBLIOGRAPHY 219
INDEX OF FIGURES 270

USC
UNIVERSIDADE DE SANTIAGO DE COMPOSTELA

ABBREVIATIONS

3'- dRP	3'-deoxyribose phosphate
5'- dRP	5'-deoxyribose phosphate
AP	Apurinic or apyrimidinic
ATI	Alternative translation initiation
ATP	Adenosine triphosphate
BER	Base excision repair
BIR	Break-induced replication
BSA	Bovine serum albumin
BTR	BLM-Topoisomerase IIIα- RMI1-RMI2
CDK	Cyclin-dependent kinase
CFSs	Common fragile sites
CO	Crossover
CPT	Camptothecin
CSM	Complete supplement mixtures
CTD	C-terminal domain
CV	Column volume
DDC	DNA damage checkpoint
DDK	Dbf4-dependent kinase
DDR	DNA damage response
DDT	DNA damage tolerance
D-loop	Displacement loop
dHJ	Double Holliday junction
DTT	Dithiothreitol
DIG	Digoxigenin
DSBR	Double-strand break repair
gDNA	Genomic DNA
HDR	Homology-directed repair
HJ	Holliday Junction
HR	Homologous recombination
HU	Hydroxyurea
IPTG	Isopropyl β- d-1-thiogalactopyranoside
IRES	Internal ribosomal entry sites
IDLs	Insertion or deletion loops
JM	Joint Molecule
LB	Lysogenic vroth
LOH	Loss of heterozygosity
MMBIR	Microhomology-mediated BIR
MMEJ	Microhomology-mediated end-joining
MMR	Mismatch repair

MMS	Methyl methanesulfonate
MTS	Mitochondrial targeting signal
NCO	Non-crossover
ND	Nuclease-dead
NER	Nucleotide excision repair
NHEJ	Non-homologous end-joining
nHJ	Nicked Holliday junction
NID	Non-ionic detergent
NLS	Nuclear localization signal
NTD	N-terminal domain
ORF	Open reading frame
PCNA	Proliferating cell nuclear antigen
PIC	Pre-initiation complex
PIKK	Phosphatidylinositol-3 kinase-related kinase
PIP	PCNA-interacting protein
Polδ	DNA polymerase δ
RDR	Recombination-dependent restart
RFB	Replication fork barrier
RFC	Replication Factor C
ROS	Reactive oxygen species
SC	Synthetic complete media
SDSA	Synthesis-dependent strand annealing
SP	Salvage pathway
SSA	Single strand annealing
SSB	Single strand breaks
SSE	Structure selective endonuclease
STR	Sgs1-Top3-Rmi1
TAE	Tris-acetate-EDTA
TBE	Tris-Borate-EDTA
TCA	Trichloroacetic acid
TLC	Thin-layer chromatography
TLS	Trans-lesion synthesis
TS	Template switching
uORF	Upstream uORF
WGD	Whole genome duplication
WT	Wild-type

USC UNIVERSIDADE DE SANTIAGO DE COMPOSTELA

EXTENDED SUMMARY EN GALICIAN

A reparación do ADN é fundamental para garantir a preservación da estabilidade xénomica e transmitir de forma fidedigna a información xenética á seguinte xeración. As células están expostas de maneira continuada a diversos axentes que comprometen a integridade do seu xenoma ao introducir modificacións que alteran a información quimicamente codificada polas súas febras. Entre os factores que constitúen un risco para o ADN inclúense axentes xenotóxicos exóxenos, como as especies reactivas de oxíxeno e diversos carcinóxenos, pero tamén procesos intrínsecos que inclúen transaccións entre moléculas ADN, como a replicación do xenoma. Un dos danos máis citotóxicos no ADN son as roturas de dobre febra (DSBs, *Double strand breaks*), que poden causar inestabilidade no xenoma se non se recupera a información xenética perdida na rotura. A reparación dos DSBs pode ser realizada por dúas vías principais: a recombinación homóloga (HR, *homologous recombination*) e a unión non homóloga de extremos (NHEJ, do inglés "*non-homologous end joining*"). A HR é un mecanismo de alta fidelidade que emprega unha molécula de ADN homóloga como modelo para a reparación dos DSBs. En particular, as células favorecen o uso da cromátide irmá como model de reparación, polo que esta ruta se encontra restrinxida ás fases S-G2-M do ciclo celular.

Dentro do proceso da HR, existen varias rutas de reparación que aseguran a eliminación de todos os intermediarios de recombinación que xorden durante o proceso de copiado da información xenética perdida, incluíndo a hibridación de cadea dependente de síntese (SDSA, *Synthesis-dependent strand-annealing*), a vía clásica de reparación de roturas de dobre cadea (DSBR, *Double Strand Break Repair*) e a replicación inducida por rotura (BIR, do inglés *Break-induced replication*). En todos os casos, o proceso de reparación comeza coa resección do DSB, un paso no que os extremos 5’ da rotura son degradados. Este paso é mediado pola acción coordinada de nucleasas e helicasas, incluíndo o complexo MRN (MRe11-Rad50-Xrs2), Exo1 e Dna2. A resección xera moléculas de cadea sinxela cun extremo 3’-OH que pode primar a síntese do ADN e, ademais, proporciona o substrato para a formación de filamentos nucleoproteicos. Os nucleofilamentos fórmanse pola unión da recombínase Rad51 sobre o ADN de cadea sinxela, iniciando a busca dunha secuencia homóloga na cromátida irmá ou no cromosoma homólogo que poida servir como molde para a reparación. Unha vez atopada a secuencia homóloga, o nucleofilamento de Rad51 é tamén capaz de invadir o dúplex de ADN homólogo, desprazando unha das cadeas do mesmo, o que resulta na formación dunha estrutura de ADN ramificada, denominada bucle de desprazamento (D-loop, *Displacement loop)*. Os D-loops son os intermediarios centrais da HR, e poden ser procesados por helicasas (Mph1, Srs2) ou primar un evento de síntese a partir do 3’-OH da cadea invasora. A súa vez, o D-loop alongado pode ser procesado pola ruta de SDSA ou, se a cadea desprazada do D-loop híbrida co segundo estremo 3’-OH da rotura, madurar nun novo intermediario de recombinación, a dobre unión de Holliday (dHJ, *Dobre unión de Holliday*). Estas estruturas cruciformes conectan covalentemente as moléculas de ADN involucradas no proceso de reparación, polo que deben ser eliminadas antes de que aconteza a división celular, para evitar comprometer a segregación cromosómica. Dada a estabilidade diste intermediario, as células contan con dous mecanismos

diferentes para garantir a pronta eliminación das dHJ: a disolución e maila resolución. Durante a disolución, un complexo constituído por Sgs1-Top3-Rmi1 (STR) dirixe a migración converxente das unións de Holliday para orixinar un hemicatenano que é seguidamente decatenado por Top3. Por outro lado, a resolución das dHJ é levada a cabo por distintas endonucleases selectivas de estrutura (SSEs, do inglés *Structure-selective endonucleases*), entre as que se inclúen Mus81-Mms4, Slx1-Slx4 e Yen1.

Dependendo da ruta de HR e das enzimas empregadas para a eliminación dos intermediarios de recombinación, a reparación dos DSB pola HR terá como produtos finais moléculas de ADN sen entrecruzamentos (CO, *crossovers*) ou con eles (NCO*, non-crossovers*). En particular, as rutas de SDSA ou disolución xeran exclusivamente NCOs, ao non producirense intercambios de dúplexes entre as moléculas donantes e receptoras a ambos lados da DSB. Pola contra, o corte das dHJ durante a resolución produce unha mestura entre CO é NCO, dependendo da orientación dos cortes requiridos para procesar as dHJs. Dado o potencial risco de perda de heterocigosidade asociada aos CO entre cromosomas homólogos, as células contan cun intricado sistema de regulación que permite canalizar os intermediarios da recombinación cara as rutas de SDSA e disolución. Durante a última década demostrouse como a maquinaria que dirixe a progresión do ciclo celular é tamén responsable de xerarquizar a activación das rutas de HR e controlar o seu acceso aos intermediarios de recombinación, incorporando unha dimensión temporal e espacial ao control da HR. O traballo de distintos grupos demostrou como quinasas e fosfatasas reguladoras da progresión do ciclo, a través de modificacións pos-traducionais, modulan a activación das rutas de procesamento de dHJs. En particular, os eventos de fosforilación e defosforilación das resolvasas Mus81-Mms4 e Yen1 pospoñen a súa activación ata a transición G2/M e fase M respectivamente, acadando así una activación secuencial que permite favorecer o procesamento de dHJs polas rutas SDSA e disolución. Ao pospoñer a activación das resolvasas ata as últimas etapas do ciclo celular, esta regulación limita a formación de COs e, ao mesmo tempo, acada a eliminación completa de tódalas dHJs antes da división celular.

Así e todo, limitar os niveis de COs podería non ser a única causa pola que as células restrinxen a actividade das resolvasas aos últimos estadios do ciclo celular. Como se mencionou ao principio deste resumo, ademais da HR, os procesos de replicación e transcrición tamén involucran transaccións entre moléculas de ADN e estruturas ramificadas como forcas de replicación, estruturas G-cuádruplex, ramificacións 5', R-Loops (híbridos entre ARN e ADN), etc. Ademais, a exposición de rexións de cadeas sinxelas de ADN e as condicións topolóxicas durante a replicación e a transcrición tamén favorecen que o ADN adquira estruturas que se desvían da conformación habitual, incluíndo G-cuádruplex ou H-DNA.

Dado que a regulación de Yen1 a inactiva e exclúe do núcleo durante as fases S-G2, cando a maioría do ADN é duplicado, a súa activación tardía, ademais de reducir os niveis de entrecruzamentos, podería ter tamén unha función protectora para evitar a súa actividade sobre

USC UNIVERSIDADE DE COMPOSTELA

intermediarios de replicación, intermediarios de recombinación temperáns, ou de estruturas secundarias. En liña con esta hipótese, demostrouse en diferentes contextos como o procesamento por SSEs de intermediarios de replicación, reparación ou estruturas secundarias leva asociados riscos para á estabilidade xenómica das células, que polo tanto promoven o desmantelamento destes intermediarios por helicasas.

Para testar a nosa hipótese, empregamos diversos alelos desregulado da nucleasa *YEN1*. Ao comezo da fase S, a fosforilación de Yen1 por Cdc28 (CDK) reduce a súa actividade catalítica e forza a súa exportación ao citoplasma ata o comezo da anafase, cando a fosfatasa Cdc14 reverte esta inactivación. Polo tanto, cara o final da fase M, Yen1 pode acceder ao núcleo nun estado activo para eliminar os intermediarios de recombinación máis persistentes. O coñecemento de esta regulación permitiu xerar un alelo desregulado baseado na mutación de nove serinas localizadas en lugares consenso de fosforilación para Cdk. Este alelo, denominado *YEN1*^{ON}, codifica unha versión de Yen1 constitutivamente activa e que localízase no núcleo ao longo de todo o ciclo celular. Este alelo constitúe unha ferramenta de extrema utilidade, xa que permite desacoplar a resolución dos intermediarios recombinatorios da progresión do ciclo celular, para estudar as posibles consequencias deletéreas da activación temperán de Yen1.

Unha aproximación inicial utilizando una versión do alelo *YEN1*^{ON} inducible por galactosa demostrou que a sobreexpresión de *YEN1*^{ON} é extremadamente prexudicial para as células, acadando a letalidade completa coa indución total do promotor *GAL1*, mentres que a sobreexpresión a niveis comparables do alelo silvestre non afecta a viabilidade. A maiores, obtivemos un resultado insospeitado co control catalíticamente inactivo da versión desregulada de *YEN1,* denominado *YEN1*$^{ON\text{-}ND}$*,* xa que a sobreexpresión diste mutante tamén deriva na morte celular. Anque este resultado indicaría que a toxicidade de Yen1^{ON} é independente da súa actividade nucleásica, propoñemos unha hipótese alternativa na que o efecto negativo dominante de *YEN1*$^{ON\text{-}ND}$ proviría da súa unión as estruturas de ADN ramificado obstaculizando o procesamento distas estruturas por outras nucleasas ou helicasas. Por lo tanto, as letalidades asociadas a sobreexpresión de Yen1^{ON} e Yen1$^{ON\text{-}ND}$ terían unha orixe distinta en cada unha das versións desreguladas.

En ambos casos, a morte celular vén acompañada dunha robusta activación do punto de control de dano ao ADN, tal e como se deduce pola fosforilación de Rad53 e a alteración do perfil normal do ciclo celular, cunha acumulación aparente de células na fase S. Isto podería ser compatible coa xeración de roturas de ADN ou a persistencia de longos tramos cadea sinxela nestes mutantes, o que concordaría coa súa capacidade para interferir na progresión normal da fase S. De importancia, un arresto prolongado do ciclo celular non é a principal causa de morte celular nestas estirpes, xa que a eliminación de *RAD53* non pode suprimir esta letalidade. Cunha aproximación similar, testamos tamén se a letalidade puidera ser consecuencia do procesamento de intermediarios de recombinación temperáns, como os D-loops. Sen embargo, a toxicidade por sobreexpresión de Yen1^{ON} e Yen1$^{ON\text{-}ND}$ non só non é suprimida no fondo xénico deficiente en recombinación *rad52*Δ, senón que agrava o efecto tóxico da desregulación de Yen1. Isto

suxire que parte do dano asociado á desregulación e sobreexpresión de Yen1 pode ser reparado pola propia ruta de HR.

Estas observacións, xunto cos resultados doutros membros do laboratorio, indicaron que a sobreexpresión de *YEN1*^{ON} provoca unha inestabilidade xenómica masiva que non pode ser suprimida por mutacións noutros xenes. Polo tanto, co fin de obter máis información sobre as vías de metabolismo do ADN que poden verse afectadas pola actividade prematura da resolvase Yen1, decidimos empregar una nova aproximación, consistente na búsqueda de interaccións xenéticas entre *YEN1*^{ON} expresada a niveis endóxenos e outros factores de reparación do ADN. Para iso, seleccionamos helicasas importantes para o procesamento de intermediarios de recombinación e replicación, cuxa deleción debería vir acompañada duns maiores niveis de potenciais substratos para Yen1^{ON}. Con esta estratexia, descubrimos dous tipos principais de interaccións. Por un lado, a presenza de Yen1^{ON} a niveis endóxenos parece ter un efecto beneficioso naquelas situacións onde a viabilidade celular se ve comprometida pola acumulación de intermediarios de recombinación sen resolver. Esta situación xorde como consecuencia da mutación simultánea de xenes de HR que levan a letalidade ou enfermidade sintética ou da combinación de mutacións individuais con axentes xenotóxicos, confirmando e ampliando resultados anteriores. Neste contexto, Yen1^{ON} suprime eficazmente o mesmo conxunto de interaccións xenéticas que a eliminación de *RAD52*, demostrando co procesamento de intermediarios de recombinación por parte de Yen1^{ON} rescata o fenotipo de morte por recombinación, pero non no contexto doutras letalidades sintéticas. Por outro lado, descubrimos que nalgúns contextos xenéticos a expresión de Yen1^{ON} provoca unha maior hipersensibilidade a axentes xenotóxicos como MMS, HU ou CPT. En particular, a interacción entre *pif1*Δ é *YEN1*^{ON} resulta especialmente interesante, xa que Pif1 é unha das principais helicasas para o procesamento de estruturas secundarias no ADN. Por tanto, decidimos afondar no mecanismo molecular subxacente desta interacción como unha forma de entender mellor a relevancia da regulación de Yen1.

Non obstante, non moi avanzada esta liña de investigación, atopamos un obstáculo técnico que impediu o seu desenvolvemento posterior: os intentos de reproducir esta interacción xenética con calquera dos dous alelos clásicos de separación de función para PIF1*, pif1-m1* (nuclear) e *pif1-m2* (mitocondrial), fallaron dunha forma sistemática na recapitulación da interacción xenética entre *pif1*Δ e *YEN1*^{ON}. Dados os efectos pleiotrópicos da eliminación completa, que combina defectos nucleares e mitocondriais, non puidemos descartar unha interacción indirecta debido a efectos metabólicos maiores causados polo fenotipo *petite* dos mutantes *pif1*Δ*,* que poderían ser pouco informativos para os nosos propósitos. Aínda que conseguimos descartar a hipótese dunha interacción xenética entre *YEN1*^{ON} e a condición *petite*, decidimos que, para entender as complexidades moleculares subxacentes a esta interacción, precisabamos as causas polas que *pif1-m1* e *pif1-m2* non reproducen a interacción *pif1*Δ *YEN1*^{ON}.

Os nosos resultados con *pif1-m2 YEN1*^{ON} confirman outros estudos publicados nos que pif1-tampouco recapitula totalmente os fenotipos *pif1*Δ atribuídos ás súas funcións nucleares, o que

USC DE COMPOSTELA

suxire novamente que a actividade nuclear de Pif1 se mantén ata certo punto nese mutante. Dado que o uso de estirpes *pif1*Δ para investigar os roles de Pif1 ou outros factores de reparación do ADN presenta importantes desvantaxes debido aos efectos pleiotrópicos da deleción completa, investigamos o grao de separación de función de *pif1-m2* en diferentes configuracións xenéticas. Os nosos experimentos co alelo *pif1-m2* indican que, calquera que sexa a cantidade de Pif1 nuclear nestes mutantes, é suficiente para enmascarar total ou parcialmente os resultados obtidos con *pif1*. Nalgúns, *pif1-m2* compórtase coma un alelo de separación de función nuclear completo. Noutros casos, *pif1-m2* aseméllase a un alelo hipomórfico, exhibindo fenotipos intermedios debido aos niveis reducidos de nPif1. Por último, *pif1-m2* pode enmascarar completamente interaccións xenéticas observadas previamente con *pif1*Δ, como no caso *pif1-m2 YEN1*^{ON} ou *pif1*Δ *dia2*Δ.

Pif1 ten dúas isoformas diferentes en *S. cerevisiae* que permiten acadar a localización dual necesaria para cumprir os seus roles tanto no núcleo (nPif1) como nas mitocondrias (mPif1). As dúas isoformas están codificadas polo mesmo xen, e prodúcense mediante un mecanismo de iniciación alternativa da tradución (ATI, do inglés *Alternative translation initiation*). Este mecanismo baséase na traducción do ARNm de PIF1 a partir do o uso alternativo dos dous primeiros codóns AUG situados na mesma pauta de lectura (AUG^{1} e AUG^{40}), entre os cales se encontra codificada un sinal de localización mitocondrial (MTS, *Mitochondrial targetting signal*). Cando a tradución comeza dende AUG1, a MTS N-terminal dirixe rapidamente a proteína cara as mitocondrias. En cambio, se a iniciación da tradución comeza en AUG^{40}, prodúcese unha isoforma máis corta que carece da MTS e é importada posteriormente ao núcleo (nPif1). O modelo ATI descrito inspirou o desenvolvemento de dúas alelos de separación de función de Pif1. En *pif1-m1*, a produción de mPif1 é eliminada pola mutación de ATG1, mentres que nPif1 aínda pode ser traducido desde o AUG^{40} intacto e importado ao núcleo, presumiblemente a través dun NLS aínda non caracterizado. Pola contra, en *pif1-m2*, a mutación de ATG^{40} anula a produción de nPif1 sen afectar a tradución de mPif1, dando lugar a cepas deficientes en nPif1.

Dado que o modelo de ATI proposto non explica o presenza de actividade nuclear no alelo *pif1-m2*, investigamos a causa de esta discrepancia. A nosa investigación levounos a descubrir una nova isoforma surxe doutro evento de ATI no AUG^{107}, xerando unha forma truncada polo N-terminal, Pif1$^{107-859}$. Esta isoforma, ademais, está especificamente enriquecida nos mutantes *pif1-m2,* é tan activa como nPif1 *in vitro*, e pode suplir algunhas das funcións de nPif1, confirmando que ista isoforma pode contribuír a enmascarar os fenotipos nucleares en estirpes *pif1-m2.* A maiores, determinamos que *leaky scanning* é o mecanismo específico de ATI responsábel da xeración de mPif1 e nPif1, a dunha terceira isoforma, Pif1$^{107-859}$. De acordo con este modelo, a presenza de secuencias Kozak pouco óptimas flanqueando aos codóns de inicio permite a unha fracción dos ribosomas continuar co seu escaneo, sen iniciar a tradución no primeiro codón de inicio que atopen. Deste xeito, os ribosomas son capaces de producir as tres isoformas de Pif1 a partir de un mesmo mRNA. Este mecanismo tamén explica que a mutación

USC UNIVERSIDADE DE SANTIAGO DE COMPOSTELA

en AUG^{40} en *pif1-m2* permite que una maior fraccións de ribosomas acaden o codón AUG^{40}, aumentando así a cantidade da isoforma Pif1$^{107-859}$.

Para xerar un alelo de separación completo para as función nucleares, identificamos e caracterizamos por primeira vez a sinal de localización nuclear (NLS, *Nuclear Localization Signal*) de Pif1, para abrogar a importación nuclear de tódalas isoformas. Este alelo, chamado *pif1^{nls}* todavía exhibe una certa actividade residual nuclear, polo que combinamos as mutacións do alelo *pif1^{nls}* co a mutación de *pif1-m2,* xerando un novo alelo, que denominamos *pif1^{mit}* , dada a súa localización mitocondrial. *pif1-mit*, comparado con *pif1-m2*, si consigue recapitular os fenotipos nucleares de *pif1*Δ, confirmando a completa separación de función deste alelo mellorado.

Durante o transcurso dos diversos experimentos realizados, tamén observamos una aparente falta de separación de separación do alelo *pif1-m1*, que non exhibe os defectos mitocondriales que sé poden observarse na deleción *pif1*Δ. A diferenza de *pif1-m2*, non se reportou na literatura ningún caso da separación incompleta de *pif1-m1,* polo que investigamos as causas dos problemas asociados a este alelo, aplicando o novo modelo de *leaky scanning*. Ante a falta de codóns de inicio que podan substituír a AUG^{1} en *pif1-m1*, centramos o noso análise nos cinco codons máis similares a AUG, os chamados *near-cognates* (nAUG), que solo defiren en un nucleótido do codón de inicio canónico, e poden ser empregados para o inicio da tradución, aunque con unha eficiencia moi baixa. Os nosos resultados a tradución a partir doestes nAUG é suficiente para a producir baixas cantidades de mPif1 que, así e todo, son capaces de manter unha función mitochondrial similar as estirpes silvestres.

Para concluír, empregamos os novos alelos de separación de función para desambiguar as interaccións xénicas entre *pif1*Δ *rad3-102* e *pif1*Δ *YEN1^{ON}*. En ambos casos, as novas ferramentas xenéticas desenvolvidas neste traballo permitiron determinar a orixe destas fenotipos. No caso de *pif1*Δ *rad3-102,* demostramos que os defectos mitochondriales, en conxunto con *rad3-102*, son os responsables da hipersensibilidade a hidroxiurea. Pola contra, tamén probamos que a hipersensibilidade das estirpes *pif1*Δ *YEN1^{ON}* veñen dadas por la ausencia de Pif1 nuclear.

USC
UNIVERSIDADE DE SANTIAGO DE COMPOSTELA

SUMMARY

Homologous recombination (HR) is regarded as an error-free pathway to repair DNA double-strand-breaks (DSBs). Despite being the main mechanism to deal with DSBs from S to M phase, HR entails the formation of several branched recombination intermediates that must be timely disengaged to safeguard chromosome segregation and cell viability. Hence, cells are endowed with DNA helicases and structure-selective endonucleases (SSEs) that sever these physical connections between DNA joint molecules prior to cell division. Strikingly, although these intermediates can arise early in the S and G2 phases, cells restrain the action of SSEs until the onset of mitosis. This is accomplished through the concerted actions of cell cycle master regulators like CDK1 or PLK1, which drive sequential waves of SSE activation or inhibition. This delay in the activation of SSEs until the final stages of cell cycle is conserved from yeast to humans, suggesting that their tight control could be crucial to prevent the unscheduled processing of DNA replication and repair intermediates.

To understand the biological relevance of this strict regulatory system, we searched for genetic interactions between a constitutively active version of the *YEN1* nuclease (*YEN1*^{ON}) and key helicases involved in DNA replication and repair. Here, we show that deletion of the conserved *PIF1* helicase in a *YEN1*^{ON} strain results in a dramatic reduction of its viability under genotoxic stress. This suggests that the unscheduled nucleolytic processing of secondary DNA structures accumulated in the absence of *PIF1* is detrimental for cells. Since the *PIF1* gene encodes both the mitochondrial and nuclear isoforms of the enzyme, we decided to take advantage of widely employed separation-of-function alleles (nuclear or mitochondrial-specific) to dissect the molecular details of this genetic interaction, but we failed to fully recapitulate it with either allele. This prompted us to delve into the translational control of the Pif1 helicase, leading us to the refinement of the molecular mechanism of alternative translation initiation for *PIF1* mRNA, the discovery of a new nuclear Pif1 isoform and the development of the first *bona-fide* nuclear-null Pif1 isoform.

USC
UNIVERSIDADE DE SANTIAGO DE COMPOSTELA

INTRODUCTION

1. GENOME INTEGRITY AND DNA REPAIR

The preservation of genome integrity, referring to the stability of the genetic material inside the cell, is essential for both its survival and the faithful transmission of hereditary information to the offspring (Kolodner 2017). This is achieved by the synergistic effect of three major molecular events: i) DNA repair, to counteract DNA lesions and sustain low variation rates, ii) DNA replication, to guarantee the accurate duplication of the genome and iii) chromosome segregation, to assemble the duplicated genome in two equal packages and symmetrically distribute them to daughter cells.

The instructions that control every cellular process in all living organisms are chemically codified in the sequence of heterocyclic bases inside the DNA double helix (Watson and Crick, 1953). However, the stability of DNA molecules is constantly threatened by both exogenous and endogenous factors. It is well established that most of the DNA damage arises from endogenous sources, with by-products of cellular metabolism and failed DNA transactions inflicting tens of thousands of DNA lesions per cell every day (Barnes and Lindahl, 2004; De Bont and van Larebeke, 2004; Tubbs and Nussenzweig, 2017; Vilenchik and Knudson, 2003). DNA is susceptible to both spontaneous decay in aqueous solutions (Lindahl, 1993) and to alterations induced by reactive oxygen species (ROS), nitrogen and carbonyl species, lipid peroxidation products, endogenous alkylating agents, or estrogen and cholesterol metabolites (Chatterjee and Walker, 2017; Hoeijmakers, 2009). Besides, the intrinsic error rates of the enzymatic machineries responsible for DNA replication, transcription and repair constitute an added burden for the integrity of the genetic material (Kunkel and Bebenek, 2000). Finally, exposure to environmental DNA-damaging agents like UV-light, ionizing radiation or genotoxic compounds in food, air, tobacco or therapeutic drugs, increases the amount and complexity of DNA lesions (Figure 1) (Chatterjee and Walker, 2017; Hoeijmakers, 2009). Independently of their origin, endogenous and exogenous factors induce different types of chemical reactions, including hydrolysis, alkylation and oxidative reactions with radicals that damage the DNA at different levels and compromise the information it encodes (Gates, 2009). These chemical reactions, together with the intrinsic error rates of enzymes during DNA transactions translate into a myriad of DNA lesions, including: abasic sites, damaged bases, bulky adducts, intra and inter-strand crosslinks, single and double strand breaks, and mismatched bases (Chatterjee and Walker, 2017; Hoeijmakers, 2009).

Therefore, it is not surprising that all organisms are endowed with a battery of DNA repair mechanisms for the continuous surveillance of DNA integrity (Figure 1). Each DNA repair pathway targets and removes specific types of lesions, minimizing the detrimental outcomes of genomic instability (Aguilera and García-Muse, 2013; Sancar et al., 2004). However, when DNA repair is impaired or cells confront high levels of stress, DNA insults may pile up and become permanent mutations (Altieri et al., 2008). Time-dependent accumulation of mutations

USC UNIVERSIDADE DE SANTIAGO DE COMPOSTELA

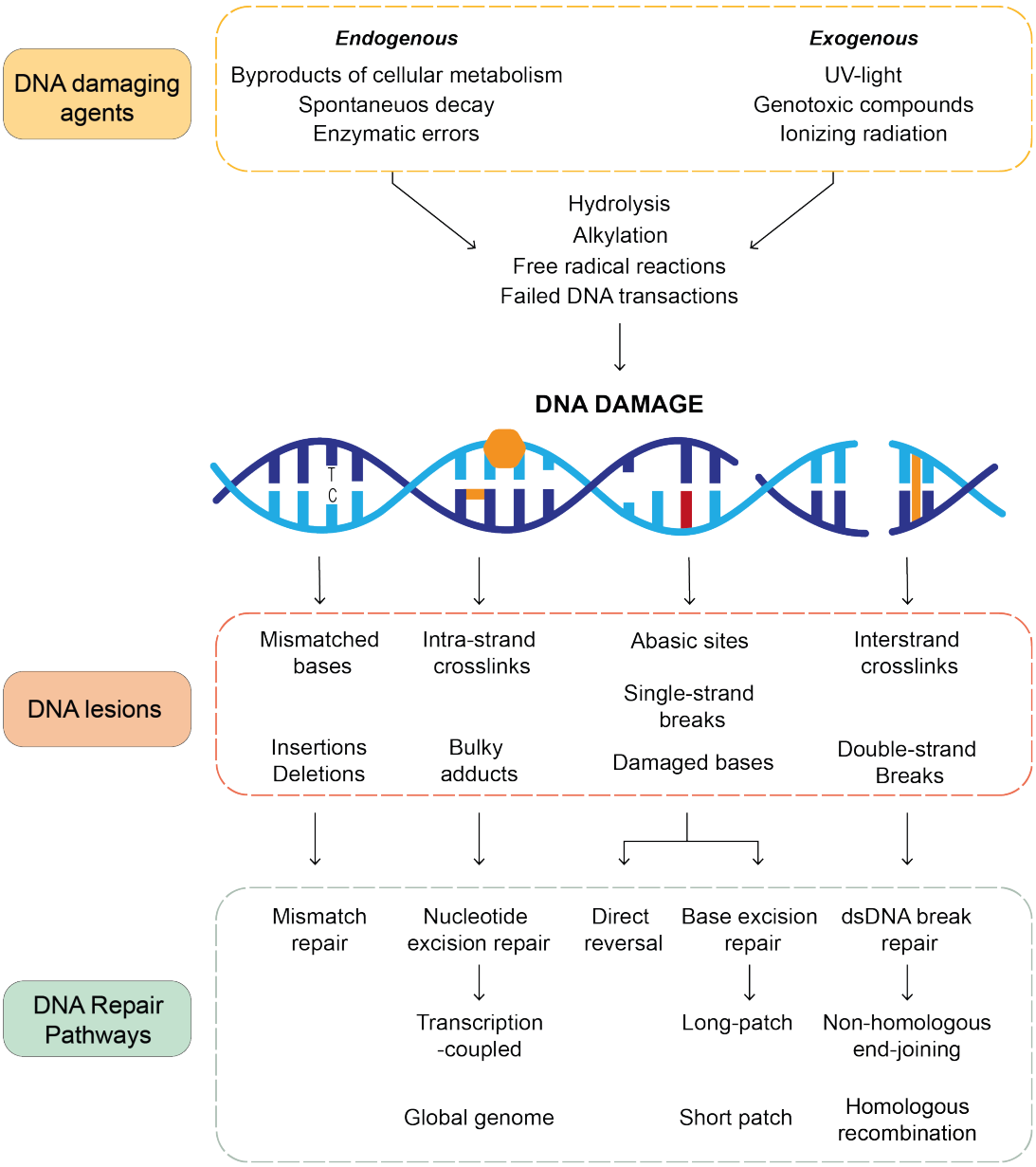


Figure 1. DNA repair overview. Schematics of common DNA damaging agents, DNA lesions, and the specific DNA repair pathways for each type of damage.

may compromise essential cellular functions and lead to uncontrolled cell division, premature cell death or senescence (Hoeijmakers, 2009). Therefore, DNA damage is considered as a key determinant in human disease. The paramount relevance of accurate DNA repair is underscored by the multiple human pathologies that stem from defects in these pathways, including neurological disorders, immunodeficiency, infertility, aging, cancer and several congenital syndromes(Freitas and de Magalhães, 2011; Hanahan and Weinberg, 2011; Jackson and Loeb, 2001; Jackson and Bartek, 2009; Rass et al., 2007; Surova and Zhivotovsky, 2013).

USC UNIVERSIDADE DE SANTIAGO DE COMPOSTELA

1.1 DNA damage response

Cells have evolved a series of sophisticated systems that work collectively to minimize the deleterious consequences of DNA damage, generally referred to as the DNA damage response (DDR). In addition to the DNA repair mechanisms themselves, the DDR includes the DNA damage tolerance (DDT) pathways and the DNA damage checkpoint (DDC). Thus, the detection of DNA lesions activates the DDR to signal their presence and promote their repair in a manner that is in accordance to the specific cell-cycle stage or the presence of ongoing DNA transactions like DNA replication or chromosome segregation (Chatterjee and Walker, 2017; Ciccia and Elledge, 2010; Jackson and Loeb, 2001). In the next sections, I will briefly describe each of these routes that contribute to the DDR in the budding yeast *Saccharomyces cerevisiae*, the model organism employed in this Thesis.

1.1.1 Direct reversal of DNA damage

This constitutes the simplest and most accurate way to repair DNA, as it solely involves the undoing of a chemical modification in a single-step reaction and without cleaving the DNA backbone. While straightforward, direct reversal of DNA damage can only deal with a minor subset of lesions, albeit quite prevalent quantitatively. In particular, this machinery is limited in *S.cerevisiae* to two different enzymes: the photolyase Phr1, which hydrolyses the cyclobutene pyrimidine dimers caused by UVB and UVC radiation, and the methyltransferase Mgt1, which removes methyl groups from modified bases (Boiteux and Jinks-Robertson, 2013). In contrast, the rest of DNA repair pathways involve sequential enzymatic reactions carried out by multiprotein complexes assembled at the lesion (Beard et al., 2019), as described in the sections below.

1.1.2 Base excision repair

Base excision repair (BER) is crucial for removing small and non-helix distorting lesions, including deaminated, oxidized and alkylated bases, as well as apurinic/apyrimidinic (AP) sites or the presence of uracil in the DNA (Beard et al., 2019). It operates in both nucleus and mitochondria, being particularly important in the latter for the maintenance of the mitochondrial DNA (mtDNA), due to the higher levels of ROS species in this organelle. Generally, BER involves four main steps (Figure 2): i) DNA damage recognition and removal; ii) DNA incision; iii) DNA synthesis and end-trimming, and iv) nick ligation. These steps are mediated by the coordinated actions of various enzymes with different types of DNA modifying activities, including: DNA N-glycosylases, AP endonucleases/lyases, 3'-phosphodiesterases or 3'-phosphatases, DNA polymerases and DNA ligases (Hoeijmakers, 2001).

First, the lesion is recognized by damage-specific DNA N-glycosylases. *S. cerevisiae* is endowed with two monofunctional glycosylases (Ung1 and Mag1) that only catalyse cleavage of N-glycosylic bonds and several bifunctional DNA N-glycosylases/AP lyases. These bifunctional glycosylases can additionally hydrolyse the phosphodiester backbone of AP sites through its AP-lyase activity and include enzymes like Ntg1, Ntg2 and Ogg1, specialized in the removal of oxidized bases (Boiteux and Guillet, 2004). Monofunctional and bifunctional DNA glycosylases start the BER pathway by severing the N-glycosylic bond linking the damaged

USC UNIVERSIDADE DE SANTIAGO DE COMPOSTELA

base to the sugar moiety, releasing the free base and leaving an AP site. Then, the AP site is either recognized and incised by AP endonucleases (Apn1, Apn2), yielding SSBs with a 5' deoxyribose phosphate (5'-dRP) end, or by bifunctional glycosylases with AP-lyase activity, generating SSBs with a 3'-deoxyribosephosphate (3'-dRP) attached (Boiteux and Guillet,

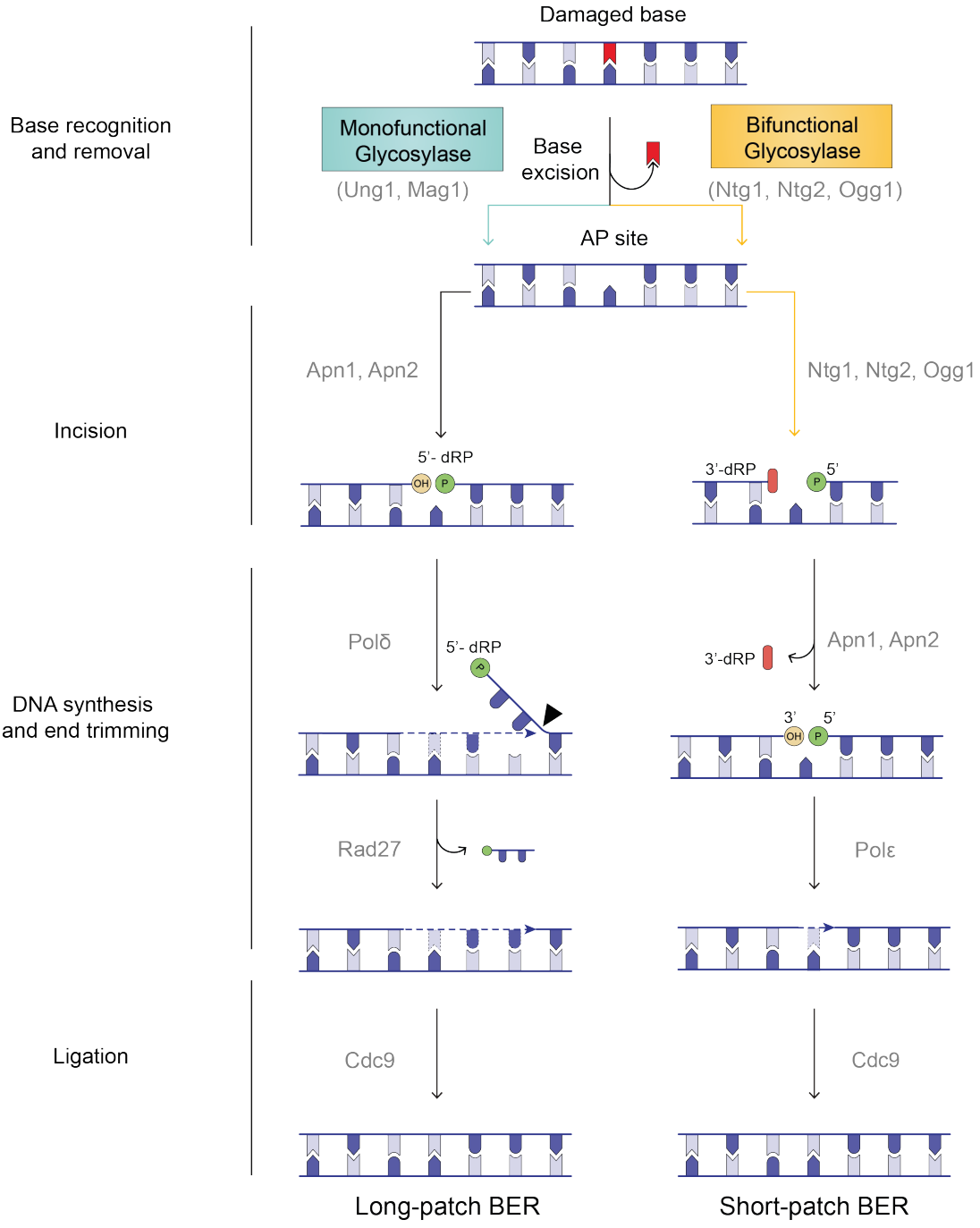


Figure 2. BER pathway. AP sites are generated by the incision of DNA N-glycosylases or by the spontaneous loss of a base (not depicted in the figure). Apn1 or Apn2 nick the DNA backbone to start the long-patch BER, generating a 5'-dRP that is removed by the sequential actions of Polδ and Rad27. Alternatively, in short-patch BER, the AP site is processed by AP lyases. The resulting 3'-dRP is trimmed by the diesterase activity of Apn1/Apn2, and the resulting gap filled by Polε. The final ligation of the compatible ends is mediated in both sub-pathways by the Cdc9 ligase

2004). These two different types of chemically modified breaks constitute the key determinant to channel these SSBs to long-patch BER (Figure 2. BER pathway, left branch) or short-patch BER (Figure 2. BER pathway, right branch), respectively. On the one hand, in long-patch BER, the presence of a 3'-hydroxyl group in SSBs with 5'-dRP primes DNA synthesis by Polδ, extending for 5-10 nucleotides. The resulting 5'-flap is processed by the 5'-flap endonuclease Rad27, leaving a nicked dsDNA molecule ready to be joined by Cdc9 ligase. On the other hand, in short-patch BER, the additional 3'-phosphodiesterase activity of AP endonucleases removes the blocked termini (3'-dRP) impeding DNA synthesis, leaving a 1-nt gap with a 3'-OH that is readily filled by Polε and subsequently ligated by Cdc9 (Boiteux and Guillet, 2004).

1.1.3 Nucleotide excision repair

Nucleotide excision repair (NER) removes a variety of helix-distorting lesions produced by bulky adducts that can block the progression of DNA and RNA polymerases. In contrast to BER, NER mainly protects the DNA from the mutagenic effects of exogenous sources, such as UV-induced lesions and carcinogen-derived bulky adducts (Cadet et al., 2005; Friedberg, 2006), although it can also neutralize intramolecular crosslinks caused by endogenous oxidative agents (Kuraoka et al., 2000). Eventually, NER also constitutes an alternative to BER for the repair of AP sites and oxidized bases (Scott et al. 1999; Swanson et al. 1999). This pathway seems to function exclusively in the nucleus, since no NER activity has been detected in mitochondria (Canugovi et al., 2010). There are two well-established routes of NER in cells: global-genome NER (GG-NER) and transcription-coupled NER (TC-NER). After the initial steps of lesion recognition and recruitment of the NER machinery, both pathways converge into the same final steps, involving a dual-incision reaction in which a ssDNA fragment of 25-30 nt is released from the helix, followed by Polδ-dependent gap-filling and ligation of the resulting nick (Boiteux and Jinks-Robertson, 2013).

GG-NER (Figure 3) operates independently of the transcription status or chromatin structure, and begins with the opening of the double helix and the formation of a pre-initiation complex. First, the Rad4-Rad23-Rad33 complex recognises the distortion of the double helix by sensing thermodynamically unstable base pairs (Min and Pavletich, 2007). Next, the complex Rad7-Rad16 remodels the chromatin through interactions with acetylating and ubiquitinating partners, while Rad4-Rad23-Rad33 recruits the transcription factor TFIIH to establish the pre-incision complex. The core repair complex is composed of 10 subunits, including the helicases Rad25 and Rad3, and three subunits with CAK kinase activity (Gibbons et al., 2012). The catalytic role of TFIIH during NER consists in unwinding the DNA flanking the lesion, which is driven by the opposing polarities of the ATPase/helicase activities of Rad3 and Rad25. After the DNA has been unwound, the pre-initiation complex is released and the single-strand binding protein RPA coats the exposed ssDNA to stabilize the pre-incision complex. The formation of the pre-incision complex is followed by the recruitment of two structure-selective endonucleases (SSEs): Rad2 and Rad1-Rad10. Rad2 and Rad1-Rad10 excise the damaged strand by dual-nicking near the branched ends of the repair bubble;

USC UNIVERSIDADE DE SANTIAGO DE COMPOSTELA

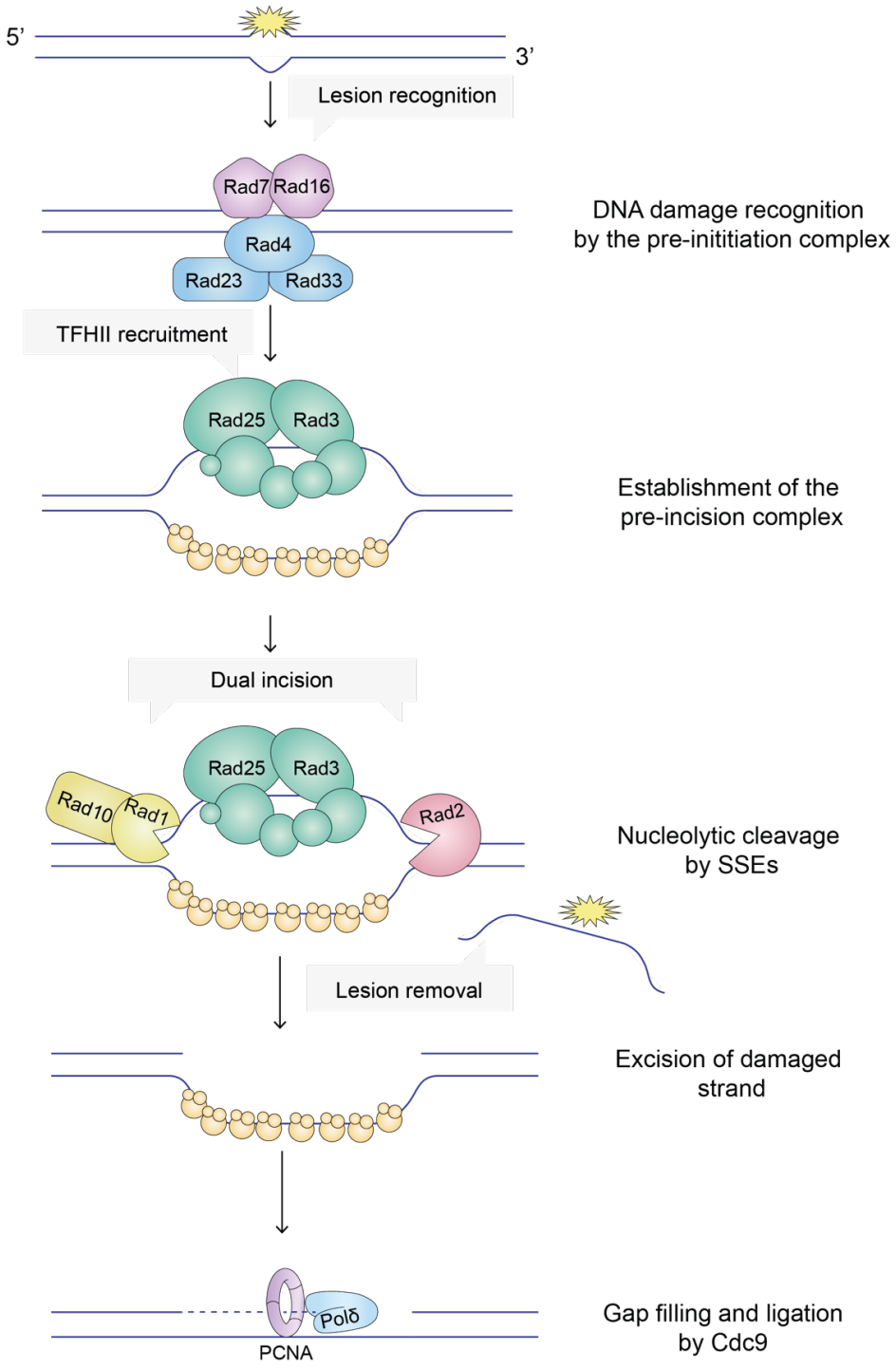


Figure 3. NER pathway. Rad23-Rad4-Rad33 recognize the distortion in the double helix caused by bulky adducts, whereas Rad7-Rad16 remodels the chromatin. Rad23-Rad4-Rad33 recruits the TFIIH complex. Two helicases of the complex, Rad25 and Rad3 unwind the DNA flaking the lesion, with RPA coating the resulting ssDNA.Dual nicking by Rad2 and Rad1-Rad10 of the bubble excises the damaged strand. Repair is completed by DNA synthesis and ligation. TC-NER, not depicted in the figure, is coupled to RNA polymerase II.

USC
UNIVERSIDADE
DE SANTIAGO
DE COMPOSTELA

Rad2 makes its incision 2–8 nt to the 3' side of the lesion, while Rad1-Rad10 does it 15–24 nt to the 5' side of the lesion (Evans et al., 1997). Once the damaged strand has been removed, the resulting gap is filled by either Polδ or Polε, and the nick ligated by Cdc9.

1.1.4 Mismatch repair

DNA mismatch repair (MMR) is a highly conserved pathway with major roles during DNA replication, repair and recombination (Liu et al., 2017), as it promotes the correction of DNA non-Watson–Crick base pairs or small loops of extrahelical nucleotides. Mismatches arise during DNA synthesis due to misincorporation of nucleotides, while small loops and hairpins are usually a consequence of replication slippage by DNA polymerases; therefore, acting as a backup for the proofreading activity of DNA polymerase, MMR contributes to increase the fidelity of replication by several orders of magnitude, ensuring that daughter cells inherit a faithful copy of the parental genome (Jiricny, 2013). Mismatches can also occur within heteroduplex DNA during homologous recombination (HR); in that context, MMR monitors the identity between DNA interacting molecules during strand exchange and limits the use of non-identical sequences as repair templates (Jiricny, 2013).

The MMR machinery detects the helical distortions caused by mismatches and excises a ssDNA tract in the newly-synthesized strands contaning the incorrect nucleotides, followed by gap fill-in and ligation steps. In *S. cerevisiae*, two heterodimeric complexes - MutSα (Msh2-Msh6) and MutLα (Mlh1-Pms1) - repair the majority of replication errors, as detailed in Figure 4a. Mismatch binding and ATP promote the activation of MutSα and allow its interaction with MutLα, which is essential to nick the nascent strand. This provides an entry point for the 5'-3' exonuclease Exo1 that will then remove a portion of the strand containing the mismatch. One of the key mechanistic steps for accurate repair is the correct discrimination between the nascent and template strands. When the mismatch occurs in the lagging strand, the discontinuity at the 5' end of the Okazaki fragment allows the recognition of the nascent strand and enables Exo1 exonuclease activity; in fact, MMR removes more efficiently those mismatches appearing in the lagging strand (Lujan et al., 2012; Pavlov et al., 2003). However, the continuous synthesis on the leading strand requires a different discrimination strategy and the deliberate generation of a nick. In this case, the recruitment of the PCNA sliding clamp by MutSα and the endonuclease activity of MutLα- dependent on PCNA interaction - fulfil both these requirements (Kadyrov et al., 2006). Since PCNA is loaded asymmetrically on the fork by the replication factor C (RFC), it can promote MutLα incision only at the nascent strand in an ATP-dependent manner (Pluciennik et al., 2010; Umar et al., 1996). The resulting nick will be used replication error after which repair will be corrected by new Polδ dependent-DNA synthesis

The MMR machinery is not limited to MutSα and MutLα. MutSβ (Msh2-Msh3) detects large insertion/deletion loops (IDLs) and, like MutSα, can also mark small IDLs for repair (Srivatsan et al., 2014) (Figure 4b). In addition, part of the MMR machinery has been adapted to recognize and cleave specific HR intermediates, like dHJ, during the meiotic cell cycle

USC UNIVERSIDADE DE SANTIAGO DE COMPOSTELA

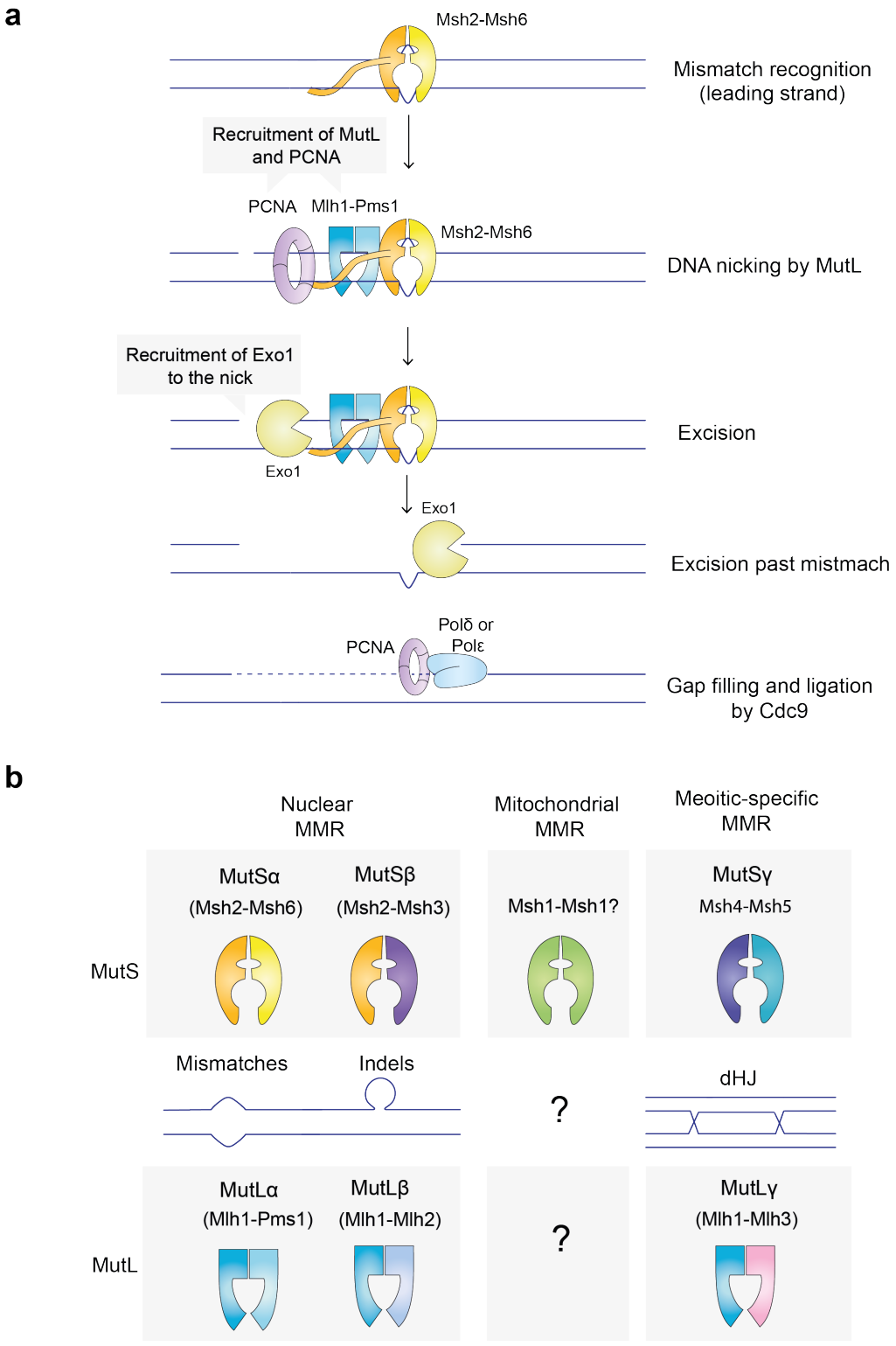


Figure 4. MMR pathway. (a) MutS (Msh2-Msh6) recognises the distortion of the double helix, and recruits PCNA and MutL (Mlh1-Pms1) to the site of mismatch. MutL creates entry points for Exo1 by nicking the damaged strand, resulting in a gap that is filled by Polδ or Polε. **(b)** MMR machinery is composed of different complexes specialized in several types of DNA damage recognition (MutSα and MutSβ), and with meiotic-specific functions (MutSγ and MutLγ). Additionally, budding yeast is endowed with a homodimeric complex for MMR in the mitochondria (Msh1-Msh1)

(Cannavo et al., 2020; Kulkarni et al., 2020; Rogacheva et al., 2014)(Figure 4b). Finally, MMR also promotes error-free replication of the mtDNA, with Msh1 being found exclusively in the yeast mitochondria (Reenan and Kolodner, 1992). While the role and activities of MMR nuclear complexes have been profusely characterized, much less is known about the putative role of this specific mitochondrial subunit (Figure 4b). The lack of a Msh1 homolog in mammalian cells could explain, at least partially, the higher mutation rates of human mtDNA (Reyes et al., 2015).

1.1.5 DSB repair: NHEJ, HR and alternative pathways

DSBs are frequently categorised as one of the most cytotoxic types of DNA lesions, since the simultaneous disruption of the continuity of both DNA strands precludes the use of the complementary strand for accurate repair. Spontaneous DSBs are mostly pathological and may be caused by the actions of ROS species from the oxidative metabolism, environmental IR, rogue endogenous nucleases or the collision of a replisome with an unrepaired SSB (Chatterjee and Walker, 2017; Lieber, 2010). However, a small subset of DSBs fulfil physiological roles by triggering programmed recombination (or other types of repair) events, such as those in meiosis, budding yeast mating-type inter-conversion, or lymphocyte and neuronal development in mammalian cells (Haber, 2012; Keeney et al., 1997; Lieber et al., 2006).

To avert the genome instability associated to DSBs, cells have evolved two main strategies: first, the direct ligation of the DNA by non-homologous end-joining (NHEJ); second, the use of homologous templates to restore genetic information by HR-dependent pathways. Additionally, two other pathways - single strand annealing (SSA) and microhomology-mediated end-joining (MMEJ) - provide alternative solutions to repair DSBs based on short homology stretches, although in yeast these are quite restricted under physiological conditions, with DSBs being primarily channelled towards NHEJ or HR (Sfeir and Symington, 2015). Pathway selection is determined by two variables: the chemical status of the DSB ends and the availability of a suitable template for HR. DSBs can be classified as chemically “clean” or “dirty”, depending on their ability to be directly religated. Clean DSBs present the canonical 5’-phosphate and 3’-hydroxyl moieties required for ligation and are usually a consequence of the unscheduled activity of endonucleases. Conversely, dirty DSBs appear mostly as by-products of radiation or abortive topoisomerase reactions. These may present chemically modified ends or protein blocks, thus requiring the end-processing activity of different enzymes before ligation (Symington and Gautier, 2011).

1.1.5.1 NHEJ

Canonical NHEJ, the simplest mechanism to rejoin DSBs, involves a set of core proteins required for religation, which in *S.cerevisiae* includes the yKu70-yKu80 (yKu) heterodimer, the Mre11-Rad50-Xrs2 (MRX) complex, Dnl4 (DNA ligase IV), as well as the accessory factors Lif1 and Nej1 (Daley et al., 2005; Lieber, 2010). Additionally, other supporting factors aid in the end-processing of chemically modified DSBs to facilitate the activities of the core proteins. Repair starts with the binding of yKu to both DNA ends to protect them from degradation (Figure 5). Then, the MRX complex is recruited to tether both ends of the DSB (Chen et al., 2001). Singularly, MRX is also involved, unlike any of the other NHEJ core

USC
DE COMPOSTELA

factors, in the early steps of HR (described in section 2.5.2). Once stabilized by yKu and MRX, the chemistry of the DNA ends will determine the ensuing repair stages. If the ends are chemically modified or blocked by a protein, an additional processing step that further trims the DNA ends is required prior to ligation. For that purpose, NHEJ is endowed – specially in human cells - with nucleases and polymerases able to act on a wide range of DNA end structures, conferring NHEJ a high degree of mechanistic flexibility (Lieber, 2010). In *S. cerevisiae*, this involves the activity of Tpp1 to remove 3'-phosphate groups; Tdp1, to hydrolyse the 3' and 5'-phosphotyrosyl bonds in topoisomerase-protein adducts; the polymerase Pol4 for gap-filling and endonuclease Fen1 for the removal of 5'-flaps (Bahmed et al., 2010; Tseng and Tomkinson, 2004). However, *S. cerevisiae* lacks specific end-processing nucleases as part of this NHEJ toolkit and, therefore, its capacity to deal with dirty DSBs is relatively limited (Symington and Gautier, 2011). In the final step , yKu recruits Dnl4-Lif1-Nej1 (Tseng and Tomkinson, 2004; Wilson et al., 1997) to catalyze the reformation of phosphodiester bonds. Interestingly, Cdc9 (DNA ligase I) cannot be used for ligation in NHEJ and, conversely, Dnl4 activity is restricted to this pathway, without any role in supporting DNA replication.

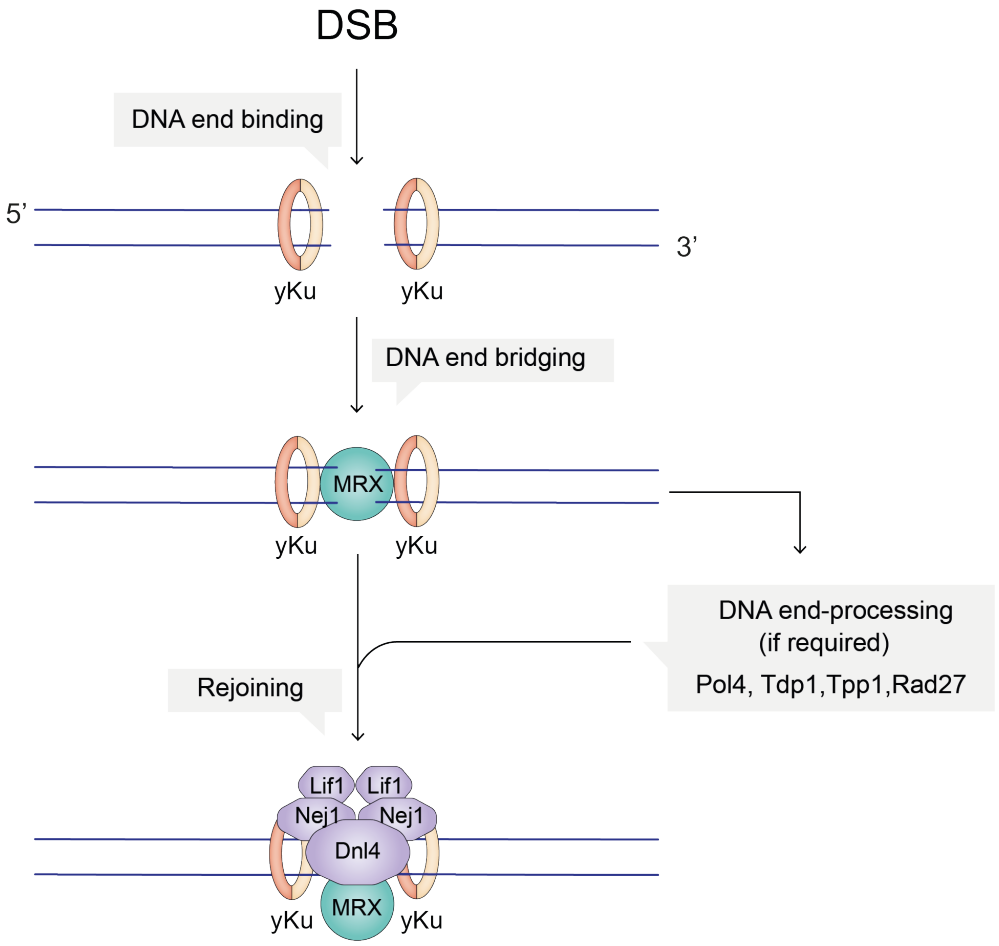


Figure 5. DSB repair by NHEJ. yKu binds dsDNA ends and protects them from degradation by nucleases. Additionally, MRX tethers both ends together, and recruit the Dnl4 ligase with its accessory factors Lif1/Nej1. If the ends cannot be directly ligated, yeast is endowed with several enzymes to process the blocked ends, such as Pol4, Tdp1, Tpp1 or Rad27.

Although NHEJ has been traditionally described as highly mutagenic, this vision has been challenged during the last decade; NHEJ, which accounts for the majority of the repair of DSBs in metazoans, is not intrinsically inaccurate (Bétermier et al., 2014). Its probability to introduce mutagenic deletions or insertions is dictated by the structure of the DNA ends, and not by the intrinsic properties of core NHEJ machinery; while DSBs with compatible ends are faithfully rejoined, the ability of NHEJ to restore DNA integrity even when the DSBs display imperfect ends comes with the risk of mutagenic insertions or deletions at the break site. In conclusion, repair by NHEJ is fast, cell cycle independent and, if no end-processing is required, highly accurate.

1.1.5.2 Homologous recombination

Homologous recombination (HR) is a high-fidelity DSB repair pathway that restores DNA continuity by retrieving any lost genetic information from a homologous donor, like the sister chromatid or the homologous chromosome. HR is tightly linked to DNA replication and the S/G2 phases of the cell cycle, since both of them cooperate to ensure faithful replication and repair. HR enables tolerance pathways to bypass damage, and participates in the protection and repair of stalled or broken forks (Heyer, 2015; Pâques and Haber, 1999). Lastly, the repair of programmed meiotic DSBs by HR generates chiasmata, the physical linkages between homologous chromosomes required for bipolar chromosome segregation during the reductional, first meiotic division (Hunter, 2015). As opposed to end-joining, HR is an intricate mechanism which entails the combined activities of various recombinases, helicases and nucleases that increase the accuracy of DSB repair at the expense of speed (Mao et al., 2008).

To fulfil its different roles, HR comprises multiple sub-pathways for repairing both one- and two-ended DSBs. In all cases, HR begins with the nucleolytic degradation of DNA ends at the break to expose long tracts of 3'-OH ssDNA, a process termed end resection. The MRX complex binds to the DNA ends and initiates resection with an endonucleolytic incision to release a 5'-ending oligonucleotide. Resected ends are further extended by Exo1 and the Sgs1 helicase working together with Dna2 nuclease (Symington and Gautier, 2011) (Figure 6, step 1). This extended DNA resection commits DSB repair to HR, since resected ends become poor substrates for yKu binding and cannot be directly ligated, hence inhibiting the NHEJ pathway. Resection is followed by RPA coating to protect the ssDNA, Rad52 recruitment, and Rad52-mediated displacement of RPA to allow the formation of the Rad51 nucleofilament, which scans the genome for homologous sequences (Figure 6, step 2). Eventually, this leads to the establishment of a synapse between the Rad51 nucleofilament and the homologous sequence, the invasion of the homologous duplex and the formation of a displacement loop (D-loop). In some cases, the Srs2 helicase can both disrupt Rad51 nucleofilaments and disengage D-loops to avoid unscheduled recombination events (Krejci et al., 2003; Veaute et al., 2003). Next, the invading strand primes DNA synthesis, extending the D-loop and copying the genetic information from the donor molecule (Figure 6, step 3). After this point, HR can follow three different routes: synthesis-dependent strand annealing (SDSA), break-induced replication (BIR) or classical double-strand break repair (DSBR) (Figure 6, step 4). Pathway selection will define the outcome of HR, which can be classified as a noncrossover (NCO) or a crossover

USC
UNIVERSIDADE DE COMPOSTELA

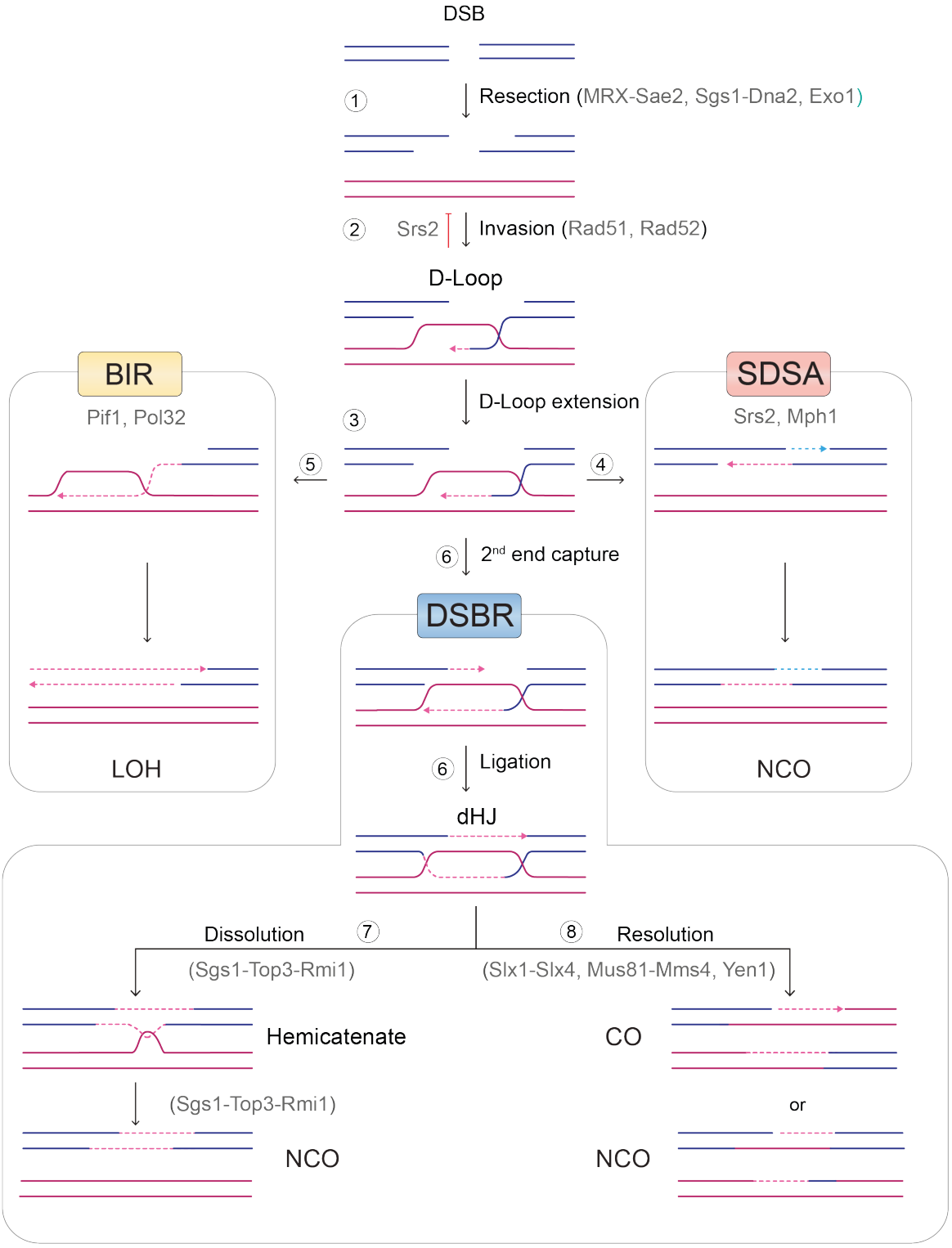


Figure 6. DSB repair by HR. (1) Resection exposes the 3'-ssDNA required to invade homologous sequences and prime DNA synthesis. (2) Invasion is mediated by Rad51 and Rad52 recombinases, whereas Srs2 strips Rad51 filament to impede D-loop formation. (3) If a second end is available, the extended D-loop can be disrupted by (4) SDSA helicases to produce NCO. Alternatively, one-ended DSBs can restore the missing genetic information via BIR (5). Finally, second-end capture, DNA synthesis and ligation leads DSBR pathway (6), characterized by the formation of a dHJ. This metastable intermediate can be eliminated via dissolution (7) or resolution (8), producing NCOs or a mixture of NCOs/COs respectively.

USC
UNIVERSIDADE DE SANTIAGO DE COMPOSTELA

(CO), depending on the absence or presence of reciprocal exchanges between the broken and donor molecules, respectively. Most of the extended D-loops in somatic cells are disrupted by the helicases Srs2 (Liu et al., 2017) or Mph1 (Ira et al., 2003; Prakash et al., 2009) and repaired via SDSA to yield exclusively NCOs. Alternatively, the second end of the broken duplex can be engaged to stabilize the D-loop (Figure 6, step 4) and ligated (Figure 6, step 6), leading to the formation of a new recombination intermediate, the double Holliday junction (dHJ) (Szostak et al., 1983). dHJs can be dissolved by the action of the STR complex to generate NCOs (Figure 6, step 7) (Cejka et al., 2010c; Ira et al., 2003, p. 2; Wu and Hickson, 2003), or undergo nucleolytic resolution to yield a mixture of NCO and CO products (Figure 6, step 8) (Wyatt and West, 2014). The third pathway, BIR (Figure 6, step 5), copes with one-ended DSBs, which appear mostly as a consequence of fork breakage during DNA replication. During BIR, the extended D-loop turns into a migrating D-loop that supports extensive recombination-coupled DNA synthesis. Two factors have been identified as essential for BIR activity: the non-essential Polδ subunit Pol32 (Lydeard et al., 2007) and the Pif1 helicase (Wilson et al., 2013). BIR implies a type of conservative DNA replication where both the newly synthesized leading and lagging strands remain associated, leading to high levels of loss of heterozygosity (LOH).

1.1.5.3 Homology-mediated repair: MMEJ and SSA

MMEJ and SSA are minor pathways that, in addition to HR and NHEJ, contribute to DSB repair. Both involve the alignment of microhomologies or homologies flanking the DSBs. Although to a different extent, they rely on the resection machinery to expose the internal homologies and, therefore, compete with HR for repair substrates. In this sense, MMEJ, SSA and HR can be grouped together as homology-directed repair (HDR) pathways. Even if MMEJ and SSA pathways are intrinsically mutagenic due to theit tendency to lose genetic information, these mechanisms could still promote a certain degree of faithful DSB repair in highly repetitive genomes (Chang et al., 2017; Sfeir and Symington, 2015).

MMEJ (Figure 7) is an error-prone, alternative route to end-joining (Yu and Gabriel, 2003), independent of canonical NHEJ factors such as the yKu heterodimer, Dnl4 or Pol4. Instead, it requires the activity of the MRX complex or the long-resection pathway (Sgs1-Dna2 and Exo1) to expose complementary regions of 6-14 nt of homology before joining (Lee and Lee, 2007; Villarreal et al., 2012); due to its unique requirements, MMEJ is considered a pathway that stands between NHEJ and HR. Following resection, the homologous regions will be paired independently of recombinases, and the Rad1-Rad10 endonuclease will remove any heterologous flaps formed during the annealing, prior to ligation (Ma et al., 2003). Otherwise, if the resection machinery exposes ends longer than 15 nt without finding microhomology repeats, the resulting ssDNA stretches will be bound by RPA, which inhibits the annealing of microhomologies and channels repair towards SSA or HR (Deng et al., 2014). The physiological relevance of MMEJ remains poorly defined in *S. cerevisiae*. In this sense, its low efficiency suggests that it could simply act as a backup mechanism, with minimal functionality unless NHEJ or HR are compromised, given that RPA both inhibits MMEJ and promotes extensive resection by removing secondary structures (Sfeir and Symington, 2015). In mammalian cells, MMEJ is more prevalent than in yeast, which is reflected by the existence of

USC
DE SANTIAGO
DE COMPOSTELA

a dedicated machinery like the MMEJ-exclusive DNA ligase III (Wang et al., 2005) and the prominent contribution of Polθ (Mateos-Gomez et al., 2015). Due to its potential to support carcinogenesis, MMEJ and Polθ have become attractive players as potentially druggable targets to restrain uncontrolled cell proliferation (Ceccaldi et al., 2015).

The SSA pathway (Figure 7), like MMEJ, starts with the end-resection machinery exposing repetitive DNA sequences flanking the DSB. After annealing of the homologous regions, the heterologous DNA 3'- flaps are trimmed by Rad1-Rad10 and the strands are ligated. Moreover, it is also error-prone, since it involves the deletion of the DNA sequence between the repeats, thus leading to mutagenic repair. However, SSA is usually described as a recombinogenic

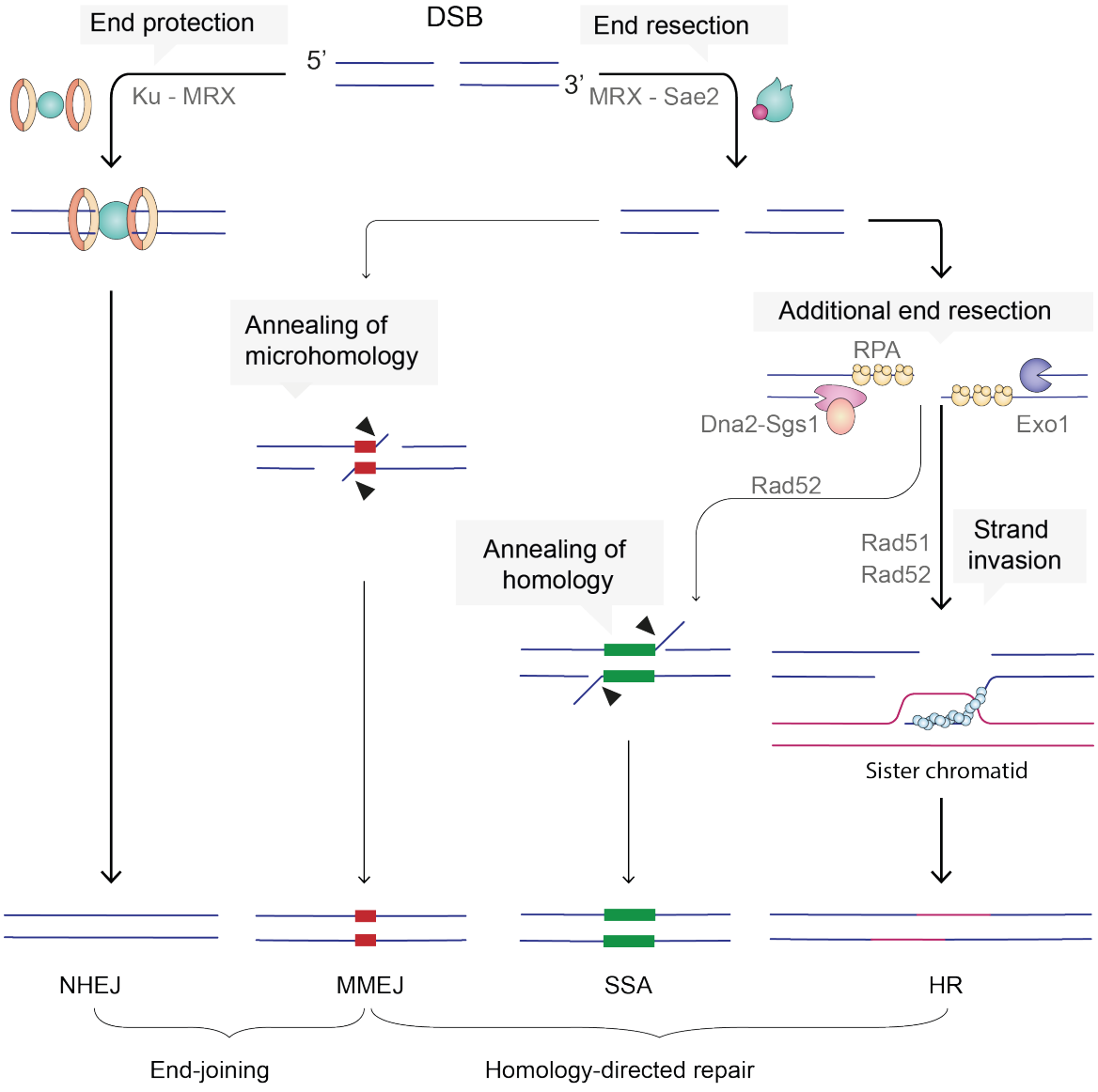


Figure 7. DSB repair pathways. End protection by yKu binding channels DSBs to NHEJ. Alternatively, resection of DSB ends by MRX-Sae2 promotes homology-directed repair. Although HR is the main homology-directed repair pathway, two alternative routes, MMEJ and SSA, can repair DSBs by using homology tracts between the same molecules (depicted as red and green boxes). These pathways are highly mutagenic, since the removal of the heterologous flaps (black arrows) formed during annealing causes the loss of genetic information.

pathway due to its specific enzymatic requirements (Ivanov et al., 1996). In particular, and in contrast to MMEJ, SSA requires more sequence homology; while MMEJ involves homology tracts shorter than 15 nt, SSA typically requires homology lengths >20 nt. To expose these homology tracts, SSA entails extensive end-resection, characteristic of all recombination pathways. Also, since long ssDNA strands are readily coated by RPA, the recombinase Rad52 is essential for annealing of the homologous sequences (Sugawara and Haber, 1992). However, unlike HR, SSA typically employs homology found in the same DNA molecule, without the need for strand invasion and D-loop formation; consistently, SSA is independent of Rad51 and Rad54, which distinguishes it from the HR pathway.

1.1.6 Replication stress: DDT and fork reversal

DNA duplication in eukaryotic cells relies on the progression of thousands of bidirectional forks (Duzdevich et al., 2015). These forks may encounter multiple physical obstacles, such as persistent lesions that escape from the DNA repair machinery, or the formation of secondary structures, as G-quadruplex or hairpins after DNA unwinding (Gaillard et al., 2015; Saxena and Zou, 2022). These impediments to DNA synthesis hinder fork progression, trigger replication stress, characterized by the slowing or stalling of the replisomes (Zeman and Cimprich, 2014),

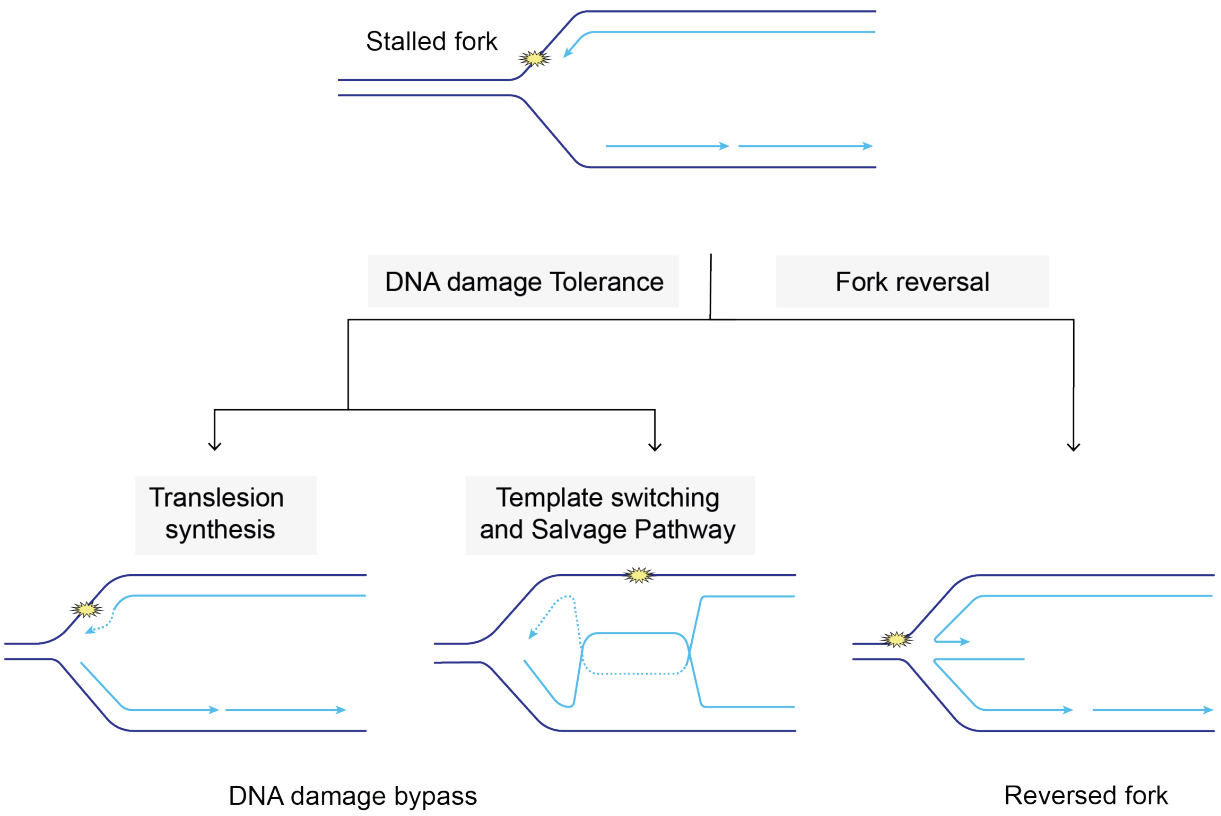


Figure 8. DDT pathways and fork reversal. During S phase, cells prioritise completion of DNA replication over repair of DNA damage. DDT pathways, such as TLS, TS and SP allow the progression of the forks by skipping the lesion and delaying its repair. Alternatively, fork reversal contributes to transiently estabilize stalled replisomes until the blocking damage has been removed.

USC UNIVERSIDADE DE SANTIAGO DE COMPOSTELA

and threaten completion of DNA replication. Under these circumstances, genetic material is particularly vulnerable, since prolonged fork stalling can cause fork collapse and DSBs, contributing to elevate the levels of genome instability (Chang and Cimprich, 2009). When a fork collides with a lesion impeding its progression, such lesion must be either repaired or bypassed to allow the completion of DNA replication. Typically, immediate repair is disfavoured for two reasons: first, it can overextend the S phase, thus triggering more instability; second, ubiquitous activity of excision-based systems during replication might lead to increased fork collapse. Consequently, repair of DNA damage in S phase is normally delayed, while lesion bypass by the replication machinery is favoured. This is accomplished by multiple DDT pathways, or, alternatively, through a DNA damage bypass or post-replication repair process (Figure 8) (Ulrich and Walden, 2010). The term post-replication repair was coined after pioneering work in *E.coli* demonstrating the presence of ssDNA gaps behind the fork that were subsequently gap-filled (Rupp et al., 1971; Rupp and Howard-flanders, 1968); nevertheless, this term is highly misleading, since the damage is initially circumvented rather than repaired (Chang and Cimprich, 2009). Moreover, it was also assumed that the process of gap filling only operates behind the replisome, a vision that was challenged by subsequent studies in eukaryotic organisms (Prado, 2014). Since DDT applies to lesions that stall DNA polymerases, but not the replicative helicase, an alternative pathway is required when the progression of the replicative helicase itself is blocked; under such circumstances, fork reversal contributes to fork stabilization and ensures replication completion (Neelsen and Lopes, 2015) (Figure 8). The replication machinery, together with its regulatory and tolerance pathways, are well conserved across eukaryotes, although the relative contribution of each one differs from yeast to humans.

1.1.6.1 DDT pathways: DNA damage bypass at the fork and behind the fork.

Three DDT pathways allow the replisome to bypass physical obstacles: the HR-independent translesion synthesis (TLS) and the HR-dependent routes template switching (TS) and salvage pathway (SP). TLS relies on specialized translesion synthesis polymerases, a subset of low-fidelity DNA polymerases characterized by its larger active site and the lack of proofreading capacity, which allows them to replicate through damaged bases at the expense of inserting mutations (Sale, 2013; Waters et al., 2009). TS, however, avoids the lesion by using the nascent sister chromatid as a homologous template for DNA synthesis. Since this route relies on the HR machinery, TS is considered a high-fidelity pathway, unlike TLS (Branzei and Szakal, 2016). Still, TS must be tightly controlled to ensure that the template used for homology is indeed the sister chromatid. Finally, SP is a genetically distinct alternative to TS that also employs the sister chromatid to recover the genetic information, but in this case it is thought to act as a last-resort bypass pathway circumscribed to late stages of the cell cycle (Branzei et al., 2008; Branzei and Szakal, 2016; Karras et al., 2013).

USC
UNIVERSIDADE DE SANTIAGO DE COMPOSTELA

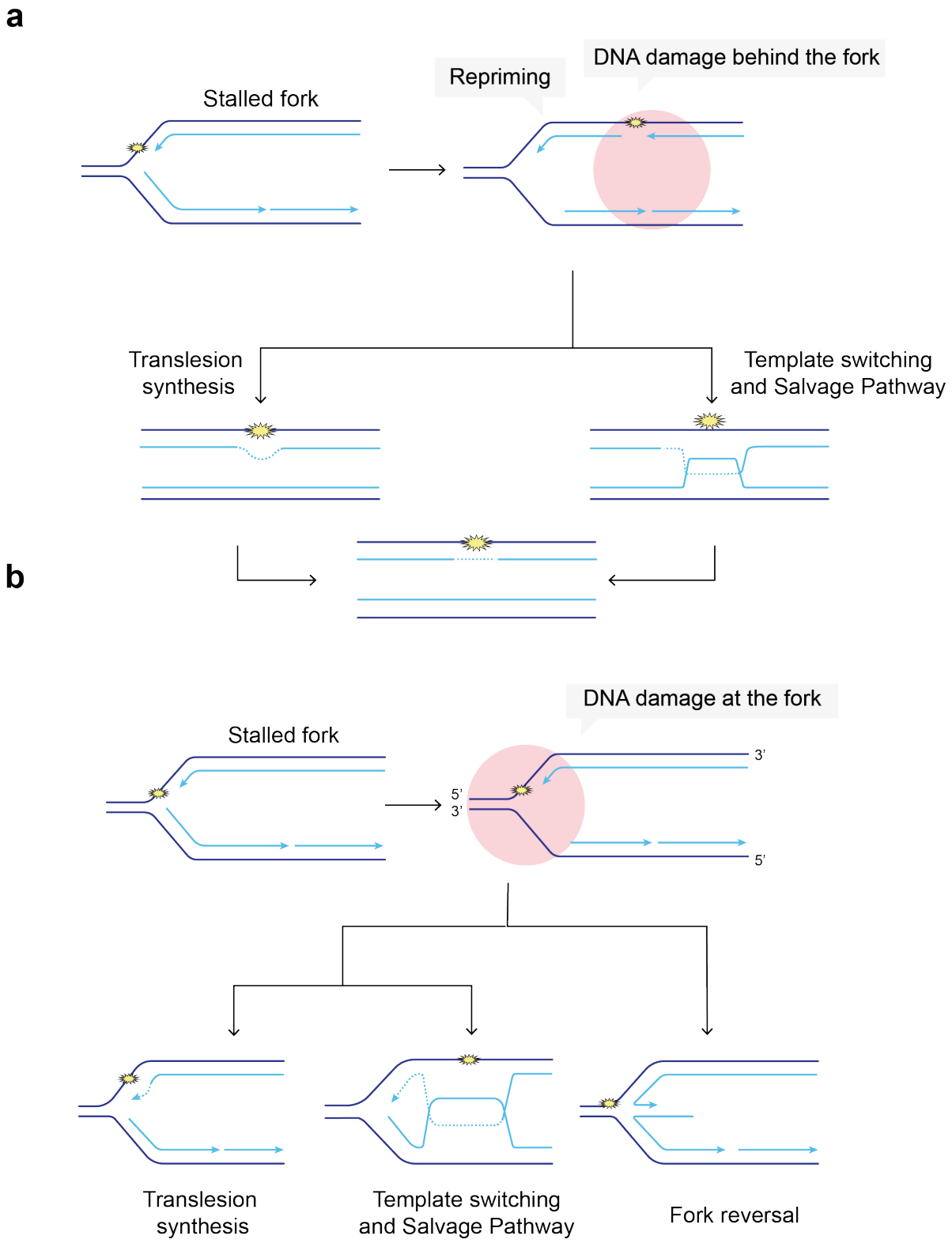


Figure 9. DDT and fork reversal at and behind the fork. (a) Repriming on the leading strand to bypass the lesion, that is repaired by post-replicative gap-filling. **(b)** In the absence of repriming or when the lesion blocks the progression of the replicative helicase, DDT pathways and fork reversal operate at the fork.

USC UNIVERSIDADE DE SANTIAGO DE COMPOSTELA

DDT pathways activate upon accumulation of ssDNA due to fork stalling and may act both at the fork or behind it. However, DDT working behind the fork is the prevailing mode of bypass when the leading strand polymerase is blocked by the lesion, while the replicative MCM helicase is able to traverse it (Daigaku et al., 2010; Karras and Jentsch, 2010). If the damage happens at the lagging strand, constant repriming through Okazaki fragment synthesis allows fork progression, leaving behind a small gap to be repaired by post-replicative DDT pathways. Although the leading strand is not constantly reprimed, under replication stress conditions, budding yeast can use repriming in the leading strand to allow fork progression (Fumasoni et al., 2015) and, similarly to the lagging strand, leave the damage behind the fork and deal with it post-replicatively by TLS, TS or SP (Figure 9a). This seems to be the case also in mammalian cells, where a specific polymerase with primase activity, PrimPol, allows efficient repriming of the leading strand after encountering a physical obstacle (García-Gómez et al., 2013; Mourón et al., 2013). A different scenario takes place when repriming is not initiated downstream the lesion in the leading strand, deriving in the accumulation of long ssDNA stretches due to the uncoupling of helicase and polymerase activities. Under these circumstances, the stalled fork is inherently fragile and prone to DNA damage, and it must be protected by fork reversal (Fumasoni et al., 2015) or DDT pathways operating at the fork (Figure 9b).

Pathway selection is strictly regulated in DDT to give priority to high-fidelity pathways like TS and, at the same stime, minimize the detrimental outcomes associated to unscheduled recombination events at the fork (Figure 10). PCNA, besides its role to increase the processivity of replicative DNA polymerases, is a molecular hub that regulates key DNA transactions during replication and repair, including DDT pathways selection (Moldovan et al., 2007). Ligation of ubiquitin and SUMO moieties to PCNA is essential to balance recombination events at the fork and dictate DDT pathway selection between TLS and TS (Figure 10). SUMOylation of PCNA occurs constitutively during the S-phase, and modifies primarily the conserved residue K164 and, to a lesser extent, K127. PCNA SUMOylation mediates the recruitment of the Srs2 helicase to counteract the formation of Rad51 nucleofilaments at ongoing replication forks (Pfander et al., 2005). Indeed, it is now generally considered that limiting the HR at active forks promotes genome integrity and protects cells from deleterious outcomes (Branzei and Szakal, 2017). Additionally, PCNA can also be ubiquitinated at K164 in a *RAD6*–dependent manner (Hoege et al., 2002). Although K164 is also a substrate for SUMO covalent attachment, the homotrimer structure of PCNA allows different posttranslational modifications to coexist in the same clamp. The *RAD6* pathway is activated during replication stress, when accumulation of ssDNA leads to the recruitment of Rad18 which, together with Rad6, leads to PCNA monoubiquitylation. Additional recruitment of Rad5 and Mms2-Ubc13 mediates further polymerization of K63-linked polyubiquitin chains at K164 (Hoege et al., 2002).

Interestingly, monoubiquitinylated PCNA promotes TLS (Stelter and Ulrich, 2003), whereas polyubiquitylation channels lesion bypass to TS (Hoege et al., 2002; Ulrich and Jentsch, 2000) Although PCNA monoubiquitinylation precedes polyubiquitylation, the concomitant recruitment of Rad18 and Rad5 to ssDNA and the upregulation of TLS factors in G2/M (Waters et al., 2009) favour the accuracy of TS over the error-proneness of TLS in S phase. Since TS

USC
DE SANTIAGO
DE COMPOSTELA

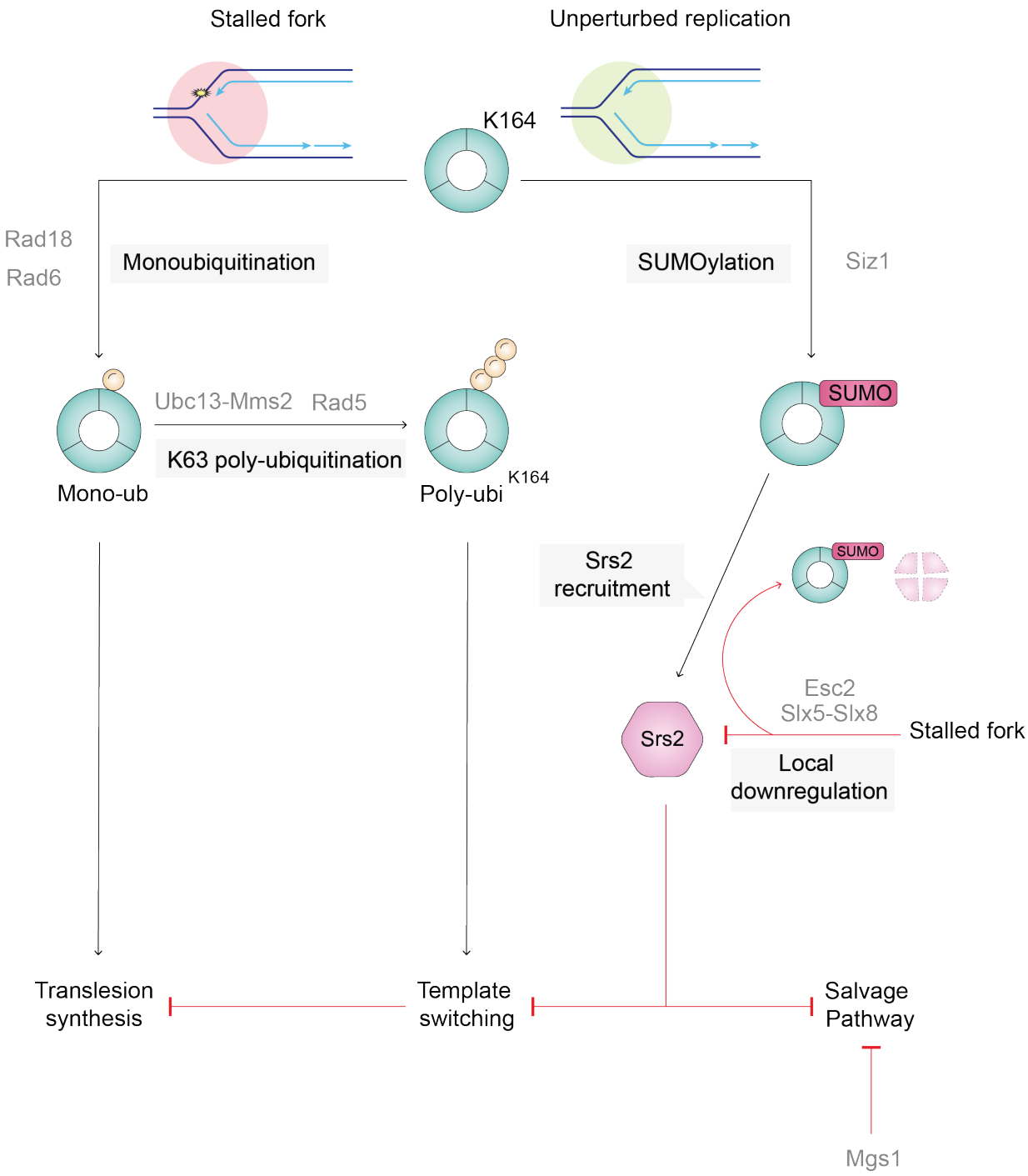


Figure 10. Regulation of DDT pathways by post-translational modifications. SUMOylation of PCNA at K164 during S-phase recruits Srs2 to prevent unscheduled recombination at the fork, inhibiting template switching and salvage pathways. Stalling of replication forks triggers mono-ubiquitination (*RAD6* pathway) and K63 poly-ubiquitination of PCNA, promoting translesion synthesis and template switching. To enforce recombination at the damaged fork, Srs2 is locally downregulated by unloading SUMOylated PCNA and by targeting Srs2 to proteosomal degradation. Absence of Srs2 at the fork is not sufficient to activate the Salvage pathway, that is inhibited by Mgs1.

USC
UNIVERSIDADE DE SANTIAGO DE COMPOSTELA

depends on the generation of a Rad51 nucleofilament to invade the sister chromatid and bypass the damage, Srs2 is locally downregulated at damaged forks to relieve its inhibition on Rad51 nucleofilament formation. This is achieved by unloading SUMOylated PCNA and by targeting Srs2 for proteasomal degradation via the E3-ligase Slx5-Slx8 complex (Fumasoni et al., 2015).

Finally, the SP is the last resort to bypass lesions during G2/M and operates independently of PCNA modifications. During a normal S phase, the presence of Srs2 inhibits this HR-dependent pathway. Moreover, even upon replication stress and downregulation of Srs2, the SP remains inactive due to an additional inhibitory layer mediated by Mgs1 that promotes the TS pathway (Jiménez-Martín et al., 2020). The stringent downregulation of this pathway in S phase suggests that toxic outcomes might ensue should SP be active during replication and points towards a specialized role in bypassing particularly persistent lesions (Branzei and Szakal, 2016). In conclusion, the DDT pathways ensure timely replication and increased resistance to genotoxic agents and replication stress. Notwithstanding, they may affect the fidelity of DNA replication. For that reason, the routes of TLS, TS and SP are tightly regulated to prevent undesired outcomes and minimize their potential to cause mutations. Since the DNA synthesized past lesions will be used as a template in the following rounds of replication, fidelity of lesion bypass and consequently, pathway selection, are essential to sustain the integrity of the genome.

1.1.6.2 Fork reversal

Replication fork reversal requires the hybridization of the two newly-synthesized strands and the re-annealing of the parental strands, hence remodelling the replication fork (a three-way junction) into the HJ-like chicken-foot structure, with a fourth regressed arm (Neelsen and Lopes, 2015). In *S. cerevisiae*, like many HR-dependent transactions at the fork, fork reversal is considered mostly pathological (Neelsen and Lopes, 2015). In this sense, fork reversal is inhibited by checkpoint kinases to maintain fork stability in response to replication stress (Sogo et al., 2002) and disfavoured by the re-priming events downstream the lesion (Fumasoni et al., 2015). Therefore, fork reversal is not considered a general mechanism to protect stalled forks in yeast, in contrast to mammalian cells where reversed forks are detected even in an unperturbed S phase. However, fork reversal may still constitute a physiological pathway to assist DNA damage bypass (Branzei and Foiani, 2010; Saugar et al., 2014) or transiently stabilize stalled forks under special circumstances (Figure 11a,b) (Branzei and Szakal, 2016), namely: i) re-priming downstream the lesion is impaired (Fumasoni et al., 2015), ii) lesions blocking the progression of the replicative MCM helicase (Carr and Lambert, 2021); iii) the presence of excessive torsional stress (Ray Chaudhuri et al., 2012); or iv) low probability of a converging fork rescuing the

USC UNIVERSIDADE DE SANTIAGO DE COMPOSTELA

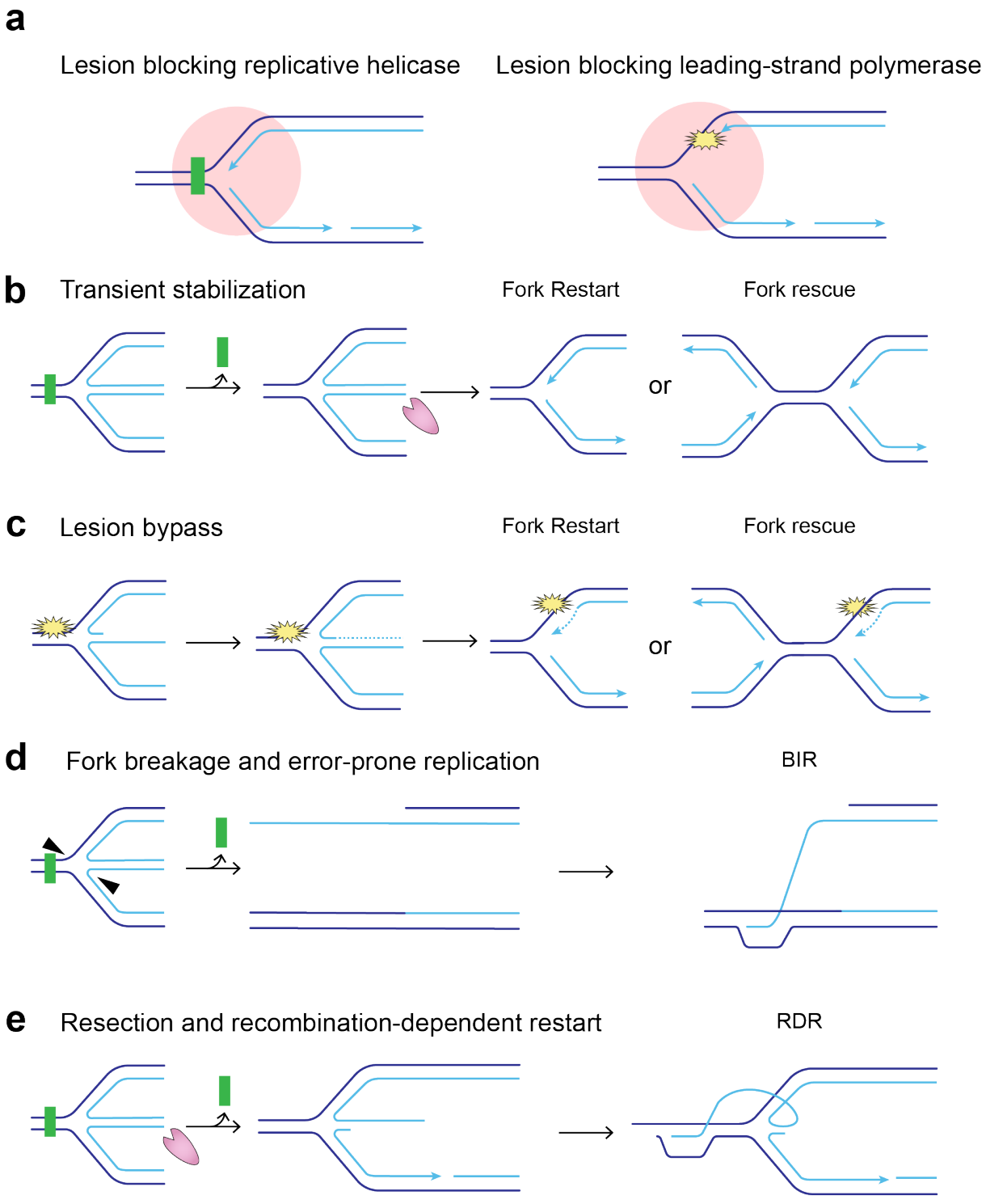


Figure 11. Possible DNA transactions during fork reversal. (a) Lesions blocking the replicative helicase (green rectangle) or the leading-strand polymerase (yellow star) may lead to fork reversal. **(b)** Fork reversal may transiently stabilize the replisome until the damage is removed. **(c)** DNA synthesis using lagging-strand as template can promote lesion bypass in lesions blocking the leading-strand polymerase. Reversed-fork breakage (d) or resection of nascent strand (e) can promote invasion to restart replication via BIR or RDR, respectively.

USC
UNIVERSIDADE DE SANTIAGO DE COMPOSTELA

stalled replisome (Figure 11a). These situations may arise when the replisome encounters DNA crosslinks, protein-DNA adducts or when it travels through highly transcribed genes, origin-poor regions or long stretches of unidirectional replication (Carr and Lambert, 2021). Alternatively, the transient nature of reversed forks may account for the low levels detected and mask a more prevalent role of this reconfiguration (Neelsen and Lopes, 2015). In yeast, fork reversal is poorly understood compared to mammalian cells, but several factors have been implicated in this process under different conditions. Various helicases and DNA translocases can drive fork reversal *in vivo* and *in vitro*, including the SWI/SNF motor protein Rad5, the FANCM homolog Mph1 and the Pif1-family helicases Pif1 and Rrm3. Contrarily, fork reversal may be counteracted by the resection activity of nucleases like Exo1, the MRX complex and Dna2 (Meng and Zhao, 2016).

After fork remodelling into a four-way junction, fork reversal may lead to different outcomes depending on the downstream molecular events and the type of lesion causing the blockage (Figure 11) (Meng and Zhao, 2016). First, reversal may have a transient, stabilizing effect, since stalled replication forks with long ssDNA regions are more susceptible to breakage (Figure 11b). Once the lesion has been removed, fork restart or rescue by a converging fork enable the completion of replication. Second, if the lesion stalls the leading strand polymerase, the nascent lagging strand can serve as a template for DNA synthesis, thus helping bypass the lesion on the parental strand (Figure 11c). Third, if the reversed fork is cleaved by a structure-selective endonuclease, further 5′-3′ resection of the one-ended DSB may recruit the HR recombinases to restart error-prone replication via BIR (Figure 11d). In the absence of fork breakage, recombination can still promote fork restart after resecting one of the nascent strands to allow binding of HR proteins and invasion ahead of the lesion. This pathway, commonly known as recombination-dependent restart (RDR) shares with BIR its dependence on Pif1 and Pol32 (Figure 11e). (Appanah et al., 2020).

1.2 Coordination of DNA repair by DNA damage checkpoint and cell cycle kinases

DNA repair must be strictly regulated to coordinate pathway selection, avoiding substrate competition and promoting high-fidelity repair, while minimizing detrimental outcomes. Extensive research over the last thirty years has unequivocally established the prominent role of post-translational modifications, such as checkpoint- and cell cycle-dependent phosphorylation, SUMOylation and ubiquitylation, in the spatio-temporal regulation of DNA repair, as already hinted in the previous sections.

1.2.1 DNA damage checkpoint

Coordination of the various DNA repair systems involves the crosstalk between the cell cycle and the DDC kinases; together, they modulate how different pathways interact to optimize the repair outcome, depending on the type of lesion and the cell-cycle-related substrate characteristics (Lanz et al., 2019). Eukaryotic cells respond to different types of DNA damage with the activation of the DDC, a signalling transduction pathway mediated by kinases that sense

USC UNIVERSIDADE DE SANTIAGO DE COMPOSTELA

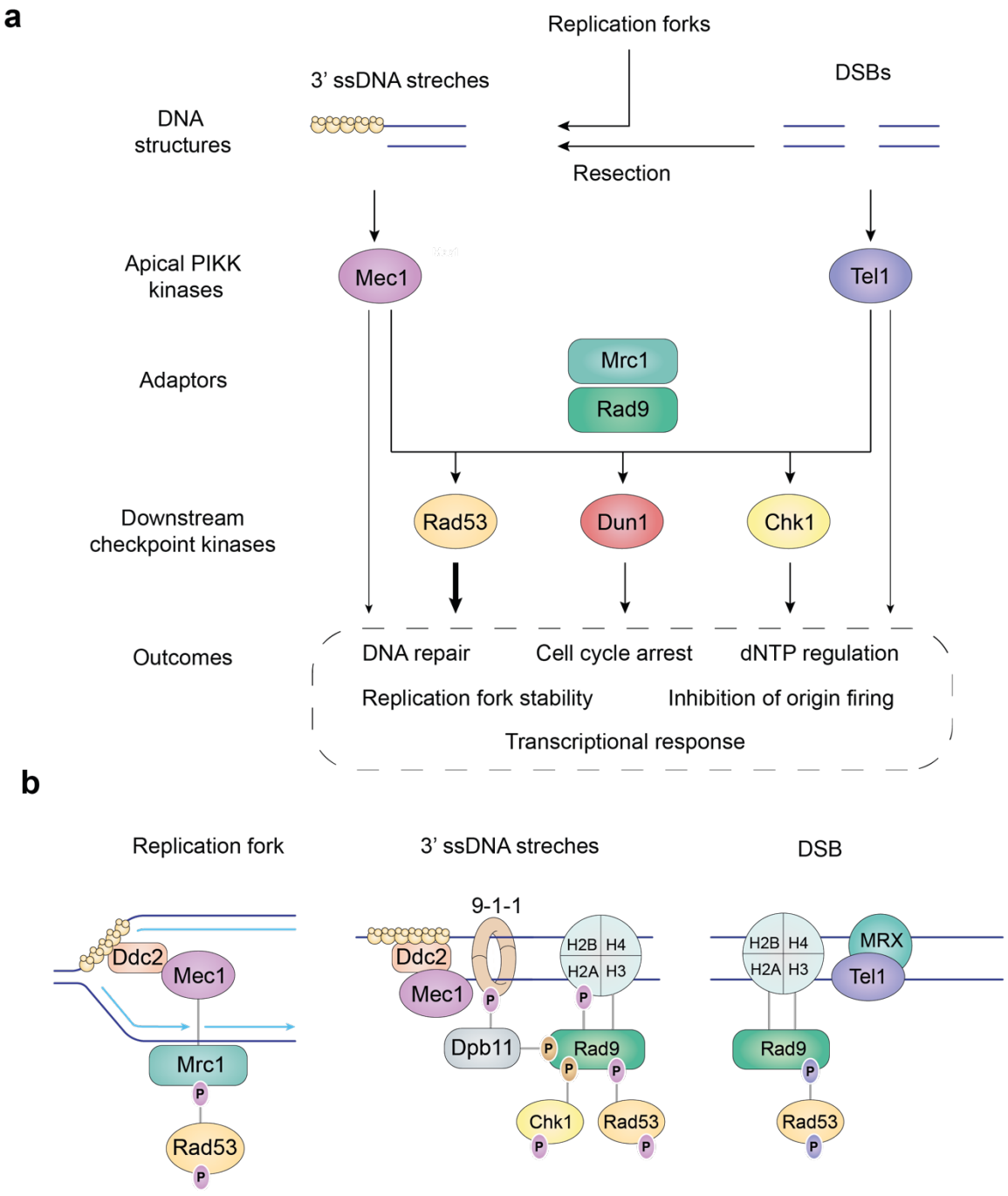


Figure 12. Overview of DDC response in budding yeast. (a) The DDC recognises DNA structures that arise during DNA damage and replication, including broken ends and 3'-ssDNA stretches coated by RPA. Signalling is started by apical PIKK kinases, with adaptor proteins facilitating phosphorylation of downstream checkpoint kinases. Both apical and downstream kinases phosphorylate multiple targets to coordinate the cellular response against DNA damage which includes cell cycle arrest, repair of the lesions and the stability of replication forks, with Rad53 participating in the majority of phosphorylation events. **(b)** Recruitment of apical kinases and activation of downstream effectors via Mrc1 and Rad9 adaptors. Ddc2 recruits Mec1 to RPA-coated ssDNA at replication forks and 3' ssDNA stretches after 5'-3' resection of broken ends, whereas interaction with the MRX complex targets Tel1 to DSBs. Adaptor proteins Mrc1 and Rad9 mediate recruitment of downstream kinases to allow their activation by Mec1/Tel1s dependent phosphorylation.

USC
UNIVERSIDADE DE SANTIAGO DE COMPOSTELA

DNA damage and coordinate DNA repair events with otherrelevant cellular processes. The DDC can be activated at three different stages of the cell cycle in budding yeast. First, DDC activation in G1 prevents entry into S phase until DNA regains a pristine condition for replication (Siede et al., 1994). Second, during S phase, the DDC coordinates fork progression and DNA repair (Paulovich and Hartwell, 1995). Third, the existence of lesions in replicated DNA triggers the G2/M checkpoint, preventing mitotic entry until the damage has been fixed (Weinert and Hartwell, 1988). However, it is important to note that checkpoint activation does not arrest cell cycle progression indefinitely; after some time, in a process commonly referred as adaptation, cells will inactivate the checkpoint signal and continue with cell division without repairing persistent DNA lesions (Paulovich et al., 1997; Sandell and Zakian, 1993).

In budding yeast, checkpoint activation is mediated by two different types of DDC kinases: the apical phosphatidylinositol-3 kinase-related kinases (PIKK) and effector checkpoint kinases (Figure 12a). As a consequence of DNA damage and/or replication stress, the apical PIKKs Mec1 and Tel1 relocate to sites containing structures like ssDNA stretches and broken DNA ends, respectively. Then they recruit and phosphoryled downstream checkpoint effector kinases (Rad53, Dun1 and Chk1) at consensus S/T-Q motives (Smolka et al., 2007), with the assistance of adaptor proteins like Mrc1 and Rad9. Mrc1 serves as a mediator during DNA replication (Alcasabas et al., 2001), whereas Rad9 has a more prominent role in G1 and G2 (Siede et al., 1993; Weinert and Hartwell, 1988). Once that apical and downstream kinases have been have been activated, they cooperate to phosphorylate key substrates for the spatiotemporal control of the checkpoint responses, including repair of DNA damage, cell-cycle arrest, regulation of dNTP levels, stabilization of replication forks, inhibition of origin firing and transcriptional control (Lanz et al., 2019). The apical PIKK kinases are recruited to damaged DNA by different mechanisms. On the one hand, Tel1 is targeted to DSBs by the MRX complex (Nakada et al., 2003). Reciprocally, Tel1 binding stabilizes MRX at the DNA ends to sustain DSB repair. On the other hand, Mec1 is loaded onto ssDNA by its integral partner Ddc2, which interacts with RPA (Rouse and Jackson, 2002); hence, the trigger for the Mec1-Ddc2 heterodimer recruitment is the presence of ssDNA stretches coated by RPA, which appear during resection of DSBs or replication stress (Figure 12a). Interestingly, Mec1 activation in S phase requires higher levels of RPA-coated ssDNA compared to G1 or G2. This specific increase in the threshold for Mec1 activation during DNA replication is most likely enforced to prevent unnecessary checkpoint activation by ssDNA generated at functional replication forks (Shimada et al., 2002; Tercero et al., 2003). Phosphorylation of downstream kinases by Mec1/Tel1 requires their physical proximity, a situation facilitated by the two checkpoint adaptors Rad9 and Mrc1 (Figure 12b). After recruitment to DNA damage sites, Mec1 and Tel1 phosphorylate proximal targets close to the lesion, like the histone H2A (Downs et al., 2000) or the Rad17-Mec3-Ddc1 (9-1-1) complex (Paciotti et al., 1998), respectively. This promotes Rad9 recruitment and subsequent phosphorylation by Mec1/Tel1 (Vialard et al., 1998) which, in turn, allows Rad53 binding (Gilbert et al., 2001; Schwartz et al., 2002) and activation by Mec1/Tel1-dependent phosphorylation (Sanchez et al., 1996; Sun et al., 1996). Alternatively,

USC UNIVERSIDADE DE SANTIAGO DE COMPOSTELA

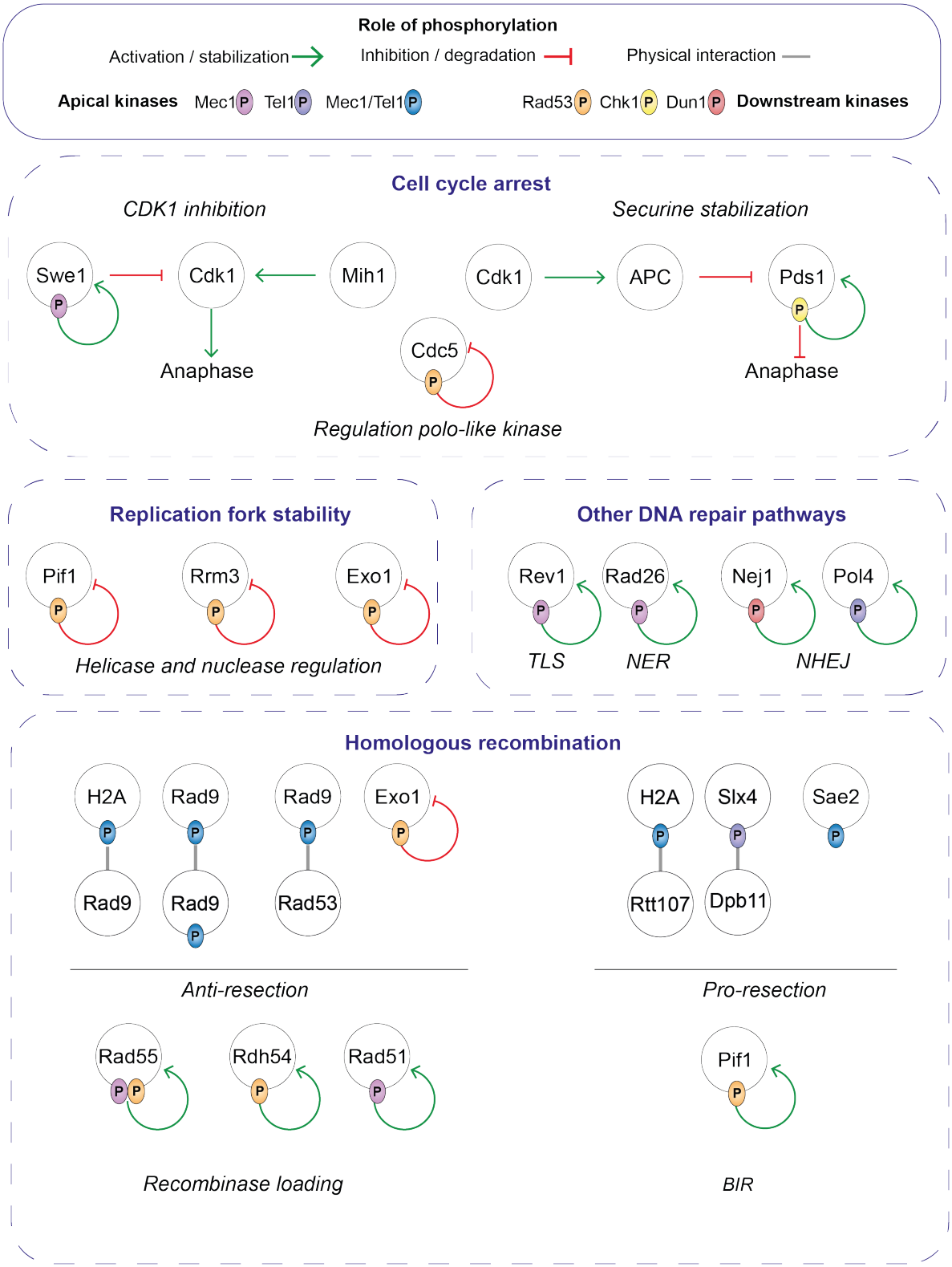


Figure 13. Phosphorylation events involved in DDC activation in budding yeast. Schematic representation of cellular targets phosphorylated by DDC kinases to regulate cell-cycle arrest, fork stability and coordinate several DNA repair pathways.

USC UNIVERSIDADE DE SANTIAGO DE COMPOSTELA

ssDNA accumulation due to replication stress does not require active mechanisms to assemble the Mrc1 adaptor at the fork, since Mrc1 is already a central component of the replisome and can be directly phosphorylated *in situ*. Analogously to Rad9, Mrc1 phosphorylation allows Mec1-dependent Rad53 phosphorylation to initiate the activation of downstream effectors (Katou et al., 2003; Osborn and Elledge, 2003). Notably, other kinases such as Cdc28 can also catalyse phosphorylation events involved in adaptor recruitment, although these events are often not induced by DNA damage.

Once active, both the effector kinases Rad53, Chk1 and Dun1, as well as the apical kinases Mec1 and Tel1, can target an extensive network of substrates involved in different cellular responses, with Rad53 mediating the majority of checkpoint-related phosphorylation events in budding yeast (Sanchez et al., 1999). Relevant pathways and particular substrates phosphorylate by checkpoint kinases are summarized in Figure 13. In addition to phosphorylating several regulators of the cell cycle to mediate its arrest, DDC kinases also phosphorylate different substrates to mediate the protection and restart of stalled replication forks. Several components of the DNA repair machinery are also regulated by checkpoint kinases to bias pathway selection or enhance repair efficiency in a context-dependent manner (Lanz et al., 2019).

1.2.2 DNA repair throughout the cell cycle

The mitotic cell cycle is defined as the ordered series of events occurring in distinct phases that ultimately results in the division of a cell into two daughters (Murray and Hunt, 1993). From a DNA-centric perspective, the cell cycle is defined by two paramount landmarks: the DNA replication in S phase, when the bulk of the nuclear genome is duplicated, and the chromosomal segregation in M phase, when the duplicated genome is condensed, sorted and equally distributed to the cellular offspring (Hustedt and Durocher, 2017; Murray and Hunt, 1993).

Cell-cycle progression is orchestrated by the periodic activation and inactivation of cyclin-dependent Ser/Thr kinases (CDKs). Budding yeast encodes five CDKs: Cdc28, Pho85, Kin28, Ssn3 and Ctk1. However, only Cdc28 (CDK1) functions as a master regulator to drive the cell cycle (Mendenhall and Hodge, 1998). Accordingly, nine cyclins are classified with respect to the main cell-cycle stage in which they interact with Cdc28: the G1-phase cyclins (Cln1, Cln2 and Cln3), the S-phase cyclins (Clb5 and Clb6), and the G2/M-phase cyclins (Clb1, Clb2, Clb3 and Clb4) (Bloom and Cross, 2007). Specific cyclin-Cdc28 heterodimeric complexes phosphorylate multiple target proteins to impel cell cycle progression in an ordered manner. In addition to this canonical role, mounting evidence from the last two decades has demonstrated further roles for the cyclin-CDK complexes in transcription, cell metabolism and DNA damage repair (Hydbring et al., 2016).

In this sense, integration of the peculiarities of different cell-cycle phases into the regulatory network that coordinates DNA replication, repair and segregation is essential to maintain genome stability. As chromatin engages in different transitions throughout the cell cycle, an accurate feedback between cell cycle progression and the various DNA repair machineries is required to adjust repair pathway selection to these different chromatin states in the G1-S-G2-M phases (Hustedt and Durocher, 2017).

The primary sources of DNA damage during G1 are endogenous ROS, chemical agents, IR or UV, leading to damaged bases, bulky adducts, nicks or DSBs. Importantly, this damage must be repaired before the onset of replication to avoid replication stress, with BER, NER and NHEJ as the main actors at this stage. While BER and NER operate throughout the cell cycle, NHEJ is specific for G 1. Despite the superior fidelity of HR, the highly compacted chromatin and the absence of sister chromatids makes NHEJ the selected DSB repair pathway during G1, as employing the homologous chromosome as a template for recombination might lead to loss of heterozygosity.

As cells enter S-phase and start replicating their genome, they face new challenges, including nucleotide misincorporations and polymerase slippage at repetitive sequences. Therefore, MMR acquires increased relevance in this phase to remove pairing mismatches and small loops due to insertions or deletions. NER and BER remain functional in this phase, with BER aiding in the removal of misincorporated uracils and ribonucleotides by replicative polymerases, a subpathway of BER known as RER (Ribonucleotide excision repair). Moreover, the S-phase is characterized by the accumulation of ssDNA nicks and gaps, fork stalling and even DSBs associated with replication stress. However, DNA replication also provides the most suitable substrate for accurate DNA repair: the sister chromatid. Therefore, during this phase, HR-dependent pathways participate both in the repair of DSBs at broken forks, but also of lesions impeding fork progression or gaps behind the fork through TS or fork reversal.

Gaps and DSBs left unattended during the S phase need to be solved before mitosis. Therefore, in G2/M, HR still mediates repair of the remaining lesions. Importantly, two additional DDT mechanisms, TLS and the salvage pathway, despite being more error-prone than HR, come into play at this stage to contribute to the removal of persistent lesions and completion of underreplicated regions. Finally, if DSBs occur arises during chromosome segregation, homology search may be impeded by the highly compact chromatin; under these circumstances, if the checkpoint does not arrest cell cycle, DSB repair will be mediated by NHEJ in the next cycle.

2. HOMOLOGOUS RECOMBINATION AND ITS CELL-CYCLE REGULATION

2.1 DSB end resection and pathway choice

The exonucleolytic degradation of the DSB 5’ ends, known as end resection, results in the generation of the 3’-ssDNA overhangs that act as a landing pad for the HR machinery and initiate the search for homology (Gnügge and Symington, 2021). Beyond its role in creating the substrate for HR, end resection is crucial to regulate DSB repair pathway choice and, through RPA coating of the 3’ ssDNA ends, to trigger the Mec1-dependent DDC (Shiotani and Zou, 2009). Currently, end resection is considered a two-step mechanism, in which the MRX-N complex -together with Sae2/CtIP- catalyses the step of DNA-end processing and resection (short-range resection). This initial step commits DSB repair to HR, whereas resected tracts are further extended in a second step mediated by the combined activities of Exo1 and Dna2-Sgs1 (long-range resection). Short resection, in contrast to long resection, is slower and restricted to the vicinity of the DNA ends. However, the short resection machinery is endowed with a high flexibility to process different types of DNA ends, including those with non-canonical

structures, such as secondary structures or protein adducts (Cejka and Symington, 2021). Due to its impact on pathway choice, the end resection machinery is tightly regulated by the DDC and cell-cycle kinases, which warrant an S- and G2-specific activation of HR, when the sister chromatid is available for repair.

The MRX/N complex and its regulatory subunit Sae2/CtIP are highly conserved from yeast to humans. The MRX/N complex is formed by two subunits of each of its components: Mre11, Rad50 and Xrs2/NBS1. *In vitro*, Mre11 is a manganese-dependent exonuclease that degrades dsDNA with 3'-5' polarity, the opposite of that expect for end-resection to yield the 3'-OH ssDNA ends capable of priming new DNA synthesis. Moreover, 5'-3' resection combined with the 3'-5' exonuclease activity of Mre11 would lead to the loss of genetic information, which has been demonstrated to be minimal *in vivo*. The solution to this apparent paradox came after the discovery of the importance of Mre11 cofactors in turning Mre11 into an endonuclease with affinity for 5'-terminated DNA strands. Structural studies have shown that Rad50 blocks Mre11 access to DNA but, upon ATP binding and hydrolysis, the complex undergoes a conformational change that displaces Rad50, allowing Mre11 to access DNA (Deshpande et al., 2014). In contrast, Xrs2 does not fulfil any catalytic function, but it is required to translocate the complex into the nucleus (Oh et al., 2016; Tsukamoto et al., 2005). However, its mammalian counterpart, NBS1, plays a more predominant role, since the physical interaction with NBS1 is required to activate MRE11 (Anand et al., 2019). Finally, the regulatory subunit Sae2/CtIP stabilizes the cutting state conformation of the MRX complex, stimulating Mre11 nuclease (Marsella et al., 2021)

As described in section (1.1.5.1), MRX/N is one of the first factors recruited to DSBs, either by direct binding or, alternatively, by sliding along the DNA due to its capacity to bypass protein barriers, including nucleosomes (Myler et al., 2017). After reaching the DSB, MRX/N initiates end resection by nicking the 5' strands upstream the DNA ends and resecting back towards the DSB with its 3'-5' exonuclease activity (Garcia et al., 2011). The distance of to 5' nick depends on the impediment blocking the ends, varying from 15-45 nt away in vitro to ~300-400 nt from the ends (Garcia et al., 2011; Reginato et al., 2017; Wang et al., 2017), and probably proceeds in a stepwise fashion (Cannavo et al., 2019). The first incision is critical in those DSBs with dirty ends; in fact, Mre11 5' nicking activity can be stimulated *in vitro* by a variety of protein blocks, including RPA, nuclease-dead restriction enzymes or yKu (Reginato et al., 2017; Wang et al., 2017). Moreover, Mre11 itself can also stimulate the endonuclease activity of close MRX complexes (Cannavo et al., 2019). Contrary to *S. cerevisiae*, MRN activity is essential for short-range resection of both dirty and clean ends in mammalian cells (Sartori et al., 2007).

MRX 5' nicking activity creates entry points for the long-resection machinery to further extend resection tracts (Figure 14). Long-resection is mediated by two partially redundant enzymatic activities, the 5'-3' exonuclease activity of Exo1, and the endonuclease activity of Dna2, which works together with the helicase Sgs1 and its accessory factors (Top3, Rmi1). Exo1/EXO1 belongs to the Rad2/XPG nuclease family and preferentially degrades DNA with 3'-protruding ends, consistent with its role in the long-resection pathway (Tran et al., 2002). Alternatively, Dna2 is a bifunctional enzyme with RecB-like nuclease and superfamily I helicase domains that

USC
DE SANTIAGO
DE COMPOSTELA

only degrades ssDNA (Kao et al., 2004a). However, the nuclease activity overpowers the Dna2 helicase activity, which can be only detected in nuclease-deficient mutants (Levikova et al., 2013). Consequently, Dna2 needs a lead helicase to perform its role in DNA resection. All the known Dna2 partners in resection belong to the RecQ helicase family; Sgs1 in *S. cerevisiae,* and BLM or WRN in human cells (Cejka et al., 2010a; Gravel et al., 2008; Mimitou and Symington, 2008; Sturzenegger et al., 2014; Zhu et al., 2008). The activity of the lead helicase creates 5' flaps that are quickly coated by RPA, which plays several roles in long resection.

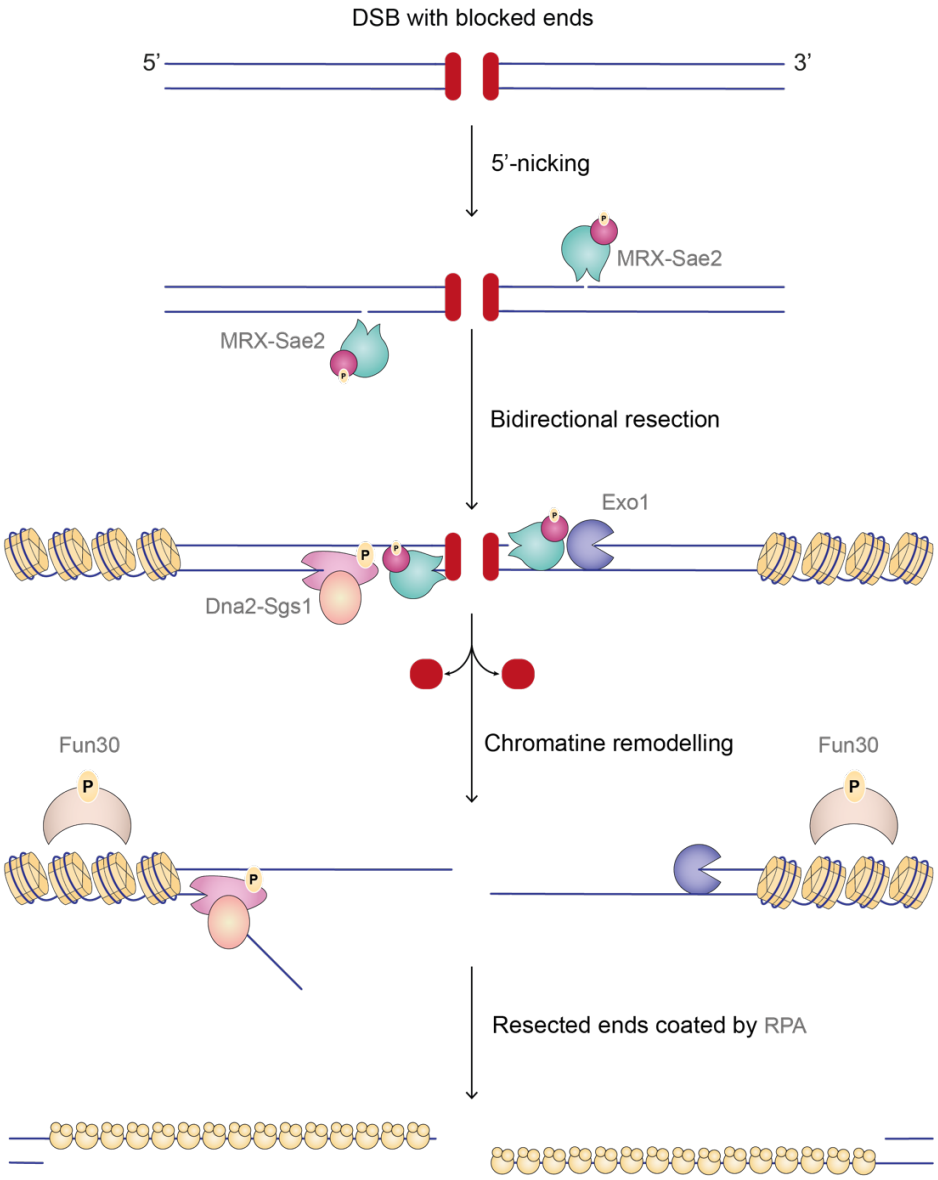


Figure 14. End-resection at blocked DSB ends. MRX-Sae2 nicks the DNA close to the ends, creating entry points needed to start resection, specially at DSBs blocked by protein adducts or secondary structures. Bidirectional resection proceeds via the exonuclease activity of the MRX complex in 3'-5' direction up to the broken end, and via long-end resection in 5'-3' direction. Long-end resection combines the exonuclease activity of Exo1, the endonuclease activity of Dna2, and chromatin remodelling by Fun30. The long 3'-OH ssDNA exposed tract is immediately coated by RPA to protect them from additional nucleolytic processing.

USC
UNIVERSIDADE DE SANTIAGO DE COMPOSTELA

First, RPA prevents the formation of secondary structures susceptible to nucleolytic attack by MRX complex (Chen et al., 2013). Second, it suppresses genomic rearrangements by inhibiting microhomology annealing (Deng et al., 2014). Third, RPA supports Dna2-Sgs1 recruitment and stimulates Sgs1 helicase activity (Chen et al., 2013; Kasaciunaite et al., 2019; Wang et al., 2018; Zhou et al., 2015). Fourth, it promotes Dna2 cleavage of the 5' flaps generated by Sgs1(Cejka et al., 2010b; Niu et al., 2010). Fifth, and as described before, RPA-coated ssDNA is essential to activate the DDC. Therefore, the current model for resection is depicted as bidirectional, in which the 5' endonuclease MRX/N activity creates initiation points for both 5'-3' degradation by Exo1/Dna2-Sgs1 and 3'-5' degradation by MRX/N exonuclease activity (Garcia et al., 2011; Shibata et al., 2014). Both Exo1 and Dna2-Sgs1 can start resecting from 5' resected, gapped or nicked DNA substrates (Wang et al., 2018) and extend the resection tracts up to several kilobases (Figure 14) (Zhu et al., 2008).

Two factors oppose to the end resection machinery: the activation of the DDC and the chromatin context. On one hand, end resection exposes ssDNA that activates the DDC via Mec1-Ddc2. This includes the phosphorylation of histone H2A and the 9-1-1 complex, leading to recruitment of the Rad9 adapter. In particular, chromatin-bound Rad9 close to DSBs inhibits long-range resection (Clerici et al., 2014; Ngo et al., 2014) and reduces Exo1 activity through its phosphorylation by Rad53 (Morin et al., 2008). On the other hand, hindrance of resection by nucleosomes is supported by *in vitro* reconstituted systems. Whereas resection of naked DNA *in vitro* proceeds much faster than *in vivo* (Zhu et al., 2008), the addition of nucleosomes to the system, in the absence of chromatin remodelers, impedes Exo1-mediated resection and, to a lesser extent, Dna2-Sgs1 resection, especially in dense nucleosome arrays. Consequently, resection is supported *in vivo* by multiple chromatin remodelers, including SRC and SWI/SNF, during short- and long-range resection (Kent et al., 2007; Peritore et al., 2021; Shim et al., 2007; Wiest et al., 2017). Another remodeler, Fun30/ SMARCD1, also promotes long-range resection by helping both Exo1 and Dna2-Sgs1 overcome the Rad9 resection barrier (Figure 14). Both the short- and long-resection pathways are positively regulated by the cell cycle machinery. First, Cdk1 phosphorylates Sae2 on serine S267 during S and G2. This facilitates MRX endonucleolytic cleavage at dirty DSBs, as reflected by the defects in resection, sporulation and resistance to camptothecin displayed by the *sae2-S267A* phosphomutant (Huertas et al., 2008). Second, Cdk1 also promotes long-end resection by phosphorylating multiple targets like Dna2, Dpb11 and Fun30. Dna2 contains three Cdk1 consensus sites (T4, S17, and S237) at its N-terminus, and is additionally phosphorylated by Mec1 upon DDC activation. S17 lies within a bipartite nuclear localization signal, and phosphorylation by Cdk1 drives nuclear accumulation of Dna2; besides, Dna2 phosphorylation at S237 is required for recruitment to DSBs (Chen et al., 2011; Kosugi et al., 2009). Fun30 also contains a cluster of N-terminal Cdk1 consensus sites (S20, S28, and S125), with serine S28 being phosphorylated *in vitro* and *in vivo* during S and G2. Phosphorylation of Fun30 allows its association with Dpb11 and tethering to the 9-1-1 complex to chromatin; in turn, this interaction promotes the spreading of Fun30 along chromatin to stimulate resection. Consistent with this model, the fun30-S28A phosphomutant displays impaired resection and DNA damage hypersensitivity. A similar phenotype is exhibited by fun30-S20A mutants, suggesting that both residues are important for Fun30 role

in resection (Bantele et al., 2017; Chen et al., 2016). Finally, the Rad9 adaptor is also a Cdk1 substrate (Ubersax et al., 2003), and Cdk1-dependent phosphorylation of Rad9 promotes its association with Dpb11 to activate DDC in G2/M (Granata et al., 2010; Pfander and Diffley, 2011).

Altogether, this cell cycle regulation of end resection coordinates its activation with the appearance of the sister chromatid after DNA replication (Figure 15). As a result, Cdk1 not only stimulates resection, but also dictates pathway choice by channelling DSBs towards HR. In yeast, CDK phosphorylation of Sae2 during S/G2 commits DSBs to HR by activating Mre11 endonuclease activity which, in turn, creates the entry points for long-end resection. Consequently, the *sae2–S237A* mutation leads to an increase in NHEJ usage (Huertas et al., 2008). Finally, CDK-dependent phosphorylation of Fun30 and Dna2 promotes long-range resection, biasing repair of DSBs to HR over other resection-dependent pathways like MMEJ or SSA. Due to the limited nucleolytic end-processing capacity exhibited by NHEJ in yeast, dirty ends in G1 also influence indirectly their mode of repair, since these DSBs persist until

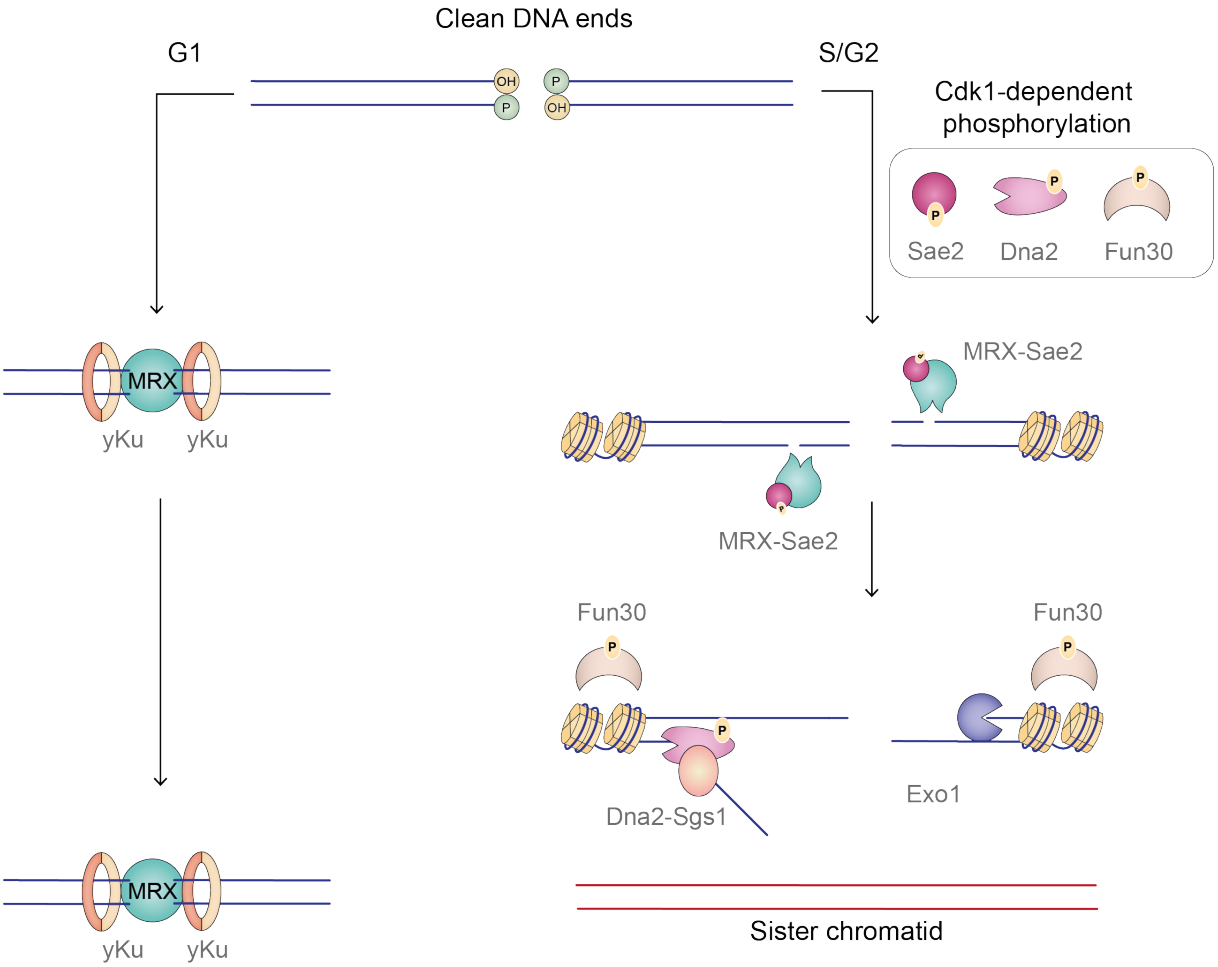


Figure 15. Cell cycle stage dictates DSBR pathway choice. Cdk1 phosphorylates Sae2, Dna3 and Fun30 to promote HR during S/G2 by promoting end resection. Additionally, if the limited end-processing machinery cannot trim dirty ends during G2, this DSBs will be left unrepaired until G2 and repaired by using the homologous chromosome.

USC
DE SANTIAGO
DE COMPOSTELA

Sae2 is phosphorylated and MRX is concomitantly activated. Cell cycle-dependent regulation of end resection and pathway choice is highly conserved between yeast and humans. CtIP, the human and *S. pombe* ortholog of Sae2 is also targeted by cell cycle kinases. During S phase, human CtIP is phosphorylated in T847 by CDK to promote end resection, RPA recruitment and repair by HR (Huertas and Jackson, 2009; Yun and Hiom, 2009). Alternatively, CtIP homolog in fission yeast is also regulated by the cell cycle, but at the transcriptional level (Limbo et al., 2007).

2.2 Nucleofilament assembly, strand invasion and D-loop formation

For recombinational repair to ensue, RPA coating the 3'-overhanging ssDNA must be replaced by the Rad51 recombinase, forming a nucleoprotein filament known as the presynaptic filament. This Rad51 filament catalyses the signature steps of HR: homology search, pairing with the intact donor template and strand invasion (Ogawa et al., 1993; Ranjha et al., 2018). The pairing with the intact donor establishes the synaptic complex, whereas the postsynaptic stage is reached after displacement of the donor's non-complementary strand to form the D-loop. The reactions during the formation of the presynaptic filament to the establishment of the D-loop are reversible and dynamically regulated, ensuring the optimal output while minimizing the deleterious effects of failed HR reactions (Piazza and Heyer, 2019).

The Rad51 recombinase, a homolog of bacterial RecA, is a strand-exchange protein with DNA-dependent ATPase activity that interacts with both ssDNA and dsDNA (Sung, 1994). Binding of ATP increases Rad51 affinity for DNA, hence stabilizing the nucleofilament and facilitating pairing and strand invasion independently of ATP hydrolysis (Sung and Stratton, 1996). *In vivo*, Rad51 binding to ssDNA is initially impeded, since RPA outcompetes Rad51 coating of resected ends due to its higher binding affinity for ssDNA. To overcome this inhibitory effect, cells employ recombination mediator proteins that assist in loading Rad51 onto ssDNA by displacing RPA in the process. In yeast, the replacement of RPA by Rad51 is carried out by Rad52 (Song and Sung, 2000). The formation of the Rad51 nucleofilament is also supported by accessory proteins, including Rad55 and Rad57, two Rad51 paralogs that, unlike Rad51, lack strand-exchange activity on their own (Figure 16) (Sung, 1997).

Homology search starts once the Rad51-ssDNA nucleoprotein filament has been formed and stabilized. This filament constitutes the active element for sequence probing and drives strand exchange with a homologous donor to form a novel heteroduplex (Renkawitz et al., 2014). Homology search is extremely challenging for cells due to the high background of heterologous sequences. Therefore, several adaptations and accessory proteins are required to increase the accuracy and speed of this process. For instance, chromatin mobility is enhanced to facilitate homology search and direct the broken molecules to specialized repair compartments at the nuclear periphery (Dion et al., 2012; Horigome et al., 2014; Oza et al., 2009). Next, the Rad51

USC UNIVERSIDADE DE SANTIAGO DE COMPOSTELA

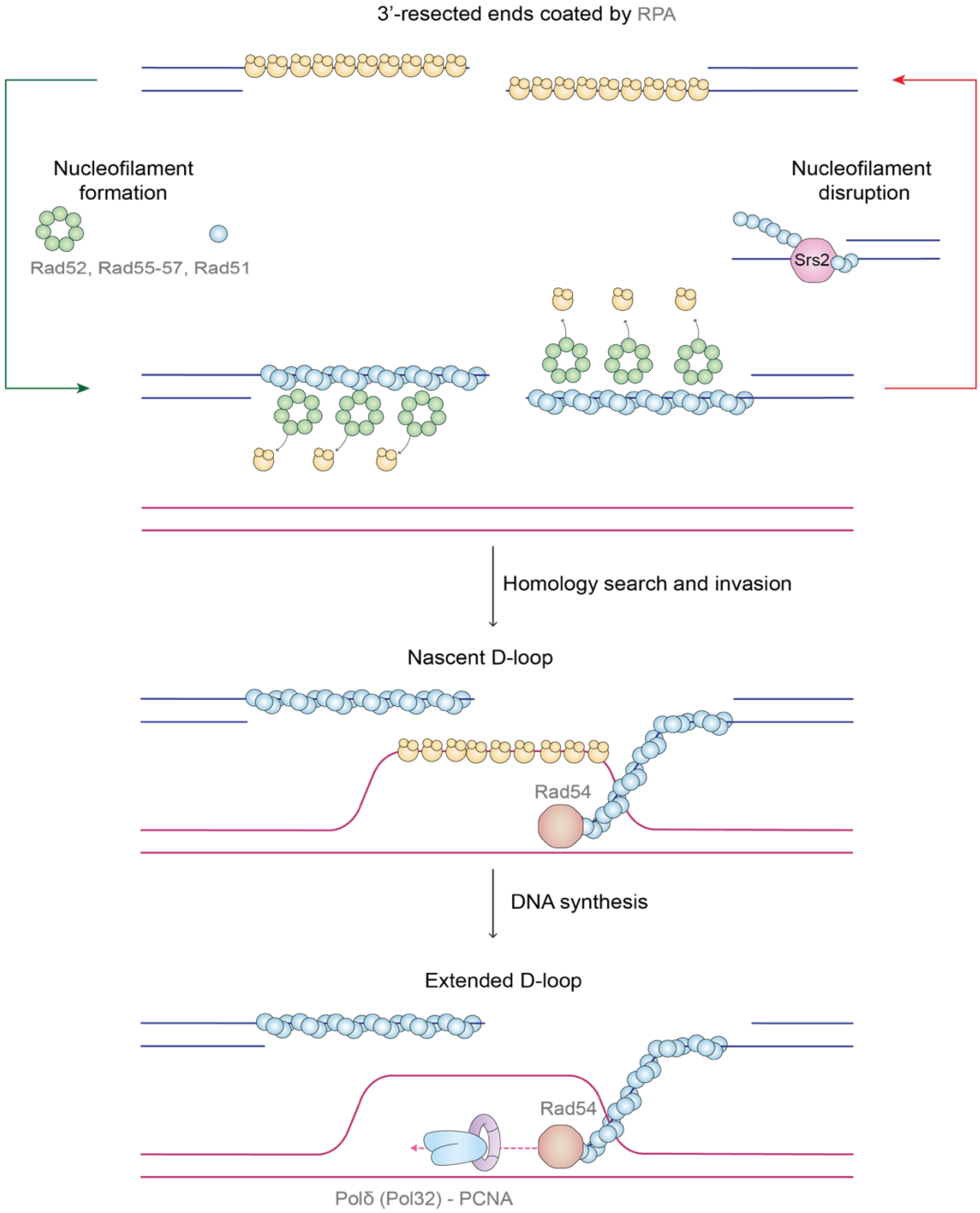


Figure 16. Rad51 nucleofilament catalyses D-loop formation. RPA bound to 3'-protruding ends impedes Rad51 nucleofilament formation. Rad52, together with Rad51 paralogs Rad55-Rad57 (not depicted in the scheme) mediate RPA displacement to allow Rad51 nucleation. Srs2 strips Rad51 from the ssDNA to limit undesired events of HR. Replacement of Rad51 at the end of the nucleofilament by Rad54 promotes homology search and, together with Rad55-Rad57, counteracts Srs2 anti-recombinase activity. The Rad51 nucleofilament, after finding a suitable template for repair, catalyses the invasion of the intact donor. The resulting nascent D-loop is further extended by Polδ to restore the genetic information compromised at the DSB.

USC DE SANTIAGO DE COMPOSTELA

nucleofilament probes the genome, diffusing in three dimensions and establishing transitory contacts with different intact donors. In addition to this, short ssDNA bubbles arising from DNA breathing facilitate the scanning of homologous regions; the role of DNA breathing is supported by the fast homology recognition occurring in AT-rich regions (Gupta et al., 1999). RecA-family proteins stretch DNA 50% more than the original B-dsDNA conformation, flanking those long tracts of stretched DNA with segments of 3 bp that remain in B-DNA-like conformations (Chen et al., 2008; Reymer et al., 2009; Xu et al., 2017; Yang et al., 2020). This over-stretched conformation still allows proper Watson–Crick base pairing and stablishes the structural basis for homology search. Triple base pairing increments between the nucleofilament and the donor facilitates homology recognition (Lee et al., 2015): a minimum of 8 paired bases is required to stabilize the transient interactions between the stretched ssDNA and the DNA duplex. Once stabilized, the nucleofilament starts to probe flanking sequences for additional homology (Qi et al., 2015).

After homologous sequence has been found, the presynaptic filament invades the donor and hybridizes with the complementary sequence, creating a D-loop. RPA then coats the displaced ssDNA, both stabilizing the structure and preventing its reversion (Eggler et al., 2002; Lavery and Kowalczykowski, 1992), whereas the Rad54 dsDNA translocase dismantles the presynaptic complex by stripping Rad51 from the DNA end in an ATP-dependent manner. This further strengthens D-loop stability and exposes the 3'-end to allow *de novo* DNA synthesis (Solinger et al., 2002). D-loop extension from the invading 3'-OH marks the onset of the post-synapsis stage, switching from a nascent to an extended D-loop. Polδ, together with the clamp loader RFC and the processivity factor PCNA, is the main polymerase involved in this step (Figure 16) (Li et al., 2009).

Both formation of the presynaptic filament and strand invasion are tightly regulated processes, with multiple factors cooperating to stimulate recombination by modulating Rad51 formation of the nucleofilament step (Figure 16). As described before in the description of DDT pathways, the Srs2 helicase is a potent disruptor of the Rad51 nucleofilament. Srs2 dismantles presynaptic filaments by the combined effect of its ATP-dependent DNA translocase activity and its physical interaction with Rad51, which stimulates the hydrolysis of its bound ATP and hence decreases the affinity of the recombinase for its substrate (Antony et al., 2009; Colavito et al., 2009; Krejci et al., 2004, 2003; Seong et al., 2009; Veaute et al., 2003). The anti-recombinogenic function of Srs2 is counteracted by the action of the Rad51 paralogs Rad55 and Rad57 and the cell-cycle dependent phosphorylation of Rad51. The precise mechanism behind the role of Rad55-Rad57 to balance Srs2 activity is still under debate. *In vitro* studies support that Rad55-Rad57 directly interact with Srs2, impeding its translocation along the Rad51-Rad55-Rad57 nucleofilament (Liu et al., 2011). Recently, single-molecule analysis of paralogs function in the presence of Srs2 have challenged that vision, favouring a model in which Rad55-Rad57 promotes rapid re-assembly of the presynaptic filament after disruption by Srs2. According to this hypothesis, Rad51 would exist in a flux between unbound and ssDNA-bound state, with Rad55-Rad57 and Srs2 controlling the equilibrium between two states (Roy et al., 2021). In contrast, the effect of Cdk1-dependent phosphorylation of Rad51

USC DE SANTIAGO DE COMPOSTELA

in G2/M is well understood, enhancing its ssDNA binding affinity and, consequently, its ability to outcompete RPA (Lim et al., 2020).

Finally, D-loop formation is also dynamically regulated. Whereas the processing of extended D-loops via SDSA ensures NCO formation, less is known about the pathways that regulate the reversibility of nascent D-loops and the purpose of such regulation. Dismantling of nascent D-loops before the DNA synthesis may result counterintuitive, since this would neither restore the lost genetic information nor repair the DSB. One possible explanation is that D-loop reversal may act as an additional regulatory layer to increase stringency of donor selection. Supporting this hypothesis, it is known that the accuracy of the homology search not only relies on the homology sampling by Rad51. In genetic set-ups where no homologous donor is available, cells reduce the threshold length of the tracts of homology that suffices to enable repair of the DSBs, demonstrating that additional mechanisms operate to regulate this process (Anand et al., 2017). Since the length of many repetitive elements in the genome is above the minimum threshold required to promote DNA strand exchange, and DNA strand invasion is not limited to the end of the filament, such sequences could mediate homology search in ectopic locations if exposed during end resection. In this context, D-loop reversal may limit the use of repetitive sequences by channelling the nucleoprotein filament to the longest available donor through iterative cycles of invasion and disruption, protecting the cells against genome rearrangements (Piazza and Heyer, 2019).

Two different pathways drive the disengagement of the majority of nascent D-loops: the main one is executed by the Mph1 helicase and the topoisomerase activity of the STR complex, whereas Srs2 is responsible for the secondary route of D-loop disruption (Figure 17). Impairment of STR and Mph1 functions displays an epistatic effect in terms of accumulation of nascent D-loops. In contrast, simultaneous disruption of the Srs2 pathway and STR or Mph1 leads to an additive interaction. Rdh54, a Rad54 paralog with a minimal role in nucleofilament formation, delineates the two pathways by funnelling nascent D-loops to the Mph1-STR axis, while escapers to Rdh54 action are dismantled by Srs2. However, it is currently unknown how Rdh54 exerts this function, as it is independent of its ATPase activity, thus complicating reasonable hypotheses such as chromatin remodelling, change in DNA supercoiling, joint molecule disruption or Rad51 stripping. Hence, further research is needed to clarify what attributes differentiate the D-loops channelled to one pathway or the other; different D-loop architecture or distinct heteroduplex length may be relevant to this process (Piazza et al., 2019; Piazza and Heyer, 2019).

When the invading strands withstands disassembly, it can prime *de novo* DNA synthesis in the D-loop. DNA synthesis extends the length of the heteroduplex, which further stabilizes the joint molecule and allows the recovery of the missing genetic information in the broken DNA molecule by using the invaded molecule as a template. Following strand invasion and DNA synthesis, recombination may proceed through three possible recombination sub-routes: BIR, SDSA, and canonical DSBR, which are discussed in the next section.

USC
UNIVERSIDADE DE SANTIAGO DE COMPOSTELA

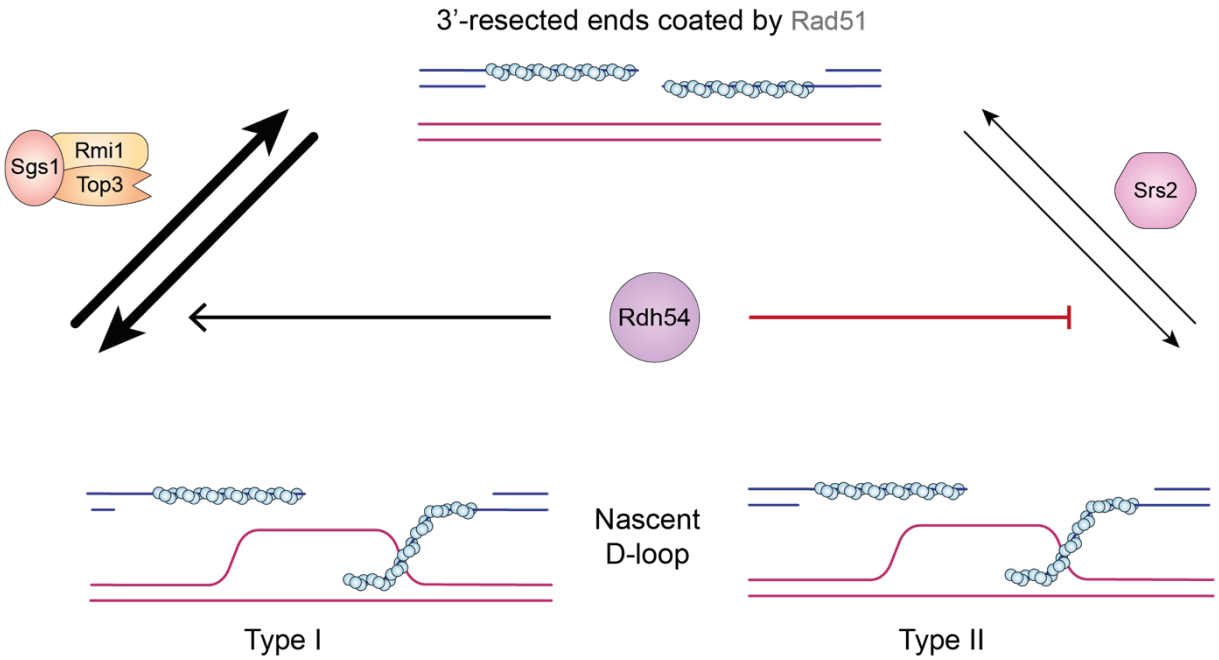


Figure 17. Regulation of nascent D-loop stability in budding yeast. Rdh54 demarcates two pathways to regulate nascent D-loop formation, promoting disruption of nascent D-loops by the STR complex. The difference between Type I and Type II nascent D-loops and the mechanism by which Rad54 delimits both pathways are presently unknown. The thickness of the arrows represents pathway usage.

2.3 Extended D-loop disruption: BIR and SDSA

SDSA and BIR share their initial steps, involving strand invasion of one DSB end, establishment of a D-loop and DNA synthesis. In SDSA, after a short stretch of DNA synthesis, the newly synthesized strand is displaced from the D-loop so it can anneal to the second DSB end. Alternatively, BIR is characterized by the absence of a second DSB end, so cells resort to multiple rounds of invasion, D-loop formation and DNA synthesis that can reach the end of the chromosome. This creates a long ssDNA strand that is later converted into a double-stranded product in a conservative replication fashion (Saini et al., 2013; Stafa et al., 2014). Although the kinetics of strand invasion and leading strand synthesis is similar in BIR and SDSA, BIR requires additional processivity factors, probably due to the longer extension of the repair synthesis. The SDSA pathway produces exclusively NCO outcomes with minimal gene conversion, being the primary HR pathway during mitotic cell cycle.

SDSA constitutes the primary HR pathway in somatic cells. Differently to the disruption of nascent D-loops, which is an inherently anti-recombination activity, disruption of extended D-loops promotes SDSA and NCO formation. SDSA starts with the previously described steps of strand invasion, formation of a nascent D-loop and extension by new DNA synthesis.

USC
UNIVERSIDADE DE SANTIAGO DE COMPOSTELA

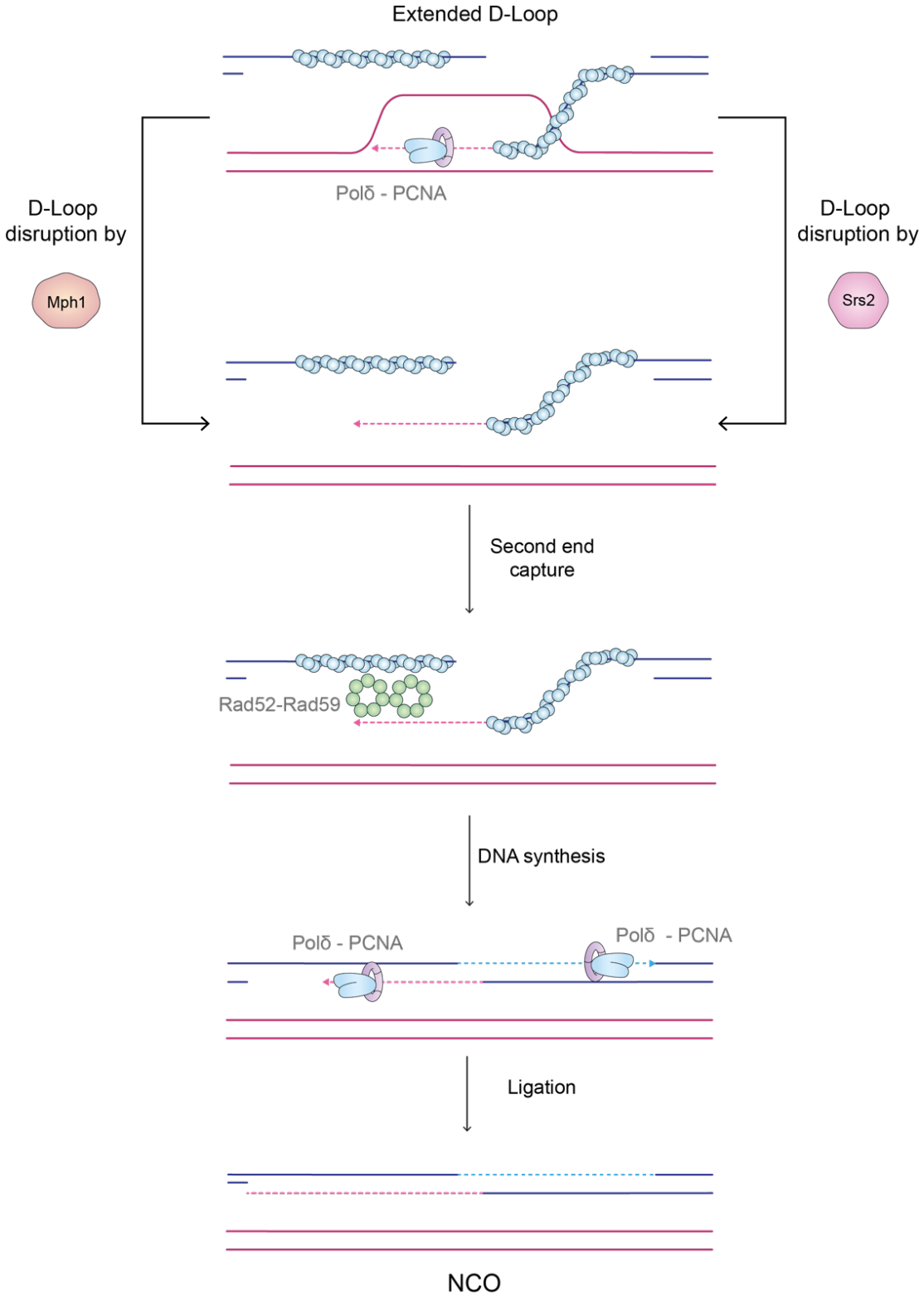


Figure 18. SDSA pathways. Srs2 and Mph1 helicases dismantle extended D-loops during SDSA to limit the extent of genetic information that is copied from the intact donor. Once the invading nucleofilament has been displaced, Rad52-Rad59 mediates re-annealing of the extended strand with its parental DNA molecule. Additional synthesis by Polδ-PCNA and ligation of the resulting nicks complete repair, yielding exclusively NCOs.

USC
UNIVERSIDADE
DE SANTIAGO
DE COMPOSTELA

DNA synthesis is initiated by Polδ, the main repair polymerase, although Polε can fulfil the same role in SDSA in the absence of Polδ (Lydeard et al., 2007). After extension, the D-loop is dismantled mainly by the 5'-3' helicases Mph1 and Srs2. Mph1 accounts for the disruption of the majority of extended D-loops in budding and fission yeasts, as supported by genetic and biochemical experiments (Prakash et al., 2009; Sebesta et al., 2011; Sun et al., 2008). Srs2 has also been implicated in SDSA, playing a partially overlapping role with Mph1 (Mitchel et al., 2013; Prakash et al., 2009). Genetic profiles of *mph1*Δ and *srs2*Δ mutants using ectopic recombination systems demonstrate their ability to direct HR intermediates to NCO through SDSA, but with some differences: *mph1*Δ mutants shift repair from NCO to CO, whereas *srs2*Δ display a decrease in the number of NCO products with a concomitant defect in repair efficiency, without altering CO proportion (Ira et al., 2003; Mitchel et al., 2013). The repair outcomes in *mph1*Δ and *srs2*Δ strains suggest that, similarly to the disruption of nascent D-loops, Mph1 and Srs2 dismantle extended D-loops differently. Again, the particular characteristics of these two helicases may account for variation in length and structure between extended D-loops *in vivo* (Liu et al., 2017; Piazza and Heyer, 2019).

Regarding one-ended DSBs, most of them arise during S-phase when the replisome encounters a nick. Alternatively, nucleolytic processing of stalled replisomes by SSEs and telomere erosion also contribute to their formation (Kockler et al., 2021). BIR was reported for the first time in the bacteriophage T4 (Kreuzer et al., 1995; Luder and Mosig, 1982), and subsequent studies in *E.coli* demonstrated its ability to restart collapsed replication forks (Asai et al., 1994; Heller and Marians, 2006) . BIR has also been extensively characterized in *S. cerevisiae*, employing genetic set-ups that unveiled the molecular mechanisms and particular enzymatic requirements of this pathway. Specifically, two BIR pathways have been described, commonly referred to as Rad51-dependent and Rad51-independent BIR. Both involve Rad52 activity, with Rad59 assisting Rad52 in strand annealing in the Rad51-independent pathway (Davis and Symington, 2004; Malkova et al., 2005, 1996). Rad51-dependent BIR is the major pathway in yeast and shares the same initial steps described for SDSA (Figure 19).

DNA synthesis in BIR is mechanistically different from unperturbed. Similar to SDSA, Polδ is the main polymerase for the synthesis of the leading and lagging strands, with a rate approximately six times slower than S-phase replication (Deem et al., 2008; Lydeard et al., 2007; Smith et al., 2009). DNA synthesis proceeds through a migrating D-loop, where the newly synthesized strand is constantly displaced from the donor and accumulated as ssDNA (Figure 19). Moreover, BIR is asynchronous and conservative, unlike S-phase replication: eventually, the leading strand serves as a template for the synthesis of the lagging strand (Saini et al., 2013; Wilson et al., 2013). This unusual mechanism of synthesis plus the extent of the DNA that needs to be copied makes BIR reliant on additional factors. Pol32, a non-essential subunit of Polδ, supports the main role of this polymerase during BIR (Lydeard et al., 2007).

Additionally, another factor essential for BIR, but dispensable for S-phase replication, is the 5'-3' helicase Pif1 (Saini et al., 2013; Wilson et al., 2013). Much like Pol32, the precise role of Pif1 is not clearly defined, with three non-mutually exclusive possibilities: i) to substitute for the Mcm2-7 replicative helicase in the unwinding of DNA ahead the migrating bubble; ii) to

USC
DE SANTIAGO
DE COMPOSTELA

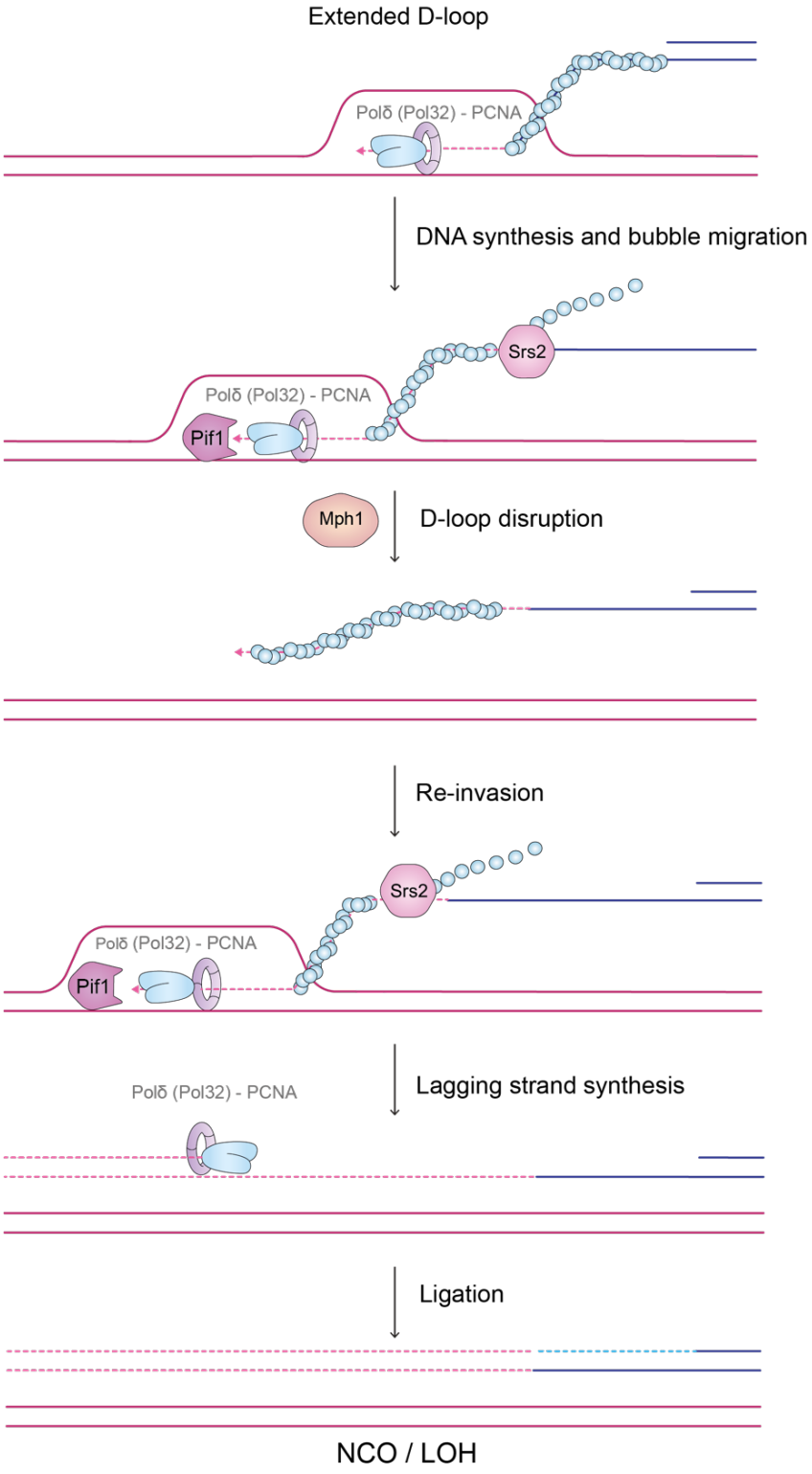


Figure 19. Rad51-dependent BIR pathway. DNA synthesis during BIR proceeds via bubble migration. Like other steps of DNA synthesis during HR, Polδ is the main polymerase in this pathway. Long-range synthesis is supported by Polδ non-essential unit Pol32, and Pif1 helicase. Lagging strand synthesis is initiated by Polα-primase using the recently synthesized strand as template, resulting in conservative inheritance of newly synthesized DNA.

USC UNIVERSIDADE DE SANTIAGO DE COMPOSTELA

unwind the newly synthesized leading strand from the donor and/or iii) to recruit Polδ to the BIR replisome. Finally, BIR is also dependent on the Polα-primase complex, which contributes to stabilize the synthesis of the leading strand. Recently, a new assay developed to monitor BIR synthesis has demonstrated that *pol32*Δ and *pif1*Δ cells are proficient in strand invasion and initiation of DNA synthesis, but the length of their BIR products is limited to 15 and 5 kb, respectively. Similarly, in cells with inactivated Polα-primase complex, BIR long-range synthesis is also affected, although synthesis can still be extended up to 25 kb (Liu et al., 2021). Interestingly, SDSA helicases Srs2 and Mph1 also play a role in BIR. Srs2 contributes to disrupting toxic intermediaries arising from the invasion of the ssDNA accumulated behind the migrating bubble (Elango et al., 2017), whereas Mph1 dissociates the invading strand, forcing BIR to proceed via multiple rounds of template switching and invasion (Stafa et al., 2014). Importantly, the basics of BIR are conserved in mammalian cells; POLD3 and PIF1, human orthologs of Pol32 and Pif1, are also essential to increase processivity during BIR replication (Costantino et al., 2014; Li et al., 2021).

Although BIR provides a solution for the problem of one-ended DSBs, it is regarded as a source of genome instability that can lead to mutagenesis and genomic rearrangements. BIR error-proneness stems from its particular mechanism of DNA synthesis, which is highly susceptible to roadblocks and implies the persistence of long ssDNA tracts (Liu et al., 2021). Therefore, BIR-related sources of genome instability include: i) the long tracts of ssDNA exposed during leading strands synthesis, which are highly susceptible to chemical modifications; ii) frequent interruptions of DNA synthesis due to template switching events or upon encountering roadblocks, such as transcription bubbles; iii) prompt dissociation of newly synthesized strand from its template, hindering correction by MMR machinery and iv) resolution of the migrating D-loop by nucleases, which can trigger translocations and cascades of genome rearrangements. In particular, the frequency of frameshift mutations and base substitutions is greatly increased during BIR (Deem et al., 2011; Saini et al., 2013).

If a second DSB end is available for repair, yeast cells employ several mechanisms to funnel extended D-loops to SDSA, diminishing BIR associated genetic instabilities. Mph1 promotes SDSA by unwinding the extended D-loop and enabling the annealing of the extended strand with the second DSB end. This step is mediated by the annealing activity of Rad52-Rad59 (Mehta et al., 2017; Pham et al., 2021). In addition, MRX contributes to sway extended D-loops towards SDSA by holding DSBs together and allowing synchronous resection of two ends (Pham et al., 2018). Cdk1-dependent phosphorylation also modulates pathway selection between BIR and SDSA. In this sense, phosphorylation of Srs2 by Cdk1 avoids its unscheduled SUMOylation and promotes its role in D-loop dismantlement for SDSA (Saponaro et al., 2010). Cdk1-dependent phosphorylation of Rad52 also assist in end-capture after D-loop formation by stimulating its strand annealing activity.

USC UNIVERSIDADE DE SANTIAGO DE COMPOSTELA

2.4 Second-end capture: Dissolution and Resolution of dHJs

When the extended D-loop is not disrupted by SDSA helicases, DNA synthesis can continue and, hence, either enlarge the D-loop or promote its migration. This allows the displaced strand to expose the sequence tract that is complementary to the second resected end. Then, Rad52/RAD52 facilitates the annealing between both strands, termed second-end capture, which further stabilises the D-loop (McIlwraith and West, 2008; Nimonkar et al., 2009; Shi et al., 2009; Sugiyama et al., 2006). Now, the 3'-OH group at the second DNA end can prime a

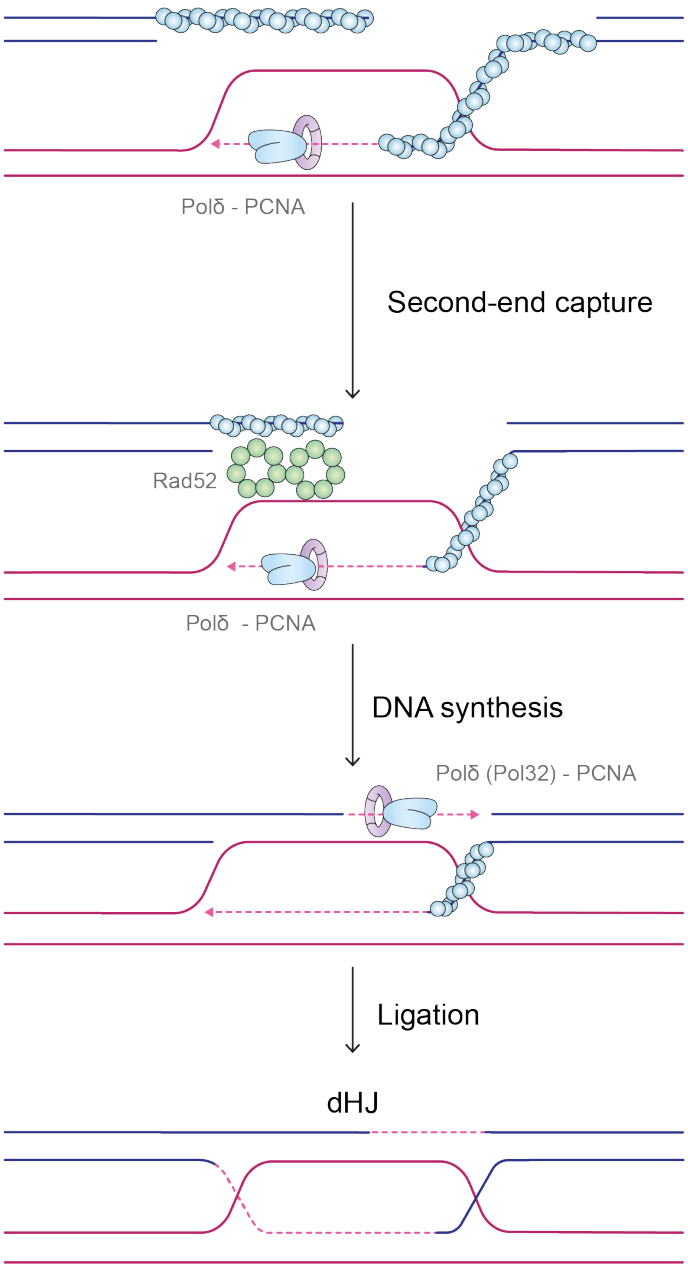


Figure 20. Second-end capture channels HR intermediates to DSBR. Rad52 stabilizes the D-loop by annealing the displaced strand to the second end of the DSB. Following second-end capture, DNA synthesis and ligation lead to the formation of a dHJ, the characteristic intermediate of DSBR.

USC UNIVERSIDADE DE SANTIAGO DE COMPOSTELA

new event of DNA synthesis using the displaced strand as a template that proceeds until the

opposite end. The ligation of the two remaining nicks leads to the formation of the characteristic intermediate of DSBR, the dHJ (Figure 20) (Bzymek et al., 2010; Duckett et al., 1988; Holliday, 1964; Szostak et al., 1983). This four-way intermediate covalently links the two recombinant DNA molecules and must be processed prior chromosome segregation. Failure to disengage dHJs leads to severe chromosome abnormalities, aneuploidies and cell death, due to the persistence of physical connections between sister chromatids or homologous chromosomes (Wechsler et al., 2011). To prevent such deleterious effects, cells can eliminate dHJs by two different mechanisms: dissolution and resolution.

2.4.1 Dissolution of dHJs

The sequence homology between the recombining molecules allows for the branch-migration of each single HJ. Although spontaneous branch-migration is limited, it can be stimulated by DNA helicases or translocases in ATP-hydrolysis-driven reactions (Tsaneva et al., 1992). Dissolution machinery takes advantage of dHJ mobility to disengage recombining molecules without reciprocal exchanges between them. In yeast, dissolution is mediated by the STR complex (Cejka et al., 2010c), while in humans it is carried out by its homologous counterparts BLM - Topoisomerase IIIα - RMI1-RMI2 (BTR) (Wu and Hickson, 2003; Xue et al., 2013). RecQ-family helicases Sgs1/BLM direct the convergent branch migration of the two HJs, with Top3/TopIIIα creating transient nicks to relax the positive supercoiling formed ahead of the migrating junctions (Chen et al., 2014). The two HJs advance towards each other until they fuse into a new type of recombination intermediate, a hemicatenane. Since the two DNA molecules are still physically linked, Top3/TOPOIIIalpha activity is required again to decatenate the junction and complete the repair (Figure 21). Absence of Top3 results in a pronounced slow-growth phenotype caused by the accumulation of converged HJs; consistently, *top3* mutants can be rescued by concomitant deletion of *SGS1*, allowing the endonucleolytic resolution of dHJs (Gangloff et al., 1994). Therefore, convergent branch migration and hemicatenane formation by Sgs1 impedes resolution and compromises repair by Top3 decatenation (Cejka et al., 2012). While Rmi1/RMI1 does not contribute significantly to the initial step of branch migration, it promotes Top3-dependent decatenation *in vitro*, although the precise role remains unknown (Bocquet et al., 2014). In line with this model, *rmi1* deletion phenocopies *top3*Δ strains, suggesting the accumulation of hemicatenanes in these cells (Mullen et al., 2005). RMI2 is only present in higher eukaryotes, supporting the activity of BTR complex in more complex genomes by targeting BLM to different intermediates (Singh et al., 2008).

Importantly, the singular mechanism of dHJ dissolution generates exclusively NCO products and, by promoting convergent migration of dHJs, impedes their resolution and hence suppresses CO formation and promotes genome stability (Ira et al., 2003; Wu and Hickson, 2003). This probably underpins why dissolution is the main DSBR sub-pathway to remove dHJs in somatic cells. Impairment of Sgs1/BLM activity *in vivo* results in higher CO levels and the concomitant increase of sister chromatid exchanges (Chaganti et al., 1974; Ira et al., 2003).

USC UNIVERSIDADE DE SANTIAGO DE COMPOSTELA

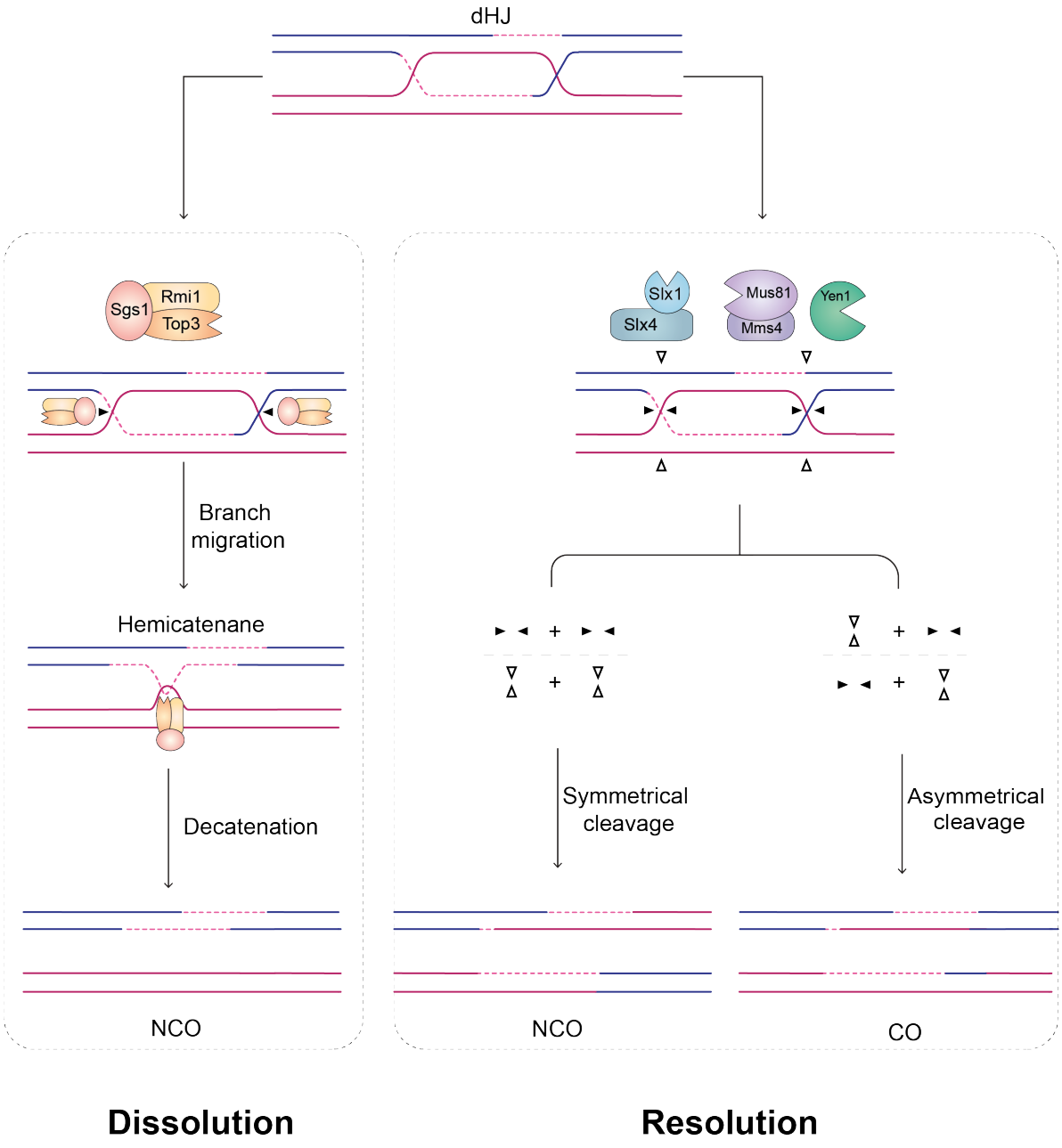


Figure 21. Schematic view of dHJ processing pathways during mitosis in *S. cerevisiae*. The STR complex disengages dHJs in a process termed dissolution to yield exclusively NCOs. Sgs1 promotes convergent migration of dHJs into a hemicatenane, which is further decatenated by Top3. Alternatively, dHJs can be processed by resolvases, producing a mixture of NCOs and COs, depending on the relative orientation of each pair of incisions. Only those resolved in the same orientation for both HJs yield a NCO configuration.

USC UNIVERSIDADE DE SANTIAGO DE COMPOSTELA

2.4.2 Resolution of dHJs

Occasionally, persistent dHJs that escape dissolution can be resolved by a specific type of SSEs, generally termed as resolvases (Blanco and Matos, 2015; Wyatt and West, 2014). Moreover, resolvases represent the only option for the elimination of single HJs, which may appear when one of the D-loop arms is cleaved prior to the second end capture, or upon fork converging during RDR or BIR (Mayle et al., 2015; Pardo et al., 2020).

Initial studies with prokaryotic resolvases, such as RuvC in *E.coli*, set the paradigm for canonical resolution of HJs, and defined how the endonucleolytic activity of resolvases generates a mixture of COs and NCOs. RuvC is a homodimeric protein in solution that introduces two symmetrical and coordinated incisions at phosphodiester bonds in opposite HJ strands, producing two nicked duplexes that can be ligated without further processing (West, 1997). In the context of dHJs, if each pair of incisions occurs on the same plane for each single HJs, a NCO product is formed, whereas cleavage on orthogonal planes results in the reciprocal exchange of the flanking DNA duplexes that characterises CO outcomes (Figure 21)(West, 1997). In eukaryotes, the search for similar resolvases first revealed the existence of mitochondrial RuvC-like enzymes both in *S. cerevisiae* (Cce1) and *S. pombe* (Ydc2)(Lilley and White, 2001). Contrarily, nuclear resolvases with similar activities proved considerably more elusive, but work from several groups over almost two decades led to the identification of a series of SSEs with the ability to process HJs *in vitro*: Slx1-Slx4, Mus81-Mms4 and Yen1 in *S.cerevisiae*, as well as their orthologs in mammals (and also in other species) SLX1-SLX4, MUS81-EME1/EME2 and GEN1 (Figure 21)(Wyatt and West, 2014). As it is described below, the function of these SSEs is highly conserved from yeast to humans.

Slx1 belongs to the GIY-YIG family of nucleases and represents the catalytic partner in the Slx1-Slx4 heterodimer (Figure 22a,b). Slx1-Slx4 displays a preference towards Y-structures, 5'-flaps and replication forks (Figure 22c). However, its role as a HJ resolvase has been questioned, given its low efficiency processing intact HJs. In this sense, Slx1-Slx4 introduces asymmetric nicks a few nucleotides away from the junction, producing a mixture of gapped and flapped products that cannot be directly ligated (Fekairi et al., 2009; Fricke and Brill, 2003; Guervilly and Gaillard, 2018; Munoz et al., 2009; Rass, 2013; Schwartz and Heyer, 2011; Svendsen and Harper, 2010; Wyatt et al., 2013). Its potential function in HJ resolution is further disputed by genetic studies demonstrating that the synthetic lethality of *sgs1*Δ *slx1*Δ or *sgs1*Δ *slx4*Δ double mutants cannot be suppressed by *rad52*Δ, suggesting that the accumulation of unresolved recombination intermediates is not the primary cause of death in these mutants (Bastin-Shanower et al., 2003; Fabre et al., 2002; Fricke and Brill, 2003). Therefore, it has been postulated that, instead, the Slx1-Slx4 complex could operate in the processing of replication intermediates (Coulon et al., 2006, 2004; Deng et al., 2005).

Mus81, the catalytic subunit of the Mus81-Mms4 complex, is a member of the XPF family of nucleases (Figure 23a,b) (Ciccia et al., 2008). Mus81-Mms4/MUS81-EME1 complexes, cleave efficiently a broad variety of structures, especially those containing a nick at the branched point, like replication forks, 3'-flaps and nicked HJs (Figure 23c) (Ehmsen and Heyer, 2009; Gaillard et al., 2003; Rass, 2013; Schwartz and Heyer, 2011). Contrarily, intact HJs constitute poor

USC UNIVERSIDADE DE COMPOSTELA

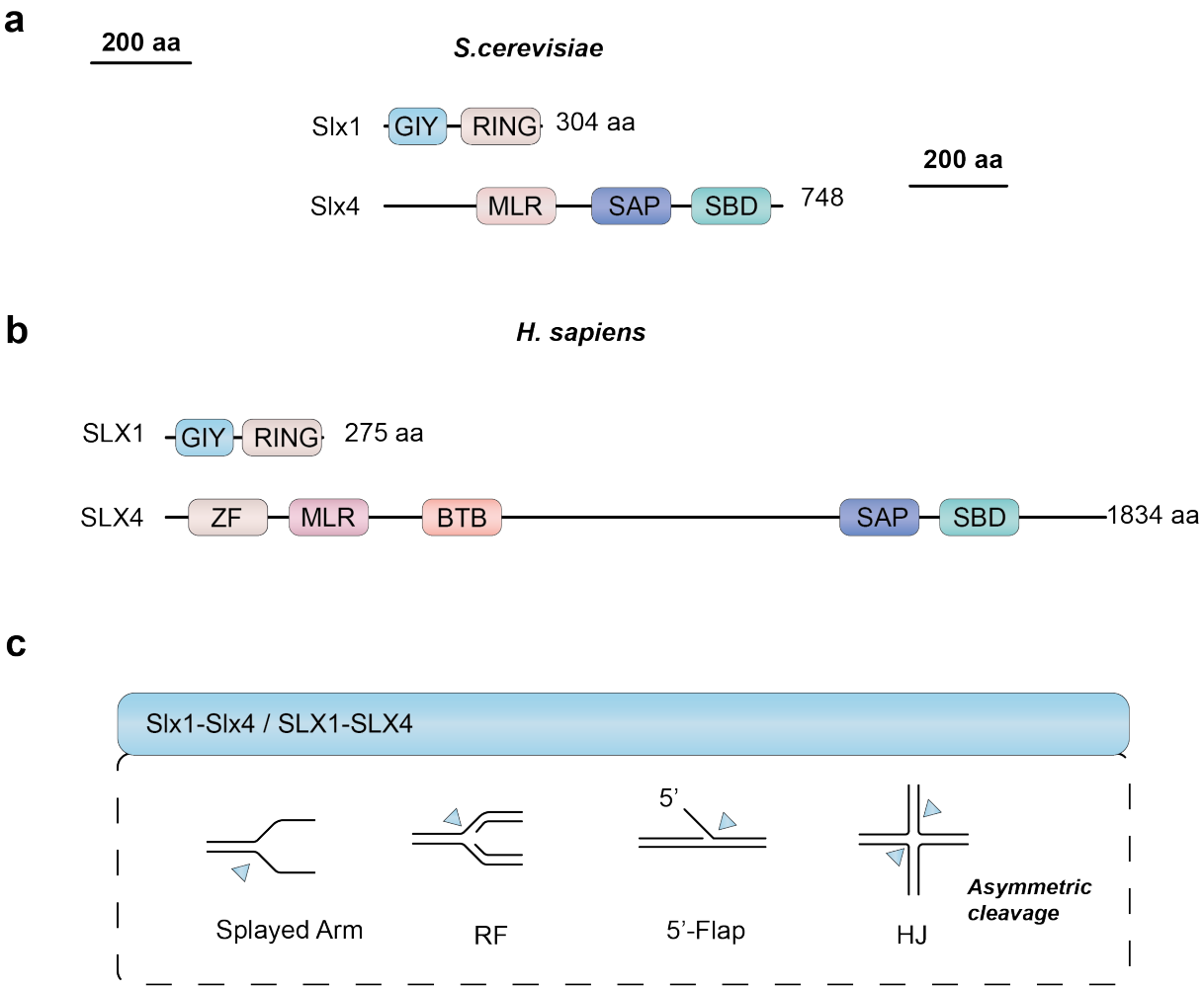


Figure 22. Domain structures of Slx1-Slx4/SLX1-SLX4 and *in vitro* DNA substrate specificities. (a,b) Slx1 is a small GIY-YIG family member with a zinc-finger motif at the C-terminus and, together with Slx4, forms a heterodimeric SSE. **(c)** Slx1-Slx4 cleaves multiple branched DNA substrates (blue arrowheads), including splayed arms, RF and 5'flaps. HJs are cleaved asymmetrically and inefficiently by Slx1-Slx4 complex in budding yeast, whereas in human cells the interaction between MUS81-EME1 and SLX4 promotes efficient HJ processing.

substrates for these enzymes *in vitro*, being cleaved asymmetrically and thus yielding products that, akin to those of Slx1-Slx4, require further processing prior to ligation. (Ciccia et al., 2003; Ehmsen and Heyer, 2008; Gaillard et al., 2003; Gaskell et al., 2007; Kaliraman et al., 2001; Ogrunc and Sancar, 2003; Osman et al., 2003; Schwartz et al., 2012). Given that both Mus81-Mms4 /MUS81-EME1/EME2 and Slx1-Slx4/SLX1-SLX4 complexes deviated from the RuvC paradigm of HJ resolution, they were dubbed as non-canonical HJ resolvases. Nonetheless, Mus81/MUS81 role in HJ resolution is supported by several *in vivo* studies. In this sense, *mus81*Δ and *mms4*Δ mutants, like *slx1*Δ and *slx4*, are essential to sustain the viability of cells lacking Sgs1 (Hickson and Mankouri, 2011). However, the lethality of *mus81*Δ*/mms4*Δ *sgs1*Δ can be suppressed in a *rad52*Δ background, proving that, in those mutants, cell death ensues from the accumulation of toxic recombination intermediates, such as dHJs. Phenotypes of single deletions of *mus81*Δ and *mms4*Δ are also consistent with its role as HJ resolvase, including a reduction in CO formation and spore viability (Boddy et al., 2001; de los Santos et

USC UNIVERSIDADE DE SANTIAGO DE COMPOSTELA

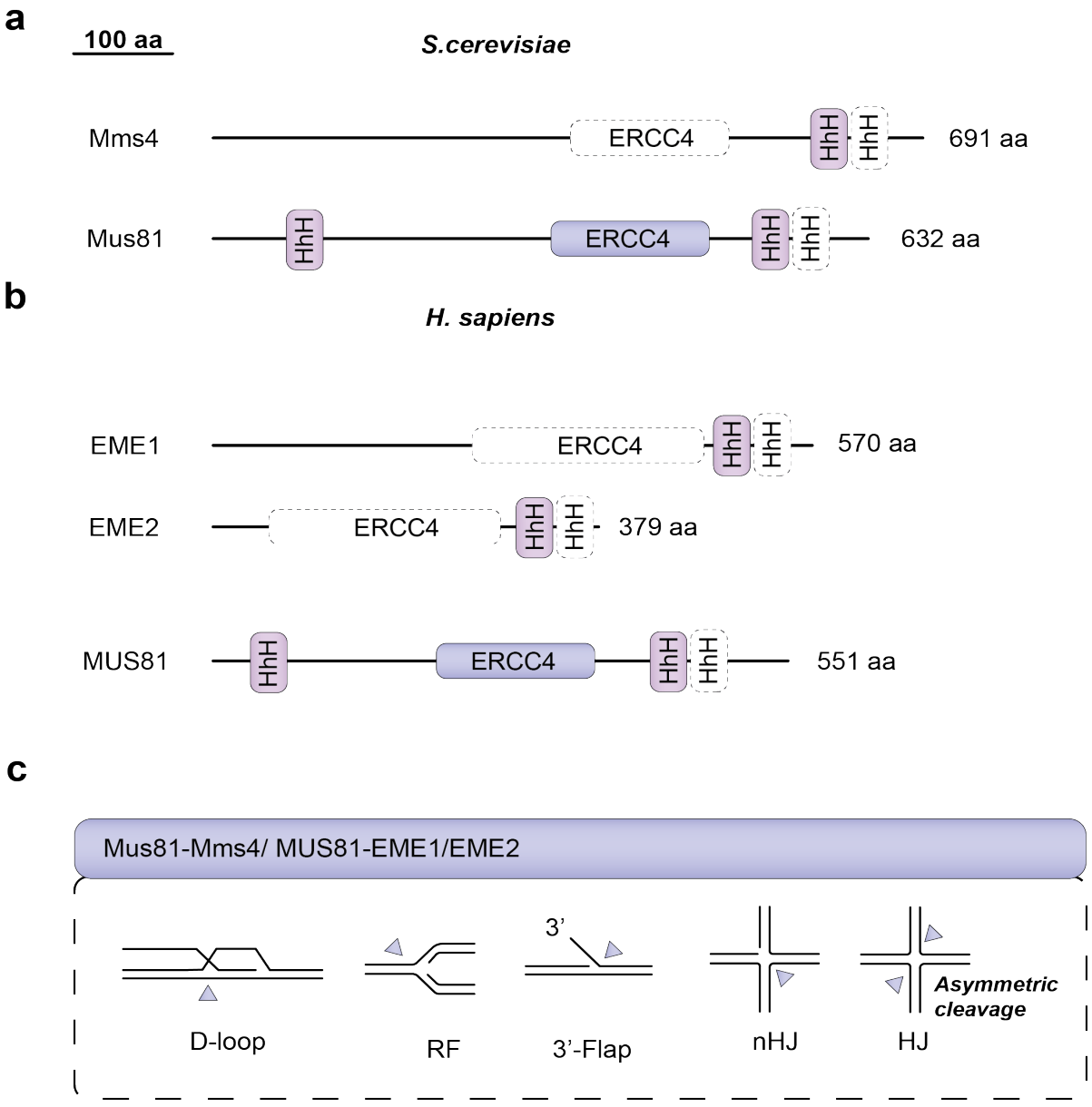


Figure 23. Domain structure of Mus81-Mms4 and MUS81-EME1/EME2 and *in vitro* DNA substrate specificities. (a,b) Mus81 and MUS81 contain an excision repair cross complementation group 4 (ERCC4) endonuclease domain and two helix-hairpin-helix (H) motifs. Mms4, EME1 and EME2 contain the same motifs, but their ERCC4 domain is catalytically inactive (dashed lines and white background boxes denote non-functional motifs). **(c)** Mus81-Mms4 and MUS81-EME1/EME2 heterodimers exhibit activity towards 3'-flaps, RFs, D-loops, and HJ substrates (purple arrowheads**).** HJs are efficiently processed only if they contain a pre-existing nick.

al., 2003, 2001; Mullen et al., 2001). Moreover, Mus81-Mms4 represents the main activity to remove X-shaped HR intermediates when the STR complex activity is compromised. Since the biochemical profile of Mus81 *in vitro* points to nicked HJs as its favourite substrate, its ability to cleave fully ligated HJs *in vivo* is still under debate. Although its role in HRR could be limited to cleave HJ precursors, accessory factors that nick or remodel mature HJs may enhance their processing by Mus81. This is the case in mammalian cells, where the interaction between SLX4 and MUS81 promotes association of SLX1-SLX4 and MUS81-EME1 into the tetrameric SM

complex; the combined activities of the two nucleases allow the efficient cleavage of fully ligated HJs (Wyatt et al., 2013). First, SLX1 nicks one strand of the intact HJ to create one of the preferred substrates for MUS81, which counter-nicks the opposite strand and thus resolves the HJ (Castor et al., 2013; Wyatt et al., 2013). The recruitment of a third nuclease, XPF-ERCC1, also contributes to stimulate HJ cleavage, although in a non-catalytic manner (Wyatt et al., 2017). In addition, SLX4 is required for targeting MUS81 to under-replicated regions (Duda et al., 2016; Guervilly et al., 2015; Minocherhomji et al., 2015). While coordination of Slx1 and Mus81 during HJ resolution has not been demonstrated in budding yeast, Mus81-Mms4 interaction with the Slx4-Dpb11 complex indicates that targeting to under-replicated regions may be also required upon replication stress in *S.cerevisiae* (Gritenaite et al., 2014).

S. cerevisiae Yen1 and human GEN1 were the first *bona-fide* canonical nuclear HJ resolvase discovered in eukaryotic cells, and belong to subclass IV of the Rad2/XPG family of nucleases (Figure 24a,b) (Blanco and Matos, 2015; Ip et al., 2008). Both these enzymes and, as demonstrated later on, their orthologs in other species, retain the characteristic 5'-flap endonuclease activity of the family, but have also evolved the ability to cleave dsDNA branched structures like replication forks, nicked HJs and HJs (Figure 24c) (Bauknecht and Kobbe, 2014; Bellendir et al., 2017; Chan and West, 2015; Freeman et al., 2014; Rass et al., 2010). Detailed biochemical characterization of human and *Chaetomium thermophilum* GEN1 proved that these enzymes fulfil all the properties of the canonical paradigm: like RuvC, GEN1 dimerizes on HJs to introduce two symmetrical and coordinated incisions across the junction, producing nicked dsDNA molecules that can be readily sealed (Chan and West, 2015; Freeman et al., 2014; Rass et al., 2010). In contrast, recent work demonstrates that Yen1 is endowed with arm-chopping and nick-exonuclease activities that yield gapped dsDNA molecules, impeding direct ligation of the molecules *in vitro*. Nevertheless, Yen1 can also process HJs via symmetrical and coordinated incisions and, since the appearance of gapped dsDNA molecules either derive from additional activities that further modify its resolution products (nick-exonuclease) or alternative ways of HJ processing (arm-chopping), its ascription to the canonical paradigm has been maintained (Carreira et al., 2022).

In budding yeast, the functional overlap between Mus81-Mms4 and Yen1 ensures the elimination of physical connections between recombining DNA molecules prior to chromosome segregation. Yen1 is considered to act as a last resort to eliminate the HJs that escape the action of Mus81-Mms4. Whereas *yen1*Δ mutants do not manifest marked DNA-damage sensitivity, cell cycle arrest or segregation defects, deletion of *YEN1* in a *mus81*Δ background intensifies all these phenotypes, leading to an increased sensitivity to several genotoxic compounds, chromosomal mis-segregation defects, cell cycle arrest and decrease in spore viability (Agmon et al., 2011; Blanco et al., 2010; Ho et al., 2010; Tay and Wu, 2010). Like *sgs1*Δ *mus81*Δ, hypersensitivity to genotoxic agents of *mus81*Δ *yen1*Δ double mutants can be partially alleviated by inactivating HR through *RAD52* deletion (Blanco et al., 2010). Expectedly from their role in HJ resolution, the simulataneous deletion of *YEN1* and *MUS81* reduces mitotic CO formation, with the excess of recombination intermediates being channelled to NCO and BIR pathways (Ho et al., 2010).

USC
DE SANTIAGO
DE COMPOSTELA

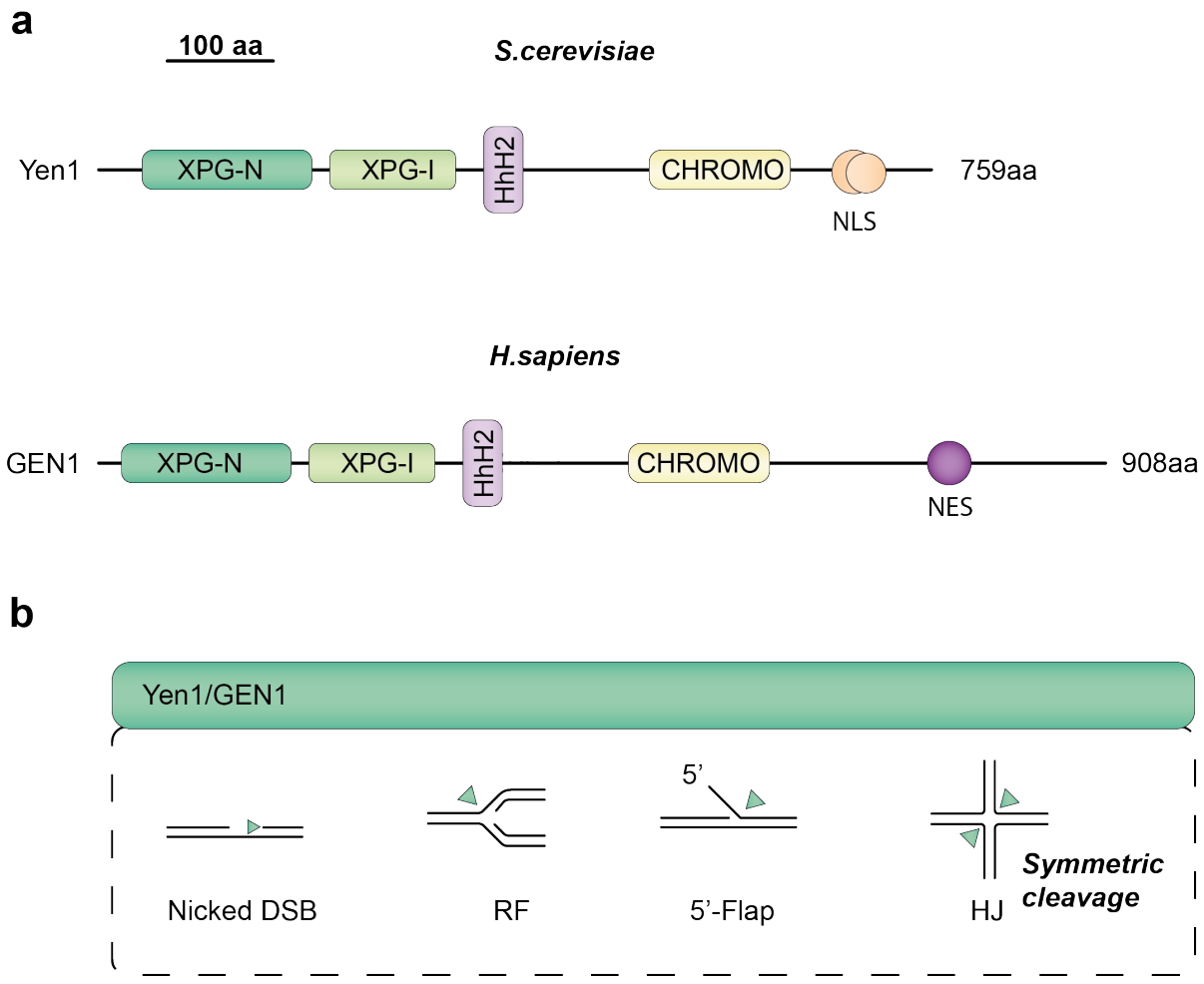


Figure 24. Domain structures of Yen1 and GEN1 and *in vitro* DNA substrate specificities. (a,b) Yen1 and GEN1 are monomeric nucleases that contain N-terminal and internal XPG nuclease motifs, followed by a HhH2 domain, and a chromodomain (CHROMO) to facilitate substrate recognition. **(c)** *In vitro*, Yen1 and GEN1 efficiently cleave 5'-flaps, RF structures and HJs. Additionally, Yen1 and, to a lesser extent, GEN1 are endowed with a weak exonuclease activity that allows them to process nicked substrates into 3-nt (Yen1) or 1nt (GEN1) gapped substrates. Similarly, Yen1 and some of its orthologs, but neither GEN1 or CtGEN1 in an overt manner, can remove one arm from cruciform structures (arm-chopping).

2.4.3 Crossover regulation

Several observations provide support for a model by which cells would resort to the DSBR pathways mediated by the STR complex, Mus81-Mms4 and Yen1 in a hierarchal manner to accomplish HJ removal: (1) the additive effects manifested by *sgs1*Δ *mus81*Δ and *mus81*Δ *yen1*Δ strains, but not in *sgs1*Δ *yen1*Δ mutants, (2) the bias of DSBR to NCO products in mitotic cells and (3) the possibility to funnel joint molecules into the resolution pathway when dissolution is compromised, but not the other way around. Such hierarchy dictating pathway choice during DSBR was confirmed upon discovery of the sequential activation profiles of Mus81-Mms4 and Yen1 late in the cell cycle (Gallo-Fernandez et al., 2012; Matos et al., 2011), and more recently, with elegant studies uncovering the mechanism promoting the early activation of Sgs1 during S-phase (Grigaitis et al., 2020).

USC UNIVERSIDADE DE SANTIAGO DE COMPOSTELA

Remarkably, the regulation of the STR complex, Mus81-Mms4 and Yen1 relies on the concerted action of two cell-cycle master regulators: Cdc28 (CDK1) and the Polo-like kinase Cdc5. The oscillating kinase activities of these enzymes impose the temporal control required to attain their sequential activation during DSBR (Blanco et al., 2014; Gallo-Fernandez et al., 2012; Grigaitis et al., 2020; Matos et al., 2011; Szakal and Branzei, 2013). In mitotic cells, Cdk1-mediated phosphorylation of Sgs1 likely initiates during the S-phase, enhancing its helicase activity. Phosphoactivation of Sgs1, and by inference, the STR complex, allows efficient dissolution of dHJs, with the exclusive production of NCO products (Figure 25a). In parallel to its meiotic regulation, Sgs1 might be inhibited by subsequent Cdc5-dependent phosphorylation at the onset of prophase, although further research is needed to confirm if this phosphoinhibition is meiotic-specific or also occurs in dividing cells (Grigaitis et al., 2020).

Mus81-Mms4 activity on HJs remains at a baseline during G1/S and peaks at the onset of mitosis, in metaphase. As cells approach M-phase, Mms4 is increasingly phosphorylated by Cdk1 and Cdc5, enhancing the catalytic activity of the complex (Figure 25a)(Gallo-Fernandez et al., 2012; Matos et al., 2013, 2011; Szakal and Branzei, 2013). *In vitro* dephosphorylation of Mus81-Mms4 decreases its nuclease activity to basal levels, confirming that hyperactivation is a direct effect of phosphorylation (Matos et al., 2011). Whereas the Cdc5 kinase suffices to activate the complex *in vitro* (Schwartz et al., 2012), the specific contribution of Cdk1 remains undetermined. It is well-documented that initial phosphorylation events by Cdk1 prime further phosphorylation by Polo-like kinases (Elia et al., 2003), but a more direct role of this kinase in activating Mus81-Mms4 cannot be discarded. Mms4 phosphorylation by Cdc5 also promotes its interaction with the Slx4-Dpb11 complex (Gritenaite et al., 2014). Slx4-Dpb11 formation is stimulated by Cdk1-dependent phosphorylation of Slx4 and in conditions of fork stalling (Ohouo et al., 2010), suggesting that this complex may target Mus81-Mms4 at M phase for resolution of recombination intermediates accumulated during lesion bypass (Gritenaite et al., 2014; Princz et al., 2015). Another central regulator of the cell cycle, the Dbf4-Cdc7 kinase (*Dbf4-dependent kinase*, DDK), cooperates with Cdc5 to enhance Mus81-Mms4 activity. DDK contributes to Mus81-Mms4 hyperactivation at M-phase, phosphorylating, like Cdc5, the Mms4 subunit (Princz et al., 2017). Since DDK can phosphorylate its targets during S-phase, Cdc5 is the key factor imposing the timely activation at the end of the cell cycle. Moreover, DDK activity is dampened by checkpoint kinases during fork stalling (Chen et al., 2013; Zegerman and Diffley, 2010). In that scenario, impairment of DDK-dependent phosphorylation may delay Mus81-Mms4 hyperactivation, restricting Mus81-Mms4 activity. According to this hypothesis, checkpoint activation delays JM resolution by Mus81-Mms4 in cells exposed to genotoxic stress (Szakal and Branzei, 2013). While the mechanistic details of how these phosphorylation events cause Mus81-Mms4 hyperactivation are still unknown, their relevance is well-supported by the hypomorphic phenotypes of several phosphomutant alleles, such as *mms4-14A, mms4-7A, mms4-8A* (Matos et al., 2011; Princz et al., 2017; Szakal and Branzei, 2013). After metaphase, Mms4 is dephosphorylated, and its activity reverted to basal levels. In this sense, hyperactivated fractions of Mus81-Mms4 can be SUMOylated and ubiquitylated on Mms4 by the Slx5-Slx8 SUMO-targeted ubiquitin ligase and an E3-ligase complex formed by the SUMO-like domain-contaning protein Esc2 and the Cullin8 complex Mms1-Cul8. These

USC UNIVERSIDADE DE SANTIAGO

post-translational modifications target the phosphorylated Mus81-Mms4 complex for proteasomal degradation, adding an extra layer of control to ensure the periodic deactivation of Mus81 in every cell cycle (Waizenegger et al., 2020).

Yen1 function is also regulated by cell-cycle stage-specific PTMs. Contrary to the STR complex and Mus81-Mms4, extensive phosphorylation imposes a dual inhibitory mechanism that holds Yen1 biochemically inactive and excluded from the nucleus until the last stages of mitosis. S-phase Cdk1 (Cdc28-Clb5) phosphorylates Yen1 at multiple CDK-consensus sites (Loog and Morgan, 2005), causing its cytoplasmic accumulation by impairment of its NLS (Kosugi et al., 2009) and reducing its DNA binding affinity and nuclease activity (Blanco et al., 2014; Eissler et al., 2014). At the onset of anaphase, the Cdc14 phosphatase reverts the effects of Cdk1 phosphorylation, allowing ingression of Yen1 into the nucleus in a biochemically active state to resolve the persistent joint molecules before chromosome segregation (Blanco et al., 2014; Eissler et al., 2014; Garcia-Luis et al., 2014; Kosugi et al., 2009). Afterwards, Yen1 remains nuclear and active until the next round of S-Cdk1 activation (Figure 25a). This probably explains why a third layer of Yen1 regulation exists, ensuring that any fraction of chromatin-bound active Yen1 will be targeted in G1 by Slx5-Slx8 to induce its proteasomal degradation before S phase, in an analogous manner to Mus81-Mms4 (Talhaoui et al., 2018).

Similar to the regulation described above for budding yeast, CDK1 and PLK1, homologs of Cdc28 and Cdc5, couple cell-cycle progression with HJ processing in human cells, even though there are several differences between the two organisms (Figure 25b). First, BLM is activated upon G2/M transition by PLK to promote BTR-dependent dissolution, and not by CDK1 at S-phase (Balbo Pogliano et al., 2022). Second, MUS81-EME1 activation relies mostly on CDK1-dependent phosphorylation, not PLK1. CDK1 phosphorylation facilitates the specific association of SLX1-SLX4 and MUS81-EME1 to promote HJ resolution at G2/M transition (Wyatt et al., 2017, 2013) and to target MUS81 to under-replicated regions (Duda et al., 2016; Guervilly et al., 2015; Minocherhomji et al., 2015). Third, although GEN1 is also phosphorylated by CDK1, it is unclear whether this phosphorylation affects its biochemical activity or subcellular localisation (Chan and West, 2014; Matos et al., 2011). Unlike Yen1, GEN1 gains access to its substrates upon envelope breakdown; since this cellular event is triggered by CDK1 at prometaphase (Heald and McKeon, 1990), GEN1 spatial control is still indirectly connected to cell cycle progression (Matos et al., 2011). The differences between Yen1 and GEN1 regulation may have evolved to adapt HJ resolution to the idiosyncrasies of organisms with open and closed mitosis (Boettcher and Barral, 2013). Strikingly, even though the regulation of dissolution and resolution do not completely mirror the sequential activation of these pathways in S. *cerevisiae*, the output of DSBR in mammalian cells is still biased towards NCO.

In summary, cell cycle kinases regulate HR at several stages, enhancing the recombinase activities of Rad51 and Rad52, and channelling recombination intermediates to NCO pathways like SDSA and dissolution (Heyer et al., 2010; Mathiasen and Lisby, 2014; Wild and Matos, 2016). Importantly, cell cycle regulation imposes a temporal control to HJ processing: first, promoting STR-mediated dissolution during S phase, and second, coordinating two

USC
DE SANTIAGO
DE COMPOSTELA

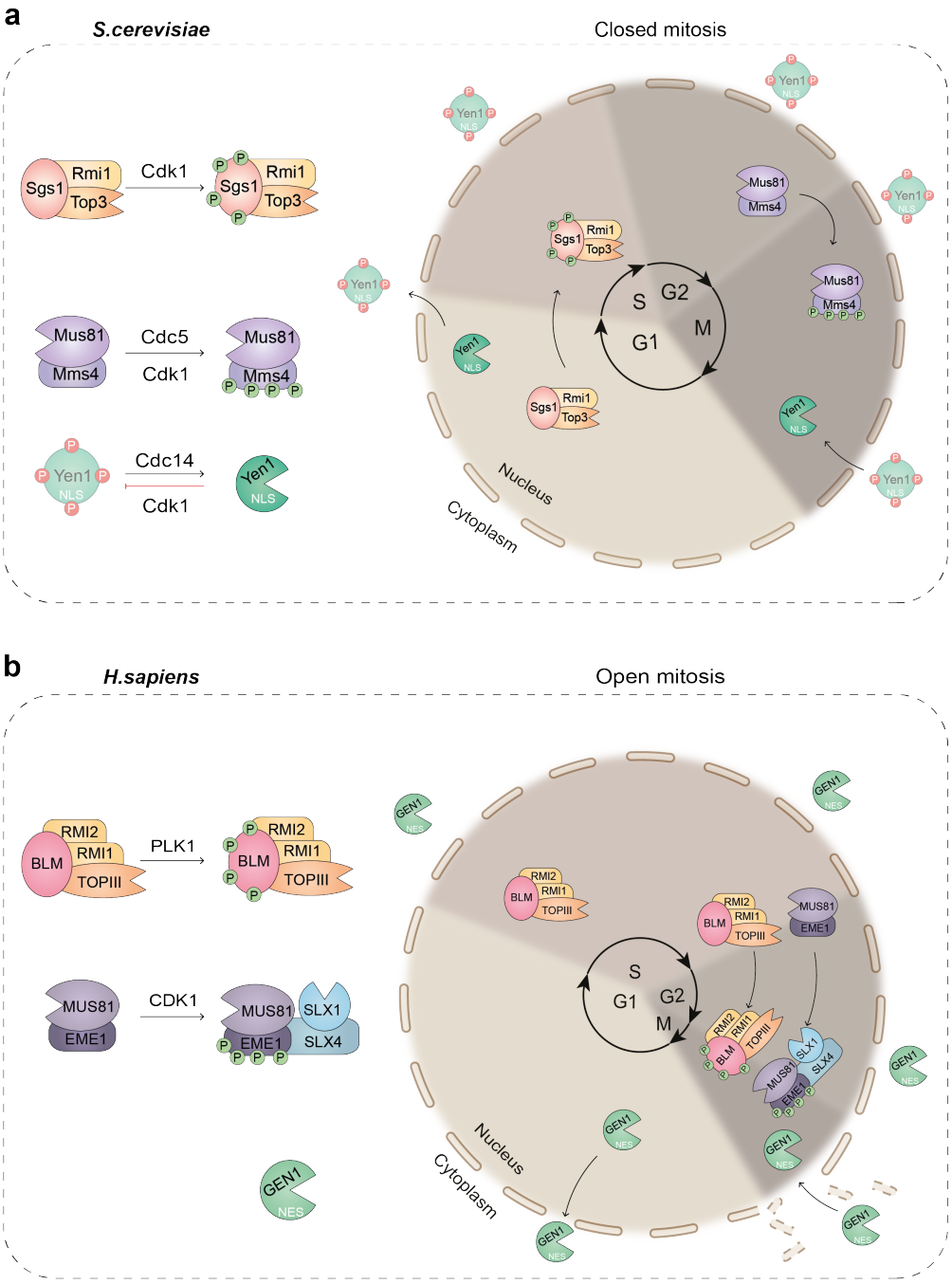


Figure 25 Control of HJ processing by the cell cycle. (a) In *S. cerevisiae*, phosphorylation of Sgs1 by Cdk1 in early S-phase promotes the activity of the STR complex to dissolve dHJs. The efficient processing of HJs during late G2 and M phases relies on the timely activation of Mus81-Mms4 and Yen1. Mms4 phosphorylation by Cdc5 and Yen1 dephosphorylation by Cdc14 sequentially activate these resolvases at the G2/M transition and at the onset of anaphase, respectively. Cdk1-mediated phosphorylation of Yen1, and proteasomal degradation of both Mus81-Mms4 and Yen1 before the S-phase restrain their activity during the bulk of DNA synthesis. **(b)** In human cells, the peak of HJ dissolution is delayed until G2/M transition, when BTR complex is fully activated by PLK1-dependent phosphorylation. Like in budding yeast, resolvases act as a backup of the dissolution pathway. Phosphorylation of EME1 and SLX4 by CDK1 enables the formation of the SM complex, composed of MUS81-EME1 and SLX1-SLX4, to efficiently remove persistent HJs. GEN1 is not directly activated by the cell cycle machinery. Instead, GEN1 control relies on a NES that prevents GEN1 from accessing to its substrates until the nuclear envelope breaks down.

USC
UNIVERSIDADE DE SANTIAGO DE COMPOSTELA

consecutive waves of HJ resolution by Mus81-Mms4 and Yen1 from the G2/M transition to the end of the cell cycle (Figure 26). The high degree of functional overlapping between these three pathways may be a consequence of the inability of cells to trigger checkpoint activation and arrest cell-cycle progression once recombination intermediates mature into dHJs (Matos et al., 2011). Therefore, mitotic cells promote STR dissolution into NCOs to maintain genome stability for most of S and G2, whereas at the end of the cell cycle, Mus81-Mms4 and Yen1 late activation safeguards chromosome segregation at the expense of CO production and, therefore, the risk of increasing loss of heterozygosity and genome rearrangements. By backing up Mus81-Mms4, Yen1 might act as a checkpoint substitute under high levels of stress, ensuring the thorough elimination of abnormal levels of single or double HJs.

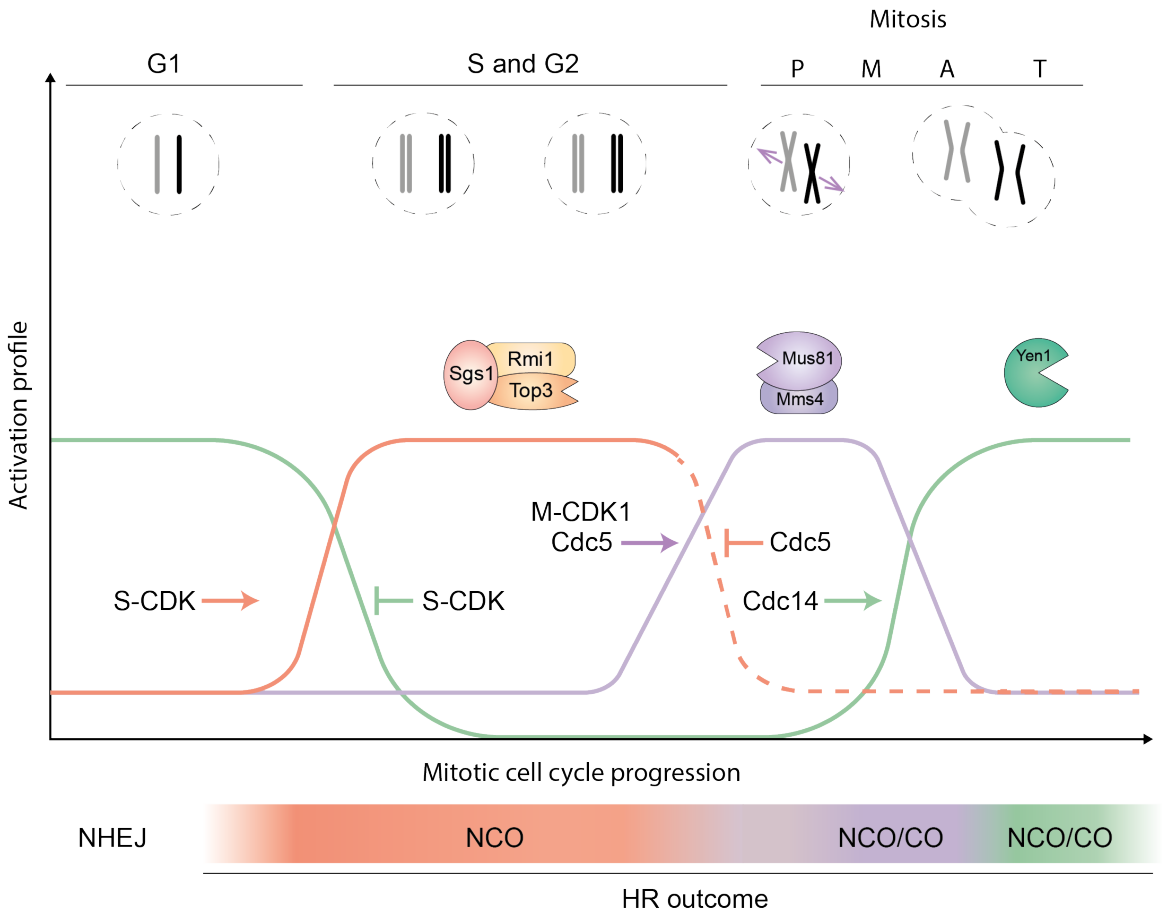


Figure 26. Schematic representation of the sequential activation of HJ processing pathways biases DSBR output towards NCO. Early phospho-stimulation of Sgs1 by Cdk1 promotes dissolution of most dHJs into NCOs. Later on, Cdc5-dependent activation of Mus81-Mms4 at G2/M and dephosphorylation of Yen1 by Cdc14 during anaphase trigger two consecutive waves of HJ resolution to remove persistent JMs, at the expense of producing a mixture of NCOs and COs. Note: All enzymes have different levels of basal activity which cannot be compared in the same graph. P, prophase/prometaphase; M, metaphase; A, anaphase; T, telophase. (Adapted from Grigaitis et al,.2020)

USC UNIVERSIDADE DE SANTIAGO DE COMPOSTELA

2.5 Modulation of SSE activity outside the NCO/CO balance

Nuclear eukaryotic resolvases are specialized flap endonucleases that recognize specific DNA secondary structures with 3' or 5' polarity, regardless of their specific sequences (Dehé and Gaillard, 2017). Resolvases -like most SSEs- can process multiple types of branched DNA molecules matching their endonuclease family preferred polarity. The versatility of Slx1-Slx4/SLX1-SLX4, Mus81-Mms4/MUS81-EME1/2 and Yen1/GEN1 debranching activities on three- and four-way DNA junctions allows them to fulfil roles beyond HJ resolution. For instance, during replication stress both the timely processing of recombination intermediates and fork cleavage to promote RDR can contribute to cell viability (Falquet and Rass, 2019).

In this sense, two main roles have been proposed for Mus81 during replication stress. First, limiting BIR mutagenesis either by cleaving the migrating D-loop to reconstitute a functional fork, or by resolving the HJ formed after the D-loop is merged with a converging replication fork (Mayle et al., 2015). Second, Mus81 could also support replication at stalled replisomes, which become stabilized by HR factors that promote D-loop formation until the arrival of a converging fork. Mus81 would then resolve the resulting HJ, in a similar scenario to the one already described for BIR (Pardo et al., 2020). In *S.pombe*, Mus81-dependent chromosomal breaks correlate with replication restart (Hanada et al., 2007), suggesting that Mus81 promotes BIR by targeting stalled RFs and converting them into one-ended DSBs. In mammalian cells under different conditions of replication stress, MUS81 activity increases cell viability by enabling replication restart at CFS (Fugger et al., 2013; Lai et al., 2017; Murfuni et al., 2013; Naim et al., 2013; Pepe and West, 2014a; Regairaz et al., 2011; Shimura et al., 2008, 2013; Ying et al., 2013). Moreover, it has been hypothesized that MUS81-EME1/EME2 complex ability to process D-loops *in vitro* is consistent with a role analogous to Mus81-Mms4 in limiting BIR mutagenicity, although more data is required to prove this model (Pepe and West, 2014b).

Yen1, given its later activation during the cell cycle, has been implicated in backing up Mus81 activities during replication stress, processing those HJs that could appear after D-loops and converging forks merge, with the additive effect of *YEN1* deletion on *mus81*Δ phenotypes supporting this model (Mayle et al., 2015). Nonetheless, recent evidence indicates that Yen1 role is not limited to process HJs that escape Mus81 during DSBR or replication stress. In human cells, DNA2 promotes DNA replication and participates in the restarting of stalled replication forks (Thangavel et al., 2015); similarly, under-replicated DNA accumulates in Dna2 helicase-defective strains. In these mutants, further deletion of *YEN1*, but not *MUS81*, results in a strong synthetic sickness that is exacerbated by exposure to genotoxic agents and aggravated by *RAD52* deletion (Olmezer et al., 2016). These results support a role for Yen1, which is not redundant with Mus81 functions, in the mitotic resolution of persistent replication intermediates by processing those DNA structures that either escape or arise in the absence of the helicase activity of Dna2 and which remain to be determined. In addition, the modelling of human CFS expression in budding yeast demonstrates that Yen1 also plays a protective role in the stability of these difficult-to-replicate regions (Kaushal et al., 2019).

USC
UNIVERSIDADE DE SANTIAGO DE COMPOSTELA

In view of this current picture where resolvases are paramount enforcers of replication completion and JM elimination, it is still quite striking that cells restrict their activities until the last stages of the cell cycle, even though under-replicated regions and persistent HJs constitute an enormous threat for chromosome segregation and viability. As described in section 2.4.3, it is well-established that the spatio-temporal regulation of resolvases is essential to bias HR outcome towards NCO pathways but, additionally, that timely activation of Mus81-Mms4/MUS81-EME1 and Yen1/GEN1 safeguards the genome from the untimely processing of physiologically relevant secondary DNA structures (Wild and Matos, 2016). Following this rationale, the delayed activation of resolvases would minimise the exposure to these enzymes of the multiple branched molecules stemming from the normal DNA metabolism during S/G2, including replication (replication forks, reversed fork, 5'-flaps, HJs, etc), transcription (R-loops), repair (D-loops or HJs), protection of chromosome ends (T-loops), etc.

Moreover, the number of possible substrates for SSEs cleavage is expanded by the potential of DNA to adopt different secondary structures that deviate from the canonical B conformation (Figure 27), like hairpins, cruciforms, G-quadruplexes and triplex DNA (Bochman et al., 2012). How DNA adopts these secondary structures depends on multiple factors, such as local base composition -symmetry, repetitiveness and GC content- and topology (Wang and Vasquez, 2017; Wickramasinghe et al., 2015), frequently arising in regions containing inverted, mirror and/or direct repeats and those with long tracts of guanines. Although these non-β DNA conformations can be readily induced *in vitro* on ssDNA, their *in vivo* relevance has been long under debate, since the duplex DNA conformation is energetically more favourable in cells. In fact, these structures are not continously present in the genome, but transiently appearing at certain genomic regions during DNA replication, repair, and transcription (Khristich and Mirkin, 2020; Krasilnikova and Mirkin, 2004), where the melting of dsDNA by helicases and the topological forces induced during such processes facilitate B-DNA to non-B DNA local transitions (Lerner and Sale, 2019).

The conservation of these branched DNA molecules and secondary structures throughout eukaryotic genomes highlights their importance in multiple aspects of DNA dynamics. T-loops protect telomeres by avoiding chromosome ends from being recognized as damaged DNA, while reversed forks stabilize replisomes during replication stress and mediate fork restart (de Lange, 2004; León-Ortiz et al., 2014; Neelsen and Lopes, 2015). G-quadruplexes have been linked to telomere maintenance, replication origin specification in mammalian cells, transcriptional regulation, and immunoglobulin class switch recombination within the IgG locus (Bochman et al., 2012; Robinson et al., 2021). However, these very structures can also trigger genomic instability (Kaushal et al., 2019; van Wietmarschen et al., 2020; Zhang and Freudenreich, 2007; Zhao et al., 2018), especially due to their intrinsic capacity to hinder fork progression (Follonier et al., 2013; Gerhardt et al., 2016; Liu et al., 2012). In fact, local sequences predicted to form non-B DNA structures correlate with translocation breakpoints, DSBs, indels, copy number variations and point mutagenesis (Wang and Vasquez, 2022).

In general terms, it appears that cells prioritise the helicase-mediated unwinding of replication and recombination intermediates, as well as secondary structures, to maintain fork progression

USC DE COMPOSTELA

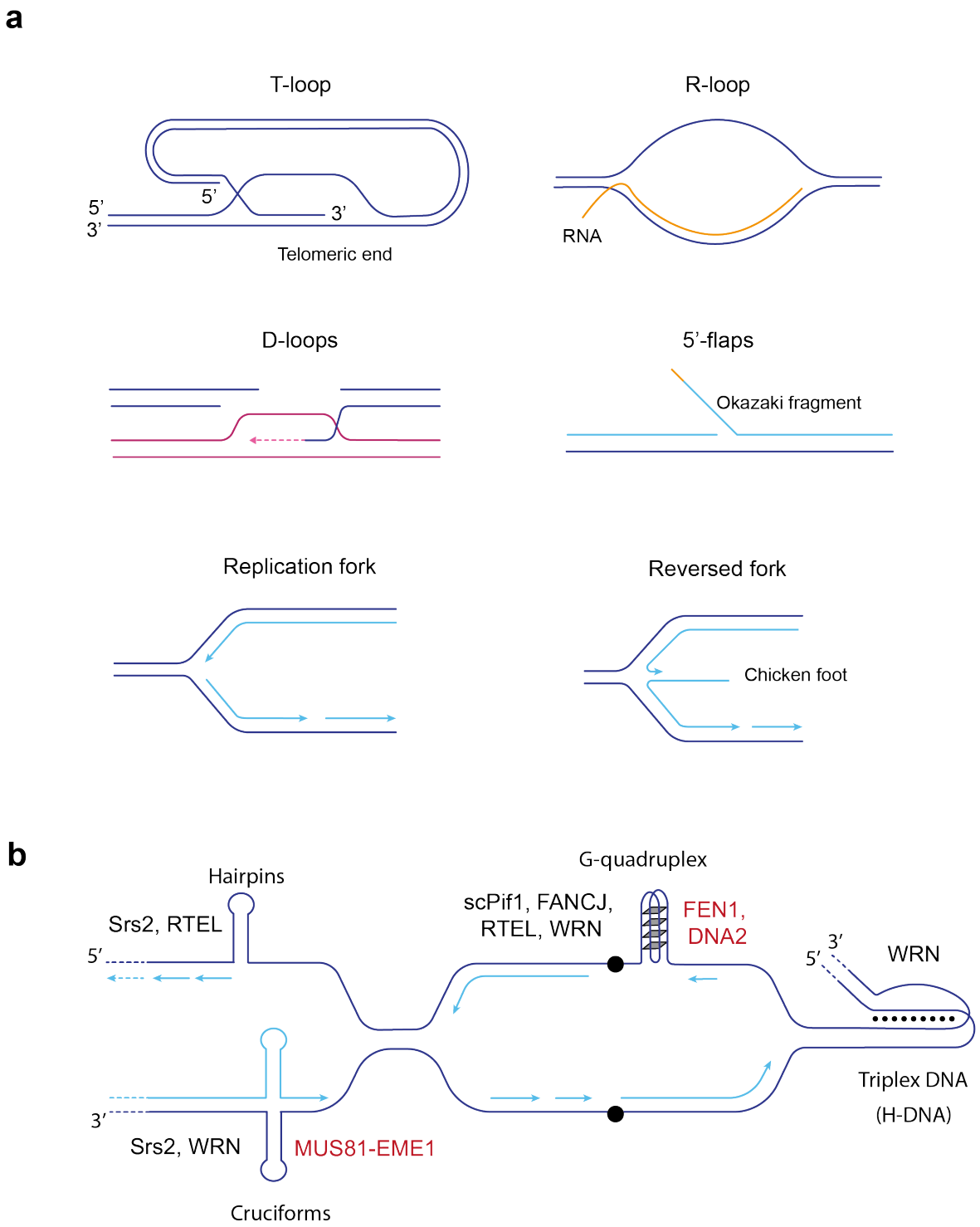


Figure 27. Schematic representation of secondary DNA structures that may serve as substrates for SSEs. (a) Replication and recombination give rise to branched intermediates that could be potentially cleaved by SSEs **(b)** Replication increases the probability of repetitive and GC rich sequences to fold into different secondary structures, such as hairpins, cruciforms, G-quadruplexes, and H-DNA. Helicases (black) and SSEs (red) that can target each structure are indicated. Black circles represent replication origins.

USC
UNIVERSIDADE DE SANTIAGO DE COMPOSTELA

and genome integrity, with the DDC extending the temporal window to remove those obstacles under situations of replication stress. However, if the intermediates or the secondary structures persist, SSEs play a critical role acting as a backup of helicase activity, albeit their nucleolytic activity is frequently associated with genomic rearrangement, insertions, deletions and telomere instability (León-Ortiz et al., 2014).

The Srs2 and WRN helicases unwind hairpins in yeast and mammalian genomes, respectively. In WRN-deficient cells, MUS81-EME1-SLX4 cooperate to cleave the excess of harpins accumulated during DNA replication (Mengoli et al., 2023; van Wietmarschen et al., 2020). Similarly, Srs2 and RTEL unwind imperfect hairpins formed at trinucleotide repeats (Bhattacharyya and Lahue, 2005, 2004; Frizzell et al., 2014), preventing their cleavage by the MMR complex MutSβ (Owen et al., 2005; van den Broek, 2002).

Numerous helicases have been implicated in dismantling G-quadruplexes *in vitro* and *in vivo*, including the Pif1-family helicases (Paeschke et al., 2011; Sabouri et al., 2012; Sanders, 2010) and FANCJ (London et al., 2008; Sarkies et al., 2012; Schwab et al., 2013; Wu and Brosh, 2009). Absence of ScPif1 and Rrm3 in *S.cerevisiae*, or FANCJ in metazoans is associated with G4-dependent rearrangements and deletions of guanine-rich sequences (Cheung et al., 2002; Kruisselbrink et al., 2008; Lopes et al., 2011; Paeschke et al., 2013; Piazza et al., 2010; Ribeyre et al., 2009; Youds et al., 2006). Some of the RecQ-family helicases (Sgs1 in budding yeast; BLM and WRN in mammals) and RTEL are necessary for efficient replication of the G-rich telomeric ends, supporting their role in dismantling G4s at chromosome ends (Crabbe et al., 2004; Kamath-Loeb et al., 2001; Sfeir et al., 2009; Vannier et al., 2013, 2012). The action of the TLS polymerase REV1 provides an alternative solution to helicase unwinding to allow G4 bypass *in vitro* and in cultured vertebrate cells (Eddy et al., 2014; Sarkies et al., 2010; Schiavone et al., 2014). In contrast, *rev1*Δ mutants in *S. cerevisiae* do not exhibit increased levels of genome instability at G4 motifs (Lopes et al., 2011). It is tempting to speculate that nucleases could also backup helicase activity to resolve persistent G4s, as supported by the *in vitro* cleavage of G4 substrates by Mre11/MRE11, Exo1/EXO1 and Dna2/DNA2 (Lin et al., 2013; Masuda-Sasa et al., 2008). Moreover, the conversion of T-loops into dsDNA required for telomere replication during S phase is mediated by RTEL, which restores the lineal configuration of chromosome ends without affecting telomere length (Brenner and Nandakumar, 2022). In contrast, SLX4 recruitment to the telomere mediates nucleolytic processing of T-loops by SLX1, resulting in telomere shortening and the appearance of T-circles in RTEL-deficient cells (Vannier et al., 2012; Wan et al., 2013).

It could be argued that the downregulation of SSEs serves a general purpose of promoting helicase-dependent dismantling of branched DNA molecules and secondary structures as a first resource. In this sense, there are several examples in the literature showing how post-translational modifications of SSEs or their interaction with specific proteins can modulate their functionality, from the direct modification of their catalytic properties to their targeting to precise locations or substrates (Dehé and Gaillard, 2017).

For instance, the activity of the NER nucleases Rad2/XPG and Rad1-Rad10/XPF-ERCC1 must be tightly controlled, since each nuclease can potentially cleave damaged and undamaged

strands on opposite sides of the distorted DNA helix, resulting in a DSB. However, in human cells, proper positioning and recruitment of both nucleases is ensured by the scaffolding effect of XPA, RPA and TFIIH, with RPA also directing the incision of XPF-ERCC1 to the damaged strand (Laat et al., 1998; Staresincic et al., 2009). XPF-ERCC1 is also important in vertebrate cells for the removal of interstrand crosslinks. In this case, the scaffold SLX4 recruits XPF-ERCC1 to the lesions and imparts structural preferences towards replication-like structures over NER common substrates, such as stem-loops or bubbles (Douwel et al., 2017, 2014; Hodskinson et al., 2014).

Another key SSE, Rad27/FEN1, interacts with PCNA to mediate its recruitment to replication sites during Okazaki fragment processing, as well as to stimulate its flap-endonuclease activity. Its timely interaction with PCNA relies on the concerted actions of two different PTMs. FEN1 methylation facilitates PCNA interaction by inhibiting phosphorylation at a nearby residue throughout S-phase. In late S phase and G2, CDK1-dependent phosphorylation both inhibits FEN1-PCNA interaction and reduces FEN1 catalytic activity. Phosphorylation also drives FEN1 SUMOylation which, in turn, allows FEN1 ubiquitination and targeting for proteasomal degradation (Guo et al., 2012, 2010). Whereas PTMs control the opportune activation of FEN1 during Okazaki fragment processing and its protein levels, additional mechanisms regulate FEN1 in the response to replication stress. In addition to its flap-endonuclease activity, FEN1 is also endowed with a gap-endonuclease activity necessary for the re-initiation of stalled replication forks. The balance between both activities is regulated by two different interactors: WRN, which promotes the gap endonuclease, and WDR4, which stimulates the flap-endonuclease activity at unstressed forks (Cheng et al., 2016; Sharma et al., 2004).

In order to understand the relevance of SSE regulation or, conversely, the consequences of their misregulation, two strategies are frequently employed: (1) the development of alleles to block or mimic the specific PTMs of the SSE of interest; (2) the overexpression of the SSE itself or the up/downregulation of its main regulators. For instance, this overexpression tactic has been employed to show that increased levels of various members of the Rad1- and Rad2-families of nucleases in budding yeast lead to genome instability, checkpoint activation, impaired DNA replication, hypersensitivity to genotoxic agents or even cell death (Becker et al., 2018; Jimeno et al., 2017; Kang et al., 2010). Similarly, overexpression of a mutant version of FEN1 that cannot be degraded upon S/G2 transition causes cell-cycle delay and abnormalities during chromosome segregation (Guo et al., 2012). Similar approaches have also been applied to Mus81-Mms4/MUS81-EME1 and Yen1/GEN1, in order to understand how their stringent cell-cycle control minimizes the risks associated to their unrestricted actions.

Regarding Mus81-Mms4, which becomes activated upon phosphorylation of Mms4 by Cdk1 and Cdc5, the two main strategies that have been employed to anticipate the action of this complex are i) the overexpression of Cdc5 by placing it under the transcriptional control of the P_{GAL1} promoter (Matos et al., 2013) and ii) the generation of phosphomimetic mutants at CDK consensus sites present on Mms4, like *mms4-S56E* and *mms4-S56E-S184D*, which complement the sensitivity of *mms4*Δ strains without affecting their sensitivity to genotoxic agents (Szakal and Branzei, 2013). Both conditions led to a significant increase in mitotic COs, which could

USC
DE SANTIAGO
DE COMPOSTELA

result in higher levels of LOH in diploid cells (Matos et al., 2013; Szakal and Branzei, 2013). It has been proposed that these higher CO levels were a direct consequence of increased interference by Mus81-Mms4 with at least two different repair pathways: dissolution of dHJs by the STR complex during HR, and the error-free DNA damage tolerance routes (Szakal and Branzei, 2013). However, it is worth mentioning that while Cdc5 overexpression led to the biochemical hyperactivation of immunoprecipitated Mus81-Mms4 in these studies (Matos et al., 2013), there is no direct evidence of increased biochemical activity of the Mus81-Mms4 phosphomimetics with respect to the wild-type enzyme. Therefore, the higher CO proportion observed in both type of strains might be a consequence of different types of perturbation to Mus81 regulation.

As aforementioned, the ability of MUS81-EME1/2 to resolve dHJs in human cells is enhanced by the nickase activity of SLX1-SLX4 (Castor et al., 2013; Fekairi et al., 2009; Gritenaite et al., 2014; Matos et al., 2011; Munoz et al., 2009; Svendsen et al., 2009; Wyatt et al., 2013) and its targeting to replication intermediates also requires its interaction with SLX4 (Guervilly et al., 2015; Minocherhomji et al., 2015, Duda et al., 2016). In this sense several lines of evidence indicate that the genome instability caused by misregulation of MUS81-EME1/2 is due to its precocious interaction with SLX4.

First, it has been shown that DNA damage induced by aberrant CDK1 levels or a defective DDC is MUS81-dependent (Beck et al., 2012; Dominguez-Kelly et al., 2011; Forment et al., 2011; Kim et al., 2013; Neelsen et al., 2013; Techer et al., 2016). Downregulation or inhibition of the WEE1 kinase, which repress CDK1, causes the breakage of replicating chromosomes, increasing DNA damage levels, checkpoint activation and S-phase cell cycle arrest (Beck et al., 2010, 2012; Dominguez-Kelly et al., 2011). This phenotype was also recapitulated by the transient overexpression of cyclin E and CDC25A phosphatase, which antagonizes WEE1 effect, except that in this case with arrest in the G2/M transition (Neelsen et al., 2013). While it was originally postulated that these results were due to a direct inhibitory effect of the WEE1 kinase on MUS81-EME1/2, it was later demonstrated that WEE1 inhibition triggers MUS81 activation indirectly. Anomalously high activity of CDK drives premature phosphorylation of SLX4 in S phase and the subsequent assembly of the hyperactive MUS81-EME1/SLX1-SLX4 complex, resulting in the cleavage of ongoing replication forks and chromosome pulverization (Duda et al., 2016). Similar phenotypes were described under conditions of checkpoint inactivation, since the CHK1 kinase directly inhibits CDC25 to avoid dephosphorylation of CDK while high levels of DNA damage persist (Beck et al., 2010, Forment et al., 2011, Syljuasen et al., 2005). In mouse embryonic cells, similar results have been obtained through the expression of a phosphomutant allele of CDK1 that cannot be inhibited by WEE1 and, indeed, the viability of the embryos harbouring this allele is severely compromised (Szmyd et al., 2019). Additionally, it has been shown that the S87D mutation in MUS81, which mimics a CK2-dependent phosphorylation event in G2/M, licenses untimely formation of the MUS81-EME1/SLX1-SLX4 complex *in vivo*, promoting DSB formation in S phase and a mild chromosome pulverization phenotype (Palma et al., 2018).

USC UNIVERSIDADE DE SANTIAGO DE COMPOSTELA

For Yen1 and GEN1, the logic behind their cell cycle-dependent regulation implies active mechanisms to inhibit their ability to access their substrates until its last stages. This has provided an exciting opportunity to understand the consequences of the premature activation of resolvases in cleaner set-ups, as relatively simple mutations in these proteins uncouple their activation from cell cycle progression without altering any of the master regulators of the cell cycle (like CDK or checkpoint kinases). In this sense, a constitutively nuclear version of GEN1 (GEN1^{nuc}) was generated by mutation of its nuclear export signal and additions of viral NLS at its C-terminus, overriding its main regulatory layer (Chan and West, 2014). Expression of GEN1^{nuc} in mammalian cells produces an increase in sister-chromatid exchanges in undamaged and cisplatin-treated cells, but not hypersensitivity to genotoxic agents like hydroxyurea, camptothecin or cisplatin. Moreover, GEN1^{nuc} is able to alleviate phenotypes associated to inactivation of MUS81 and BLM, like chromosomal defects and decreased viability (Chan and West, 2014).

In budding yeast, Yen1 activity and localization is directly controlled by Cdk1-dependent phosphorylation. Mutation of all nine serines in CDK consensus sites to alanines resulted in a version of Yen1, Yen1^{ON}, that is constitutively active and nuclear at all stages and, therefore, fully refractory to cell cycle control (Blanco et al., 2014). This mutant has already been widely employed to demonstrate the detrimental effects of the aberrant accumulation of recombination and replication intermediates by relieving the phenotypes of mutant strains with reduction or loss of function in genes like *MUS81*, *SGS1*, *SRS2*, *MLH1/MLH3* or *DNA2*, in both mitotic and meiotic contexts (Alonso-Ramos et al., 2021; Arter et al., 2018; Bittmann et al., 2020; Elango et al., 2017; Grigaitis et al., 2020; Michel et al., 2017; Olmezer et al., 2016). However, its utility as a tool to understand the requirement for the stringent control of resolvase activation has been considerably less exploited. In mitotic cells, Yen1^{ON} expression increases sensitivity to MMS, CO formation and total loss-of-heterozigosity (Blanco et al., 2014) while in meiosis it produces not only higher CO/NCO ratios, but also the loss of CO interference (Arter et al., 2018). Taking into account the plethora of different recombination/replication intermediates and other non-B DNA secondary structures that can potentially be hydrolysed by Yen1, it remains of great interest to determine which of them could be specifically compromised by its unrestricted activity in S/G2.

Therefore, the concept driving the present PhD research project is to uncover the specific pathways or structures disrupted by Yen1 misregulation. To achieve this, we will combine previously described strategies, such as altering the expression levels of both wild-type and regulation-deficient *YEN1* alleles with mutations in several candidate DNA helicases involved in genome integrity maintenance. Our focus will be on the Pif1 family of DNA helicases, given their crucial functions in DNA secondary structure metabolism in budding yeast.

3. PIF1 FAMILY OF HELICASES

The Pif1 family, found in some bacteria, archaea, and virtually in all eukaryotes, belongs to the superfamily IB of 5'-3' directed, ATP-dependent, P-loop helicases (Berger, 2008; Bochman et al., 2011). *Saccharomyces cerevisiae PIF1* (*ScPIF1*), the founding member of the Pif1 family, was identified in a genetic screen searching for nuclear mutations affecting the recombination

USC DE COMPOSTELA

frequency of the mtDNA; three allelic mutants were discovered and assigned to the *PIF1* locus (*petite integration frequency*) (Foury and Kolodynski, 1983). Further research showed that *PIF1* encodes an enzyme with ssDNA-dependent ATPase and 5'-3' helicase activities, and confirmed its predominant role in sustaining the integrity of the mtDNA (Foury and Lahaye, 1987; A. Lahaye et al., 1991; Lahaye et al., 1993a). Shortly after, *PIF1* mutations were isolated in another screening designed to identify mutants influencing the loss of expression of subtelomeric genes (Schulz and Zakian, 1994a), initiating a long-lasting research line on the functions of Pif1 helicases in the maintainance of nuclear genome stability.

S. cerevisiae harbours a second *PIF1*-like gene, named *ribosomal DNA recombination mutation* (*ScRRM3*), after its discovery in an independent screening for factors suppressing recombination at loci with tandem repeats, such as the rDNA and *CUP1* genes. It was later identified as a member of Pif1 helicase family based on sequence similarity with ScPif1 (Ivessa et al., 2000; Keil and McWilliams, 1993). Whereas other fungal species, such as *Candida albicans* or *Cryptococcus neoformans* also contain two Pif1 family helicases, the distantly related fungi *Schizosacchromyces pombe* and metazoans contain only one. Importantly, the presence of two Pif1 helicases in *S. cerevisiae* is not related to the ancient whole-genome duplication (WGD) that occurred in the ancestor of the yeast WGD clade within the *Saccharomycetaceae* family (Dujon et al., 2004; Kellis et al., 2004). This suggests that one of the two Pif1 helicases was lost in a common ancestor of metazoans and in some fungal taxons. Phylogenetic analyses support that ScRrm3 may have evolved first (Bochman et al., 2010).

3.1 Structural motifs and protein isoforms of Pif1-family helicases

Pif1-like helicases conserve the seven SFI family characteristic motifs (I, Ia, II, III, IV, V, and VI) and present three *E. coli* RecD motifs (A, B and C). In addition, they present a distinctive 21-aminoacid sequence, the Pif1 signature motif, located between regions II and III, which differentiates Pif1-family members from other helicases of the IB superfamily (Figure 28). This Pif1 signature motif is required for optimal ATPase and helicase activities *in vitro* and, consequently, for all *in vivo* functions requiring the catalytic activity of these proteins (Bochman et al., 2010; Geronimo et al., 2018; Mohammad et al., 2018; Zhou et al., 2016). As the founding member of the family, ScPif1 has been deeply characterized both *in vitro* and *in vivo*. In contrast, ScRrm3 research has been limited to *in vivo* approaches for decades, largely due to the difficulties to purify the full-length protein. ScRrm3 is expressed at low levels and forms insoluble aggregates when overexpressed in *E. coli,* yeast and Sf9 insect cells (Ivessa et al., 2002). Besides studies in budding yeast, SpPfh1 from *S. pombe* and PIF1 from *Mus musculus* and *Homo sapiens* (HsPIF1) have also been widely studied to interrogate the properties and functions of Pif1 helicases.

ScPif1, ScRrm3, SpPfh1 and HsPIF1 present a central helicase domain flanked by N-terminal and C-terminal domains of variable length, hereinafter NTD and CTD, respectively (Andis et al., 2018; Bessler et al., 2001; Byrd and Raney, 2017) (Figure 28). The highly conserved helicase domain is required for both the ATP binding and hydrolysis as well as the ssDNA binding and translocation activities required to unwind duplex DNA, unfold G4s or displace non-nucleosomal protein complexes bound to DNA. The NTD and CTD domains are

USC DE COMPOSTELA

intrinsically disordered and have diverged to fulfil specific roles in different Pif1 helicases by expanding their biochemical properties (Andis et al., 2018; Gu et al., 2008), mediating diverse protein-protein interactions (Syed et al., 2016) or reacting to specific post-translational modifications (Makovets and Blackburn, 2009a; Rossi et al., 2015). In this sense, the NTDs of ScPif1 and SpPfh1 also contain mitochondrial targeting signals (MTS), whereas in HsPIF1 the NLS and MTS localise at the NTD and CTD, respectively (Figure 28) (Futami et al., 2007). The NTD of ScPif1 is responsible for its preferential unwinding of RNA-DNA hybrids as well as for its specific interaction with the mitochondrial SSB Rim1. Acetylation of ScPif1 NTD and CTD enhances its helicase activity (Onyekachi E Ononye et al., 2020), while phosphorylation of both ScPif1 and ScRrm3 NTDs inhibits fork reversal during replication stress (Rossi et al., 2015). ScRrm3 NTD is indispensable for ScRrm3 functions *in vivo* and, like SpPfh1 NTD, contains a PIP box to interact with PCNA, as well as the residues that mediate ScRrm3 interaction with Orc5 (Schmidt et al., 2002; Syed et al., 2016). ScPif1 contains two PIP boxes that control its interaction with PCNA in the contexts of replication and DSB repair (Buzovetsky et al., 2017; Dahan et al., 2018), and its Mec1-dependent phosphorylation is necessary to recruit ScPif1 to DSBs (Makovets and Blackburn, 2009a). Similarly, the human HsPIF1 CTD is important to mediate physical interactions its post-translationally modified, while its NTD is required for strand annealing activity *in vitro* (Gu et al., 2008).

All *ScPIF1*, *SpPFH1* and *HsPIF1* encode at least two different protein isoforms, allowing the dual-targeted localization required to fulfil their multiple roles in the nucleus and the mitochondria. In budding and fission yeast, the mitochondrial and nuclear isoforms are produced by Alternative Translation Initiation (ATI) at two in-frame AUG codons: AUG^{1} - AUG^{40} in *S. cerevisiae* and AUG^{1} - AUG^{21} in *S. pombe.* Importantly, in both cases, these AUG codons flank the sequence for an MTS (Sabouri et al., 2012; Schulz and Zakian, 1994a). If translation starts from AUG^{1}, the MTS drives the mitochondrial import of the full-length isoform; instead, translation initiation from the second AUG produces shorter isoforms lacking the MTS. These are thus targeted to the nucleus, presumably through yet-uncharacterized NLSs. In contrast, HsPIF1 mitochondrial and nuclear isoforms are a consequence of mRNA alternative splicing, although the same rationale prevails: the presence of an MTS outcompetes the NLS, while the shorter isoform lacking the MTS is imported into the nucleus (Futami et al., 2007). Moreover, upon DNA damage, the nuclear isoform is replaced by a third HsPIF1 isoform, also generated by alternative splicing, that improves cell survival. Both the cytoplasmic location of

USC
UNIVERSIDADE DE SANTIAGO DE COMPOSTELA

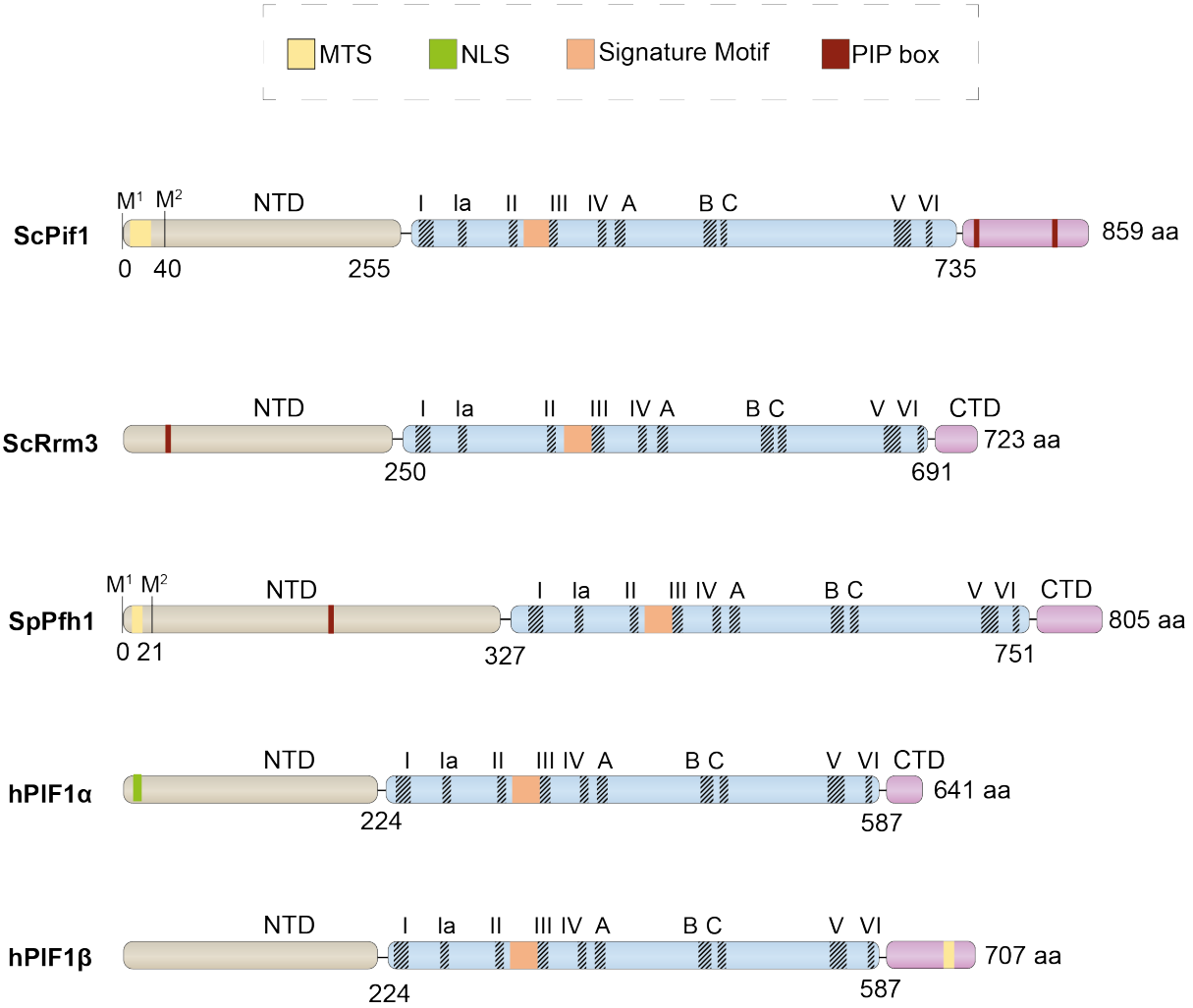


Figure 28. Structural motifs in the Pif1 family helicases. Pif1-family members share a conserved helicase domain with an exclusive signature. NTD and CTD are intrinsically disordered, and usually contain targeting signals or interaction motifs.

this third isoform, as well as the truncation of its helicase domain, suggest that human cells may downregulate the active pool of nuclear HsPIF1 under stress conditions (Prados-Carvajal et al., 2020)

To analyse the roles of ScPif1 and SpPfh1 in the two subcellular compartments, two separation-of-function alleles were designed following the described ATI rationale. Hence, mutations of the first (*pif1-m1, pfh1-m1)* or the second *(pif1-m2, pfh1-m21 and pfh1-mt**) AUG site in their respective open reading frames were introduced (Pinter et al., 2008; Schulz and Zakian, 1994). The lethality of *pfh1-m1* in *S. pombe* and the *petite* phenotype of *pif1-m1* mutants in *S. cerevisiae* confirmed the paramount role of these isoforms to maintain mtDNA integrity. It is important to note that fission yeast, unlike budding yeast, requires functional mitochondria for survival, explaining the differences in viability between these two organisms in the absence of mitochondrial Pif1 (Haffter and Fox, 1992). Similarly, nuclear SpPfh1 is also essential in *S. pombe* (Pinter et al., 2008). Since *S. cerevisiae* harbours two Pif1-like helicases involved in

nuclear functions, lethality in *S. pombe* can only be compared with *S. cerevisiae* mutants lacking both ScRrm3 and the nuclear isoform of ScPif1. Interestingly, despite their slow growth, the *rrm3*Δ *pif1*Δ and *rrm3*Δ *pif1-m2* double mutants are still viable, suggesting either that SpPfh1 fulfils additional roles in *S. pombe*, or that some nuclear functions of the Pif1-like helicases have become essential in this organism. In this sense, heterologous expression of ScRrm3, but not ScPif1 or HsPIF1, can compensate the absence of nuclear Pfh1 (Pinter et al., 2008). Some of the known functions of these helicases are described in the next sections.

3.2 Pif1-helicases in DNA replication through physical barriers

Progression of replisomes throughout the genome can be hindered by various protein-DNA complexes and DNA secondary structures, particularly at highly transcribed genes, dormant replication origins, centromeres, telomeres, and GC-rich tracts. Therefore, Pif1-family members, by removing non-histone protein-DNA complexes and secondary structures, play a critical role in promoting fork advance during replication (Alzu et al., 2012; Azvolinsky et al., 2009; Chen et al., 2019; Ivessa et al., 2003; McDonald et al., 2014; Osmundson et al., 2017; Paeschke et al., 2013, 2011; Sabouri et al., 2012; Tran et al., 2017).

3.2.1 G-quadruplex structures

The ability to unfold G4 structures is highly conserved among the different members of Pif1 helicases, as all ScPif1, SpPfh1 and HsPIF1 can efficiently unwind them *in vitro* (Byrd and Raney, 2015; Wallgren et al., 2016; L. Wang et al., 2018). G4s can adopt antiparallel and parallel conformations, with the latter being predominant in *S. cerevisiae*. *In vitro*, ScPif1 displays a higher unwinding activity towards antiparallel G4s, probably due to the lower thermal stability of this conformation. While ScPif1 has also been proposed to unfold the majority of parallel G4s *in vivo*, its poor *in vitro* activity on such structures suggests that additional helicases or other factors may cooperate with ScPif1 for disruption of G4s with high thermal stability (Wang et al., 2018). Importantly, ScPif1 strand-annealing activity may also contribute to preclude G4 formation by promoting the reassociation of ssDNA strand into dsDNA (Byrd and Raney, 2015).

In support of the *in vitro* data, absence of nuclear ScPif1 or SpPfh1correlates with higher levels of broken forks and replisome stalling at G4 motifs (Paeschke et al., 2011; Sabouri et al., 2014). Moreover, in *pif1*Δ mutants DNA damage accumulates specifically at loci predicted to form G4 structures, leading to mutations and gross chromosomal rearrangements (Lopes et al., 2011; Paeschke et al., 2013, 2011; Ribeyre et al., 2009; Sabouri et al., 2014). Similarly, HsPIF1 is required in human cells to facilitate resection through sequences prone to G4 formation (Jimeno et al., 2018), although, in contrast to fungi, metazoans rely on non-Pif1 family helicases, such as FANCJ, to promote replication across G4 structures (Castillo Bosch et al., 2014; Sarkies et al., 2012). Importantly, ScPif1 cooperates with several factors to improve replication through G4 motifs. For instance, RPA assists ScPif1 in G4 unfolding at both the lagging and leading strands (George et al., 2009; Maestroni et al., 2020) whereas its interaction with PCNA -mediated by the canonical PIP box located at ScPif1 CTD- is specifically required for efficient G4 unwinding at the lagging strand (Dahan et al., 2018). While the predominant role of ScPif1 in dismantling G4s *in vivo* is well established, the enrichment of ScRrm3 at G4s in *pif1-m2*

USC

mutants indicates that ScRrm3 may serve as a backup to reduce G4-induced genome instability (Azvolinsky et al., 2009; Paeschke et al., 2013)

3.2.2 Highly transcribed genes and protein barriers

Simultaneous replication and transcription, which is more likely to occur in highly transcribed loci, may lead to collisions between both molecular machineries that result in fork pausing in wild-type cells (Deshpande and Newlon, 1996). The Pif1-family helicases contribute to fork progression through these hard-to-replicate regions genome-wide, since both depletion of SpPfh1 and *ScRRM3* knockout exacerbate fork stalling (Ivessa et al., 2003; Sabouri et al., 2012). Budding yeast transfer RNA (tRNA) genes (tDNAs) constitute the most-studied model system for transcription-replication conflicts; tRNAs account for ~15% total cellular RNA, and tDNAs are well-known sites of replication fork pausing (Azvolinsky et al., 2009; Deshpande and Newlon, 1996; Ivessa et al., 2003). ScRrm3 and ScPif1 redundant activities alleviate replication-fork pausing and genome instability at tDNAs, with ScPif1 supporting fork progression in *rrm3*Δ cells (Osmundson et al., 2017; Tran et al., 2017). Similarly, SpPfh1 also promotes replication at highly transcribed genes (Sabouri et al., 2012). However, how Pif1-family helicases contribute to fork progression is still under debate. Both head-on and co-directional conflicts induce fork pausing, but head-on collisions are specially severe: they are associated with higher levels of R-loop formation, mutagenesis and fork stalling (Hamperl et al., 2017; Lang et al., 2017; Osmundson et al., 2017). Accordingly with the *in vitro* preference of scPif1 for RNA:DNA hybrids over DNA duplexes (Chib et al., 2016). Consequently, it has been proposed that ScRrm3 and ScPif1 could dismantle R-loops at these loci (Tran et al., 2017). However, R-loop disruption might not be the main function of these helicases, since i) replication fork arrest in *rrm3*Δ strains is not affected by increased or reduced levels of RNase H activity, and ii) the decrease in the overall frequency of fork arrest is independent of the relative orientation of replication and transcription machineries (Osmundson et al., 2017). Therefore, an alternative model was postulated based on the ability of Pif1-family helicases -specially ScRrm3 and SpPfh1- to act as replisome-accessory *"sweepases"*, enzymes that could avoid replication-transcription conflicts by displacing the transcription machinery (Osmundson et al., 2017)m

Besides promoting replication through tDNA, ScRrm3 and ScPif1 also associate to active centromeres in a cell cycle-dependent manner. ScRrm3 is enriched at centromeres during S-phase, before centromere replication, whereas ScPif1 association peaks at late S/G2. Similar to its role at other loci enriched in protein complexes, ScRrm3 promotes fork progression probably by displacing the kinetochore complex bound to the centromere; indeed, in *rrm3*Δ strains, the transient pause at centromeres observed in WT cells is increased two- to three-fold (Chen et al., 2019; Ivessa et al., 2000). ScPif1 also supports centromere replication, but this function is only relevant in *rrm3*Δ cells, while its specific role at S/G2 has not been defined yet. However, whichever task ScPif1 performs at the centromeres, it can be also carried out by ScRrm3. Importantly, even if the simplest explanation for the increased rate of centromeric plasmid loss in *rrm3*Δ *pif1-m2* strains are replication defects across centromeric regions, this phenotype

USC UNIVERSIDADE DE SANTIAGO DE COMPOSTELA

could also arise as a consequence of a hypothetic contribution of Pif1 helicases to chromosome segregation (Chen et al., 2019).

Finally, Pif1 helicases also participate in the replication of the rDNA, which accounts for 60% of total transcription in cycling yeasts. To meet the high cellular demand for rRNA, the rDNA is organised as a cluster of tandem repeats in all eukaryotic genomes (Warner, 1999). This high transcriptional activity makes these loci especially vulnerable to collisions between the replication and transcription machineries that, given the repetitive nature of the region, could lead to HR-mediated rearrangements. To minimize this risk, yeasts have evolved polar barriers to block replisome progression in a directional manner, commonly known as the replication fork barriers (RFB) (Kobayashi et al., 1998). The RFBs are located in the non-transcribed intergenic regions at every rDNA repeat, contain two termination sites for replication -Ter1 and Ter2- bound by the Fob1 protein, and ensure the co-directional progression of replication and transcription within each repeat. It is important to note that, unlike HU-induced fork stalling, pausing at the RFBs is independent of the DDC kinases and the DNA synthesis resumes without recombination or breakage, suggesting that RFB pausing sites are processed differently than those arising during general replication stress (Calzada et al., 2005).

Curiously, ScRrm3 and ScPif1 play opposite parts in the rDNA loci. ScPif1 cooperates with Fob1 to maintain the RFB, as inferred by the decrease in RFB efficacy in *pif1*Δ mutants, although the precise underlying mechanism remains undetermined. On the contrary, ScRrm3 is required to displace the protein-DNA complexes, removing Fob1 from the RFB to allow replisome progression (Ivessa et al., 2003, 2000). Accordingly, *rrm3*Δ strains display impaired fork progression, causing fork stalling and the accumulation of ssDNA gaps (Fritsch et al., 2010). *FOB1* deletion does not completely suppress fork pausing in *rrm3*Δ strains, suggesting that additional protein barriers may be present at inactive ARS and that transcription of the 35S and 5S loci also compromises fork movement at the rDNA copies (Mohanty et al., 2006; Torres et al., 2004). In addition to the helicase domain, the ScRrm3 NTD is indispensable for its function at the RFB, since deletion of residues 134-196 increases fork stalling at levels comparable to *RRM3* deletion (Bessler and Zakian, 2004). In *S. pombe*, SpPfh1 also ensures genome stability at the RFB, similarly to ScRrm3 in budding yeast, by displacing proteins from the RFB, such as Sap1 or Reb1 to promote fork progression (Sabouri et al., 2012).

3.3 Pif1-helicases in Okazaki fragment maturation

In eukaryotic cells, DNA synthesis of both the leading and lagging strands is initiated by the activity of the low fidelity DNA polymerase α/RNA-primase, which synthesizes a short RNA primer followed by 10-20 nt of DNA (Waga and Stillman, 1994). As opposed to the leading strand, the lagging strand in each replication bubble is synthesized discontinuously, with the complex between PCNA and DNA polymerase δ (Polδ) extending these RNA-DNA primers into the so-called Okazaki fragments. In *S. cerevisiae*, it is estimated that Polδ produces around 100,000 Okazaki fragments of ~250 nt during DNA replication. Upon encountering the downstream Okazaki fragment, the strand-displacement activity of Polδ creates short 5'-ssDNA flaps that include the initial RNA portion of each primer and are subsequently removed by the action of the Rad27 SSE. This leaves a small ssDNA gap that is then re-filled by Polδ

USC DE COMPOSTELA

and finally ligated by Cdc9. Hence, the coordinated activities of Rad27, Polδ and Cdc9 efficiently remove the ribonucleotides incorporated into DNA during the priming event and restore the continuity of the lagging strands (Garg et al., 2004). Occasionally, the strand displacement activity can generate 5'-flaps that are long enough to recruit RPA. The coating of the 5'-flap by RPA inhibits Rad27, but in turn stimulates the endonuclease activity of the nuclease/helicase Dna2, which can shorten the RPA-coated 5'-flaps and make them susceptible again to Rad27 (Bae et al., 2001; Kao et al., 2004a, 2004b).

A role for ScPif1 in this two-nuclease pathway of Okazaki fragment maturation was proposed after discovering that both *pif1*Δ and *pif1-m2,* but not *rrm3*Δ, can suppress *dna2*Δ lethality (Budd et al., 2006). *In vivo* and *in vitro* evidence suggests that lethality in the absence of *DNA2* is caused by the accumulation of long 5'-flaps during Okazaki fragment processing (Burgers, 2011; Fiorentino and Crabtree, 1997; Rossi et al., 2018). According to this model, ScPif1 stimulates long flap formation, increasing the dependency of the Dna2 backup pathway to cleave those flaps that are resistant to Rad27 action (Pike et al., 2009; Rossi et al., 2008). In support of this interpretation, it has been also adduced that additional deletion of *POL32*, the non-essential subunit of Polδ that promotes strand displacement, suppresses the residual defects in *dna2*Δ *pif1*Δ strains, completely channelling the processing of Okazaki fragments towards the Dna2-independent Rad27 pathway (Budd et al., 2006). SpPfh1 has been also implicated in Okazaki fragment maturation, due to its biochemical activity on 5'-flaps and the suppression of the temperature-sensitivity of *dna2-C2 S. pombe* strains by mutations (Ryu et al., 2004).

3.4 Pif1-helicases in fork convergence during replication termination

In addition to their ability to promote replication progression, ScPif1 and ScRrm3 share an overlapping role in the convergence of replication forks during replication termination. Full-length ScRrm3 has been recently purified for the first time, demonstrating that ScRrm3 and ScPif1 are required to complete DNA replication in an *in vitro*-reconstituted eukaryotic replication system (Deegan et al., 2019). *In vivo*, fork convergence is delayed in *rrm3*Δ *pif1-m2* cells, but not completely abolished, since additional pathways involving the removal of precatenates by Top2 operate to ensure termination (Fachinetti et al., 2010). Consistent with this model, Top2 is upregulated in *rrm3*Δ strains (Syed et al., 2016). This role may be conserved in *S. pombe*, where impairment of SpPfh1 activity leads to the accumulation of short stretches

3.5 Pif1-helicases in telomere length homeostasis

Telomeres are essential nucleoprotein structures evolved to maintain the integrity of the linear chromosomal ends in eukaryotes, allowing cells to distinguish intact from broken chromosomes and thus protect chromosome ends from degradation and fusions. Moreover, telomeres participate in the regulation of gene expression, chromosome positioning, as well as in cell division. Telomeric DNA is composed of short tandem repeats of 6-8 bp sequence that vary between eukaryotic organisms. *S. cerevisiae* telomerase contain approximately 60-100 copies of the sequence $TG_{1–3}$, whereas human telomeres are longer and more homogenous, with thousands of repeats of the hexameric sequence (TTAGGG). Telomeres are normally elongated by telomerase, a specialized reverse transcriptase that counteracts the progressive telomeric

shortening associated to the replication of DNA ends, although telomerase-independent, recombination-dependent mechanisms for telomere elongation have also been described (Blackburn, 1991; Wellinger and Zakian, 2012; Zakian, 1995).

Pif1-family helicases contribute to telomere homeostasis in yeast, and possibly in human cells, through different mechanisms. ScPif1 is one of the major negative regulators of telomerase activity in budding yeast, acting as a catalytic inhibitor of telomerase. This function requires its helicase activity to displace telomerase from chromosome ends, either by disrupting the *TLC1* RNA:DNA hybrid or by directly stripping Est2 (the reverse transcriptase subunit of the telomerase holoenzyme) from telomeric ends. Consistent with this model, the absence of nuclear ScPif1 in *pif1*Δ and *pif1-m2* strains leads to telomere elongation, while overexpression of *PIF1* results in shorter telomeres (Schulz and Zakian, 1994a; Zhou, 2000a). Truncation of its NTD partially suppresses telomere shortening upon *PIF1* overexpression, even though deletion of the NTD enhances *in vitro* inhibition of telomerase, suggesting an additional, uncharacterized mode to restrict telomere lengthening *in vivo* (Nickens et al., 2019). ScPif1 is also required to inhibit telomerase activity at DSBs. In addition to the normal DSB repair by HR or NHEJ, DNA ends can be recognized and processed by telomerase, leading to the addition of telomeric repeats at the break site, a phenomenon referred to as *de novo* telomere addition. This mechanism is especially relevant at those DSBs where resection exposes telomeric-like repeats that facilitate telomerase recruitment. To counteract this, ScPif1 also localizes at DSBs and, like at chromosome ends, displaces telomerase to restrict telomere addition and, indirectly, promote high-fidelity repair by HR (Mangahas et al., 2001; Myung et al., 2001; Schulz and Zakian, 1994a). ScPif1 inhibition of telomerase at DSBs requires phosphorylation at its CTD by the Mec1/Rad53 signalling pathway; deletion of *PIF1* or the mutation of C-terminal residues increases significantly the frequency and distribution of *de novo* telomere additions at DSBs (Makovets and Blackburn, 2009a).

*rrm3*Δ mutants also present elongated telomeres, but this phenotype is unrelated to the inhibition of telomerase. Instead, ScRrm3 promotes normal semi-conservative replication of telomeres by facilitating unperturbed replisome progression through telomeric and subtelomeric DNA. SpPfh1, like ScRrm3, also supports telomere replication in *S. pombe* but, unlike ScPif1 or HsPIF1, cannot inhibit telomerase activity *in vitro*. The aforementioned capacity of ScRrm3 and SpPfh1 to displace non-histone protein complexes bound to DNA is key to successful replication of telomere sequences, since chromosome ends are protected by multiple proteins (Ivessa et al., 2002; McDonald et al., 2014). Finally, no phenotype related with telomere homeostasis has been reported for mammalian PIF1; interestingly, human PIF1 also inhibits telomerase *in vitro* (Zhang et al., 2006), and both murine and human helicases interact *in vivo* with telomerase (Mateyak and Zakian, 2006; Reynolds et al., 2011; Snow et al., 2007). These data suggest that mammalian telomere homeostasis and stability may not depend on PIF1 or, alternatively, that its role is masked due to genetic redundancy with other DNA helicases or repair factors.

3.6 Pif1-helicases in DSB repair

USC UNIVERSIDADE DE SANTIAGO DE COMPOSTELA

As described in the 2.3 section, ScPif1, together with Pol32, is essential to promote long-track DNA synthesis during BIR. ScPif1 is recruited to the migrating D-loop through its interaction with PCNA, mediated by a non-canonical PIP domain located at ScPif1 CTD and mutation of this domain (Buzovetsky et al., 2017) or deletion of *PIF1* in yeast, *D. melanogaster* or mammalian cells greatly impairs BIR completion (Kocak et al., 2019; Li et al., 2021; Wilson et al., 2013). It is considered that ScPif1 may promote BIR synthesis in two different ways: i) acting as the replicative helicase during D-loop-associated DNA synthesis and ii) releasing the newly synthesized strand to prevent topological stress and promote D-loop migration. Besides BIR, both mechanisms could also promote DNA synthesis during gene conversion. Indeed, ScPif1 activity is inhibited during meiosis to limit long-tract gene conversion, with its ability to support DNA synthesis in this context also relying on the PCNA interaction through its non-canonical PIP box (Vernekar et al., 2021). In contrast, *rrm3*Δ mutants do not exhibit any deficiency in repair by BIR (Muñoz-Galván et al., 2017; Wilson et al., 2013). Instead, ScRrm3 contributes to the repair of replication-dependent DSBs, consistent with its ability to move with the replisome (Azvolinsky et al., 2006; Schmidt et al., 2002). The repair of this subset of DSBs requires sister-chromatid exchange, but how ScRrm3 contributes to this process is currently unknown (Muñoz-Galván et al., 2017).

3.7 Pif1-helicases in mtDNA maintenance

Pif1-family helicases are essential to maintain the integrity of mtDNA in most eukaryotic cells. In *S.cerevisiae*, mtDNA of *pif1*Δ strains is highly unstable due to fragmentation and mutagenesis, leading to the loss of a functional mitochondrial genome, depicted by the rho^- or rho^0 (commonly known as cytoplasmic *petite* phenotype) exhibited by these cells (Cheng et al., 2007; Foury and Van Dyck, 1985; O'Rourke et al., 2005). Like *pif1*Δ cells, strains harbouring the *pif1-m1* allele have been reported to quickly acquire this *petite* phenotype and are more sensitive to genotoxic agents, such as EtBr, than wild-type cells (Cheng et al., 2007; O'Rourke et al., 2005; Schulz and Zakian, 1994a). *PIF1*$^{-/-}$ knockout mice develop mitochondrial myopathy with respiratory chain deficiency, accompanied by mutations of the mtDNA, supporting a conserved role for these enzymes in mtDNA maintenance in mammalian cells (Bannwarth et al., 2016). While the precise mechanisms by which these helicases operate in mitochondria is still unknown, several phenotypes support the notion that, like their nuclear isoforms, they could be involved in multiple steps of mitochondrial DNA replication and repair. ScPif1, together with the Ntg1 glycosylase/AP-lyase, protects mtDNA from oxidative damage (Doudican et al., 2005; O'Rourke et al., 2002). Similarly, murine PIF1 is also important to safeguard mtDNA from the action of ROS (Bannwarth et al., 2016). Moreover, ScPif1 has been also implicated in promoting mtDNA recombination and replication (Foury and Van Dyck, 1985) and scPif1 and SpPfh1 catalytic activity is required for efficient mtDNA replication (Cheng et al., 2009; Pinter et al., 2008). This suggests that akin to the nuclear roles of Pif1 helicases, both scPif1 and SpPfh1 may support mtDNA replication by displacing protein-DNA complexes or unwinding G4 structures.

*rrm3*Δ mutants do not manifest visible mitochondrial defects, but the presence of a putative MTS in its sequence, and its identification -while not individually verified- in a screen for

USC DE SANTIAGO DE COMPOSTELA

mitochondria-localized proteins were compatible with a role of ScRrm3 in the mitochondria. Indeed, *RRM3* deletion partially suppresses the *petite* phenotype of *pif1*Δ cells. However, this suppression may be an indirect consequence of altered dNTP pools in these mutants, since the absence of ScRrm3 activates the DDC response via Rad53 phosphorylation, which, in turn, increases the activity of the ribonucleotide reductase. This leads to an increment of dNTPs concentration, which is known to promote replication under stress conditions; consistently, higher Rnr1 levels partially alleviate respiratory deficiency and mtDNA copy number in *pif1*Δ mutants to the same extent as *RRM3* deletion (O'Rourke et al., 2005; Taylor et al., 2005). The lack of a direct role for ScRrm3 in mitochondria is also supported by experiments in fission yeast, where the heterologous expression of ScRrm3 can only compensate for the nuclear defects of *pfh1* mutants (Pinter et al., 2008).

USC
UNIVERSIDADE DE SANTIAGO DE COMPOSTELA

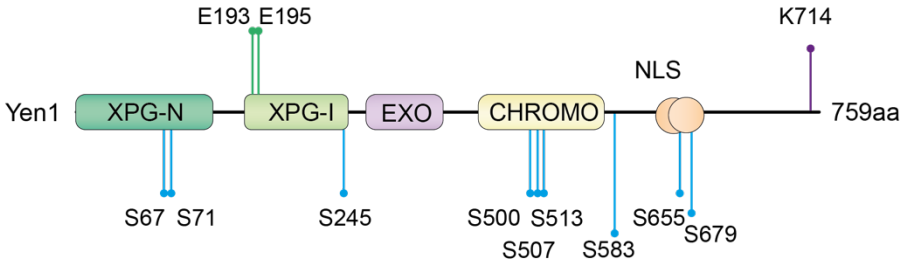
CHAPTER 1: ANALYSIS OF YEN1 PREMATURE ACTIVATION

The discovery of the late activation of Yen1 and its orthologs has prompted several lines of research to understand the benefits of its regulation to cell cycle progression. In addition to cell-cycle dependent phosphorylation, Yen1 SUMOylation at K714 also contributes to restrain its activity by triggering SUMOylation-dependent ubiquitination and proteasomal degradation of chromatin-bound Yen1 during G1 (Figure 29a), adding another regulatory layer to minimize the presence of active Yen1 in the nucleus when S phase begins (Talhaoui et al., 2018)). Here, we will employ *YEN1* alleles deficient for one or both types of regulatory PTMs to explore the potential detrimental outcomes of premature resolvase activity during S and G2 phases. As described in the introduction, abrogation of Cdk1-dependent phosphorylation by nine Ser to Ala mutations in CDK consensus sites (Figure 29b, Yen1^{ON}) renders the protein nuclear and active through the cell cycle (Figure 29c), while a K714R mutation (Figure 29b, Yen1^{KR}) prevents its proteasomal degradation in G1 when bound to chromatin.

The use of the Yen1^{ON} phosphomutant presents several advantages to establish genetic set-ups with well-defined variables in the context of premature HJ resolution activities if compared to systems based on Mus81-Mms4 or MUS81-EME1/EME2 deregulation. First, premature hyperactivation of Mus81/MUS81 is achieved either through unrestrained CDK1 activation during S phase (Beck et al., 2012; Duda et al., 2016; Forment et al., 2011; Neelsen and Lopes, 2015) or with phosphomimetic alleles (Palma et al., 2018; Szakal and Branzei, 2013). However, both experimental approaches present limitations that complicate the interpretation of genetic results. On the one hand, extensive CDK1 activity during replication can affect multiple cellular processes, given its role as a cell-cycle master regulator. On the other hand, serine and threonine phosphorylation is usually mimicked by their substitution with negatively charged amino acids, such as aspartate and glutamate, respectively. It has been proven that these acidic amino acids are rather poor pSer/pThr mimetics, since their charge (-1 vs -2 for pSer/pThr at physiological pH), shape and hydrogen-bond geometry differ considerably (Cerulli and Kritzer, 2020; Chen and Cole, 2015). Consequently, Asp/Glu mutations frequently fail to fully recapitulate the functional effects of phosphorylation events. Second, despite recent reports hinting at potential SUMO-mediated interactions of Yen1 with other proteins (Dorison et al., 2022), no stable interaction partners that may influence its activity have been detected for Yen1 (Wild et al., 2019), unlike for Mus81-Mms4 and MUS81-EME1/2. Therefore, a Yen1 phosphomutant refractory to cell cycle-dependent downregulation may more realistically imitate a fully active version of Yen1 *in vivo* during S and G2. We will focus on Yen1^{ON} and, similarly, Yen1^{KR} to investigate the protective role of Yen1 cell cycle regulation by applying the approaches described in the introduction, including alteration of their expression levels and/or interaction with DNA helicases to specifically increase the cellular load of secondary structures and recombination or replication intermediates.

USC
UNIVERSIDADE DE SANTIAGO DE COMPOSTELA

a



b

Mutant	Mutations	Effect
$Yen1^{KR}$	K714R	Attenuates Yen1 degradation at G1/S transition
$Yen1^{ON}$	S67A, S71A, S245A S500A, S507A, S513A S583A, S655A, S679A	Constitutively active
$Yen1^{ND}$	E193A, E195A	Catalytically inactive, binding proficient

c

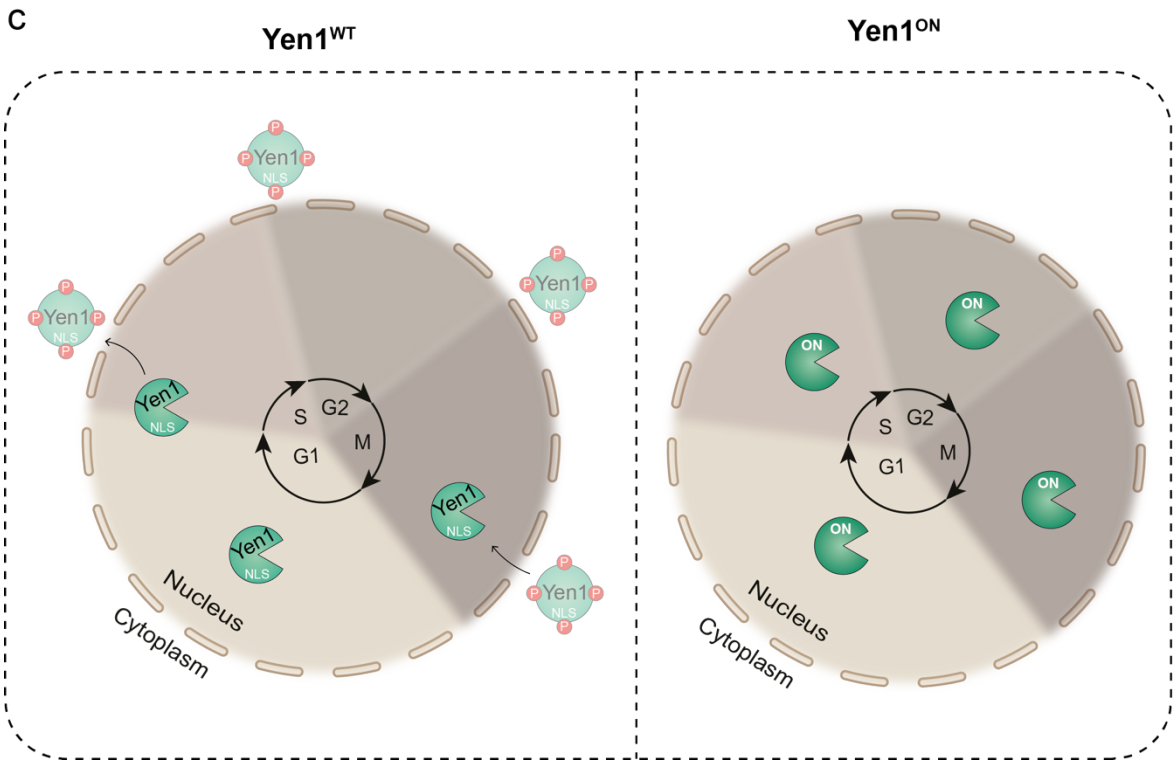


Figure 29. Mutant variants of Yen1 to study the regulation of HJ resolution. (a) Schematic representation of Yen1 domains, depicting those residues modified in various Yen1 mutants: blue, serines in CDK consensus sites; green, residues required for catalytic activity; purple, residue required for SUMOylation-dependent proteasomal degradation. **(b)** Description of the Yen1 mutants employed in this work. **(c)** Illustrative summary of Yen1 cell-cycle regulation by CDK-dependent phosphorylation (left panel), as opposed to the regulation-insensitive $Yen1^{ON}$ mutant (right panel), employed in this work as a tool to study the consequences of Yen1 premature activation.

USC UNIVERSIDADE DE SANTIAGO DE COMPOSTELA

1. OBJECTIVES

Aim 1. To analyse the consequences of the overexpression of *YEN1*^{ON} on viability, cell-cycle progression and DDC activation.

Aim 2. To search for genetic interactions between *YEN1*^{ON} expressed at endogenous levels and helicases involved in DNA replication and repair.

Aim 3. To characterise novel genetic interactions at the molecular level for the identification of potential substrates targeted by *YEN1*^{ON} *in vivo*.

USC
UNIVERSIDADE DE SANTIAGO DE COMPOSTELA

2. RESULTS

2.1 Overexpression of *YEN1* deregulated alleles results in lethality, cell cycle arrest and Rad53 phosphorylation

In our first approach to understanding the importance of an adequate control of HJ resolvases, we started by asking whether elevated levels of different *YEN1* alleles could have a detrimental effect on cell viability. Hence, derivatives of the integrative plasmid pAG306GAL-YEN1-FTH were inserted at the endogenous *ura3-52* locus for inducible overexpression of Yen1 by addition of galactose. Then, cell survival was tested by spotting serial dilutions of each strain on YPDA (repression conditions) or YPRaff+GAL (induction conditions) solid medium plates. While the overexpression of the wild-type and $YEN1^{KR}$ alleles did not cause cell mortality when compared to an unmodified strain, the strain harbouring $YEN1^{ON}$ was not viable under induction conditions (Figure 30a). This indicates that, even when overexpressed, wild-type Yen1 activity is efficiently curtailed by its regulatory network, as inactivation of this inhibitory system is lethal to cells. Since the overexpression of the $YEN1^{KR}$ allele did not cause any overt effects, we decided to combine this mutation with those of $YEN1^{ON}$ to create a new allele, $YEN1^{ON\text{-}KR}$, which should be deficient in all its regulatory layers (catalytic, localization, degradation) and ask whether it can further enhance the toxic effects of $YEN1^{ON}$. Indeed, $YEN1^{ON\text{-}KR}$ overexpression phenotype is slightly more severe that of $YEN1^{ON}$, specially at lower galactose concentrations (Figure 30b). This indicates that all regulatory layers contribute to cellular resistance to *YEN1* overexpression, even if at different extents. During the course of these experiments, we decided to generate catalytically inactive versions of all the described *YEN1* alleles by mutating the catalytic glutamate residues E193 and E195 to alanines, generating nuclease-dead (ND) versions for each. Surprisingly, we found that the expression of $YEN1^{ON\text{-}ND}$ and $YEN1^{-ON\text{-}KR\text{-}ND}$ resulted in comparable levels of cell death with respect to their catalytically proficient counterparts (Figure 30b).

To ensure that this result was not due to residual catalytic activity in these mutants, $Yen1^{ON\text{-}ND}$ was purified to near-homogeneity (Figure 30c) and compared to $Yen1^{ON}$ in *in vitro* nuclease activity assays employing various fluorescently-labelled DNA substrates. As opposed to $Yen1^{ON}$, which readily digested both HJ and 5'-flap synthetic substrates, no traces of endonucleolytic activity could be detected with $Yen1^{ON\text{-}ND}$ (Figure 30d). As expected, a linear dsDNA substrate did not reveal any non-specific exonucleolytic activity for either enzyme. These results imply that we cannot formally rule out that the underlying mechanism driving cellular lethality in strains overexpressing $YEN1^{ON}$ or $YEN1^{ON\text{-}KR}$ is catalysis-independent. Notwithstanding, it is also reasonable to speculate that different mechanisms are responsible for cell death in the $YEN1^{ON}$ or $YEN1^{ON\text{-}KR}$ mutants as opposed to those harbouring $YEN1^{ON\text{-}ND}$ or $YEN1^{ON\text{-}KR\text{-}ND}$.

These observations prompted us to test whether the observed lethality phenotype would be equally accompanied by an activation of the DDC in our overexpression system. Therefore, we induced asynchronous cultures in YPRaff with 2% galactose and took samples at 0, 3 and 5h after induction. Western blot analysis of protein whole-cell extracts revealed that all strains

USC UNIVERSIDADE DE SANTIAGO DE COMPOSTELA

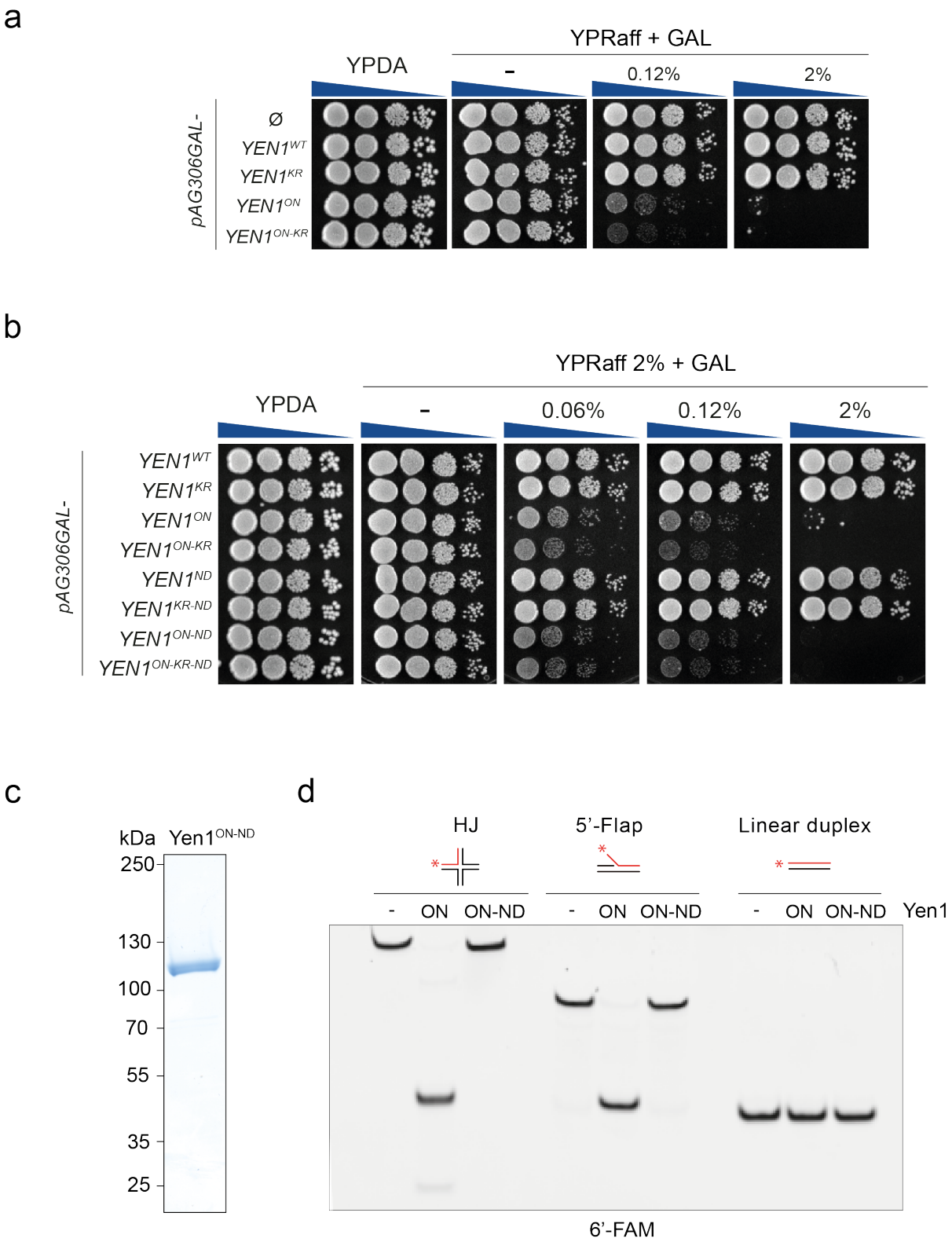


Figure 30. Overexpression of catalytically active and nuclease-dead versions of deregulated Yen1 causes cell death in a dose-dependent manner. (a,b) Ten-fold serial dilutions of strains with the indicated genotypes were spotted on YPDA or YPRaff containing different galactose concentrations and photographed after 2 days of incubation at 30 ºC. **(c)** SDS-PAGE analysis of purified Yen1^{ON-ND} stained with Coomassie. **(d)** Verification of the absence of nuclease activity for Yen1^{ON-ND} on three different substrates, using Yen1^{ON} as a positive control. After native PAGE, fresh gels were scanned for 5'-6FAM signal in a Typhoon FLA 9500. (-) No enzyme.

express relatively comparable amounts of their corresponding Yen1 version. Moreover, only the strains with *YEN1* alleles that caused cell death in our previous assays ($YEN1^{ON}$, $YEN1^{ON\text{-}KR}$, $YEN1^{ON\text{-}ND}$ and $YEN1^{ON\text{-}KR\text{-}ND}$) displayed an activated checkpoint 5h after induction, as denoted by Rad53 phosphorylation (Figure 31a). Interestingly, mild phosphorylation of Rad53 can already be observed at 3h after induction in those strains harbouring catalytically active alleles, suggesting a faster checkpoint activation that relies on Yen1 nuclease activity.

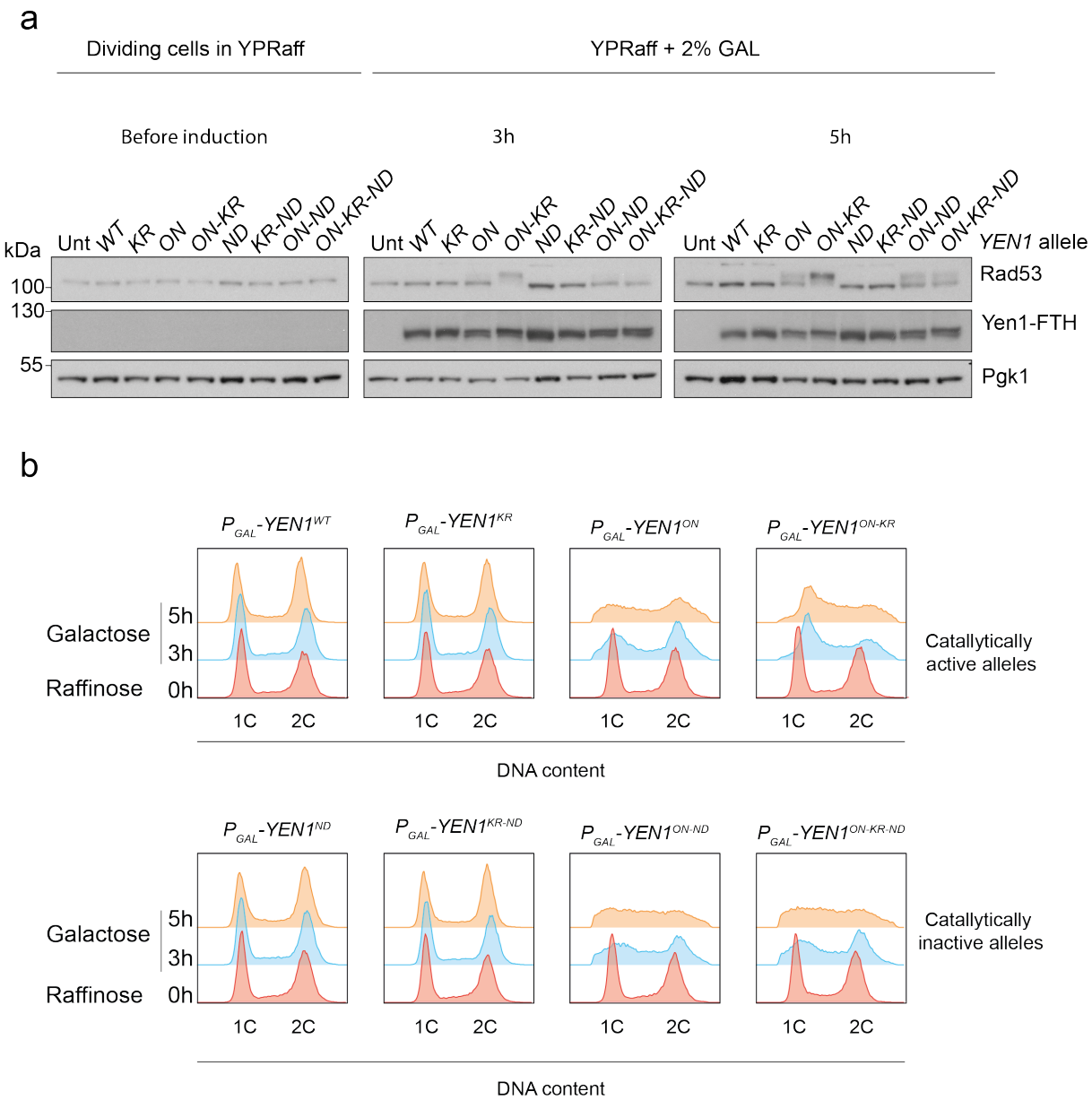


Figure 31. Overexpression of deregulated versions of Yen1 leads to checkpoint activation and disrupts cell cycle progression. (a) Protein extracts were prepared from liquid cultures of strains overexpressing the indicted *YEN1* allele grown in YPRaff and induced for 3-5h by addition of 2% galactose. Abundance of different overexpressed versions of Yen1 was compared by western blotting using anti-Flag antibodies. Activation of the DDC response was assessed by phosphorylation of Rad53 with anti-Rad53 antibodies. Pgk1 was employed as a loading control. **(b)** FACS analysis of DNA content in samples collected at the indicated timepoints for the same strains employed in (a).

Additionally, FACS analysis of DNA content in these strains indicated that the overexpression of lethal alleles disrupts normal cell-cycle progression, displaying a flattened profile without clear 1C and 2C peaks after 5h, and with more cells apparently stuck with an intermediate DNA content (Figure 31b).

2.2 The lethality at strain overexpressing deregulated *YEN1* is not dependent on checkpoint activation or homologous recombination,

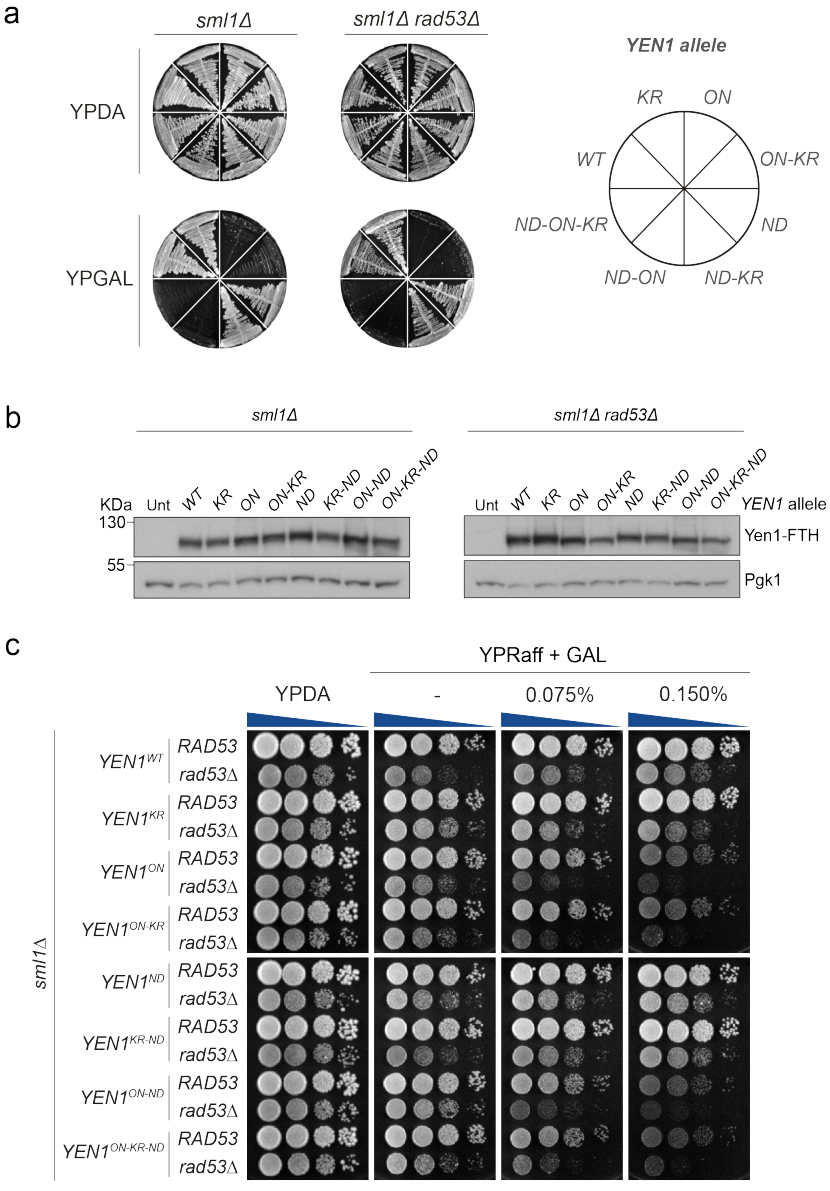


Figure 32. Prolonged cell cycle arrest by DDC activation is not the main cause of cell death in strains overexpressing *YEN1^{ON}* variants. (a) Strains expressing different *YEN1* mutant alleles in *sml1Δ* or *sml1Δ rad53Δ* backgrounds were streaked and examined for growth on solid medium in the absence (YPDA) or presence of galactose (YPGAL). Pictures were taken after 3 days at 30 ºC. **(b)** Abundance of Yen1 variants in the strains from (a) was compared by western blotting using anti-flag antibodies. Protein extracts were prepared from liquid cultures grown in YPRaff and induced for 3 h by addition of 2% galactose. **(c)** Ten-fold serial dilutions of strains with the indicated genotypes were spotted on YPDA or YPRaff with the indicated concentrations of galactose and photographed after 2 days of incubation at 30 ºC.

Given the observation of Rad53 phosphorylation after overexpression of misregulated *YEN1* alleles, we next asked whether checkpoint activation itself was the cause of cell death in these strains. Therefore, we created a set of *rad53*Δ strains in a *sml1*Δ background (deletion of *SML1*, coding for an inhibitor of the ribonucleotide reductase, suppresses the lethality of *RAD53* deletion (Zhao et al., 1998) that carrying a similar set of integrative plasmids as described above. While all strains were viable under non-inducing conditions, overexpression of $YEN1^{ON}$, $YEN1^{ON\text{-}KR}$, $YEN1^{ON\text{-}ND}$ and $YEN1^{ON\text{-}KR\text{-}ND}$ led again to cellular death in both the *sml1*Δ and *sml1*Δ *rad53*Δ backgrounds (Figure 32a,b). This indicates that an aberrant activation of the checkpoint by Yen1 deregulation is not the main cause of lethality in these strains. Contrarily, induction with lower galactose concentrations demonstrated that, in fact, checkpoint abrogation led to a slight decrease in the survival of these strains, suggesting that an intact checkpoint may contribute to counter the toxic effects of a mild overexpression of $YEN1^{ON}$, $YEN1^{ON\text{-}KR}$, $YEN1^{ON\text{-}ND}$ and $YEN1^{ON\text{-}KR\text{-}ND}$ (Figure 32c).

Taking into account that Yen1 can process a number of different HR intermediates (Blanco et al., 2014; Carreira et al., 2022; Ip et al., 2008)), we employed a similar approach to assess if the observed cause of lethality was the untimely processing or blockage of recombination intermediates. We thus deleted the *RAD52* gene, required for most forms of homologous recombination, in the same set of strains employed in Figure 30, but abrogation of recombination did not prevent the lethality associated to the overexpression of the $YEN1^{ON}$, $YEN1^{ON\text{-}KR}$, $YEN1^{ON\text{-}ND}$ and $YEN1^{ON\text{-}KR\text{-}ND}$ alleles (Figure 33a). Additionally, akin to our observations with checkpoint mutants, the presence of Rad52 reduces the toxic effects of weak overexpression of these alleles (Figure 33b). Altogether these results indicate that an incorrect processing of physiological HR intermediates is not the fundamental cause of the death in these strains and that, most likely, recombination plays a role in alleviating the detrimental consequences derived from uninhibited Yen1 actions.

2.3 Expression of $Yen1^{ON}$ at endogenous levels displays genetic interactions with HR helicases

The lethal effect of high overexpression of the indicated regulation-refractory *YEN1* alleles seems to lead to an "overkill" situation that cells cannot easily adapt to. In this sense, on top of the recombination- and checkpoint inactivation experiments shown here, an unbiased screening of spontaneous suppressors of $YEN1^{ON}$ overexpression only found mutations that either directly inactivated $YEN1^{ON}$ or that impaired the galactose-dependent overexpression system (like *GAL4* mutants), which drastically reduced the cellular levels of $Yen1^{ON}$ (Vanesa Hurtado-Nieves and Miguel G. Blanco, unpublished results). Therefore, in order to gather insight on the potential targets of unrestricted Yen1 activity *in vivo*, we decided to resort to a strategy based on combining a strain expressing $YEN1^{ON}$ from its endogenous promoter with deletions in a series of candidate DNA repair genes. To test the feasibility of this approach, we first decided to investigate whether unrestricted $YEN1^{ON}$ would display any synthetic genetic interaction with the deletion of various candidate helicases involved in the processing of HR intermediates. We thus generated diploid strains carrying homozygous *YEN1* or $YEN1^{ON}$ alleles and heterozygous deletions for various combinations of the *SGS1*, *SRS2* and *MPH1* helicases, *MUS81* and/or

USC
DE SANTIAGO
DE COMPOSTELA

RAD52. We then induced them to undergo meiosis and analysed the viability or colony growth defects of the spores after tetrad dissection (Figure 34). The presence of *YEN1*^{ON} was able to partially suppress the synthetic lethality of the *sgs1*Δ *srs2*Δ double mutants (Figure 34a), as well as the synthetic sickness of the *srs2*Δ *mph1*Δ and *mus81*Δ *srs2*Δ strains (Figure 34c,e). In line with previous results in mus81Δ sgs1Δ strains (Blanco et al., 2014), all these genetic interactions can be alleviated by *rad52*Δ (Figure 34b,d,f), suggesting that in these backgrounds

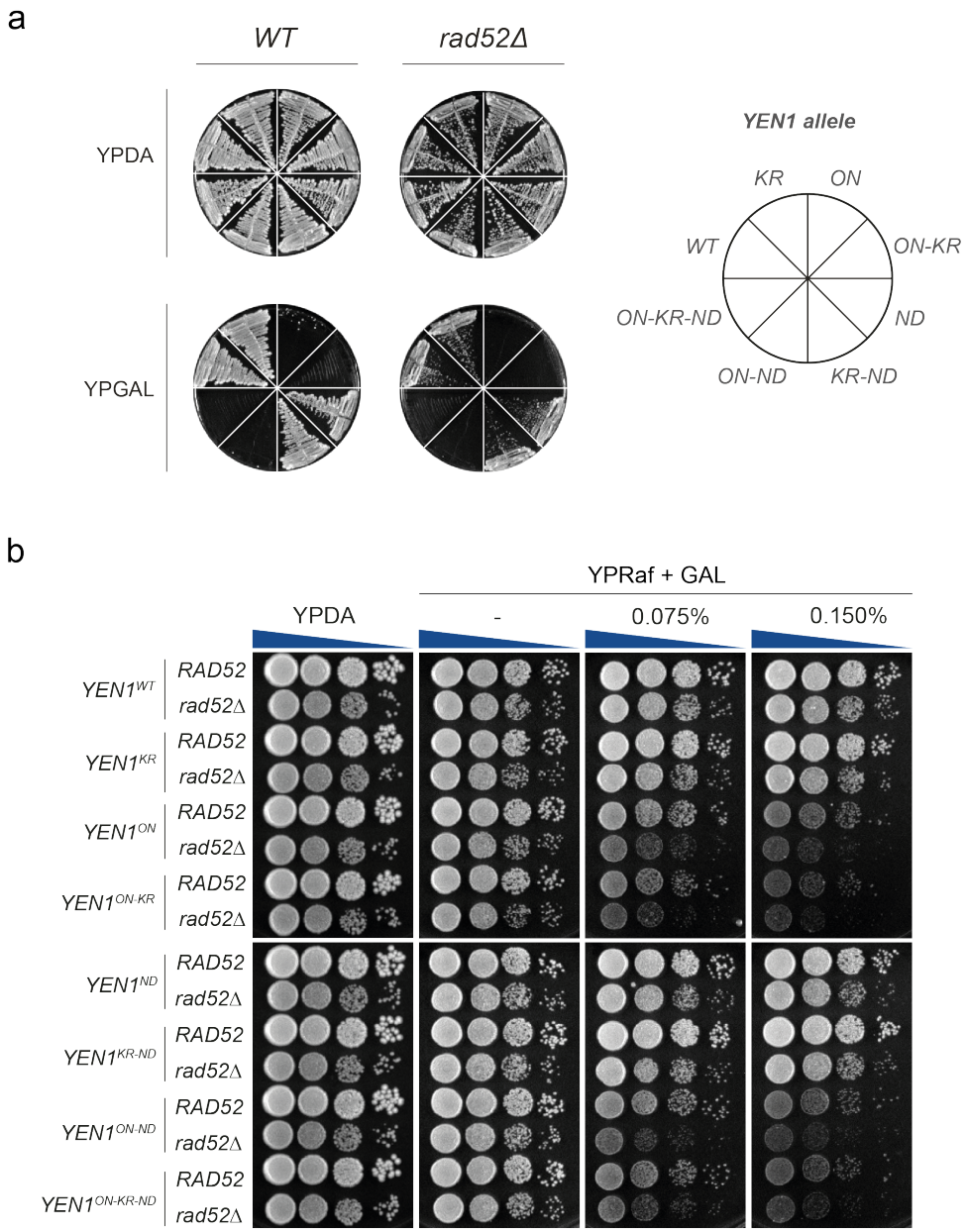


Figure 33 Abrogation of HR pathways does not suppress *YEN1*^{ON}-dependent lethality. a) Strains expressing different *YEN1* alleles in wild-type or *rad52Δ* backgrounds were streaked and examined for growth on solid medium in the absence (YPDA) or presence of galactose (YPGAL). Pictures were taken after 3 days at 30 ºC. **(b)** Ten-fold serial dilutions of strains with the indicated genotypes were spotted on YPDA or YPRaff with the indicated concentrations of galactose and photographed after 2 days of incubation at 30 ºC.

USC DE SANTIAGO DE COMPOSTELA

YEN1^{ON} is providing an alternative route for the removal of toxic recombination intermediates. The *sgs1*Δ *mph1*Δ double mutants did not show any clear proliferation defects when compared to the single *sgs1*Δ and therefore, no overt effects on *YEN1*^{ON} expression were detected in this

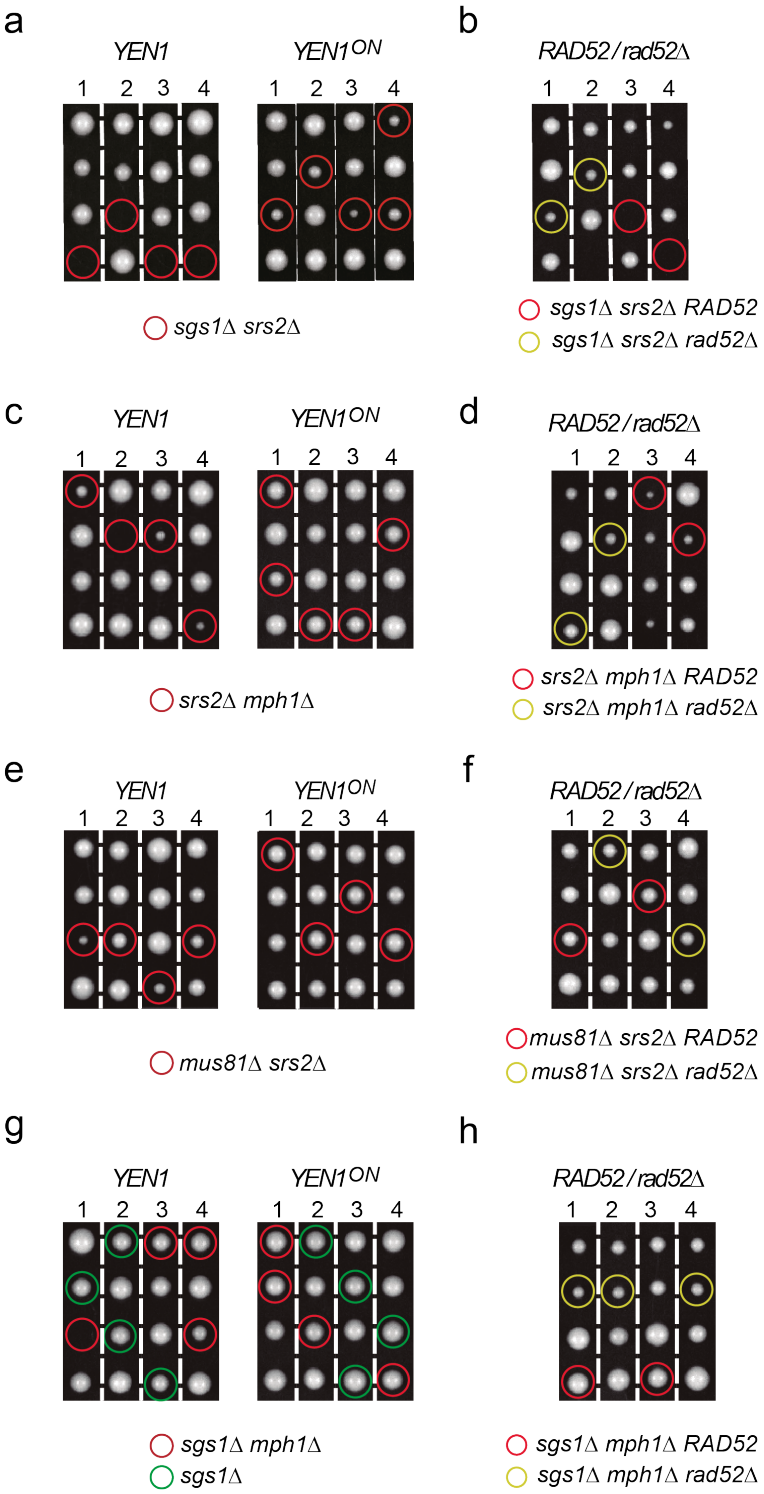


Figure 34. Premature activation of Yen1 is beneficial in strains with an excess of toxic recombination intermediates. (a-h) Tetrad microdissection of diploid strains carrying heterozygous mutations for the indicated genes in *YEN1* or *YEN1*^{ON} homozygous backgrounds **(a, c, g, e)** or *RAD52/rad52Δ* heterozygous backgrounds (**b, d, f, h**). Plates were photographed after 3 days of incubation at 30 ºC.

USC UNIVERSIDADE DE SANTIAGO DE COMPOSTELA

case (Figure 34g). Indeed, further deletion of *RAD52* in this context created a slow growth defect (Figure 34h), suggesting that *sgs1*Δ *mph1*Δ do not suffer from an excessive accumulation of HR intermediates. Importantly, *YEN1*^{ON} could not suppress the synthetic lethality of *sgs1*Δ *slx1*Δ or *sgs1*Δ *slx4*Δ (Figure 35a,c), which is neither rescued by *rad52*Δ (Figure 35b,d) and, hence, does not ensue from accumulation of recombination-dependent joint molecules. Altogether, these results confirm that Yen1^{ON} can target and reduce the excess of HR intermediates that compromise cellular fitness in some specific backgrounds.

We next investigated if this alternative route provided by Yen1^{ON} to the processing of repair

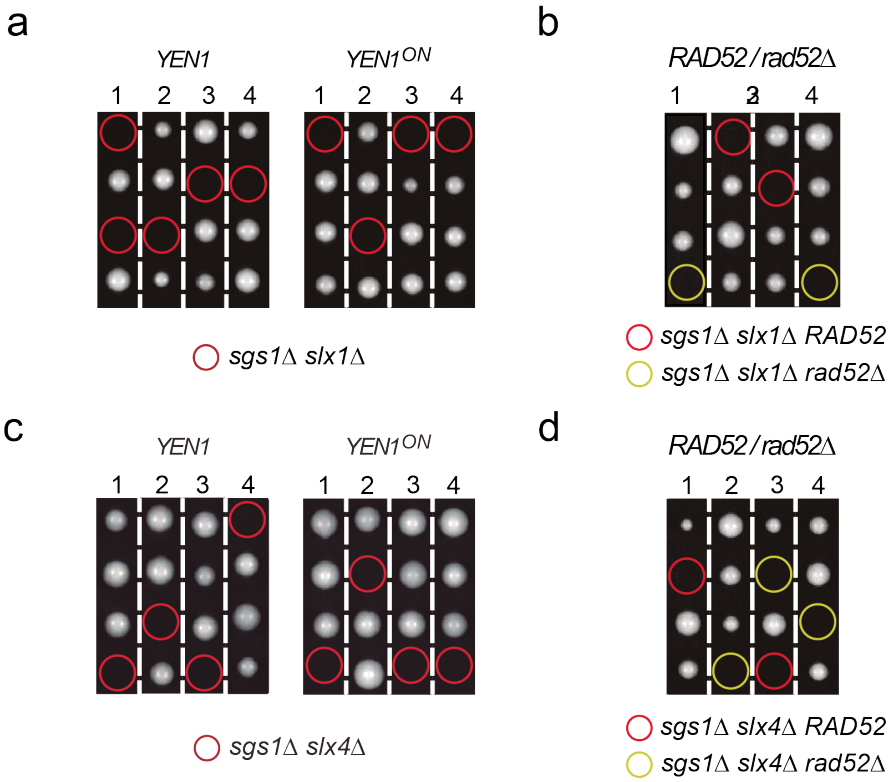


Figure 35. *YEN1*^{ON} does not suppress the synthetic lethality of *sgs1Δ slx1Δ* and *sgs1Δ slx4Δ*. **(a-d)** Tetrad microdissection of diploid strains carrying heterozygous mutations of the indicated genes in *YEN1* and *YEN1*^{ON} homozygous backgrounds **(a, c)** or *RAD52/rad52Δ* heterozygous backgrounds **(b, d)**. Plates were photographed after 3 days of incubation at 30 ºC.

intermediates could also diminish the hypersensitivity of the *sgs1*Δ, *srs2*Δ and *mph1*Δ single mutants to exogenous genotoxic agents. For this purpose, we employed haploid strains carrying one of these deletions and *YEN1*^{ON} expressed from its endogenous promoter. Cells were then subjected to growth under chronic exposure to the alkylating agent methyl methanesulphonate (MMS), the ribonucleotide reductase inhibitor hydroxyurea (HU) or the Top1 inhibitor camptothecin (CPT) by spotting them on solid media containing different doses of each drug (Figure 36). *YEN1*^{ON} was able to slightly ameliorate the proliferation of *sgs1*Δ strains in the presence of all three agents, while for *srs2*Δ this effect was particularly evident under CPT treatment (Figure 36a,b). No overt changes were observed for *mph1*Δ strains in the presence of HU or CPT, but, strikingly, *YEN1*^{ON} increased their hypersensitivity to MMS in a

USC DE SANTIAGO DE COMPOSTELA

considerable manner (Figure 36c). Altogether these results indicate that the premature activation of Yen1 may contribute to the successful processing of repair intermediates under particular types of genotoxic stress in the absence of Sgs1 and Srs2. However, those DNA species that accumulate in *mph1*Δ mutants under MMS treatment might be suffering an aberrant endonucleolytic disruption by Yen1^{ON} that increases the severity of the original lesion.

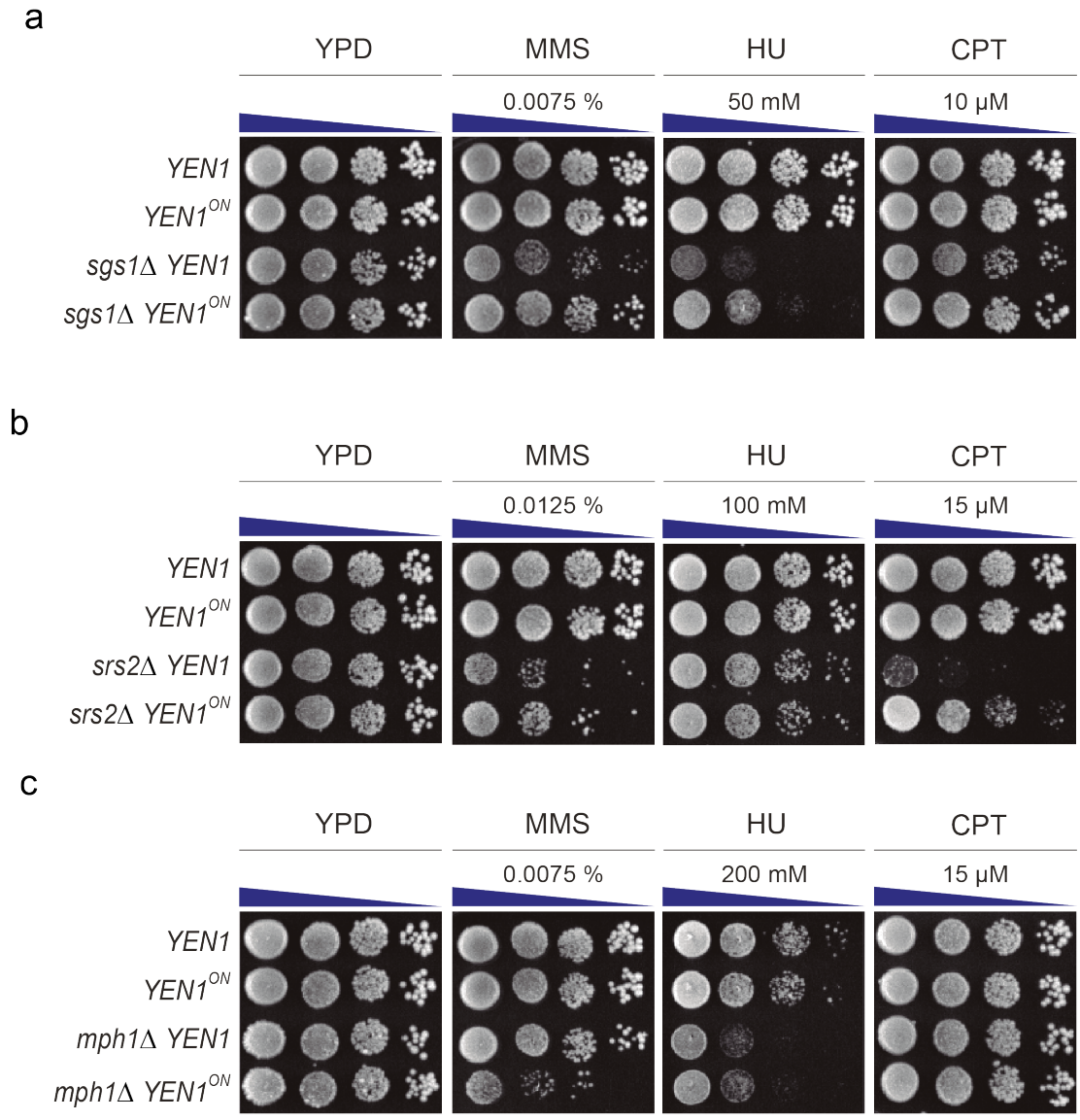


Figure 36. *YEN1^{ON}* alters the hypersensitivity of mutants for HR-related helicases to DNA-damaging agents. Ten-fold serial dilutions of strains with the indicated genotypes were spotted on YPD with various concentrations of MMS, HU or CPT. An illustrative concentration is shown for each. Plates were photographed after 2 days of incubation at 30 ºC.

USC UNIVERSIDADE DE SANTIAGO DE COMPOSTELA

2.4 Cells deficient in nuclear Pif1 become hypersensitive to HU upon expression of Yen1^{ON}

In addition to these genes, we wanted to extend our analyses about the effect of *YEN1*^{ON} expression to the absence of other helicases generally considered to act on a wider spectrum of secondary DNA structures, the Pif1-family helicases, which in budding yeast are represented by the ScPif1 and ScRrm3 paralogs (hereinafter, simply Pif1 and Rrm3). Therefore, we created double-mutant strains and carried out genotoxicity assays as described above, employing MMS and HU (Figure 37). Interestingly, while no synthetic defects could be observed between *YEN1*^{ON} and *rrm3*Δ in the presence of MMS or HU (Figure 37a,b), the *pif1*Δ *YEN1*^{ON} double mutants displayed a strong hypersensitivity to both genotoxic agents when compared to any of the single mutants (Figure 37c,d). Quite remarkably, at the tested MMS and HU doses, the single *pif1*Δ and *YEN1*^{ON} mutants do not display any hypersensitivity when compared to the wild-type strain, underscoring the specificity of their synthetic interaction under these conditions.

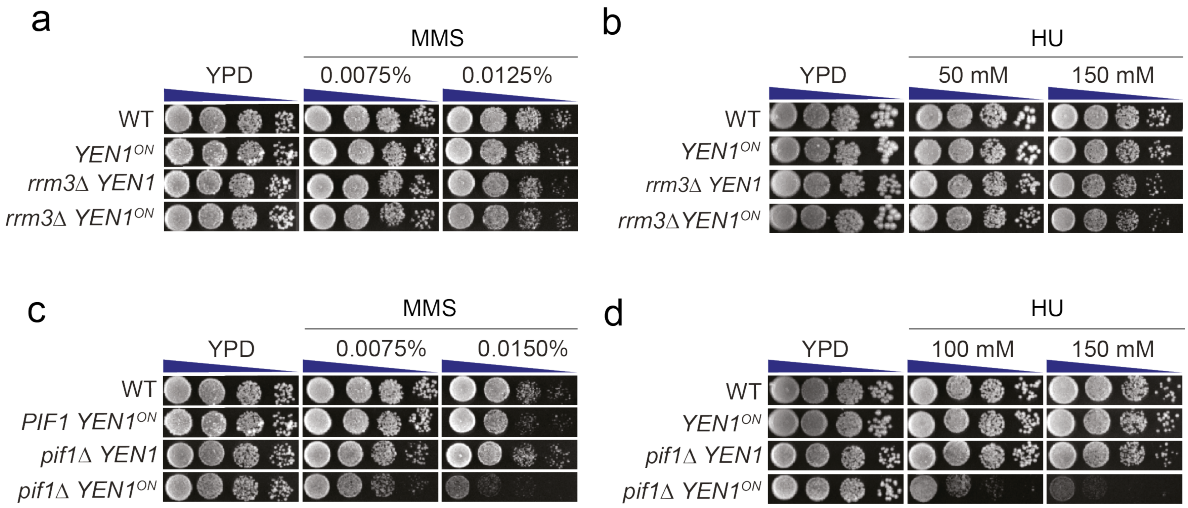


Figure 37. Genetic interaction between *YEN1*^{ON} and absence of *PIF1*-family helicases in the presence of MMS or HU. Ten-fold serial dilutions of strains with the indicated genotypes were spotted on YPD containing different concentrations of MMS **(a, c)** or HU **(b, d)** and photographed after 2 days of incubation at 30 ºC. Two illustrative doses are shown for each condition.

The simplest, but not unique, explanation for these results would be that, in the absence of Pif1, some of the multiple secondary structures that it normally targets in the nucleus under replication or genotoxic stress, either directly become substrates for Yen1^{ON} or indirectly contribute to their appearance. Given the continuous presence of active Yen1^{ON} in the nucleus, it could compete with the optimal repair machinery for these structures and lead to their untimely processing and further contribute to genome instability and cellular viability. Therefore, we first decided to confirm that the observed interaction was specifically related to the loss of Pif1 nuclear functions, since *pif1*Δ mutants also lack mitochondrial Pif1 and display a *petite* phenotype, which could lead to confounding effects. For this purpose, we resorted to the classical separation-of-function *PIF1* alleles *pif1-m1* and *pif1-m2* (Schulz and Zakian, 1994a), deficient in mitochondrial and nuclear Pif1, respectively (Figure 38a). Quite to our surprise,

USC UNIVERSIDADE DE SANTIAGO DE COMPOSTELA

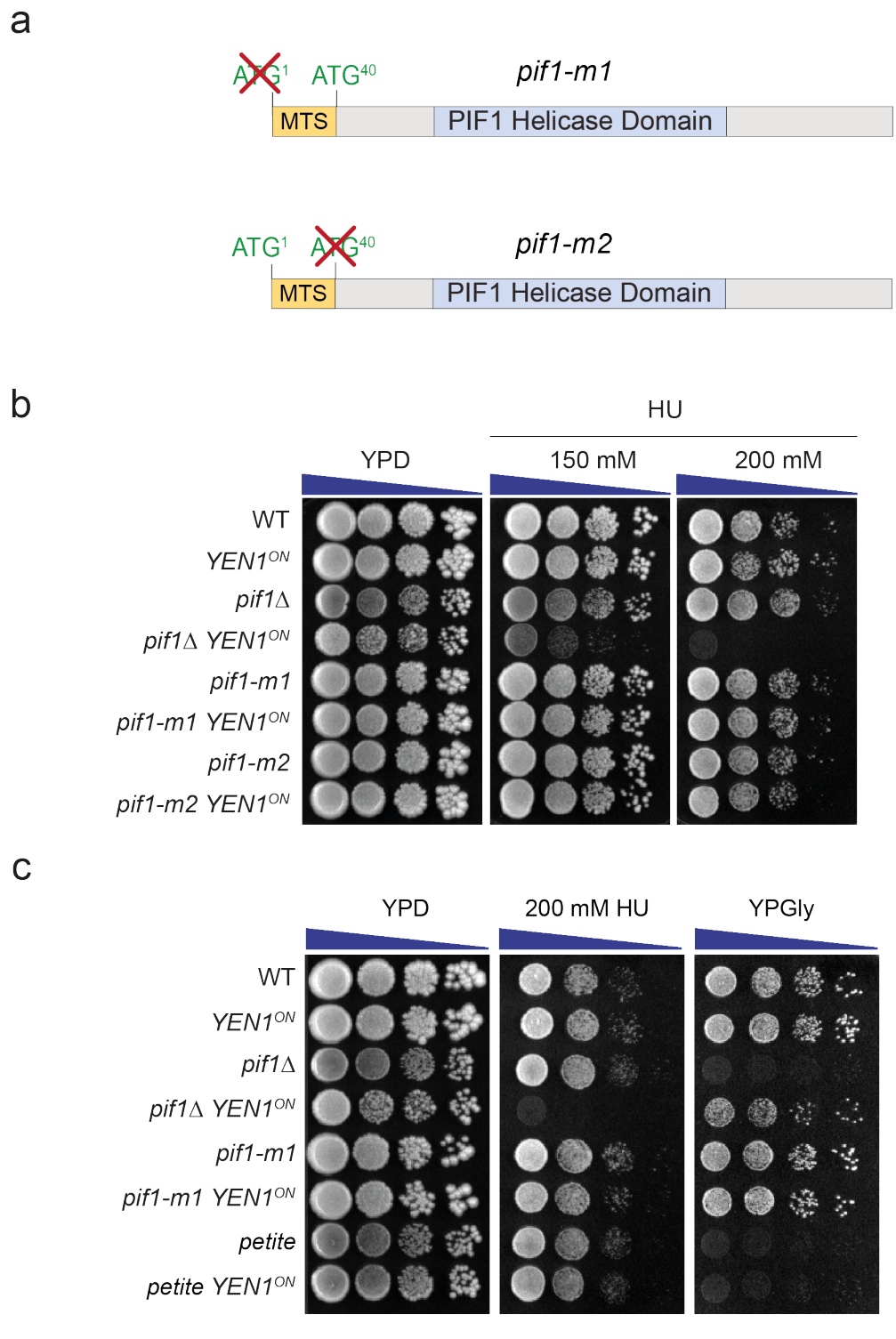


Figure 38. ***PIF1*** **mitochondrial and nuclear separation-of-function alleles fail to recapitulate the genetic interaction in** ***pif1Δ YEN1ON*****. (a)** Schematic representation of *pif1-m1* (mitochondrial-defective) and *pif1-m2* (nuclear-defective) alleles. **(b)** Ten-fold serial dilutions of strains with the indicated genotypes were spotted on YPD plates containing different HU concentrations and photographed after 2 days of incubation at 30 ºC. **(c)** As in (b), but employing YPD, with or without HU, and YPGly plates.

USC UNIVERSIDADE DE SANTIAGO DE COMPOSTELA

when we tested the hypersensitivity to HU of the strains combining *YEN1^{ON}* with each of these alleles, neither *pif1-m1* nor *pif1-m2* recapitulated the synthetic interaction observed with *pif1*Δ (Figure 38b). This result, together with the known *petite* phenotype of *pif1*Δ strains, would be compatible with a scenario where the observed interaction with *YEN1^{ON}* might be due to a general lack of mitochondrial respiratory functions, rather than the specific absence of Pif1. To test this hypothesis, we isolated spontaneous *petites* in the *YEN1* and *YEN1^{ON}* strains, where Pif1 is both present at nucleus and mitochondria, and compared their HU hypersensitivity to that of *pif1*Δ *YEN1^{ON}* strains. As shown in Figure 38c, the *petite YEN1^{ON}* strains grew comparably to wild-type cells in the presence of HU, unlike the *pif1*Δ *YEN1^{ON}* mutants, indicating that this synthetic interaction is specific for the loss of Pif1. Quite remarkably, subjecting the same set of strains to growth in medium containing glycerol (a non-fermentable carbon source) instead of glucose, led to two important observations. First, while the *pif1*Δ and the spontaneous *petite* strains failed to proliferate in this medium due to their disabled respiratory functions, *pif1-m1* strains were able to grow normally, even when they should also display a *petite* phenotype (Figure 38c). This pointed to an incomplete separation-of-function in this mutant, which will be further explored in the next chapter of this PhD Thesis. Second, the double mutant *pif1*Δ *YEN1^{ON}*, despite its hypersensitivity to HU, quite unexpectedly showed an increased proliferation capacity in glycerol-containing medium compared to *pif1*Δ, suggesting some compensatory effect by Yen1^{ON} in cells without mitochondrial function or preventing its loss in the absence of Pif1. This observation and its potential implications are being explored by other members of the laboratory at the time of writing this PhD Thesis and will not be further discussed here.

Both our own results during the generation and handling of strains carrying the *pif1-m1* and *pif1-m2* alleles, as well as a thorough revision of the Pif1 literature led us to the conclusion that the most likely explanation for the failure of these alleles to recapitulate the *pif1*Δ synthetic interaction with *YEN1^{ON}* was that the *pif1-m2* mutants still retained a phenotypically relevant level of nuclear Pif1 activity. Therefore, we decided to generate improved separation-of-function alleles in order to ascertain the precise molecular intricacies behind the strong *pif1*Δ *YEN1^{ON}* interaction. The rationale employed to generate those refined alleles, now termed *pif1^{nuc}* and *pif1^{mit}* (Figure 39a), will be addressed in the next chapter of this PhD Thesis. Importantly, by combining *YEN1^{ON}* with these new set of alleles, we could confirm that the hypersensitivity of *pif1*Δ *YEN1^{ON}* strains to HU is specifically due to the loss of Pif1 nuclear functions, since only the *pif1^{mit} YEN1^{ON}* strain can phenocopy this deficiency (Figure 39b). Altogether, our findings support that downregulation of HJ resolvases during S phase prevents the aberrant processing of replication or repair intermediates. Further characterization of the phenotypes associated to *YEN1^{ON}* overexpression, or its hypersensitivity to genotoxic agents when combined with loss of nuclear Pif1, may help to elucidate the precise DNA structures that could be targeted by premature Yen1 activation.

USC UNIVERSIDADE DE SANTIAGO DE COMPOSTELA

a

Separation-of-function alleles

Classical	Improved	Expected location
pif1-m1	*pif1^{nuc}*	Nucleus
pif1-m2	*pif1^{mit}*	Mitochondria

b

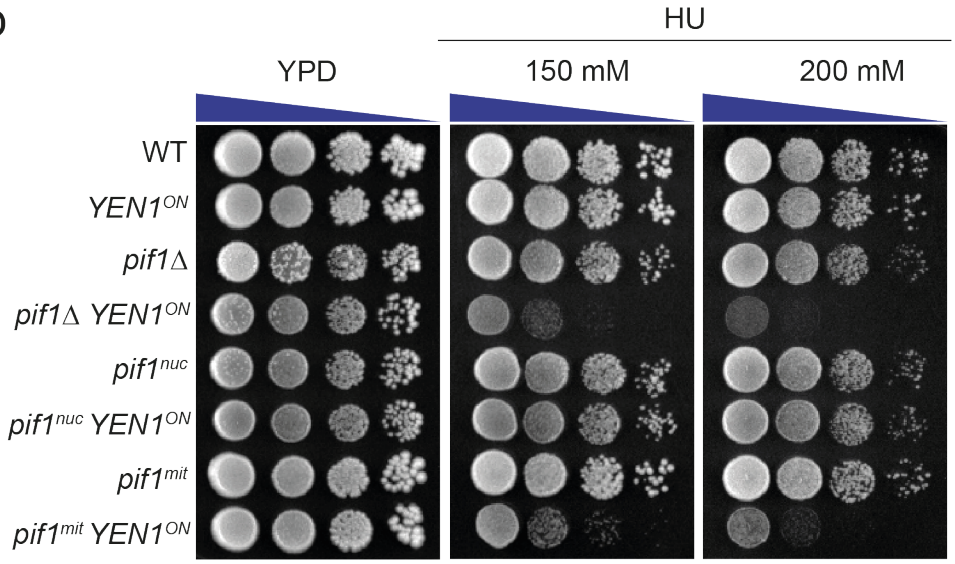


Figure 39. Hypersensitivity of *pif1Δ YEN1^{ON}* strains to HU is caused by the loss of Pif1 nuclear function. (a) *pif1^{nuc}* and *pif1^{mit}* represent improved versions of *pif1-m1* and *pif1-m2*, respectively. **(b)** Ten-fold serial dilutions of strains with the indicated genotypes were spotted on YPD containing HU and photographed after 2 days of incubation at 30 °C.

3. Discussion

3.1 Cell-cycle regulation of Yen1 prevents genome instability.

Work from several groups has established that downregulation of HJ resolvases during S-phase is an evolutionarily conserved strategy to preserve genome integrity, even if its mechanistic implementation for specific nucleases in different organisms may vary. A general interpretation of this observation is that these restrictions prevent the aberrant processing of replication or repair intermediates. However, the precise DNA structures that could be targeted by precocious HJ resolvases remains unclear. In this work, we have carried out a preliminary characterization of the impact of premature activation of the *S. cerevisiae* Yen1 resolvase by taking advantage of the regulation-refractory *YEN1^{ON}* mutant, which is constitutively active and nuclear throughout the cell cycle.

An initial approach using galactose-inducible constructs demonstrated that overexpression of *YEN1^{ON}* induces cell death in a dose-dependent manner, reaching complete lethality with full induction of the *GAL1* promoter (Figure 30a), whereas similar overexpression of the wild-type enzyme is inconsequential. Interestingly, we expected such phenotype to be dependent on

UCC UNIVERSIDAD CATÓLICA DE CHILE

Yen1^{ON} catalytic activity, but much to our surprise, we found that overexpression of the catalytically inactive, but still nuclear and DNA binding-proficient, *YEN1^{ON-ND}* mutant also derived in cell death (Figure 30b). Taken at face value, this result would indicate that Yen1^{ON} toxicity is independent of its nuclease activity. However, we favour an alternative explanation in which lethality upon *YEN1^{ON}* overexpression does depend on its nuclease activity to process yet-undetermined branched DNA structures aberrantly, while the dominant negative effect of *YEN1^{ON-ND}* would stem from a "*Dog in the Manger*"-like behaviour, by tightly binding to physiologically relevant branched DNA structures and preventing their normal processing by other enzymes.

In both cases, cell death is accompanied by robust checkpoint activation, as judged by Rad53 phosphorylation (Figure 31a), and disruption of the normal cell-cycle profile, with an apparent accumulation of cells in S phase (Figure 31b). This could be compatible with the generation of DNA breaks or the persistence of long ssDNA tracts in these mutants, which would be in agreement with their ability to interfere with normal S-phase progression. Importantly, a prolonged cell-cycle arrest is not the main cause of cell death in these strains, as deletion of *RAD53* cannot suppress it (Figure 32a,c).

Since Yen1 is not only able to process HJs, but also other branched structures that may appear during HR, like D-loops, we employed a similar simplistic rationale to verify if the primary cause of lethality in these cells was the unscheduled processing of recombination intermediates. However, overexpression of *YEN1^{ON}* and *YEN1^{ON-ND}* was not only still deleterious in a *rad52*Δ background (Figure 33a), but in fact HR seems to counter the toxic effect of Yen1 misregulation (Figure 33b).

3.2 Upon genotoxic stress, nuclear Pif1 may prevent the accumulation of DNA secondary structures that Yen1^{ON} could hydrolyse.

These observations, together with results from other members of the lab, indicated that *YEN1^{ON}* overexpression leads to massive genome instability that cannot be suppressed by mutations in other genes. Therefore, in order to gain further information on the DNA metabolism pathways that may be disrupted by premature resolvase activity, we changed our approach and started to search for genetic interactions between *YEN1^{ON}* expressed at endogenous levels and other DNA repair factors, unveiling two main types of interactions. On the one hand, the presence of Yen1^{ON} at endogenous levels seems to have a beneficial effect in those situations where cellular viability is compromised by the accumulation of unresolved recombination intermediates. This situation arises as consequence of either the simultaneous mutations of HR genes leading to synthetic lethality or sickness (Figure 34) or the combination of single mutations with genotoxic agents (Figure 36 and Figure 37), confirming and extending previous results (Blanco et al., 2014; Elango et al., 2017). In this context, *YEN1^{ON}* could efficiently suppress the same set of genetic interactions as *RAD52* deletion, confirming that Yen1^{ON} provides an alternative therapeutic route against the "sickness/death-by-recombination" phenotype, but not in the context of other synthetic lethalities (Figure 35). On the other hand, we found that in some genetic backgrounds expression of *YEN1^{ON}* leads to increased hypersensitivity to genotoxic agents like MMS, HU or CPT (Figure 36 and Figure 37),). In particular, the *YEN1^{ON} pif1*Δ

interaction (Figure 37c,d) was particularly exciting due to its strong synthetic effect and that the Pif1 helicase is one of the main actors in the handling of multiple secondary DNA structures. Therefore, we decided to further delve into the underpinning molecular mechanism of this interaction as a way to better understand the relevance of Yen1 regulation.

However, not far into this line of research we encountered a technical obstacle that prevented its further development: attempts to recapitulate this genetic interaction with any of the two classical separation-of-function alleles for *PIF1*, *pif1-m1* (nuclear) and *pif1-m2* (mitochondrial), systematically failed to recapitulate the genetic interaction between *pif1*Δ and *YEN1*^{ON} (Figure 38a,b). Given the pleiotropic effects of the full deletion, (nuclear defects and loss of mitochondrial DNA), we could not rule out an indirect interaction caused by the petite phenotype of *pif1*Δ mutants, which could be uninformative for our purposes. Although we managed to discard the hypothesis of a genetic interaction between *YEN1*^{ON} and the *petite* condition (Figure 38a,b), we decided that, in order to understand the underlying molecular intricacies of this interaction, we needed to find out the reason behind the failure of *pif1-m1* and *pif1-m2* to recapitulate the *YEN1*^{ON} *pif1*Δ interaction. This ultimately became the focus for the rest of my PhD Thesis, which will be laid out in Chapter 2. Importantly, once we had managed to generate improved separation-of-function alleles for nuclear and mitochondrial Pif1, we demonstrated that the increase in hypersensitivity to genotoxic agents in *YEN1*^{ON} *pif1*Δ mutants is specifically connected to the loss of Pif1 nuclear function (Figure 39).

The most intuitive explanation for such results would be that in the absence of nuclear Pif1 those DNA secondary structures that this helicase contributes to unwind persist for longer times, either becoming substrates themselves or indirectly contributing to the appearance of new substrates for Yen1^{ON} activity. Alternatively, we cannot formally rule out that, as in the case of Rad52, nuclear Pif1 is important to avert the damage generated by Yen1^{ON} under genotoxic stress.

3.3 Future plans

While, due to time constraints, we could not reach further conclusions at this point, I would like to lay out some of our future plans to delineate the molecular mechanism that underpins the lethality of *YEN1*^{ON} overexpression, as well as the hypersensitivity to DNA damaging agents of Yen1^{ON} strains in the absence of nuclear Pif1. Since the still inceptive stage of this project complicates the elaboration of data-driven hypothesis, for the remaining part of this discussion I will focus on different experimental approaches that could be useful to address some relevant questions.

Firstly, it would be of interest to investigate whether the overexpression of both *YEN1*^{ON} and *YEN1*$^{ON\text{-}ND}$ is concomitant with the occurrence of DNA breaks that could explain the subsequent lethality under these conditions. For this, physical analysis of chromosomal breakage by pulsed-field electrophoresis would be employed, both in asynchronous and synchronous cultures, followed by general DNA staining and/or probing for particular loci. If the integrity of a specific chromosome is compromised, it could point towards a particular genomic region (like the rDNA array in chromosome XII (Petes, 1979) being affected by Yen1 unscheduled activity. Alternatively, if all chromosomes are affected, resembling a chromosome pulverization

phenotype (Crasta et al., 2012; Duda et al., 2016), it would imply the unscheduled cleavage of widespread secondary structures arising during S phase, such as replication forks, hairpins or G4s. Similarly, bidimensional gel electrophoresis analysis followed by southern blotting could be employed to examine the accumulation and processing of ongoing replication intermediates upon premature activation of Yen1. Finally, it would be also interesting to tease out the route for checkpoint activation after *YEN1*^{ON} or *YEN1*$^{ON\text{-}ND}$ overexpression. This could be determined by assessing the phosphorylation status of Rad53 in our assays in strains lacking the checkpoint apical kinases Mec1 and Tel1 or the Rad9 and Mrc1 mediators (Waterman et al., 2020)

Ideally, genome-wide techniques could be applied to map the binding and cleavage sites of prematurely activated Yen1 in phases when it does not normally have access to the nucleus. In this sense, the lethality of overexpressed Yen1$^{ON\text{-}ND}$ suggests a very tight binding to its substrates, in line with the previously described dominant negative effect of *YEN1*ND expression in *mus81*Δ strains (Blanco et al., 2010). This "substrate-trapping" behaviour could be exploited to interrogate the *in vivo* binding sites of Yen1 in S phase by ChIP-seq, which would hint at particular secondary DNA structures targeted by this nuclease. Moreover, it would be also interesting to obtain a genome-wide profiling of Yen1-dependent incisions, taking advantage of the explosion of techniques to map DNA breaks that have been developed in the recent years, including BLESS (Crosetto et al., 2013), END-seq (Canela et al., 2016), DSB-capture (Lensing et al., 2016), BLISS (Yan et al., 2017), i-BLESS (Biernacka et al., 2018), qDSB-seq (Zhu et al., 2019), CNN-seq and sBLISS (Bouwman et al., 2020) for DSBs and SSiNGLe (Cao et al., 2019), GLOE-seq (Sriramachandran et al., 2020), Nick-seq (Cao et al., 2020) and TRAEL-seq (Kara et al., 2021) for mapping of SSBs (Cao et al., 2019; Kara et al., 2021; Sriramachandran et al., 2020). Importantly, some of these methodologies have already been successfully applied to the identification of cleavage sites by other SSEs, like Mus81, even in a quantitative manner… Algunas técnicas y han demostrado los cortes de Mus81, y variants cuantitivvas.

Most of the techniques described to characterize the reason behind *YEN1*^{ON} overexpression-dependent lethality could be similarly employed to unravel the underlying mechanism for the hypersensitivity of *pif1*^{mit} *YEN1*^{ON} strains to DNA damaging agents, such as pulse-field electrophoresis and mapping of binding sites with Yen1$^{ON\text{-}ND}$. In the latter case, it would be interesting to employ for comparison purposes the *pif1*^{K264A} allele, which renders a catalytically inactive, but binding proficient version of Pif1 that has already been employed in ChIP-seq experiments to map its binding sites genome-wide (Paeschke et al., 2011). Similarly, mapping of DNA breaks produced by Yen1^{ON} in a *pif1-*^{mit} background could also help to delineate the structures disrupted in *pif1*^{mit} *YEN1*^{ON} mutants upon HU treatment.

Given the multiple factes of DNA metabolism where Pif1 plays a role, we will also take advantage of *PIF1* mutants defective in pathway-specific protein-protein interactions, like *pif1-R3E*, *pif1-PIPmut* or *pif1-4A*. *pif1-R3E* impairs the PCNA-Pif1 interaction required to promote DNA synthesis during BIR, whereas *pif1-PIPmut* is necessary for Pif1-assisted replisome progression through G4s (Buzovetsky et al., 2017; Dahan et al., 2018). Since the DDR phosphorylates Pif1 at is CTD to promote BIR and, at the same time, prevent telomerization of DSBs, the *pif1-4A* phosphomutant allele is both defective at BIR stimulation and inhibition of

USC
DE COMPOSTELA

telomerase activity at chromosomal breaks (Makovets and Blackburn, 2009a; Vasianovich et al., 2014). A specific interaction of *YEN1^{ON}* with any of these alleles could also pinpoint the pathways affected by the premature activation of Yen1. However, it is important to consider that the interaction of *YEN1^{ON}* with this type of alleles might not resemble that with *pif1^{mit}* because of two main reasons: i) a complex/additive effect of *YEN1^{ON}* through the disruption of multiple pathways in which nPif1 is involved under replicative stress, including the repair of *YEN1^{ON}*-dependent DNA break; ii) incomplete separation of function of those alleles, as in the case of *pif1-m2*.

Given such potential limitations, we also intend to combine *YEN1^{ON}* with mutations in other genes that render cells deficient in specific pathways in which Pif1 plays a role. For instance, the lack of interaction between *rrm3*Δ and *YEN1^{ON}* indicates that the underlying cause of the *pif1^{mit} YEN1^{ON}* phenotype can be attributed to Pif1-specific functions or those in which Rrm3 plays a backup role, such as fork progression through G4-rich regions, inhibition of telomerase, support of the RFB and BIR. To determine whether impairment of fork progression through G4s underlies the interaction of *pif1^{mit} YEN1^{ON}*, we propose several strategies. First, we will combine *pif1^{mit}* allele with *rrm3*Δ and *YEN1^{ON}*, considering Rrm3 back-up role in promoting genome stability at G4 motifs (Paeschke et al., 2013). Furthermore, we will combine *YEN1^{ON}* with deletions of *MMS1* and the hypomorphic RPA allele *rfa1-D228Y*. Mms1, a subunit of an E3 ubiquitin-ligase complex, binds G4 structures and recruits Pif1 to those regions (Wanzek et al., 2017), whereas RPA cooperates with Pif1 to remove G4-quadruplex structures. In particular, the *rfa1-D228Y* mutant reduces RPA ssDNA binding activity, especially to G-rich tracts (Audry et al., 2015; Maestroni et al., 2020). Finally, we will test the effects of G4 chemical stabilisers, such as Phen-DC3 (Lopes et al., 2011; Piazza et al., 2010) in *YEN1^{ON}* and *pif1^{mit} YEN1^{ON}* strains, both in terms of cell viability and chromosomal integrity. To address if Pif1-dependent telomere homeostasis or telomere healing at DSBs is altered in the presence of *YEN1^{ON}*, the separation-of-function alleles *cdc13-S306A* and *est2-up34* could be employed. Mec1 phosphorylates Cdc13 at S306 to prevent its accumulation at DSBs, and the S306A substitution increases telomere healing to levels comparable to *PIF1*-deficient strains (Zhang and Durocher, 2010). In contrast, *est2-up34,* a mutant version of the catalytic subunit of telomerase, prevents the Pif1-dependent downregulation of Est2 activity, leading to extended telomeres (Eugster et al., 2006). Similarly, a possible effect on the stability of the rDNA or the maintenance of the replication fork barrier, which is partially dependent on Pif1 could be assessed in *fob1*Δ mutants. Finally, a potential interference by *YEN1^{ON}* with the repair of single-end DSBs by BIR, which requires Pif1 for extensive D-loop-associated DNA synthesis, could also be revealed in mutants of the *POL32*, the subunit of Polδ indispensable for this repair pathway (Lydeard et al., 2007; Wilson et al., 2013).

We believe that with such results in hand we could compose a more precise picture of the physiological events that cells are shielding from the action of SSEs by delaying their activation until the late stages of the cell cycle.

USC
UNIVERSIDADE DE SANTIAGO DE COMPOSTELA

CHAPTER 2: PIF1 TRANSLATIONAL MECHANISM

Pif1 has two different isoforms in *S. cerevisiae*, allowing the dual-targeted localization required to fulfil its roles in both nucleus and mitochondria. This is achieved by ATI of *PIF1* mRNA from the first two in-frame AUG codons (AUG^1 and AUG^{40}), which flank a MTS. When translation starts from AUG^1, the N-terminal MTS quickly directs the full-length precursor (98 kDa) to the mitochondria. Once imported into the matrix, the MTS is proteolytically removed, rendering the mature mitochondrial isoform (mPif1, 92 kDa), starting at arginine 46 (Lahaye et al., 1993b). Instead, if translation initiation starts at AUG^{40}, a 93 kDa isoform lacking the MTS is produced and subsequently imported into the nucleus (nPif1) (Figure 40).

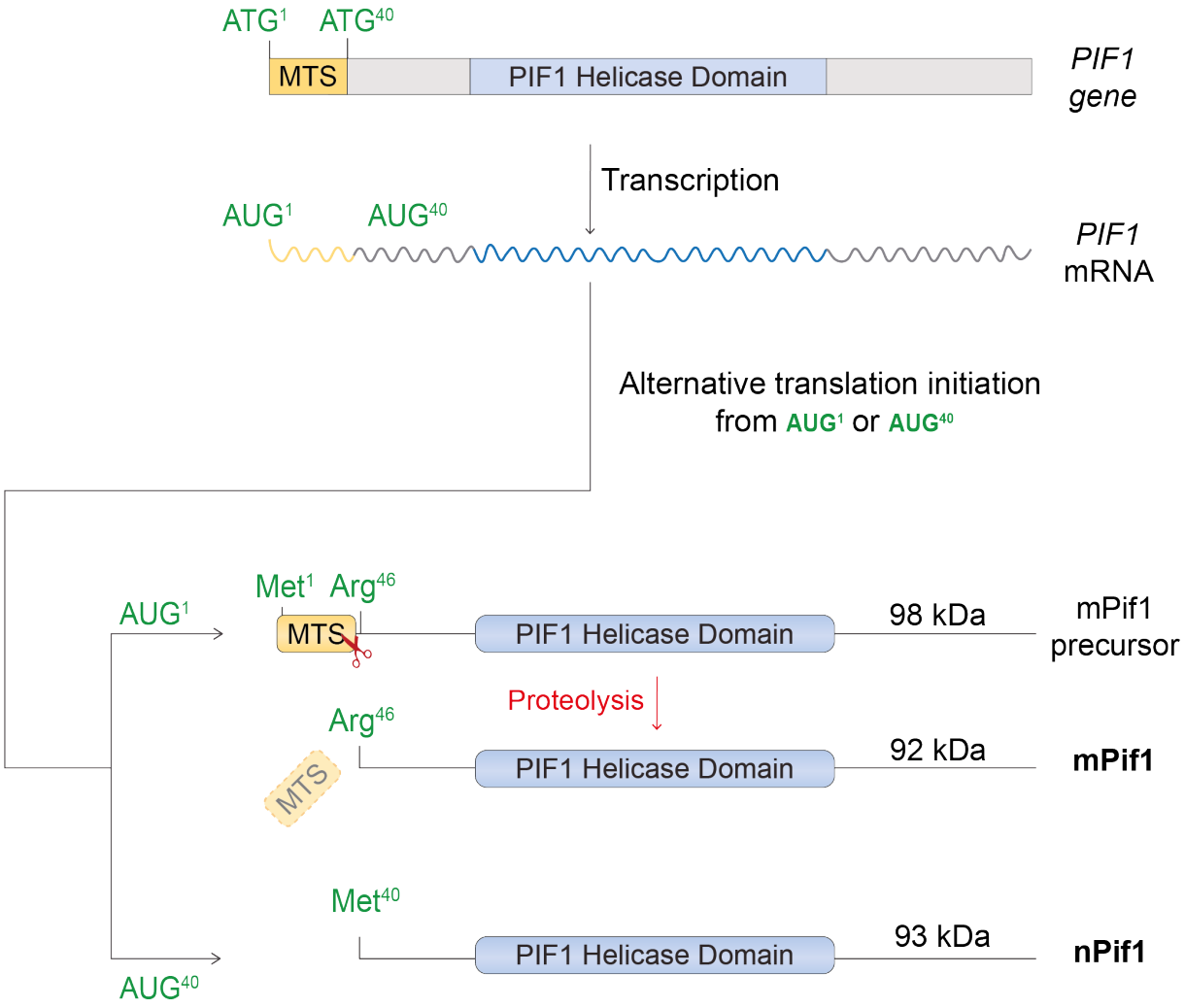


Figure 40. ATI from AUG^1 and AUG^{40} produces Pif1 mitochondrial and nuclear isoforms. Translation initiation from the first start codon (AUG^1) renders the full-length precursor of mPif1. Alternatively, translation from the second in-frame AUG (AUG^{40}) produces nPif1. After proteolytical cleavage of the mPif1 precursor before Arg^{46}, both mature isoforms will differ only in 6 amino acids. mPif1, mitochondrial isoform of Pif1; nPif1, nuclear isoform of Pif1; MTS, mitochondrial targeting signal.

USC UNIVERSIDADE DE SANTIAGO DE COMPOSTELA

The described ATI model inspired the development of two separation-of-function alleles for the mitochondrial (*pif1-m1*) and nuclear (*pif1-m2*) functions of Pif1 (Schulz and Zakian, 1994a). In *pif1-m1*, the production of mPif1 is abolished by mutation of ATG^{1}, whereas nPif1 can still be translated from the intact AUG^{40} and imported into the nucleus, presumably through a yet-uncharacterized NLS (Figure 41a). Conversely, in *pif1-m2*, the mutation of ATG^{40} abrogates the production of nPif1 without affecting the translation of mPif1, resulting in nPif1-deficient strains (Figure 41b). Given the extensive research into the molecular mechanisms that ensure the stability of the nuclear genome, *pif1-m2* has been widely exploited to interrogate the roles

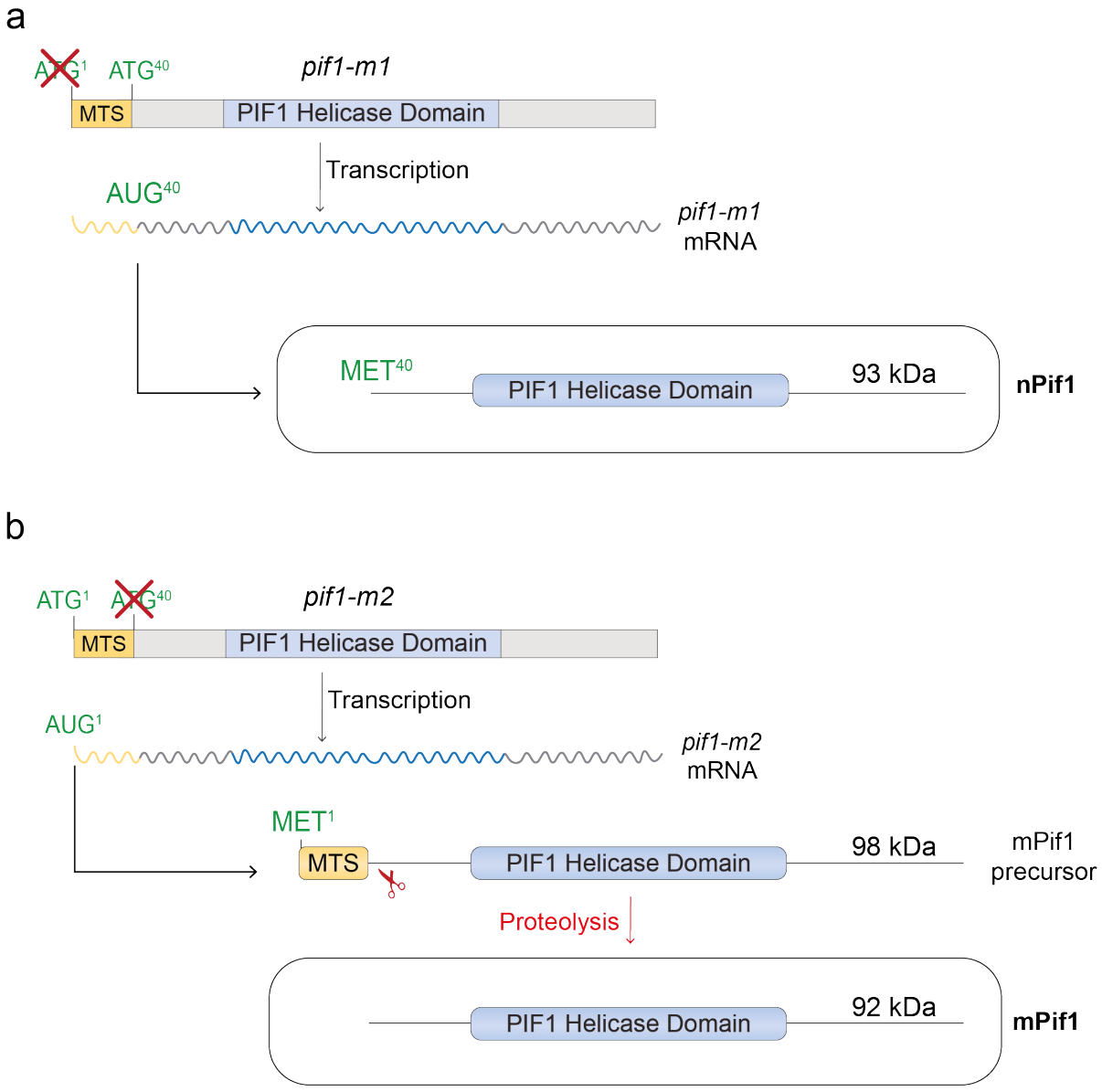


Figure 41. Schematic representation of *PIF1* separation of function alleles with their predicted molecular weight and subcellular localization. (a) *m1* indicates mutation of the first ATG codon. *pif1-m1* produces exclusively a nuclear isoform starting at Met^{40}. **(b)** *m2* stands for mutation of the second ATG codon, at position 40. *pif1-m2* mRNA is only translated as the mitochondrial Pif1 full-length precursor. Like in wild-type cells, mPif1 precursor is proteolytically cleaved upon mitochondrial import. mPif1, mitochondrial isoform of Pif1; nPif1, nuclear isoform of Pif1; MTS, mitochondrial targeting signal.

USC UNIVERSIDADE DE SANTIAGO DE COMPOSTELA

of nPif1 in nuclear DNA replication and repair, avoiding the slow growth and *petite* phenotypes conferred by the loss of mitochondrial Pif1 activity (Bochman et al., 2010).

Despite being frequently mislabelled in the literature as a nuclear-null allele, it was acknowledged since their initial description (Schulz and Zakian, 1994a) that *pif1-m2* mutants could retain traces of nuclear protein, as inferred from their partial suppression of some of the *pif1*Δ phenotypes in different genetic set-ups. In this sense, published data indicate that *pif1-m2* consistently behaves as a poor separation-of-function allele in three specific contexts. First, the extended telomere length of *pif1*Δ strains is only partially recapitulated by *pif1-m2* mutants, suggesting a partial inhibition of telomerase by nuclear Pif1 (Schulz and Zakian, 1994a). Also related to telomeric phenotypes, presence of *pif1-m2* inhibits the growth of *exo1*Δ *cdc13-1* strains when compared to the full knockout or the expression of the helicase-dead version *pif1-K264A* (Dewar and Lydall, 2010). Second, *pif1-m2* can promote stability at G4 tracts. Replication time through G4 regions is significantly slower in *pif1*Δ than in *pif1-m2* cells (Dahan et al., 2018), and the elevated rate of GCRs at the GC-rich CEB1 minisatellite decreases from 20-fold in *pif1*Δ to wild-type levels in *pif1-m2* cells (Ribeyre et al., 2009). This has led other authors to acknowledge that G4-dependent GCRs are probably underestimated in *pif1-m2* strains (Paeschke et al., 2013). Third, the reduction in BIR efficiency, with a concomitant increase in aberrant half-crossovers, is more pronounced in *pif1*Δ than in *pif1-m2* cells (Buzovetsky et al., 2017). Likewise, whereas *PIF1* deletion, in addition to half-crossovers, also leads to microhomology-mediated-BIR (MMBIR) upon BIR collapse, *pif1-m2* cells minimize MMBIR by promoting longer-tracts of BIR synthesis (Sakofsky et al., 2015). Moreover, one screening employing *pif1-m2* to search for novel interactions of *PIF1* failed to report several of the previously described interactions of *pif1*Δ; importantly, as pointed out in the same study, this could be explained either by remnants of nPif1 in *pif1-m2* mutants, or because some synthetic phenotypes described for *pif1*Δ are caused by its mitochondrial defects (Stundon and Zakian, 2015a). Given the suspected presence of nPif1 derived from *pif1-m2*, alternatives like placing *PIF1* under the control of the *CLB2* promoter have been employed to suppress its expression during the meiotic cell cycle (Vernekar et al., 2021; Ziesel et al., 2022). However, when no alternative to *pif1-m2* is available, *pif1*Δ is still widely employed, either on its own or with *pif1-m2* to compare the phenotypes of both alleles.

Our own results in the context of *YEN1*^{ON} mutants described at the end of Chapter 1 (Figure 38) confirm those in the literature showing that the commonly employed *pif1-m2* allele does not fully recapitulate the *pif1*Δ phenotypes ascribed to its nuclear functions, suggesting again that Pif1 nuclear activity is retained to some extent in those mutants. Since employing *pif1*Δ strains to investigate the roles of Pif1 or other DNA repair factors raises important caveats due to the pleiotropic effects of the full deletion, in this Chapter 2 we investigated the extent of separation of function of *pif1-m2* in different genetic set-ups, the potential source of nuclear activity from the *pif1-m2* alleles, and the basis of the molecular mechanism of ATI for Pif1. Finally, we took advantage of our better understanding of those questions to develop improved separation-of-function alleles for *PIF1*.

USC UNIVERSIDADE DE SANTIAGO DE COMPOSTELA

1. OBJECTIVES

Aim 1. To compare *pif1*Δ phenotypes with those of *pif1-m2* in different genetic set-ups.

Aim 2. To search for potential novel isoforms of Pif1 with nuclear activity.

Aim 3. To characterise the molecular mechanism controlling the production of Pif1 isoforms.

Aim 4. To generate improved separation-of-function alleles for *PIF1*.

USC
UNIVERSIDADE DE SANTIAGO DE COMPOSTELA

2. RESULTS

2.1 The *pif1-m2* allele does not fully recapitulate the phenotypes derived from loss of Pif1 nuclear functions in *pif1*Δ mutants.

To analyse the impact of the residual nuclear activity in *pif1-m2* mutants, we started by directly comparing the phenotypes of *pif1-m2* and *pif1*Δ strains in different biological contexts. Importantly, we also employed *pif1-m1* in our experiments to assess whether any phenotypic differences between *pif1-m2* and *pif1*Δ arise from the residual nuclear activity of *pif1-m2* mutants, the mitochondrial defects of *pif1*Δ strains, or the combined effect of simultaneous Pif1 loss at both nucleus and mitochondria. First, given Pif1 role as the main inhibitor of telomerase activity (Schulz and Zakian, 1994b; Zhou, 2000b), we analysed telomeric length in these mutants by "teloblotting", a southern blotting-based technique in which XhoI-digested genomic DNA is hybridized with a probe targeting the Y' subtelomeric elements (Figure 42a). These experiments showed the characteristic extended telomeres in *pif1*Δ mutants with respect to those in wild-type and *pif1-m1* strains (Zhou, 2000b), while *pif1-m2* mutants displayed intermediate telomere lengthening (Figure 42b).

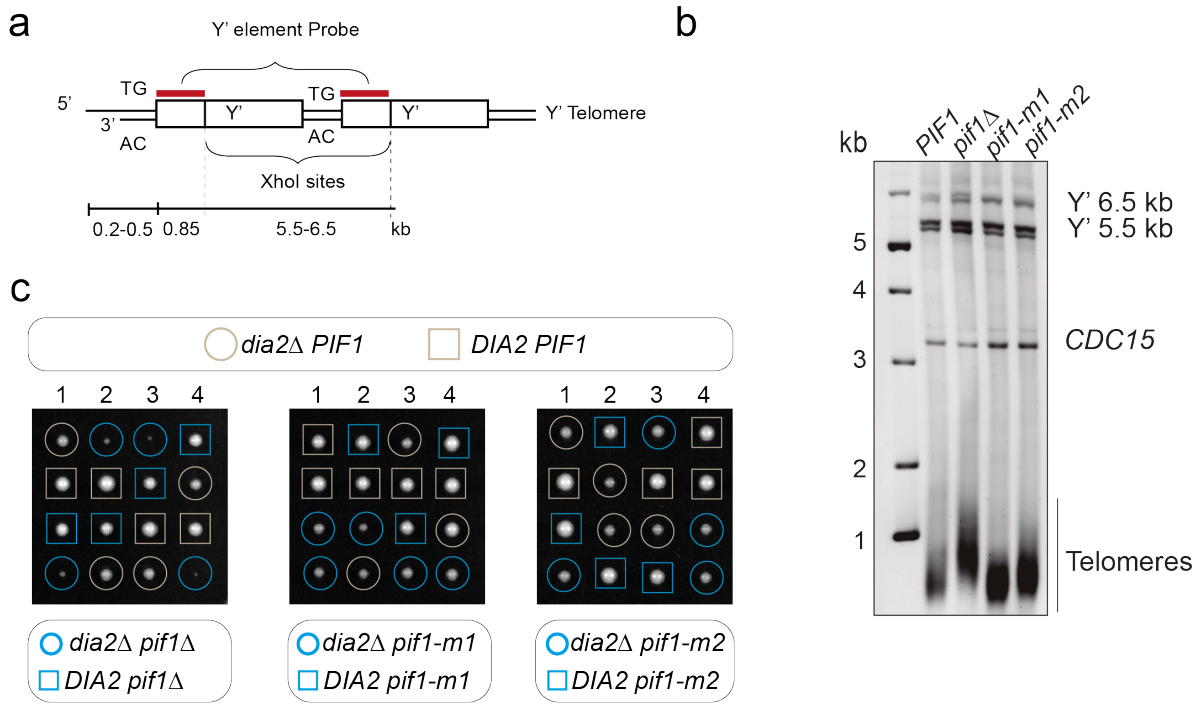


Figure 42. *pif1-m2* recapitulates neither *pif1Δ* telomere lengthening nor its synthetic sickness with *dia2Δ*. **(a)** Schematic representation of a yeast telomere containing a subtelomeric Y' repetitive element. The Y' probe (red line) detects two fragments upon XhoI digestion: i) a fragment including 0.85 kb from the Y' element plus a variable amount of telomeric TG repeats and ii) a fragment of 5.5 or 6.5 kb (depending on each telomere) devoid of telomeric DNA. Changes in the length of TG repeats adjacent to the 0.85 kb fragment of the Y'element will result in variations in the average length of the smaller fragment. **(b)** Southern blot of XhoI-digested DNA from strains carrying the indicated *PIF1* alleles. Telomeric DNA can be observed as a smeared band at the bottom to the blot. A second probe targeted to *CDC15* was employed as a loading control. **(c)** Tetrad microdissection of diploid strains carrying heterozygous mutations for the indicated wild-type and mutant alleles of *DIA2* and *PIF1*. Images were taken after 2 days of incubation at 30ºC.

USC UNIVERSIDADE DE SANTIAGO DE COMPOSTELA

Next, we tested the synthetic sickness between *pif1*Δ and the absence of *DIA2*, a member of the E3 ligase SCF complex (Blake et al., 2006; Pan et al., 2006). Tetrad dissection analyses of *DIA2/dia2*Δ heterozygous diploids in combination with *PIF1*, *pif1*Δ, *pif1-m1* or *pif1-m2* alleles confirmed the overt synthetic sickness of *pif1*Δ *dia2*Δ colonies. In contrast, neither the *pif1-m1* or *pif1-m2* alleles increased the slow-growth phenotype of *dia2*Δ single mutants (Figure 42c), consistently with previous results from a screening searching for *pif1-m2* genetic interactions (Stundon and Zakian, 2015b). As opposed to the previous case, where *pif1-m2* mutants still exhibit partial defects in telomere homeostasis, the lack of phenotypic differences between *pif1-m1* or *pif1-m2* in combination with *dia2*Δ prevents the ascription of *pif1*Δ *dia2*Δ synthetic sickness to the nuclear or mitochondrial functions of Pif1.

We next compared how these separation-of-function alleles suppressed the lethality caused by the absence of the essential Dna2 nuclease-helicase. Although this suppression of *dna2*Δ lethality by *pif1-m2* and *pif1*Δ is well-documented (Budd et al., 2006; Falquet et al., 2020; Rossi et al., 2018)), and many studies have taken advantage of *pif1*Δ or *pif1-m2* to understand *DNA2* nuclear functions, we could not find in the literature a side-by-side tetrad analysis of *DNA2/dna2*Δ diploids harbouring *pif1*Δ*, pif1-m1* or *pif1-m2* alleles. In agreement with previous works (Budd et al., 2006), the deletion of *PIF1* also provided in our hands a robust suppression of *dna2*Δ lethality, unlike the *pif1-m1* allele (Figure 43a). However, the growth of *dna2*Δ *pif1-m2* colonies is severely impaired with respect to the *dna2*Δ *pif1*Δ, indicative of functionally relevant amounts of nuclear Pif1 in those cells (Figure 43a). To test if higher levels of *pif1-m2* mRNA could increase nuclear levels of functional Pif1 and aggravate the phenotype of *dna2*Δ *pif1-m2* strains, we decided to place *pif1-m2* allele under the control of the constitutive *ADH1* promoter. Tetrad analysis of *DNA2/dna2*Δ *pif1-m2/*P_{ADH1}*-pif1-m2* heterozygous diploids showed that replacement of the endogenous *pif1-m2* promoter with the constitutive *ADH1* promoter is sufficient to restore *dna2*Δ lethality, supporting the hypothesis that *pif1-m2* mRNA can still produce functional nuclear Pif1 (Figure 43b).

Interestingly, the synthetic lethality observed between *pif1*Δ and *top3*Δ (Wagner et al., 2006) is fully recapitulated by *pif1-m2*, but not *pif1-m1* (Figure 43c). Following the same rationale, lethality of *pif1-m2 top3*Δ strains suggests that nuclear levels of Pif1 in *pif1-m2* cells are insufficient to support viability of *top3*Δ mutans. Given that overexpression of *PIF1* ameliorates the slow growth of *top3*Δ strains (Wagner et al., 2006), we took advantage again of P_{ADH1}*-pif1-m2* to test if increased levels of *pif1-m2* could support the growth of *top3*Δ strains. Unlike *pif1-m2,* P_{ADH1}*-pif1-m2* restored the viability of *top3*Δ strains (Figure 43d), confirming that some *pif1*Δ phenotypes can be reproduced in *pif1-m2* even in the presence of reduced nPif1 levels.

Finally, we addressed if the hypersensitivity to HU of *pif1*Δ *rad3-102* strains (a hypomorphic allele of the essential Rad3 helicase) could also be recapitulated in the *pif1-m1* or *pif1-m2* mutants (Moriel-Carretero and Aguilera, 2010) (Figure 43e). Like our own results with *pif1*Δ $YEN1^{ON}$*,* neither *pif1-m1* or *pif1-m2* exacerbated the mild sensitivity of *rad3-102* strains to HU. Altogether, these results demonstrate that the separation-of-function allele *pif1-m2* still retains an undetermined, but functionally significant, level of nuclear activity that can be sufficient to mask some of the phenotypes observed in the complete absence of *PIF1*. Importantly, for those

USC
DE SANTIAGO
DE COMPOSTELA

*pif1*Δ genetic interactions not recapitulated by *pif1-m1* or *pif1-m2*, such as *dia2*Δ and *rad3-102*, it cannot be formally disambiguated whether this is a consequence of the incomplete separation-of-function of *pif1-m2*, or whether such interactions require the simultaneous loss of nuclear and mitochondrial Pif1 isoforms.

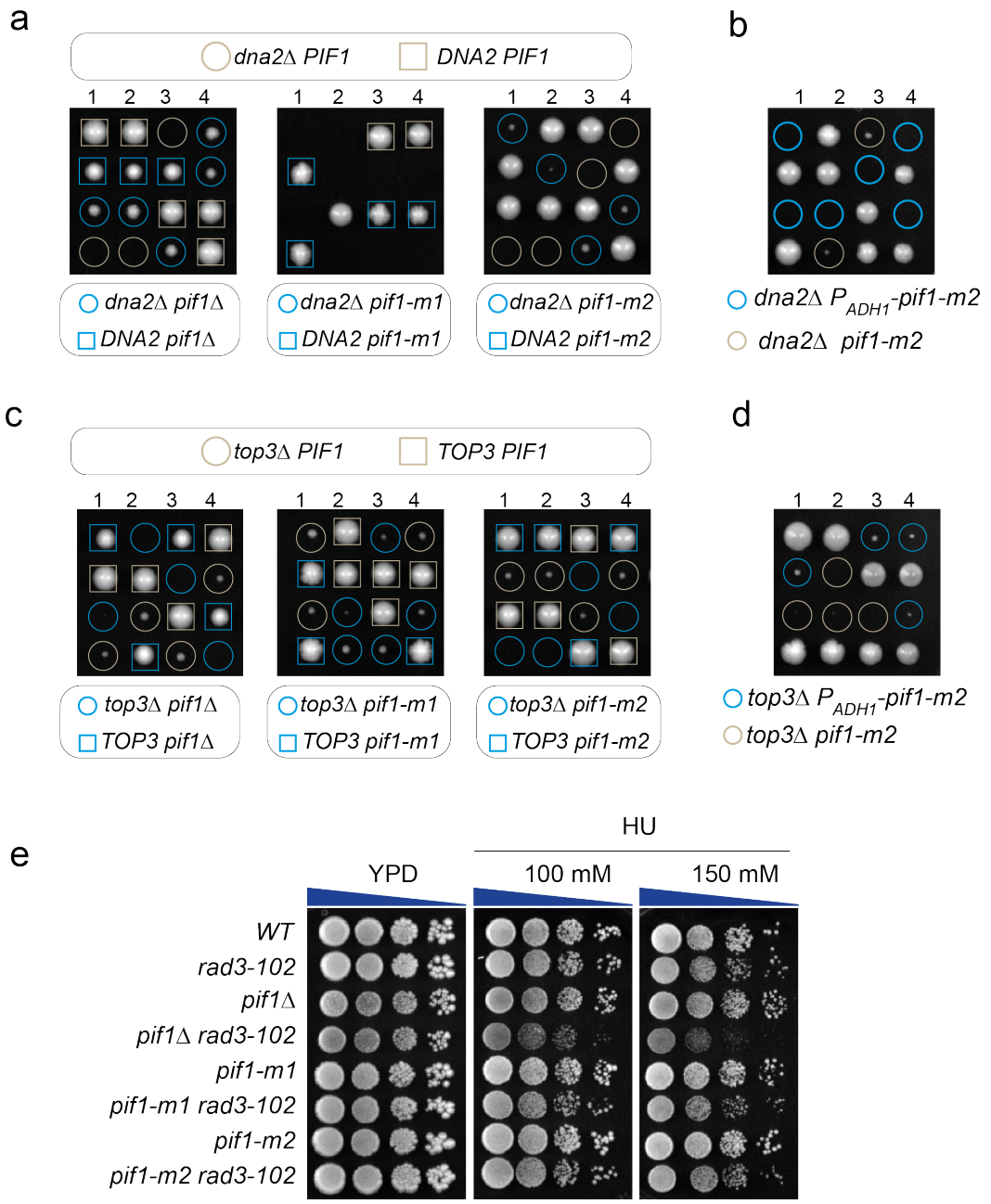


Figure 43. *pif1-m2* does not fully recapitulate *pif1Δ* genetic interactions with *dna2Δ* and *rad3-102*. (a) Tetrad microdissection of diploid strains carrying heterozygous mutations for the indicated wild-type and mutant alleles of *DNA2* and *PIF1*. **(b)** Same as (a), but employing the constitutively overexpressed allele P_{ADH1}-*pif1-m2*. **(c)** Tetrad microdissection of diploid strains carrying heterozygous mutations for the indicated wild-type and mutant alleles of *TOP3* and *PIF1*. **(d)** Same as (c), but employing the constitutively overexpressed allele P_{ADH1}-*pif1-m2* **(e)** Ten-fold serial dilutions of strains with the indicated genotypes were plated on YPD containing different concentrations of hydroxyurea (HU) and imaged after 2 days of incubation at 30 ºC.

2.2 A novel, fast-migrating isoform of Pif1 produced by alternative translation initiation

Although the presence of residual nuclear Pif1 in *pif1-m2* strains has been previously acknowledged, so far only one hypothesis to explain its source has been formally put forward, proposing that traces of mitochondrial Pif1 isoform could leak into the nucleus (Bochman et al., 2010). If a fraction of full-length Pif1 harbouring the MTS is imported into the nucleus, three isoforms should be detected in wild-type strains (mPif1 precursor, mPif1 and nPif1), and two in *pif1-m2* strains (mPif1 precursor, mPif1). However, in the few reports in which Pif1 isoforms have been electrophoretically separated, only two isoforms migrating as a tight doublet are detected in protein extracts from wild-type strains (mPif1 and nPif1), while a single band is observed in both *pif1-m1* (nPif1) and *pif1-m2* (mPif1) strains (Crider et al., 2012; Rossi et al., 2015; Vega et al., 2007). We envisage three hypothesis that could explain these results and still account for the presence of nuclear Pif1 activity in *pif1-m2* cells. First, the levels of mPif1 precursor may be too low to be detected by western blotting in wild-type cells, since full-length Pif1 has been only detected upon *GAL1* overexpression (Lahaye et al., 1993a). Second, an undetermined fraction of proteolytically cleaved mPif1 could return to the cytoplasm by reverse translocation, a process that has been already described for other yeast mitochondrial proteins, such as fumarase (Sass et al., 2003, 2001; Stein et al., 1994; Yogev et al., 2007); after reverse translocation, the lack of the MTS could facilitate the nuclear import of mPif1. Third, residual nuclear activity may stem from an alternative nuclear isoform that has not been previously detected. This isoform could either be constitutively expressed or induced in *pif1-m2* cells to compensate for the absence of nPif1.

To scrutinize these three possibilities, we C-terminally tagged endogenous *PIF1, pif1-m1* and *pif1-m2* with 6 copies of the flag epitope (6flag), and optimized our SDS-PAGE running conditions to achieve the separation between isoforms previously reported by (Vega et al., 2007). We noticed the presence of a mild, but specific, third band in all *PIF1* alleles displaying faster electrophoretic mobility than the nPif1/mPif1 doublet. Interestingly, this band is particularly enriched in strains harbouring the *pif1-m2* allele (Figure 44a). Therefore, we speculated that it could represent a different Pif1 isoform that accounts for the residual nuclear activity. We also confirmed that this fast-migrating band is not exclusive of the W303 background, since it can be also detected in YPH derivative strains (Figure 44b). Quantification by fluorescent western-blotting confirmed a significant enrichment of this fast-migrating band in *pif1-m2* cells, being over 3 times more abundant than in *PIF1* or *pif1-m1* cells and representing around 30% of total Pif1 (Figure 44c,d).

Among the three hypothesis presented above, this result is most compatible with the existence of an additional, uncharacterized nuclear isoform that is expressed at low levels in *PIF1* and *pif1-m1* cells, but induced in *pif1-m2* cells. Therefore, we investigated the origin of this potential isoform and tested if it could be responsible for the nuclear levels of Pif1 in *pif1-m2* strains. Since this novel isoform migrates faster than mPif1 and nPif1, we reasoned that it could arise from an additional alternative translation initiation (ATI) event downstream from AUG[40] (Figure 45a). Since the next in-frame AUG codon is located at position 107, we decided to

USC DE COMPOSTELA

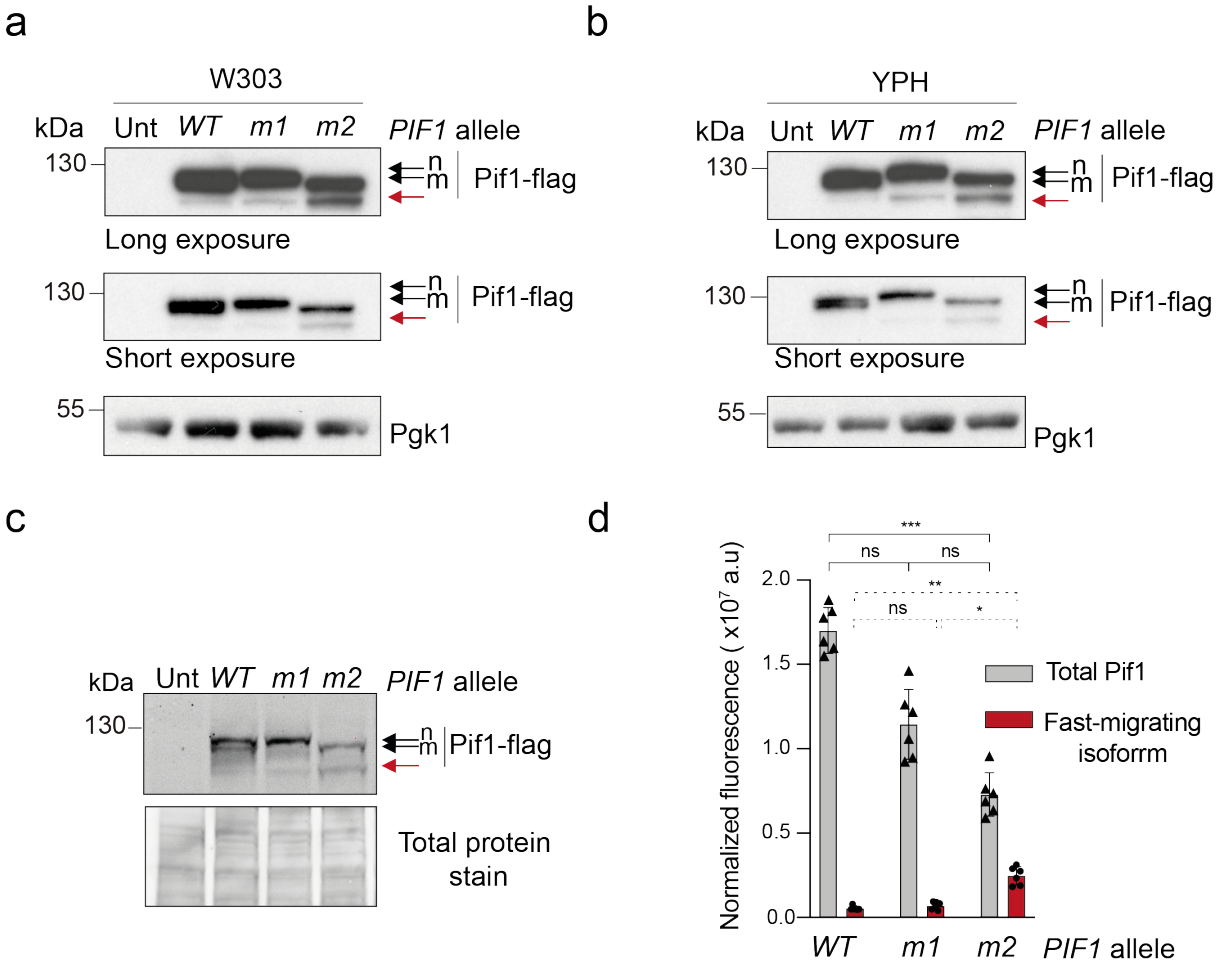


Figure 44. A fast-migrating isoform is enriched in *pif1-m2* mutants. (a) Protein extracts were prepared from untagged *PIF1* (Unt), *PIF1-6flag* (*WT*), *pif1-m1-6flag* (*m1*) and *pif1-m2-6flag* (*m2*) strains. Pif1-6flag isoforms were detected by western blotting. Black arrows mark the nuclear (n) and mitochondrial isoforms (m). Red arrows mark the fast-migrating isoform. Pgk1 was employed as a loading control. **(b)** As in (a), but with strains derived from the YPH background. **(c)** As in a (a), but employing fluorescent secondary antibodies to detect Pif1 isoforms and total protein stain as a loading control (*See materials and methods, 3.1.2.3*) for quantification purposes. **(d)** Quantification of the fluorescence corresponding to total Pif1 or the fast-migrating isoform in *PIF1-6flag, pif1-m1-6flag and pif1-m2-6flag* strains. Histograms represent mean values ± standard deviation (n = 6). Statistical analysis was performed using ANOVA Kruskal-Wallis test followed by Dunn's post hoc multiple comparison analysis. P-value represented by ns, *p<0.05, ** p<0.005, and *** p<0.005.

compare the migration of a Pif1$^{107-859}$ truncation and the fast-migrating isoform enriched in *pif1-m2* mutants. We started by cloning the C-terminally, 6flag-tagged versions of *PIF1*, *pif1-m1*, *pif1-m2* and the N-terminal truncation *pif1*$^{107-859}$ under the control of the *PIF1* promoter into pRSII406 vectors for integration at the *ura3-52* locus. We first compared the abundance of ectopically expressed Pif1 isoforms against their endogenously-tagged counterparts to validate our set-up and confirm similar expression levels (Figure 45b). Unless otherwise stated, all the integrative vectors used in this work were integrated in untagged *pif1-m2* strains to avoid the slow growth of *pif1*Δ mutants. We next employed this array of ectopically expressed *PIF1* alleles to contrast the electrophoretical migration of the novel isoform in *PIF1, pif1-m1* and *pi1f-m2* strains with the truncated Pif1$^{107-859}$ (Figure 45c). Indeed, Pif1$^{107-859}$ truncation co-

migrates with the fast-migrating isoform expressed in all *PIF1* alleles, strongly suggesting that alternative translation initiation from AUG^{107} may produce a previously undetected Pif1

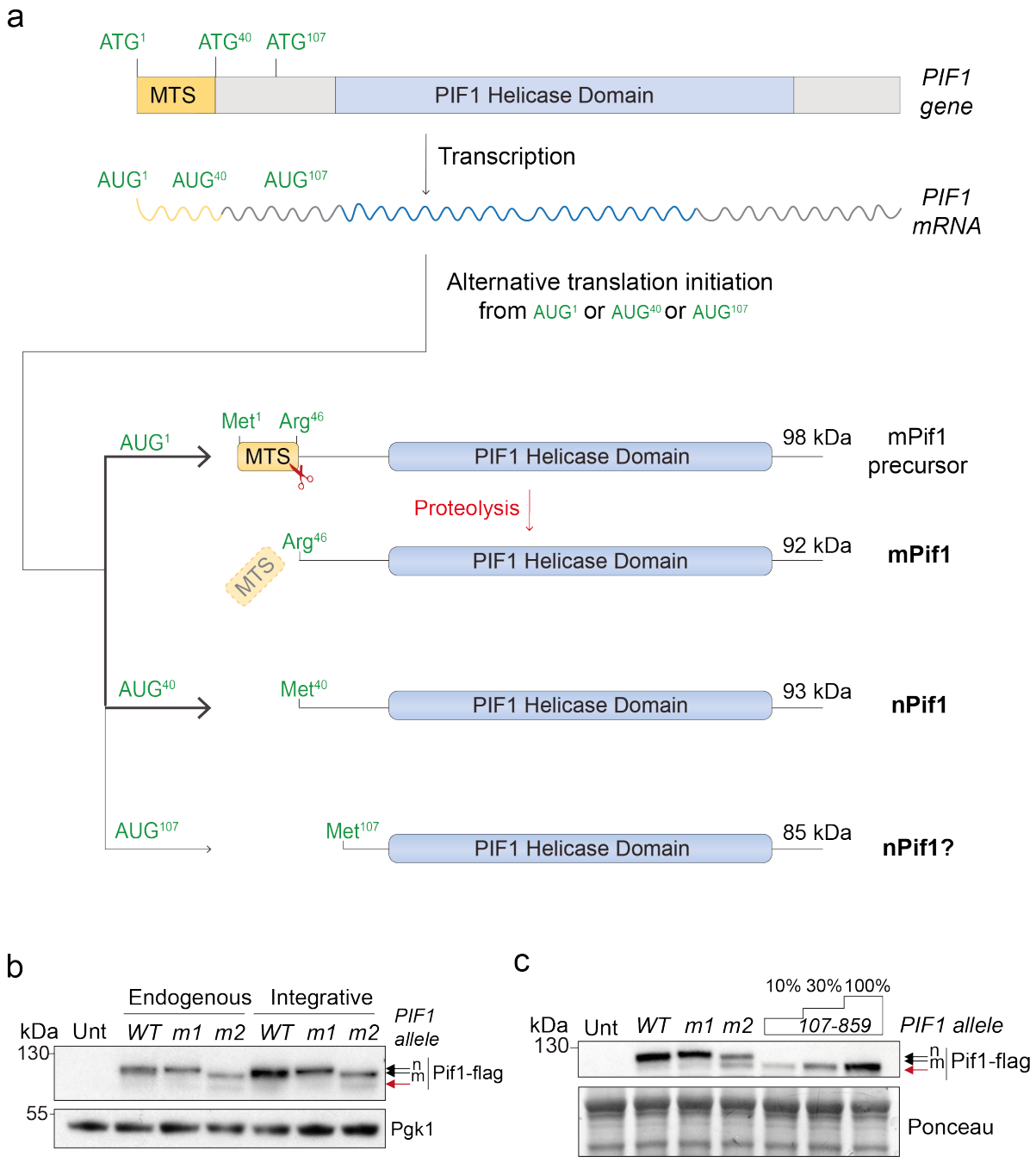


Figure 45. The fast-migrating Pif1 isoform could arise by ATI from downstream AUG codons. Schematic view of *PIF1* mRNA ATI, including the putative start site (AUG^{107}) for the fast-migrating isoform. **(b)** Western blot analysis of Pif1, comparing the expression levels of endogenously tagged strains with the ectopic expression of *PIF1* alleles cloned into integrative vectors under the control of their native *PIF1* promoter. Pgk1 was employed as a loading control. **(c)** Western blot analysis of ectopically expressed Pif1-6flag in strains with the indicated genotypes. To minimize variations in migration, different amounts of Pif1$^{107-859}$ protein extract were mixed with the protein extract of the untagged strain. PVDF membranes were stained with Ponceau as a loading control. Black arrows indicate the nPif1 and mPif1 isoforms. Red arrows indicate the fast-migrating isoform, which co-migrates with Pif1$^{107-859}$.

USC UNIVERSIDADE DE SANTIAGO DE COMPOSTELA

isoform. However, the underlying mechanism controlling start codon selection in *PIF1* mRNA, which could be relevant for the design of improved separation-of-function alleles, was still unknown.

2.3 Pif1 isoforms are produced through ribosomal leaky scanning

Translation involves four main steps: initiation, elongation, termination and recycling. Here, we will focus on the initiation step to investigate how different AUG codons are employed in order to produce three Pif1 isoforms from the same mRNA. During the canonical cap-dependent translation, eukaryotic initiation factors (eIFs) interact with the mRNA to initiate the process (Figure 46). In particular, one member of the eIF4F complex, eIF4E, recognizes the m^7G cap structure at the 5' end of the mRNA. Separately, the ternary complex comprising eIF2 complex, initiator tRNA, and GTP binds the 40S ribosomal subunit together with eIF3, forming the 43S pre-initiation complex (PIC). Next, the interaction between another member of the eIF4F complex (eIF4G) and eIF2 recruits the PIC to the 5'end of the mRNA (Hinnebusch, 2011;

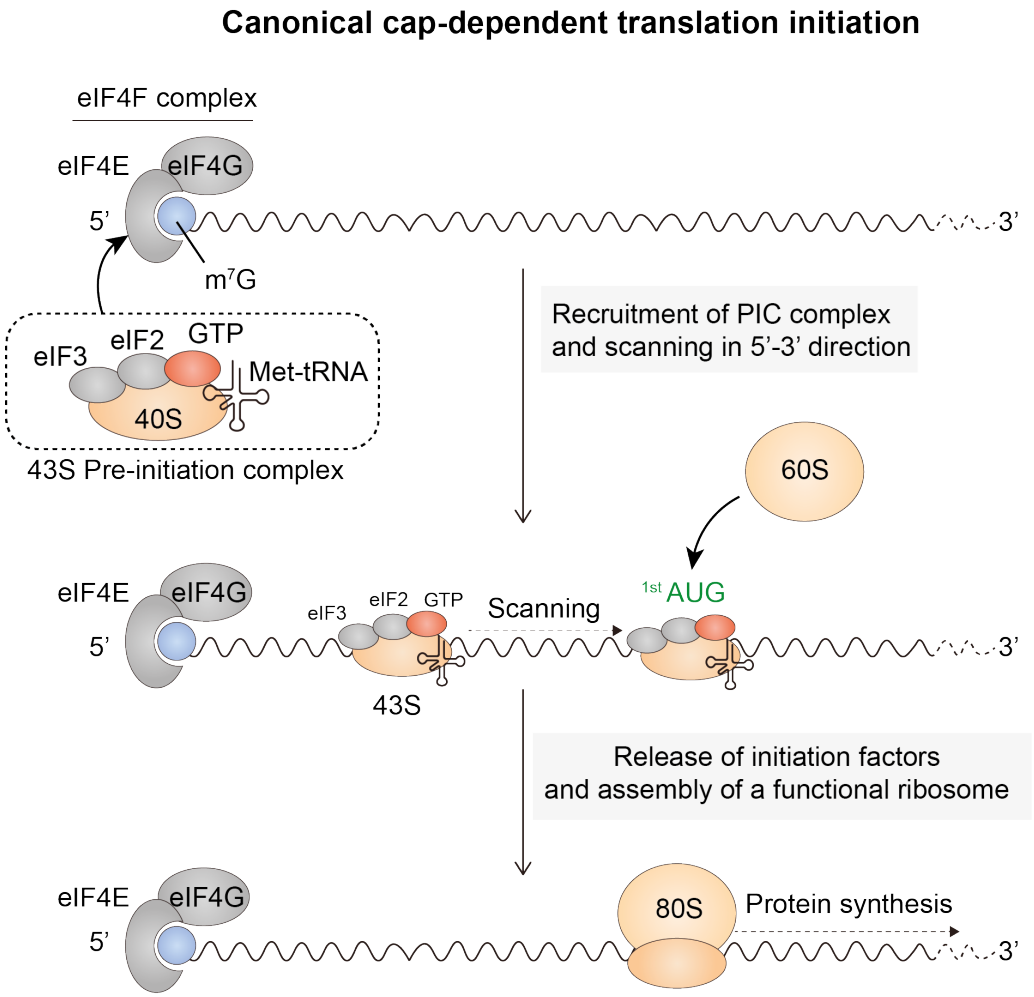


Figure 46. Schematic representation of canonical cap-dependent translation initiation. The eIF4F complex recognizes the m^7G cap and recruits the PIC to the 5' end of the mRNA. The PIC scans the mRNA in 5'-3' direction until the Met-tRNA recognizes the start codon, which promotes the assembly of the 60s subunit and beginning of protein synthesis.

Leppek et al., 2018). The scanning model postulates that the PIC moves along the mRNA in the 5'-3' direction, aided by ATP-powered helicases (Figure 46). Once the first AUG codon is encountered, the Met-tRNA pre-loaded in the PIC complex recognizes it and halts the scanning, leading to the release and recycling of eIF2 and other initiation factors. The dissociation of initiation factors allows the engagement of the 60S large ribosomal subunit with the remaining of the PIC complex, resulting in a functional ribosome ready for protein synthesis (Figure 46). The elongation phases proceed with the addition of codon-dependent amino acids to generate a polypeptide chain. Finally, during termination and recycling, the polypeptide is released and the ribosomes are dissociated from the mRNA.

Importantly, according to the "first-AUG rule" in the canonical cap-dependent mechanism, translation is initiated at the AUG codon closest to the 5' end of the mRNA (Kozak, 1989; Kozak and Shatkin, 1978). Nonetheless, various mechanisms of alternative translation initiation in eukaryotes enable novel initiation events to occur downstream of the first AUG (Figure 47), including reinitiation, ribosomal shunting, internal ribosomal entry sites (IRES), and ribosomal leaky scanning (Hinnebusch, 2011a; Sriram et al., 2018).

Reinitiation (Figure 47a) facilitates the translation of two or more consecutive open reading frames (ORF) from a single mRNA. It involves the recycling of the translational machinery upon termination of the upstream ORF (uORF) by reinitiation factors that allow the 40S subunit to remain bound to the mRNA and reacquire the initiator tRNA, thus resuming 5'-3' scanning and enabling the translation of the downstream ORF (Hinnebusch, 2011a; Sriram et al., 2018). In yeast, *GCN4* constitutes the best characterized example of how reinitiation operates to regulate protein expression. Reinitiation is generally inefficient, suggesting that uORFs are regulatory elements that limit production of the protein encoded by the downstream ORF. Consequently, this mechanism leads to the production of two different peptides, but it cannot generate two dual-targeted isoforms from a single mRNA that differ only in the N-terminal region.

Ribosome shunting is another cap-dependent translation mode initially discovered in viruses. The PIC complex is recruited to the mRNA in a cap-dependent manner and starts scanning in 5'-3' direction. Upon encountering a stem-loop structure (Figure 47b), the 40S subunit bypasses or shunts over the obstacle and lands at a downstream start codon to initiate translation (Kwan and Thompson, 2019; Sriram et al., 2018). Although ribosomal shunting is both rare and the less studied ATI mechanism in eukaryotic cells, it has been demonstrated that it can operate in budding yeast (Chappell et al., 2006)). However, we could not find any yeast mRNA that relies exclusively on this mechanism for the generation of alternative protein isoforms. Interestingly, ribosome shunting can be relevant in mRNAs with a short uORF, facilitating reinitiation by allowing the 40S subunit to shunt other short ORF or secondary structure to reinitiate at a downstream ORF. However, as a facilitator of reinitiation, ribosomal shunting raises the same caveats described above to produce dual targeted isoforms.

IRESs are RNA sequences that can recruit 40S ribosomal subunits internally to the mRNA, independently of the 5' cap-dependent initiation (Figure 47c). IRESs can be unstructured or contain stable secondary and tertiary structures, and their lengths vary from 9 to 1000 nt (Kwan

USC DE COMPOSTELA

and Thompson, 2019; Sriram et al., 2018). Like ribosome shunting, IRES were initially discovered in viruses, but they were also later identified in eukaryotic mRNAs (Johannes and Sarnow, 1998), where they mediate translation of different protein isoforms from important genes, such as *TP53* (Ray et al., 2006) or *DMD* (Wein et al., 2014). In Pif1, an IRES located between AUG^{1} and AUG^{40} might recruit 40S subunit to initiate the translation of the nuclear isoform at AUG^{40}, and mutation in *pif1-m2* could result in ribosome scanning until the next AUG. However, IRES are specially relevant upon situations of cellular stress when 5' cap-dependent translation is impaired; for example, in yeast, IRES are particularly relevant upon glucose starvation (Gilbert et al., 2007), whereas both Pif1 isoforms are constitutively produced in unperturbed conditions. Moreover the majority of experimentally validated IRES in yeast from IRESbase (Zhao et al., 2020) are longer than 150 bp, compared to the 114 bp between AUG^{1} and AUG^{40} in Pif1. Hence, it seems unlikely that an IRES is mediating isoform production in Pif1.

Finally, leaky scanning (Figure 47d) involves the ribosomal skipping of the first AUG codon and initiation of translation at a downstream, in-frame AUG codon (Kozak, 2002). In leaky scanning, the efficiency of any given AUG for translation initiation depends on the sequence context around this codon, commonly known as the Kozak sequence. Interestingly, the AUG^{1} in *PIF1* mRNA is flanked by a suboptimal Kozak sequence, which would increase the probability of the ribosome to bypass AUG^{1} (that produces mPif1) and reach AUG^{40} to start the translation of nPif1. Moreover, the context around AUG^{40} is also suboptimal, which suggests that another event of leaky scanning might allow a minor fraction of scanning ribosomes to reach AUG^{107}. This scenario seems both compatible with the low amounts of $Pif1^{107\text{-}859}$ produced in *PIF1* and *pif1-m1* cells and with the selective enrichment of this isoform in *pif1-m2* cells due to mutation of AUG^{40} (Figures 44 and 45). Therefore, we decided to investigate if indeed a leaky scanning mechanism is regulating the abundance of Pif1 isoforms.

In addition to AUG^{107}, there are other four in-frame AUG codons downstream AUG^{40} and upstream the Pif1 helicase domain, which begins at Phe^{255}. The first cluster would include AUG^{107} itself, together with AUG^{113} and AUG^{127}, while the second one comprises AUG^{187} and AUG^{196}. Initiation of translation from any of these positions would result in a Pif1 isoform that retains an intact helicase domain (Figure 48a). Given the also suboptimal Kozak context of AUG^{107} and the proximity of downstream codons, we cannot rule out that a fraction of scanning ribosomes could also skip AUG^{107} and reach AUG^{113}, specially in *pif1-m2* cells. Importantly, as we aim to improve the *pif1-m2* allele, the scanning model predicts that mutation of ATG^{107} in the *pif1-m2* would result in ATI from the next downstream AUG.

To test the leaky scanning model, we took two complementary approaches. First, we ectopically expressed *PIF1* alleles with single conservative methionine-to-isoleucine mutations at positions 107, 113, 127, 187 and 196 and determined whether the expression of the fast-migrating isoform was affected, but none of these single mutations eliminated the fast-migrating band (Figure 48b). This could be coherent with the proposed model of leaky scanning, as mutations in a given AUG would simply enable the scanning ribosomes to reach the next downstream

USC UNIVERSIDADE DE SANTIAGO DE COMPOSTELA

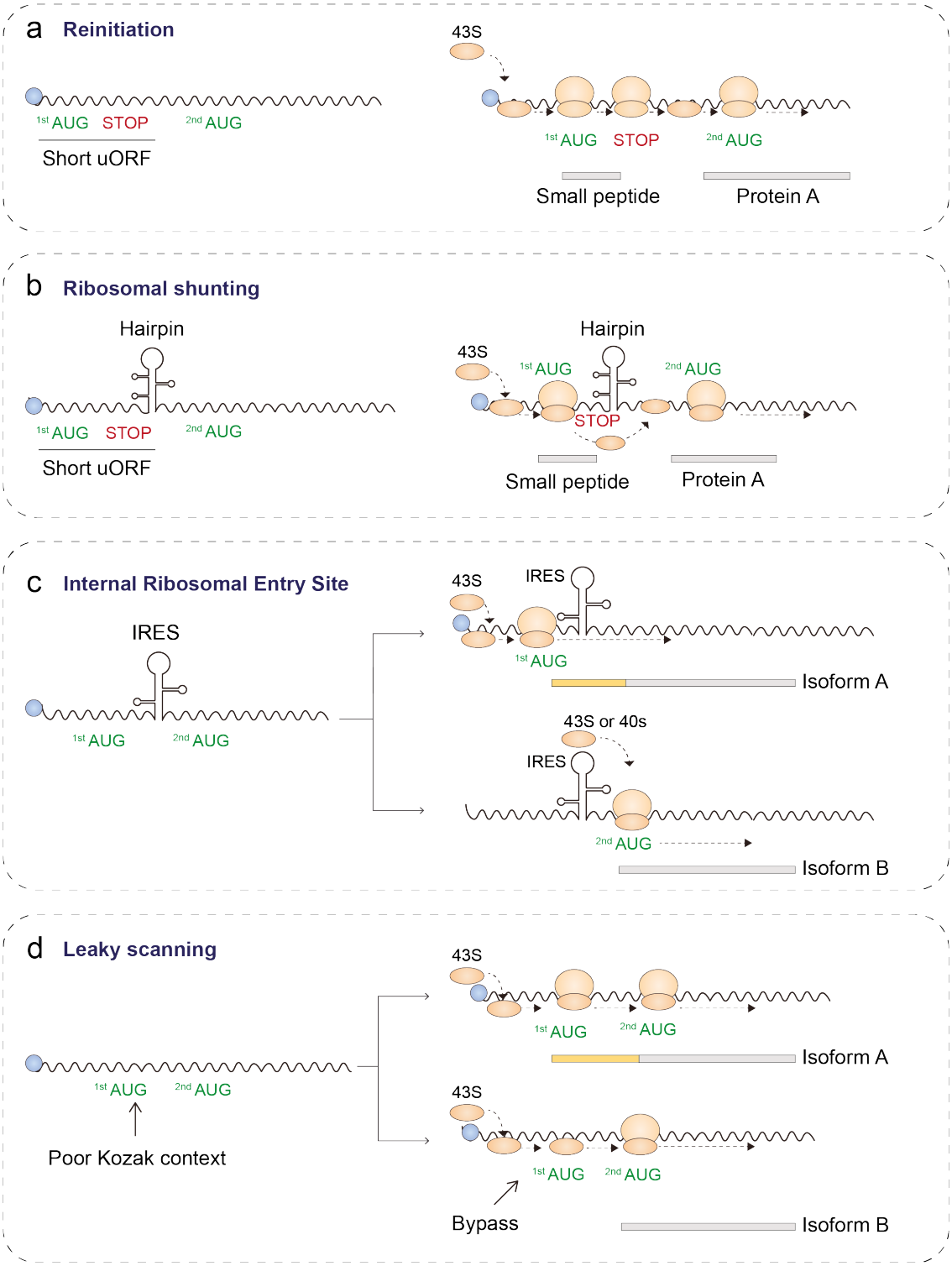


Figure 47. Schematic overview of the main mechanisms of ATI from different AUGs. (a) Reinitiation after translation of the uORF creates two different peptides. **(b)** Shunting of the 40S subunit upon encountering a stable secondary structure can favour translation reinitiation at a distant downstream AUG. **(c)** An IRES located between the first two AUGs could lead to the production of two isoforms. Translation from the first AUG would produce a full-length isoform, whereas the IRES could recruit 40S subunits to the downstream AUG, producing shorter isoforms lacking N-terminal regions that could contain targeting sequences or other functional domains. **(d)** In leaky scanning, the suboptimal context surrounding the first AUG allows a fraction of ribosomes to skip it and continue scanning until a downstream AUG is reached, generating an N-terminal truncated isoform. Alternatively, some ribosomes start translation even in the presence of a poor Kozak sequence, producing the full-length isoform.

methionine. In contrast, double Met-to-Ile substitutions in the first cluster revealed both changes in the relative amounts and mobility of the fast-migrating band, demonstrating that translation initiation may occur from any of these AUGs, albeit M107 appears as the most relevant, followed by M113 (Figure 48c). Crucially, the fast-migrating band became undetectable when these three methionines were simultaneously mutated, without further detection of smaller bands (Figure 48d). Therefore, the amount of scanning ribosomes reaching AUG^{187} or AUG^{196} in the triple mutant is not enough to produce a detectable band, in accordance with the reported decay of ribosomes after scanning ~150 triplets (Chappell et al., 2006). These results confirm the existence of, at least, a third cellular Pif1 isoform that is translated from M107 (hereinafter, Pif1$^{107\text{-}859}$) and demonstrate that M113 and M127 can also function as alternative starting points upon mutation of upstream start codons.

To verify that Pif1 translation is specifically under the control of a leaky scanning mechanism, we mutated the sequences surrounding the AUG^{1} and AUG^{40} codons to match the best Kozak consensus sequence in *S. cerevisiae* (Figure 49a). According to the leaky scanning model, improving the Kozak context should reduce the ribosomal skipping of AUG^{40}, and, as a consequence, the translation of Pif1$^{107\text{-}859}$. We mutated the Kozak contexts around AUG^{1} in *PIF1* or AUG^{40} in both *PIF1* and *pif1-m1*. For AUG^{1}, we only optimized the upstream nucleotides at the highly conserved -4, -3 and -2 positions (Hamilton et al., 1987; Hernández et al., 2019), but we did not mutate the +4 residue since there is no conservative change for proline.

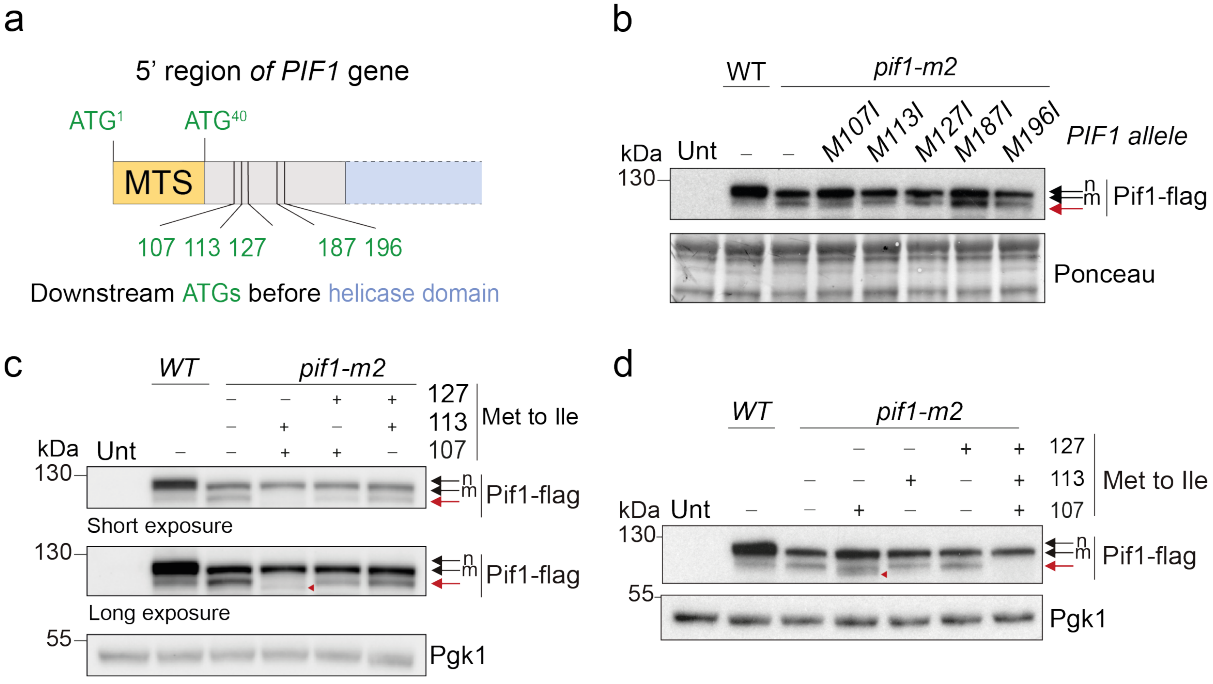


Figure 48. ATI can initiate translation from a cluster of ATGs downstream ATG40. (a) Schematic representation of the 5' region of *PIF1*, depicting the ATGs before the helicase domain, whose expression could give rise to N-terminal truncated -but still catalytically active- isoforms. **(b,c,d)** Western blot analyses of the changes in the abundance and electrophoretic mobility of the fast-migrating isoform in single **(b)**, double **(c)** and triple **(d)** mutants of downstream methionines to isoleucines. Protein extracts were prepared from strains ectopically expressing different variants of *pif1-m2* with the indicated Met to Ile substitutions. Red arrowheads in (c) and (d) point to changes in the electrophoretic mobility of the fast-migrating isoform.

UNIVERSIDADE DE SANTIAGO DE COMPOSTELA

With respect to AUG^{40}, we designed synonymous changes in its two surrounding amino acids to match the Kozak consensus in the two key positions -3 and +4. Next, we ectopically expressed these *PIF1* and *pif1-m1* alleles and verified the expression of Pif1$^{107-859}$ by western-blotting. Confirming our hypothesis, Pif1$^{107-859}$ could not be detected in those cells harboring constructs with optimal Kozak contexts at AUG^{40} (Figure 49b). Also, optimization of AUG^{1} in *PIF1* cells produced an apparent increase in mobility of the Pif1 doublet that would be consistent with increased proportion of mPif1 over nPif1. Overall, our data demonstrate that the mechanism controlling the alternative translation of Pif1 isoforms is ribosomal leaky scanning.

2.4 Pif1$^{107-859}$ is catalytically active and retains partial functionality in the nucleus.

After identifying the underlying mechanism of ATI in *PIF1*, we investigated if the increased abundance of Pif1$^{107-859}$ accounts for residual Pif1 activity described for *pif1-m2*. Although the NTD is dispensable for Pif1 activity, its *in vivo* roles may be affected by an N-terminal truncation, given that the NTD, in addition to containing Pif1 MTS, is post-translationally modified to control Pif1 nuclear activities (Ononye et al., 2020; Rossi et al., 2015). Consistent with the lack of MTS, cells harbouring exclusively the *pif1$^{107-859}$* allele display a *petite* phenotype and are unable to grow on non-fermentable carbon sources (Figure 50a). Moreover, we integrated fusion constructs with various *PIF1-eGFP* alleles under the control of the inducible *GAL1* promoter in a strain with endogenous, untagged *pif1-m2,* to assess the subcellular localization of *pif1$^{107-859}$* by fluorescence microscopy. *pif1-m1* and *pif1-m2* were employed as controls for nuclear and mitochondrial localization, respectively. As expected, Pif1-eGFP signal could be detected both in the nucleus and mitochondria in *PIF1* cells, while in those with *pif1-m1* or *pif1$^{107-859}$* a clear nuclear enrichment was observed, confirming that nuclear localization is not impaired in *pif1$^{107-859}$* (Figure 50b). In agreement with the presence

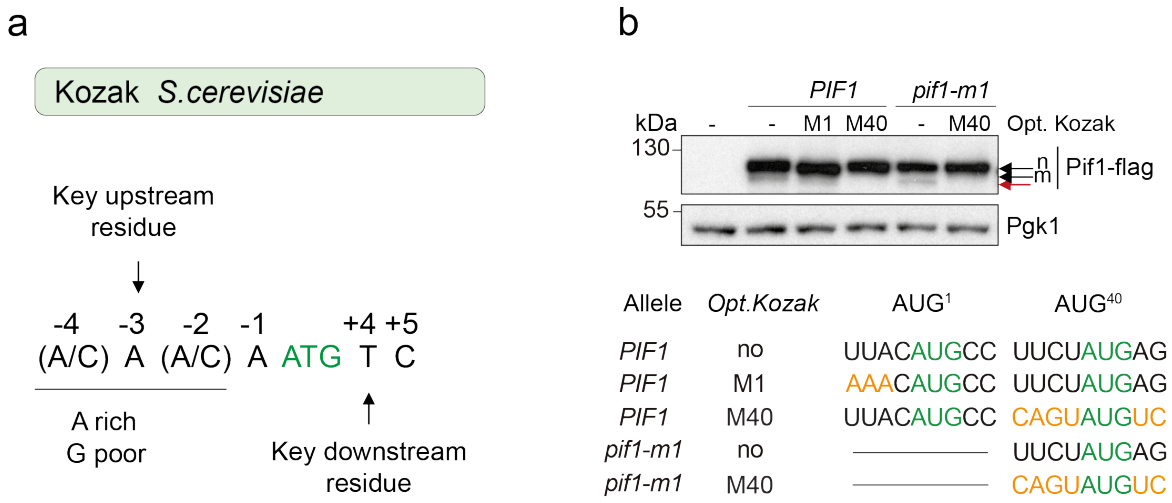


Figure 49. Optimization of Kozak context surrounding AUG^{40} abrogates the expression of the fast-migrating isoform. (a) Kozak consensus sequence in *S. cerevisiae* according to Hamilton et al.,1987 **(b)** Changes in the expression of Pif1$^{107-859}$ (red arrow) in *PIF1* and *pif1-m1* strains with improved Kozak sequences were assayed by western blotting, as described for previous Figures. The specific mutations introduced to optimize the Kozak context of AUG^{1} and AUG^{40} are shown in yellow.

of increased levels of Pif1$^{107-859}$ in *pif1-m2* strains, these mutants displayed a mild accumulation of nuclear Pif1, in addition to the predicted mitochondrial localization (Figure 50b).

Next, we investigated if the cause of the incomplete separation of function in *pif1-m2* alleles is due to the increased levels of nuclear Pif1$^{107-859}$. Since its NTD is relevant for Pif1 function in different contexts, we first decided determined the biological functionality of Pif1$^{107-859}$ using

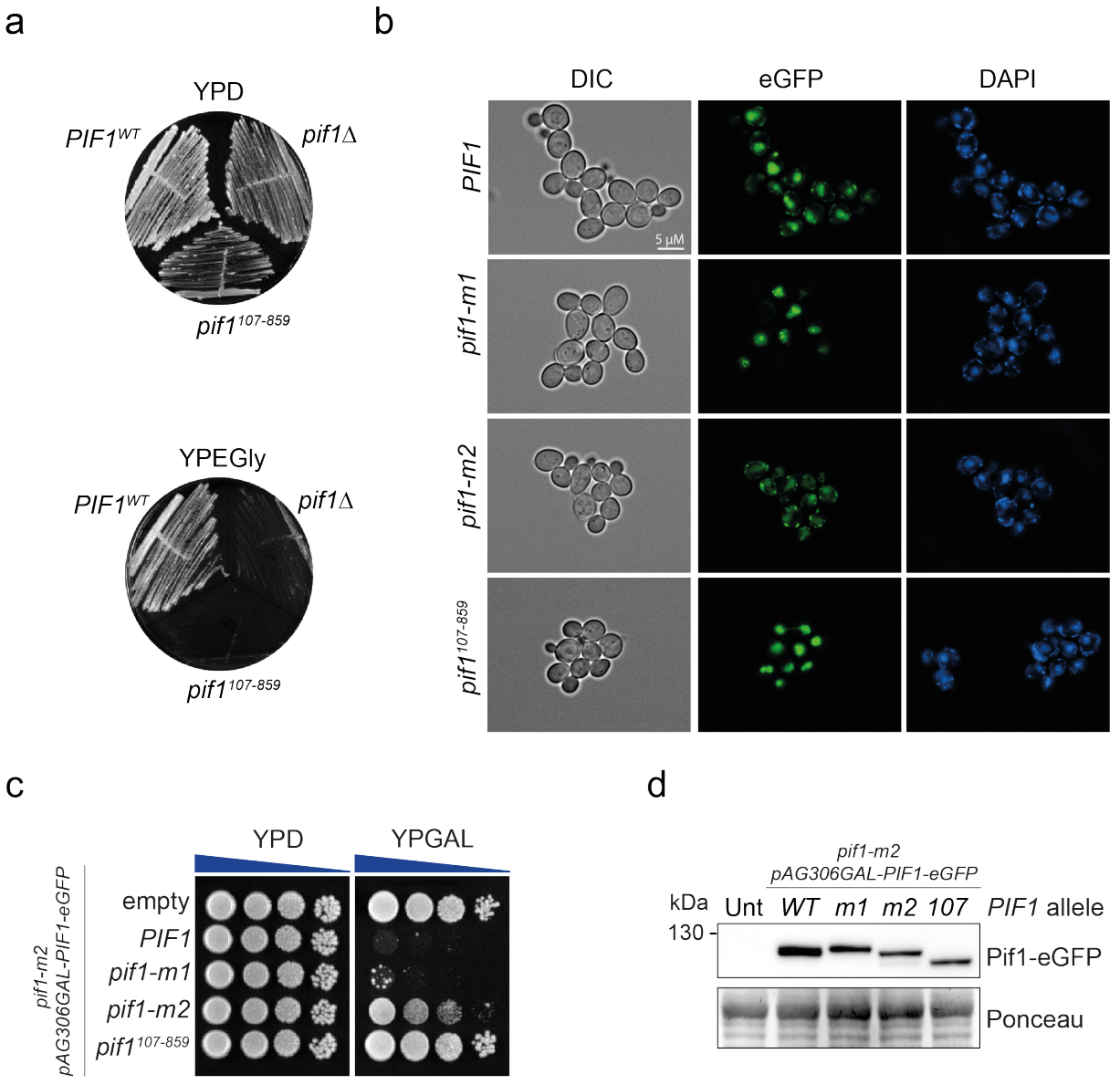


Figure 50. *In vivo* characterization of Pif1$^{107-859}$ localization, mitochondrial functionality, and toxicity by overexpression. (a) The indicated strains were streaked and examined for growth on solid medium containing fermentable (YPD, 2% glucose) or non-fermentable carbon sources (YPEGly, 3% ethanol, 3% glycerol). Pictures were taken after 4 days at 30 ºC. **(b)** Subcellular localization of Pif1 isoforms in live yeast cells overexpressing different *PIF1-eGFP* alleles. DNA was visualized with DAPI staining and cell contour by DIC microscopy. **(c)** Ten-fold dilutions of strains with the indicated genotypes were plated on YPD or YPGAL plates and imaged after 2 days of incubation at 30 ºC. **(d)** Abundance of Pif1 isoforms in the strains from (c) was compared by western blotting using anti-GFP antibodies. Protein extracts were prepared from liquid cultures grown in YPRaff and induced for 3 h by addition of 2% galactose. Ponceau staining of the PVDF membrane was used as a loading control.

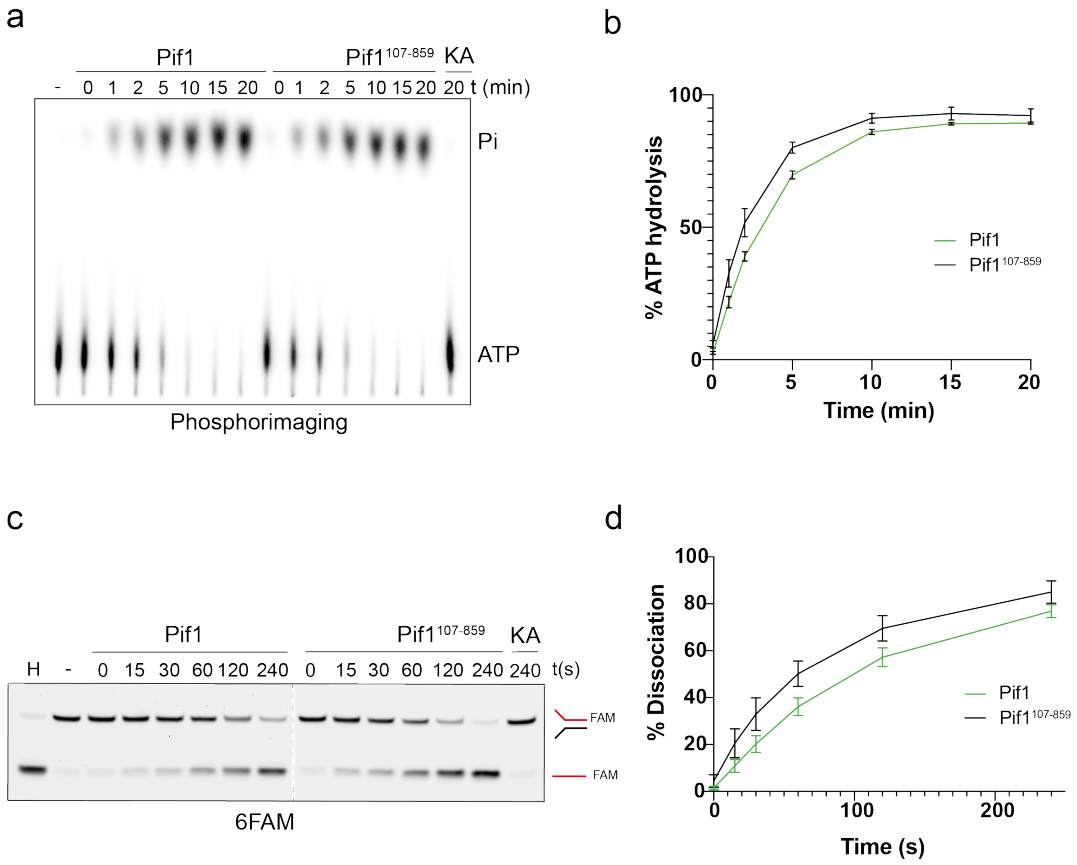


Figure 51. Functional characterization of purified Pif1$^{107-859}$. a) ATP hydrolysis by Pif1 and Pif1$^{107-859}$ was measured by TLC and phosphorimaging. The catalytically inactive Pif1^{KA} mutant was employed as a negative control. **(b)** Quantification of ATPase activity assays as displayed in (a). Data are represented as mean values ± standard deviation (n = 3). **(c)** Native PAGE analysis of the unwinding of a 5'-6FAM-splayed arm substrate by Pif1 and Pif1$^{107-859}$, using Pif1^{KA} as a negative control. Gels were scanned for 6FAM signal in a Typhoon FLA 9500. **(d)** Quantification DNA unwinding activity as displayed in (c). Data are represented as mean values ± standard deviation (n = 3). H, heat-denatured substrate. (-), no enzyme. Dashed line indicates splices lanes from the same gel.

as a proxy the lethality caused by the overexpression of nuclear Pif1 (Chang et al., 2009; Lahaye et al., 1991; Ononye et al., 2020). For that, we employed the same *P$_{GAL1}$-PIF1-eGFP* expressing constructs to assess cell viability under overexpression conditions of different *PIF1* alleles in galactose-containing medium. While the overexpression of *PIF1* or *pif1-m1* derived in extensive cell death, overexpression of *pif1*$^{107-859}$ caused no detectable reduction in cell viability when compared to an empty vector (Figure 50c), despite their comparable protein levels (Figure 50d).

Since the lack of toxicity of the overexpression of Pif1$^{107-859}$ could be indicative of a loss of function of this isoform, we decided to analyse its catalytic activity *in vitro*. For this purpose, we expressed Pif1, Pif1$^{107-859}$ and the catalytically inactive Pif1^{KA} (Zhou, 2000b) as N-terminally 6His-tagged fusion proteins in *E. coli* and purified them to compare their ATPase and helicase activities. ATP hydrolysis time-courses with the three Pif1 variants were analysed by thin-layer chromatography (TLC) and phosphorimaging to detect radioactively labelled ATP or free inorganic phosphate (Figure 51a,b). Helicase activity was measured by strand

USC UNIVERSIDADE DE SANTIAGO DE COMPOSTELA

displacement assays with fluorescently labelled splayed-arm substrates (Figure 51c,d). Pif1$^{107-859}$ displayed at least comparable (or higher) catalytic activity to Pif1 in both ATPase (Figure 51b) and helicase assays (Figure 51d), confirming that this isoform is fully functional *in vitro*.

Given these results, we next addressed if Pif1$^{107-859}$ could substitute for nPif1 specifically in those genetic interactions where the *pif1-m2* allele did not recapitulate the *pif1*Δ phenotypes (Figure 42 and Figure 43). We included *pif1-m1* as a control of Pif1 nuclear activity since the *petite* phenotype of cells harboring *pif1*$^{107-859}$ complicates its comparison with nPif1 expressed from *PIF1*. First, tetrad dissection analyses showed that *dia2*Δ *pif1*$^{107-859}$ mutants displayed reduced synthetic sickness compared to *dia2*Δ *pif1*Δ mutants, indicating that Pif1$^{107-859}$ can support cell growth similarly to Pif1 in *dia2*Δ mutants (Figure 52a). Second, compared to the lethality of *dna2*Δ in *PIF1* and *pif1-m1* strains, *dna2*Δ *pif1*$^{107-859}$ mutants are able to grow. However, they form smaller colonies than *dna2*Δ *pif1*Δ mutants, indicating that in this context Pif1$^{107-859}$ is partially functional (Figure 52b). Third, *top3*Δ *pif1*$^{107-859}$ strains failed to grow after tetrad dissection, similarly to *top3*Δ *pif1*Δ strains, suggesting that Pif1$^{107-859}$ cannot substitute for Pif1 in these conditions (Figure 52c). Finally, *pif1*$^{107-859}$ could not reduce the hypersensitivity to HU observed in *rad3-102 pif1*Δ mutants, unlike *pif1-m1* (Figure 52d). Therefore, *pif1*$^{107-859}$ resembles *pif1-m2* in *dia2*Δ, *top3*Δ and *dna2*Δ mutants, confirming that

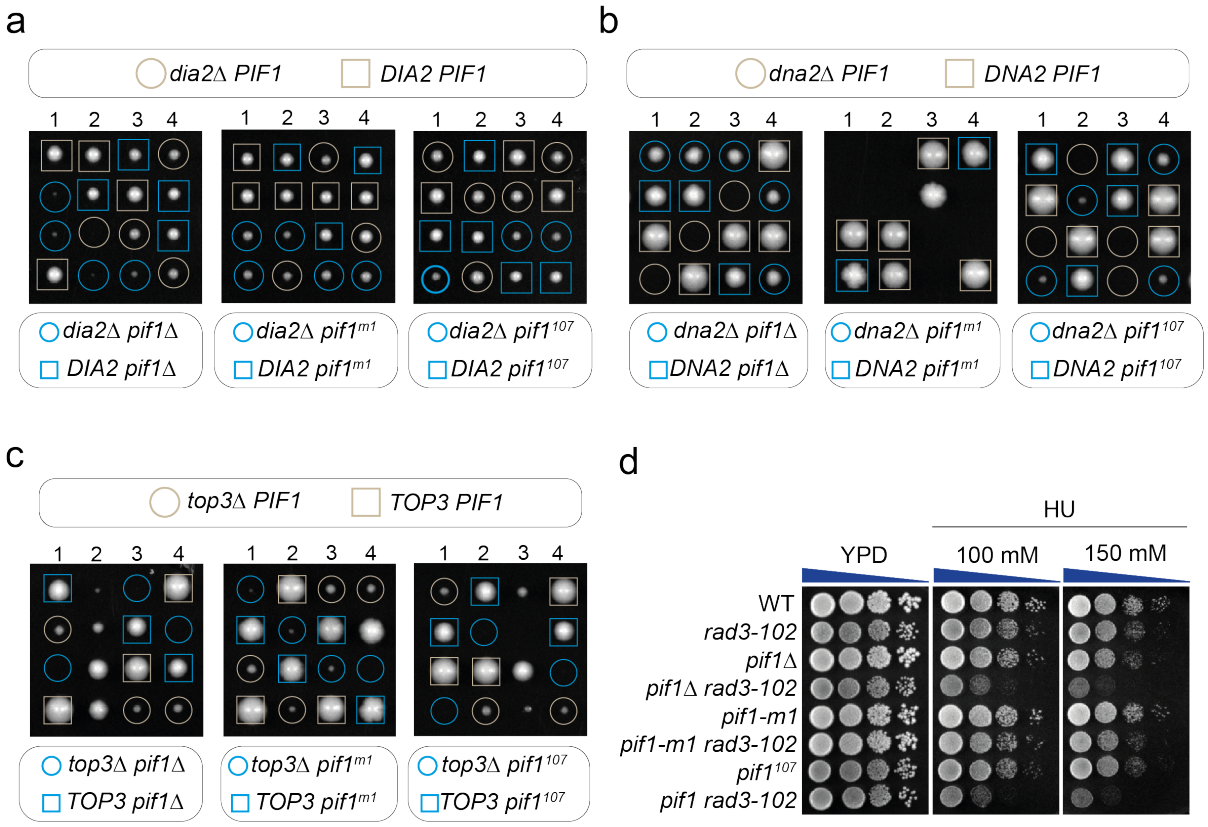


Figure 52. *In vivo* characterization of *pif1*$^{107-859}$. For simplicity, *pif1*$^{107-859}$ is labelled as *pif1*^{107}. Microdissection of diploid strains carrying heterozygous mutations for the indicated wild-type and mutant alleles of *PIF1* and **(a)** *DIA2*, **(b)** *DNA2* or **(c)** *TOP3*. Plates were incubated at 30 ºC for 2 days (a) or 4 days (b) and (c). **(d)** Ten-fold dilutions of strains with the indicated genotypes were plated in YPD with different HU concentrations, incubated for 2 days at 30 ºC and photographed.

the increased level of this isoform impinges on the separation of function of *pif1-m2* alleles. In contrast, the hypersensitivity of *pif1*$^{107-859}$ *rad3-102* strains to HU is difficult to explain with our current model, in which the nuclear levels of Pif1$^{107-859}$ in *pif1-m2* should derive in mild to complete suppression of *pif1*Δ phenotype. The failure of our model to explain this result led us to explore different possibilities for this particular interaction, as described in section 2.7.

Taken together, our data indicate that in *pif1-m2* mutants there is an increase in the translation of the partially functional Pif1$^{107-859}$ isoform, which is able to enter the nucleus and fulfil some of the roles of nuclear Pif1.

2.5 Identification of the nuclear localization signal in Pif1

Once we have shown that alternative nuclear Pif1 isoforms may lead to the misinterpretation of genetic results obtained with the classical *pif1-m2* allele, we reasoned that a better separation-of-function allele could be attained by blocking the nuclear import of all isoforms. Since the upper limit of protein diffusion through the nuclear pore complex is around 60 kDa (Wang and Brattain, 2007), the size of Pif1 suggests that it should contain an NLS that has not been identified so far. To begin with, we employed an *in-silico* analysis to search for potential NLSs in the Pif1 sequence. In addition, we also performed two extra *in silico* analyses, PSIPRED (Buchan and Jones, 2019; McGuffin et al., 2000) (data not shown) and DISOPRED (Ward et al., 2004) to obtain a structural profile of Pif1 (Figure 53a). The intrinsic disordered profile obtained with DISOPRED predicts three unstructured regions, including both the NTD and the CTD, as well as a sharp peak centered around position 600, in thePif1 helicase domain (Figure 53a). Given that the NLSs mediates nuclear import through karyopherins, they tend to locate in the surface of the protein at disordered regions. Therefore, we combined the information of DISOPRED and NLS mappers to filter different putative NLSs, selecting four for further analysis (Figure 53b): two located at the CTD and two around the most disordered region inside the helicase domain (Figure 53c). Next, we deleted in our P_{GAL}-*PIF1-eGFP* vectors regions encompassing those putative NLSs, employing the structural information of PSIPRED to minimally disrupt the secondary structure of each region, thus reducing the probabilities to generate complete loss-of-function mutants (Figure 53d).

As a first approach to test their functionality, we took advantage again of the lethality of P_{GAL1}-*PIF1* overexpression, which is mostly linked to aberrant increases in the nuclear isoform. Therefore, blocking Pif1 nuclear import should preserve cell viability in this assay. We observed that overexpression of *pif1*$^{\Delta 814-834}$ is as deleterious as that of *PIF1* and *pif1-m1*, whereas the absence of the 623-646 region only slightly alleviates the lethality of Pif1 overexpression. Interestingly, two different alleles (*pif1*$^{\Delta 650-663}$ and *pif1*$^{\Delta 775-803}$) resulted in a marked increase in survival compared to *PIF1*, *pif1-m1* and even *pif1-m2* (Figure 54a). These differences in cell viability are not likely due to gross variations in the expression of each

USC UNIVERSIDADE DE SANTIAGO DE COMPOSTELA

mutant, given their comparable levels (Figure 54b). As none of the tools detected a bipartite signal comprising those two regions, we decided to analyse the subcellular localization by fluorescence microscopy of these *PIF1* variants. Only deletion of the 775-803 region resulted in loss of nuclear accumulation of Pif1 with a concomitant increase in cytoplasmic signal, consistently with the disruption of a functional NLS (Figure 54c). These results indicate that

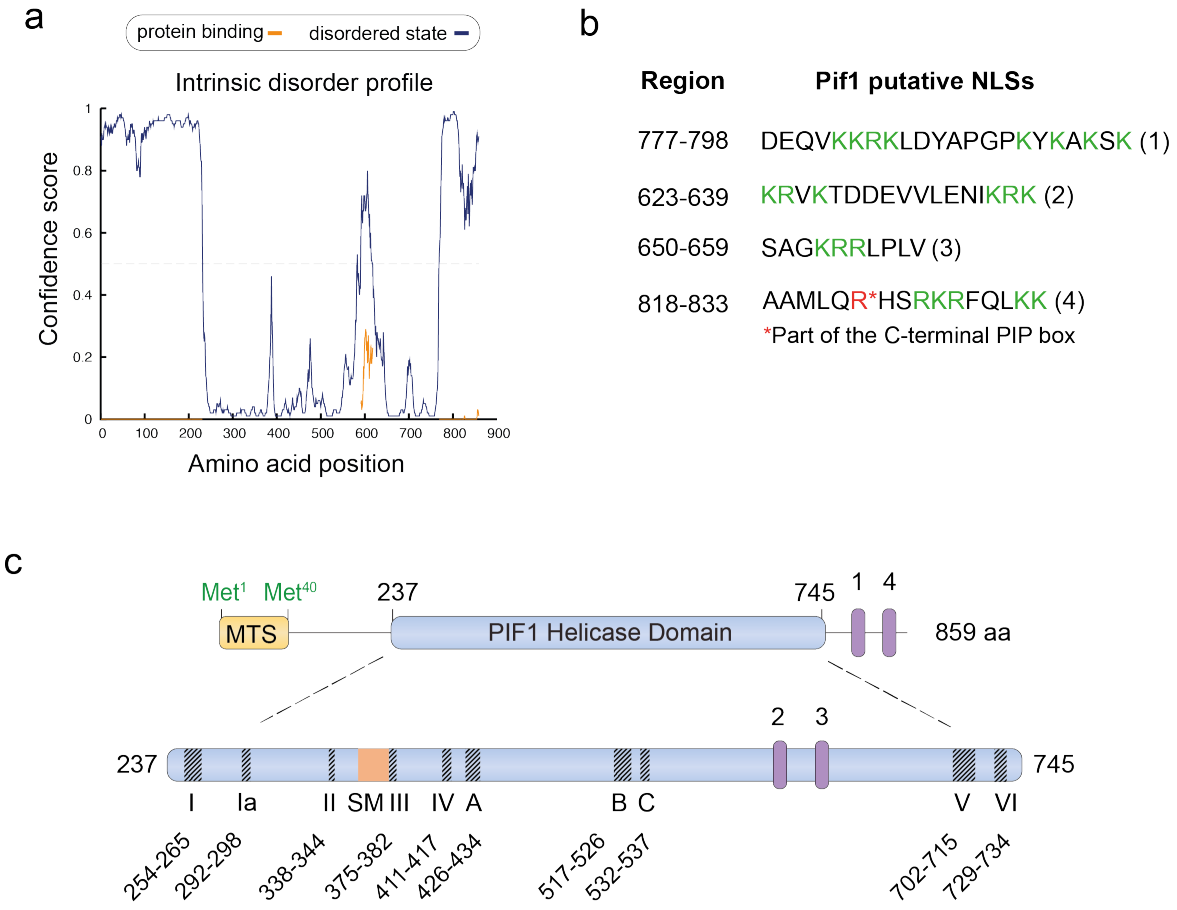


Figure 53. Putative NLS in Pif1. (a) Disorder profile of Pif1 obtained with DISOPRED3. **(b)** Putative NLS sequences selected according to *in silico* analyses. **(c)** Schematic representation of Pif1 depicting the localization of the four candidate NLSs (purple) relative to the helicase domain (blue) and the conserved SFB motifs (shaded boxes). **(d)** *PIF1* alleles with different deleted regions employed in the analysis of Pif1 nuclear import.

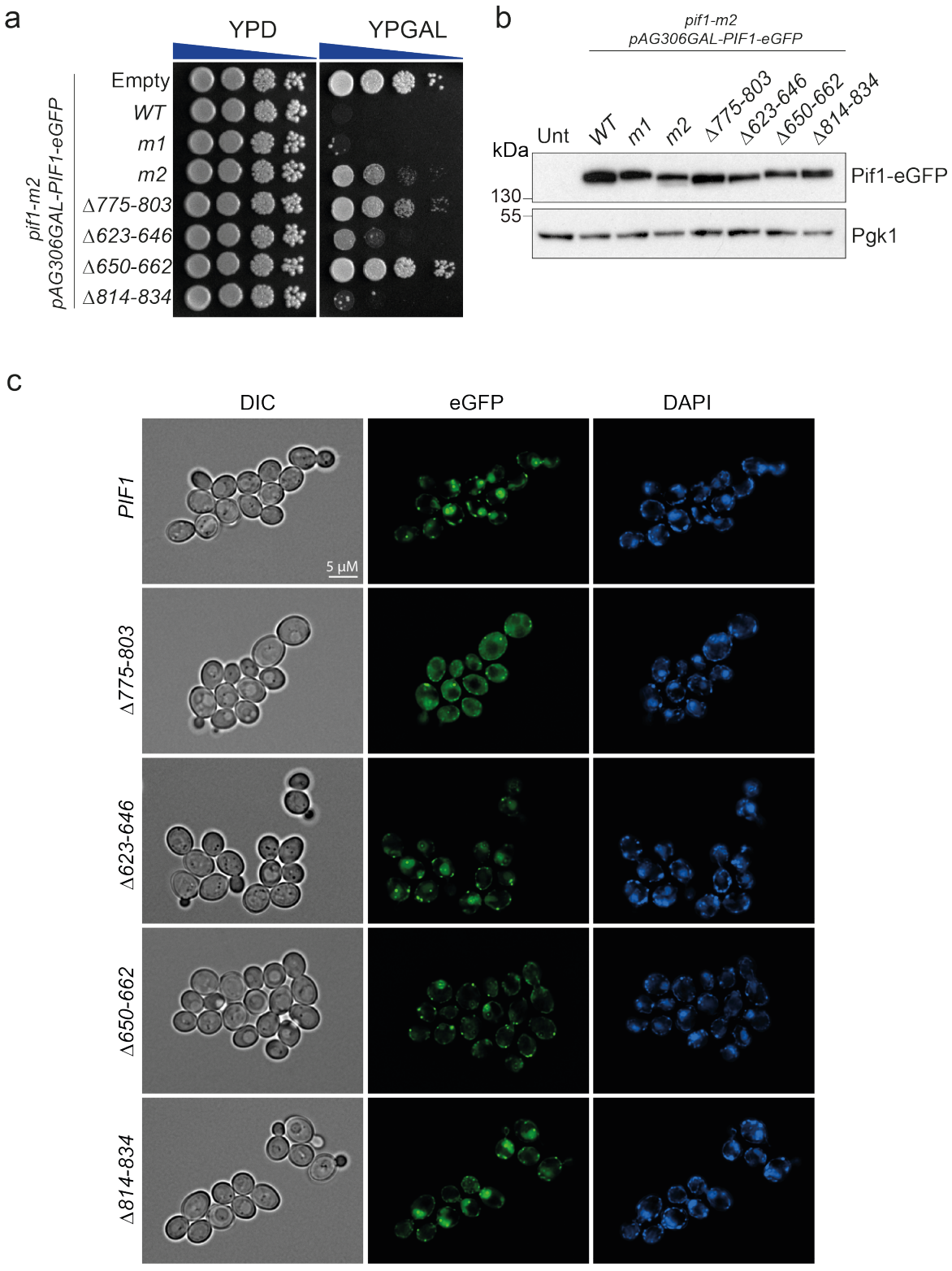


Figure 54. Importing of Pif1 nuclear isoform is impaired in Pif1$^{\Delta 775\text{-}803}$. (a) Ten-fold serial dilutions of strains with the indicated genotypes were spotted on YPD and YPGAL plates and photographed after 2 days of incubation at 30 °C. **(b)** Abundance of Pif1 variants in the strains from (a) was compared by western blotting using anti-GFP antibodies. Protein extracts were prepared from liquid cultures grown in YPRaff and induced for 3 h by addition of 2% galactose. Pgk1 was used as a loading control. **(c)** Subcellular localization of Pif1 variants in live yeast cells overexpressing the indicated *PIF1-eGFP* alleles. Mitochondrial and nuclear DNA was visualized with DAPI and cell contour with DIC microscopy.

UFAL

the 775-803 region is required for the nuclear import of Pif1, while the elimination of 650-662 tract probably results in a general loss of function of the protein due to its location in the helicase domain. This could also explain the modest improvement in cell viability of cells lacking 623-646, since this region is also found inside the helicase domain, although closer to the peak of the disordered region. In order to produce a less disruptive NLS-deficient allele, we then mutated the nine basic residues in the 775-803 region and tested whether such *pif1*^{9A} mutant could phenocopy *pif1*$^{\Delta 775\text{-}803}$ for impaired nuclear import (Figure 55a). We additionally engineered two additional alleles, *pif1*^{4A} and *pif1*^{5A} to identify which of the two basic residue clusters are required for nuclear import (Figure 55a). Next, we tested the functionality of these mutated NLSs for both overexpression-dependent lethality of P_{GAL1}-*PIF1-eGFP* variants and Pif1 subcellular localization by fluorescence microscopy. Upon galactose induction, growth of cells expressing *pif1*^{9A} was comparable to those harbouring the *pif1*$^{\Delta 775\text{-}803}$ allele, suggesting that the basic amino acids present in this region are required to mediate nuclear import (Figure 55b). In particular, our results indicate that only the first basic patch (^{781}KKRK^{784}; Pif1^{4A}) is relevant for the nuclear import of Pif1, as judged by tolerance to overexpression of Pif1^{4A} (Figure 55b). Importantly, differences in viability cannot be attributed to different expression levels (Figure 55c). Cytoplasmic accumulation of both Pif1^{4A} and Pif1^{9A} confirmed that ^{781}KKRK^{784} is necessary for Pif1 nuclear import (Figure 56). Whereas all cells expressing *pif1-m2* exhibit some extent of nuclear Pif1, in the NLS mutants some of the cells also display a faint eGFP signal co-localizing with DAPI nuclear staining. Whether this minor nuclear

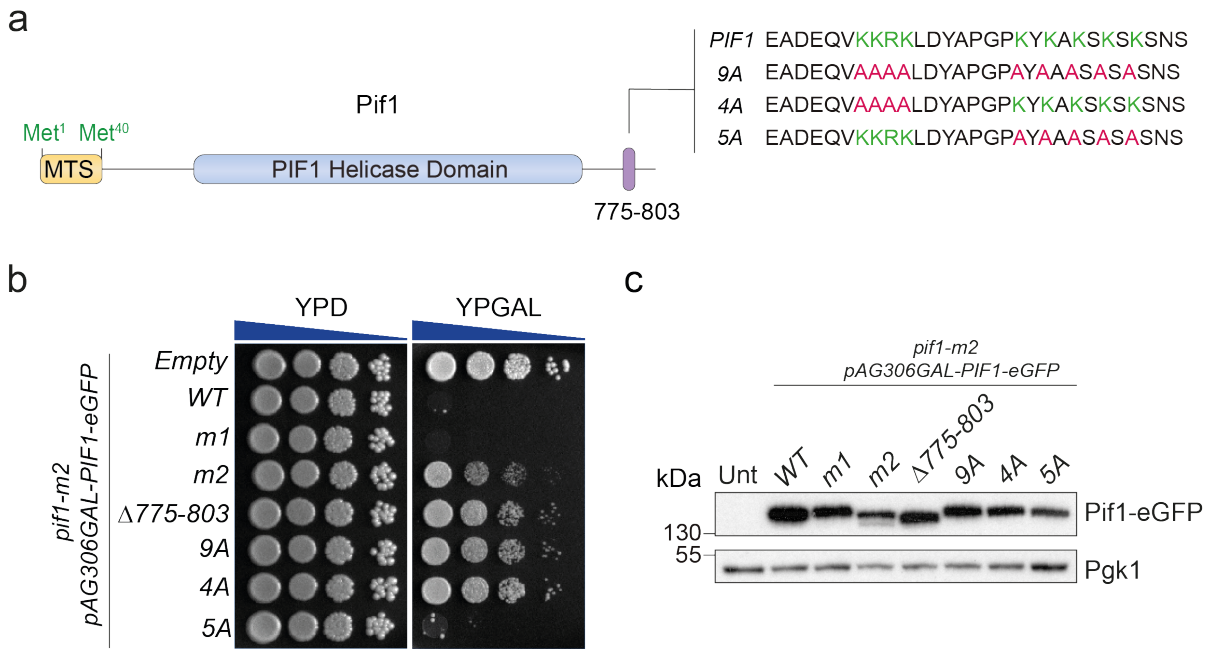


Figure 55. Mutation of ^{781}KKRK^{784} basic patch located at position 781-784 suppress *PIF1* overexpression toxicity. (a) Schematic representation of the 775-803 region of Pif1 (purple), highlighting the amino acids substituted to alanine (green/red) in the indicated mutants. **(b)** Ten-fold serial dilutions of strains with the indicated genotypes were spotted on YPD and YPGAL plates and photographed after 2 days of incubation at 30 ºC. **(c)** Abundance of Pif1 variants in the strains from (b) was compared by western blotting using anti-GFP antibodies. Protein extracts were prepared from liquid cultures grown in YPRaff and induced for 3 h by addition of 2% galactose. Pgk1 was used as a loading control.

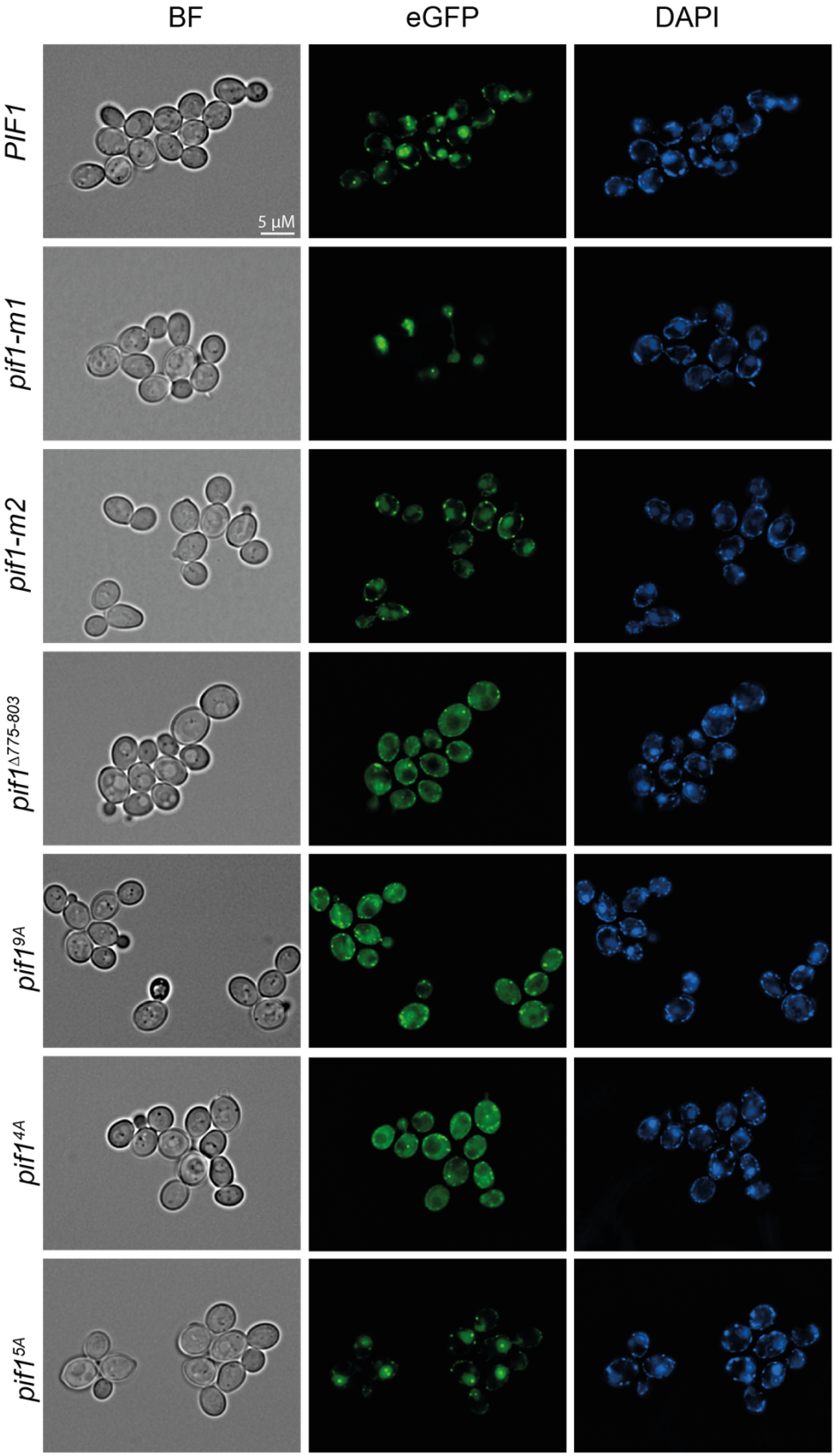


Figure 56. ^{781}**KKRK**^{784} **is necessary to mediate import of Pif1 nuclear isoforms.**Subcellular localization of Pif1 variants in live yeast cells overexpressing the indicated *PIF1-eGFP* alleles. Mitochondrial and nuclear DNA was visualized with DAPI and cell contour with DIC microscopy.

enrichment is higher or lower than *pif1-m2* cells is difficult to estimate, given the disperse cytoplasmatic signal on NLS mutants. Consequently, these alleles must be further characterized *in vivo* and at endogenous levels, to verify if they still conserve traces of nuclear Pif1 activity.

Finally, to determine if this region constitutes a fully functional NLS in itself, we fused the wild-type and 4A versions of the Pif1 775-803 fragment to eGFP and asked whether this small peptide is sufficient to drive nuclear accumulation of eGFP (Figure 57a). Indeed, while eGFP displays a cytoplasmic distribution, its fusion to the 775-803 fragment drives its nuclear accumulation (Figure 57b). Moreover, this nuclear enrichment was impaired by mutation of

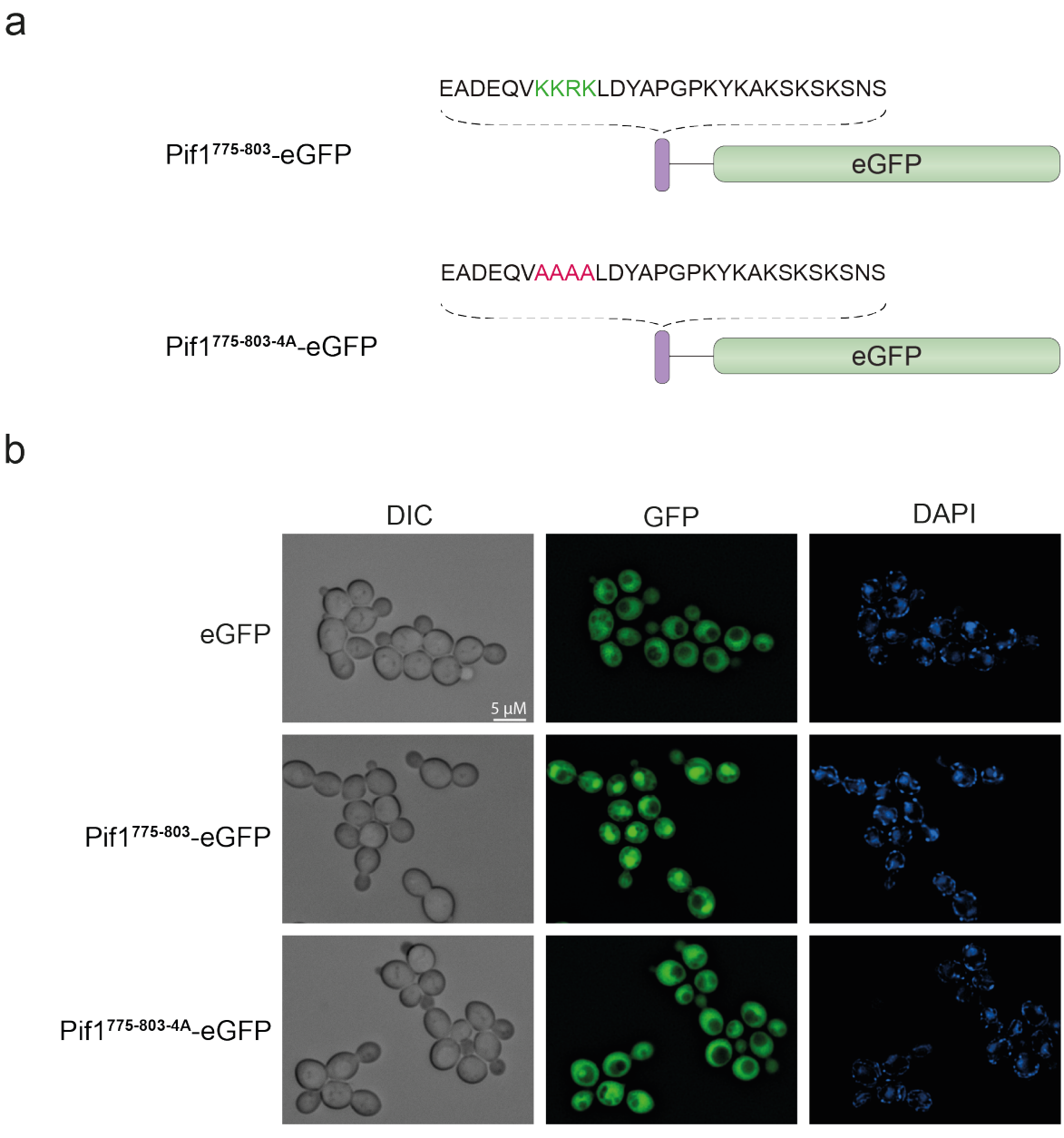


Figure 57. ^{781}KKRK^{784} is sufficient to drive the nuclear accumulation of eGFP. (a) Schematic representation of eGFP fusions employed. **(b)** Subcellular localization of the indicated eGFP overexpressed fusions in live yeast cells. Mitochondrial and nuclear DNA was visualized with DAPI and cell contour with DIC microscopy.

^{781}KKRK^{784} to alanines. Altogether, these results demonstrate the existence of a C-terminal NLS in Pif1 and that the ^{781}KKRK^{784} basic patch is required for the nuclear import of Pif1.

2.6 Generation of an improved nuclear-null *PIF1* allele

Following the identification of Pif1 NLS, we focused on the consequences of impairing Pif1 nuclear import and tested if disruption of its NLS represented a better strategy for the abrogation of Pif1 nuclear function than the use of *pif1-m2*. For this, we resorted to our NLS-mutant *pif1^{4A}* allele, which hereinafter we will rename as *pif1^{nls}* to avoid nomenclature overlapping with the previously described *pif1*^{T763A,S765A,S766A,S769A} phosphomutant allele, also referred to as *pif1^{4A}* (Makovets and Blackburn, 2009b). To exclude an effect on the catalytical activities of Pif1 caused by the amino acid substitutions in Pif1^{nls}, we purified Pif1^{nls} as described for Pif1 and Pif1$^{107-859}$, and compared its ATPase (Figure 58a,b) and helicase activities (Figure 58c,d) to the

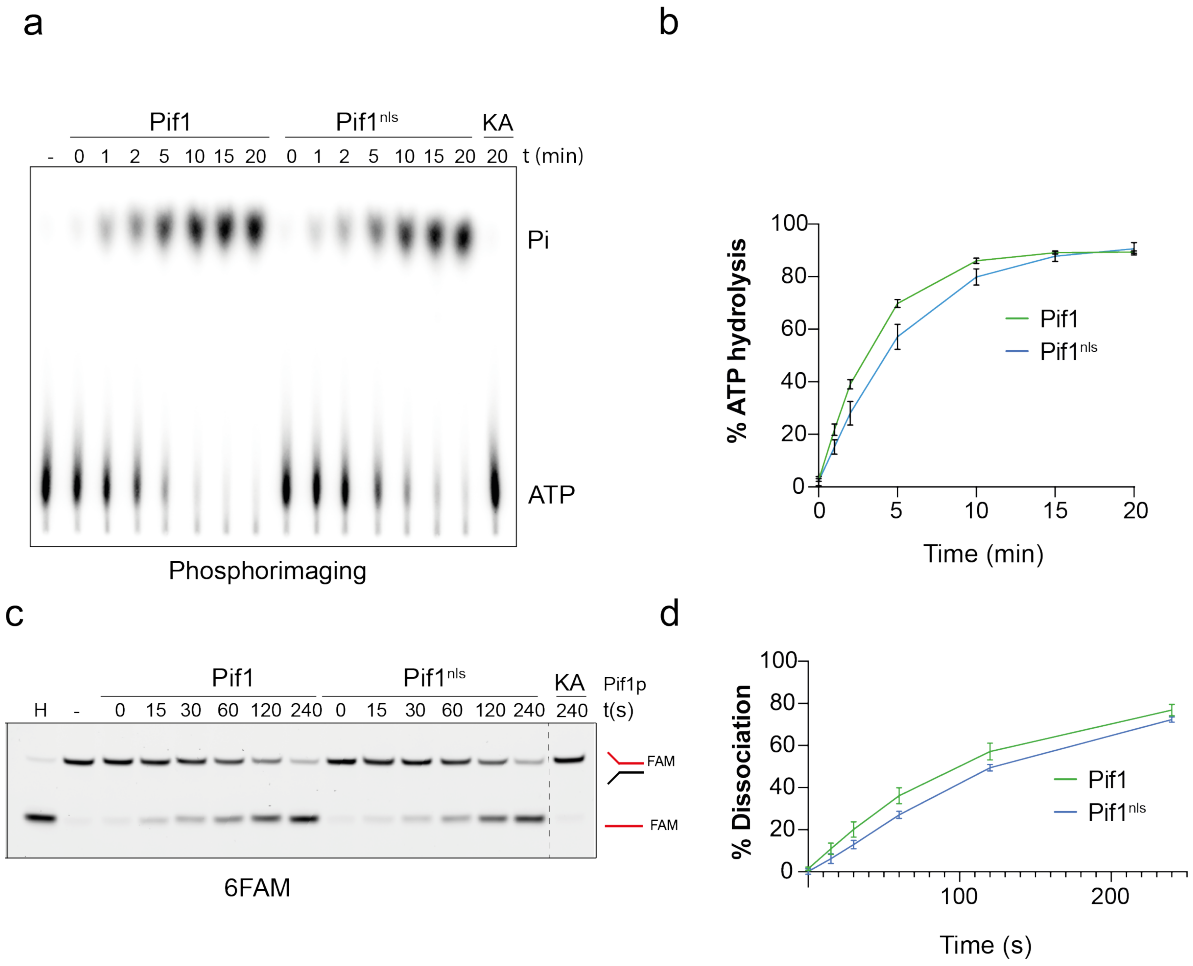


Figure 58.Functional characterization of purified Pif1^{nls}.(a) ATP hydrolysis by Pif1 and Pif1^{nls} was measured by TLC and phosphorimaging. The catalytically inactive Pif1^{KA} mutant was employed as a negative control. **(b)** Quantification of ATPase activity assays as displayed in (a). Data are represented as mean values ± standard deviation (n = 3). **(c)** Native PAGE analysis of the unwinding of a 5'-6FAM-splayed arm substrate by Pif1 and Pif1^{nls}, using Pif1^{KA} as a negative control. Gels were scanned for 6FAM signal in a Typhoon FLA 9500. The dotted line denotes the splicing of irrelevant lanes. **(d)** Quantification of DNA unwinding activity as displayed in (c). Data are represented as mean values ± standard deviation (n = 3). H, heat-denatured substrate. (-), no enzyme. Dashed line indicates splices lanes from the same gel.

USC
DE COMPOSTELA

wild-type protein. In both cases, Pif1^{nls} displayed similar reaction kinetics to Pif1, indicating that the four mutations in the NLS do not interfere with its enzymatic activity.

We then estimated the impact of *PIF1* NLS disruption (Figure 59a) on its genetic interactions with *top3*Δ, *dia2*Δ, and *dna2*Δ mutants by tetrad dissection analyses. Our findings indicate that the disrupted nuclear import of Pif1^{nls} leads to synthetic lethality with *TOP3* deletion, which mimics the phenotype of both *pif1*Δ (Figure 59b) and *pif1-m2* (Figure 43). Similar to the results obtained with *pif1-m2* (Figure 42), *pif1^{nls}* does not display such an overt synthetic sickness with *dia2*Δ as *pif1*Δ (Figure 59c) and produces only a modest suppression of *dna2*Δ lethality (Figure 59d), implying residual nuclear Pif1 activity like in *pif1-m2* strains (Figure 43). These results demonstrate that even the disruption of the NLS in an otherwise wild-type allele diminished nuclear Pif1 only to levels functionally comparable to those of *pif1-m2*, rather than behaving like the full *PIF1* deletion.

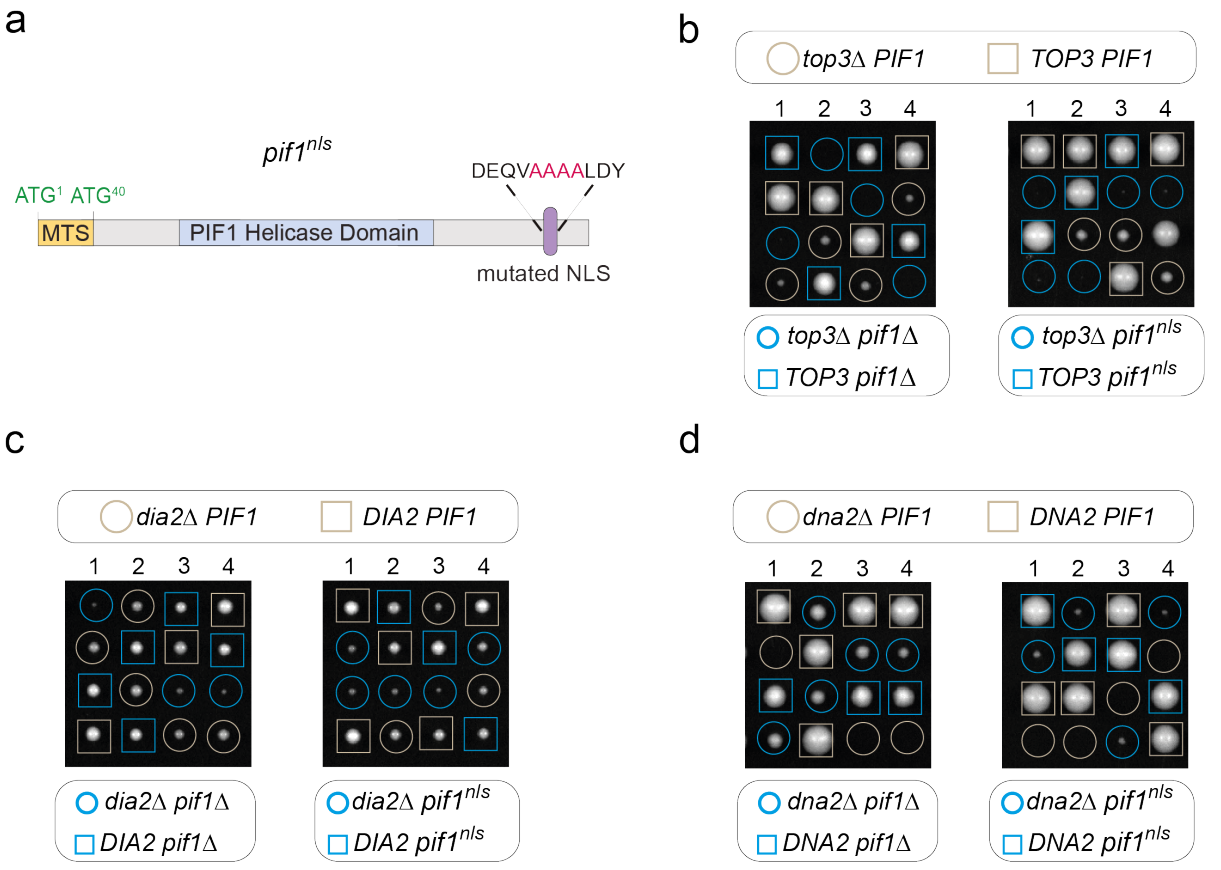


Figure 59. Disruption of Pif1 NLS does not completely abolish nuclear function. (a) Schematic representation of *pif1^{nls}*. **(b)** Microdissection of diploid strains carrying heterozygous mutations for the indicated wild-type and mutant alleles of *PIF1* and **(b)** *TOP3*, **(c)** *DIA2* and **(d)** *DNA2*. Plates were incubated at 30 ºC for 2 days (c) or 4 days (b) and (d).

USC UNIVERSIDADE DE SANTIAGO DE COMPOSTELA

Given such unexpected results with *pif1*^{nls}, we set out to further minimize this residual nuclear Pif1 activity by combining the mutations in both *pif1*^{nls} (impaired nuclear import) and *pif1-m2* (reduced nPif1) into a new allele that we have termed *pif1*^{mit} (Figure 60a). In this case, tetrad dissection analyses demonstrated that when combined with *dia2*Δ, *pif1*^{mit} phenocopies *pif1*Δ

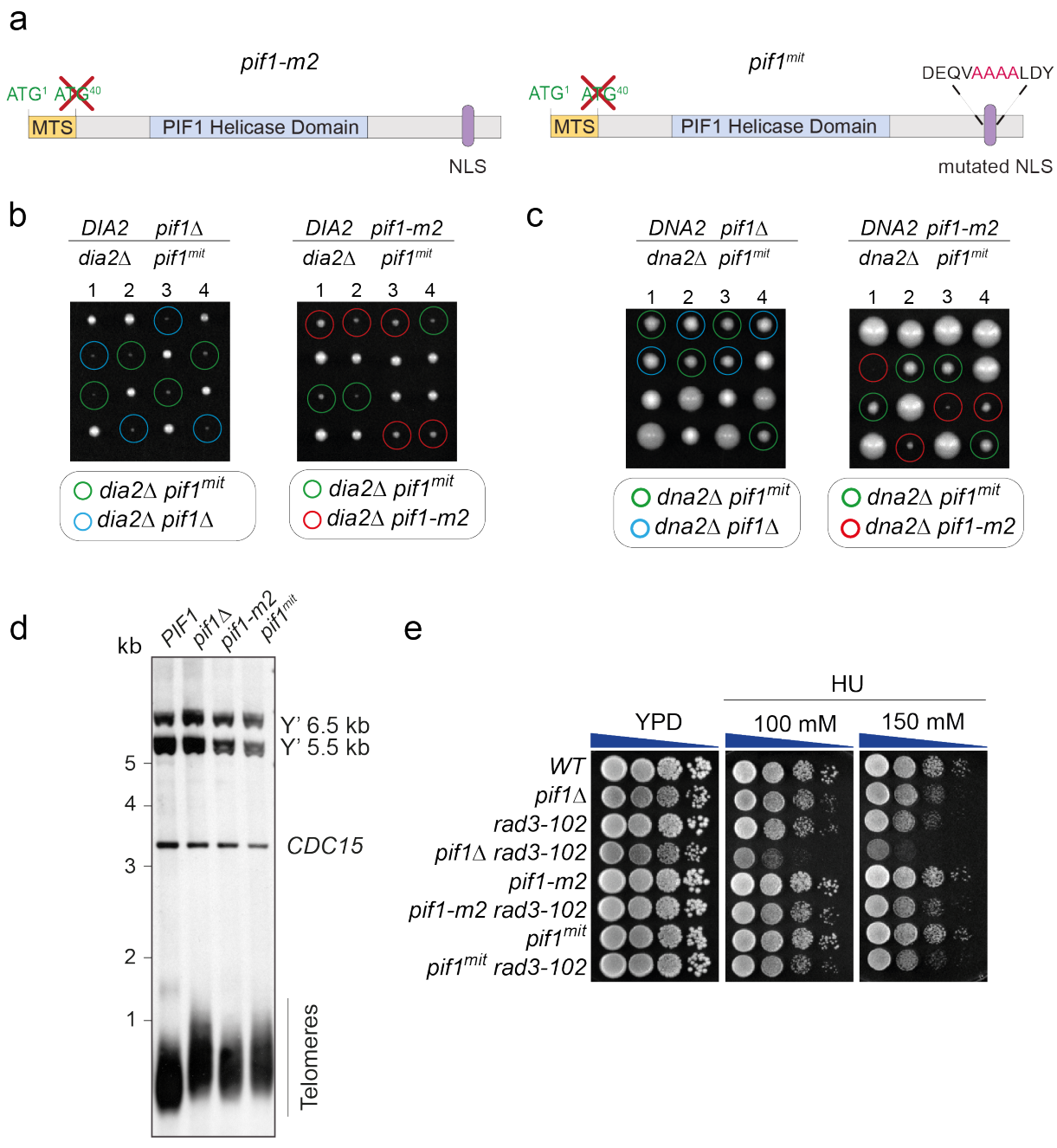


Figure 60. *pif1*^{mit} recapitulates the nuclear phenotypes of *pif1Δ*. **(a)** Schematic representation of the *pif1-m2* and *pif1*^{mit} alleles. **(b)** Tetrad microdissection analyses of diploid strains carrying heterozygous mutations for the indicated wild-type and mutant alleles of *DIA2* **and** *PIF1*. Images were taken after 2 days incubation at 30 ºC. **(c)** As in (b), but for the indicated wild-type and mutant alleles of *DNA2* **and** *PIF1*. Images were taken after 4 days incubation at 30 ºC. **(d)** Telomeric southern blot of different *PIF1* **alleles** to assess the telomeric length. A probe targeting ***CDC15*** probe was employed as a loading control. **(e)** Ten-fold serial dilutions of strains with the indicated genotypes were plated in YPD containing HU and photographed after 2 days at 30 ºC.

USC UNIVERSIDADE DE SANTIAGO DE COMPOSTELA

synthetic sickness more closely than *pif1-m2* (Figure 60b). Likewise, the suppression of *dna2*Δ lethality by *pif1*^{mit} is similar to that of *pif1*Δ, and much more robust than for *pif1-m2* mutants (Figure 60c). Moreover, *pif1*^{mit} strains also resemble *pif1*Δ in telomeric lengthening, exhibiting a slight increase with respect to *pif1-m2* mutants (Figure 60d).

These results indicate that *pif1*^{mit} represents an improved separation-of-function allele that translates almost exclusively into mitochondrial Pif1, with almost no functional traces of nuclear Pif1. However, we were surprised that *pif1*^{mit} was still unable to recapitulate the increased HU hypersensitivity conferred by *pif1*Δ to *rad3-102* mutants (Figure 60e), an observation that will be further explored in the next section.

2.7 Residual mitochondrial activity is present in *pif1-m1* mutants

During the course of our studies, we noticed an anomalous behaviour of the *pif1-m1* strains with respect to their expected loss of mitochondrial function. While haploid *pif1*Δ strains freshly generated by tetrad dissection of *PIF1/pif1*Δ diploids acquire an unmistakable *petite* phenotype by the time the colony is visible, *pif1-m1* colonies arising from *PIF1/pif1-m1* diploids do not. To formally validate this observation, we generated diploid *PIF1/pif1*Δ strains with one additional copy of the *pif1-m1* allele under the control of its endogenous promoter, integrated at the *ura3-52* locus (Figure 61a), and analysed their meiotic progeny by tetrad dissection. Confirming our previous observations, *pif1*Δ colonies displayed a clear *petite* phenotype as judged by their lack of pigmentation in YPD plates and inability to grow in a medium without a fermentable carbon source (Figure 61b,c). Contrarily, when *pif1*Δ co-segregated with the ectopic *pif1-m1* allele, normal pigmentation and the ability to grow on YPEGly were restored.

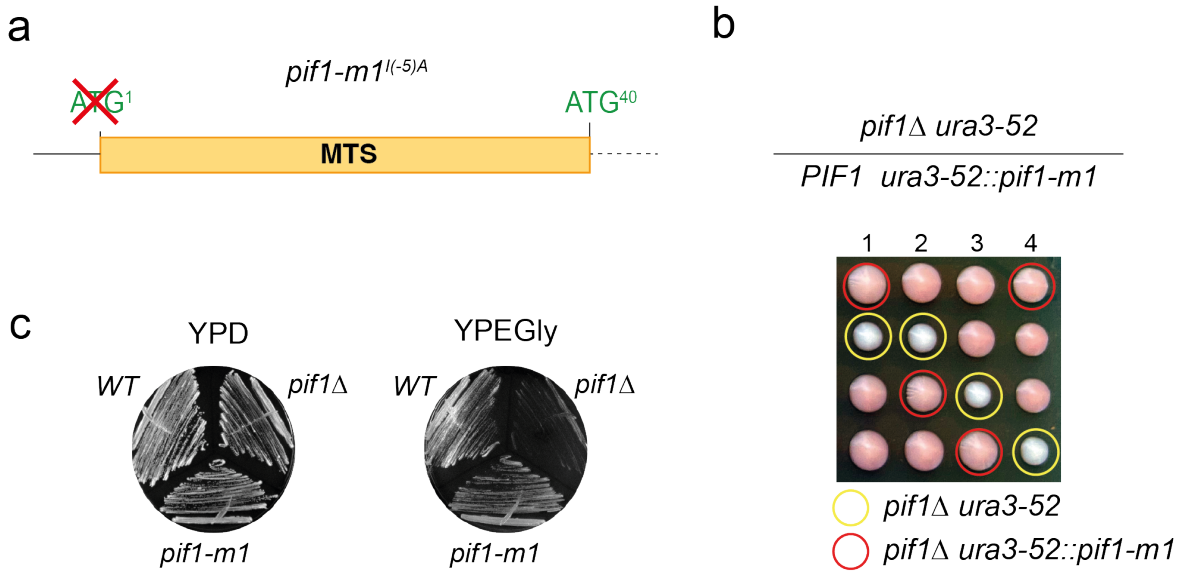


Figure 61. *pif1-m1* retains functional mitochondria. (a) Schematic representation of the N-terminal MTS region in *pif1-m1* integrated at the *ura3-52* locus. **(b)** Tetrad microdissection of a diploid strain carrying heterozygous deletion of *PIF1* and an ectopic *pif1-m1* allele integrated at *ura3-52*. YPD plates were not supplemented with adenine to allow for colour discrimination of *petite* colonies. (c) Strains harbouring the indicated *PIF1* alleles were streaked on rich medium with a fermentable (YPD, 2% glucose) or non-fermentable (YPEGly, 3% ethanol, 3% glycerol) carbon source. Plates were incubated at 30 ºC for 2 days and photographed.

Interestingly, colonies where *pif1*Δ and *pif1-m1* co-segregate exhibit a rough border, suggesting that mitochondrial function could still be partially compromised in *pif1-m1* cells (Figure 61b).

These results suggested that the *pif1-m1* allele may also be subject to some sort of genetic bypass. While this situation could seem reminiscent of the ATI by ribosomal leaky scanning observed for *pif1-m2*, there are no additional in-frame start codons in the vicinity of AUG^{1} that could initiate translation of isoforms with a functional MTS. However, there is an additional mechanism of ATI by leaky scanning involving the use of "near-cognate" triplets as start codons. In this sense, it is well established that ribosomes can initiate translation at near-cognate start codons, although these triplets function at frequencies of <1 to 10% compared to canonical AUGs, according to *in vivo* and *in vitro* studies (Clements et al., 1988; Ingolia et al., 2009; Kolitz et al., 2009; Peabody, 1989). To maximize the likelihood of translation initiation, near-cognates require to be embedded within a robust Kozak context (Chen et al., 2008; Kearse and Wilusz, 2017). In *S. cerevisiae*, mitochondrial isoforms of the glycyl- and alanyl-tRNA synthetases (Grs1 and Ala1, respectively) are generated upon translation iniation from non-AUG codons (Chang and Wang, 2004; Tang et al., 2004), illustrating the ability of this mechanism to produce mitochondrial isoforms in dual-targeted proteins.

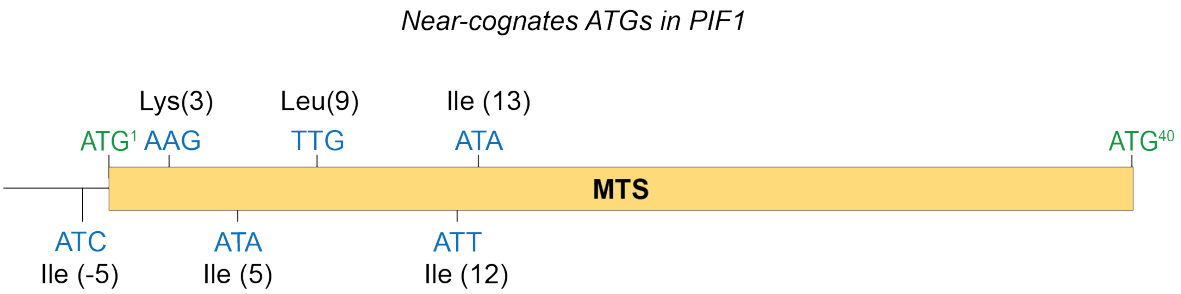
In the case of Pif1, such mode of ATI had not been previously considered when ATI mechanisms were described, since the existing model for Pif1 translation postulated that two consecutive AUG codons were the only responsible for ATI events in Pif1 mRNA. Consistent with this potential role of near cognates in Pif1 ATI, we identified six in-frame near-cognate codons in the vicinity of ATG^{1} that could give rise to Pif1 isoforms with potentially functional MTSs (Figure 62a). One is located upstream - ATC^{-5} (Ile) -, while the remaining five are downstream ATG^{1}: AAG^{3} (Lys), ATA^{5} (Ile), TTG^{9} (Leu), ATT^{12} (Ile), ATA^{13} (Ile). According to the scanning model, the mutation of ATG^{1} in *pif1-m1* would significantly increase the fraction of PICs reaching the downstream non-AUG codons. Indeed, computational analysis of the putative MTSs generated from some of this near-cognate codons predicts a high (ATA^{5}) or very high (ATC^{-5}, AAG^{3}, ATA^{5}) probability of MTS functionality, which coherently decreases with their distance from ATG^{1} (Figure 62b).

Therefore, to challenge our model of residual mitochondrial activity in *pif1-m1* mutants due to ATI from near-cognate start codons, we mutated some of these codons in a *pif1-m1* construct, being as conservative as possible with respect to amino acid changes in those downstream ATG^{1}. In particular, we replaced all the downstream near-cognates coding for leucine or isoleucine to TTA leucine codons, since all codons for isoleucine are near cognates (Figure 62c). We did not mutate AAG^{3}, since near cognates with purine substitutions at the second position cannot initiate translation (Clements et al., 1988; Kolitz et al., 2009)

Next, we ectopically integrated the new alleles into heterozygous *PIF1*/*pif1*Δ strains to evaluate their respective mitochondrial phenotypes in *pif1*Δ backgrounds. Crucially, we carefully selected clones with expression levels equal to or higher than our *pif1-m1* strain (Figure 62d),

USC UNIVERSIDADE DE SANTIAGO DE COMPOSTELA

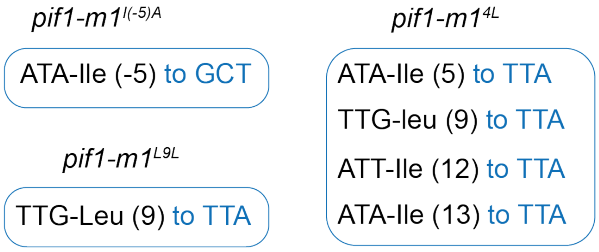
a



b

Start codon	Probability of MTS
AUC-Ile (-5)	0.844
AUG-Met (1)	0.996
AAG-Lys (3)	0.948
AUA-Ile (5)	0.911
UUG-Leu (9)	0.627
AUU-Ile (12)	0.465
AUA-Ile (13)	0.383

c



d

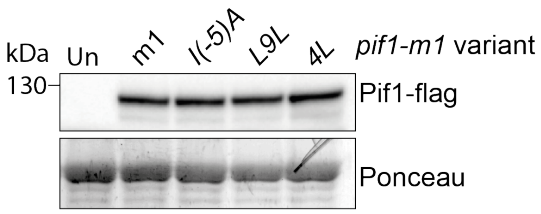


Figure 62. In-frame near-cognate start codons surrounding AUG[1] could produce mitochondrial-targeted isoforms. (a) ATG-like near-cognate codons upstream and downstream ATG[1] in *PIF1*. **(b)** Probability of functional MTS in extended or truncated peptides arising from ATI at non-AUG codons. **(c)** Mutations introduced in near-cognate ATGs in various *pif1-m1* alleles. **(d)** Western blot analysis of Pif1-flag in protein extracts from strains ectopically expressing the indicated *pif1-m1* variants. Unt, untagged. Ponceau staining of the PVDF membrane was employed as a loading control.

as our hypothesis suggests that minute mPif1 amounts, undetectable by western blot, could still support mitochondrial function.

First, we employed *pif1-m1*$^{I(-5)A}$ allele to assess the influence of the upstream near-cognate codon for mitochondrial function (Figure 63a). When co-segregating with *pif1*Δ, mutation of ATC^{-5} to GCA^{-5} in *pif1*-m1 had only a minor detrimental effect on mitochondrial proficiency (Figure 63b,c). While we did notice an increase in the rugged morphology of yeast colonies (Figure 63b), these mutants still sustained an apparently robust respiratory metabolism (Figure 63c). Given that the number of scanning ribosomes along the upstream near-cognates start codons should not be affected by the ATG^{1} mutation, this finding suggests that this particular ATC^{-5} triplet should contribute to produce minor fractions of mPif1 even in WT cells.

Next, we evaluated the effect of the single TTG^{9} to TTA^{9} mutation (*pif1-m1*^{L9L}; Figure 63d) , since among all the downstream near-cognate codons, this is the only one embedded in an optimal Kozak sequence (AACA**UUG**A). Consistent with our prediction, expression of this mutant as the only source of cellular Pif1 derived in the distinctive slow growth and white

colour of *petite* colonies (Figure 63e). Moreover, the ability of these strains to employ non-fermentable carbon sources was greatly reduced, although they exhibited a slightly superior growth compared to *pif1*Δ strains (Figure 63f).

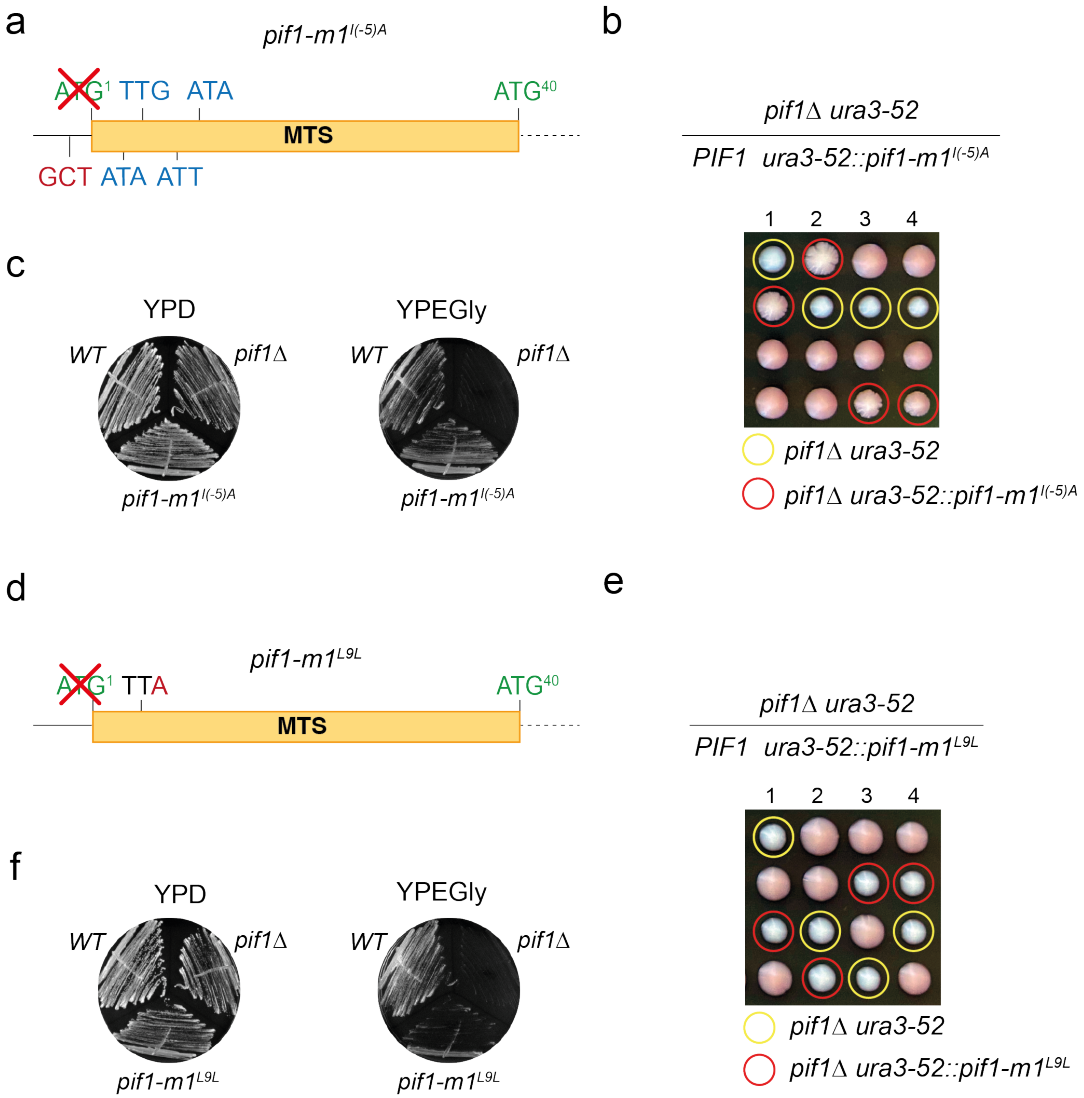


Figure 63. Translation initiation from near-cognates AUGs can sustain mitochondrial function in the absence of AUG[1]. (a) Schematic representation of the N-terminal part of the *pif1-m1*$^{I(-5)A}$ allele. Red colour designates the near-cognate ATG mutated in this allele. Blue colour indicates the near-cognate ATGs downstream ATG[1]. **(b)** Tetrad microdissection of a diploid strain carrying a heterozygous deletion of *PIF1* and an ectopic *pif1-m1*$^{I(-5)A}$ allele integrated at the *ura3-52* locus. **(c)** Strains harbouring the indicated *PIF1* alleles were streaked in rich medium with a fermentable (YPD, 2% glucose) or non-fermentable (YPEGly, 3% glycerol + 3% ethanol) carbon source. Plates were incubated at 30 ºC for 2 days and photographed. **(d)** As in (a), but indicating the mutation of the *pif1-m1*^{L9L} allele. **(e)** As in (b), but the diploid strain harbours an ectopic copy of *pif1-m1*^{L9L}. **(f)** As in (c), but with *pif1-m1*^{L9L}.

USC UNIVERSIDADE DE SANTIAGO DE COMPOSTELA

Next, we attempted to fully recapitulate the *pif1*Δ mitochondrial phenotype through the mutation of all the downstream near-cognate codons that could still yield a functional MTS (*pif1-m1*^{4L}; Figure 62b,c). Importantly, we first ruled out a potential effect of some of these non-synonymous changes on the functionality of MTS itself by introducing the same set of mutations in an otherwise wild-type *PIF1* allele (*pif1*^{4L}) and testing its mitochondrial functions (Figure 64a). *pif1*^{4L} strains exhibit the typical pink hue and morphology of wild-type cells after

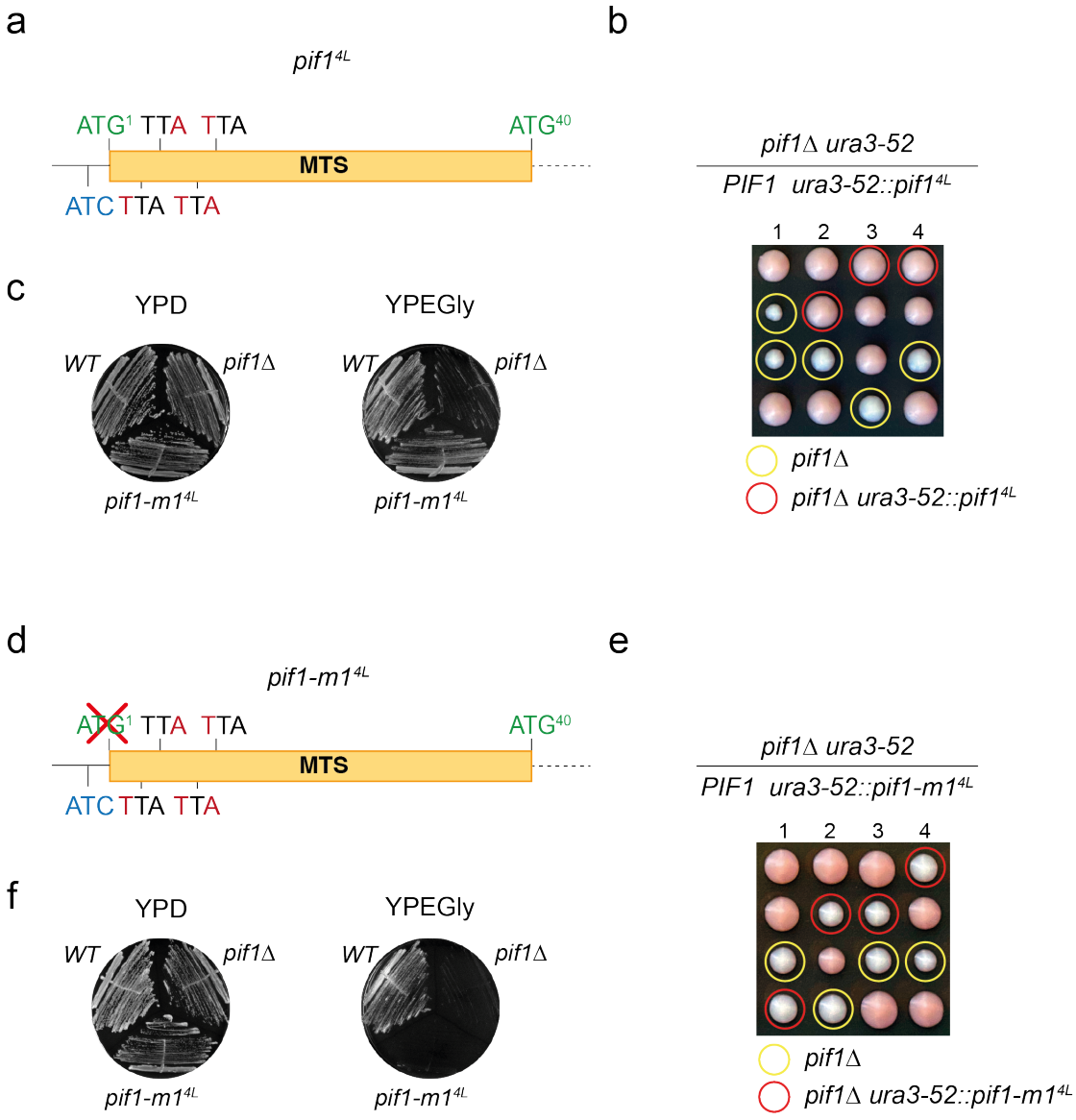


Figure 64. Mutations of four near-cognates in *pif1-m1* phenocopies *pif1Δ* mitochondrial defects. (a) Schematic representation of the N-terminal part of *pif1*^{4L} allele. Red colour designates the near-cognate ATGs mutated in this allele. Blue colour indicates the near-cognate codon still present upstream ATG^{1}. **(b)** Tetrad microdissection of a diploid strain carrying heterozygous deletion of *PIF1* and an ectopic *pif1*^{4L} allele integrated at the *ura3-52* locus. **(c)** Strains harbouring the indicated *PIF1* alleles were streaked in rich medium with a fermentable (YPD, 2% glucose) or non-fermentable (YPEGly, 3% glycerol + 3% ethanol) carbon source. Plates were incubated at 30 ºC for 2 days and photographed. **(d)** As in (a), but indicating the mutations of the *pif1-m1*^{4L} allele. **(e)** As in (b), but the diploid strain harbours an ectopic copy of *pif1-m1*^{4L}. **(f)** As in (c), but with *pif1-m1*^{4L}.

USC UNIVERSIDADE DE SANTIAGO DE COMPOSTELA

tetrad dissection analyses (Figure 64b), as well as a similar capacity to grow on YPEGly (Figure 64c), hence demonstrating that these mutations do not interfere with the mitochondrial import of mPif1. Importantly the combination of the *pif1*^{4L} and *m1* mutations into the *pif1-m1*^{4L} allele (Figure 64d) not only results in typical *petite* colonies after tetrad dissection experiments (Figure 64e), but also completely abrogates the residual growth on non-fermentable carbon sources previously described for *pif1-m1*^{L9L} (Figure 64f). This confirms the loss of Pif1 mitochondrial function in *pif1-m1*^{4L} strains. Collectively, these results demonstrate that translation initiation from near-cognate start codons in the vicinity of AUG^{1} can give rise to phenotypically relevant amounts of mitochondrial Pif1, suppressing the mitochondrial defects predicted for *pif1-m1*.

Finally, we took advantage of these improved mitochondrial-deficient *PIF1* alleles, *pif1-m1*^{L9L} and *pif1-m1*^{4L}, to revisit the genetic interaction between *pif1*Δ and *rad3-102*, which could not be recapitulated by the nuclear-deficient *pif1*^{mit} allele. Therefore, we decided to test whether the hypersensitivity of *pif1*Δ *rad3-102* mutants to HU derives from the loss of mitochondrial Pif1. Indeed, both *pif1-m1*^{4L} or *pif1-m1*^{L9L} expression in *rad3-102* mutants resulted in similar HU sensitivity to the *pif1*Δ *rad3-102* strain (Figure 65), demonstrating a counterintuitive mitochondrial connection between Pif1 and Rad3 in their response to genotoxic agents. These results underscore the advantages of the improved *PIF1* separation-of-alleles generated as part of this PhD Thesis to potentially disambiguate previously misascribed interactions between DNA repair/replication genes and the nuclear or mitochondrial roles of the pleiotropic Pif1 helicase.

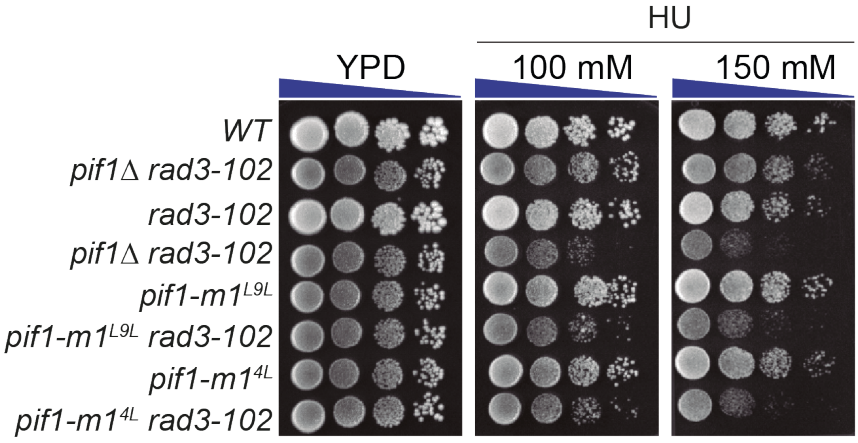


Figure 65. Improved, mitochondrial-deficient *pif1-m1*^{L9L} and *pif1-m1*^{4L} alleles phenocopy the HU hypersensitivity of *pif1Δ* in *rad3-102* mutants. Ten-fold serial dilutions of strains with the indicated genotypes were plated on YPD containing different concentrations of hydroxyurea (HU) and imaged after 2 days of incubation at 30 ºC.

USC UNIVERSIDADE DE SANTIAGO DE COMPOSTELA

3. DISCUSSION

This PhD Thesis constitutes the first comprehensive characterization of the translational mechanism controlling start codon selection in *PIF1* mRNA. Soon after Pif1 identification in yeast, it was shown that its dual targeting to mitochondria and nucleus is dependent on ATI of its mRNA from AUG^{1} and AUG^{40}, resulting in two different isoforms: mPif1 or nPif1. However, the underlying leaky scanning mechanism that dictates the choice between the two start codons involved remained unproven. This refinement in the model for Pif1 ATI led us to the discovery of a new nuclear Pif1 isoform translated from AUG^{107} that explains the incomplete loss of Pif1 nuclear function of *pif1-m2* strains. To our knowledge, we have also provided the first evidence of *pif1-m1* defective behaviour as a mitochondrial-null separation-of-function allele by revealing its inability to recapitulate some of the mitochondrial phenotypes of *pif1*Δ. In contrast to *pif1-m2*, the residual mitochondrial activity of *pif1-m1* derives from multiple ATI events starting at non-AUG codons. Importantly, this deeper understanding of the intricacies of the leaky scanning model for *PIF1* mRNA, together with our identification of Pif1 NLS, allowed us to develop improved versions of the classical *pif1-m1* and *pif1-m2* separation-of-function alleles, which we have successfully employed to disambiguate *pif1*Δ genetic interactions with $YEN1^{ON}$ and *rad3-102*. Still, we consider that some of our observations as well as remaining open questions merit further discussion in the following sections.

3.1 Variable phenotypic impact of the residual nuclear Pif1 activity in *pif1-m2* mutants

Our experiments with *pif1-m2* alleles indicate that whatever the proportion of nuclear Pif1 in these mutants, it produces a considerably different phenotypic outcome depending on the biological context (Figure 42 and Figure 43). In some genetic set-ups, *pif1-m2* behaves like a genuine nuclear-null allele, as exemplified by its recapitulation of the synthetic lethality of *pif1*Δ *top3*Δ strains (Figure 43c). In other cases, *pif1-m2* resembles a hypomorphic allele, exhibiting intermediate phenotypes due to the reduced levels nPif1, such as its incomplete suppression of *dna2*Δ lethality or its intermediate telomeric lengthening compared to *PIF1* and *pif1*Δ strains (Figure 42b and Figure 43a). Lastly, as described in Chapter 1 for $YEN1^{ON}$ (Figure 38b) and in Chapter 2 for *dia2*Δ (Figure 42c), *pif1-m2* can completely mask genetic interactions previously observed with *pif1*Δ.

Such variations on the impact of *pif1-m2* between the different genetic set-ups tested indicate that a reduced concentration of nuclear Pif1 impairs to a different extent the multiple functions of this helicase in the nucleus. Thus, Pif1 nuclear levels in *pif1-m2* would be sufficient to fulfil some of the nPif1 roles, but not enough for others, thus distinctly impinging on the genetic interactions of *pif1-m2* with other genes. Consistent with this hypothesis, a constitutively overexpressed P_{ADH1}-*pif1-m2* allele restores both the viability of *top3*Δ and the lethality of *dna2*Δ mutants, mimicking the phenotypes of strains harbouring *PIF1* or *pif1-m1* alleles (Figure 43b,d).

USC UNIVERSIDADE DE SANTIAGO DE COMPOSTELA

3.2 Pervasive ribosomal leaky scanning of *PIF1* mRNA facilitates ATI from AUG^{1}, AUG^{40} and AUG^{107}

In this work, we have determined that ribosomal leaky scanning is the specific ATI mechanism responsible for the generation of mPif1 an nPif1. Under this model, there is a high probability for the scanning of the 43S PIC to skip the first AUG codon in *PIF1* mRNA due to the suboptimal Kozak sequence around it, hence enabling translation from downstream AUG codons. Accordingly, two lines of evidence support that the suboptimal Kozak context surrounding AUG^{1}, responsible for the translation of mPif1, allows a significant fraction of the scanning ribosomes to bypass AUG^{1} and reach AUG^{40}, resulting in the translation of nPif1. First, various western blots in this PhD Thesis (Figure 44) and other published works point at a roughly similar abundance of mPif1 and nPif1 (Crider et al., 2012; Vega et al., 2007). If we assume similar translational efficiencies for ribosomes engaging at AUG^{1} or AUG^{40}, as well as similar protein turnover rates for mPif and nPif1, this alone would imply that fewer than 50% of total ribosomes initiate translation at AUG^{1}. Second, the optimization of the AUG^{1} Kozak context in *PIF1* strains could be leading to a slight increase in mPif1, as judged by a subtle change in the electrophoretic migration of the tight nPif1/mPif1 doublet (Figure 49b, compare second and third lanes). Moreover, the Kozak motif surrounding AUG^{40} is also permissive enough to allow a minor fraction of scanning ribosomes to read through and traverse to the next in-frame start codon (AUG^{107}), producing detectable amounts of the shorter Pif1$^{107\text{-}859}$ isoform even in wild-type cells (Figure 44, Figure 45, Figure 46, Figure 48 and Figure 49). Again, in agreement with the leaky scanning model, mutations in the preceding start codon, as those in the *pif1-m2* allele, enable a higher proportion of ribosomes reaching AUG^{107} and increase the abundance of Pif1$^{107\text{-}859}$ (Figure 44). Conversely, optimization of the Kozak context surrounding AUG^{40} results in increased engagement of ribosomes at this start codon, rendering this isoform undetectable (Figure 49). In fact, the commonality of suboptimal Kozak sequences at *PIF1* AUG codons implies that the sole mutation of AUG^{107} is not sufficient to abrogate the generation of a fast-migrating isoform. Instead, the complete disappearance of these smaller isoforms requires the concomitant mutation of the clustered AUG^{107}, AUG^{113} and AUG^{127} codons, further substantiating the intrinsic tendency of *PIF1* mRNA to undergo ATI by leaky scanning (Figure 48).

3.3 The intrinsic ATI mechanism operating on *PIF1* mRNA constrains the efficiency of *pif1-m1* and *pif1-m2* as separation-of-function alleles.

Under the light of our results, we argue that the incomplete separation of function observed for the classical *pif1-m1* and *pif1-m2* alleles is a consequence, at least partially, of the ATI mechanism by ribosomal leaky scanning mediating translational start from AUGs and near-cognates AUGs on *PIF1* mRNA. In the case of *pif1-m1* strains, *a priori* lacking mPif1 due to AUG^{1} elimination, the characteristic *petite* phenotype of *pif1*Δ mutants was not reproduced, as cells maintained both their ability to grow on non-fermentable carbon sources and the typical red pigmentation of W303 strains in YPD, both proxies for respiration-proficient mitochondria (Figure 61). Given the absence of any in-frame AUG codon that would allow the translation of MTS-containing Pif1 isoforms (Figure 62), we demonstrated that near-cognate start codons in

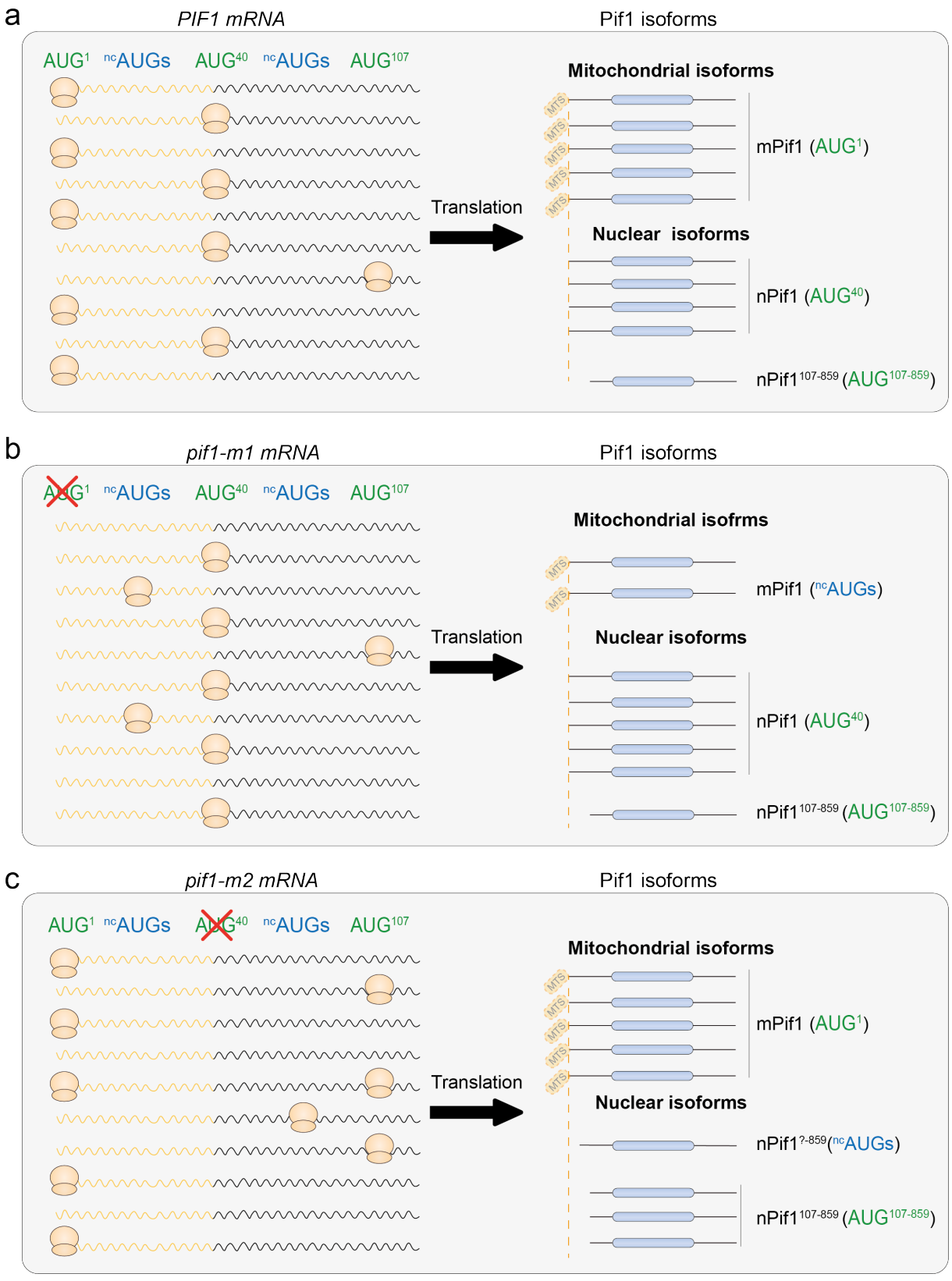
USC
UNIVERSIDADE DE SANTIAGO DE COMPOSTELA

the vicinity of AUG^{1} may serve as alternative translation initiation codons. It is important to note that, upon proteolytic removal of the MTS of the mPif1 precursor in the mitochondrial matrix, mature mPif1 produced from AUG^{1} or any of those near-cognate start codons would be undistinguishable. Despite being undetectable by western blot, the amount of mPif1 translated from these non-AUG codons is sufficient to prevent overt mitochondrial phenotypes in *pif1-m1* mutants (Figure 61, Figure 63 and Figure 64). Therefore, our model (Figure 66) proposes that the elimination of AUG^{1} in *pif1*-m1 facilitates that the fraction of the PICs that would normally engage at this first start codon can continue their scanning process, thus increasing the probability of ATI at downstream near-cognate start codons, specially at UUG^{9} due to its optimal Kozak sequence (Figure 63).

In *pif1-m2* mutants, the increased abundance of the biochemically-proficient (Figure 51) and nuclear Pif1$^{107-859}$ isoform (Figure 50b) provides a plausible explanation for the oft-invoked residual nuclear function of these mutants, as suggested by the similar restoration of cell growth produced by the expression of *pif1*$^{107-859}$ or *PIF1/pif1-m1* in *dia2*Δ mutants (Figure 52a). However, our results are more compatible with a scenario where the remaining nuclear activity in *pif1-m2* mutants derives from a combined effect between the increased levels of *pif1*$^{107-859}$ and, akin to *pif1-m1* mutants, the existence of other undetectable isoforms produced by translation initiation from non-AUG codons (Figure 66). This is supported by the presence of nine near-cognate codons between AUG^{40} and AUG^{107} and the reduced functionality of *pif1*$^{107-859}$ compared to *PIF1* in two different contexts: i) *pif1*$^{107-859}$ overexpression does not impair cell growth (Figure 50c); ii) *dna2*Δ cells maintain viability in the presence of *pif1*$^{107-859}$ (Figure 52b). Hence, translation from these near-cognates would result in Pif1 isoforms that retain a longer portion of its N-terminal domain. Then, it is arguable that *pif1*$^{107-859}$ might lack a portion of a regulatory region located between amino acids 40-107. Similar to *pif1-m1,* mutation of AUG^{40} may increase the amount of these isoforms arising from non-AUG codons, which would contain most of the region that is missing in *pif1*$^{107-859}$ and thus being capable to fulfil to some extent those functions that *pif1*$^{107-859}$ cannot satisfy.

Figure 66. Integrated model of Pif1 isoforms production mediated by leaky scanning in different *PIF1* alleles. **(a)** Weak Kozak context of AUG^{1} in *PIF1* allows a significant number of ribosomes to bypass the first start codon and initiate translation at AUG^{40}, producing similar amounts of mPif1 and nPif1. The weak context in which AUG^{40} is also embedded enables a small fraction of scanning PIC to undergo a second event of AUG bypass and start translation at AUG^{107}, to generate N-terminal truncated and nuclear isoforms. **(b)** Mutation of AUG^{1} in *pif1-m1* increases the number of PICs scanning between the mutated AUG^{1} and AUG^{40}, leading to the production of residual functional mPif1 from near-cognates AUGs located between the first two start codons, impairing the separation-of-function of this allele. **(c)** After mutation of AUG^{40} in *pif1-m2*, those PICS that have bypassed AUG^{1} to continue their scanning downstream, increasing the translation from AUG^{107}. Akin to *pif1-m1*, the higher number of PICs scanning downstream AUG^{40} may also produce nuclear isoforms expressed for near-cognates situated between mutated AUG^{40} and AUG^{107}. The pool of N-terminally truncated isoforms subverts the separation-of-function of *pif1-m2*. Different to *pif1-m1*, where the MTS cleavage upon mitochondrial import homogenizes the final protein product, in *pif1-m2*, translation from near-cognates or AUG^{107} may lead to isoforms with different N-terminal truncations that could impact differently on the biological functions of these isoforms.

USC UNIVERSIDADE DE SANTIAGO DE COMPOSTELA



USC
UNIVERSIDADE DE SANTIAGO DE COMPOSTELA

3.4 On the novel Pif1 isoform and the functionality of the N-terminal domain

The identification of Pif1$^{107\text{-}859}$ as a minor, but constitutively expressed Pif1 isoform raises interesting caveats. First, it is striking that it has remained undetected until now, given that Pif1 has been extensively studied for the last 30 years. However, we have only found a handful of reports in which Pif1 levels are analysed under conditions that permit the discrimination between isoforms of very similar sizes. In the first report, a polyclonal antibody was employed to detect mPif1 and nPif1 in cells harboring *PIF1, pif1-m1* and *pif1-m2* alleles (Vega et al., 2007). Given the low levels of Pif1$^{107\text{-}859}$ in *pif1-m2* cells and, specially, in *PIF1* and *pif1-m1*, such polyclonal antibody might have been too inefficient to detect this isoform, in contrast to our set-up where Pif1 is C-terminally fused to six copies of the Flag epitope. Additionally, the polyclonal antibody may recognise epitopes on the N-terminal region truncated in Pif1$^{107\text{-}859}$, hence diminishing its capacity to detect it. In the second report, anti-myc antibodies were employed to detect a wild-type version of Pif1 tagged with thirteen myc epitopes. However, since *pif1-m2* was not tested, visualizing Pif1$^{107\text{-}859}$ would have probably required longer exposures and could have easily been mistaken for a degradation product (Crider et al., 2012).

Another interesting question is the putative *in vivo* role of this isoform. The leaky scanning model for the production of dual-targeted isoforms would predict a poor Kozak context in the first AUG, but not in the next in-frame start codon. While the low levels of these isoforms suggest that its importance *in vivo* could be negligible, our work also demonstrates how undetectable amounts of Pif1 translated from near-cognates can still support mitochondrial function (Figure 61) and, possibly, compromise the cell viability of *dna2*Δ cells. In this sense, although our *in vivo* data suggest that Pif1$^{107\text{-}859}$ is only partially functional, its helicase activity is not affected, and it is still endowed with at least three interaction motifs located at its CTD that could recruit this isoform to sites of DNA damage or replisomes. The non-canonical PIP-box that facilitates recruitment of Pif1 via PCNA interaction could allow this isoform to promote DNA synthesis during TS and BIR (Buzovetsky et al., 2017; Garcia-Rodriguez et al., 2018), whereas the checkpoint-phosphorylated TLSSAES motif could recruit Pif1$^{107\text{-}859}$ to DSBs to inhibit their telomerization and promote BIR (Falquet et al., 2020; Makovets and Blackburn, 2009a). Likewise, Pif1$^{107\text{-}859}$ also possesses the canonical PIP-box that mediates Pif1-PCNA interaction to promote Polδ synthesis through G4s (Dahan et al., 2018). The presence of this interaction motifs in Pif1$^{107\text{-}859}$ is compatible with the intermediate phenotypes published for *pif1-m2* in G4-associated instability and BIR, and also suggests that some of these domains could be relevant to suppress *YEN1^{ON}*-dependent toxicity upon replication stress.

Following this rationale and taking into account the absence of cell death under *pif1$^{107\text{-}859}$* overexpression conditions (as opposed to Pif1), it is tempting to propose that the suboptimal Kozak context of AUG^{40} could be an adaptation to finely downregulate nPif1 by substituting a small fraction of it for Pif1$^{107\text{-}859}$. This shorter isoform, while preserving its catalytic activity and functional elements on its CTD, would be devoid of potentially deleterious activities associated to the N-terminal region of nPif1 upon high expression levels.

As previously mentioned, post-translational modifications like acetylation or checkpoint-dependent phosphorylation of Pif1 NTD have been reported (Ononye et al., 2020; Rossi et al.,

2015), although their significance is not fully understood. However, all the reported PTMs in those studies are also present in Pif1$^{107-859}$, suggesting than an additional motif or PTM located between amino acids 40-106 could regulate Pif1 activity or mediate some of its functions in vivo. Moreover, a global analysis of Cdk1 substrates described the phosphorylation of the S70 and S72 residues *in vivo* (Holt et al., 2009). In this study, the authors employed quantitative mass spectrometry to identify phosphosites affected by specific inhibition of Cdk1. On top of a direct role of Cdk1 in the phosphorylation of these residues, it could also be envisaged that Cdk1 stimulates a second kinase that subsequently phosphorylates S70 and S72, especially since none of them constitute a minimal Cdk1 consensus site (S/T-P). Together, these observations indicate that there could exist an active regulation (cell cycle-dependent, checkpoint-dependent, etc) of potential, yet-uncharacterised functional elements in Pif1 NTD. Although further work is required to prove that phosphorylation of S70 and S72 is relevant for Pif1 function, we consider the characterization of the possible roles of PTMs in the 40-106 region in Pif1 regulation as an exciting line of research that other members of the lab are starting to pursue.

Remarkably, the viability of *dna2*Δ *pif1*$^{107-859}$ cells suggests that the missing part of the N-terminal may be required for the 2-step pathway of Okazaki processing. As detailed in the introduction (section 3.3), the two-step pathway propose that Rad27 process the short flaps on Okazaki fragments created by the strand displacement activity of Polδ. In this process, Pif1 can potentially increase the flap length by and promoting the aforementioned strand displacement of Polδ or by dismantling secondary structures present in the flap. Elongated flaps are then coated by RPA, which inhibits Fen1 while promoting Dna2 cleavage. According to this model, *dna2*Δ lethality is a direct consequence of the accumulation of a high load of long 5'-flaps on the lagging strand, leading to checkpoint hyperactivation and cell death. Two alternative models have been suggested to explain source of those long flaps. On one hand, the Dna2 activity may be required to process 5'-flaps originated Polδ–Pif1 strand displacement activity at the lagging strand during BIR (Rossi et al., 2018). On the other hand, the absence of helicase activity in DNA2 could promote the accumulation of reversed forks, enabling pervasive RDR upon replication stress. Given the instability of DNA synthesis during this processes, the migrating D-loop could collapse, generating long stretches of ssDNA(Appanah et al., 2020; Falquet et al., 2020). Characterization of N-terminal activities of Pif1 may allow to generate a specific separation-of-function allele that could be instrumental to further investigate the source of *dna2*Δ lethality.

USC
UNIVERSIDADE DE SANTIAGO DE COMPOSTELA

3.5 *pif1^{nuc}* and *pif1^{mit}* as valuable tools for the DNA repair field.

In our efforts to generate a nuclear-null *PIF1* allele to substitute for *pif1-m2* and given the possibility of multiple nuclear isoforms produced by ATI, we decided to block the nuclear import of all isoforms. Through our investigation, we demonstrated that a small C-terminal region (^{781}KKRK^{784}) is necessary for the nuclear localization of Pif1 both through fluorescence microscopy (Figure 54c and Figure 56) and by employing the toxicity of the overexpression of several *PIF1* alleles with mutations in various putative NLSs as proxy for functional nuclear Pif1 (Figure 54a and Figure 55). Furthermore, we found that fusion of a fragment containing the Pif1 NLS (775-803) was sufficient to enrich the nuclear localization of eGFP (Figure 57). When tested *in vivo*, a ^{781}AAAA^{784} mutation in Pif1 NLS (*pif1^{nls}*) recapitulated the synthetic lethality of *pif1*Δ *top3*Δ strains, but was unable to suppress *dna2*Δ lethality to the same extent as *pif1*Δ (Figure 59). We envisaged two possible explanations for these striking observations: i) a fraction of Pif1 can reach the nucleus even in the absence of a functional NLS, due to the limited, but non-zero, ability of proteins up to 90 kDa to diffuse through the nuclear pore (Wang and Brattain, 2007); ii) upon NLS mutation, another patch of basic residues located in any of the disordered regions of the NTD or CTD acts as a cryptic NLS to mediate nuclear import, albeit inefficiently. In this sense, some of the other regions that we initially considered as putative NLSs display relatively high-confidence scores in our *in silico* analyses.

To overcome this problem, we developed a novel allele, *pif1^{mit}*, by combining the mutation of AUG^{40} (*pif1-m2*), which is responsible for nPif1 translation, with the disruption of the NLS. As a result, the only potential source of nuclear activity in the *pif1^{mit}* strains stems from minor isoforms translated from non-AUG codons or AUG^{107}, which might either diffuse or undergo inefficient nuclear import. *pif1^{mit}* provides more stringent phenotypes than *pif1-m2* and successfully recapitulates various genetic interactions previously described for *pif1*Δ (Figure 39 and Figure 60). Similarly, we built on *pif1-m1* to generate a mitochondrial-null allele by mutating four downstream near-cognates, which abrogates any residual translation of mPif1 from these triplets upon mutation of AUG^{1}. As a proof of principle of the usefulness of these improved alleles, we have disambiguated the hypersensitivity of *pif1*Δ *rad3-102* mutants to HU (Moriel-Carretero and Aguilera, 2010) which arises, quite unexpectedly, from the loss of Pif1 mitochondrial activity, rather than nuclear (Figure 65).

We believe that *pif1^{nuc}* and *pif1^{mit}* may enable the discovery of subtle genetic interactions that could have been previously overlooked due to the residual activities of *pif1-m1* and *pif1-m2* or the confounding effect of *pif1*Δ pleiotropy. Whereas *pif1-m2* has been instrumental in characterizing the nuclear functions of Pif1, we anticipate that *pif1^{mit}* and, particularly, *pif1^{nuc}* will be instrumental to shed light on the less explored mitochondrial roles of this helicase. Moreover, these alleles may contribute to establish more controlled genetic set-ups for the study of Pif1-dependent pathways involved in the maintenance mitochondrial and nuclear genomes and, therefore, reassess or disambiguate previously described *pif1*Δ genetic interactions.

3.6 Extensibility of our model to other genes

Alternative intron splicing and alternative translation initiation (ATI) are two essential mechanisms that contribute to proteome diversity by enabling the production of multiple

protein variants from one original gene, including dual-targeted isoforms that perform their functions in different subcellular compartments (Cai et al., 2006; Hinnebusch, 2011b; Kazak et al., 2013; Touriol et al., 2003). Since *S. cerevisiae* contains only ~300 spliceosomal introns, distributed among just 5% of its genes, and mRNA alternative-splicing events are rare, this organism is specially reliant on ATI to increase protein diversity (Davis, 2000; Juneau et al., 2007; Spingola et al., 1999). Although not always formally demonstrated, ribosomal leaky scanning is possibly the most prevalent pathway for ATI in unperturbed eukaryotic cells (Kozak, 2002). In budding yeast, leaky scanning mediates the production of nuclear and cytoplasmic isoforms of the histone methyl transferase Dot1 (Frederiks et al., 2009), and the mitochondrial and cytoplasmic isoforms of the tRNA dimethylallyltransferase Mod5 (Slusher et al., 1991). Here, we have refined the existing model of ATI for *PIF1* mRNA by demonstrating the involvement of not only ribosomal leaky scanning, but also initiation at non-AUG codons, in the generation of dual-targeted Pif1 isoforms. Moreover, this plasticity in the translation initiation step has important implications for the design of separation-of-function alleles that are likely applicable to other dual-targeted DNA repair factors.

In *S. pombe*, the *PIF1* ortholog *Pfh1* also encodes two differentially targeted Pfh1 isoforms through ATI (Pinter et al., 2008). Akin to the strategy in *S. cerevisiae*, *pfh1* separation-of-function alleles were also created by mutating its two alternative start codons. Despite the essential nuclear function of Pfh1 (Zhou et al., 2002), cells harbouring a *pfh1-mt* (nuclear-deficient) allele can sustain cell division indefinitely (Pinter et al., 2008), suggesting that, like *pif1-m2* mutants in *S. cerevisiae*, a significant amount of Pfh1 can still access the nucleus. Even after the generation of an improved version of nuclear-deficient *pfh1* by the combined mutation of downstream ATG codons and the addition of a viral nuclear export signal to *pfh1-mt*, these new mutants (*pfh1-mt**) were still viable (Pinter et al., 2008). These results are consistent with the leaky scanning mechanism controlling start codon selection in Pfh1, as described for its budding yeast counterpart. As depicted in Figure X, the N-terminus of Pfh1 extends over the first 345 amino acids, with the ATG^{1} and ATG^{21} delimiting the MTS. Additionally, three downstream ATGs at positions 170, 265 and 320 might serve as start codons for the translation of truncated isoforms after mutation of ATG^{21} in *pfh1-mt*. The fact that even after mutation of these three ATGs and addition of a viral NES, the new allele *pfh1-mt** still fails to recapitulate the *pfh1*Δ phenotypes strongly suggests that near-cognate start codons, like in *PIF1*, could act as ATI sites of functional Pfh1. In this sense, we have listed up to ten near-cognates located between AUG^{21} and AUG^{170} that could produce Pfh1 truncated isoforms with a functional helicase domain (data not shown). Moreover, although it has not been demonstrated, the best candidates for Pif1 NLS are located downstream these near-cognates, implying that this isoform could be efficiently imported into the nucleus, impairing the separation of function of *pfh1-mt**.

Interestingly, in two separate studies aimed at understanding the roles of Pfh1 in replisome progression, Pfh1 was downregulated either by using a repressible promoter (Sabouri et al., 2012) or employing the *pfh1-mt** allele (Steinacher et al., 2012), reaching different conclusions. Indeed, the two strategies used for depletion of Pfh1 were proposed to explain the discrepancies between both reports (Shimada and Gasser, 2012), underscoring the misleading effects of

USC
DE SANTIAGO
DE COMPOSTELA

suboptimal separation-of-function alleles and the phenotypical relevance of residual amounts of some DNA repair factors.

The relevance of the ATI consequences can be intuitively expanded to other dual-targeted genes in budding and fission yeast, like *S. cerevisiae CDC9 / S. pombe cdc17*, which code for the conserved Ligase I. Ligase I is involved in the joining of Okazaki fragments during S phase and required for sealing nicked dsDNA molecules in multiple DNA repair pathways, with the notable exception of NHEJ. Consequently, Ligase I is essential for viability of yeast cells. Analogously to Pif1/Pfh1, its dual targeting to nucleus and mitochondria is achieved by the alternative use of two in-frame start codons (Willer et al., 1999). Although it has not been formally demonstrated that translational control of *CDC9/cdc17* relies on a ribosomal leaky scanning mechanism, the phenotypes exhibited by the separation-of-function alleles suggest that again, individual mutations of the first and second start codons do not completely abolish the production of mitochondrial or nuclear isoforms. In budding yeast, mutation of the second ATG, which should abrogate the expression of the nuclear isoform, still yields viable cells and, like in *pif1-m2*, correlates with the appearance of a fast-migrating isoform (Willer et al., 1999). In *S. pombe*, the MTS region of *cdc17* is flanked by AUG^{1} and AUG^{20}, whereas a basic patch of three amino acids at positions 62 to 64 is required for the nuclear import of Cdc17 (Martin and MacNeill, 2004). Reminiscent of the results with *pif1-m2*, a Met^{20} to Ala^{20} substitution decreased the nuclear signal for Cdc17, but nuclear localization was completely abolished only when this mutation was combined with that of the downstream basic patch. Since the next in-frame ATG is located at position 170, the most likely source of the nuclear signal upon mutation of ATG^{20} are ATI events from two near-cognates at positions 27 and 32 (Martin and MacNeill, 2004).

We have noticed that other DNA repair genes could also be good candidates for regulation by leaky scanning in *S. cerevisiae*. As described in the introduction, the BER pathway operates at both nuclear and mitochondrial compartments (section 1.1.2) and important BER glycosylases, such as Ung1 and Ntg1 (Figure 2), present dual-targeted localization that is also achieved through ATI (Bauer et al., 2013; Chatterjee, 2001). According to the leaky scanning model, genes that drive the production of dual-targeted proteins should display a suboptimal Kozak context around the first ATG codon. In a speculative manner, we decided to categorize the Kozak sequences around the AUGs mediating ATI in both *NTG1* and *UNG1*. For this, we adapted to *S. cerevisiae* a pre-existent model for vertebrates to classify Kozak sequences that deviate from the optimal (Meijer and Thomas, 2002) (Figure 67a,b). This classification focuses primarily on the two key residues at positions -3 and +4. A strong Kozak context will display optimal nucleotides at both key residues, whereas a moderate Kozak will display only one and a weak Kozak none of them. It is important to mention that while the optimal 5' portion of the

USC UNIVERSIDADE DE SANTIAGO DE COMPOSTELA

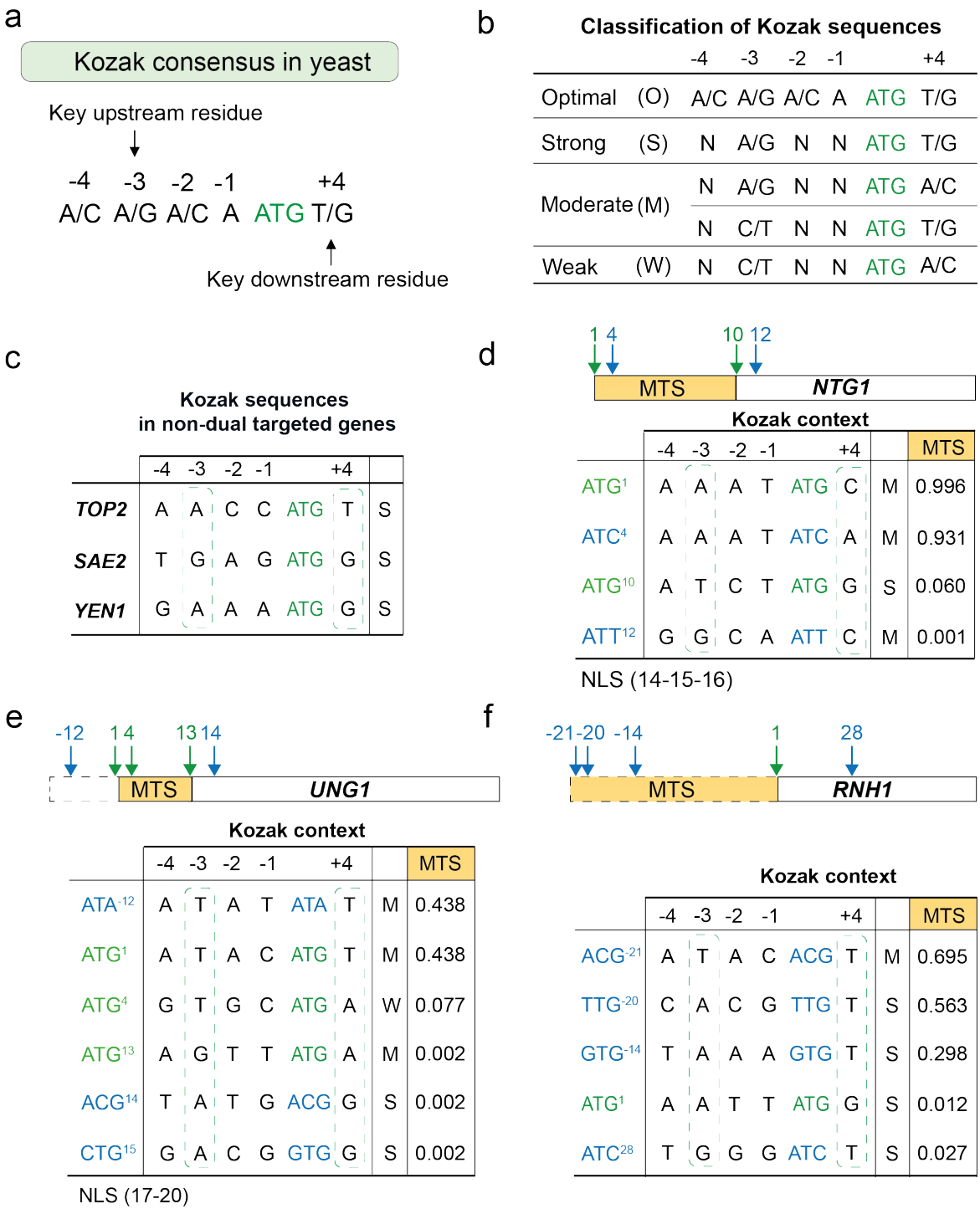
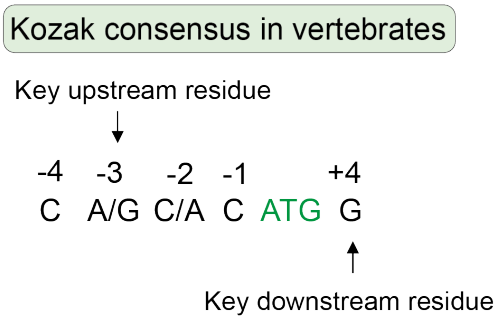


Figure 67. Analysis of the Kozak context in dual-targeted genes in *S. cerevisiae*. **(a)** Schematic representation of the optimal Kozak sequence in yeast. **(b)** Classification of Kozak sequences according to the nucleotides in the positions -3 and +4. **(c)** Classification of Kozak sequences around ATG[1] in three DNA repair factors without dual targeted isoforms. **(d)** Analysis of the Kozak sequence contexts for various ATG and near-cognate codons in the 5' region of *NTG1*, **(e)** *UNG1* and **(f)** *RNH1*, three DNA repair factors with dual-targeted isoforms to nucleus and mitochondria. ATGs are depicted in green. Blue denotes near-cognate ATGs. Probability of MTS was calculated with Mitofates (Fukasawa et al.,2015). Where relevant, the 5'-UTR is represented by black-dashed boxes adjacent to the beginning of the first exon. Green-dashed boxes highlight the key residues for Kozak classification. O, optimal; S, strong, M, moderate, W; weak.

USC UNIVERSIDADE DE SANTIAGO DE COMPOSTELA

Kozak sequence has been well characterized in yeast (Figure 67a), some controversy exists with respect to the relevance of position +4. As a simple proof of concept, we started by analysing the Kozak context of three other DNA repair factors without dual-targeting (Figure 67c) and all of them displayed a strong Kozak context around their first ATG. In contrast, *NTG1* and *UNG1* presented moderate Kozak sequences at their respective first ATGs (Figure 67d,e), which would facilitate that a fraction of ribosomes bypasses that start codon. Interestingly, both genes present near-cognates or downstream ATGs with moderate or strong Kozak sequences which, akin to the *pif1-m1* and *pif1-m2* situation, could still produce relevant amounts of functional isoforms should the main ATGs be mutated (Figure 67d,e). Recently, it was also demonstrated how ATI from an upstream near-cognate start codon generates a mitochondrial isoform of Rnh1 (Monteuuis et al., 2019). According to the predictions of the leaky scanning model, the inefficiency of translation from non-AUGs is partially compensated by the presence of two consecutive in-frame, near-cognates with moderate and strong context, respectively, in the

a

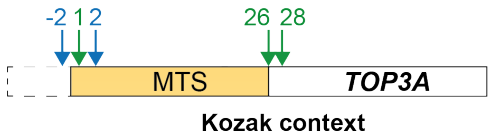


b

Classification of Kozak sequences

		-4	-3	-2	-1		+4
Optimal	(O)	C	A/G	C/A	C	ATG	G
Strong	(S)	N	A/G	N	N	ATG	G
Moderate	(M)	N	A/G	N	N	ATG	A/C/T
		N	C/T	N	N	ATG	T/G
Weak	(W)	N	C/T	N	N	ATG	A/C/T

c

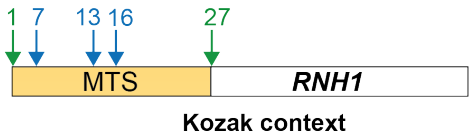


Kozak context

	-4	-3	-2	-1		+4		MTS
CTG^{-2}	A	G	G	T	CTG	A	M	0.917
ATG^{1}	G	A	G	G	ATG	A	M	0.863
ATC^{2}	G	A	T	G	ATC	T	M	0.893
ATG^{26}	C	G	C	C	ATG	G	O	0.012
ATG^{28}	G	G	A	G	ATG	G	S	0.027

NLS (965-966)

d



Kozak context

	-4	-3	-2	-1		+4		MTS
ATG^{1}	A	G	C	G	ATG	A	M	0.542
CTG^{7}	T	T	C	C	CTG	G	M	0.647
TTG^{13}	C	G	C	C	TTG	G	O	0.622
TTG^{16}	C	G	C	C	TTG	C	M	0.388
ATG^{27}	C	G	G	G	ATG	T	M	0.163

Figure 68. Analysis of the Kozak context in dual-targeted genes in *H. sapiens*. **(a)** Schematic representation of the optimal Kozak sequence in vertebrates. **(b)** Classification of Kozak sequences according to the nucleotides located at positions -3 and +4. **(c)** Analysis of Kozak sequence for various ATG and near-cognate codons in the 5' region of *TOP3A* and **(d)** *RNH1*. ATGs are depicted in green. Blue denotes near-cognate ATGs. Probability of MTS was calculated with Mitofates (Fukasawa et al.,2015). Where relevant, the 5'-UTR is represented by black-dashed boxes adjacent to the beginning of the first exon. Green-dashed boxes highlight the key residues for Kozak classification. O, optimal; S, strong, M, moderate, W; weak.

RNH1 5'-UTR region (Figure 67f). The frequent bypass of these AUGs would still allow a significant fraction of scanning PICs to reach the first AUG and mediate translation of the nuclear isoform.

Alternative translation initiation also contributes to enrich the pool of dual-targeted proteins in higher eukaryotes, including humans. Therefore, we repeated this simple analysis of the Kozak sequence in human DNA repair factors with dual-targeted localization nucleus-mitochondria (Figure 68a,b), such as TOP3α (Wang et al., 2002) and RNAseH1 (Suzuki et al., 2010). Interestingly, both genes present a moderate Kozak context in the first ATG, but a strong one

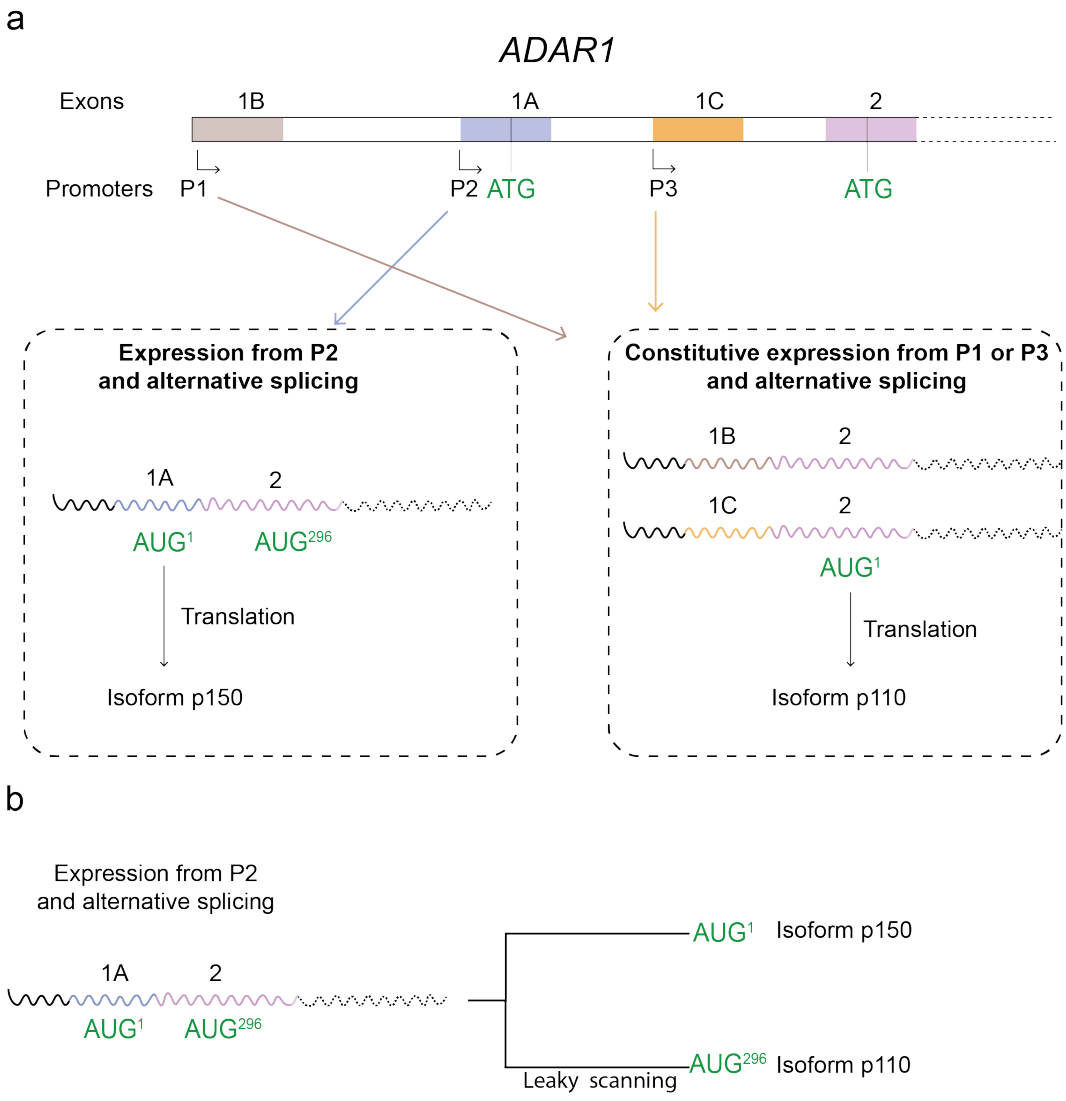


Figure 69. Isoform p110 of *ADAR1* is produced by both alternative splicing and leaky scanning. (a) Schematic representation of the 5' region of the human *ADAR1* locus, depicting the relative positions of the three alternative Exons 1 (1B, 1A, 1C), each controlled by its own promoter. P1 and P3 are constitutive promoters, whereas P2 is inducible by type I interferon. Exon 2 is the common splice acceptor for exon 1B, 1A or 1C. Exons 1B and 1C lack start codons and rely on an AUG in exon 2 to start translation. Alternative splicing generates the two isoforms of ADAR, p150 and p110. **(b)** The suboptimal Kozak sequence around the AUG codon in Exon 1A allows a fraction of scanning ribosomes to reach the next AUG, located in Exon 2, to produce minor fractions of p110 isoform by ATI.

USC
DE COMPOSTELA

around the next in-frame ATG (Figure 68c,d), reinforcing the notion of an adaptation of the ribosomal leaky scanning mechanism to the production of protein isoforms with different subcellular localization. It is remarkable again the presence in these genes of both downstream ATGs and near cognates with strong or even optimal Kozak contexts that could sustain a relevant amount of translation initiation in mutants of the primary start codons, which should be taken into account for the design of separation-of-function alleles for these genes. In this sense, it has been recently reported that to achieve the exclusive expression of the mitochondrial isoform of human TOP3α the mutation of both its second ATG (which drives the translation of the nuclear isoform) and its NLS is required (Hangas et al., 2022).

Interestingly, leaky scanning can be also relevant in mRNAs that also undergo alternative splicing to produce different protein isoforms, such as human ADAR1. Transcription of this RNA adenosine deaminase is controlled by three different promoters: two constitutive, P1 and P3, upstream exons 1B and 1C respectively, and one additional promoter, P2, inducible by the interferon response and upstream exon 1A (Figure 69a). After transcription from each of those promoters, alternative splicing results in linkages between exon 1B, 1C, or 1A with exon 2. Differently to exon 1B and 1C, exon 1A contains an AUG that initiates translation within this exon, producing the interferon-inducible p150 isoform. Alternatively, exon 1B and 1C lack AUG codons in the correct reading frame, so translation starts from an AUG at exon 2, creating the constitutively expressed, shorter isoform known as p110 (Figure 69a) (Baker and Slack, 2022). However, it was recently demonstrated that the mRNA containing exon 1A can also generate minor fractions of the p110 isoform by a leaky scanning mechanism, since the Kozak context surrounding the AUG at exon 1A is suboptimal, allowing a fraction of ribosomes to scan through and engage translation from the AUG in exon 2 (Figure 69b) (Sun et al., 2021).

Likewise, hPIF1 provides another example of how alternative splicing and leaky scanning can coexist in the same gene. The hPIF1α and hPIF1ß isoforms are produced by alternative splicing: a short transcript of 2295 nt is translated into a longer isoform (hPIF1ß), targeted to the by leaky scanning, add another source of mitochondrial PIF1 independent of hPIF1ß, targeted to mitochondria, whereas the longer transcript produces a shorter isoform, without MTS, that translocates into the nucleus (hPIF1α) (Futami et al., 2007). Nevertheless, it was later demonstrated how ATI at AUG^{54} exposes a functional MTS (Figure 70), while simultaneously removing the NLS (Kazak et al., 2013). This event of ATI, probably mediated by leaky scanning, adds another source of mitochondrial PIF1 independent of hPIF1ß, which should be considered for the design of specific alleles to study the mitochondrial roles of hPIF1.

USC
UNIVERSIDADE DE SANTIAGO DE COMPOSTELA

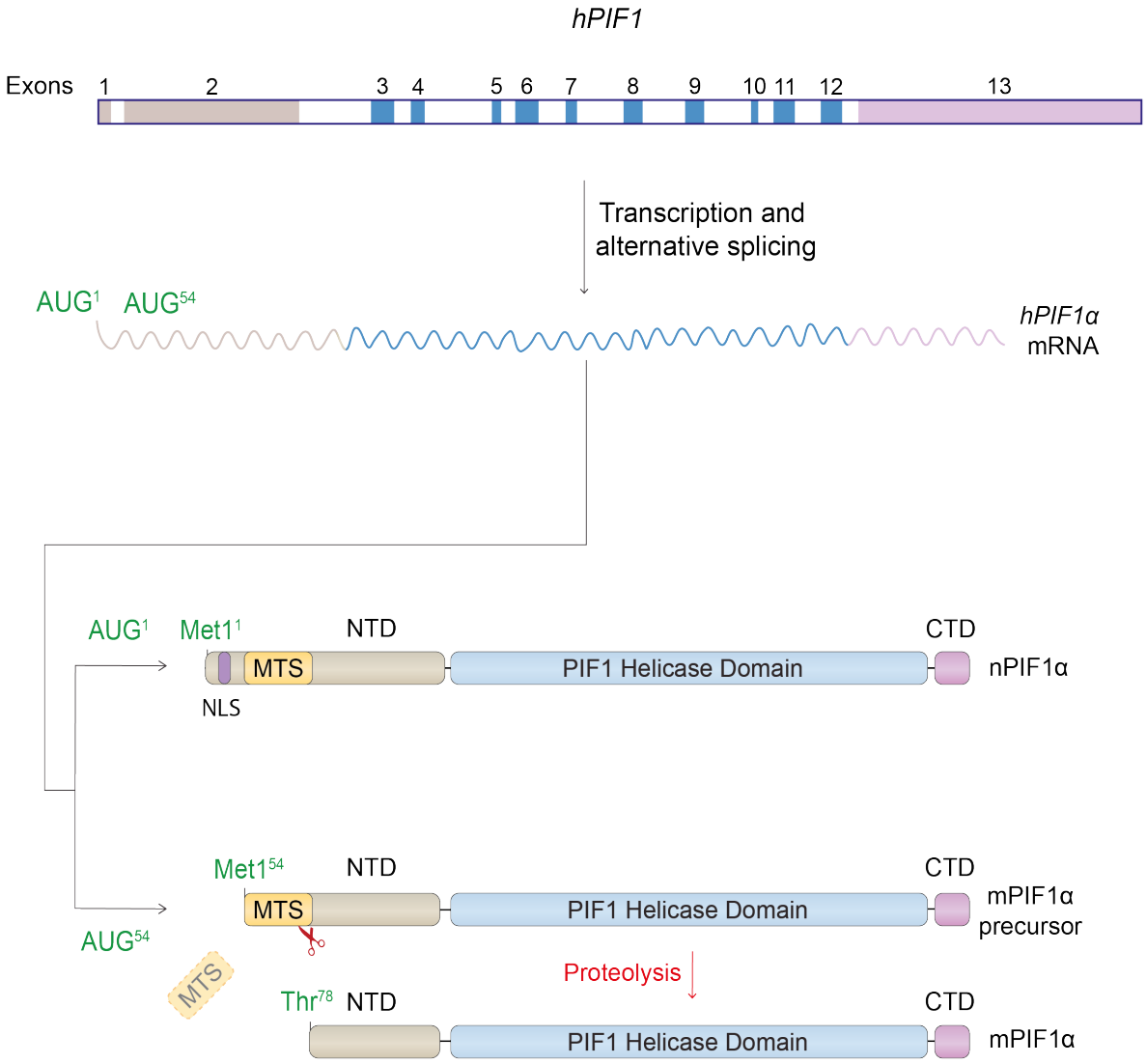


Figure 70. hPIF1α produces two isoforms by ATI with dual-targeted localization. In addition of the well-characterised nuclear isoform of hPIF1α, another isoform is produced by ATI at AUG^{54}, exposing a cryptic MTS that is buried in the full length isoform. When located at the beginning of the NTD, this MTS directs PIF1α to the mitochondria, where it is imported and processed by mitochondrial proteases. For simplicity, the second mitocondrial isoform produced by alternative splicing, hPIF1ß, is not depicted in this Figure.

USC
UNIVERSIDADE DE SANTIAGO DE COMPOSTELA

CONCLUSIONS

1. Overexpression of prematurely activated Yen1 leads to cell death, perturbed cell-cycle progression and DNA-damage checkpoint activation.
2. *YEN1^{ON}* displays synthetic genetic interactions with several helicases involved in DNA replication and repair.
3. Endogenous expression of *YEN1^{ON}* with a concomitant loss of nuclear Pif1 functions derives in synthetic hypersensitivity to genotoxic agents.
4. Neither of the classical separation-of-function alleles, *pif1-m1* and *pif1-m2*, recapitulates the *pif1*Δ genetic interaction with *dia2*Δ*, rad3-102* or *YEN1^{ON}*.
5. Pif1$^{107-859}$ is a novel, nuclear and catalytically active Pif1 isoform that arises as a consequence of ATI by ribosomal leaky scanning.
6. Specific enrichment of Pif1$^{107-859}$ in *pif1-m2* strains can partially suppress some of the *pif1*Δ phenotypes.
7. Identification of the previously uncharacterized Pif1 NLS enables the generation of *PIF1* mutants with impaired nuclear import.
8. Disruption of the NLS in *pif1-m2* mutants results in a novel allele that successfully recapitulates those *pif1*Δ phenotypes specifically due to the loss of its nuclear functions.
9. ATI events from non-AUG codons produce biologically relevant amounts of mPif1 that sustain mitochondrial function in *pif1-m1* mutants.
10. The consequences of ATI events by leaky scanning can be extended to other dual-targeted DNA repair factors and should be considered for the design of complete separation-of-function alleles.

USC
UNIVERSIDADE DE SANTIAGO DE COMPOSTELA

USC
UNIVERSIDADE
DE SANTIAGO
DE COMPOSTELA

MATERIALS

1. Bacterial Strains

The genotypes of all the *E. coli* strains used in this Thesis are listed in Table 1. For routine laboratory work, like cloning or vector propagation, the DH5alpha strain was used. Gateway vectors encoding the toxic *ccdB* gene were propagated using *One shot*^{TM}*ccdB* Survival™ 2 T1^{R}. For efficient overexpression of heterologous proteins, the BL21-CodonPlus (DE3)-RIL strain was employed; this strain lacks the Lon and OmpT proteases to avoid protein degradation and it harbours a plasmid that codes for additional copies of limiting tRNAs in bacteria and confers chloramphenicol resistance.

Table 1. *E. coli* strains used in this study.

***E. coli* strain**	**Genotype**
DH5α	(F – ϕ80lacZΔM15 Δ(lacZYAargF)U169 recA1 endA1 hsdR17(rK – , mK +) phoA supE44 λ – thi-1 gyrA96 relA1)
One shotTMccdB Survival™ 2 T1R	(F-mcrA Δ(mrr-hsdRMS-mcrBC) Φ80lacZΔM15 ΔlacX74 recA1 araΔ139 Δ(ara-leu)7697 galU galK rpsL (StrR) endA1 nupG fhuA:IS),
BL21-CodonPlus (DE3)-RIL	[E. coli B F – ompT hsdS(r B – mB –) dcm + Tet r gal λ(DE3) endA Hte [argU ileY leuW CamR].

2. Yeast strains

Unless indicated, all strains used in this work are derivatives W303 derivatives (*MATa leu2-3,112 trp1-1 can1-100 ura3-1 ade2-1 his3-11,15 RAD5+*) or (*MATa ura3-52 trp1Δ2 leu2-3_112 his3-11 ade2-1 can1-100 RAD5+*).

** YPH background

Strain (YTL)	**Genotype**
216	*MATa/MATalpha sgs1Δ::TRP1 srs2Δ::his3MX6 YEN1-ON-myc9::NATMX4*
218	*MATa/MATalpha sgs1Δ::TRP1 srs2Δ::his3MX6 rad52Δ::LEU2 YEN1-WT-myc9::NATMX4*
402	*MATa/MATalpha mph1Δ::TRP1 srs2Δ::his3MX6 YEN1-WT-myc9::NATMX4*
403	*MATa/MATalpha mph1Δ::TRP1 srs2Δ::his3MX6 YEN1-ON-myc9::NATMX4*

USC UNIVERSIDADE DE SANTIAGO DE COMPOSTELA

Strain (YTL)	Genotype
413	*MATa/MATalpha mph1Δ::TRP1 sgs1Δ::his3MX6 YEN1-WT-myc9::NATMX4*
414	*MATa/MATalpha mph1Δ::TRP1 sgs1Δ::his3MX6 YEN1-ON-myc9::NATMX4*
528	*MATa/MATalpha mus81Δ::TRP1 srs2Δ::his3MX6 rad52Δ::LEU2 YEN1-WT-myc9::NATMX4*
530	*MATa/MATalpha mph1Δ::TRP1 srs2Δ::his3MX6 rad52Δ::LEU2 YEN1-WT-myc9::NATMX4*
532	*MATa/MATalpha sgs1Δ::TRP1 srs2Δ::his3MX6 rad52Δ::LEU2 YEN1-WT-myc9::NATMX4*
533	*MATa/MATalpha sgs1Δ::TRP1 slx1Δ::kanMX4 rad52Δ::LEU2 YEN1-WT-myc9::NATMX4*
534	*MATa/MATalpha mph1Δ::TRP1 sgs1Δ::his3MX6 rad52Δ::LEU2 YEN1-WT-myc9::NATMX4*
535	*MATa/MATalpha sgs1Δ::TRP1 slx4Δ::kanMX4 rad52Δ::LEU2 YEN1-WT-myc9::NATMX4*
597	*pif1Δ::HIS3MX6*
760	*PIF1-6xHIS-6xFLAG::klTRP1*
764	*pif1-m1-6xHIS-6xFLAG::klTRP1*
765	*pif1-m2-6xHIS-6xFLAG::klTRP1*
834	*pif1-m2-6xHIS-6xFLAG::klTRP1 rad3-102::hyg*
835	*rad3-102::hyg*
841	*pif1-m1-6xHIS-6xFLAG::klTRP1*
844	*pif1-m2-6xHIS-6xFLAG::klTRP1*
847	*PIF1-6xHIS-6xFLAG::klTRP1*
885	*MATa/MATalpha dia2Δ::kanMX pif1-m2-6xHIS-6xFLAG::klTRP1*
924	*pif1-m2 ura3-52::pRSII406-PIF1-WT-6h6flag*
927	*pif1-m2 ura3-52::pRSII406-PIF1-M1-6h6flag*
930	*MATa pif1-m2 ura3-52::pRSII406-PIF1-M2-6h6flag*
933	*pif1-m2 ura3-52::pRSII406-PIF1-WT-K1-6h6flag*

USC UNIVERSIDADE DE SANTIAGO DE COMPOSTELA

Strain (YTL)	Genotype
936	*pif1-m2 ura3-52::pRSII406-PIF1-WT-K40-6h6flag*
942	*pif1-m2 ura3-52::pRSII406-PIF1-M1-K40-6h6flag*
967	*pif1-m2 ura3-52::pRSII406-PIF1-M2-M107I-6h6flag*
970	*pif1-m2 ura3-52::pRSII406-PIF1-M2-M113I-6h6flag*
972	*pif1-m2 ura3-52::pRSII406-PIF1-M2-M127I-6h6flag*
976	*pif1-m2 ura3-52::pRSII406-PIF1-M2-M187I-6h6flag*
978	*pif1-m2 ura3-52::pRSII406-PIF1-M2-M196I-6h6flag*
1089	*MATa/MATalpha dna2Δ::LEU2 kanMX::pADH1-pif1-m2-6h6flag::klTRP1 / pif1-m2-6h6flag::klTRP1*
1097	*pif1Δ::HIS3MX6 PIF1-107-859-WT-6h6Flag::pRSII406*
1108	*MATa/MATalpha dia2Δ::kanMX pif1Δ::HIS3MX6 PIF1-107-859-WT-6h6Flag::pRSII406*
1111	*pif1Δ::HIS3MX6 PIF1-107-859-WT-6h6Flag::pRSII406*
1115	*rad3-102::hyg pif1Δ::HIS3MX6 PIF1-107-6h6Flag::pRSII406*
1163	*pif1-m2 ura3-52::pRSII406-PIF1-M2-M107-M113-M127-6h6flag*
1178	*MATa/MATalpha top3Δ::LEU2 pif1Δ::his3MX6*
1180	*MATa/MATalpha top3Δ::LEU2 pif1-m1-6xHIS-6xFLAG::klTRP1*
1182	*MATa/MATalpha top3Δ::LEU2 pif1-m2-6xHIS-6xFLAG::klTRP1*
1193	*MATa/MATalpha dia2Δ::kanMX pif1Δ::his3MX6*
1194	*MATa/MATalpha dia2Δ::kanMX pif1-m1-6xHIS-6xFLAG::klTRP1*
1203	*pif1-m2 ura3-1::pAG306GAL-775-803-NLS-PIF1-eGFP*
1209	*pif1-m2 ura3-1::pAG306GAL-775-803-NLS-4A-eGFP*
1230	*MATa/MATalpha top3Δ::LEU2 kanMX::pADH1-pif1-m2-6h6flag::klTRP1 / pif1-m2-6h6flag::klTRP1*
1237	*MATa/MATalpha dna2Δ::LEU2 pif1Δ::his3MX6*

USC UNIVERSIDADE DE SANTIAGO DE COMPOSTELA

Strain (YTL)	Genotype
1239	*MATa/MATalpha dna2Δ::LEU2 pif1-m1-6xHIS-6xFLAG::klTRP1*
1242	*MATa/MATalpha dna2Δ::LEU2 pif1-m2-6xHIS-6xFLAG::klTRP1*
1273	*MATa/MATalpha top3Δ::LEU2 pif1Δ::HIS3MX6 PIF1-107-859-WT-6h6Flag::pRSII406*
1274	*MATa/MATalpha dna2Δ::LEU2 pif1Δ::HIS3MX6 PIF1-107-859-WT-6h6Flag::pRSII406*
1278	*MATa/MATalpha top3Δ::LEU2 PIF1-NLS-6xHIS-6xFLAG::klTRP1*
1280	*MATa/MATalpha dna2Δ::LEU2 PIF1-NLS-6xHIS-6xFLAG::klTRP1*
1283	*MATa/MATalpha dia2Δ::kanMX PIF1-NLS-6xHIS-6xFLAG::klTRP1*
1492	*MATa/MATalpha dia2Δ::kanMX pif1Δ::his3MX pif1-mit-6xHIS-6xFLAG::klTRP1*
1527	*rad3-102::hyg pif1Δ::HIS3MX6*
1650	*pif1-m2 ura3-1::pAG306GAL-PIF1-eGFP*
1651	*pif1-m2 ura3-1::pAG306GAL-pif1-m1-eGFP*
1652	*pif1-m2 ura3-1::pAG306GAL-pif1-m2-eGFP*
1653	*pif1-m2 ura3-1::pAG306GAL-pif1-107-859-eGFP*
1654	*pif1-m2 ura3-1::pAG306GAL-pif1-Δ775-803-eGFP*
1655	*pif1-m2 ura3-1::pAG306GAL-pif1-Δ623-646-eGFP*
1656	*pif1-m2 ura3-1::pAG306GAL-pif1-Δ650-662-eGFP*
1657	*pif1-m2 ura3-1::pAG306GAL-pif1-Δ814-834-eGFP*
1658	*pif1-m2 ura3-1::pAG306GAL-pif1-9A-eGFP*
1659	*pif1-m2 ura3-1::pAG306GAL-pif1-4A-eGFP*
1660	*pif1-m2 ura3-1::pAG306GAL-pif1-5A-eGFP*
1700	*ura3-52::pAG306GAL-YEN1-WT-FTH*
1701	*ura3-52::pAG306GAL-YEN1-ND-FTH*

USC UNIVERSIDADE DE SANTIAGO DE COMPOSTELA

Strain (YTL)	Genotype
1702	*ura3-52::pAG306GAL-YEN1-KR-FTH*
1703	*ura3-52::pAG306GAL-YEN1-ON-FTH*
1704	*ura3-52::pAG306GAL-YEN1-ON-KR-FTH*
1705	*ura3-52::pAG306GAL-YEN1-KR-ND-FTH*
1706	*ura3-52::pAG306GAL-YEN1-ON-ND-FTH*
1707	*ura3-52::pAG306GAL-YEN1-ON-KR-ND-FTH*
1708	*sml1Δ ura3-52::pAG306GAL-YEN1-WT-FTH*
1709	*sml1Δ ura3-52::pAG306GAL-YEN1-ND-FTH*
1710	*sml1Δ ura3-52::pAG306GAL-YEN1-KR-FTH*
1711	*sml1Δ ura3-52::pAG306GAL-YEN1-ON-FTH*
1712	*sml1Δ ura3-52::pAG306GAL-YEN1-ON-KR-FTH*
1713	*sml1Δ ura3-52::pAG306GAL-YEN1-KR-ND-FTH*
1714	*sml1Δ ura3-52::pAG306GAL-YEN1-ON-ND-FTH*
1715	*sml1Δ ura3-52::pAG306GAL-YEN1-ON-KR-ND-FTH*
1716	*sml1Δ rad53Δ ura3-52::pAG306GAL-YEN1-WT-FTH*
1717	*sml1Δ rad53Δ ura3-52::pAG306GAL-YEN1-ND-FTH*
1718	*sml1Δ rad53Δ ura3-52::pAG306GAL-YEN1-KR-FTH*
1719	*sml1Δ rad53Δ ura3-52::pAG306GAL-YEN1-ON-FTH*
1720	*sml1Δ rad53Δ ura3-52::pAG306GAL-YEN1-ON-KR-FTH*
1721	*sml1Δ rad53Δ ura3-52::pAG306GAL-YEN1-KR-ND-FTH*
1722	*sml1Δ rad53Δ ura3-52::pAG306GAL-YEN1-ON-ND-FTH*
1723	*sml1Δ rad53Δ ura3-52::pAG306GAL-YEN1-ON-KR-ND-FTH*

USC UNIVERSIDADE DE SANTIAGO DE COMPOSTELA

Strain (YTL)	Genotype
1724	*rad52Δ ura3-52::pAG306GAL-YEN1-WT-FTH*
1725	*rad52Δ ura3-52::pAG306GAL-YEN1-ND-FTH*
1726	*rad52Δ ura3-52::pAG306GAL-YEN1-KR-FTH*
1727	*rad52Δ ura3-52::pAG306GAL-YEN1-ON-FTH*
1728	*rad52Δ ura3-52::pAG306GAL-YEN1-ON-KR-FTH*
1729	*rad52Δ ura3-52::pAG306GAL-YEN1-KR-ND-FTH*
1730	*rad52Δ ura3-52::pAG306GAL-YEN1-ON-ND-FTH*
1731	*rad52Δ ura3-52::pAG306GAL-YEN1-ON-KR-ND-FTH*
3000	*MATa*

3. PLASMIDS

All plasmids used in this thesis are listed on Table 2.

Table 2. List of plasmids used in this study.

Alias	Name	Source
pTL1	pUC19-6xHIS6xFLAG::klTRP1	Kind gift from Joao Matos
pTL2	pUC19-9xMyc::KANMX	Lab collection
pTL24	pAG306GAL1-YEN1_WT-FTH	Lab collection
pTL26	pAG306GAL1-YEN1_ON-FTH	Lab collection
pTL34	pFA6a-LEU2	(Longtine et al., 1998)
pTL35	pFA6-scTRP1	(Longtine et al., 1998)
pTL38	pFA6a-hphMX6	(Longtine et al., 1998)
pTL40	pFA6a-kanMX4	(Longtine et al., 1998)
pTL41	pFA6a-HIS3MX6	(Longtine et al., 1998)

USC UNIVERSIDADE DE SANTIAGO DE COMPOSTELA

Alias	Name	Source
pTL42	pCORE-UH	(Storici and Resnick, 2006)
pTL61	p4339-natMX	Lab collection
pTL64	pYES-DEST52-YEN1-V5-HIS	Lab collection
pTL65	pYES-DEST52-YEN1^{ON}-V5-HIS	Lab collection
pTL68	pENTR221-YEN1^{ON-ND}	Lab collection
pTL70	pENTR221-YEN1^{ON-ND}-FTH	This work
pTL74	pAG306GAL-YEN1^{ON-ND}-FTH	This work
pTL95	pENTR221-PIF1_WT	This work
pTL97	pENTR221-PIF1_M2	This work
pTL106	pUC19-Myc9-klTRP1	Lab collection
pTL127	pRS306GAL1,10-YEN1^{ON-ND}-FTH	This work
pTL147	pFA6a-klTRP1	This work
pTL154	pENTR221-YEN1^{KR}-FTH	This work
pTL157	pENTR221-YEN1^{ON-KR}-FTH	This work
pTL161	pENTR221-YEN1^{ND-KR}-FTH	This work
pTL165	pENTR221-YEN1$^{ON-ND-KR}$-FTH	This work
pTL198	pAG306GAL-ccdB-eGFP	(Alberti et al., 2007)
pTL206	pRSII406-PIF1-WT-6h6flag	This work
pTL207	pRSII406-PIF1-M1-6h6flag	This work
pTL208	pRSII406-PIF1-M2-6h6flag	This work
pTL212	pRSII406-PIF1-M107I-6h6flag	This work
pTL213	pRSII406-PIF1-M113I-6h6flag	This work
pTL214	pRSII406-PIF1-M127I-6h6flag	This work
pTL215	pRSII406-PIF1-M187I-6h6flag	This work
pTL216	pRSII406-PIF1-M196I-6h6flag	This work

USC UNIVERSIDADE DE SANTIAGO DE COMPOSTELA

Alias	Name	Source
pTL217	pRSII406-PIF1-M2-M107I-6h6flag	This work
pTL218	pRSII406-PIF1-M2-M113I-6h6flag	This work
pTL219	pRSII406-PIF1-M2-M127I-6h6flag	This work
pTL220	pRSII406-PIF1-M2-M187I-6h6flag	This work
pTL221	pRSII406-PIF1-M2-M196I-6h6flag	This work
pTL222	pRSII406-PIF1-Kozak-MET1-6h6flag	This work
pTL223	pRSII406-PIF1-Kozak-MET40-6h6flag	This work
pTL224	pRSII406-PIF1-Kozak-MET40-ST-6h6flag	This work
pTL225	pRSII406-PIF1-M1-Kozak-MET40-6h6flag	This work
pTL226	pRSII406-PIF1-M1-Kozak-MET40-ST-6h6flag	This work
pTL227	pRSII406-PIF1-M2-Kozak-MET1-6h6flag	This work
pTL228	pRSII406-PIF1-R3E-6h6flag	This work
pTL229	pRSII406-PIF1-TLSSAES-4A-6h6flag	This work
pTL230	pRSII406-PIF1-K264A-6h6flag	This work
pTL231	pRSII406-PIF1-NLS-4A-6h6flag	This work
pTL232	pAG306GAL-YEN1-ON-KR-FTH	This work
pTL234	pAG306GAL-YEN1-WT-KR-FTH	This work
pTL236	pET28b-6xHis-nPIF1-WT	(Boulé et al., 2005) Addgene (#60547)
pTL237	pET28b-6xHis-nPIF1-K264A	This work
pTL238	pET28b-6xHis-nPIF1-4A-NLS	This work
pTL241	pRSII406-PIF1-WT-M107I-M127I-6h6flag	This work
pTL242	pRSII406-PIF1-M2-M107I-M127I-6h6flag	This work
pTL243	pRSII406-PIF1-WT-M187I-M196I-6h6flag	This work
pTL244	pRSII406-PIF1-M2-M187I-M196I-6h6flag	This work
pTL245	pRSII406-PIF1-WT-M107I-M113I-M127I-6h6flag	This work

USC UNIVERSIDADE DE SANTIAGO DE COMPOSTELA

Alias	Name	Source
pTL246	pRSII406-PIF1-M2-M107I-M113I-M127I-6h6flag	This work
pTL247	pET28b-6xHis-Pif1-107-859	This work
pTL248	pRSII406-PIF1-107-859-WT-6h6Flag	This work
pTL250	pBluescriptII-yeast-telomere	Kind gift from David Lydall
pTL255	pRSII406-PIF1-PIP-6h6flag	This work
pTL257	pENTR221-PIF1-WT-GO	This work
pTL258	pENTR221-PIF1-M1-GO	This work
pTL259	pENTR221-PIF1-M2-GO	This work
pTL260	pENTR221-PIF1-WT-NLS-4A-GO	This work
pTL262	pENTR221-PIF1-WT-5A-GO	This work
pTL265	pENTR221-PIF1-WT-9A-GO	This work
pTL266	pENTR221-PIF1-WT-NLS1Δ-775-789-GO	This work
pTL268	pENTR221-PIF1-WT-NLS2Δ-623-646-GO	This work
pTL270	pENTR221-PIF1-WT-NLS3Δ-650-662-GO	This work
pTL272	pENTR221-PIF1-WT-ΔNLS4-814-834	This work
pTL274	pAG306GAL-PIF1-WT-eGFP	This work
pTL275	pAG306GAL-PIF1-M1-eGFP	This work
pTL276	pAG306GAL-PIF1-M2-eGFP	This work
pTL277	pAG306GAL-PIF1-WT-Δ775-803-eGFP	This work
pTL278	pAG306GAL-PIF1-WT-775-789-4A-eGFP	This work
pTL281	pAG306GAL-PIF1-WT-9A-eGFP	This work
pTL282	pAG306GAL-PIF1-NLS1Δ-eGFP	This work
pTL284	pAG306GAL-PIF1-WT-NLS2-eGFP	This work
pTL286	pAG306GAL-PIF1-ΔNLS3-eGFP	This work
pTL288	pAG306GAL-PIF1-ΔNLS4-eGFP	This work

USC UNIVERSIDADE DE SANTIAGO DE COMPOSTELA

Alias	Name	Source
pTL290	pAG306GAL-PIF1-107-859-eGFP	This work
pTL291	pENTR221-PIF1-Δ775-803-GO	This work
pTL295	pENTR221-775-803-PIF1-GO	This work
pTL297	pENTR221-647-668-PIF1-GO	This work
pTL303	pRSII406-PIF1-M107-M113-M127-6h6flag	This work
pTL306	pAG306GAL-775-803-NLS-PIF1-eGFP	This work
pTL307	pAG306GAL-647-668-PIF1-eGFP	This work
pTL312	pENTR221-775-803-NLS-4A-PIF1-GO	This work
pTL313	pAG306GAL-775-803-NLS-4A-PIF1-eGFP	This work
pTL315	pAG306GAL-MET-linker-gateway-eGFP	This work
pTL320	pRSII406-PIF1-WT-L-(-8)A-IL(-5)A-6h6flag	This work
pTL321	pRSII406-PIF1-WT-IL(-5)A-6h6flag	This work
pTL322	pRSII406-PIF1-M1-L-(-8)A-IL(-5)A-6h6flag	This work
pTL323	pRSII406-PIF1-M1-IL(-5)A-6h6flag	This work
pTL324	pRSII406-PIF1-WT-IL5L-6h6flag	This work
pTL325	pRSII406-PIF1-WT-L9L-6h6flag	This work
pTL326	pRSII406-PIF1-WT-IL5L-L9L-IL12L-IL13L-6h6flag	This work
pTL327	pRSII406-PIF1-M1-IL5L-6h6flag	This work
pTL328	pRSII406-PIF1-M1-L9L-6h6flag	This work
pTL329	pRSII406-PIF1-M1-IL5L-L9L-IL12L-IL13L-6h6flag	This work
pTL331	pFA6a-hphNT1	(Janke et al., 2004)
pTL332	pFA6a-natNT2	(Janke et al., 2004)
pTL338	pRSII406-PIF1-M2-M107I-M113I-6h6flag	This work
pTL339	pRSII406-PIF1-M2-M113I-M127I-6h6flag	This work

USC UNIVERSIDADE DE SANTIAGO DE COMPOSTELA

4. OLIGONUCLEOTIDES

Oligonucleotides employed for plasmid mutagenesis, Gateway cloning, PCR cassettes for gene-editing and verification of gene-edited strains are listed in Table 3. Oligonucleotides used to prepare synthetic DNA substrates for *in vitro* helicase and nuclease assays are listed in Table 4.

Table 3. List of oligonucleotides for PCR amplification, mutagenesis and Gateway cloning used in this study.

Alias	Name	Sequence (5´-3´)
OTL9	RRM3 FW (-336)	CTAACACAGACCCTTGACAAATC
OTL10	RRM3 FW (-93)	CGTCAAAGAATATGTAAATAAACATCATC
OTL11	RRM3 RV (+125)	GATGGCTTCTAGATGAATATTTCGG
OTL12	RRM3 RV (+266)	CGATATATTCCTGGCTAGATCTCC
OTL13	SLX1 FW (-333)	CCAACAATGTACTCATCGAGG
OTL14	SLX1 FW (-160)	GAGTGCCTTGTCTTCTATGG
OTL15	SLX1 RV (+88)	TTCTTACAAAGTAAACGTAAAAATATCCG
OTL16	SLX1 RV (+221)	TGCCGACTAGATCGTCATATG
OTL17	SLX4 FW (-409)	GTGAACAAACTGAATTACAAGGC
OTL18	SLX4 FW (-84)	GAATGGAACTCCGAACAAGC
OTL19	SLX4 RV (+78)	GTGTACGTGTATTCTTCATCTATACG
OTL20	SLX4 RV (+293)	TTGCAGAGAATGACCTGGTG
OTL29	MPH1 FW (-140)	GGCATCACGAAGAGATCAATAG
OTL30	MPH1 FW (-110)	GTGCCCTATGCTCTATCACG
OTL31	MPH1 RV (+210)	GATTGTACTCGTCGTTGGCTC
OTL32	MPH1 RV (+380)	GGAGTGTAGGAAATTGTTGCG
OTL41	PIF1 FW (-309)	ATCAGGACGCTTCAAATGCC
OTL42	PIF1 FW (-226)	TTACATTAAGAAAGGCGCGTC
OTL43	PIF1 RV (+70)	GAACTATGTATCTCGGCCTTG
OTL44	PIF1 RV (+274)	GGCATTGTGAGTTAGTCTCC

USC UNIVERSIDADE DE SANTIAGO DE COMPOSTELA

Alias	Name	Sequence (5´-3´)
OTL55	delPIF1 FW	TGTAATATTATCCATTGAGCGATTAGCTTACTTGTATCAATCAAT TTTAC CGTACGCTGCAGGTCGAC
OTL56	delPIF1 RV	GATTATTATAGCAGTTTGTATTCTATATAACTATGTGTATTAATAT GTAC ATCGATGAATTCGAGCTCG
OTL57	OJM1	CAGTCGACCGGTTTGTAGCCTGTGACAGTGATAGCAGTAGCAC TATTGAA TCCGGTTCTGCTGCTAG
OTL58	OJM2	TCGGCGCGATCAACTGTGGTGGCGGATTTTTTGACGCTGTGCC CGTTAAC CCTCGAGGCCAGAAGAC
OTL62	5'-MPH1	AGACATAAACCGGGTAACGG
OTL63	delMPH1 FW	ATTCAACACATTCCGGTTCTGTTTTATTTTAGTGTCCTTTTTTCT CTCTG CGTACGCTGCAGGTCGAC
OTL64	delMPH1 RV	ATTACAGCAGCGTTATTTTTGTATAGACGCCGACGTATAAGAGT CTCCTA ATCGATGAATTCGAGCTCG
OTL65	MPH1 RV (+171)	TTCAAAAACAGTGCCGTATCC
OTL66	MPH1 RV (+325)	TTCATATCCTCCAAGAAACAAGC
OTL75	PIF1 tag FW	TGGTTTCCGACGAACCTCGTGGTCAGGATACCGAAGACCACAT CTTAGAA TCCGGTTCTGCTGCTAG
OTL76	PIF1 tag RV	GATTATTATAGCAGTTTGTATTCTATATAACTATGTGTATTAATAT GTAC CCTCGAGGCCAGAAGAC
OTL79	RAD52 FW (-320)	TCGCTAAAGATGGTATGGTACG
OTL80	RAD52 FW (-196)	CTCTTCCCGTTAGTGATTCTCG
OTL81	RAD52 RV (+312)	ATCTATTGTTTTTCCGAGTTGCC
OTL82	RAD52 RV (+427)	AATGTTGGGAATGGATAGGTCC
OTL83	DNA2 FW (-437)	CCGTCGTAGTTGCTACCTACC
OTL84	DNA2 FW (-157)	AACTGATCTTACGCTATTTATGGC
OTL85	DNA2 RV (+114)	CGAACCTCAGATGCTAATATTACG
OTL86	DNA2 RV (+347)	CAGAATCACCTTCACTCTGCC
OTL87	delDNA2 FW	GAGTACTCATTTTGTGCAAGCAAACACTGACAATTGAAGAGATC GTCAGG CGTACGCTGCAGGTCGAC
OTL88	delDNA2 RV	TATGCTGTGATAGCTTTCCTGTTATGGAGAAGCTCTTCTTATTC CCCCTG ATCGATGAATTCGAGCTCG
OTL114	K714R-FW	ATGTTGCCTCCAAACTTGAC
OTL115	K714R-Mut-RV	CCTAGTACCTTGAAGGCGAGC
OTL118	AsiSI-PIF1-FW	ACCTTAGCGATCGC ATGCCAAAGTGGATAAGATCAAC
OTL119	PIF1-GO-MluI-RV	ACCTTAACGCGTTTCTAAGATGTGGTCTTCGG

USC UNIVERSIDADE DE SANTIAGO DE COMPOSTELA

Alias	Name	Sequence (5´-3´)
OTL120	AttB1-SD-Kozak-PIF1-FW	GGGGACAAGTTTGTACAAAAAAGCAGGCTTCGAAGGAGATAGAACCATGCCAAAGTGGATAAGATCAAC
OTL121	AttB2-PIF1-(+STOP)-RV	GGGGACCACTTTGTACAAGAAAGCTGGGTCTTATTCTAAGATGTGGTCTTCGG
OTL122	AttB2-PIF1-(-STOP)-RV	GGGGACCACTTTGTACAAGAAAGCTGGGTCTTCTAAGATGTGGTCTTCGG
OTL127	delNLS-Pif1-FW (777-798)	GTCAAAGTCAAATTCTCCAGCACC
OTL128	delNLS-Pif1-RV (777-798)	AAGTTGCTTATAGGCACTTTCGG
OTL129	delNLS-Pif1-FW (623-646)	CATCAAAACTCTGCAGGAAAACG
OTL130	delNLS-Pif1-RV (623-646)	CATGAAGTCAAAAACTGAGGAATCTAGG
OTL131	delNLS-Pif1-FW (650-662)	GCTTCTGATATGAGTACGAGGATGG
OTL132	delNLS-Pif1-RV (650-662)	GTTTTGATGTATGGTCTGCATCAG
OTL133	delNLS-Pif1-FW (818-833)	TCTAATAGTAATCAAGTTCATTCATTGG
OTL134	delNLS-Pif1-RV (818-833)	AGATTGTGTGGTCGCTG
OTL135	delNLS-Pif1-FW (162-173)	CTTCAAAATAATTCTATATCTCAAGAGAG
OTL136	delNLS-Pif1-RV (162-173)	TAATGGATTCTTGAATCCTGTCG
OTL137	delNLS-Pif1-FW (315-334)	ATTGGTGCTTTGGTTGTCG
OTL138	delNLS-Pif1-RV (315-334)	ATCACCTTTTCCTAATCCTATACC
OTL139	delNLS-Pif1-FW (417-450)	TTGCCAGACGATGAAATTATTCCC
OTL140	delNLS-Pif1-RV (417-450)	AAAAACCTTTTGTAGCATAATCGTC
OTL141	E193A/E195A RV	ACCACAAGCGATAACGTAGG
OTL142	E193A/E195A FW	GCTGGTGCTGCTCAATGTGTTTGGTTGC
OTL153	AsiSI-PIF1-M1-FW	ACCTTAGCGATCGCGCCCCAAAGTGGATAAGATCAAC
OTL181	delNLS-Pif1-FW (777-798)	TCAAAGTCAAATTCTCCAGCACC
OTL206	attb1-PIF1-FW	GGGGACAAGTTTGTACAAAAAAGCAGGCTTCATGCCAAAGTGGATAAGATCAAC
OTL207	attB2-PIF1-RV-GO	GGGGACCACTTTGTACAAGAAAGCTGGGTCTTCTAAGATGTGGTCTTCGG
OTL208	PIF1-NLS-775-803-FW	CCAGCACCCATATCAGC
OTL209	PIF1-NLS-775_803-RV	AAGTTGCTTATAGGCACTTTCG

USC UNIVERSIDADE DE SANTIAGO DE COMPOSTELA

Alias	Name	Sequence (5´-3´)
OTL210	PIF1-4A-FW	TTAGACTACGCACCAGGC
OTL211	PIF1-4A-RV	TGCTGCAGCAGCCACTTGCTCATCTGCCTC
OTL212	PIF1-5A-FW	CCTGCATATGCAGCTGCTTCCGCATCAGCTTCAAATTCTCCAG CACCC
OTL213	PIF1-5A-RV	GCCTGGTGCGTAGTCTAAC
OTL228	AttB1-PIF1-M1-FW	GGGGACAAGTTTGTACAAAAAAGCAGGCTTCGCCCCAAAGTGG ATAAGATCAAC
OTL237	6his6Flag-ter	CAGCAGGCCTCTCAATAGAGG
OTL238	PIF1 P.I	TTCTAAGATGTGGTCTTCGGTATCCTGACCACGAGGTTCGTCG GAAACCA TTCGTACGCTGCAGGTCGAC
OTL239	PIF1 P.II	ATGCCAAAGTGGATAAGATCAACATTGAATCATATTATACCAAG AAGGCC CCGCGCGTTGGCCGATTCAT
OTL241	PIF1-M107I-FW	AGGGATAAAAATGTCATGAATTTTATC
OTL242	PIF1-M107I-RV	AATAGGCTTTTTGTCCACC
OTL243	PIF1-M113I-FW	AATTTTATCAATAAAGACAGTCCTTTATCC
OTL244	PIF1-M113I-RV	AATGACATTTTTATCCCTCATAGG
OTL245	PIF1-M127I-FW	TTTAAACCCAGTATAATACAACCAC
OTL246	PIF1-M127I-RV	AATATCGTTCCAGGATAAAGG
OTL247	PIF1-M187I-FW	ATAAATGAAAACGAAAAGAAGAAAATG
OTL248	PIF1-M187I-RV	AATTTCCAAACTTCTCTCTTGAG
OTL249	PIF1-M196I-FW	CAATTTGGAGAAAAGATTGCTG
OTL250	PIF1-M196I-RV	AATTTTCTTCTTTTCGTTTTCATTTATC
OTL251	DIA2 (-287) FW	CATTGATCGTTTGAGTATCTGCG
OTL252	DIA2 (-101) FW	TTGGTAACACTAGCTTTAAACCG
OTL253	DIA2 (+91) FW	AGCTTTCTATATTCTCACCTCC
OTL254	DIA2 (+213) RV	TTGGTAACACTAGCTTTAAACCG
OTL261	PIF1-MET1-Kozak-RV	GTTTAATTGATTGATACAAGTAAGCTAATCG
OTL262	PIF1-MET1-Kozak-FW	ATGCCAAAGTGGATAAGATC
OTL263	PIF1-MET2-Kozak-RV	ACTGAACGATAGTTTGGCGTGC

USC UNIVERSIDADE DE SANTIAGO DE COMPOSTELA

Alias	Name	Sequence (5´-3´)
OTL264	PIF1-MET2-Kozak-S39T-RV	TGTGAACGATAGTTTGGCGTGC
OTL265	PIF1-MET2-Kozak-FW	ATGTCTAGTCGTGGTTTCAGGTCTAATAAC
OTL270	PIF1-TLSSAES-4A-FW	GAAGCTGCCTATAAGCAACTTGAGGC
OTL271	PIF1-TLSSAES-4A-RV	GGCTGCAGCTAAAGCAAGATAAAAATCAATTACCTTTTGATG
OTL275	PIF1-K264-mut-RV	GGCACTCCCTGTATAAAAAATGTTGTG
OTL276	PIF1-K264A-mut-FW	GGTACCGGTGCATCCATTCTTTTACGTGAAATG
OTL277	PIF1-K264R-mut-FW	GGTACCGGTAGATCCATTCTTTTACGTGAAATG
OTL278	PIF1-R3E-mut-RV	CGCTGCTCTACCATTATTAGATTGTGTGGTCG
OTL279	PIF1-R3E-mut-FW	AGAAGACAAGAACACAGTAGGAAGAGATTTCAGTTG
OTL286	PIF1-S1	TTTGTAATATTATCCATTGAGCGATTAGCTTACTTGTATCAATCAATTTTACATGCGTACGCTGCAGGTCGAC
OTL287	PIF1-S4	AATGGCCTTCTTGGTATAATATGATTCAATGTTGATCTTATCCACTTTGGCATCGATGAATTCTCTGTCG
OTL288	PIF1-8A-9A-RV	GCCTGGTGCGTAGTCTAATGC
OTL304	delRRM3-FW	GAGGAGAACAAGCTCAAAAGTCGAGAGATTTGTTCTTATAAGACATCCCGCGTACGCTGCAGGTCGAC
OTL305	delRRM3-RV	AACAAGAAAAGAAAACTTCAACTAGAGTATATGCATTTATTCGTTGCAAGATCGATGAATTCGAGCTCG
OTL314	PIF1-M107I-M113I-RV	AATGACATTTTTATCCCTAATAGGC
OTL315	PIF1-M107I-M113I-FW	AATTTTATCAATAAAGACAGTCCTTTATCC
OTL316	PIF1-M187I-M196I-RV	GTTTTCATTTATAATTTCCAAACTTCTCTCTTGAG
OTL317	PIF1-M187I-M196I-FW	GAAAAGAAGAAAATTCAATTTGGAGAAAAGATTGCTG
OTL320	attB1-MET-Linker-gateway-cter-attB2-FW	GGGGACAAGTTTGTACAAAAAAGCAGGCTTCATGGGTGCTTCTGCAGACCCAGCTTTCTTGTACAAAGTGGTCCCC
OTL321	attB1-MET-Linker-gateway-cter-attB2-RV	GGGGACCACTTTGTACAAGAAAGCTGGGTCTGCAGAAGCACCCATGAAGCCTGCTTTTTTGTACAAACTTGTCCCC
OTL322	attB1-NLS1-775-803-PIF1-FW	GGGGACAAGTTTGTACAAAAAAGCAGGCTTCATGGAGGCAGATGAGCAAGTG
OTL323	attB2-NLS1-775-803-PIF1-RV	GGGGACCACTTTGTACAAGAAAGCTGGGTCAGAATTTGACTTTGACTTGG
OTL324	attB1-NLS3-647-668-FW	GGGGACAAGTTTGTACAAAAAAGCAGGCTTCATGCATCAAAACTCTGCAGGAAAACG
OTL325	attB2-NLS3-647-668-RV	GGGGACCACTTTGTACAAGAAAGCTGGGTCCGTACTCATATCAGAAGCTTTGAATC
OTL338	M107-PIF1-pRS-RV	GTAAAATTGATTGATACAAGTAAGC

Alias	Name	Sequence (5´-3´)
OTL339	M107-PIF1-FW	ATGAGGGATAAAAATGTCATG
OTL340	NdeI-M107-PIF1-pET28b-FW	ATCGATCATATGAGGGATAAAAATGTCATG
OTL341	M107-PIF1-pET28b-RV	AAGCTTGTCGACTTATTCTAAG
OTL342	M107-PIF1-pAG-RV	GAAGCCTGCTTTTTTGTAC
OTL343	RRM3-C-term-tag-FW	GCACCAATGAAAGAGTAAAAGATTTCTATAAACGTTTAGAAACT TTGAAATCCGGTTCTGCTGCTAG
OTL344	RRM3-C-term-tag-RV	AACAAGAAAAGAAAACTTCAACTAGAGTATATGCATTTATTCGTT GCAAGCCTCGAGGCCAGAAGAC
OTL347	PIF1-F760A-Y761A-RV	ATCAATTACCTTTTGATGTGCTTTG
OTL348	PIF1-F760A-Y761A-FW	GCTGCACTTACTTTATCTTCAGCCGAAAGTGC
OTL349	m1045	CTGCATTTGGCTCCATTTT
OTL350	m1046	TGTTGTAATGGGGACGGAAA
OTL363	Telomeric-Probe-Y-FW	GCGTTTGCGTTCCATGACGAG
OTL364	Telomeric-Probe-Y-RV	CTGCCGTGCAACAAACACTAAATC
OTL365	5'-SGS1	GCCAGCTTGGAGTCATTGGC
OTL366	delSGS1-FW	ATTATTGTTGTATATATTTAAAAAATCATACACGTACACACAAGG CGGTA CGTACGCTGCAGGTCGAC
OTL367	delSGS1-RV	TTGGCGAATGGTGTCGTAGTTATAAGTAACACTATTTATTTTTCT ACTCT ATCGATGAATTCGAGCTCG
OTL394	delSML1-FW	GATCTTACGGTCTCACTAACCTCTCTTCAACTGCTCAATAATTT CCCGCTCGTACGCTGCAGGTCGAC
OTL395	delSML1-RV	CAGAACTAGTGGGAAATGGAAAGAGAAAAGAAAAGAGTATGAA AGGAACTATCGATGAATTCGAGCTCG
OTL396	delTEL1-FW	TTCGAAAAAAAAAGCCTTCAAAGAAAAAGGGAAATCAGTGTAACA TAGACGCGTACGCTGCAGGTCGAC
OTL397	delTEL1-RV	TTCGTATTTCTATAAACAAAAAAAAGAAGTATAAAGCATCTGCAT AGCAAATCGATGAATTCGAGCTCG
OTL399	delMEC1-RV	TGGTTAGATCAAGAGGAAGTTCGTCTGTTGCCGAAAATGGTGG AAAGTCGATCGATGAATTCGAGCTCG
OTL400	delRAD53-FW	TAAAAGAGAGAATAGTGAGAAAAGATAGTGTTACACAACATCAA CTAAAACGTACGCTGCAGGTCGAC
OTL401	delRAD53-RV	ATCTTCTCTCTTAAAAAGGGGCAGCATTTTCTATGGGTATTTGT CCTTGGATCGATGAATTCGAGCTCG
OTL402	TEL1 FW (-154)	AGAAACAAGTATGGCACCAGCC
OTL403	TEL1 RV (+96)	AGTAATGGTAGCTTCACTATCAGC
OTL404	MEC1 FW (-127)	AATCAAATAGATGGAACGCACG

USC UNIVERSIDADE DE SANTIAGO DE COMPOSTELA

Alias	Name	Sequence (5´-3´)
OTL405	MEC1 RV (+114)	GTGTCAACATCCCTGTTAAGAGAG
OTL408	PIF1-N-term P.I	CGTGCGATACGTTTTTGAGTAAAAGAAAACTGTTGAAACTACAG ATAAAT TTCGTACGCTGCAGGTCGAC
OTL409	PIF1-N-term P.II	TGTAATATTATCCATTGAGCGATTAGCTTACTTGTATCAATCAAT TTTAC CCGCGCGTTGGCCGATTCAT
OTL416	PIF1-WT-IL5L-RV	TGTTGATCTTAACCACTTTGGCATGTAAAATTG
OTL417	PIF1-L9L-IL12L-IL13L-FW	TTAAATCATTTATTACCAAGAAGGCCATTTATCTG
OTL418	PIF1-IL5L-FW	TTGAATCATATTATACCAAGAAGGC
OTL419	PIF1-L9L-RV	TGTTGATCTTATCCACTTTGG
OTL420	PIF1-L9L-FW	TTAAATCATATTATACCAAGAAGGC
OTL421	PIF1-M1-IL5-9-12-13L-RV	TGATCTTAACCACTTTGGGGCCCAAAATTG
OTL422	PIF1-M1-IL5-9-12-13L-FW	ACATTAAATCATTTATTACCAAGAAGGCCATTTATCTG
OTL423	PIF1-M1-IL5L-RV	TCTTAACCACTTTGGGGCCCAAAATTG
OTL424	PIF1-M1-IL5L-FW	TCAACATTGAATCATATTATACCAAGAAGGC
OTL425	PIF1-L-(-8)A-IL-(-5)A-RV	AGTAGCCTAATCGCTCAATGGATAATATTAC
OTL426	PIF1-WT-L-(-8)A-IL-(-5)A-FW	TGTGCTAATCAATTTTACATGCCAAAGTGG
OTL427	PIF1-IL-(-5)A-RV	ACAAGTAAGCTAATCGCTCAATGG
OTL428	PIF1-WT-IL-(-5)A-FW	GCTAATCAATTTTACATGCCAAAGTGG
OTL429	PIF1-M1-L-(-8)A-IL-(-5)A-RV	ACAAGTAGCCTAATCGCTCAATGGATAATATTAC
OTL430	PIF1-M1-IL-(-5)A-FW	GCTAATCAATTTTGGGCCCCAAAGTGG

Table 4. List of oligonucleotides used in this study to generate substrates for *in vitro* assays.

Oligo	Length	Sequence (5'-3')
A6-3'-6FAM	31	ATTGGTTATTTACCGAGCTCGAATTCACTGG-6FAM
A9	42	CCAGTGAATTCGAGCTCGGTACCCGCTAGCGGGGATCCTCTA
A6-Comp	31	CCAGTGAATTCGAGCTCGGTAAATAACCAAT

USC UNIVERSIDADE DE SANTIAGO DE COMPOSTELA

Poli-dT	60	TTTTTTTTTTTTTTTTTTTTTTTTTTTTTTTTTTTTTTTT TTTTTTTTTTTTTTTTTTT
X01	60	6FAM-ACGCTGCCGAATTCTACCAGTGCCTTGCTAGGACATC TTTGCCCACCTGCAGGTTCACCC
X02	60	GGGTGAACCTGCAGGTGGGCAAAGATGTCCATCTGTTGTAATCGTC AAGCTTTATGCCGT
X03	60	ACGGCATAAAGCTTGACGATTACAACAGATCATGGAGCTGTCTAGA GGATCCGACTATCG
X04	60	CGATAGTCGGATCCTCTAGACAGCTCCATGTAGCAAGGCACTGGTA GAATTCGGCAGCGT
X02-(1/2)	30	GGGTGAACCTGCAGGTGGGCAAAGATGTCC

5. Antibodies

All the antibodies used during this thesis are listed in Table 5.

Table 5. List of antibodies used in this study.

Antibody	Type	Host	Source	Identifier
Monoclonal ANTI-FLAG® M2	Primary	Mouse	Merck	F1084
ANTI-FLAG®M2-HRP	Primary	Mouse	Merck	A8592
Anti-GFP	Primary	Mouse	Roche	11814460001
Anti-myc-9E10	Primary	Mouse	CRUK	
HRP Anti-Myc tag antibody	Primary	Rabbit	Abcam	ab1326
Anti-Rad53	Primary	Rabbit	Abcam	ab104232
Anti-Pgk1-HRP	Primary	Rabbit	Abcam	ab197960
Anti-Mouse Alexa Fluor™ Plus 800	Secondary	Goat	Invitrogen	A32730
Anti-mouse-HRP	Secondary	Goat	Invitrogen	31430
Anti-rabbit-HRP	Secondary	Mouse	Santa Cruz	sc-2357

6. Media

All bacterial and yeast media were prepared in milli-Q water and sterilized by autoclaving (121°C, 20 min) or filtration. Bacteria were grown in standard Lysogenic Broth (LB) complex media (10 g/L NaCl, 10 g/L tryptone, 5 g/L yeast extract) and supplemented with 50-100 µg/ml ampicillin, 34 µg/ml chloramphenicol or 50 µg/ml kanamycin for antibiotic selection whenever required.

All the media and antibiotics employed for yeast growth were purchased from Formedium. Yeast cells were routinely grown in complex media composed of a mixture of yeast extract and peptone (YEP), supplemented with different carbon sources, including glucose, raffinose,

USC DE COMPOSTELA

galactose, glycerol and ethanol. Carbon sources were typically used at final concentration of 20 g/L and prepared as 10X stocks; raffinose and galactose were sterilized by filtration through 0.22 µm filters (15206869 Fisher Scientific), while glucose and glycerol were autoclaved as described above. Solid media was prepared by adding agar to a final concentration of 20 g/L whenever required. For antibiotic selection, the medium was supplemented with 100 µg/ml clonNAT, 150 µg/ml G418 or 200 µg/ml hygromycin B. All the complex media employed are listed in Table 6. Synthetic defined media for *S. cerevisiae* were based on Synthetic Minimal Media (SD media), composed of Yeast Nitrogen Base (YNB) plus the desired carbon source at final concentration of 20 g/L. Synthetic complete media (SC) were prepared by supplementing SD media with all the essential amino acids, minerals and vitamins at known concentrations with complete supplement mixtures (CSM), or CSMs lacking a particular essential nutrient (CSM Drop-Outs) for auxotrophic selection. Solid media was prepared by adding agar to a final concentration of 20 g/L. All the complex media employed are listed in Table 6.

Table 6. List of media used in this study for bacterial and yeast growth.

Media	Composition
Bacteria complex media	
LB	10 g/L NaCl, 10 g/L tryptone, 5 g/L yeast extract
SOB	0.5 g/L NaCl, 20 g/L tryptone, 5 g/L yeast extract, 2.5 mM KCl, 10 mM $MgCl_2$
Yeast complex media	
YEP	10 g/L yeast extract, 20 g/L peptone.
YPD	YEP supplemented with 20 g/L glucose.
YPAD	YEP supplemented with 20 g/L glucose and 0.04 g/L adenine.
YPRAFF	YEP supplemented with 20 g/L raffinose.
YPGAL	YEP supplemented with 20 g/L galactose.
YPRAFF-GAL	YEP supplemented with 20 g/L raffinose and 20 g/L galactose.
YPGly	YEP supplemented with 2% (v/v) glycerol.
YPEGly	YEP supplemented with 3% (v/v) ethanol and 2% (v/v) glycerol.
Yeast synthetic media	
SD-Glucose	YNB[a] with 20 g/L glucose.
SD-Raffinose	YNB[a] with 20 g/L raffinose.

USC UNIVERSIDADE DE SANTIAGO DE COMPOSTELA

Media	Composition
SC-Glucose	SD-Glucose + CSM[b]
SC-Raff-Gal	SD-Raffinose + 20 g/L galactose + CSM[b]
SC-URA	SD-Glucose + CSM, single drop out -Ura[c]
SPO	3 g/L CH_3COOK supplemented with 10 mg/L Uracil, 10 ml/L adenine 10 mg/L histidine, 10 mg/ml leucine and 10 mg/ml tryptophane,

[a]YNB: Histidine HCl 10 mg/L, Methionine 20 mg/L, Tryptophane 20 mg/L, Biotin 0.002 mg/L, Ca-Panthotenate 0.4 mg/L, Folic acid 0.002 mg/L, Inositol 2 mg/L, Nicotinic Acid 0.4 mg/L, p-Aminobenzoic Acid 0.2 mg/L, Pyridoxine HCl 0.4 mg/L, Riboflavin 0.2 mg/L, Thiamine HCl 0.4 mg/L,Boric Acid 0.5 mg/L, Copper Sulphate 0.04 mg/L, Potassium Iodide 0.1 mg/L, Ferric Chloride 0.2 mg/L, Manganese Sulfate 0.4 mg/L, Sodium Molybdate 0.2 mg/L, Zinc Sulfate 0.4 mg/L, Potassium Phosphate monobasic 1000 mg/L, Magnesium Sulphate anh 500 mg/L Sodium Chloride 100 mg/L, Calcium Chloride. anh 100 mg/L and Ammonium Sulphate 5000 mg/L as nitrogen source.

[b]CSM: L-arginine 50 mg/L, L-aspartic acid 80 mg/L, L-Histidine HCl 20 mg/L, L-Isoleucine 50 mg/L, L-Leucine 100 mg/L, L-lysine-HCl 50 mg/L, L-methionine 20mg/L, L-phenylalanine 50 mg/L, L-threonine 100 mg/L, L-tryptophane 50 mg/L, L-tyrosine 50 mg/L, valine 140 mg/L, adenine 10 mg/L and 20 mg/L uracil.

[c]CSM, single drop-out -Ura: CSM without uracil.

7. Reagents

Relevant and specific reagents will be listed at the beginning of each protocol. Common reagents are listed in Table 7.

Table 7. List of common reagents used in this study.

Reagent	Source	Identifier
Chemicals		
PIPES	Sigma-Aldrich	P6757
Acrylamide:Bis-Acrylamide 19:1 40%	Thermo Fisher Scientific	BP1406-1
Acrylamide:Bis-Acrylamide 29:1 40%	Thermo Fisher Scientific	BP1408-1
Agarose	Thermo Fisher Scientific	A3054

USC UNIVERSIDADE DE SANTIAGO DE COMPOSTELA

Reagent	Source	Identifier
Ammonium persulfate (APS)	Thermo Fisher Scientific	BP179-100
Boric acid	Honeywell	31146
Bovine Serum Albumin (BSA)	Thermo Fisher Scientific	BP8805-100
Bromophenol Blue	Sigma-Aldrich	114391
Calcium chloride dihydrate	Acros organics	207780010
Camptothecin	Selleck Chemicals	NSC-100880
DAPI	Invitrogen	D3571
dATP	Sigma-Aldrich	11277049001
EDTA	Formedium	EDTA1000
Dithiothreitol (DTT)	Formedium	DTT025
DMSO	Thermo Fisher Scientific	F-515
Ethanol absolute	VWR	20.821.330
Ethidium Bromide	Sigma-Aldrich	E7637
Ficoll, Biotech grade	Thermo Fisher Scientific	BP525-10
Formamide, 99%	Acros organics	327235000
Formic acid	Sigma-Aldrich	33015-1L-M
Glycerol	Thermo Fisher Scientific	BP229-4
Glycine	Thermo Fisher Scientific	BP381-5
Hydrochloric acid 37%	VWR	20.252.295
Hydrogen peroxide 30%	Fisher BioRagents	
Hydroxyurea	USBiological	H9120
IGEPAL® CA-630	Sigma-Aldrich	I8896-50ML
Imidazole	Thermo Fisher Scientific	I/0010/53
Isopropanol	Sigma-Aldrich	33539-2.5L-GL-R
Isopropyl-thiogalactopyranoside (IPTG)	Thermo Fisher Scientific	BP1755-10

USC UNIVERSIDADE DE SANTIAGO DE COMPOSTELA

Reagent	Source	Identifier
Lanolin	Alfa Aesar	A16902
Lithium Acetate dihydrate	Sigma-Aldrich	L4158
Lithium Chloride, 99%	Acros Organics	449041000
Luminol, >97%	Sigma-Aldrich	A8511
Magnesium Chloride hexa-hydrate	Sigma-Aldrich	M2670
Manganese (II) chloride tetrahydrate	Thermo Fisher Scientific	M/1800/52
Methanol	Thermo Fisher Scientific	BP1105-4
Methyl methanesulfonate	Sigma-Aldrich	129925-5G
TEMED	Thermo Fisher Scientific	BP150-100
Nonidet P-40 Substitute	Sigma-Aldrich	74385-1L
Orange G	Sigma-Aldrich	7252
p-Coumaric acid, >98,0% (HPLC)	Sigma-Aldrich	C9008
Paraffin 52-54ºC pellets	VWR	26.157.291
Phenol/Chloroform/Isoamyl Alcohol	Thermo Fisher Scientific	BP1752I-400
Phenylmethylsulfonyl fluoride (PMSF)	Thermo Fisher Scientific	36978
Poly(ethylene glycol) 4000 (PEG4000)	Sigma-Aldrich	95904
Potassium chloride	Sigma-Aldrich	60130
Potassium Hydroxide	Thermo Fisher Scientific	P/5640/60
Potassium phosphate dibasic, >99%	Thermo Fisher Scientific	BP363-1
Sodium Acetate Trihydrate	Sigma-Aldrich	32318
Sodium chloride	Thermo Fisher Scientific	S/3160/60
Sodium Dodecylsulfate (SDS)	Thermo Fisher Scientific	BP166-500
Sodium Fluoride, >99%	Sigma-Aldrich	S7920
Sodium Hydroxide	Thermo Fisher Scientific	BP359
Sodium phosphate, monobasic dihydrate	Acros Organics	271750010

USC UNIVERSIDADE DE SANTIAGO DE COMPOSTELA

Reagent	Source	Identifier
Stains-All	Sigma-Aldrich	E9379-1G
Sytox Green Nucleic Acid Stain	Invitrogen	S7020
Trichloroacetic acid, 99-100,5%	Sigma-Aldrich	27242
Tris Base	Thermo Fisher Scientific	BP152-1
Trisodium citrate dihydrate	Thermo Fisher Scientific	BP327-1
Triton X-100	Sigma-Aldrich	X100-500ML
TWEEN 20	Sigma-Aldrich	P7949-500ML
Urea	Sigma-Aldrich	33247
Vaseline white	VWR	28.908.290
Xylene-cyanole FF	Bio-Rad	M1777
β-glycerophosphate disodium salt hydrate	Sigma-Aldrich	G9422
Enzymes		
BseRI	NEB	R0581
Eco1471-FD	Thermo Fisher Scientific	FD1471
FastAP Thermosensitive Alkaline Phosphatase	Thermo Fisher Scientific	EF0654
Lysozyme	Sigma-Aldrich	62970-5G-F
NcoI-FD	Thermo Fisher Scientific	FD0574
Pepsine	Sigma-Aldrich	P6887-1G
Proteinase K	Thermo Fisher Scientific	BP-1700-500
Rnase A solution	Sigma-Aldrich Aldrich	R6148-25ML
Rnase A solution	Invitrogen	8003088
XhoI-FD	Fisher Scientific	FD0694
Zymolyase 20T	Amsbio	120491-1
Media and antibiotics		

USC DE SANTIAGO DE COMPOSTELA

Reagent	Source	Identifier
Ampicillin Sodium	Formedium	AMP25
Chloramphenicol	Formedium	CLA01
clonNAT	Jena Bioscience	AB-102L
Complete supplement (CSM) Drop-out: -URA	Formedium	DCS0169
D(+) raffinose pentahydrate	Formedium	RAF04
D(+) galactose	Formedium	GAL03
D(+) glucose anhydrous	Formedium	GLU03
G418 Sulphate	Corning	30-234-CR
Hygromycin B	Invitrogen	10687-010
Kanamycin Monosulphate	Formedium	KAN0005
L-adenine sulphate	Formedium	DOC0229
SD Agar 2% glucose	Formedium	CSM0110
SD Broth 2% galactose and 1% raffinose	Formedium	CSM1010
SD Broth 2% glucose	Formedium	CSM0205
SD Broth 2% raffinose	Formedium	CSM0605
Sucrose, Rnase & Dnase free	VWR Chemicals	0335-500G
YNB without aminoacids and ammonium sulphate	Formedium	CYN00510
YEP agar	Formedium	CCM0310
YEP broth	Formedium	CCM0410

USC UNIVERSIDADE DE SANTIAGO DE COMPOSTELA

METHODS

1. MICROBIOLOGY

1.1 Bacterial methods

1.1.1 Bacterial inoculation and stocks

All the bacterial strains used in this work were routinely grown in liquid LB media, or supplemented with 2% agar when required, with the corresponding antibiotic for plasmid selection. For small scale plasmid preparation (minipreps), 5 ml cultures of LB with antibiotic were inoculated with single colonies and incubated overnight (12-16 h) a 37 °C. For long-term storage of bacterial stocks, 500 µl of an overnight culture were added to cryovials with 500 µl of pre-aliquoted 50% glycerol. Glycerol stock vials were frozen and stored at -80 °C.

1.1.2 Preparation and transformation of competent cells

Protocols for preparation and transformation of DH5alpha and BL21 strains were adapted from the classical high efficiency transformation protocol (Inoue et al., 1990). This protocol is based on chemical treatment with Ca^{2+} and Mn^{2+} ions of cells grown at low temperature (16 °C) which is thought to increase efficiency transformation by opening pores in the bacterial membranes and masking the negative charge of DNA.

Solutions and reagents:

- Transformation Buffer: 10 mM PIPES, 15 mM $CaCl^2$, 250 mM KCL. Adjust the pH to 6.7 with KOH, then add $MnCl_2$ at 55 mM final concentration. Filter sterilized.
- SOB medium
- LB medium

Procedure: preparation of competent cells

1. Pick a few colonies (3-4) from a fresh plate, incubated for 16-20 h at 37 °C and transfer them into a 250 ml flask with 25 ml of SOB medium. Incubate the culture for 6-8 h at 37 °C with vigorous shaking (250-300 rpm).
2. Use this starter culture to inoculate three flasks with 250 ml of SOB with different amounts of starter cultures (10 ml, 4 ml and 2 ml, respectively). Incubate overnight at 18 °C with shaking at 200 rpm.
3. Next morning measure the OD_{600}. If one of the three cultures is at OD_{600} = 0.55-0.6, start the protocol with that flask. Otherwise, monitor the OD_{600} every 30-45 min until one of them reaches the desired OD.
4. When the OD_{600} reaches 0.55-0.6 (it usually takes around 30 hours), place the flask on ice for 10 min, and then spin down cells at 2000 g for 10 minutes at 4 °C.
5. Remove supernatant and resuspend gently in 80 ml of ice-cold Transformation Buffer. Incubate on ice for 10 min.

USC UNIVERSIDADE DE SANTIAGO DE COMPOSTELA

6. Spin down cells at 800 g and resuspend the pellet gently in 20 ml of ice-cold Transformation Buffer. Add DMSO to a final concentration of 7 %. Mix the bacterial suspension by swirling and incubate on ice for further 10 min.
7. Quickly, dispense aliquots into pre-chilled, sterile tubes. Immediately snap-freeze the competent cells in liquid nitrogen. Store tubes at -80 °C until needed.

Procedure: transformation of competent cells

For transformation, 50-100 µl of DH5alpha or BL21 cells were thawed on ice for 10 min. After adding plasmid DNA (1-10 ng) or ligation reactions (1-2 % total volume transformation reaction), cells were incubated on ice for additional 30 min, followed by a short heat shock (42 °C, 45 s), and 2 min on ice for recovery. Finally, cells were incubated for 45 min at 37 °C in 1 ml of LB to allow for the expression of proteins responsible for antibiotic selection before plating on LB with 2% agar with the suitable antibiotic.

1.2 Yeast methods

1.2.1 Yeast cultures and stocks

Yeast manipulations were generally performed according to standard procedures (Sherman, 2002). Yeast were routinely grown in YPAD broth or 2 % agar plates. Drop-out synthetic media was employed for selection purposes, maintenance of strains transformed with episomal plasmids (centromeric or 2µ plasmids) and for yeast live-cell imaging to avoid YPAD autofluorescence. Glycerol yeast stocks for long term storage were prepared in 15% glycerol, frozen and kept at -80 °C.

1.2.2 Yeast mating, sporulation and tetrad dissection

Patches of yeast of opposite mating types (*MATa* and *MATalpha*) were mixed and incubated together in YPDA plates for 4 h at 30 °C . Diploids were selected by consecutive streaks in selective media, or by micromanipulation under the dissection microscope. Once selected, diploids were plated in patches and incubated for 24 h in YPAD, followed by their transfer as highly dense patches to SPO plates to induce meiotic entry and sporulation. SPO plates were incubated 3 days at 30 °C prior to allow the formation of asci containing the spore tetrads.

For tetrad dissections, a sterile 10 µl tip was used to transfer a small amount of sporulated cells from the plate into 15 µl of Zymolyase 20T to degrade the asci. Resuspended cells were incubated for 10 min at RT, before diluting the cell suspension 1:10 with 135 µl of water. 20 µl of cell suspension was spread in a straight-line on YPD plates to isolate tetrads. The four spores of each tetrad were dissected using the dissection microscope (SporePlay, Singer Instruments).

1.2.3 Yeast transformation

Intact yeast cells were transformed with exogenous DNA (PCR cassettes for gene editing or plasmids) with a high-efficiency protocol based on cell treatment with lithium acetate and adapted from (Storici and Resnick, 2006)

Solutions and reagents:

- Solution 1: LiAc 0.1 M, TE 1X pH 7.5.
- Solution 2: LiAc 0.1 M, TE 1X pH 7.5 in PEG 4000 40%.

USC UNIVERSIDADE DE SANTIAGO DE COMPOSTELA

Procedure:

1. Inoculate 5 ml YPDA with one yeast colony and incubate with shaking (200 rpm) at 30 °C overnight (typically to saturation).
2. Refresh cells by diluting the starter culture in 50 ml YPDA at a final OD_{600} ~ 0.25. If collected at OD_{600} = 0.5-0.6, this amount of culture is sufficient for 8 transformations; increase the volume during this step if required.
3. Incubate with vigorous shaking for 3 h at 30 °C. For slow-growth strains, extend the incubation time until cells reach an OD_{600} = 0.5-0.6.
4. Transfer the culture to a 50 ml centrifuge tube and spin down the cells at 2000 x g for 2 min.
5. Discard the supernatant, wash the pellet with 50 ml of sterile water and spin down again as stated previously.
6. Discard the supernatant again and wash the pellet with 5 ml of Solution I. Harvest cells as stated previously.
7. Resuspend the pellet in 250 µl of Solution I.
8. Aliquot 50 µl of the cell suspension in 1.5 ml centrifuge tubes and add 10 µl of concentrated PCR product (or 0.2-0.5 µg plasmid DNA in 10 µl), 5 µl of denatured carrier DNA, and 300 µl of Solution II for each transformation reaction. Mix briefly by vortexing.
9. Incubate transformation reactions at 30 °C for 30 min with shaking.
10. Heat shock at 42 °C for 15 min with shaking.
11. Collect cells by centrifugation at 2500 x *g* for 4 min.
12. Discard supernatant and resuspend cells in 1 ml of YPD.
13. Incubate the resuspended cells at 30 °C for 1 h with shaking. This step can be omitted for auxotrophic selection if high transformation efficiency is not required.
14. Collect cells as in Step 11, discard supernatant and resuspend in 100-200 µl of sterile water for plating on the corresponding media.
15. Once colonies appear, streak the desired number on a suitable medium to obtain single colony isolates.

2. MOLECULAR BIOLOGY

2.1 Isolation of plasmid DNA from bacteria

2.1.1 Isolation of plasmid DNA by alkaline lysis

Plasmid DNA was purified by alkaline lysis (Birnboim and Doly, 1979) from 5 ml of bacterial cultures using the E.Z.N.A. Plasmid Mini Kit I (Omega, #D6942-01), following the manufacturer´s protocol. Plasmid DNA was quantified by spectrophotometry in a NanoDrop 200 (Thermo Fisher) and verified on agarose gel after digestion with restriction enzymes.

2.1.2 Isolation of plasmid DNA by non-ionic detergent (NID) boiling.

Screening of multiple clones transformed with small plasmids (~10kb) was done by NID boiling lysis (Lezin et al., 2011). This method is more time-efficient than commercial kits based on alkaline lysis and DNA retention in silica columns. In fact, NID crude lysate obtained before ethanol precipitation is sufficiently pure to be used in both sanger sequencing reaction and digestion with restriction enzymes.

Solutions and reagents

- 100X enzyme stock: 50 mM Tris pH 8.0, 50% (v/v) Glycerol, 10 mg/ml lysozyme, 2.5 mg/ml RNase A. Store at -20ºC.
- Extraction Buffer: 5% sucrose, 50 mM EDTA, 50 mM Tris-HCl pH 8, 0.5 M NaCl, 0.5% Triton X-100, 20 mM $CaCl_2$, 100 µg/ml lysozyme, 25 µg/ml RNase A. RNase and lysozyme are added from the 100X enzyme stock just before use.
- Ethanol 70%
- TE buffer

Procedure

1. Pellet 1.5-2 ml of bacterial cultures 4500 x *g* for 1 min. Discard the supernatant. Draw 150 µl of extraction buffer (containing lysozyme and RNaseA) and loosen off the pellet with the tip before releasing the buffer. Resuspend the pellet in extraction buffer.
2. Incubate the bacterial suspension at 65 °C for 5 min.
3. Centrifuge at maximum speed (21000 x g) for 10 min and remove the pellet with a toothpick. At this point, the DNA in solution in the supernatant can be digested with restriction enzymes without further purification.
4. Add 110 µl isopropanol, mix and centrifuge at 4500 x *g* for 10 min.
5. Discard supernatant. Add 500 µl 70% ethanol and spin 1 min (>13000 x g).
6. Discard ethanol. Dissolve DNA pellet in 50 µl TE buffer.

2.2 Isolation of yeast genomic DNA

Yeast genomic DNA (gDNA) was routinely isolated by adapting the commercial kit used to purify plasmid DNA from bacteria E.Z.N.A. Plasmid Mini Kit I (Omega, #D6942-01), adding an initial step of mechanical lysis in a BeadBeater (1 volume of glass beads, 3 cycles of 30 sec).

Alternatively, for large screenings and genotyping tetrads, gDNA was isolated by a modified protocol based on phenol : chloroform extraction of DNA (Green and Sambrook, 2018). gDNAs isolated by this method have been used as templates for PCRs up to 8 kb in length.

Solutions and reagents

- STES buffer: 200 mM Tris-HCl pH 7.6, 0.5 M NaCl, 10 mM EDTA, 0.1% (w/v) SDS.
- Ethanol (70% and 100%).

USC UNIVERSIDADE DE SANTIAGO DE COMPOSTELA

- 3 M sodium acetate, pH 5.2.
- TE buffer pH 7.6.

Procedure

1. Transfer 1 ml of yeast cells from an overnight culture to a microcentrifuge tube
2. Pellet the cells by centrifuging at maximum speed for 1 min at room temperatur
3. Replace the screw cap of every tube, and harvest the cells by centrifugation at 10000 x *g* for 1 min at RT.
4. Remove supernatant by aspiration and resuspend the pellet in 50 µl of STES buffer. Add µl of TE to each tube and 50 µl of acid-washed glass beads.
5. Add 60 µl of phenol:chloroform and mix the organic and aqueous phases by vortexing for 1 min.
6. Centrifuge the tubes at 12000 x *g* for 5 min at RT.
7. Transfer 40 µl of the upper aqueous phase to a fresh tube.
8. Add 3 µl of 1 mg/ml RNase A solution to the aqueous phase and incubate 15 min at 37 °C.
9. Purify the gDNA by standard ethanol precipitation.
10. Resuspend the pellet in 40 µl of TE pH 7.6/

2.3 Polymerase chain reaction (PCR)

DNA was routinely amplified using Phusion Green Hot Start II High-Fidelity PCR Master Mix (Thermo Scientific™, F566L), following manufacturer's instructions. Extension time was adjusted to 30 s/kb. Template amount adapted to the starting material: 1-5 ng for plasmid DNA and 50-100 ng for gDNA. The volume was set considering the final application of PCR product: generation of deletion and tagging cassettes, 100-200 µl; mutagenesis by inverse PCR, 50-75 µl; genotyping, 15-20 µl. For GC-rich templates, DMSO was added to a final concentration of 3% (v/v).

2.4 DNA purifications

2.4.1 PCR cassettes

PCR products were purified using the commercial kit E.Z.N.A.® MicroElute® Gel Extraction Kit (D6294-01), following the manufacturer's instructions.

2.4.2 Gel extraction

Bands of interest were excised from agarose gels with sterile scalpel blades in a blue-light transilluminator. DNA was purified from the excised band with the commercial kit E.Z.N.A.® MicroElute® Gel Extraction Kit (D6294-02), following the manufacturer's instructions.

2.4.3 Ethanol precipitation

Ethanol precipitation was employed as part of several protocols to purify DNA from different contaminants.

Solutions and reagents:

- Glycogen (Thermo Scientific™, #R0561)
- 3 M sodium acetate pH 5.2
- 100% ice-cold ethanol
- 70% ice-cold ethanol

Procedure:

1. Optional: To help visualize the pellet, add 1 µl of 1 mg/ml glycogen to the DNA solution prior precipitation. If the DNA concentration in the solution is very low, add 1 µl of 5 mg/ml glycogen stock. Glycogen does not interfere with downstream applications like PCRs or electrophoretic analysis.
2. Add 0.1 volumes of 3 M sodium acetate pH 5.2.
3. Add 2 volumes of cold 100% ethanol. For small fragments (~50-200 bp), add 3 volumes of cold 100% ethanol to increase the yield.
4. Mix by vortexing and incubate at -20 °C (20 min). This incubation was occasionally extended to overnight to increase yield, specially of small DNA fragments.
5. Centrifuge at >12000 x *g*, 15 min at 4 °C. Extend the centrifugation step to 30 min for small fragments.
6. Carefully remove the supernatant by vacuum.
7. Wash the pellet with 1 ml of cold 70% ethanol and mix by inversion.
8. Centrifuge at >12000 x *g*, 1 min at 4 °C.
9. Carefully remove the supernatant by vacuum.
10. To remove the last traces of ethanol, leave the tube open in an inverted position (do not over dry).
11. Resuspend the pellet in the desired amount of 10 mM Tris-HCl pH 8.0 or TE by vortexing.

2.5 DNA sequencing

Sanger sequencing of PCR products and plasmids was outsourced to STAB VIDA (www.stabvida.com). Analysis of the sequencing results was done by aligning the curated sequence from chromatograms (ab1 files) with a reference sequence using SnapGene® software (from Insightful Science; available at snapgene.com).

2.6 Cloning and mutagenesis of DNA fragments

2.6.1 Cloning with restriction enzymes

For cloning with restriction enzymes, Fast-Digest enzymes (Themo Fisher) were routinely employed, following manufacturer's recommendations. When required, plasmid backbones were simultaneously digested and dephosphorylated by addition of 1U of FastAP

thermosensitive alkaline phosphatase in the digestion reaction. Digested backbone and inserts were separated in 0.7% (w/v) agarose gels stained with 0.5 µg/ml ethidium bromide and purified as described before. For ligations, the DNA ligation kit Mighty Mix (Takara Bio, #6023) was employed, following manufacturer's instructions, and using a vector: insert ratio ranging from 1:3 to 1:5.

2.6.2 Gateway cloning

The protocol for standard LR and BP reactions was modified and downscaled from the manufacturer's recommended instructions. For BP reactions, 0.5 µl of the DNA flanked by attB sites (60 ng/µl) was mixed with 0.5 µl of pDONR221 (60 ng/µl) and 0.35 µl of Gateway™ BP Clonase™ II Enzyme Mix (Invitrogen, #11789020). Reactions were incubated for 1 h at 25 °C before transforming DH5alpha cells. LR were set up like BP reactions but combining entry vectors (pENTR221 derivatives with attL sites) with destination vectors (pAG306-GAL-ccdB-eGFP, pAG306GAL-eGFP-ccdB, PAG306GAL) and Gateway™ LR Clonase™ II Enzyme Mix (Invitrogen, #11791020).

Occasionally, one-tube BP-LR reactions were performed, following the manufacturer's instructions, to generate both entry and expression vectors in a single reaction.

2.6.3 Mutagenesis by inverse PCR

Mutagenesis for single or clustered mutations was achieved by inverse PCR, adding the required sequence to introduce the mutations at the 5' end of the primers used during the amplification step. Linear products obtained by inverse PCR were purified as described in Section 2.4, eluted in 30 µl of 10 mM Tris-HCl pH 8.0 and phosphorylated with T4 polynucleotide kinase (Thermo Scientific™, EK0031) following manufacturer instructions. T4 was heat-inactivated and 10 fmol of PCR product were circularized by adding 1 volume of DNA ligation kit Mighty Mix (Takara Bio, #6023), followed by incubation at 16 °C for 30 min. Ligation reactions were then employed to transform DH5alpha cells.

2.6.4 Gene editing of *S. cerevisiae*

2.6.4.1 Integration of plasmids in the host chromosomes

Integrative plasmids from the pAG306 (Alberti et al., 2007) and pRSII406 (Chee and Haase, 2012) series were linearized with restriction enzymes to target their integration into the desired locus (Table 8).

Table 8. List of integrative vectors used in this work and the enzymes employed to linearize them.

Backbone	Insert	Enzyme	Integration locus
pAG306	YEN1	StuI	Ectopic (*URA3*)
pRS306	YEN1	StuI	Ectopic (*URA3*)
pAG306	PIF1	NcoI	Ectopic (*URA3*)

USC UNIVERSIDADE DE SANTIAGO DE COMPOSTELA

pRSII406	PIF1	NcoI	Ectopic (*URA3*)
pRSII406	PIF1	BseRI	*PIF1* promoter

2.6.4.2 Knockouts, promoter replacement and epitope tagging.

Yeast knockouts, promoter replacement and C-terminal epitope tagging were done by PCR-based gene targeting (Wach et al., 1994). Briefly, cells were transformed with 1 µg purified PCR cassettes with drug-selectable or auxotrophic nutritional markers flanked by 50 bp of homologous sequence. Additionally, some knockouts were made by extracting gDNA from the desired strain of the Yeast Knockout collection (Giaever et al., 2002; Winzeler et al., 1999)) and preparing PCR cassettes using primers the deleted locus.

PCR cassettes for knockouts and promoter replacement were amplified from pFA6a derivatives (Janke et al., 2004; M. I. Longtine et al., 1998)). For C-terminal epitope tagging of Yen1 and Pif1, we used a set of unpublished plasmids, developed during this Thesis, with different combinations of epitopes and genetic markers cloned into pUC19 backbones, including pUC19-6xHis-6xFlag::klTRP1 and pUC19-9xMyc::KANMX.

2.7 Determination of telomere length by Southern Blot.

Telomeric length in various yeast strains was determined by Southern blotting, employing XhoI-digested gDNA from a pool of three biological replicates and a probe targeting the subtelomeric Y´elements.

Reagents and buffers

- Zeta-Probe nylon membrane (Bio-Rad, #1620159)
- Whatman™ 3MM Chr Chromatography Paper (Cytiva)
- 12 N HCl
- 2 N NaOH
- 20X SSC (3 M NaCl, 0.3 M trisodium citrate).
- DIG-High Prime DNA Labelling and Detection Starter Kit II (Roche, #11585614910)

Procedure: *DNA preparation*

PIF1/ *pif1*Δ diploid strains carrying an additional copy of different *PIF1* alleles, ectopically integrated in *ura3-52*, were sporulated and dissected at the same time. After replica-plating (1st passage), strains with genotypes of interest were selected (2nd passage) and re-streaked again (3rd passage) to allow telomere elongation in *PIF1*-deficient strains. Starter cultures were prepared by pooling three biological replicates for each genotype. High-molecular weight gDNA was purified by phenol: chloroform and ethanol precipitation. DNA was further purified using silica-columns. Finally, 1 µg of gDNA for each genotype was digested with XhoI overnight at 37 °C.

Procedure: *electrophoresis and transfer*

Once DNA has been prepared, the DNA fragments are separated by electrophoresis and blotted to nylon membranes by the alkaline transfer method.

1. Load 1 µg of each XhoI digested sample in a 1% agarose gel (20 cm length) in TBE 0.5X for 18h at 1.5 V/cm, using the as a molecular-weight marker.
2. After electrophoresis, depurinate the DNA by soaking the gel in 0.25 M HCl for 10 min. Rinse the gel 3 times with distilled water.
3. Prewet the Zeta-Probe membrane in distilled water and cut four sheets of Whatman 3MM paper so they overhang the bottom of the gel tray by 5 cm on each end.
4. Place the inverted gel casting tray inside a deep tray and put the four sheets of 3MM paper on top of the inverted gel casting tray.
5. Saturate the 3MM paper with 0.4 M NaOH. Remove the bubbles by rolling a pipette over the soaked 3MM paper. Pour enough 0.4 M NaOH into the deep tray so that the 3MM wick ends are immersed in NaOH.
6. Carefully place the gel on top of the wick. Make sure that no bubbles are trapped between the gel and the wick. Cover the gel with a small amount of 0.4 M NaOH.
7. Place plastic wrap over the entire 3MM wick - gel stack. Cut out a window with a clean razor blade, exposing only the gel.
8. Lower the sheet of pre-wetted Zeta-Probe membrane onto the gel surface. Carefully flood the surface with 0.4 M NaOH. Make sure again that no bubbles are present between the gel and the Zeta-Probe membrane. Cut two sheets of 3MM paper to the same size as the membrane, saturate in 0.4 M NaOH and place them on top the membrane, making sure no bubbles are trapped.
9. Place a 15 cm stack of paper towels with a plastic plate and aprox. 500 g weigh on top. Allow the capillary transfer to proceed overnight.
10. After transfer, remove the Whatman sheets covering the Zeta-Probe. With the DNA surface still facing down, draw with a pencil the position of the wells for future reference. Then, place the Zeta-Probe membrane (DNA surface facing up) on a pad of 3MM paper saturated with 0.4 M NaOH for 10 min.
11. Rinse the membrane 3 times in 2x SSC and air dry. Annotate in one of the corners in which since the DNA surface is facing up. The dried membranes are stable at room temperature. The membranes can be stored between two pieces of filter paper in zipped plastic bags at 23–25 °C.

Procedure: *hybridization and detection*

All the solutions for hybridization and detection steps are included in DIG-High Prime DNA Labeling and Detection Starter Kit II (Roche, #11585614910).

USC UNIVERSIDADE DE SANTIAGO DE COMPOSTELA

1. Pre-heat DIG Easy Hyb Buffer to hybridization temperature. A temperature of 44 °C was established as optimal for the Y'probe, calculated following the manufacturer's recommendation.

   Tm = 49.82 + 0.41 (% G + C) - (600/l) [l = length of hybrid in base pairs]

   Topt. = Tm- 20 to 25°C.

2. Place the membrane in a roller bottle and prehybridize the membrane for at least 30 min in an incubation oven.
3. Denature the DIG-labeled DNA probe by boiling for 5 min followed by cooling in ice.
4. Remove the prehybridization solution and add the denatured DIG-labeled DNA probe to pre-heated DIG Easy Hyb Buffer at a final concentration of 10 ng/ml of probe. For a typical 170 cm^2 membrane, 6 ml of hybridization solution were employed.
5. Incubate 4h to o/n in the incubation oven at 44 °C.
6. After incubation, discard the hybridization solution and wash the membrane twice in 250 ml 2X SSC with 0.1 SDS (w/v) for 5 min at RT.
7. Wash the membrane twice in pre-warmed 200 ml 0.5X SSC with 0.1 SDS (w/v) for 15 min at 65 °C. The membrane is now ready for blocking and detection of the probe.
8. Rinse the membrane twice in Wash Buffer for 2 min.
9. Incubate for 30 min in 100 ml of Blocking solution
10. Incubate for 30 min in 20 ml of Blocking solution containing 1 µl of the Anti-Digoxigenin-AP antibody provided with the kit (1:20000 dilution).
11. Wash the membrane twice in 100 ml Washing Buffer for 15 min at RT.
12. Equilibrate the membrane for 5 min in 50 ml detection buffer at RT
13. Place membrane with DNA side facing up on a plastic sheet and apply 1 ml CSPD ready-to-use reagent. Cover the membrane with a second plastic to spread the substrate evenly and without air bubbles over the membrane. Seal the plastic sheets and incubate for 5 min at +15 to +25 °C.
14. Incubate the membranes for further 10 min at 37 °C to enhance luminescence
15. Detect luminescence in an imager (ChemiDoc, Bio-Rad) for 5-30 min, acquiring cumulative exposures every 5 min. Alternatively, expose to X-ray films for 2-10 min.

2.8 Purification of synthetic DNA substrates

2.8.1 Purification of unlabelled and fluorescently labelled oligos

Long oligonucleotides usually contain a significant amount of incomplete-synthesis by-products that must be removed to prepare high-quality substrates enriched in full-length species. Although commercial PAGE-purified oligonucleotides are suitable for preparing high-quality

USC DE COMPOSTELA

substrates, it is time and cost-effective to order them desalted and purify them in the lab by denaturing PAGE.

Solutions and reagents

- 1X TBE: 90 mM boric acid, 90 mM Tris base, 2 mM EDTA.
- Stains-all solution: 0.01% (w/v), 10% formamide (v/v), 20% isopropanol (v/v). Dissolve 0.01 g of Stains-all in 10 ml of deionized formamide, and then dilute it with 2 volumes of isopropanol and 7 volumes of H_20.
- TE: 10 mM Tris-HCl pH 8.0, 1 mM EDTA.
- TMgN: 10 mM Tris-HCl pH 8.0, 1 mM $MgCl_2$, 50 mM NaCl.
- 2X formamide loading buffer: 1X TBE, 80% formamide, 0.15% Orange G.
- 6X Ficoll loading buffer: 15% Ficoll-400 in 60 mM EDTA, 20 mM Tris–HCl pH 8.0, 0.48% SDS, also containing 0.15% Orange G, 0.05% xylene-cyanol FF, 0.05% bromophenol blue.

Procedure

1. Prepare the denaturing gel mixture (7 M UREA – 15% acrylamide-bysacrilamide) and filter the solution to eliminate urea crystals before pouring the gel into the casting system (Protean II, Bio-Rad)
2. Once polymerized, add TBE running buffer heated to 60 °C to the electrophoresis tank and pre-run the gel for 1 h. Just before loading the samples, flush the wells of the gel to remove the excess urea and unpolymerized acrylamide.
3. Mix 15 nmol of each oligonucleotide (75 µl from 200 µM stock) with 1 volume of 2X formamide loading buffer. Heat the mix for 3 min at 99 °C.
4. Spin the samples and load on the gel quickly, while still hot.
5. Run the electrophoresis at 300 V for 4 h. This should keep the gel at around 55 °C.
6. Once the electrophoresis is finished, transfer the gel to a glass tray with 100 mL of Stains-all solution and incubate for 10 min at RT with gentle agitation on an orbital shaker. Alternatively, when purifying 6´-FAM labelled DNA can be easily visualized without staining using a blue-light transilluminator (SAFEVIEW-MINI2, Cleaver Scientific) or even to the naked eye.
7. Discard the staining solution and wash the gel with 100 ml of water for 10 min at RT with gentle agitation on an orbital shaker. Bands containing the oligonucleotides should be clearly visible as dark patches, with a ladder of incomplete-synthesis by-products below them.
8. Using a scalpel, cut only the upper two thirds of the band corresponding to each full-length oligonucleotide to avoid contamination with species of smaller sizes. Place each excised band in a sterile 1.5 mL microcentrifuge tube.

USC UNIVERSIDADE DE SANTIAGO DE COMPOSTELA

9. Push gently the bands to the bottom, and then crush the acrylamide band with the help of a minipestle. Add 1 mL TE directly to the pestle to remove the acrylamide attached to it.
10. Let the oligonucleotide elute for 24 h at 4 °C on a rotary wheel.
11. Centrifuge the tubes at 15,000 x *g* for 1 min to pellet the gel pieces and transfer supernatant to a fresh 2 ml microcentrifuge tube, and split half of it into another 2 ml tube to accommodate the volume for ethanol precipitation.
12. Precipitate the DNA with 2 volumes of 100% ethanol and 0.1 volume of 3 M sodium acetate pH 5.2. Wash the pellet once with 1 mL 70% ethanol, air-dry it briefly and resuspend in 100 µl of 10 mM Tris–HCl pH 8.0.
13. Quantify by spectrophotometry or fluorescence, and store at 20 ºC until required. With this method, we typically obtain purified oligonucleotides at concentrations between 20 and 50 µM.

2.8.2 Hybridization of oligonucleotides and purification of fluorescentlylabeled substrates

Once oligonucleotides have been PAGE-purified, they can be employed to assemble various DNA substrates (splayed arm or Holliday junction) by hybridization. The fully assembled substrates must be purified from partial-hybridization species present in the mixture by native PAGE.

Solutions and reagents:

- 1X TBE: 90 mM boric acid, 90 mM Tris base, 2 mM EDTA.
- 5X annealing buffer: 0.1 M Tris-HCl pH 7.5, 0.5 M NaCl, 10 mM EDTA.
- 6X Ficoll-Orange-G: 15% Ficoll-400 in 60 mM EDTA, 20 mM Tris–HCl pH 8.0, 0.48% SDS, also containing 0.15% Orange G.
- PAGE-purified oligos
- TMgN buffer:10 mM Tris-HCl pH 8.0, 1 mM $MgCl_2$, 50 mM NaCl.

Procedure:

1. In 0.2 ml microcentrifuge tube, mix 600 pmol of the fluorescently labelled oligonucleotides with a two-molar excess of the appropriate unlabelled ones.
2. Boil the samples at 99 °C for 3 min in a thermocycler, allowing the temperature to decrease gradually to favor the hybridization (140 cycles, decreasing the temperature -0.5°C/min until RT is reached).
3. Add 6X Ficoll-Orange G loading buffer to the oligonucleotide mixture to a final concentration of 1X.
4. Load the sample on a 10% native polyacrylamide gel (29:1) in 1X TBE. Fill the empty wells with a mixture of 1X Ficoll-Orange-G and 1X Annealing Buffer.

USC UNIVERSIDADE DE SANTIAGO DE COMPOSTELA

5. Run the electrophoresis at 250 V for 3 h at 4 °C in 1X TBE.
6. Excise the bands corresponding to the fully assembled substrate with a clean scalpel blade.
7. Crush the acrylamide using a minipestle and add 200 µl – 300 µl of TMgN buffer.
8. Let the substrate elute at least for 24 h at 4 °C, with gentle agitation. Store the mix as it is at 4 °C or centrifuge the tubes at 15000 x *g* for 1 min at 4 °C to pellet the gel pieces and transfer the supernatant to a fresh tube.

USC
UNIVERSIDADE DE SANTIAGO DE COMPOSTELA

3. BIOCHEMICAL TECHNIQUES

3.1 Preparation and analysis of protein extracts

3.1.1 Preparation of denatured protein extracts with trichloroacetic acid (TCA)

Acidic extraction with 10% TCA was used to precipitate protein from yeast cell extracts, especially in those cases when high protein integrity or preservation of post-translational modifications is important, but analysis of enzymatic activities was not required ((Koontz, 2014).

Solutions and reagents:

- 0.5 mm glass beads (BioSpec, #11079105).
- Ice-cold TCA 10%.
- 4X SDS Sample Buffer: 200 mM Tris-HCl pH 6.8, 8%(w/v) SDS, 0.2% (w/v) bromophenol blue, 40% (v/v) glycerol.
- 4X NuPAGE™ LDS Sample Buffer (Invitrogen, NP0008).
- 1 M DTT
- 1 M Tris base
- Bio-Rad Protein Assay Dye Reagent Concentrate (Bio-Rad, #5000006)

Procedure:

1. Harvest 5-10 ml of exponential yeast cell culture at OD_{600} = 0.3-0.6 at 2000 x g.
2. Pre-wash cell pellet once with TCA 10% and transfer it to a 1.5 ml screw cap centrifuge tube (compatible with mini-Bead Beater). At this point, cell pellet can be snap froze in liquid N_2 or directly processed for extract preparation.
3. Resuspend the cell pellet in 400 µl of ice-cold 10% TCA
4. Add ~ 1 vol glass beads.
5. Lyse cells with 2 x 30 s cycles in the mini–Bead Beater at full speed.
6. Transfer lysate to a fresh 1.5 ml centrifuge tube.
7. Centrifuge at 1000 x *g* for 10 min at 4 °C.
8. Remove all the supernatants. It is critical to remove all TCA to ensure good protein migration.
9. Add 50 µl of 2X SDS Sample Buffer containing freshly added 200 mM DTT from the 1 M stock. For protein extracts that will be run in Tris – Acetate gels, use instead the 2X NuPAGE™ LDS Sample Buffer with 200 mM DTT.
10. Add 25 µl 1M Tris base and resuspend cells by vortexing.
11. Boil for 5 min at 99 °C and centrifuge at >15.000 x *g* for 10 min at RT.

USC UNIVERSIDADE DE SANTIAGO DE COMPOSTELA

12. Transfer supernatant to a fresh tube and store at -20 °C until required. Total protein quantification of these extracts was carried out by Bradford assay using the Bio-Rad Protein Assay Dye Reagent, following manufacturer instructions.

3.1.2 Total Protein detection by direct staining

3.1.2.1 Ponceau staining

Ponceau S was employed to detect total protein in PVDF membranes.

Solutions and reagents:

- Ponceau S (BP103-10, Fisher Scientific)
- Acetic Acid glacial (20104.312, VWR chemicals)
- Ponceau S staining: 0.1% (w/v) Ponceau S, 1% (v/v) Acetic Acid.
- TBS-T: 20 mM Tris-HCl pH 7.6, 150 mM NaCl, 0.1% (v/v) Tween 20.

Procedure:

Add Ponceau S staining solution and incubate the PVD membrane for1 min with gentle agitation. Distain with water until the background becomes clear. Let the membrane dry between two Whatman papers to increase the contrast between lanes and background. Destain with TBS-T to remove Ponceau staining from the membrane.

3.1.2.2 Coomassie staining

Polyacrylamide gels were stained with Coomassie Protein Stain (Abcam, #ab119211) following manufacturer's instructions.

3.1.2.3 Total protein staining

For quantitative western blotting, PVDF membranes were stained after semi-dry transfer by using No-Stain Reagent (Invitrogen, #A44449) following manufacturer's instructions, and imaged with ChemiDoc™ MP (Bio-Rad).

3.1.3 Protein detection by Western blot

Solutions and reagents:

- Amersham™ Hybond® P western blotting membranes, PVDF, pore size 0.45 µm (GE Healthcare, #10600023) for chemiluminescent detection or Immobilon® - FL PVDF Membrane (Immobilon®, #PFL00010) for fluorescent detection.
- Amersham™ Hyperfilm™ MP (Cytiva, #28-9068-44).
- Fujifilm Medical X-raySuper RX-N (Fuji, #47410)
- Western blotting filter paper, extra thick (Thermo ScientificTM, #10675935).
- Transfer Buffer: 20% (v/v) methanol, 192 mM glycine, 25 mM Tris base, 0.05% (w/v) SDS).
- Running Buffer: 192 mM glycine, 25 mM Tris base, 0.1% (w/v) SDS.

USC DE COMPOSTELA

- TBS-T: 20 mM Tris-HCl pH 7.6, 150 mM NaCl, 0.1% (v/v) Tween 20.
- Blocking Buffer: TBS-T containing either 5% (w/v) fat-free milk powder or 1X BlockerTM FL Fluorescent Blocking Buffer (Thermo ScientificTM, #15929152).
- ECL Solution 1: 100 mM Tris-HCl pH 8.5, 2.5 mM luminol, 0.4 mM p-coumaric acid.
- ECL solution 2: 100 mM Tris-HCl pH 8.5, 0.02 % (v/v) H_2O_2.

Procedure:

1. Once the electrophoresis has finished, transfer the gel to a box with 100 ml ice-cold Transfer Buffer.
2. Soak Western Blotting Filter Paper with ice-cold Transfer Buffer (only 2 per gel with the extra thick paper).
3. Activate PVDF membrane in methanol for 2 min, discard the methanol, and incubate in ice-cold transfer buffer for 2 additional min.
4. Using a semidry transfer Semiphor system (#TE77X, Hoefer), assemble sequentially the transfer sandwich by placing one sheet of the western blotting filter paper in direct contact with the anode plate, the PVDF membrane, the gel and a second sheet of filter paper that will be in contact with the cathode when the system is closed. Ensure that no bubbles are trapped in between the layers.
5. Transfer for 90 min at a constant amperage of 0.8 mA/cm^2 (typically 40 mA per minigel).
6. After transfer, incubate the membrane in Blocking Buffer for 20 minutes at RT with gentle shaking.
7. Incubate the membrane with the primary antibody solution for 1h at RT or overnight at 4 °C.
8. Wash the membrane with TBS-T (3 x 5 min). If the primary antibody is already conjugated to HRP, proceed directly to step 11.
9. Incubate the membrane with the secondary antibody for 1h at RT.
10. Wash the membrane with TBS-T (3 x 5 min).
11. Remove excess TBS-T. For chemiluminescent detection, incubate the membrane with mixture of ECL solution 1 and ECL solution 2 (vol 1:1) for 1 min. Image the membrane using a ChemiDoc™ MP (Bio-rad) or alternatively expose X-ray films to the membrane and develop using an automatic film processor (Fuji Medical Film Processor FPM-100A). For fluorescent detection, allow the membrane to dry and image using the ChemiDoc™ MP.

3.2 Protein purifications

3.2.1 Purification of scPif1 in *E. coli*.

USC UNIVERSIDADE DE SANTIAGO DE COMPOSTELA

Solutions and reagents:

- Buffer B (20 mM K_2HPO_4 pH 7.5, 10% (v/v) glycerol, 0.01% (v/v)) Igepal
- Lysis Buffer: Buffer B supplemented with 0.5 mM EDTA, 10% (v/v) glycerol, 2 mM DTT, 100 mM KCl, 1mM PMSF, 1X EDTA-free Protease Inhibitor Cocktail tablets (Roche, #11873580001). DTT, PMSF and protease inhibitors must be added freshly before use.
- HiTrap™ Capto™ Q ImpRes IEX Columns (5 ml) (Cytiva, #17-5470-55).
- HiTrap™ Capto™ SP ImpRes IEX Columns (5 ml) (Cytiva, #17-5468-5).
- HisTrap™ HP Prepacked Columns (1 ml) (Cytiva, #17-5247-01).
- InstantBlue® Coomassie Protein Stain (Abcam, #ab119211).
- Novex™ WedgeWell™ 4 to 12%, Tris-Glycine, 1.0 mm, Mini Protein Gels (InvitrogenTM, #XP04122BOX).
- 1 M imidazole.
- 1 M IPTG.
- 2X SDS Sample Buffer (100 mM Tris-HCl pH 6.8, 4% (w/v) SDS, 0.1% (w/v) bromophenol blue, 20% (v/v) glycerol).

3.2.1.1 Optimization of induction conditions and solubility tests

Pif1 was purified from *E. coli*, adapting the protocol from (Buzovetsky et al., 2017). Prior to big-scale purification, we tested two different *E. coli* strains engineered to facilitate the overexpression of heterologous proteins: BL21-CodonPlus(DE3)-RIL strain (Agilent, #230245) and Rosetta(DE3) Competent Cells (Novagen, 70954-3). Both strains were transformed with pET28-nPIF1 to optimize both total yield and protein solubility.

1. Inoculate cells in 5 ml of LB containing 50 µg/ml kanamycin and 34 µg/ml chloramphenicol and incubate overnight at 37 °C with agitation (200 rpm).
2. Next morning, measure OD_{600} and normalize cell cultures to OD_{600} = 0.05 in a final volume of 10 ml LB with kanamycin and chloramphenicol.
3. Once they reach OD_{600} ~ 0.5 (usually 2.5 - 3 h after refresh), induce protein expression by adding 0.1 mM IPTG for 20h at 16 °C.
4. Centrifuge cultures at 4500 x *g*, for 15 min, 4 °C.
5. Remove supernatant and resuspend the cell pellet in 900 µl of Lysis Buffer. Incubate for 20 min on ice and transfer to a 1.5 ml microcentrifuge tube.
6. Sonicate the cell suspension with 3 cycles of 5 s at 15% amplitude in a sonicator (Branson 450 digital sonifier), keeping samples on ice between cycles.

USC UNIVERSIDADE DE SANTIAGO DE COMPOSTELA

7. Centrifuge lysates at 16000 x *g* for 30 min at 4 °C. Transfer supernatant (soluble fraction) to a new centrifuge tube. Take a 20 µl sample and add 1 vol of 2X SDS Sample Buffer for SDS-PAGE analysis.
8. Resuspend the pellet from step 7 (insoluble fraction) in 900 µl of 2X SDS Sample Buffer by incubation at 65 °C for 30 min with agitation. Take a 20 µl sample and add 1 volume of Lysis Buffer to make soluble and insoluble fractions comparable.
9. Boil samples for 3 min at 99 °C.
10. Run samples in a 4-12% Tris-Glycine gel at 200V for 40 min.
11. Stain gel with Coomassie to analyse fractions.

3.2.1.2 Purification of Pif1

After protein expression optimization experiments, we decided to employ E. coli BL21-CodonPlus (DE3)-RIL cells to express and purify different variants of the Pif1 nuclear isoform (amino acids 40–859) cloned into the low-copy plasmid pET28b-6xHis: nPif1, nPif1nls, nPif1107-850 and the ATPase-deficient mutant nPif1K264A as a negative control. Protein induction was performed as described in the previous section but increasing the cultures volumes to 2.4 L (3x 800 ml cultures in 2 L flasks) per variant.

1. Harvest cells from the 2.4 L by centrifugation at 10000 x *g*, 10 min, 4 °C (Avanti J26-XPI with JA-10 rotor, Beckman) and wash once with H_2O containing 1 mM PMSF. Centrifuge in the same conditions and remove supernatant. Freeze pellets at -80 °C or proceed with lysis in step 2.
2. Resuspend the cell pellet from a 2.4 L culture in 70 ml Lysis Buffer.
3. Lyse cells in the Branson Digital Sonifier with 7 cycles at 15% amplitude for 5 s, followed by 1 additional cycle at 25% amplitude for 2 s, keeping samples on ice for 1 min between cycles.
4. Pre-clear the lysate by centrifugation at 12000 x *g* for 10 min, 4 °C (Avanti J26-XPI with JA-20 rotor, Beckman). Transfer supernatant to pre-cooled ultracentrifuge tubes. Resuspend pellet in 2% SDS (insoluble fraction) and proceed to the next step with the supernatant.
5. Clarify lysate by ultracentrifugation at 100000 x *g* for 40 min, 4 °C (Optima L-100 XP with a Type 45 Ti rotor, Beckman). Save a sample (50 µl) of the supernatant for final analysis (soluble input fraction).
6. Load lysate onto a 5 ml HiTrap™ Capto™ Q ImpRes IEX column connected to an ÄKTA™ start FPLC system (GE Healthcare). Collect the flow-through and save a 50 µl sample.
7. Load flow-through from the Q column onto a 5 ml HiTrap™ Capto™ SP ImpRes IEX column. Wash the column with 5 vol of Lysis Buffer and elute proteins into 3 ml fractions over a 90-ml gradient of 100–660 mM KCl in Buffer B.

USC UNIVERSIDADE DE SANTIAGO DE COMPOSTELA

8. Analyse 10 µl of each fraction by SDS-PAGE and Coomassie staining. Pool the fractions enriched in Pif1 (usually fraction 15-22 in our conditions) and adjust imidazole to a final concentration of 10 mM.
9. Load pooled fractions containing Pif1 onto the 1 ml HisTrap column and collect a flow-through sample.
10. Wash the column with 15 CV of buffer B containing 1 M KCl, 1 mM ATP, 8 mM $MgCl_2$ and 10 mM imidazole.
11. Wash with 10 CV of buffer B + 150 mM KCl + 20 mM Imidazole
12. Elute the bound proteins with 10 CV of buffer B containing 150 mM KCl and 500 mM imidazole.
13. Analyse elution fractions by SDS-PAGE and Coomassie staining.
14. Pool the peak fractions and dialyze twice against 500 vol of Buffer B containing 150 mM KCl and 1 mM DTT at 4 °C (first overnight, second for 2-3 h).
15. Centrifuge the dialyzed protein at 13.000 x *g*, for 10 min at 4 °C, aliquot into pre-chilled 0.5 ml tubes and snap freeze in liquid nitrogen. Store at -80 °C.

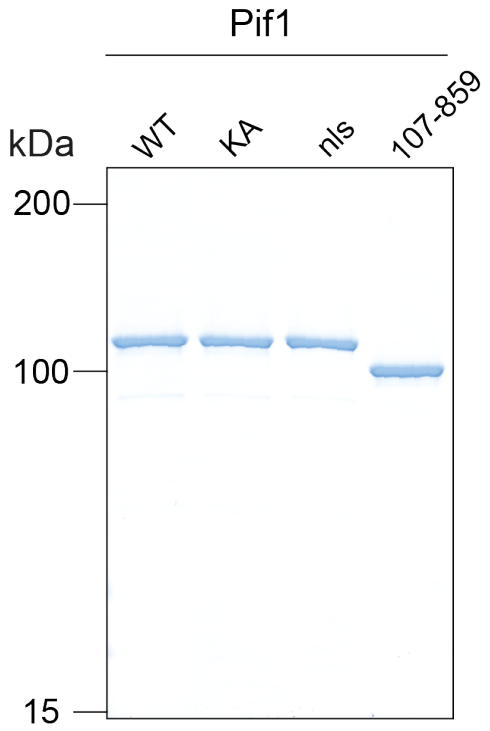


Figure 71. Coomassie staining of all Pif1 variants purified in this study. Pif1, the ATPase-dead version $Pif1^{KA}$, $Pif1^{nls}$ and the truncated isoform $Pif1^{107-859}$ were purified, analysed by SDS-PAGE and stained with Coomassie.

3.2.2 Purification of Yen1

This protocol was adapted from (Carreira et al., 2021)

Solutions and reagents

- Buffer A: 40 mM Tris-HCl pH 7.5, 500 mM NaCl, 20% (v/v) glycerol, 0.1% (v/v) Nonidet P-40, 1 mM DTT.
- Lysis Buffer: Buffer A containing 5 mM NaF, 5 mM H2NaPO4, 5 mM β-glycerophosphate, 1 mM PMSF, 1X EDTA-free Protease Inhibitor Cocktail tablets (Roche, #11873580001) and 1X Sigma yeast Protease Inhibitor Cocktail (Sigma, #P8215).
- FLAG Elution buffer: Buffer A containing 0.5 mg/ml 3xFLAG peptide (Sigma, #F4799). Check pH of Buffer A with 300 mM imidazole, usually requires a few drops of concentrated HCl to adjust.
- Imidazole Elution buffer: Buffer A + 300 mM Imidazole.
- M2 anti-FLAG agarose affinity gel (Sigma, #A2220).
- Lambda protein phosphatase (New England BioLabs, #P0753S).
- SuperFlow His-Pur Ni-NTA agarose beads (Thermo, #25215).
- Coomassie Protein Stain (InstantBlue®, ab119211).

Procedure:

1. Freshly streak yeast strain W2507 (*MATa ura3-52::P_{GAL1}-YEN1^{ON-ND}-FLAG3-TEV2-HIS10::URA3 yen1Δ::HIS3 pep4Δ::KANMX4 bar1Δ::HPHNT1*) on YPD agar plates and incubate at 25 °C to isolate red colonies. Ensure the absence of petite cells by re-streaking on YPGly agar plates and once more in YPAD plates.
2. Inoculate 100 ml YPARaff (for a final 10L preparative culture) in a 500 ml flask with several individual colonies from the YPAD plates using sterile technique. Let cells grow at 30 °C, 200 rpm until they reach approximately 108 cells/ml.
3. In the meanwhile, prepare 9L of sterile YPARaff and set up the fermentor (we use a custom-made, 10L glass fermentor) using sterile techniques. Pre-warm medium in the fermentor to 30 °C
4. When ready, transfer cells to the fermentor and grow until cell density reaches around 5 x 107 cells/ml.
5. After reaching the desired density, add 1 L sterile 20% galactose and incubate for an additional 3 h. (Probably I did a longer induction, gotta check)
6. Harvest cells in 500 ml centrifuge bottles at 5000 x g for 5 min in a JA-10 rotor. Weigh pellets, resuspend them in sterile cold water containing 1 mM PMSF and pool them in batches containing approximately 70-80 g cells. Collect cells again under the same conditions and resuspend them in cold 200 ml Buffer A containing 1 mM PMSF. Centrifuge cells once more under the same conditions, remove supernatant and proceed to lysis using a BeadBeater or freeze the pellet in dry ice and store at -80 °C until needed.

USC UNIVERSIDADE DE SANTIAGO DE COMPOSTELA

7. Set up BeadBeater according to manufacturer´s instructions. Pour around 200 ml of 0.5 mm glass in its 350 ml stainless steel chamber jar and pre-cool them in the fridge. Unless indicated, all steps are carried out at 4 °C.
8. Resuspend a pellet of up to 80 g cells in a final volume of cold 200 ml of Lysis Buffer and pour it in the chamber (if thawing the pellet, assist resuspension by pipetting up and down on ice). Assemble the BeadBeater and grind 8 x 1 min with 1 min breaks, replenishing the ice if required. Carefully decant the lysate into a 500 ml centrifuge bottle to minimize carrying over glass beads. Wash beads with 2 x 50 ml Lysis Buffer and combine with the crude lysate.
9. Pre-clear the lysate by centrifugation at 10000 x g for 10 min at 4°C (Avanti J26-XPI with JA-20 rotor, Beckman). Decant the supernatant into ultracentrifuge bottles.
10. Clear the lysate by centrifugation at 125000 x g for 45 min at 4°C (Optima L-100 XP with a Type 45 Ti rotor, Beckman).
11. During the centrifugation, wash the required amount of anti-FLAG M2 resin that will be used in the next step. For a prep starting with 80 g cells, we routinely use 2.5 ml of M2 beads. Thaw the 50% M2 resin slurry and resuspend it homogeneously. Transfer 5 ml of the 50% slurry to a 100 ml chromatography column and let the resin storage buffer flow through. Wash the beads with 10 CV of Buffer A and then 3 CV of Lysis Buffer, leaving a small amount of buffer on top of the column bed to avoid dehydration. Close the column until the lysate is ready.
12. After centrifugation, carefully transfer the clean supernatant to the 100 ml column (Bio-Rad, #7372522) with a 25 ml serological pipette, avoiding both the cloudy upper layer and the viscous bottom layer as much as possible. Save a sample (200µl) of the lysate. Incubate with gentle rolling for 1h at 4°C.
13. After incubation, let the column stand for 5 min and then open the end and collect the flow-through (save a 200 µl sample to assess binding efficiency).
14. Wash the column with 10 CV of Lysis Buffer and then 20 CV of Buffer A + 1mM DTT. Save 200 µl samples of both washes.
15. Elute the bound proteins in protein low-binding tubes with 3 x 1 CV of FLAG Elution buffer. For each elution, close the bottom of column, add the FLAG Elution buffer, place the column top cap, and incubate for 5 min with gentle rotation at 4°C. Then, let the column stand for 1 min and open it to collect the elution. In general, 3 elutions are enough to recover most of the protein bound to the beads.
16. Combine the three eluates (take 10 µl sample)
17. During the incubation, prepare the Ni-NTA resin that will be used in the next step. Resuspend the resin and dispense 400 µl of the 50% Ni-NTA slurry (200 µl packed beads) into one 10 ml disposable columns (Thermo, #89898) and let the storage buffer flow

USC UNIVERSIDADE DE SANTIAGO DE COMPOSTELA

through. Equilibrate the beads with 30 CV of Buffer A containing 5 mM imidazole. Cap the columns until needed.

18. After incubation, adjust the sample to 5 mM imidazole, keeping a 20 µl sample for later analysis and transfer the rest to the column containing the Ni-NTA beads.
19. Incubate with gentle rotation on a roller for 1h at 4 °C.
20. Once finished, let the column stand for a few minutes and collect the flow-through. Wash the beads with 2 x 20 CV of Buffer A containing 5 mM and 20 mM imidazole, respectively. Keep the washes for analysis.
21. To elute the bound protein, add 3 x 2 CV of Buffer A containing 300 mM imidazole, incubating with gentle rotation for 5 min as described above. Collect each elution separately for analysis in protein low-binding tubes.
22. Analyse 10 µl of the aliquots from each step of the purification by SDS-PAGE and Coomassie staining to assess the efficiency of the protocol and select the final peak fractions.
23. Pool the selected fractions and dialyze twice against 500 vol Buffer A at 4 °C in a Slide-A-LyzerTM MINI dialysis device with a 10 kDa cut-off (Thermo ScientificTM, # 69570). Typically, the first dialysis is performed overnight and the second one for 3-4 h in the next morning, both with gentle stirring.
24. After dialysis, centrifuge the samples at 16,000 x g for 15 min at 4°C to eliminate possible insoluble aggregates that may have formed during the
25. Recover the supernatant and distribute in small (10-20 µl) aliquots. Flash-freeze in liquid nitrogen and store at -80°C.
26. Quantify protein by Bradford assay and/or densitometry against BSA standards in SDS-PAGE gels and Coomassie staining.

3.3 Biochemical assays

3.3.1 ATPase assays

The capacity of different Pif1 mutants to hydrolyse ATP for unwinding DNA was tested by Thin Layer Chromatography (TLC). This method is based on the different partition coefficients of the inorganic phosphate (Pi) and ATP between the mobile phase (formic acid and lithium chloride solution) and the stationary phase (a positively charged polyethyleneimine cellulose membrane), resulting in the faster migration of the Pi. This protocol was adapted from (Sausen et al., 2019).

Solutions and reagents:

- Running Buffer: 1M formic acid, 400 mM LiCl.
- 2X ATPase Buffer: 70 mM Tris-HCl pH 7.5, 84 mM KCl, 10 mM MgCl2, 200 ng/µl BSA, 2 mM DTT.
- 2X Stop solution: 2% (v/v) SDS, 40 mM EDTA.

USC UNIVERSIDADE DE SANTIAGO DE COMPOSTELA

- ATP [γ-32P]- 3000Ci/mmol 10mCi/ml (Perkin Elmer, NEG002A250UC).
- TLC plate (Sigma-Aldrich® Z122882-25EA).

Procedure

1. Prepare the TLC PEI cellulose sheet. Delineate lanes for your reactions with a blunt pencil without scratching the surface; draw a line across the TLC sheet 2 cm from the bottom edge and mark every 1 cm along the line, with 0.5 cm margins from the edges.
2. In a fume-hood, add approximately 100 ml of Running buffer to the TLC tank. This should fill it approximately 0.5-1 cm from the bottom.
3. Pre-aliquot 2 µl of 2X Stop solution into as many tubes (on ice) as required (one per time-point).
4. For 7 time-points, prepare a mix of 15 µl divided in two tubes. In Tube 1, add 2.25 µl of H20 + 0.6 µl [^{32}P]-ATP. In tube 2, add 3.75 µl 2X ATPase Buffer +1.5 µl 10 µM oligo (poli-T) + 7.5 µl 20 nM Pif1 in ATPase Buffer
5. Start the reactions while transferring all the volume from tube 2 to tube 1. Take time-point 0 immediately and incubate the reaction at 30 °C.
6. Take 2 µl of sample at every timepoint (1 min – 2 min – 5 min – 10 min – 15 min – 20 min) and add it to the tube with pre-aliquoted stop solution. Incubate all reactions for 30 min at 37 °C.
7. Spot 1 µl of every stopped reaction onto a mark on the TLC plate. Allow the spots to dry until they are not visible (it takes less than 2 min).
8. Place the TLC plate into the tank, carefully submerging the bottom edge in Running buffer. Apply vacuum grease to the lid to ensure a tight seal and cover the tank. Develop the plate for 80 min, allowing the solvent front to reach ~1 cm from the top of the TLC plate.
9. Take out the TLC plate from the tank, place it on top of a few layers of paper and allow it to dry (cellulose side up) for 30 min.
10. Wrap the TLC in plastic and expose to a Phosphor Screen (Fujifilm, #BASMP-2040P) for 3-4h.
11. Scan the phosphor screen using a Typhoon FLA9500 scanner (GE Healthcare). The Pi will have migrated towards the top of the plate, while the ATP remains close to the original spot.
12. Quantify the ATP hydrolysis by densitometry using ImgeQuant™ software using the following equation: % Hydrolysis = (Pi) / (ATP + Pi) * 100. The amount of Pi hydrolyzed in the no protein control was subtracted from each reaction.

3.3.2 DNA unwinding assays

USC UNIVERSIDADE DE SANTIAGO DE COMPOSTELA

Helicase activity was analysed by time-course experiments in DNA unwinding assays. Pif1 (4 nM) was incubated with a 10-molar excess of a fluorescent Splayed Arm substrate and 100-molar excesses of an unlabelled ssDNA trap to avoid reannealing of the fluorescent-labelled oligo.

Solutions and reagents:

- Helicase Buffer: 35 mM Tris HCl pH 7.5, 5 mM MgCl2, 60 mM KCl, 100 ng/µl BSA, 1 mM DTT, 5 mM ATP
- 5X Stop solution: 10 mg/ml Proteinase K, 0.5% SDS.
- 6X Ficoll loading buffer: 15% (w/v) Ficoll-400 in 60 mM EDTA, 20 mM Tris-HCl pH 8.0, 0.48% (w/v) SDS, 0.15% (w/v) Orange G.

Procedure:

The procedure to set up a time-course for 6 points (10 µl each) is described below:

1. Set up time course reactions on ice. Dilute protein to 40 nM in Helicase Buffer.
2. Prepare a volume of 1.1X reaction mix equivalent to seven time points (63 µl), for a final 40 nM of Splayed Arm and 400 nM Cold-Trap in Helicase Buffer (see Table 4).
3. Start time course by adding 7 µl 40 nM Pif1 to the reaction mix to a final concentration of 4 nM.
4. Draw a 10 µl aliquot at each time point (0, 15, 30, 60, 120, 240 sec) and mix with 2.5 µl of pre-aliquoted 5X stop solution. Incubate for a further 30 min at 37 °C.
5. Mix each reaction with 2.5 µl of 6X Ficoll loading buffer and analyse the products by 12% (29:1) native PAGE in 1xTBE. Gels (Cambridge electrophoresis LTD) were run in 1X TBE buffer at 150 V for 75 min and imaged while fresh by scanning at 488 nm in a Typhoon FLA 9500.
6. Quantification by densitometry was carried out with the ImageQuant software. The percent of DNA unwound was with the following equation: % unwinding = ssDNA / (ssDNA + Splayed Arm) * 100. The amount of ssDNA present in the no protein control was subtracted from each reaction.

4. CELL BIOLOGY TECHNIQUES

4.1 Fluorescence microscopy

Pif1 subcellular localization was addressed by fluorescence microscopy in live yeast cells since fixation procedures may generate artifacts. Different mutant versions of *PIF1* cloned into pAG306GAL-ccdB-eGFP were integrated in *pif1-m2* strains to avoid the slow growth of *pif1*Δ strains. SC-Raf-Gal supplemented with a high concentration of adenine was employed instead of YPD to avoid the high autofluorescence of both YP-based media and the red pigment accumulated in the W303 background in the absence of adenine due to the *ade2-1* mutation (Smirnov et al., 1967).

Solutions and reagents:

- SC-Raff + 100 µg/ml of adenine
- SC-Raff-Gal + 100 µg/ml of adenine
- 1.2% (w/v) agarose dissolved in SC-Raf-Gal + 100 µg/ml adenine
- DAPI solution: 5 mg/ml stock solution in deionized water (500X).
- Valap: mixture of equal volumes of paraffin, petroleum jelly and lanolin.

Procedure: *preparation of agarose patches*

Prepare a microscope slide. Add 150 µl of melted 1.2% agarose in SC-Raf-Gal + 100 µg/ml adenine to the center of a microscope slide. Then cover with another slide and wait 7 min for the agarose to solidify. Remove the top slide very carefully. It is recommended to start preparing the agarose patches 30 min before harvesting the cells.

Procedure: *mounting cells*

1. Inoculate cells in 5 ml SC-Raf + 100 µg/ml adenine and incubate at 30 °C with shaking overnight.
2. Next morning, if the cultures are in mid-log phase, normalize to OD_{600} = 0.2 and induce 3 h in SC-Raf-Gal + 100 µg/ml adenine. If the cultures are saturated, normalize to OD_{600} = 0.1, let them cycle once to reach OD_{600} = 0.2 and induce cells as stated above.
3. Transfer 1 ml of each culture to 1.5 microcentrifuge tubes, and add DAPI to final concentration of 10 µg/ml. Incubate cells with shaking at 30 °C for additional 30 min.
4. Harvest cells by low-speed centrifugation (1500 x *g*) to preserve the organelles position.
5. Wash cells once with SC-Raf-Gal + 100 µg/ml adenine and resuspend in 100 µl of the same media.
6. Transfer cells 3.5 µl of the cell suspension to a microscope slide with a solidified patch of 1.2% agarose SC-Raf-Gal + 100 µg/ml Ade.
7. Cover with a coverslip. Seal the edges using melted valap and proceed to imaging.

Procedure: *mounting cells*

Cells were imaged using a THUNDER Imager Tissue (Leica Microsystems) with the following parameters: refractive index 1.34, Thunder algorithm enabled for background subtraction.

4.2 Flow cytometry

A classic flow cytometry protocol based on fixation and permeabilization with ethanol, RNase A treatment and the use of DNA-specific intercalating dye was employed to analyze the cell-cycle profile of different yeast strains.

Solutions and reagents:

- 70% Ethanol (cold, 4 °C)

- 50 mM Tris-HCl pH 8.0
- RNase A (10 mg/ml in 10 mM sodium acetate pH 5.2)
- 55 mM HCl.
- Pepsin (5 mg/ml in 55 mM HCl).
- Sytox Green 5 mM in DMSO (Invitrogen™ , #S7020).

Procedure:

1. Transfer 1 ml of the culture (about 107 cell/ml or OD600 = 0.5-1.0) to a 2.2 ml Eppendorf tube. Centrifuge cells for 1 min at 10000 x g, remove supernatant and resuspend cells in the remaining liquid (dry vortex). Add 1 ml of cold 70% ethanol and mix by vortexing. Store at 4 °C overnight or until required.
2. Harvest cells at 5000 x g for 5 min, discard the supernatant and wash them once with 1 ml of 50 mM Tris-HCl pH 8.
3. Pellet cells again and resuspend the cell pellet in 1 ml 50 mM Tris-HCl pH 8 containing 0.1 mg/ml RNase A (DNase-free). Incubate 4 h to overnight at 37 °C, with agitation.
4. Harvest cells at 5000 x g for 5 min. Discard supernatant and resuspend cells in 0.5 ml of 5 mg/ml pepsin, freshly dissolved in 55 mM HCl. Incubate at 37 °C for 30 min.
5. Harvest cells at 5000 x g for 5 min, discard supernatant and resuspend cells in 50 mM Tris-HCl pH 8. Store unstained cells at 4 °C until required.
6. Transfer 50-100 µl cells into an optically clear polystyrene tube (Corning™ Falcon™ Round-Bottom Polystyrene Test Tubes, 10579511) that contains 0.5 ml 50 mM Tris-HCl pH 8 with 1 µM SYTOX Green. Mix the cells and sonicate for 3 s at 15% amplitude (Branson Digital Sonifier 250 Cell Disruptor) just before running the samples.
7. Acquire data within the flow cytometer (BD AccuriTM C6 Flow Cytometer, BD Biosciences), using excitation at 488 nm and collecting fluorescence emission at 525 nm. Gating conditions were applied to eliminate doubles and debris from analysis, 10000 cells were measured per condition.
8. Analyze data with FlowJo™ software (BD Biosciences).

4.3 Genotoxicity assays

Viability and DNA damage sensitivity of different strains was tested by exposure to different DNA damage agents, including hydroxyurea (HU, an inhibitor of the ribonucleotide reductase), camptothecin (CPT, a Topoisomerase I inhibitor) and the alkylating agent methyl methanesulfonate (MMS). Different strains were grown overnight to saturation and then normalized to OD_{600} = 0.5; 200 µl of each culture were transferred to a sterile 96-well microplate (Corning®, 3879) and three 1:10 serial dilutions were made prepared. 4 µl drops from each dilution were spotted onto a suitable solid medium containing different concentrations of genotoxic drugs. Plates were allowed to dry before inverting and then

USC DE COMPOSTELA

incubated at 30 °C for 3 days. Pictures were taken at 48 and 72 h using a Gel-Doc XR+ system (Bio-rad) with epi-white illumination and 0.5 s exposure.

5. *IN SILICO* ANALYSES

To identify potential regions functioning as nuclear localization sequences in Pif1, we primarily employed the cNLS mapper software (Table 9) to scan for both monopartite and bipartite signals, using the software's default parameters, and manually setting the discovery threshold at 4.0. Additionally, we complemented our search with two other packages optimized for NLS prediction, NucPred and NLStradamus, employing their default parameters (Table). A total of 4 regions were selected for mutagenesis and further analysis.

For the prediction of potential mitochondrial pre-sequences and their cleavage positions we employed the Mitofates software (Table 9), using fungal or metazoan parameters where applicable. The minimum probability a sequence as a functional MTS was the recommended threshold of 0.385.

For the prediction of secondary structures and disordered regions in Pif1, we employed the PSIPRED package including PSIPRED 4.0 and DISOPRED3 with the default parameters (Table 9).

Table 9. Software used in this study for the *in silico* analyses.

Software	Source or reference	Link
Web server		
Mitofates	(Fukasawa et al., 2015)	https://mitf.cbrc.pj.aist.go.jp/MitoFates/cgi-bin/top.cgi
cNLS mapper	(Kosugi et al., 2009)	http://nls-mapper.iab.keio.ac.jp/
DISOPRED3	(Jones and Cozzetto, 2015)	http://bioinf.cs.ucl.ac.uk/psipred
PSIPRED	(McGuffin et al., 2000)	http://bioinf.cs.ucl.ac.uk/psipred
Commercial software		
FlowJo 10.4	BD Biosciences	https://www.flowjo.com/
LasX	Leica Microsystems	https://www.leica-microsystems.com/
GraphPad Prism9	GraphPad	https://www.graphpad.com/
ImageQuant	Cytiva	https://www.cytivalifesciences.com
Snapgene 4.3.11	Domatics	https://www.snapgene.com/
ImageLab 6.1	Bio-rad	https://www.bio-rad.com/es-es/product/image-lab-software

USC UNIVERSIDADE DE SANTIAGO DE COMPOSTELA

BIBLIOGRAPHY

Agmon, N., Yovel, M., Harari, Y., Liefshitz, B., Kupiec, M., 2011. The role of Holliday junction resolvases in the repair of spontaneous and induced DNA damage. Nucleic Acids Res. 39, 7009–7019. https://doi.org/10.1093/nar/gkr277

Aguilera, A., García-Muse, T., 2013. Causes of Genome Instability. Annu. Rev. Genet. 47, 1–32. https://doi.org/10.1146/annurev-genet-111212-133232

Alberti, S., Gitler, A.D., Lindquist, S., 2007. A suite of Gateway® cloning vectors for high-throughput genetic analysis in Saccharomyces cerevisiae. Yeast 24, 913–919. https://doi.org/10.1002/yea.1502

Alcasabas, A.A., Osborn, A.J., Bachant, J., Hu, F., Werler, P.J.H., Bousset, K., Furuya, K., Diffley, J.F.X., Carr, A.M., Elledge, S.J., 2001. Mrc1 transduces signals of DNA replication stress to activate Rad53. Nat. Cell Biol. 3, 958–965. https://doi.org/10.1038/ncb1101-958

Alonso-Ramos, P., Álvarez-Melo, D., Strouhalova, K., Pascual-Silva, C., Garside, G.B., Arter, M., Bermejo, T., Grigaitis, R., Wettstein, R., Fernández-Díaz, M., Matos, J., Geymonat, M., San-Segundo, P.A., Carballo, J.A., 2021. The Cdc14 Phosphatase Controls Resolution of Recombination Intermediates and Crossover Formation during Meiosis. Int. J. Mol. Sci. 22, 9811. https://doi.org/10.3390/ijms22189811

Altieri, F., Grillo, C., Maceroni, M., Chichiarelli, S., 2008. DNA Damage and Repair: From Molecular Mechanisms to Health Implications. Antioxid. Redox Signal. 10, 891–938. https://doi.org/10.1089/ars.2007.1830

Alzu, A., Bermejo, R., Begnis, M., Lucca, C., Piccini, D., Carotenuto, W., Saponaro, M., Brambati, A., Cocito, A., Foiani, M., Liberi, G., 2012. Senataxin Associates with Replication Forks to Protect Fork Integrity across RNA-Polymerase-II-Transcribed Genes. Cell 151, 835–846. https://doi.org/10.1016/j.cell.2012.09.041

Anand, R., Beach, A., Li, K., Haber, J., 2017. Rad51-mediated double-strand break repair and mismatch correction of divergent substrates. Nature 544, 377–380. https://doi.org/10.1038/nature22046

Anand, R., Jasrotia, A., Bundschuh, D., Howard, S.M., Ranjha, L., Stucki, M., Cejka, P., 2019. NBS1 promotes the endonuclease activity of the MRE11-RAD50 complex by sensing CtIP phosphorylation. EMBO J. 38, e101005. https://doi.org/10.15252/embj.2018101005

Andis, N.M., Sausen, C.W., Alladin, A., Bochman, M.L., 2018. The WYL Domain of the PIF1 Helicase from the Thermophilic Bacterium Thermotoga elfii is an Accessory Single-Stranded DNA Binding Module. Biochemistry 57, 1108–1118. https://doi.org/10.1021/acs.biochem.7b01233

USC UNIVERSIDADE DE SANTIAGO DE COMPOSTELA

Antony, E., Tomko, E.J., Xiao, Q., Krejci, L., Lohman, T.M., Ellenberger, T., 2009. Srs2 disassembles Rad51 filaments by a protein-protein interaction triggering ATP turnover and dissociation of Rad51 from DNA. Mol. Cell 35, 105–115. https://doi.org/10.1016/j.molcel.2009.05.026

Appanah, R., Jones, D., Falquet, B., Rass, U., 2020. Limiting homologous recombination at stalled replication forks is essential for cell viability: DNA2 to the rescue. Curr. Genet. 66, 1085–1092. https://doi.org/10.1007/s00294-020-01106-7

Arter, M., Hurtado-Nieves, V., Oke, A., Zhuge, T., Wettstein, R., Fung, J.C., Blanco, M.G., Matos, J., 2018. Regulated Crossing-Over Requires Inactivation of Yen1/GEN1 Resolvase during Meiotic Prophase I. Dev. Cell 45, 785-800.e6. https://doi.org/10.1016/j.devcel.2018.05.020

Asai, T., Bates, D.B., Kogoma, T., 1994. DNA replication triggered by double-stranded breaks in E. coli: Dependence on homologous recombination functions. Cell 78, 1051–1061. https://doi.org/10.1016/0092-8674(94)90279-8

Audry, J., Maestroni, L., Delagoutte, E., Gauthier, T., Nakamura, T.M., Gachet, Y., Saintomé, C., Géli, V., Coulon, S., 2015. RPA prevents G-rich structure formation at lagging-strand telomeres to allow maintenance of chromosome ends. EMBO J 34, 1942–58. https://doi.org/10.15252/embj.201490773

Azvolinsky, A., Dunaway, S., Torres, J.Z., Bessler, J.B., Zakian, V.A., 2006. The S. cerevisiae Rrm3p DNA helicase moves with the replication fork and affects replication of all yeast chromosomes. Genes Dev. 20, 3104–3116. https://doi.org/10.1101/gad.1478906

Azvolinsky, A., Giresi, P.G., Lieb, J.D., Zakian, V.A., 2009. Highly Transcribed RNA Polymerase II Genes Are Impediments to Replication Fork Progression in Saccharomyces cerevisiae. Mol. Cell 34, 722–734. https://doi.org/10.1016/j.molcel.2009.05.022

Bae, S.-H., Bae, K.-H., Kim, J.-A., Seo, Y.-S., 2001. RPA governs endonuclease switching during processing of Okazaki fragments in eukaryotes. Nature 412, 456–461. https://doi.org/10.1038/35086609

Bahmed, K., Nitiss, K.C., Nitiss, J.L., 2010. Yeast Tdp1 regulates the fidelity of nonhomologous end joining. Proc. Natl. Acad. Sci. 107, 4057–4062. https://doi.org/10.1073/pnas.0909917107

Baker, A.R., Slack, F.J., 2022. ADAR1 and its implications in cancer development and treatment. Trends Genet. 38, 821–830. https://doi.org/10.1016/j.tig.2022.03.013

Balbo Pogliano, C., Ceppi, I., Giovannini, S., Petroulaki, V., Palmer, N., Uliana, F., Gatti, M., Kasaciunaite, K., Freire, R., Seidel, R., Altmeyer, M., Cejka, P., Matos, J., 2022. The CDK1-TOPBP1-PLK1 axis regulates the Bloom's syndrome helicase BLM to suppress crossover recombination in somatic cells. Sci. Adv. 8, eabk0221. https://doi.org/10.1126/sciadv.abk0221

Bannwarth, S., Berg-Alonso, L., Auge, G., Fragaki, K., Kolesar, J.E., Lespinasse, F., Lacas-Gervais, S., Burel-Vandenbos, F., Villa, E., Belmonte, F., Michiels, J.-F., Ricci, J.-E.,

Gherardi, R., Harrington, L., Kaufman, B.A., Paquis-Flucklinger, V., 2016. Inactivation of Pif1 helicase causes a mitochondrial myopathy in mice. Mitochondrion 30, 126–137. https://doi.org/10.1016/j.mito.2016.02.005

Bantele, S.C., Ferreira, P., Gritenaite, D., Boos, D., Pfander, B., 2017. Targeting of the Fun30 nucleosome remodeller by the Dpb11 scaffold facilitates cell cycle-regulated DNA end resection. eLife 6, e21687. https://doi.org/10.7554/eLife.21687

Barnes, D.E., Lindahl, T., 2004. Repair and Genetic Consequences of Endogenous DNA Base Damage in Mammalian Cells. Annu. Rev. Genet. 38, 445–476. https://doi.org/10.1146/annurev.genet.38.072902.092448

Bastin-Shanower, S.A., Fricke, W.M., Mullen, J.R., Brill, S.J., 2003. The mechanism of Mus81-Mms4 cleavage site selection distinguishes it from the homologous endonuclease Rad1-Rad10. Mol. Cell. Biol. 23, 3487–3496. https://doi.org/10.1128/mcb.23.10.3487-3496.2003

Bauer, N.C., Corbett, A.H., Doetsch, P.W., 2013. Automated Quantification of the Subcellular Localization of Multicompartment Proteins via Q-SCAn. Traffic 14, 1200–1208. https://doi.org/10.1111/tra.12118

Bauknecht, M., Kobbe, D., 2014. AtGEN1 and AtSEND1, two paralogs in Arabidopsis, possess holliday junction resolvase activity. Plant Physiol. 166, 202–216. https://doi.org/10.1104/pp.114.237834

Beard, W.A., Horton, J.K., Prasad, R., Wilson, S.H., 2019. Eukaryotic Base Excision Repair: New Approaches Shine Light on Mechanism. Annu. Rev. Biochem. 88, 137–162. https://doi.org/10.1146/annurev-biochem-013118-111315

Beck, H., Nahse-Kumpf, V., Larsen, M.S.Y., O'Hanlon, K.A., Patzke, S., Holmberg, C., Mejlvang, J., Groth, A., Nielsen, O., Syljuasen, R.G., Sorensen, C.S., 2012. Cyclin-dependent kinase suppression by WEE1 kinase protects the genome through control of replication initiation and nucleotide consumption. Mol. Cell. Biol. 32, 4226–4236. https://doi.org/10.1128/MCB.00412-12

Becker, J.R., Gallo, D., Leung, W., Croissant, T., Thu, Y.M., Nguyen, H.D., Starr, T.K., Brown, G.W., Bielinsky, A.-K., 2018. Flap endonuclease overexpression drives genome instability and DNA damage hypersensitivity in a PCNA-dependent manner. Nucleic Acids Res. 46, 5634–5650. https://doi.org/10.1093/nar/gky313

Bellendir, S.P., Rognstad, D.J., Morris, L.P., Zapotoczny, G., Walton, W.G., Redinbo, M.R., Ramsden, D.A., Sekelsky, J., Erie, D.A., 2017. Substrate preference of Gen endonucleases highlights the importance of branched structures as DNA damage repair intermediates. Nucleic Acids Res. 45, 5333–5348. https://doi.org/10.1093/nar/gkx214

Berger, J.M., 2008. SnapShot: Nucleic Acid Helicases and Translocases. Cell 134, 888-888.e1. https://doi.org/10.1016/j.cell.2008.08.027

Bessler, J.B., Torres, J.Z., Zakian, V.A., 2001. The Pif1p subfamily of helicases: region-specific DNA helicases? Trends Cell Biol. 11, 60–65. https://doi.org/10.1016/s0962-8924(00)01877-8

USC UNIVERSIDADE DE SANTIAGO DE COMPOSTELA

Bessler, J.B., Zakian, V.A., 2004. The amino terminus of the Saccharomyces cerevisiae DNA helicase Rrm3p modulates protein function altering replication and checkpoint activity. Genetics 168, 1205–18. https://doi.org/10.1534/genetics.104.028035

Bétermier, M., Bertrand, P., Lopez, B.S., 2014. Is Non-Homologous End-Joining Really an Inherently Error-Prone Process? PLOS Genet. 10, e1004086. https://doi.org/10.1371/journal.pgen.1004086

Bhattacharyya, S., Lahue, R.S., 2005. Srs2 helicase of Saccharomyces cerevisiae selectively unwinds triplet repeat DNA. J. Biol. Chem. 280, 33311–33317. https://doi.org/10.1074/jbc.M503325200

Bhattacharyya, S., Lahue, R.S., 2004. Saccharomyces cerevisiae Srs2 DNA helicase selectively blocks expansions of trinucleotide repeats. Mol. Cell. Biol. 24, 7324–7330. https://doi.org/10.1128/MCB.24.17.7324-7330.2004

Biernacka, A., Zhu, Y., Skrzypczak, M., Forey, R., Pardo, B., Grzelak, M., Nde, J., Mitra, A., Kudlicki, A., Crosetto, N., Pasero, P., Rowicka, M., Ginalski, K., 2018. i-BLESS is an ultra-sensitive method for detection of DNA double-strand breaks. Commun. Biol. 1, 1–9. https://doi.org/10.1038/s42003-018-0165-9

Birnboim, H.C., Doly, J., 1979. A rapid alkaline extraction procedure for screening recombinant plasmid DNA. Nucleic Acids Res. 7, 1513–1523. https://doi.org/10.1093/nar/7.6.1513

Bittmann, J., Grigaitis, R., Galanti, L., Amarell, S., Wilfling, F., Matos, J., Pfander, B., 2020. An advanced cell cycle tag toolbox reveals principles underlying temporal control of structure-selective nucleases. eLife 9, e52459. https://doi.org/10.7554/eLife.52459

Blackburn, E.H., 1991. Structure and function of telomeres. Nature 350, 569–573. https://doi.org/10.1038/350569a0

Blake, D., Luke, B., Kanellis, P., Jorgensen, P., Goh, T., Penfold, S., Breitkreutz, B.-J., Durocher, D., Peter, M., Tyers, M., 2006. The F-Box Protein Dia2 Overcomes Replication Impedance to Promote Genome Stability in *Saccharomyces cerevisiae*. Genetics 174, 1709–1727. https://doi.org/10.1534/genetics.106.057836

Blanco, M.G., Matos, J., 2015. Hold your horSSEs: controlling structure-selective endonucleases MUS81 and Yen1/GEN1. Front. Genet. 6, 253. https://doi.org/10.3389/fgene.2015.00253

Blanco, M.G., Matos, J., Rass, U., Ip, S.C.Y., West, S.C., 2010. Functional overlap between the structure-specific nucleases Yen1 and Mus81-Mms4 for DNA-damage repair in S. cerevisiae. DNA Repair 9, 394–402. https://doi.org/10.1016/j.dnarep.2009.12.017

Blanco, M.G., Matos, J., West, S.C., 2014. Dual control of Yen1 nuclease activity and cellular localization by Cdk and Cdc14 prevents genome instability. Mol. Cell 54, 94–106. https://doi.org/10.1016/j.molcel.2014.02.011

Bloom, J., Cross, F.R., 2007. Multiple levels of cyclin specificity in cell-cycle control. Nat. Rev. Mol. Cell Biol. 8, 149–160. https://doi.org/10.1038/nrm2105

USC UNIVERSIDADE DE SANTIAGO DE COMPOSTELA

Bochman, M.L., Judge, C.P., Zakian, V.A., 2011. The Pif1 family in prokaryotes: what are our helicases doing in your bacteria? Mol. Biol. Cell 22, 1955–1959. https://doi.org/10.1091/mbc.E11-01-0045

Bochman, M.L., Paeschke, K., Zakian, V.A., 2012. DNA secondary structures: stability and function of G-quadruplex structures. Nat. Rev. Genet. 13, 770–780. https://doi.org/10.1038/nrg3296

Bochman, M.L., Sabouri, N., Zakian, V.A., 2010. Unwinding the functions of the Pif1 family helicases. DNA Repair 9, 237–249. https://doi.org/10.1016/j.dnarep.2010.01.008

Bocquet, N., Bizard, A.H., Abdulrahman, W., Larsen, N.B., Faty, M., Cavadini, S., Bunker, R.D., Kowalczykowski, S.C., Cejka, P., Hickson, I.D., Thoma, N.H., 2014. Structural and mechanistic insight into Holliday-junction dissolution by topoisomerase IIIalpha and RMI1. Nat. Struct. Mol. Biol. 21, 261–268. https://doi.org/10.1038/nsmb.2775

Boddy, M.N., Gaillard, P.-H.L., McDonald, W.H., Shanahan, P., Yates, J.R. 3rd, Russell, P., 2001. Mus81-Eme1 are essential components of a Holliday junction resolvase. Cell 107, 537–548. https://doi.org/10.1016/s0092-8674(01)00536-0

Boettcher, B., Barral, Y., 2013. The cell biology of open and closed mitosis. Nucleus 4, 160–165. https://doi.org/10.4161/nucl.24676

Boiteux, S., Guillet, M., 2004. Abasic sites in DNA: repair and biological consequences in Saccharomyces cerevisiae. DNA Repair 3, 1–12. https://doi.org/10.1016/j.dnarep.2003.10.002

Boiteux, S., Jinks-Robertson, S., 2013. DNA Repair Mechanisms and the Bypass of DNA Damage in *Saccharomyces cerevisiae*. Genetics 193, 1025–1064. https://doi.org/10.1534/genetics.112.145219

Bouwman, B.A.M., Agostini, F., Garnerone, S., Petrosino, G., Gothe, H.J., Sayols, S., Moor, A.E., Itzkovitz, S., Bienko, M., Roukos, V., Crosetto, N., 2020. Genome-wide detection of DNA double-strand breaks by in-suspension BLISS. Nat. Protoc. 15, 3894–3941. https://doi.org/10.1038/s41596-020-0397-2

Branzei, D., Szakal, B., 2017. Building up and breaking down: mechanisms controlling recombination during replication. Crit. Rev. Biochem. Mol. Biol. 52, 381–394. https://doi.org/10.1080/10409238.2017.1304355

Branzei, D., Szakal, B., 2016. DNA damage tolerance by recombination: Molecular pathways and DNA structures. DNA Repair, Cutting-edge Perspectives in Genomic Maintenance III 44, 68–75. https://doi.org/10.1016/j.dnarep.2016.05.008

Branzei, D., Vanoli, F., Foiani, M., 2008. SUMOylation regulates Rad18-mediated template switch. Nature 456, 915–920. https://doi.org/10.1038/nature07587

Brenner, K.A., Nandakumar, J., 2022. Consequences of telomere replication failure: the other end-replication problem. Trends Biochem. Sci. 47, 506–517. https://doi.org/10.1016/j.tibs.2022.03.013

Buchan, D.W.A., Jones, D.T., 2019. The PSIPRED Protein Analysis Workbench: 20 years on. Nucleic Acids Res. 47, W402–W407. https://doi.org/10.1093/nar/gkz297

USC DE SANTIAGO DE COMPOSTELA

Budd, Martin E., Reis, C.C., Smith, S., Myung, K., Campbell, J.L., 2006. Evidence suggesting that Pif1 helicase functions in DNA replication with the Dna2 helicase/nuclease and DNA polymerase delta. Mol. Cell. Biol. 26, 2490–2500. https://doi.org/10.1128/MCB.26.7.2490-2500.2006

Budd, M. E., Reis, C.C., Smith, S., Myung, K., Campbell, J.L., 2006. Evidence suggesting that Pif1 helicase functions in DNA replication with the DNA2 helicase/nuclease and DNA polymerase delta. Mol Cell Biol 26, 2490–2500.

Burgers, P.M., 2011. It's all about flaps. Cell Cycle 10, 2417–2418. https://doi.org/10.4161/cc.10.15.15851

Buzovetsky, O., Kwon, Y., Pham, N.T., Kim, C., Ira, G., Sung, P., Xiong, Y., 2017. Role of the Pif1-PCNA Complex in Pol delta-Dependent Strand Displacement DNA Synthesis and Break-Induced Replication. Cell Rep. 21, 1707–1714. https://doi.org/10.1016/j.celrep.2017.10.079

Byrd, A.K., Raney, K.D., 2017. Structure and function of Pif1 helicase. Biochem. Soc. Trans. 45, 1159–1171. https://doi.org/10.1042/BST20170096

Byrd, A.K., Raney, K.D., 2015. A parallel quadruplex DNA is bound tightly but unfolded slowly by pif1 helicase. J. Biol. Chem. 290, 6482–6494. https://doi.org/10.1074/jbc.M114.630749

Bzymek, M., Thayer, N.H., Oh, S.D., Kleckner, N., Hunter, N., 2010. Double Holliday junctions are intermediates of DNA break repair. Nature 464, 937–941. https://doi.org/10.1038/nature08868

Cadet, J., Sage, E., Douki, T., 2005. Ultraviolet radiation-mediated damage to cellular DNA. Mutat. Res. Mol. Mech. Mutagen., Biological Effects of Ultraviolet Radiation 571, 3–17. https://doi.org/10.1016/j.mrfmmm.2004.09.012

Cai, J., Huang, Y., Li, F., Li, Y., 2006. Alteration of protein subcellular location and domain formation by alternative translational initiation. Proteins Struct. Funct. Bioinforma. 62, 793–799. https://doi.org/10.1002/prot.20785

Calzada, A., Hodgson, B., Kanemaki, M., Bueno, A., Labib, K., 2005. Molecular anatomy and regulation of a stable replisome at a paused eukaryotic DNA replication fork. Genes Dev. 19, 1905–1919. https://doi.org/10.1101/gad.337205

Canela, A., Sridharan, S., Sciascia, N., Tubbs, A., Meltzer, P., Sleckman, B.P., Nussenzweig, A., 2016. DNA Breaks and End Resection Measured Genome-wide by End Sequencing. Mol. Cell 63, 898–911. https://doi.org/10.1016/j.molcel.2016.06.034

Cannavo, E., Reginato, G., Cejka, P., 2019. Stepwise 5′ DNA end-specific resection of DNA breaks by the Mre11-Rad50-Xrs2 and Sae2 nuclease ensemble. Proc. Natl. Acad. Sci. 116, 5505–5513. https://doi.org/10.1073/pnas.1820157116

Canugovi, C., Maynard, S., Bayne, A.-C.V., Sykora, P., Tian, J., de Souza-Pinto, N.C., Croteau, D.L., Bohr, V.A., 2010. The mitochondrial transcription factor A functions in mitochondrial base excision repair. DNA Repair 9, 1080–1089. https://doi.org/10.1016/j.dnarep.2010.07.009

USC UNIVERSIDADE DE SANTIAGO DE COMPOSTELA

Cao, B., Wu, X., Zhou, J., Wu, H., Liu, L., Zhang, Q., DeMott, M.S., Gu, C., Wang, L., You, D., Dedon, P.C., 2020. Nick-seq for single-nucleotide resolution genomic maps of DNA modifications and damage. Nucleic Acids Res. 48, 6715–6725. https://doi.org/10.1093/nar/gkaa473

Cao, H., Salazar-García, L., Gao, F., Wahlestedt, T., Wu, C.-L., Han, X., Cai, Y., Xu, D., Wang, F., Tang, L., Ricciardi, N., Cai, D., Wang, H., Chin, M.P.S., Timmons, J.A., Wahlestedt, C., Kapranov, P., 2019. Novel approach reveals genomic landscapes of single-strand DNA breaks with nucleotide resolution in human cells. Nat. Commun. 10, 5799. https://doi.org/10.1038/s41467-019-13602-7

Carr, A., Lambert, S., 2021. Recombination-dependent replication: new perspectives from site-specific fork barriers. Curr. Opin. Genet. Dev., Mechanisms of Homologous Recombination 71, 129–135. https://doi.org/10.1016/j.gde.2021.07.008

Carreira, R., Aguado, F.J., Hurtado-Nieves, V., Blanco, M.G., 2022. Canonical and novel non-canonical activities of the Holliday junction resolvase Yen1. Nucleic Acids Res. 50, 259–280. https://doi.org/10.1093/nar/gkab1225

Carreira, R., Aguado, F.J., Lama-Diaz, T., Blanco, M.G., 2021. Holliday Junction Resolution, in: Aguilera, A., Carreira, A. (Eds.), Homologous Recombination: Methods and Protocols, Methods in Molecular Biology. Springer US, New York, NY, pp. 169–185. https://doi.org/10.1007/978-1-0716-0644-5_12

Castillo Bosch, P., Segura-Bayona, S., Koole, W., van Heteren, J.T., Dewar, J.M., Tijsterman, M., Knipscheer, P., 2014. FANCJ promotes DNA synthesis through G-quadruplex structures. EMBO J. 33, 2521–2533. https://doi.org/10.15252/embj.201488663

Castor, D., Nair, N., Declais, A.-C., Lachaud, C., Toth, R., Macartney, T.J., Lilley, D.M.J., Arthur, J.S.C., Rouse, J., 2013. Cooperative control of holliday junction resolution and DNA repair by the SLX1 and MUS81-EME1 nucleases. Mol. Cell 52, 221–233. https://doi.org/10.1016/j.molcel.2013.08.036

Ceccaldi, R., Liu, J.C., Amunugama, R., Hajdu, I., Primack, B., Petalcorin, M.I.R., O'Connor, K.W., Konstantinopoulos, P.A., Elledge, S.J., Boulton, S.J., Yusufzai, T., D'Andrea, A.D., 2015. Homologous-recombination-deficient tumours are dependent on Polθ-mediated repair. Nature 518, 258–262. https://doi.org/10.1038/nature14184

Cejka, P., Cannavo, E., Polaczek, P., Masuda-Sasa, T., Pokharel, S., Campbell, J.L., Kowalczykowski, S.C., 2010a. DNA end resection by Dna2-Sgs1-RPA and its stimulation by Top3-Rmi1 and Mre11-Rad50-Xrs2. Nature 467, 112–116. https://doi.org/10.1038/nature09355

Cejka, P., Cannavo, E., Polaczek, P., Masuda-Sasa, T., Pokharel, S., Campbell, J.L., Kowalczykowski, S.C., 2010b. DNA end resection by Dna2-Sgs1-RPA and its stimulation by Top3-Rmi1 and Mre11-Rad50-Xrs2. Nature 467, 112–116. https://doi.org/10.1038/nature09355

USC UNIVERSIDADE DE SANTIAGO DE COMPOSTELA

Cejka, P., Plank, J.L., Bachrati, C.Z., Hickson, I.D., Kowalczykowski, S.C., 2010c. Rmi1 stimulates decatenation of double Holliday junctions during dissolution by Sgs1-Top3. Nat. Struct. Mol. Biol. 17, 1377–1382. https://doi.org/10.1038/nsmb.1919

Cejka, P., Plank, J.L., Dombrowski, C.C., Kowalczykowski, S.C., 2012. Decatenation of DNA by the S. cerevisiae Sgs1-Top3-Rmi1 and RPA complex: a mechanism for disentangling chromosomes. Mol. Cell 47, 886–896. https://doi.org/10.1016/j.molcel.2012.06.032

Cejka, P., Symington, L.S., 2021. DNA End Resection: Mechanism and Control. Annu. Rev. Genet. 55, 285–307. https://doi.org/10.1146/annurev-genet-071719-020312

Cerulli, R.A., Kritzer, J.A., 2020. Phosphotyrosine isosteres: past, present and future. Org. Biomol. Chem. 18, 583–605. https://doi.org/10.1039/C9OB01998G

Chaganti, R.S.K., Schonberg, S., German, J., 1974. A Manyfold Increase in Sister Chromatid Exchanges in Bloom's Syndrome Lymphocytes. Proc. Natl. Acad. Sci. 71, 4508–4512. https://doi.org/10.1073/pnas.71.11.4508

Chan, Y.W., West, S., 2015. GEN1 promotes Holliday junction resolution by a coordinated nick and counter-nick mechanism. Nucleic Acids Res. 43, 10882–10892. https://doi.org/10.1093/nar/gkv1207

Chan, Y.W., West, S.C., 2014. Spatial control of the GEN1 Holliday junction resolvase ensures genome stability. Nat. Commun. 5, 4844. https://doi.org/10.1038/ncomms5844

Chang, D.J., Cimprich, K.A., 2009. DNA damage tolerance: when it's OK to make mistakes. Nat. Chem. Biol. 5, 82–90. https://doi.org/10.1038/nchembio.139

Chang, H.H.Y., Pannunzio, N.R., Adachi, N., Lieber, M.R., 2017. Non-homologous DNA end joining and alternative pathways to double-strand break repair. Nat. Rev. Mol. Cell Biol. 18, 495–506. https://doi.org/10.1038/nrm.2017.48

Chang, K.-J., Wang, C.-C., 2004. Translation Initiation from a Naturally Occurring Non-AUG Codon in Saccharomyces cerevisiae*. J. Biol. Chem. 279, 13778–13785. https://doi.org/10.1074/jbc.M311269200

Chang, M., Luke, B., Kraft, C., Li, Z., Peter, M., Lingner, J., Rothstein, R., 2009. Telomerase Is Essential to Alleviate Pif1-Induced Replication Stress at Telomeres. Genetics 183, 779–791. https://doi.org/10.1534/genetics.109.107631

Chappell, S.A., Dresios, J., Edelman, G.M., Mauro, V.P., 2006. Ribosomal shunting mediated by a translational enhancer element that base pairs to 18S rRNA. Proc. Natl. Acad. Sci. 103, 9488–9493. https://doi.org/10.1073/pnas.0603597103

Chatterjee, A., 2001. Uracil-DNA glycosylase-deficient yeast exhibit a mitochondrial mutator phenotype. Nucleic Acids Res. 29, 4935–4940. https://doi.org/10.1093/nar/29.24.4935

Chatterjee, N., Walker, G.C., 2017. Mechanisms of DNA damage, repair, and mutagenesis. Environ. Mol. Mutagen. 58, 235–263. https://doi.org/10.1002/em.22087

Chee, M.K., Haase, S.B., 2012. New and Redesigned pRS Plasmid Shuttle Vectors for Genetic Manipulation of Saccharomyces cerevisiae. G3 GenesGenomesGenetics 2, 515–526. https://doi.org/10.1534/g3.111.001917

USC UNIVERSIDADE DE SANTIAGO DE COMPOSTELA

Chen, C.-F., Pohl, T.J., Pott, S., Zakian, V.A., 2019. Two Pif1 Family DNA Helicases Cooperate in Centromere Replication and Segregation in Saccharomyces cerevisiae. Genetics 211, 105–119. https://doi.org/10.1534/genetics.118.301710

Chen, H., Lisby, M., Symington, L.S., 2013. RPA Coordinates DNA End Resection and Prevents Formation of DNA Hairpins. Mol. Cell 50, 589–600. https://doi.org/10.1016/j.molcel.2013.04.032

Chen, L., Trujillo, K., Ramos, W., Sung, P., Tomkinson, A.E., 2001. Promotion of Dnl4-Catalyzed DNA End-Joining by the Rad50/Mre11/Xrs2 and Hdf1/Hdf2 Complexes. Mol. Cell 8, 1105–1115. https://doi.org/10.1016/S1097-2765(01)00388-4

Chen, S.H., Plank, J.L., Willcox, S., Griffith, J.D., Hsieh, T., 2014. Top3α Is Required during the Convergent Migration Step of Double Holliday Junction Dissolution. PLOS ONE 9, e83582. https://doi.org/10.1371/journal.pone.0083582

Chen, S.-J., Lin, G., Chang, K.-J., Yeh, L.-S., Wang, C.-C., 2008. Translational Efficiency of a Non-AUG Initiation Codon Is Significantly Affected by Its Sequence Context in Yeast *. J. Biol. Chem. 283, 3173–3180. https://doi.org/10.1074/jbc.M706968200

Chen, X., Niu, H., Chung, W.-H., Zhu, Z., Papusha, A., Shim, E.Y., Lee, S.E., Sung, P., Ira, G., 2011. Cell cycle regulation of DNA double-strand break end resection by Cdk1-dependent Dna2 phosphorylation. Nat. Struct. Mol. Biol. 18, 1015–1019. https://doi.org/10.1038/nsmb.2105

Chen, X., Niu, H., Yu, Y., Wang, J., Zhu, S., Zhou, J., Papusha, A., Cui, D., Pan, X., Kwon, Y., Sung, P., Ira, G., 2016. Enrichment of Cdk1-cyclins at DNA double-strand breaks stimulates Fun30 phosphorylation and DNA end resection. Nucleic Acids Res. 44, 2742–2753. https://doi.org/10.1093/nar/gkv1544

Chen, Y.-C., Kenworthy, J., Gabrielse, C., Hänni, C., Zegerman, P., Weinreich, M., 2013. DNA Replication Checkpoint Signaling Depends on a Rad53–Dbf4 N-Terminal Interaction in *Saccharomyces cerevisiae*. Genetics 194, 389–401. https://doi.org/10.1534/genetics.113.149740

Chen, Z., Cole, P.A., 2015. Synthetic approaches to protein phosphorylation. Curr. Opin. Chem. Biol., Synthetic biology • Synthetic biomolecules 28, 115–122. https://doi.org/10.1016/j.cbpa.2015.07.001

Chen, Z., Yang, H., Pavletich, N.P., 2008. Mechanism of homologous recombination from the RecA–ssDNA/dsDNA structures. Nature 453, 489–494. https://doi.org/10.1038/nature06971

Cheng, I.-C., Chen, B.C., Shuai, H.-H., Chien, F.-C., Chen, P., Hsieh, T., 2016. Wuho Is a New Member in Maintaining Genome Stability through its Interaction with Flap Endonuclease 1. PLOS Biol. 14, e1002349. https://doi.org/10.1371/journal.pbio.1002349

Cheng, X., Dunaway, S., Ivessa, A.S., 2007. The role of Pif1p, a DNA helicase in Saccharomyces cerevisiae, in maintaining mitochondrial DNA. Mitochondrion 7, 211–22. https://doi.org/10.1016/j.mito.2006.11.023

USC UNIVERSIDADE DE SANTIAGO DE COMPOSTELA

Cheng, X., Qin, Y., Ivessa, A.S., 2009. Loss of mitochondrial DNA under genotoxic stress conditions in the absence of the yeast DNA helicase Pif1p occurs independently of the DNA helicase Rrm3p. Mol Genet Genomics 281, 635–45. https://doi.org/10.1007/s00438-009-0438-6

Cheung, I., Schertzer, M., Rose, A., Lansdorp, P.M., 2002. Disruption of dog-1 in Caenorhabditis elegans triggers deletions upstream of guanine-rich DNA. Nat. Genet. 31, 405–409. https://doi.org/10.1038/ng928

Chib, S., Byrd, A.K., Raney, K.D., 2016. Yeast Helicase Pif1 Unwinds RNA:DNA Hybrids with Higher Processivity than DNA:DNA Duplexes. J. Biol. Chem. 291, 5889–5901. https://doi.org/10.1074/jbc.M115.688648

Ciccia, A., Constantinou, A., West, S.C., 2003. Identification and characterization of the human mus81-eme1 endonuclease. J. Biol. Chem. 278, 25172–25178. https://doi.org/10.1074/jbc.M302882200

Ciccia, A., Elledge, S.J., 2010. The DNA Damage Response: Making It Safe to Play with Knives. Mol. Cell 40, 179–204. https://doi.org/10.1016/j.molcel.2010.09.019

Ciccia, A., McDonald, N., West, S.C., 2008. Structural and functional relationships of the XPF/MUS81 family of proteins. Annu. Rev. Biochem. 77, 259–287. https://doi.org/10.1146/annurev.biochem.77.070306.102408

Clements, J.M., Laz, T.M., Sherman, F., 1988. Efficiency of translation initiation by non-AUG codons in Saccharomyces cerevisiae. Mol. Cell. Biol. 8, 4533–4536. https://doi.org/10.1128/mcb.8.10.4533-4536.1988

Clerici, M., Trovesi, C., Galbiati, A., Lucchini, G., Longhese, M.P., 2014. Mec1/ATR regulates the generation of single-stranded DNA that attenuates Tel1/ATM signaling at DNA ends. EMBO J. 33, 198–216. https://doi.org/10.1002/embj.201386041

Colavito, S., Macris-Kiss, M., Seong, C., Gleeson, O., Greene, E.C., Klein, H.L., Krejci, L., Sung, P., 2009. Functional significance of the Rad51-Srs2 complex in Rad51 presynaptic filament disruption. Nucleic Acids Res. 37, 6754–6764. https://doi.org/10.1093/nar/gkp748

Costantino, L., Sotiriou, S.K., Rantala, J.K., Magin, S., Mladenov, E., Helleday, T., Haber, J.E., Iliakis, G., Kallioniemi, O.P., Halazonetis, T.D., 2014. Break-Induced Replication Repair of Damaged Forks Induces Genomic Duplications in Human Cells. Science 343, 88–91. https://doi.org/10.1126/science.1243211

Coulon, S., Gaillard, P.-H.L., Chahwan, C., McDonald, W.H., Yates, J.R. 3rd, Russell, P., 2004. Slx1-Slx4 are subunits of a structure-specific endonuclease that maintains ribosomal DNA in fission yeast. Mol. Biol. Cell 15, 71–80. https://doi.org/10.1091/mbc.e03-08-0586

Coulon, S., Noguchi, E., Noguchi, C., Du, L.-L., Nakamura, T.M., Russell, P., 2006. Rad22Rad52-dependent repair of ribosomal DNA repeats cleaved by Slx1-Slx4 endonuclease. Mol. Biol. Cell 17, 2081–2090. https://doi.org/10.1091/mbc.e05-11-1006

USC UNIVERSIDADE DE SANTIAGO DE COMPOSTELA

Crabbe, L., Verdun, R.E., Haggblom, C.I., Karlseder, J., 2004. Defective Telomere Lagging Strand Synthesis in Cells Lacking WRN Helicase Activity. Science 306, 1951–1953. https://doi.org/10.1126/science.1103619

Crasta, K., Ganem, N.J., Dagher, R., Lantermann, A.B., Ivanova, E.V., Pan, Y., Nezi, L., Protopopov, A., Chowdhury, D., Pellman, D., 2012. DNA breaks and chromosome pulverization from errors in mitosis. Nature 482, 53–58. https://doi.org/10.1038/nature10802

Crider, D.G., García-Rodríguez, L.J., Srivastava, P., Peraza-Reyes, L., Upadhyaya, K., Boldogh, I.R., Pon, L.A., 2012. Rad53 is essential for a mitochondrial DNA inheritance checkpoint regulating G1 to S progression. J. Cell Biol. 198, 793–798. https://doi.org/10.1083/jcb.201205193

Crosetto, N., Mitra, A., Silva, M.J., Bienko, M., Dojer, N., Wang, Q., Karaca, E., Chiarle, R., Skrzypczak, M., Ginalski, K., Pasero, P., Rowicka, M., Dikic, I., 2013. Nucleotide-resolution DNA double-strand break mapping by next-generation sequencing. Nat. Methods 10, 361–365. https://doi.org/10.1038/nmeth.2408

Dahan, D., Tsirkas, I., Dovrat, D., Sparks, M.A., Singh, S.P., Galletto, R., Aharoni, A., 2018. Pif1 is essential for efficient replisome progression through lagging strand G-quadruplex DNA secondary structures. Nucleic Acids Res. 46, 11847–11857. https://doi.org/10.1093/nar/gky1065

Daigaku, Y., Davies, A.A., Ulrich, H.D., 2010. Ubiquitin-dependent DNA damage bypass is separable from genome replication. Nature 465, 951–955. https://doi.org/10.1038/nature09097

Daley, J.M., Palmbos, P.L., Wu, D., Wilson, T.E., 2005. Nonhomologous End Joining in Yeast. Annu. Rev. Genet. 39, 431–451. https://doi.org/10.1146/annurev.genet.39.073003.113340

Davis, C.A., 2000. Test of intron predictions reveals novel splice sites, alternatively spliced mRNAs and new introns in meiotically regulated genes of yeast. Nucleic Acids Res. 28, 1700–1706. https://doi.org/10.1093/nar/28.8.1700

De Bont, R., van Larebeke, N., 2004. Endogenous DNA damage in humans: a review of quantitative data. Mutagenesis 19, 169–185. https://doi.org/10.1093/mutage/geh025

de Lange, T., 2004. T-loops and the origin of telomeres. Nat. Rev. Mol. Cell Biol. 5, 323–329. https://doi.org/10.1038/nrm1359

de los Santos, T., Hunter, N., Lee, C., Larkin, B., Loidl, J., Hollingsworth, N.M., 2003. The Mus81/Mms4 endonuclease acts independently of double-Holliday junction resolution to promote a distinct subset of crossovers during meiosis in budding yeast. Genetics 164, 81–94.

de los Santos, T., Loidl, J., Larkin, B., Hollingsworth, N.M., 2001. A Role for MMS4 in the Processing of Recombination Intermediates During Meiosis in Saccharomyces cerevisiae. Genetics 159, 1511–1525. https://doi.org/10.1093/genetics/159.4.1511

USC UNIVERSIDADE DE SANTIAGO DE COMPOSTELA

Deegan, T.D., Baxter, J., Ortiz Bazan, M.A., Yeeles, J.T.P., Labib, K.P.M., 2019. Pif1-Family Helicases Support Fork Convergence during DNA Replication Termination in Eukaryotes. Mol. Cell 74, 231-244.e9. https://doi.org/10.1016/j.molcel.2019.01.040

Deem, A., Barker, K., VanHulle, K., Downing, B., Vayl, A., Malkova, A., 2008. Defective Break-Induced Replication Leads to Half-Crossovers in *Saccharomyces cerevisiae*. Genetics 179, 1845–1860. https://doi.org/10.1534/genetics.108.087940

Deem, A., Keszthelyi, A., Blackgrove, T., Vayl, A., Coffey, B., Mathur, R., Chabes, A., Malkova, A., 2011. Break-Induced Replication Is Highly Inaccurate. PLOS Biol. 9, e1000594. https://doi.org/10.1371/journal.pbio.1000594

Dehé, P.-M., Gaillard, P.-H.L., 2017. Control of structure-specific endonucleases to maintain genome stability. Nat. Rev. Mol. Cell Biol. 18, 315–330. https://doi.org/10.1038/nrm.2016.177

Deng, C., Brown, J.A., You, D., Brown, J.M., 2005. Multiple endonucleases function to repair covalent topoisomerase I complexes in Saccharomyces cerevisiae. Genetics 170, 591–600. https://doi.org/10.1534/genetics.104.028795

Deng, S.K., Gibb, B., de Almeida, M.J., Greene, E.C., Symington, L.S., 2014. RPA antagonizes microhomology-mediated repair of DNA double-strand breaks. Nat. Struct. Mol. Biol. 21, 405–412. https://doi.org/10.1038/nsmb.2786

Deshpande, A.M., Newlon, C.S., 1996. DNA Replication Fork Pause Sites Dependent on Transcription. Science 272, 1030–1033. https://doi.org/10.1126/science.272.5264.1030

Deshpande, R.A., Williams, G.J., Limbo, O., Williams, R.S., Kuhnlein, J., Lee, J.-H., Classen, S., Guenther, G., Russell, P., Tainer, J.A., Paull, T.T., 2014. ATP-driven Rad50 conformations regulate DNA tethering, end resection, and ATM checkpoint signaling. EMBO J. 33, 482–500. https://doi.org/10.1002/embj.201386100

Dewar, J.M., Lydall, D., 2010. Pif1- and Exo1-dependent nucleases coordinate checkpoint activation following telomere uncapping. EMBO J. 29, 4020–4034. https://doi.org/10.1038/emboj.2010.267

Dion, V., Kalck, V., Horigome, C., Towbin, B.D., Gasser, S.M., 2012. Increased mobility of double-strand breaks requires Mec1, Rad9 and the homologous recombination machinery. Nat. Cell Biol. 14, 502–509. https://doi.org/10.1038/ncb2465

Dorison, H., Talhaoui, I., Mazón, G., 2022. SUMO-mediated recruitment allows timely function of the Yen1 nuclease in mitotic cells. PLOS Genet. 18, e1009860. https://doi.org/10.1371/journal.pgen.1009860

Doudican, N.A., Song, B., Shadel, G.S., Doetsch, P.W., 2005. Oxidative DNA damage causes mitochondrial genomic instability in Saccharomyces cerevisiae. Mol Cell Biol 25, 5196–204. https://doi.org/10.1128/MCB.25.12.5196-5204.2005

Douwel, D.K., Boonen, R.A.C.M., Long, D.T., Szypowska, A.A., Raschle, M., Walter, J.C., Knipscheer, P., 2014. XPF-ERCC1 acts in Unhooking DNA interstrand crosslinks in cooperation with FANCD2 and FANCP/SLX4. Mol. Cell 54, 460–471. https://doi.org/10.1016/j.molcel.2014.03.015

USC UNIVERSIDADE DE SANTIAGO DE COMPOSTELA

Douwel, D.K., Hoogenboom, W.S., Boonen, R.A., Knipscheer, P., 2017. Recruitment and positioning determine the specific role of the XPF-ERCC1 endonuclease in interstrand crosslink repair. EMBO J. 36, 2034–2046. https://doi.org/10.15252/embj.201695223

Duckett, D.R., Murchie, A.I.H., Diekmann, S., von Kitzing, E., Kemper, B., Lilley, D.M.J., 1988. The structure of the holliday junction, and its resolution. Cell 55, 79–89. https://doi.org/10.1016/0092-8674(88)90011-6

Duda, H., Arter, M., Gloggnitzer, J., Teloni, F., Wild, P., Blanco, M.G., Altmeyer, M., Matos, J., 2016. A Mechanism for Controlled Breakage of Under-replicated Chromosomes during Mitosis. Dev. Cell 39, 740–755. https://doi.org/10.1016/j.devcel.2016.11.017

Dujon, B., Sherman, D., Fischer, G., Durrens, P., Casaregola, S., Lafontaine, I., de Montigny, J., Marck, C., Neuvéglise, C., Talla, E., Goffard, N., Frangeul, L., Aigle, M., Anthouard, V., Babour, A., Barbe, V., Barnay, S., Blanchin, S., Beckerich, J.-M., Beyne, E., Bleykasten, C., Boisramé, A., Boyer, J., Cattolico, L., Confanioleri, F., de Daruvar, A., Despons, L., Fabre, E., Fairhead, C., Ferry-Dumazet, H., Groppi, A., Hantraye, F., Hennequin, C., Jauniaux, N., Joyet, P., Kachouri, R., Kerrest, A., Koszul, R., Lemaire, M., Lesur, I., Ma, L., Muller, H., Nicaud, J.-M., Nikolski, M., Oztas, S., Ozier-Kalogeropoulos, O., Pellenz, S., Potier, S., Richard, G.-F., Straub, M.-L., Suleau, A., Swennen, D., Tekaia, F., Wésolowski-Louvel, M., Westhof, E., Wirth, B., Zeniou-Meyer, M., Zivanovic, I., Bolotin-Fukuhara, M., Thierry, A., Bouchier, C., Caudron, B., Scarpelli, C., Gaillardin, C., Weissenbach, J., Wincker, P., Souciet, J.-L., 2004. Genome evolution in yeasts. Nature 430, 35–44. https://doi.org/10.1038/nature02579

Duzdevich, D., Warner, M.D., Ticau, S., Ivica, N.A., Bell, S.P., Greene, E.C., 2015. The Dynamics of Eukaryotic Replication Initiation: Origin Specificity, Licensing, and Firing at the Single-Molecule Level. Mol. Cell 58, 483–494. https://doi.org/10.1016/j.molcel.2015.03.017

Eddy, S., Ketkar, A., Zafar, M.K., Maddukuri, L., Choi, J.-Y., Eoff, R.L., 2014. Human Rev1 polymerase disrupts G-quadruplex DNA. Nucleic Acids Res. 42, 3272–3285. https://doi.org/10.1093/nar/gkt1314

Eggler, A.L., Inman, R.B., Cox, M.M., 2002. The Rad51-dependent Pairing of Long DNA Substrates Is Stabilized by Replication Protein A *. J. Biol. Chem. 277, 39280–39288. https://doi.org/10.1074/jbc.M204328200

Ehmsen, K.T., Heyer, W.-D., 2009. A junction branch point adjacent to a DNA backbone nick directs substrate cleavage by Saccharomyces cerevisiae Mus81-Mms4. Nucleic Acids Res. 37, 2026–2036. https://doi.org/10.1093/nar/gkp038

Ehmsen, K.T., Heyer, W.-D., 2008. Saccharomyces cerevisiae Mus81-Mms4 is a catalytic, DNA structure-selective endonuclease. Nucleic Acids Res. 36, 2182–2195. https://doi.org/10.1093/nar/gkm1152

Eissler, C.L., Mazon, G., Powers, B.L., Savinov, S.N., Symington, L.S., Hall, M.C., 2014. The Cdk/cDc14 module controls activation of the Yen1 holliday junction resolvase to

USC UNIVERSIDADE DE SANTIAGO DE COMPOSTELA

promote genome stability. Mol. Cell 54, 80–93. https://doi.org/10.1016/j.molcel.2014.02.012

Elango, R., Sheng, Z., Jackson, J., DeCata, J., Ibrahim, Y., Pham, N.T., Liang, D.H., Sakofsky, C.J., Vindigni, A., Lobachev, K.S., Ira, G., Malkova, A., 2017. Break-induced replication promotes formation of lethal joint molecules dissolved by Srs2. Nat. Commun. 8, 1790. https://doi.org/10.1038/s41467-017-01987-2

Elia, A.E.H., Cantley, L.C., Yaffe, M.B., 2003. Proteomic Screen Finds pSer/pThr-Binding Domain Localizing Plk1 to Mitotic Substrates. Science 299, 1228–1231. https://doi.org/10.1126/science.1079079

Eugster, A., Lanzuolo, C., Bonneton, M., Luciano, P., Pollice, A., Pulitzer, J.F., Stegberg, E., Berthiau, A.-S., Förstemann, K., Corda, Y., Lingner, J., Géli, V., Gilson, E., 2006. The finger subdomain of yeast telomerase cooperates with Pif1p to limit telomere elongation. Nat Struct Mol Biol 13, 734–9. https://doi.org/10.1038/nsmb1126

Evans, E., Fellows, J., Coffer, A., Wood, R.D., 1997. Open complex formation around a lesion during nucleotide excision repair provides a structure for cleavage by human XPG protein. EMBO J. 16, 625–638. https://doi.org/10.1093/emboj/16.3.625

Fabre, F., Chan, A., Heyer, W.-D., Gangloff, S., 2002. Alternate pathways involving Sgs1/Top3, Mus81/ Mms4, and Srs2 prevent formation of toxic recombination intermediates from single-stranded gaps created by DNA replication. Proc. Natl. Acad. Sci. U. S. A. 99, 16887–16892. https://doi.org/10.1073/pnas.252652399

Fachinetti, D., Bermejo, R., Cocito, A., Minardi, S., Katou, Y., Kanoh, Y., Shirahige, K., Azvolinsky, A., Zakian, V.A., Foiani, M., 2010. Replication Termination at Eukaryotic Chromosomes Is Mediated by Top2 and Occurs at Genomic Loci Containing Pausing Elements. Mol. Cell 39, 595–605. https://doi.org/10.1016/j.molcel.2010.07.024

Falquet, B., Ölmezer, G., Enkner, F., Klein, D., Challa, K., Appanah, R., Gasser, S.M., Rass, U., 2020. Disease-associated DNA2 nuclease-helicase protects cells from lethal chromosome under-replication. Nucleic Acids Res 48, 7265–7278. https://doi.org/10.1093/nar/gkaa524

Falquet, B., Rass, U., 2019. Structure-Specific Endonucleases and the Resolution of Chromosome Underreplication. Genes 10, 232. https://doi.org/10.3390/genes10030232

Fekairi, S., Scaglione, S., Chahwan, C., Taylor, E.R., Tissier, A., Coulon, S., Dong, M.-Q., Ruse, C., Yates, J.R. 3rd, Russell, P., Fuchs, R.P., McGowan, C.H., Gaillard, P.-H.L., 2009. Human SLX4 is a Holliday junction resolvase subunit that binds multiple DNA repair/recombination endonucleases. Cell 138, 78–89. https://doi.org/10.1016/j.cell.2009.06.029

Fiorentino, D.F., Crabtree, G.R., 1997. Characterization of Saccharomyces cerevisiae dna2Mutants Suggests a Role for the Helicase Late in S Phase. Mol. Biol. Cell 8, 2519–2537. https://doi.org/10.1091/mbc.8.12.2519

USC UNIVERSIDADE DE SANTIAGO DE COMPOSTELA

Follonier, C., Oehler, J., Herrador, R., Lopes, M., 2013. Friedreich's ataxia–associated GAA repeats induce replication-fork reversal and unusual molecular junctions. Nat. Struct. Mol. Biol. 20, 486–494. https://doi.org/10.1038/nsmb.2520

Forment, J.V., Blasius, M., Guerini, I., Jackson, S.P., 2011. Structure-specific DNA endonuclease Mus81/Eme1 generates DNA damage caused by Chk1 inactivation. PloS One 6, e23517. https://doi.org/10.1371/journal.pone.0023517

Foury, F., Kolodynski, J., 1983. pif mutation blocks recombination between mitochondrial rho+ and rho- genomes having tandemly arrayed repeat units in Saccharomyces cerevisiae. Proc. Natl. Acad. Sci. 80, 5345–5349. https://doi.org/10.1073/pnas.80.17.5345

Foury, F., Lahaye, A., 1987. Cloning and sequencing of the PIF gene involved in repair and recombination of yeast mitochondrial DNA. EMBO J. 6, 1441–1449. https://doi.org/10.1002/j.1460-2075.1987.tb02385.x

Foury, F., Van Dyck, E., 1985. A PIF-dependent recombinogenic signal in the mitochondrial DNA of yeast. EMBO J. 4, 3525–3530. https://doi.org/10.1002/j.1460-2075.1985.tb04112.x

Frederiks, F., Heynen, G.J.J.E., van Deventer, S.J., Janssen, H., van Leeuwen, F., 2009. Two Dot1 isoforms in Saccharomyces cerevisiae as a result of leaky scanning by the ribosome. Nucleic Acids Res. 37, 7047–7058. https://doi.org/10.1093/nar/gkp765

Freeman, A.D.J., Liu, Y., Declais, A.-C., Gartner, A., Lilley, D.M.J., 2014. GEN1 from a thermophilic fungus is functionally closely similar to non-eukaryotic junction-resolving enzymes. J. Mol. Biol. 426, 3946–3959. https://doi.org/10.1016/j.jmb.2014.10.008

Freitas, A.A., de Magalhães, J.P., 2011. A review and appraisal of the DNA damage theory of ageing. Mutat. Res. Mutat. Res. 728, 12–22. https://doi.org/10.1016/j.mrrev.2011.05.001

Fricke, W.M., Brill, S.J., 2003. Slx1-Slx4 is a second structure-specific endonuclease functionally redundant with Sgs1-Top3. Genes Dev. 17, 1768–1778. https://doi.org/10.1101/gad.1105203

Friedberg, E.C. (Ed.), 2006. DNA repair and mutagenesis, 2nd ed. ed. ASM Press, Washington, D.C.

Fritsch, O., Burkhalter, M.D., Kais, S., Sogo, J.M., Schär, P., 2010. DNA ligase 4 stabilizes the ribosomal DNA array upon fork collapse at the replication fork barrier. DNA Repair 9, 879–888. https://doi.org/10.1016/j.dnarep.2010.05.003

Frizzell, A., Nguyen, J.H.G., Petalcorin, M.I.R., Turner, K.D., Boulton, S.J., Freudenreich, C.H., Lahue, R.S., 2014. RTEL1 inhibits trinucleotide repeat expansions and fragility. Cell Rep. 6, 827–835. https://doi.org/10.1016/j.celrep.2014.01.034

Fugger, K., Kit Chu, W., Haahr, P., Nedergaard Kousholt, A., Beck, H., Payne, M.J., Hanada, K., Hickson, I.D., Storgaard Sørensen, C., 2013. FBH1 co-operates with MUS81 in inducing DNA double-strand breaks and cell death following replication stress. Nat. Commun. 4, 1423. https://doi.org/10.1038/ncomms2395

USC UNIVERSIDADE DE SANTIAGO DE COMPOSTELA

Fumasoni, M., Zwicky, K., Vanoli, F., Lopes, M., Branzei, D., 2015. Error-Free DNA Damage Tolerance and Sister Chromatid Proximity during DNA Replication Rely on the Polα/Primase/Ctf4 Complex. Mol. Cell 57, 812–823. https://doi.org/10.1016/j.molcel.2014.12.038

Futami, K., Shimamoto, A., Furuichi, Y., 2007. Mitochondrial and nuclear localization of human Pif1 helicase. Biol. Pharm. Bull. 30, 1685–1692. https://doi.org/10.1248/bpb.30.1685

Gaillard, H., García-Muse, T., Aguilera, A., 2015. Replication stress and cancer. Nat. Rev. Cancer 15, 276–289. https://doi.org/10.1038/nrc3916

Gaillard, P.-H.L., Noguchi, E., Shanahan, P., Russell, P., 2003. The endogenous Mus81-Eme1 complex resolves Holliday junctions by a nick and counternick mechanism. Mol. Cell 12, 747–759. https://doi.org/10.1016/s1097-2765(03)00342-3

Gallo-Fernandez, M., Saugar, I., Ortiz-Bazan, M.A., Vazquez, M.V., Tercero, J.A., 2012. Cell cycle-dependent regulation of the nuclease activity of Mus81-Eme1/Mms4. Nucleic Acids Res. 40, 8325–8335. https://doi.org/10.1093/nar/gks599

Gangloff, S., McDonald, J.P., Bendixen, C., Arthur, L., Rothstein, R., 1994. The yeast type I topoisomerase Top3 interacts with Sgs1, a DNA helicase homolog: a potential eukaryotic reverse gyrase. Mol. Cell. Biol. 14, 8391–8398. https://doi.org/10.1128/mcb.14.12.8391

Garcia, V., Phelps, S.E.L., Gray, S., Neale, M.J., 2011. Bidirectional resection of DNA double-strand breaks by Mre11 and Exo1. Nature 479, 241–244. https://doi.org/10.1038/nature10515

García-Gómez, S., Reyes, A., Martínez-Jiménez, M.I., Chocrón, E.S., Mourón, S., Terrados, G., Powell, C., Salido, E., Méndez, J., Holt, I.J., Blanco, L., 2013. PrimPol, an Archaic Primase/Polymerase Operating in Human Cells. Mol. Cell 52, 541–553. https://doi.org/10.1016/j.molcel.2013.09.025

Garcia-Luis, J., Clemente-Blanco, A., Aragon, L., Machin, F., 2014. Cdc14 targets the Holliday junction resolvase Yen1 to the nucleus in early anaphase. Cell Cycle 13, 1392–1399. https://doi.org/10.4161/cc.28370

Garcia-Rodriguez, N., Wong, R.P., Ulrich, H.D., 2018. The helicase Pif1 functions in the template switching pathway of DNA damage bypass. Nucleic Acids Res. 46, 8347–8356. https://doi.org/10.1093/nar/gky648

Garg, P., Stith, C.M., Sabouri, N., Johansson, E., Burgers, P.M., 2004. Idling by DNA polymerase δ maintains a ligatable nick during lagging-strand DNA replication. Genes Dev. 18, 2764–2773. https://doi.org/10.1101/gad.1252304

Gaskell, L.J., Osman, F., Gilbert, R.J.C., Whitby, M.C., 2007. Mus81 cleavage of Holliday junctions: a failsafe for processing meiotic recombination intermediates? EMBO J. 26, 1891–1901. https://doi.org/10.1038/sj.emboj.7601645

USC UNIVERSIDADE DE SANTIAGO DE COMPOSTELA

Gates, K.S., 2009. An Overview of Chemical Processes That Damage Cellular DNA: Spontaneous Hydrolysis, Alkylation, and Reactions with Radicals. Chem. Res. Toxicol. 22, 1747–1760. https://doi.org/10.1021/tx900242k

George, T., Wen, Q., Griffiths, R., Ganesh, A., Meuth, M., Sanders, C.M., 2009. Human Pif1 helicase unwinds synthetic DNA structures resembling stalled DNA replication forks. Nucleic Acids Res. 37, 6491–6502. https://doi.org/10.1093/nar/gkp671

Gerhardt, J., Bhalla, A.D., Butler, J.S., Puckett, J.W., Dervan, P.B., Rosenwaks, Z., Napierala, M., 2016. Stalled DNA Replication Forks at the Endogenous GAA Repeats Drive Repeat Expansion in Friedreich's Ataxia Cells. Cell Rep. 16, 1218–1227. https://doi.org/10.1016/j.celrep.2016.06.075

Geronimo, C.L., Singh, S.P., Galletto, R., Zakian, V.A., 2018. The signature motif of the Saccharomyces cerevisiae Pif1 DNA helicase is essential in vivo for mitochondrial and nuclear functions and in vitro for ATPase activity. Nucleic Acids Res. 46, 8357–8370. https://doi.org/10.1093/nar/gky655

Giaever, G., Chu, A.M., Ni, L., Connelly, C., Riles, L., Véronneau, S., Dow, S., Lucau-Danila, A., Anderson, K., André, B., Arkin, A.P., Astromoff, A., El Bakkoury, M., Bangham, R., Benito, R., Brachat, S., Campanaro, S., Curtiss, M., Davis, K., Deutschbauer, A., Entian, K.-D., Flaherty, P., Foury, F., Garfinkel, D.J., Gerstein, M., Gotte, D., Güldener, U., Hegemann, J.H., Hempel, S., Herman, Z., Jaramillo, D.F., Kelly, D.E., Kelly, S.L., Kötter, P., LaBonte, D., Lamb, D.C., Lan, N., Liang, H., Liao, H., Liu, L., Luo, C., Lussier, M., Mao, R., Menard, P., Ooi, S.L., Revuelta, J.L., Roberts, C.J., Rose, M., Ross-Macdonald, P., Scherens, B., Schimmack, G., Shafer, B., Shoemaker, D.D., Sookhai-Mahadeo, S., Storms, R.K., Strathern, J.N., Valle, G., Voet, M., Volckaert, G., Wang, C., Ward, T.R., Wilhelmy, J., Winzeler, E.A., Yang, Y., Yen, G., Youngman, E., Yu, K., Bussey, H., Boeke, J.D., Snyder, M., Philippsen, P., Davis, R.W., Johnston, M., 2002. Functional profiling of the Saccharomyces cerevisiae genome. Nature 418, 387–391. https://doi.org/10.1038/nature00935

Gibbons, B.J., Brignole, E.J., Azubel, M., Murakami, K., Voss, N.R., Bushnell, D.A., Asturias, F.J., Kornberg, R.D., 2012. Subunit architecture of general transcription factor TFIIH. Proc. Natl. Acad. Sci. 109, 1949–1954. https://doi.org/10.1073/pnas.1105266109

Gilbert, W.V., Zhou, K., Butler, T.K., Doudna, J.A., 2007. Cap-Independent Translation Is Required for Starvation-Induced Differentiation in Yeast. Science 317, 1224–1227. https://doi.org/10.1126/science.1144467

Gnügge, R., Symington, L.S., 2021. DNA end resection during homologous recombination. Curr. Opin. Genet. Dev., Mechanisms of Homologous Recombination 71, 99–105. https://doi.org/10.1016/j.gde.2021.07.004

Granata, M., Lazzaro, F., Novarina, D., Panigada, D., Puddu, F., Abreu, C.M., Kumar, R., Grenon, M., Lowndes, N.F., Plevani, P., Muzi-Falconi, M., 2010. Dynamics of Rad9 Chromatin Binding and Checkpoint Function Are Mediated by Its Dimerization and Are

USC UNIVERSIDADE DE SANTIAGO DE COMPOSTELA

Cell Cycle–Regulated by CDK1 Activity. PLOS Genet. 6, e1001047. https://doi.org/10.1371/journal.pgen.1001047

Gravel, S., Chapman, J.R., Magill, C., Jackson, S.P., 2008. DNA helicases Sgs1 and BLM promote DNA double-strand break resection. Genes Dev. 22, 2767–2772. https://doi.org/10.1101/gad.503108

Green, M.R., Sambrook, J., 2018. Rapid Isolation of Yeast DNA. Cold Spring Harb. Protoc. 2018, pdb.prot093542. https://doi.org/10.1101/pdb.prot093542

Grigaitis, R., Ranjha, L., Wild, P., Kasaciunaite, K., Ceppi, I., Kissling, V., Henggeler, A., Susperregui, A., Peter, M., Seidel, R., Cejka, P., Matos, J., 2020. Phosphorylation of the RecQ Helicase Sgs1/BLM Controls Its DNA Unwinding Activity during Meiosis and Mitosis. Dev. Cell 53, 706-723.e5. https://doi.org/10.1016/j.devcel.2020.05.016

Gritenaite, D., Princz, L.N., Szakal, B., Bantele, S.C.S., Wendeler, L., Schilbach, S., Habermann, B.H., Matos, J., Lisby, M., Branzei, D., Pfander, B., 2014. A cell cycle-regulated Slx4-Dpb11 complex promotes the resolution of DNA repair intermediates linked to stalled replication. Genes Dev. 28, 1604–1619. https://doi.org/10.1101/gad.240515.114

Gu, Y., Masuda, Y., Kamiya, K., 2008. Biochemical analysis of human PIF1 helicase and functions of its N-terminal domain. Nucleic Acids Res. 36, 6295–6308. https://doi.org/10.1093/nar/gkn609

Guervilly, J.-H., Gaillard, P.H., 2018. SLX4: multitasking to maintain genome stability. Crit. Rev. Biochem. Mol. Biol. 53, 475–514. https://doi.org/10.1080/10409238.2018.1488803

Guervilly, J.-H., Takedachi, A., Naim, V., Scaglione, S., Chawhan, C., Lovera, Y., Despras, E., Kuraoka, I., Kannouche, P., Rosselli, F., Gaillard, P.-H.L., 2015. The SLX4 complex is a SUMO E3 ligase that impacts on replication stress outcome and genome stability. Mol. Cell 57, 123–137. https://doi.org/10.1016/j.molcel.2014.11.014

Guo, Z., Kanjanapangka, J., Liu, N., Liu, S., Liu, C., Wu, Z., Wang, Y., Loh, T., Kowolik, C., Jamsen, J., Zhou, M., Truong, K., Chen, Y., Zheng, L., Shen, B., 2012. Sequential Posttranslational Modifications Program FEN1 Degradation during Cell-Cycle Progression. Mol. Cell 47, 444–456. https://doi.org/10.1016/j.molcel.2012.05.042

Guo, Z., Zheng, L., Xu, H., Dai, H., Zhou, M., Pascua, M.R., Chen, Q.M., Shen, B., 2010. Methylation of FEN1 suppresses nearby phosphorylation and facilitates PCNA binding. Nat. Chem. Biol. 6, 766–773. https://doi.org/10.1038/nchembio.422

Gupta, R.C., Folta-Stogniew, E., O'Malley, S., Takahashi, M., Radding, C.M., 1999. Rapid Exchange of A:T Base Pairs Is Essential for Recognition of DNA Homology by Human Rad51 Recombination Protein. Mol. Cell 4, 705–714. https://doi.org/10.1016/S1097-2765(00)80381-0

Haber, J.E., 2012. Mating-Type Genes and MAT Switching in Saccharomyces cerevisiae. Genetics 191, 33–64. https://doi.org/10.1534/genetics.111.134577

USC UNIVERSIDADE DE SANTIAGO DE COMPOSTELA

Haffter, P., Fox, T.D., 1992. Nuclear mutations in the petite-negative yeast Schizosaccharomyces pombe allow growth of cells lacking mitochondrial DNA. Genetics 131, 255–260. https://doi.org/10.1093/genetics/131.2.255

Hamilton, R., Watanabe, C.K., de Boer, H.A., 1987. Compilation and comparison of the sequence context around the AUG startcodons in *Saccharomyces cerevisiae* mRNAs. Nucleic Acids Res. 15, 3581–3593. https://doi.org/10.1093/nar/15.8.3581

Hamperl, S., Bocek, M.J., Saldivar, J.C., Swigut, T., Cimprich, K.A., 2017. Transcription-Replication Conflict Orientation Modulates R-Loop Levels and Activates Distinct DNA Damage Responses. Cell 170, 774-786.e19. https://doi.org/10.1016/j.cell.2017.07.043

Hanada, K., Budzowska, M., Davies, S.L., van Drunen, E., Onizawa, H., Beverloo, H.B., Maas, A., Essers, J., Hickson, I.D., Kanaar, R., 2007. The structure-specific endonuclease Mus81 contributes to replication restart by generating double-strand DNA breaks. Nat. Struct. Mol. Biol. 14, 1096–1104. https://doi.org/10.1038/nsmb1313

Hanahan, D., Weinberg, R.A., 2011. Hallmarks of Cancer: The Next Generation. Cell 144, 646–674. https://doi.org/10.1016/j.cell.2011.02.013

Hangas, A., Kekäläinen, N.J., Potter, A., Michell, C., Aho, K.J., Rutanen, C., Spelbrink, J.N., Pohjoismäki, J.L., Goffart, S., 2022. Top3α is the replicative topoisomerase in mitochondrial DNA replication. Nucleic Acids Res. 50, 8733–8748. https://doi.org/10.1093/nar/gkac660

Heald, R., McKeon, F., 1990. Mutations of phosphorylation sites in lamin A that prevent nuclear lamina disassembly in mitosis. Cell 61, 579–589. https://doi.org/10.1016/0092-8674(90)90470-Y

Heller, R.C., Marians, K.J., 2006. Replisome assembly and the direct restart of stalled replication forks. Nat. Rev. Mol. Cell Biol. 7, 932–943. https://doi.org/10.1038/nrm2058

Hernández, G., Osnaya, V.G., Pérez-Martínez, X., 2019. Conservation and Variability of the AUG Initiation Codon Context in Eukaryotes. Trends Biochem. Sci. 44, 1009–1021. https://doi.org/10.1016/j.tibs.2019.07.001

Heyer, W.-D., 2015. Regulation of Recombination and Genomic Maintenance. Cold Spring Harb. Perspect. Biol. 7, a016501. https://doi.org/10.1101/cshperspect.a016501

Heyer, W.-D., Ehmsen, K.T., Liu, J., 2010. Regulation of Homologous Recombination in Eukaryotes. Annu. Rev. Genet. 44, 113–139. https://doi.org/10.1146/annurev-genet-051710-150955

Hickson, I.D., Mankouri, H.W., 2011. Processing of homologous recombination repair intermediates by the Sgs1-Top3-Rmi1 and Mus81-Mms4 complexes. Cell Cycle Georget. Tex 10, 3078–3085. https://doi.org/10.4161/cc.10.18.16919

Hinnebusch, A.G., 2011a. Molecular mechanism of scanning and start codon selection in eukaryotes. Microbiol. Mol. Biol. Rev. MMBR 75, 434–467, first page of table of contents. https://doi.org/10.1128/MMBR.00008-11

USC UNIVERSIDADE DE SANTIAGO DE COMPOSTELA

Hinnebusch, A.G., 2011b. Molecular Mechanism of Scanning and Start Codon Selection in Eukaryotes. Microbiol. Mol. Biol. Rev. 75, 434–467. https://doi.org/10.1128/MMBR.00008-11

Ho, C.K., Mazon, G., Lam, A.F., Symington, L.S., 2010. Mus81 and Yen1 promote reciprocal exchange during mitotic recombination to maintain genome integrity in budding yeast. Mol. Cell 40, 988–1000. https://doi.org/10.1016/j.molcel.2010.11.016

Hodskinson, M.R.G., Silhan, J., Crossan, G.P., Garaycoechea, J.I., Mukherjee, S., Johnson, C.M., Scharer, O.D., Patel, K.J., 2014. Mouse SLX4 is a tumor suppressor that stimulates the activity of the nuclease. Mol. Cell 54, 472–484. https://doi.org/10.1016/j.molcel.2014.03.014

Hoege, C., Pfander, B., Moldovan, G.-L., Pyrowolakis, G., Jentsch, S., 2002. RAD6-dependent DNA repair is linked to modification of PCNA by ubiquitin and SUMO. Nature 419, 135–141. https://doi.org/10.1038/nature00991

Hoeijmakers, J.H.J., 2009. DNA Damage, Aging, and Cancer. N. Engl. J. Med. 361, 1475–1485. https://doi.org/10.1056/NEJMra0804615

Hoeijmakers, J.H.J., 2001. Genome maintenance mechanisms for preventing cancer. Nature 411, 366–374. https://doi.org/10.1038/35077232

Holliday, R., 1964. A mechanism for gene conversion in fungi. Genet. Res. 5, 282–304. https://doi.org/10.1017/S0016672300001233

Holt, L.J., Tuch, B.B., Villén, J., Johnson, A.D., Gygi, S.P., Morgan, D.O., 2009. Global Analysis of Cdk1 Substrate Phosphorylation Sites Provides Insights into Evolution. Science 325, 1682–1686. https://doi.org/10.1126/science.1172867

Horigome, C., Oma, Y., Konishi, T., Schmid, R., Marcomini, I., Hauer, M.H., Dion, V., Harata, M., Gasser, S.M., 2014. SWR1 and INO80 Chromatin Remodelers Contribute to DNA Double-Strand Break Perinuclear Anchorage Site Choice. Mol. Cell 55, 626–639. https://doi.org/10.1016/j.molcel.2014.06.027

Huertas, P., Cortés-Ledesma, F., Sartori, A.A., Aguilera, A., Jackson, S.P., 2008. CDK targets Sae2 to control DNA-end resection and homologous recombination. Nature 455, 689–692. https://doi.org/10.1038/nature07215

Huertas, P., Jackson, S.P., 2009. Human CtIP Mediates Cell Cycle Control of DNA End Resection and Double Strand Break Repair *. J. Biol. Chem. 284, 9558–9565. https://doi.org/10.1074/jbc.M808906200

Hunter, N., 2015. Meiotic Recombination: The Essence of Heredity. Cold Spring Harb. Perspect. Biol. a016618. https://doi.org/10.1101/cshperspect.a016618

Hustedt, N., Durocher, D., 2017. The control of DNA repair by the cell cycle. Nat. Cell Biol. 19, 1–9. https://doi.org/10.1038/ncb3452

Hydbring, P., Malumbres, M., Sicinski, P., 2016. Non-canonical functions of cell cycle cyclins and cyclin-dependent kinases. Nat. Rev. Mol. Cell Biol. 17, 280–292. https://doi.org/10.1038/nrm.2016.27

USC UNIVERSIDADE DE SANTIAGO DE COMPOSTELA

Ingolia, N.T., Ghaemmaghami, S., Newman, J.R.S., Weissman, J.S., 2009. Genome-Wide Analysis in Vivo of Translation with Nucleotide Resolution Using Ribosome Profiling. Science 324, 218–223. https://doi.org/10.1126/science.1168978

Inoue, H., Nojima, H., Okayama, H., 1990. High efficiency transformation of Escherichia coli with plasmids. Gene 96, 23–28. https://doi.org/10.1016/0378-1119(90)90336-P

Ip, S.C.Y., Rass, U., Blanco, M.G., Flynn, H.R., Skehel, J.M., West, S.C., 2008. Identification of Holliday junction resolvases from humans and yeast. Nature 456, 357–361. https://doi.org/10.1038/nature07470

Ira, G., Malkova, A., Liberi, G., Foiani, M., Haber, J.E., 2003. Srs2 and Sgs1-Top3 suppress crossovers during double-strand break repair in yeast. Cell 115, 401–411. https://doi.org/10.1016/s0092-8674(03)00886-9

Ivanov, E.L., Sugawara, N., Fishman-Lobell, J., Haber, J.E., 1996. Genetic Requirements for the Single-Strand Annealing Pathway of Double-Strand Break Repair in Saccharomyces cerevisiae. Genetics 142, 693–704. https://doi.org/10.1093/genetics/142.3.693

Ivessa, A.S., Lenzmeier, B.A., Bessler, J.B., Goudsouzian, L.K., Schnakenberg, S.L., Zakian, V.A., 2003. The Saccharomyces cerevisiae Helicase Rrm3p Facilitates Replication Past Nonhistone Protein-DNA Complexes. Mol. Cell 12, 1525–1536. https://doi.org/10.1016/S1097-2765(03)00456-8

Ivessa, A.S., Zhou, J.-Q., Schulz, V.P., Monson, E.K., Zakian, V.A., 2002. Saccharomyces Rrm3p, a 5' to 3' DNA helicase that promotes replication fork progression through telomeric and subtelomeric DNA. Genes Dev 16, 1383–96. https://doi.org/10.1101/gad.982902

Ivessa, A.S., Zhou, J.Q., Zakian, V.A., 2000. The Saccharomyces Pif1p DNA helicase and the highly related Rrm3p have opposite effects on replication fork progression in ribosomal DNA. Cell 100, 479–89. https://doi.org/10.1016/s0092-8674(00)80683-2

Jackson, A.L., Loeb, L.A., 2001. The contribution of endogenous sources of DNA damage to the multiple mutations in cancer. Mutat. Res. Mol. Mech. Mutagen., Analysis and Prevention of Carcinogenesis in Animal Models 477, 7–21. https://doi.org/10.1016/S0027-5107(01)00091-4

Jackson, S.P., Bartek, J., 2009. The DNA-damage response in human biology and disease. Nature 461, 1071–1078. https://doi.org/10.1038/nature08467

Janke, C., Magiera, M.M., Rathfelder, N., Taxis, C., Reber, S., Maekawa, H., Moreno-Borchart, A., Doenges, G., Schwob, E., Schiebel, E., Knop, M., 2004. A versatile toolbox for PCR-based tagging of yeast genes: new fluorescent proteins, more markers and promoter substitution cassettes. Yeast 21, 947–962. https://doi.org/10.1002/yea.1142

Jiménez-Martín, A., Saugar, I., Joseph, C.R., Mayer, A., Lehmann, C.P., Szakal, B., Branzei, D., Tercero, J.A., 2020. The Mgs1/WRNIP1 ATPase is required to prevent a recombination salvage pathway at damaged replication forks. Sci. Adv. 6, eaaz3327. https://doi.org/10.1126/sciadv.aaz3327

USC UNIVERSIDADE DE SANTIAGO DE COMPOSTELA

Jimeno, S., Camarillo, R., Mejias-Navarro, F., Fernandez-Avila, M.J., Soria-Bretones, I., Prados-Carvajal, R., Huertas, P., 2018. The Helicase PIF1 Facilitates Resection over Sequences Prone to Forming G4 Structures. Cell Rep. 25, 3543. https://doi.org/10.1016/j.celrep.2018.12.029

Jimeno, S., Herrera-Moyano, E., Ortega, P., Aguilera, A., 2017. Differential effect of the overexpression of Rad2/XPG family endonucleases on genome integrity in yeast and human cells. DNA Repair 57, 66–75. https://doi.org/10.1016/j.dnarep.2017.06.030

Jiricny, J., 2013. Postreplicative Mismatch Repair. Cold Spring Harb. Perspect. Biol. 5, a012633–a012633. https://doi.org/10.1101/cshperspect.a012633

Johannes, G., Sarnow, P., 1998. Cap-independent polysomal association of natural mRNAs encoding c-myc, BiP, and eIF4G conferred by internal ribosome entry sites. RNA 4, 1500–1513. https://doi.org/10.1017/S1355838298981080

Juneau, K., Palm, C., Miranda, M., Davis, R.W., 2007. High-density yeast-tiling array reveals previously undiscovered introns and extensive regulation of meiotic splicing. Proc. Natl. Acad. Sci. 104, 1522–1527. https://doi.org/10.1073/pnas.0610354104

Kadyrov, F.A., Dzantiev, L., Constantin, N., Modrich, P., 2006. Endonucleolytic Function of MutLα in Human Mismatch Repair. Cell 126, 297–308. https://doi.org/10.1016/j.cell.2006.05.039

Kaliraman, V., Mullen, J.R., Fricke, W.M., Bastin-Shanower, S.A., Brill, S.J., 2001. Functional overlap between Sgs1-Top3 and the Mms4-Mus81 endonuclease. Genes Dev. 15, 2730–2740. https://doi.org/10.1101/gad.932201

Kamath-Loeb, A.S., Loeb, L.A., Johansson, E., Burgers, P.M.J., Fry, M., 2001. Interactions between the Werner Syndrome Helicase and DNA Polymerase δ Specifically Facilitate Copying of Tetraplex and Hairpin Structures of the d(CGG)n Trinucleotide Repeat Sequence *. J. Biol. Chem. 276, 16439–16446. https://doi.org/10.1074/jbc.M100253200

Kang, M.-S., Yu, S.-L., Lim, H.-S., Choi, B., Park, C.-S., Kang, J.-H., Lee, S.-K., 2010. Mitotic catastrophe induced by overexpression of budding yeast Rad2p. Yeast 27, 399–411. https://doi.org/10.1002/yea.1764

Kao, H.-I., Campbell, J.L., Bambara, R.A., 2004a. Dna2p Helicase/Nuclease Is a Tracking Protein, Like FEN1, for Flap Cleavage during Okazaki Fragment Maturation *. J. Biol. Chem. 279, 50840–50849. https://doi.org/10.1074/jbc.M409231200

Kao, H.-I., Veeraraghavan, J., Polaczek, P., Campbell, J.L., Bambara, R.A., 2004b. On the Roles of Saccharomyces cerevisiae Dna2p and Flap Endonuclease 1 in Okazaki Fragment Processing *. J. Biol. Chem. 279, 15014–15024. https://doi.org/10.1074/jbc.M313216200

Kara, N., Krueger, F., Rugg-Gunn, P., Houseley, J., 2021. Genome-wide analysis of DNA replication and DNA double-strand breaks using TrAEL-seq. PLOS Biol. 19, e3000886. https://doi.org/10.1371/journal.pbio.3000886

USC UNIVERSIDADE DE SANTIAGO DE COMPOSTELA

Karras, G.I., Fumasoni, M., Sienski, G., Vanoli, F., Branzei, D., Jentsch, S., 2013. Noncanonical Role of the 9-1-1 Clamp in the Error-Free DNA Damage Tolerance Pathway. Mol. Cell 49, 536–546. https://doi.org/10.1016/j.molcel.2012.11.016

Karras, G.I., Jentsch, S., 2010. The RAD6 DNA Damage Tolerance Pathway Operates Uncoupled from the Replication Fork and Is Functional Beyond S Phase. Cell 141, 255–267. https://doi.org/10.1016/j.cell.2010.02.028

Kasaciunaite, K., Fettes, F., Levikova, M., Daldrop, P., Anand, R., Cejka, P., Seidel, R., 2019. Competing interaction partners modulate the activity of Sgs1 helicase during DNA end resection. EMBO J. 38, e101516. https://doi.org/10.15252/embj.2019101516

Kaushal, S., Wollmuth, C.E., Das, K., Hile, S.E., Regan, S.B., Barnes, R.P., Haouzi, A., Lee, S.M., House, N.C.M., Guyumdzhyan, M., Eckert, K.A., Freudenreich, C.H., 2019. Sequence and Nuclease Requirements for Breakage and Healing of a Structure-Forming (AT)n Sequence within Fragile Site FRA16D. Cell Rep. 27, 1151-1164.e5. https://doi.org/10.1016/j.celrep.2019.03.103

Kazak, L., Reyes, A., Duncan, A.L., Rorbach, J., Wood, S.R., Brea-Calvo, G., Gammage, P.A., Robinson, A.J., Minczuk, M., Holt, I.J., 2013. Alternative translation initiation augments the human mitochondrial proteome. Nucleic Acids Res 41, 2354–69. https://doi.org/10.1093/nar/gks1347

Kearse, M.G., Wilusz, J.E., 2017. Non-AUG translation: a new start for protein synthesis in eukaryotes. Genes Dev. 31, 1717–1731. https://doi.org/10.1101/gad.305250.117

Keeney, S., Giroux, C.N., Kleckner, N., 1997. Meiosis-specific DNA double-strand breaks are catalyzed by Spo11, a member of a widely conserved protein family. Cell 88, 375–384.

Keil, R.L., McWilliams, A.D., 1993. A gene with specific and global effects on recombination of sequences from tandemly repeated genes in Saccharomyces cerevisiae. Genetics 135, 711–718. https://doi.org/10.1093/genetics/135.3.711

Kellis, M., Birren, B.W., Lander, E.S., 2004. Proof and evolutionary analysis of ancient genome duplication in the yeast Saccharomyces cerevisiae. Nature 428, 617–624. https://doi.org/10.1038/nature02424

Kent, N.A., Chambers, A.L., Downs, J.A., 2007. Dual Chromatin Remodeling Roles for RSC during DNA Double Strand Break Induction and Repair at the Yeast MAT Locus *. J. Biol. Chem. 282, 27693–27701. https://doi.org/10.1074/jbc.M704707200

Khristich, A.N., Mirkin, S.M., 2020. On the wrong DNA track: Molecular mechanisms of repeat-mediated genome instability. J. Biol. Chem. 295, 4134–4170. https://doi.org/10.1074/jbc.REV119.007678

Kobayashi, T., Heck, D.J., Nomura, M., Horiuchi, T., 1998. Expansion and contraction of ribosomal DNA repeats in Saccharomyces cerevisiae: requirement of replication fork blocking (Fob1) protein and the role of RNA polymerase I. Genes Dev. 12, 3821–3830. https://doi.org/10.1101/gad.12.24.3821

Kocak, E., Dykstra, S., Nemeth, A., Coughlin, C.G., Rodgers, K., McVey, M., 2019. The Drosophila melanogaster PIF1 Helicase Promotes Survival During Replication Stress

USC UNIVERSIDADE DE SANTIAGO DE COMPOSTELA

and Processive DNA Synthesis During Double-Strand Gap Repair. Genetics 213, 835–847. https://doi.org/10.1534/genetics.119.302665

Kockler, Z.W., Osia, B., Lee, R., Musmaker, K., Malkova, A., 2021. Repair of DNA Breaks by Break-Induced Replication. Annu. Rev. Biochem. 90, 165–191. https://doi.org/10.1146/annurev-biochem-081420-095551

Kolitz, S.E., Takacs, J.E., Lorsch, J.R., 2009. Kinetic and thermodynamic analysis of the role of start codon/anticodon base pairing during eukaryotic translation initiation. RNA 15, 138–152. https://doi.org/10.1261/rna.1318509

Koontz, L., 2014. Chapter One - TCA Precipitation, in: Lorsch, J. (Ed.), Methods in Enzymology, Laboratory Methods in Enzymology: Protein Part C. Academic Press, pp. 3–10. https://doi.org/10.1016/B978-0-12-420119-4.00001-X

Kosugi, S., Hasebe, M., Tomita, M., Yanagawa, H., 2009. Systematic identification of cell cycle-dependent yeast nucleocytoplasmic shuttling proteins by prediction of composite motifs. Proc. Natl. Acad. Sci. U. S. A. 106, 10171–10176. https://doi.org/10.1073/pnas.0900604106

Kozak, M., 2002. Pushing the limits of the scanning mechanism for initiation of translation. Gene 299, 1–34. https://doi.org/10.1016/s0378-1119(02)01056-9

Kozak, M., 1989. The scanning model for translation: an update. J. Cell Biol. 108, 229–241. https://doi.org/10.1083/jcb.108.2.229

Kozak, M., Shatkin, A.J., 1978. Migration of 40 S ribosomal subunits on messenger RNA in the presence of edeine. J. Biol. Chem. 253, 6568–6577. https://doi.org/10.1016/S0021-9258(19)46969-X

Krasilnikova, M.M., Mirkin, S.M., 2004. Replication Stalling at Friedreich's Ataxia (GAA)n Repeats In Vivo. Mol. Cell. Biol. 24, 2286–2295. https://doi.org/10.1128/MCB.24.6.2286-2295.2004

Krejci, L., Macris, M., Li, Y., Van Komen, S., Villemain, J., Ellenberger, T., Klein, H., Sung, P., 2004. Role of ATP hydrolysis in the antirecombinase function of Saccharomyces cerevisiae Srs2 protein. J. Biol. Chem. 279, 23193–23199. https://doi.org/10.1074/jbc.M402586200

Krejci, L., Van Komen, S., Li, Y., Villemain, J., Reddy, M.S., Klein, H., Ellenberger, T., Sung, P., 2003. DNA helicase Srs2 disrupts the Rad51 presynaptic filament. Nature 423, 305–309. https://doi.org/10.1038/nature01577

Kreuzer, K.N., Saunders, M., Weislo, L.J., Kreuzer, H.W., 1995. Recombination-dependent DNA replication stimulated by double-strand breaks in bacteriophage T4. J. Bacteriol. 177, 6844–6853. https://doi.org/10.1128/jb.177.23.6844-6853.1995

Kruisselbrink, E., Guryev, V., Brouwer, K., Pontier, D.B., Cuppen, E., Tijsterman, M., 2008. Mutagenic capacity of endogenous G4 DNA underlies genome instability in FANCJ-defective C. elegans. Curr. Biol. CB 18, 900–905. https://doi.org/10.1016/j.cub.2008.05.013

USC UNIVERSIDADE DE SANTIAGO DE COMPOSTELA

Kunkel, T.A., Bebenek, K., 2000. DNA Replication Fidelity. Annu. Rev. Biochem. 69, 497–529. https://doi.org/10.1146/annurev.biochem.69.1.497

Kuraoka, I., Bender, C., Romieu, A., Cadet, J., Wood, R.D., Lindahl, T., 2000. Removal of oxygen free-radical-induced 5′,8-purine cyclodeoxynucleosides from DNA by the nucleotide excision-repair pathway in human cells. Proc. Natl. Acad. Sci. 97, 3832–3837. https://doi.org/10.1073/pnas.070471597

Kwan, T., Thompson, S.R., 2019. Noncanonical Translation Initiation in Eukaryotes. Cold Spring Harb. Perspect. Biol. 11, a032672. https://doi.org/10.1101/cshperspect.a032672

Laat, W.L. de, Appeldoorn, E., Sugasawa, K., Weterings, E., Jaspers, N.G.J., Hoeijmakers, J.H.J., 1998. DNA-binding polarity of human replication protein A positions nucleases in nucleotide excision repair. Genes Dev. 12, 2598–2609. https://doi.org/10.1101/gad.12.16.2598

Lahaye, A., Leterme, S., Foury, F., 1993a. PIF1 DNA helicase from Saccharomyces cerevisiae. Biochemical characterization of the enzyme. J. Biol. Chem. 268, 26155–26161. https://doi.org/10.1016/S0021-9258(19)74294-X

Lahaye, A., Leterme, S., Foury, F., 1993b. PIF1 DNA helicase from Saccharomyces cerevisiae. Biochemical characterization of the enzyme. J. Biol. Chem. 268, 26155–26161. https://doi.org/10.1016/S0021-9258(19)74294-X

Lahaye, A., Stahl, H., Thines-Sempoux, D., Foury, F., 1991. PIF1: a DNA helicase in yeast mitochondria. EMBO J. 10, 997–1007.

Lahaye, A, Stahl, H., Thines-Sempoux, D., Foury, F., 1991. PIF1: a DNA helicase in yeast mitochondria. EMBO J. 10, 997–1007.

Lai, X., Broderick, R., Bergoglio, V., Zimmer, J., Badie, S., Niedzwiedz, W., Hoffmann, J.-S., Tarsounas, M., 2017. MUS81 nuclease activity is essential for replication stress tolerance and chromosome segregation in BRCA2-deficient cells. Nat. Commun. 8, 15983. https://doi.org/10.1038/ncomms15983

Lang, K.S., Hall, A.N., Merrikh, C.N., Ragheb, M., Tabakh, H., Pollock, A.J., Woodward, J.J., Dreifus, J.E., Merrikh, H., 2017. Replication-Transcription Conflicts Generate R-Loops that Orchestrate Bacterial Stress Survival and Pathogenesis. Cell 170, 787-799.e18. https://doi.org/10.1016/j.cell.2017.07.044

Lanz, M.C., Dibitetto, D., Smolka, M.B., 2019. DNA damage kinase signaling: checkpoint and repair at 30 years. EMBO J. 38. https://doi.org/10.15252/embj.2019101801

Lavery, P.E., Kowalczykowski, S.C., 1992. Enhancement of recA protein-promoted DNA strand exchange activity by volume-occupying agents. J. Biol. Chem. 267, 9307–9314. https://doi.org/10.1016/S0021-9258(19)50424-0

Lee, J.Y., Terakawa, T., Qi, Z., Steinfeld, J.B., Redding, S., Kwon, Y., Gaines, W.A., Zhao, W., Sung, P., Greene, E.C., 2015. Base triplet stepping by the Rad51/RecA family of recombinases. Science 349, 977–981. https://doi.org/10.1126/science.aab2666

USC UNIVERSIDADE DE SANTIAGO DE COMPOSTELA

Lee, K., Lee, S.E., 2007. Saccharomyces cerevisiae Sae2- and Tel1-Dependent Single-Strand DNA Formation at DNA Break Promotes Microhomology-Mediated End Joining. Genetics 176, 2003–2014. https://doi.org/10.1534/genetics.107.076539

Lensing, S.V., Marsico, G., Hänsel-Hertsch, R., Lam, E.Y., Tannahill, D., Balasubramanian, S., 2016. DSBCapture: in situ capture and sequencing of DNA breaks. Nat. Methods 13, 855–857. https://doi.org/10.1038/nmeth.3960

León-Ortiz, A.M., Svendsen, J., Boulton, S.J., 2014. Metabolism of DNA secondary structures at the eukaryotic replication fork. DNA Repair 19, 152–162. https://doi.org/10.1016/j.dnarep.2014.03.016

Lerner, L.K., Sale, J.E., 2019. Replication of G Quadruplex DNA. Genes 10, 95. https://doi.org/10.3390/genes10020095

Levikova, M., Klaue, D., Seidel, R., Cejka, P., 2013. Nuclease activity of Saccharomyces cerevisiae Dna2 inhibits its potent DNA helicase activity. Proc. Natl. Acad. Sci. 110, E1992–E2001. https://doi.org/10.1073/pnas.1300390110

Lezin, G., Kosaka, Y., Yost, H.J., Kuehn, M.R., Brunelli, L., 2011. A One-Step Miniprep for the Isolation of Plasmid DNA and Lambda Phage Particles. PLoS ONE 6, e23457. https://doi.org/10.1371/journal.pone.0023457

Li, S., Wang, H., Jehi, S., Li, J., Liu, S., Wang, Zi, Truong, L., Chiba, T., Wang, Zefeng, Wu, X., 2021. PIF1 helicase promotes break-induced replication in mammalian cells. EMBO J 40, e104509. https://doi.org/10.15252/embj.2020104509

Li, X., Stith, C.M., Burgers, P.M., Heyer, W.-D., 2009. PCNA Is Required for Initiation of Recombination-Associated DNA Synthesis by DNA Polymerase δ. Mol. Cell 36, 704–713. https://doi.org/10.1016/j.molcel.2009.09.036

Lieber, M.R., 2010. The Mechanism of Double-Strand DNA Break Repair by the Nonhomologous DNA End-Joining Pathway. Annu. Rev. Biochem. 79, 181–211. https://doi.org/10.1146/annurev.biochem.052308.093131

Lieber, M.R., Yu, K., Raghavan, S.C., 2006. Roles of nonhomologous DNA end joining, V(D)J recombination, and class switch recombination in chromosomal translocations. DNA Repair, Mechanisms of chromosomal translocation 5, 1234–1245. https://doi.org/10.1016/j.dnarep.2006.05.013

Lilley, D.M.J., White, M.F., 2001. The junction-resolving enzymes. Nat. Rev. Mol. Cell Biol. 2, 433–443. https://doi.org/10.1038/35073057x

Lim, G., Chang, Y., Huh, W.-K., 2020. Phosphoregulation of Rad51/Rad52 by CDK1 functions as a molecular switch for cell cycle–specific activation of homologous recombination. Sci. Adv. 6, eaay2669. https://doi.org/10.1126/sciadv.aay2669

Limbo, O., Chahwan, C., Yamada, Y., de Bruin, R.A.M., Wittenberg, C., Russell, P., 2007. Ctp1 Is a Cell-Cycle-Regulated Protein that Functions with Mre11 Complex to Control Double-Strand Break Repair by Homologous Recombination. Mol. Cell 28, 134–146. https://doi.org/10.1016/j.molcel.2007.09.009

USC UNIVERSIDADE DE SANTIAGO DE COMPOSTELA

Lin, W., Sampathi, S., Dai, H., Liu, C., Zhou, M., Hu, J., Huang, Q., Campbell, J., Shin-Ya, K., Zheng, L., Chai, W., Shen, B., 2013. Mammalian DNA2 helicase/nuclease cleaves G-quadruplex DNA and is required for telomere integrity. EMBO J. 32, 1425–1439. https://doi.org/10.1038/emboj.2013.88

Lindahl, T., 1993. Instability and decay of the primary structure of DNA. Nature 362, 709–715. https://doi.org/10.1038/362709a0

Liu, D., Keijzers, G., Rasmussen, L.J., 2017. DNA mismatch repair and its many roles in eukaryotic cells. Mutat. Res. Mutat. Res. 773, 174–187. https://doi.org/10.1016/j.mrrev.2017.07.001

Liu, G., Myers, S., Chen, X., Bissler, J.J., Sinden, R.R., Leffak, M., 2012. Replication Fork Stalling and Checkpoint Activation by a PKD1 Locus Mirror Repeat Polypurine-Polypyrimidine (Pu-Py) Tract*. J. Biol. Chem. 287, 33412–33423. https://doi.org/10.1074/jbc.M112.402503

Liu, J., Ede, C., Wright, W.D., Gore, S.K., Jenkins, S.S., Freudenthal, B.D., Todd Washington, M., Veaute, X., Heyer, W.-D., 2017. Srs2 promotes synthesis-dependent strand annealing by disrupting DNA polymerase delta-extending D-loops. eLife 6. https://doi.org/10.7554/eLife.22195

Liu, J., Renault, L., Veaute, X., Fabre, F., Stahlberg, H., Heyer, W.-D., 2011. Rad51 paralogues Rad55-Rad57 balance the antirecombinase Srs2 in Rad51 filament formation. Nature 479, 245–248. https://doi.org/10.1038/nature10522

Liu, L., Yan, Z., Osia, B.A., Twarowski, J., Sun, L., Kramara, J., Lee, R.S., Kumar, S., Elango, R., Li, H., Dang, W., Ira, G., Malkova, A., 2021. Tracking break-induced replication shows that it stalls at roadblocks. Nature 590, 655–659. https://doi.org/10.1038/s41586-020-03172-w

London, T.B.C., Barber, L.J., Mosedale, G., Kelly, G.P., Balasubramanian, S., Hickson, I.D., Boulton, S.J., Hiom, K., 2008. FANCJ is a structure-specific DNA helicase associated with the maintenance of genomic G/C tracts. J. Biol. Chem. 283, 36132–36139. https://doi.org/10.1074/jbc.M808152200

Longtine, M.I., Demarini, S., Wach, B., Philippsen, P., 1998. Additional modules for versatile and economical PCR-based gene deletion and modification in Saccharomyces cerevisiae 9.

Longtine, M.S., Iii, A.M., Demarini, D.J., Shah, N.G., Wach, A., Brachat, A., Philippsen, P., Pringle, J.R., 1998. Additional modules for versatile and economical PCR-based gene deletion and modification in Saccharomyces cerevisiae. Yeast 14, 953–961. https://doi.org/10.1002/(SICI)1097-0061(199807)14:10<953::AID-YEA293>3.0.CO;2-U

Loog, M., Morgan, D.O., 2005. Cyclin specificity in the phosphorylation of cyclin-dependent kinase substrates. Nature 434, 104–108. https://doi.org/10.1038/nature03329

USC UNIVERSIDADE DE SANTIAGO DE COMPOSTELA

Lopes, J., Piazza, A., Bermejo, R., Kriegsman, B., Colosio, A., Teulade-Fichou, M.-P., Foiani, M., Nicolas, A., 2011. G-quadruplex-induced instability during leading-strand replication. EMBO J 30, 4033–46. https://doi.org/10.1038/emboj.2011.316

Luder, A., Mosig, G., 1982. Two alternative mechanisms for initiation of DNA replication forks in bacteriophage T4: priming by RNA polymerase and by recombination. Proc. Natl. Acad. Sci. 79, 1101–1105. https://doi.org/10.1073/pnas.79.4.1101

Lujan, S.A., Williams, J.S., Pursell, Z.F., Abdulovic-Cui, A.A., Clark, A.B., McElhinny, S.A.N., Kunkel, T.A., 2012. Mismatch Repair Balances Leading and Lagging Strand DNA Replication Fidelity. PLOS Genet. 8, e1003016. https://doi.org/10.1371/journal.pgen.1003016

Lydeard, J.R., Jain, S., Yamaguchi, M., Haber, J.E., 2007. Break-induced replication and telomerase-independent telomere maintenance require Pol32. Nature 448, 820–823. https://doi.org/10.1038/nature06047

Ma, J.-L., Kim, E.M., Haber, J.E., Lee, S.E., 2003. Yeast Mre11 and Rad1 Proteins Define a Ku-Independent Mechanism To Repair Double-Strand Breaks Lacking Overlapping End Sequences. Mol. Cell. Biol. 23, 8820–8828. https://doi.org/10.1128/MCB.23.23.8820-8828.2003

Maestroni, L., Audry, J., Luciano, P., Coulon, S., Géli, V., Corda, Y., 2020. RPA and Pif1 cooperate to remove G-rich structures at both leading and lagging strand. Cell Stress 4, 48–63. https://doi.org/10.15698/cst2020.03.214

Makovets, S., Blackburn, E.H., 2009a. DNA damage signalling prevents deleterious telomere addition at DNA breaks. Nat. Cell Biol. 11, 1383–1386. https://doi.org/10.1038/ncb1985

Makovets, S., Blackburn, E.H., 2009b. DNA damage signalling prevents deleterious telomere addition at DNA breaks. Nat. Cell Biol. 11, 1383–1386. https://doi.org/10.1038/ncb1985

Mangahas, J.L., Alexander, M.K., Sandell, L.L., Zakian, V.A., 2001. Repair of chromosome ends after telomere loss in Saccharomyces. Mol Biol Cell 12, 4078–89. https://doi.org/10.1091/mbc.12.12.4078

Mao, Z., Bozzella, M., Seluanov, A., Gorbunova, V., 2008. Comparison of nonhomologous end joining and homologous recombination in human cells. DNA Repair 7, 1765–1771. https://doi.org/10.1016/j.dnarep.2008.06.018

Marsella, A., Gobbini, E., Cassani, C., Tisi, R., Cannavo, E., Reginato, G., Cejka, P., Longhese, M.P., 2021. Sae2 and Rif2 regulate MRX endonuclease activity at DNA double-strand breaks in opposite manners. Cell Rep. 34, 108906. https://doi.org/10.1016/j.celrep.2021.108906

Martin, I.V., MacNeill, S.A., 2004. Functional analysis of subcellular localization and protein–protein interaction sequences in the essential DNA ligase I protein of fission yeast. Nucleic Acids Res. 32, 632–642. https://doi.org/10.1093/nar/gkh199

USC UNIVERSIDADE DE SANTIAGO DE COMPOSTELA

Masuda-Sasa, T., Polaczek, P., Peng, X.P., Chen, L., Campbell, J.L., 2008. Processing of G4 DNA by Dna2 Helicase/Nuclease and Replication Protein A (RPA) Provides Insights into the Mechanism of Dna2/RPA Substrate Recognition *. J. Biol. Chem. 283, 24359–24373. https://doi.org/10.1074/jbc.M802244200

Mateos-Gomez, P.A., Gong, F., Nair, N., Miller, K.M., Lazzerini-Denchi, E., Sfeir, A., 2015. Mammalian polymerase θ promotes alternative NHEJ and suppresses recombination. Nature 518, 254–257. https://doi.org/10.1038/nature14157

Mateyak, M.K., Zakian, V.A., 2006. Human PIF helicase is cell cycle regulated and associates with telomerase. Cell Cycle 5, 2796–804. https://doi.org/10.4161/cc.5.23.3524

Mathiasen, D.P., Lisby, M., 2014. Cell cycle regulation of homologous recombination in *Saccharomyces cerevisiae*. FEMS Microbiol. Rev. 38, 172–184. https://doi.org/10.1111/1574-6976.12066

Matos, J., Blanco, M.G., Maslen, S., Skehel, J.M., West, S.C., 2011. Regulatory control of the resolution of DNA recombination intermediates during meiosis and mitosis. Cell 147, 158–172. https://doi.org/10.1016/j.cell.2011.08.032

Matos, J., Blanco, M.G., West, S.C., 2013. Cell-Cycle Kinases Coordinate the Resolution of Recombination Intermediates with Chromosome Segregation. Cell Rep. 4, 76–86. https://doi.org/10.1016/j.celrep.2013.05.039

Mayle, R., Campbell, I.M., Beck, C.R., Yu, Y., Wilson, M., Shaw, C.A., Bjergbaek, L., Lupski, J.R., Ira, G., 2015. Mus81 and converging forks limit the mutagenicity of replication fork breakage. Science 349, 742–747. https://doi.org/10.1126/science.aaa8391

McDonald, K.R., Sabouri, N., Webb, C.J., Zakian, V.A., 2014. The Pif1 family helicase Pfh1 facilitates telomere replication and has an. DNA Repair 24, 80–86. https://doi.org/10.1016/j.dnarep.2014.09.008

McGuffin, L.J., Bryson, K., Jones, D.T., 2000. The PSIPRED protein structure prediction server. Bioinformatics 16, 404–405. https://doi.org/10.1093/bioinformatics/16.4.404

McIlwraith, M.J., West, S.C., 2008. DNA Repair Synthesis Facilitates RAD52-Mediated Second-End Capture during DSB Repair. Mol. Cell 29, 510–516. https://doi.org/10.1016/j.molcel.2007.11.037

Mehta, A., Beach, A., Haber, J.E., 2017. Homology Requirements and Competition between Gene Conversion and Break-Induced Replication during Double-Strand Break Repair. Mol. Cell 65, 515-526.e3. https://doi.org/10.1016/j.molcel.2016.12.003

Meijer, H.A., Thomas, A.A.M., 2002. Control of eukaryotic protein synthesis by upstream open reading frames in the 5′-untranslated region of an mRNA. Biochem. J. 367, 1–11. https://doi.org/10.1042/bj20011706

Mendenhall, M.D., Hodge, A.E., 1998. Regulation of Cdc28 Cyclin-Dependent Protein Kinase Activity during the Cell Cycle of the Yeast Saccharomyces cerevisiae. Microbiol. Mol. Biol. Rev. 62, 1191–1243. https://doi.org/10.1128/MMBR.62.4.1191-1243.1998

Meng, X., Zhao, X., 2016. Replication fork regression and its regulation. FEMS Yeast Res. fow110. https://doi.org/10.1093/femsyr/fow110

USC DE SANTIAGO DE COMPOSTELA

Mengoli, V., Ceppi, I., Sanchez, A., Cannavo, E., Halder, S., Scaglione, S., Gaillard, P.-H., McHugh, P.J., Riesen, N., Pettazzoni, P., Cejka, P., 2023. WRN helicase and mismatch repair complexes independently and synergistically disrupt cruciform DNA structures. EMBO J. 42, e111998. https://doi.org/10.15252/embj.2022111998

Michel, A.H., Hatakeyama, R., Kimmig, P., Arter, M., Peter, M., Matos, J., De Virgilio, C., Kornmann, B., 2017. Functional mapping of yeast genomes by saturated transposition. eLife 6, e23570. https://doi.org/10.7554/eLife.23570

Mimitou, E.P., Symington, L.S., 2008. Sae2, Exo1 and Sgs1 collaborate in DNA double-strand break processing. Nature 455, 770–774. https://doi.org/10.1038/nature07312

Min, J.-H., Pavletich, N.P., 2007. Recognition of DNA damage by the Rad4 nucleotide excision repair protein. Nature 449, 570–575. https://doi.org/10.1038/nature06155

Minocherhomji, S., Ying, S., Bjerregaard, V.A., Bursomanno, S., Aleliunaite, A., Wu, W., Mankouri, H.W., Shen, H., Liu, Y., Hickson, I.D., 2015. Replication stress activates DNA repair synthesis in mitosis. Nature 528, 286–290.

Mitchel, K., Lehner, K., Jinks-Robertson, S., 2013. Heteroduplex DNA position defines the roles of the Sgs1, Srs2, and Mph1 helicases in promoting distinct recombination outcomes. PLoS Genet. 9, e1003340. https://doi.org/10.1371/journal.pgen.1003340

Mohammad, J.B., Wallgren, M., Sabouri, N., 2018. The Pif1 signature motif of Pfh1 is necessary for both protein displacement and helicase unwinding activities, but is dispensable for strand-annealing activity. Nucleic Acids Res. 46, 8516–8531. https://doi.org/10.1093/nar/gky654

Mohanty, B.K., Bairwa, N.K., Bastia, D., 2006. The Tof1p–Csm3p protein complex counteracts the Rrm3p helicase to control replication termination of Saccharomyces cerevisiae. Proc. Natl. Acad. Sci. 103, 897–902. https://doi.org/10.1073/pnas.0506540103

Moldovan, G.-L., Pfander, B., Jentsch, S., 2007. PCNA, the Maestro of the Replication Fork. Cell 129, 665–679. https://doi.org/10.1016/j.cell.2007.05.003

Monteuuis, G., Miścicka, A., Świrski, M., Zenad, L., Niemitalo, O., Wrobel, L., Alam, J., Chacinska, A., Kastaniotis, A.J., Kufel, J., 2019. Non-canonical translation initiation in yeast generates a cryptic pool of mitochondrial proteins. Nucleic Acids Res. 47, 5777–5791. https://doi.org/10.1093/nar/gkz301

Moriel-Carretero, M., Aguilera, A., 2010. A Postincision-Deficient TFIIH Causes Replication Fork Breakage and Uncovers Alternative Rad51- or Pol32-Mediated Restart Mechanisms. Mol. Cell 37, 690–701. https://doi.org/10.1016/j.molcel.2010.02.008

Morin, I., Ngo, H.-P., Greenall, A., Zubko, M.K., Morrice, N., Lydall, D., 2008. Checkpoint-dependent phosphorylation of Exo1 modulates the DNA damage response. EMBO J. 27, 2400–2410. https://doi.org/10.1038/emboj.2008.171

Mourón, S., Rodriguez-Acebes, S., Martínez-Jiménez, M.I., García-Gómez, S., Chocrón, S., Blanco, L., Méndez, J., 2013. Repriming of DNA synthesis at stalled replication forks by human PrimPol. Nat. Struct. Mol. Biol. 20, 1383–1389. https://doi.org/10.1038/nsmb.2719

USC UNIVERSIDADE DE SANTIAGO DE COMPOSTELA

Mullen, J.R., Kaliraman, V., Ibrahim, S.S., Brill, S.J., 2001. Requirement for three novel protein complexes in the absence of the Sgs1 DNA helicase in Saccharomyces cerevisiae. Genetics 157, 103–118.

Mullen, J.R., Nallaseth, F.S., Lan, Y.Q., Slagle, C.E., Brill, S.J., 2005. Yeast Rmi1/Nce4 controls genome stability as a subunit of the Sgs1-Top3 complex. Mol. Cell. Biol. 25, 4476–4487. https://doi.org/10.1128/MCB.25.11.4476-4487.2005

Munoz, I.M., Hain, K., Declais, A.-C., Gardiner, M., Toh, G.W., Sanchez-Pulido, L., Heuckmann, J.M., Toth, R., Macartney, T., Eppink, B., Kanaar, R., Ponting, C.P., Lilley, D.M.J., Rouse, J., 2009. Coordination of structure-specific nucleases by human SLX4/BTBD12 is required for DNA repair. Mol. Cell 35, 116–127. https://doi.org/10.1016/j.molcel.2009.06.020

Muñoz-Galván, S., García-Rubio, M., Ortega, P., Ruiz, J.F., Jimeno, S., Pardo, B., Gómez-González, B., Aguilera, A., 2017. A new role for Rrm3 in repair of replication-born DNA breakage by sister chromatid recombination. PLOS Genet. 13, e1006781. https://doi.org/10.1371/journal.pgen.1006781

Murfuni, I., Nicolai, S., Baldari, S., Crescenzi, M., Bignami, M., Franchitto, A., Pichierri, P., 2013. The WRN and MUS81 proteins limit cell death and genome instability following oncogene activation. Oncogene 32, 610–620. https://doi.org/10.1038/onc.2012.80

Murray, A.W., Hunt, T., 1993. The Cell Cycle: An Introduction. Oxford University Press.

Myler, L.R., Gallardo, I.F., Soniat, M.M., Deshpande, R.A., Gonzalez, X.B., Kim, Y., Paull, T.T., Finkelstein, I.J., 2017. Single-Molecule Imaging Reveals How Mre11-Rad50-Nbs1 Initiates DNA Break Repair. Mol. Cell 67, 891-898.e4. https://doi.org/10.1016/j.molcel.2017.08.002

Myung, K., Chen, C., Kolodner, R.D., 2001. Multiple pathways cooperate in the suppression of genome instability in Saccharomyces cerevisiae. Nature 411, 1073–6. https://doi.org/10.1038/35082608

Naim, V., Wilhelm, T., Debatisse, M., Rosselli, F., 2013. ERCC1 and MUS81–EME1 promote sister chromatid separation by processing late replication intermediates at common fragile sites during mitosis. Nat. Cell Biol. 15, 1008–1015. https://doi.org/10.1038/ncb2793

Nakada, D., Matsumoto, K., Sugimoto, K., 2003. ATM-related Tel1 associates with double-strand breaks through an Xrs2-dependent mechanism. Genes Dev. 17, 1957–1962. https://doi.org/10.1101/gad.1099003

Neelsen, K.J., Lopes, M., 2015. Replication fork reversal in eukaryotes: from dead end to dynamic response. Nat. Rev. Mol. Cell Biol. 16, 207–220. https://doi.org/10.1038/nrm3935

Ngo, G.H.P., Balakrishnan, L., Dubarry, M., Campbell, J.L., Lydall, D., 2014. The 9-1-1 checkpoint clamp stimulates DNA resection by Dna2-Sgs1 and Exo1. Nucleic Acids Res. 42, 10516–10528. https://doi.org/10.1093/nar/gku746

USC UNIVERSIDADE DE SANTIAGO DE COMPOSTELA

Nickens, D.G., Sausen, C.W., Bochman, M.L., 2019. The Biochemical Activities of the Saccharomyces cerevisiae Pif1 Helicase Are Regulated by Its N-Terminal Domain. Genes 10. https://doi.org/10.3390/genes10060411

Nimonkar, A.V., Sica, R.A., Kowalczykowski, S.C., 2009. Rad52 promotes second-end DNA capture in double-stranded break repair to form complement-stabilized joint molecules. Proc. Natl. Acad. Sci. 106, 3077–3082. https://doi.org/10.1073/pnas.0813247106

Niu, H., Chung, W.-H., Zhu, Z., Kwon, Y., Zhao, W., Chi, P., Prakash, R., Seong, C., Liu, D., Lu, L., Ira, G., Sung, P., 2010. Mechanism of the ATP-dependent DNA end-resection machinery from Saccharomyces cerevisiae. Nature 467, 108–111. https://doi.org/10.1038/nature09318

Ogawa, T., Yu, X., Shinohara, A., Egelman, E.H., 1993. Similarity of the Yeast RAD51 Filament to the Bacterial RecA Filament. Science 259, 1896–1899. https://doi.org/10.1126/science.8456314

Ogrunc, M., Sancar, A., 2003. Identification and characterization of human MUS81-MMS4 structure-specific endonuclease. J. Biol. Chem. 278, 21715–21720. https://doi.org/10.1074/jbc.M302484200

Oh, J., Al-Zain, A., Cannavo, E., Cejka, P., Symington, L.S., 2016. Xrs2 Dependent and Independent Functions of the Mre11-Rad50 Complex. Mol. Cell 64, 405–415. https://doi.org/10.1016/j.molcel.2016.09.011

Ohouo, P.Y., Bastos de Oliveira, F.M., Almeida, B.S., Smolka, M.B., 2010. DNA damage signaling recruits the Rtt107-Slx4 scaffolds via Dpb11 to mediate replication stress response. Mol. Cell 39, 300–306. https://doi.org/10.1016/j.molcel.2010.06.019

Olmezer, G., Levikova, M., Klein, D., Falquet, B., Fontana, G.A., Cejka, P., Rass, U., 2016. Replication intermediates that escape Dna2 activity are processed by Holliday junction resolvase Yen1. Nat. Commun. 7, 13157. https://doi.org/10.1038/ncomms13157

Ononye, Onyekachi E, Sausen, C.W., Balakrishnan, L., Bochman, M.L., 2020. Lysine acetylation regulates the activity of nuclear Pif1. J Biol Chem 295, 15482–15497. https://doi.org/10.1074/jbc.RA120.015164

Ononye, Onyekachi E., Sausen, C.W., Balakrishnan, L., Bochman, M.L., 2020. Lysine acetylation regulates the activity of nuclear Pif1. J. Biol. Chem. 295, 15482–15497. https://doi.org/10.1074/jbc.RA120.015164

O'Rourke, T.W., Doudican, N.A., Mackereth, M.D., Doetsch, P.W., Shadel, G.S., 2002. Mitochondrial dysfunction due to oxidative mitochondrial DNA damage is reduced through cooperative actions of diverse proteins. Mol Cell Biol 22, 4086–93. https://doi.org/10.1128/MCB.22.12.4086-4093.2002

O'Rourke, T.W., Doudican, N.A., Zhang, H., Eaton, J.S., Doetsch, P.W., Shadel, G.S., 2005. Differential involvement of the related DNA helicases Pif1p and Rrm3p in mtDNA point mutagenesis and stability. Gene 354, 86–92. https://doi.org/10.1016/j.gene.2005.03.031

USC UNIVERSIDADE DE SANTIAGO DE COMPOSTELA

Osman, F., Dixon, J., Doe, C.L., Whitby, M.C., 2003. Generating crossovers by resolution of nicked Holliday junctions: a role for Mus81-Eme1 in meiosis. Mol. Cell 12, 761–774. https://doi.org/10.1016/s1097-2765(03)00343-5

Osmundson, J.S., Kumar, J., Yeung, R., Smith, D.J., 2017. Pif1-family helicases cooperatively suppress widespread replication-fork arrest at tRNA genes. Nat. Struct. Mol. Biol. 24, 162–170. https://doi.org/10.1038/nsmb.3342

Owen, B.A.L., Yang, Z., Lai, M., Gajek, M., Badger, J.D., Hayes, J.J., Edelmann, W., Kucherlapati, R., Wilson, T.M., McMurray, C.T., 2005. (CAG)n-hairpin DNA binds to Msh2–Msh3 and changes properties of mismatch recognition. Nat. Struct. Mol. Biol. 12, 663–670. https://doi.org/10.1038/nsmb965

Oza, P., Jaspersen, S.L., Miele, A., Dekker, J., Peterson, C.L., 2009. Mechanisms that regulate localization of a DNA double-strand break to the nuclear periphery. Genes Dev 23, 912–27. https://doi.org/10.1101/gad.1782209

Paeschke, K., Bochman, M.L., Garcia, P.D., Cejka, P., Friedman, K.L., Kowalczykowski, S.C., Zakian, V.A., 2013. Pif1 family helicases suppress genome instability at G-quadruplex motifs. Nature 497, 458–462. https://doi.org/10.1038/nature12149

Paeschke, K., Capra, J.A., Zakian, V.A., 2011. DNA replication through G-quadruplex motifs is promoted by the Saccharomyces cerevisiae Pif1 DNA helicase. Cell 145, 678–691. https://doi.org/10.1016/j.cell.2011.04.015

Palma, A., Pugliese, G.M., Murfuni, I., Marabitti, V., Malacaria, E., Rinalducci, S., Minoprio, A., Sanchez, M., Mazzei, F., Zolla, L., Franchitto, A., Pichierri, P., 2018. Phosphorylation by CK2 regulates MUS81/EME1 in mitosis and after replication stress. Nucleic Acids Res. 46, 5109–5124. https://doi.org/10.1093/nar/gky280

Pan, X., Ye, P., Yuan, D.S., Wang, X., Bader, J.S., Boeke, J.D., 2006. A DNA Integrity Network in the Yeast Saccharomyces cerevisiae. Cell 124, 1069–1081. https://doi.org/10.1016/j.cell.2005.12.036

Pâques, F., Haber, J.E., 1999. Multiple Pathways of Recombination Induced by Double-Strand Breaks in Saccharomyces cerevisiae. Microbiol. Mol. Biol. Rev. 63, 349–404. https://doi.org/10.1128/MMBR.63.2.349-404.1999

Pardo, B., Moriel-Carretero, M., Vicat, T., Aguilera, A., Pasero, P., 2020. Homologous recombination and Mus81 promote replication completion in response to replication fork blockage. EMBO Rep. 21. https://doi.org/10.15252/embr.201949367

Paulovich, A.G., Hartwell, L.H., 1995. A checkpoint regulates the rate of progression through S phase in S. cerevisiae in Response to DNA damage. Cell 82, 841–847. https://doi.org/10.1016/0092-8674(95)90481-6

Paulovich, A.G., Toczyski, D.P., Hartwell, L.H., 1997. When Checkpoints Fail. Cell 88, 315–321. https://doi.org/10.1016/S0092-8674(00)81870-X

Pavlov, Y.I., Mian, I.M., Kunkel, T.A., 2003. Evidence for Preferential Mismatch Repair of Lagging Strand DNA Replication Errors in Yeast. Curr. Biol. 13, 744–748. https://doi.org/10.1016/S0960-9822(03)00284-7

USC UNIVERSIDADE DE SANTIAGO DE COMPOSTELA

Peabody, D.S., 1989. Translation Initiation at Non-Aug Triplets in Mammalian Cells. J. Biol. Chem. 264, 5031–5035. https://doi.org/10.1016/S0021-9258(18)83694-8

Pepe, A., West, S.C., 2014a. MUS81-EME2 promotes replication fork restart. Cell Rep. 7, 1048–1055. https://doi.org/10.1016/j.celrep.2014.04.007

Pepe, A., West, S.C., 2014b. Substrate specificity of the MUS81-EME2 structure selective endonuclease. Nucleic Acids Res. 42, 3833–3845. https://doi.org/10.1093/nar/gkt1333

Peritore, M., Reusswig, K.-U., Bantele, S.C.S., Straub, T., Pfander, B., 2021. Strand-specific ChIP-seq at DNA breaks distinguishes ssDNA versus dsDNA binding and refutes single-stranded nucleosomes. Mol. Cell 81, 1841-1853.e4. https://doi.org/10.1016/j.molcel.2021.02.005

Petes, T.D., 1979. Yeast ribosomal DNA genes are located on chromosome XII. Proc. Natl. Acad. Sci. 76, 410–414. https://doi.org/10.1073/pnas.76.1.410

Pfander, B., Diffley, J.F.X., 2011. Dpb11 coordinates Mec1 kinase activation with cell cycle-regulated Rad9 recruitment: Dpb11 in checkpoint activation. EMBO J. 30, 4897–4907. https://doi.org/10.1038/emboj.2011.345

Pfander, B., Moldovan, G.-L., Sacher, M., Hoege, C., Jentsch, S., 2005. SUMO-modified PCNA recruits Srs2 to prevent recombination during S phase. Nature 436, 428–433. https://doi.org/10.1038/nature03665

Pham, N., Yan, Z., Yu, Y., Faria Afreen, M., Malkova, A., Haber, J.E., Ira, G., 2021. Mechanisms restraining break-induced replication at two-ended DNA double-strand breaks. EMBO J. 40, e104847. https://doi.org/10.15252/embj.2020104847

Pham, V.N., Xu, X., Huq, E., 2018. Molecular bases for the constitutive photomorphogenic phenotypes in Arabidopsis. Dev. Camb. Engl. 145. https://doi.org/10.1242/dev.169870

Piazza, A., Boulé, J.-B., Lopes, J., Mingo, K., Largy, E., Teulade-Fichou, M.-P., Nicolas, A., 2010. Genetic instability triggered by G-quadruplex interacting Phen-DC compounds in Saccharomyces cerevisiae. Nucleic Acids Res. 38, 4337–4348. https://doi.org/10.1093/nar/gkq136

Piazza, A., Heyer, W.-D., 2019. Moving forward one step back at a time: reversibility during homologous recombination. Curr. Genet. 65, 1333–1340. https://doi.org/10.1007/s00294-019-00995-7

Piazza, A., Shah, S.S., Wright, W.D., Gore, S.K., Koszul, R., Heyer, W.-D., 2019. Dynamic Processing of Displacement Loops during Recombinational DNA Repair. Mol. Cell 73, 1255-1266.e4. https://doi.org/10.1016/j.molcel.2019.01.005

Pike, J.E., Burgers, P.M.J., Campbell, J.L., Bambara, R.A., 2009. Pif1 helicase lengthens some Okazaki fragment flaps necessitating Dna2 nuclease/helicase action in the two-nuclease processing pathway. J. Biol. Chem. 284, 25170–25180. https://doi.org/10.1074/jbc.M109.023325

Pinter, S.F., Aubert, S.D., Zakian, V.A., 2008. The Schizosaccharomyces pombe Pfh1p DNA Helicase Is Essential for the Maintenance of Nuclear and Mitochondrial DNA. Mol. Cell. Biol. 28, 6594–6608. https://doi.org/10.1128/MCB.00191-08

Pluciennik, A., Dzantiev, L., Iyer, R.R., Constantin, N., Kadyrov, F.A., Modrich, P., 2010. PCNA function in the activation and strand direction of MutLα endonuclease in mismatch repair. Proc. Natl. Acad. Sci. 107, 16066–16071. https://doi.org/10.1073/pnas.1010662107

Prado, F., 2014. Homologous recombination maintenance of genome integrity during DNA damage tolerance. Mol. Cell. Oncol. 1, e957039. https://doi.org/10.4161/23723548.2014.957039

Prados-Carvajal, R., Rodriguez-Real, G., Gutierrez-Pozo, G., Huertas, P., 2020. CtIP -mediated alternative mRNA splicing finetunes the DNA damage response. RNA. https://doi.org/10.1261/rna.078519.120

Prakash, R., Satory, D., Dray, E., Papusha, A., Scheller, J., Kramer, W., Krejci, L., Klein, H., Haber, J.E., Sung, P., Ira, G., 2009. Yeast Mph1 helicase dissociates Rad51-made D-loops: implications for crossover control in mitotic recombination. Genes Dev. 23, 67–79. https://doi.org/10.1101/gad.1737809

Princz, L.N., Gritenaite, D., Pfander, B., 2015. The Slx4-Dpb11 scaffold complex: coordinating the response to replication fork stalling in S-phase and the subsequent mitosis. Cell Cycle Georget. Tex 14, 488–494. https://doi.org/10.4161/15384101.2014.989126

Princz, L.N., Wild, P., Bittmann, J., Aguado, F.J., Blanco, M.G., Matos, J., Pfander, B., 2017. Dbf4-dependent kinase and the Rtt107 scaffold promote Mus81-Mms4 resolvase activation during mitosis. EMBO J. 36, 664–678. https://doi.org/10.15252/embj.201694831

Qi, Z., Redding, S., Lee, J.Y., Gibb, B., Kwon, Y., Niu, H., Gaines, W.A., Sung, P., Greene, E.C., 2015. DNA Sequence Alignment by Microhomology Sampling during Homologous Recombination. Cell 160, 856–869. https://doi.org/10.1016/j.cell.2015.01.029

Ranjha, L., Howard, S.M., Cejka, P., 2018. Main steps in DNA double-strand break repair: an introduction to homologous recombination and related processes. Chromosoma 127, 187–214. https://doi.org/10.1007/s00412-017-0658-1

Rass, U., 2013. Resolving branched DNA intermediates with structure-specific nucleases during replication in eukaryotes. Chromosoma 122, 499–515. https://doi.org/10.1007/s00412-013-0431-z

Rass, U., Ahel, I., West, S.C., 2007. Defective DNA Repair and Neurodegenerative Disease. Cell 130, 991–1004. https://doi.org/10.1016/j.cell.2007.08.043

Rass, U., Compton, S.A., Matos, J., Singleton, M.R., Ip, S.C.Y., Blanco, M.G., Griffith, J.D., West, S.C., 2010. Mechanism of Holliday junction resolution by the human GEN1 protein. Genes Dev. 24, 1559–1569. https://doi.org/10.1101/gad.585310

Ray Chaudhuri, A., Hashimoto, Y., Herrador, R., Neelsen, K.J., Fachinetti, D., Bermejo, R., Cocito, A., Costanzo, V., Lopes, M., 2012. Topoisomerase I poisoning results in PARP-mediated replication fork reversal. Nat. Struct. Mol. Biol. 19, 417–423. https://doi.org/10.1038/nsmb.2258

USC UNIVERSIDADE DE SANTIAGO DE COMPOSTELA

Ray, P.S., Grover, R., Das, S., 2006. Two internal ribosome entry sites mediate the translation of p53 isoforms. EMBO Rep. 7, 404–410. https://doi.org/10.1038/sj.embor.7400623

Reenan, R.A., Kolodner, R.D., 1992. Characterization of insertion mutations in the Saccharomyces cerevisiae MSH1 and MSH2 genes: evidence for separate mitochondrial and nuclear functions. Genetics 132, 975–985. https://doi.org/10.1093/genetics/132.4.975

Regairaz, M., Zhang, Y.-W., Fu, H., Agama, K.K., Tata, N., Agrawal, S., Aladjem, M.I., Pommier, Y., 2011. Mus81-mediated DNA cleavage resolves replication forks stalled by topoisomerase. J. Cell Biol. 195, 739–749. https://doi.org/10.1083/jcb.201104003

Reginato, G., Cannavo, E., Cejka, P., 2017. Physiological protein blocks direct the Mre11–Rad50–Xrs2 and Sae2 nuclease complex to initiate DNA end resection. Genes Dev. 31, 2325–2330. https://doi.org/10.1101/gad.308254.117

Renkawitz, J., Lademann, C.A., Jentsch, S., 2014. Mechanisms and principles of homology search during recombination. Nat. Rev. Mol. Cell Biol. 15, 369–383. https://doi.org/10.1038/nrm3805

Repair of Oxidative DNA Damage in Saccharomyces cerevisiae, 2017. . DNA Repair 51, 2–13. https://doi.org/10.1016/j.dnarep.2016.12.010

Reyes, G.X., Schmidt, T.T., Kolodner, R.D., Hombauer, H., 2015. New insights into the mechanism of DNA mismatch repair. Chromosoma 124, 443–462. https://doi.org/10.1007/s00412-015-0514-0

Reymer, A., Frykholm, K., Morimatsu, K., Takahashi, M., Nordén, B., 2009. Structure of human Rad51 protein filament from molecular modeling and site-specific linear dichroism spectroscopy. Proc. Natl. Acad. Sci. 106, 13248–13253. https://doi.org/10.1073/pnas.0902723106

Reynolds, G.E., Gao, Q., Miller, D., Snow, B.E., Harrington, L.A., Murnane, J.P., 2011. PIF1 disruption or NBS1 hypomorphism does not affect chromosome healing or fusion resulting from double-strand breaks near telomeres in murine embryonic stem cells. DNA Repair 10, 1164–1173. https://doi.org/10.1016/j.dnarep.2011.09.002

Ribeyre, C., Lopes, J., Boule, J.-B., Piazza, A., Guedin, A., Zakian, V.A., Mergny, J.-L., Nicolas, A., 2009. The yeast Pif1 helicase prevents genomic instability caused by. PLoS Genet. 5, e1000475. https://doi.org/10.1371/journal.pgen.1000475

Robinson, J., Raguseo, F., Nuccio, S.P., Liano, D., Di Antonio, M., 2021. DNA G-quadruplex structures: more than simple roadblocks to transcription? Nucleic Acids Res. 49, 8419–8431. https://doi.org/10.1093/nar/gkab609

Rossi, M.L., Pike, J.E., Wang, W., Burgers, P.M.J., Campbell, J.L., Bambara, R.A., 2008. Pif1 helicase directs eukaryotic Okazaki fragments toward the two-nuclease cleavage pathway for primer removal. J. Biol. Chem. 283, 27483–27493. https://doi.org/10.1074/jbc.M804550200

Rossi, S.E., Ajazi, A., Carotenuto, W., Foiani, M., Giannattasio, M., 2015. Rad53-Mediated Regulation of Rrm3 and Pif1 DNA Helicases Contributes to Prevention of Aberrant

Fork Transitions under Replication Stress. Cell Rep. 13, 80–92. https://doi.org/10.1016/j.celrep.2015.08.073

Rossi, S.E., Foiani, M., Giannattasio, M., 2018. Dna2 processes behind the fork long ssDNA flaps generated by Pif1 and replication-dependent strand displacement. Nat. Commun. 9, 4830. https://doi.org/10.1038/s41467-018-07378-5

Rouse, J., Jackson, S.P., 2002. Lcd1p Recruits Mec1p to DNA Lesions In Vitro and In Vivo. Mol. Cell 9, 857–869. https://doi.org/10.1016/S1097-2765(02)00507-5

Roy, U., Kwon, Y., Marie, L., Symington, L., Sung, P., Lisby, M., Greene, E.C., 2021. The Rad51 paralog complex Rad55-Rad57 acts as a molecular chaperone during homologous recombination. Mol. Cell 81, 1043-1057.e8. https://doi.org/10.1016/j.molcel.2020.12.019

Rupp, W.D., Howard-flanders, P., 1968. Discontinuities in the DNA synthesized in an Excision-defective strain of Escherichia coli following ultraviolet irradiation. J. Mol. Biol. 31, 291–304. https://doi.org/10.1016/0022-2836(68)90445-2

Rupp, W.D., Wilde, C.E., Reno, D.L., Howard-Flanders, P., 1971. Exchanges between DNA strands in ultraviolet-irradiated Escherichia coli. J. Mol. Biol. 61, 25–44. https://doi.org/10.1016/0022-2836(71)90204-X

Ryu, G.-H., Tanaka, H., Kim, D.-H., Kim, J.-H., Bae, S.-H., Kwon, Y.-N., Rhee, J.S., MacNeill, S.A., Seo, Y.-S., 2004. Genetic and biochemical analyses of Pfh1 DNA helicase function in fission yeast. Nucleic Acids Res 32, 4205–16. https://doi.org/10.1093/nar/gkh720

Sabouri, N., Capra, J.A., Zakian, V.A., 2014. The essential Schizosaccharomyces pombe Pfh1 DNA helicase promotes fork movement past G-quadruplex motifs to prevent DNA damage. BMC Biol 12, 101. https://doi.org/10.1186/s12915-014-0101-5

Sabouri, N., McDonald, K.R., Webb, C.J., Cristea, I.M., Zakian, V.A., 2012. DNA replication through hard-to-replicate sites, including both highly transcribed RNA Pol II and Pol III genes, requires the S. pombe Pfh1 helicase. Genes Dev 26, 581–93. https://doi.org/10.1101/gad.184697.111

Saini, N., Ramakrishnan, S., Elango, R., Ayyar, S., Zhang, Y., Deem, A., Ira, G., Haber, J.E., Lobachev, K.S., Malkova, A., 2013. Migrating bubble during break-induced replication drives conservative DNA synthesis. Nature 502, 389–92. https://doi.org/10.1038/nature12584

Sakofsky, C.J., Ayyar, S., Deem, A.K., Chung, W.-H., Ira, G., Malkova, A., 2015. Translesion Polymerases Drive Microhomology-Mediated Break-Induced Replication Leading to Complex Chromosomal Rearrangements. Mol. Cell 60, 860–872. https://doi.org/10.1016/j.molcel.2015.10.041

Sale, J.E., 2013. Translesion DNA Synthesis and Mutagenesis in Eukaryotes. Cold Spring Harb. Perspect. Biol. 5, a012708–a012708. https://doi.org/10.1101/cshperspect.a012708

USC UNIVERSIDADE DE SANTIAGO DE COMPOSTELA

Sancar, A., Lindsey-Boltz, L.A., Ünsal-Kaçmaz, K., Linn, S., 2004. Molecular Mechanisms of Mammalian DNA Repair and the DNA Damage Checkpoints. Annu. Rev. Biochem. 73, 39–85. https://doi.org/10.1146/annurev.biochem.73.011303.073723

Sanchez, Y., Bachant, J., Wang, H., Hu, F., Liu, D., Tetzlaff, M., Elledge, S.J., 1999. Control of the DNA Damage Checkpoint by Chk1 and Rad53 Protein Kinases Through Distinct Mechanisms. Science 286, 1166–1171. https://doi.org/10.1126/science.286.5442.1166

Sandell, L.L., Zakian, V.A., 1993. Loss of a yeast telomere: Arrest, recovery, and chromosome loss. Cell 75, 729–739. https://doi.org/10.1016/0092-8674(93)90493-A

Sanders, C.M., 2010. Human Pif1 helicase is a G-quadruplex DNA-binding protein with G-quadruplex. Biochem. J. 430, 119–128. https://doi.org/10.1042/BJ20100612

Saponaro, M., Callahan, D., Zheng, X., Krejci, L., Haber, J.E., Klein, H.L., Liberi, G., 2010. Cdk1 targets Srs2 to complete synthesis-dependent strand annealing and to promote recombinational repair. PLoS Genet. 6, e1000858. https://doi.org/10.1371/journal.pgen.1000858

Sarkies, P., Murat, P., Phillips, L.G., Patel, K.J., Balasubramanian, S., Sale, J.E., 2012. FANCJ coordinates two pathways that maintain epigenetic stability at G-quadruplex DNA. Nucleic Acids Res. 40, 1485–1498. https://doi.org/10.1093/nar/gkr868

Sarkies, P., Reams, C., Simpson, L.J., Sale, J.E., 2010. Epigenetic Instability due to Defective Replication of Structured DNA. Mol. Cell 40, 703–713. https://doi.org/10.1016/j.molcel.2010.11.009

Sartori, A.A., Lukas, C., Coates, J., Mistrik, M., Fu, S., Bartek, J., Baer, R., Lukas, J., Jackson, S.P., 2007. Human CtIP promotes DNA end resection. Nature 450, 509–514. https://doi.org/10.1038/nature06337

Sass, E., Blachinsky, E., Karniely, S., Pines, O., 2001. Mitochondrial and Cytosolic Isoforms of Yeast Fumarase Are Derivatives of a Single Translation Product and Have Identical Amino Termini *. J. Biol. Chem. 276, 46111–46117. https://doi.org/10.1074/jbc.M106061200

Sass, E., Karniely, S., Pines, O., 2003. Folding of Fumarase during Mitochondrial Import Determines its Dual Targeting in Yeast *. J. Biol. Chem. 278, 45109–45116. https://doi.org/10.1074/jbc.M302344200

Sausen, C.W., Rogers, C.M., Bochman, M.L., 2019. Thin-Layer Chromatography and Real-Time Coupled Assays to Measure ATP Hydrolysis, in: Balakrishnan, L., Stewart, J.A. (Eds.), DNA Repair, Methods in Molecular Biology. Springer New York, New York, NY, pp. 245–253. https://doi.org/10.1007/978-1-4939-9500-4_15

Saxena, S., Zou, L., 2022. Hallmarks of DNA replication stress. Mol. Cell 82, 2298–2314. https://doi.org/10.1016/j.molcel.2022.05.004

Schiavone, D., Guilbaud, G., Murat, P., Papadopoulou, C., Sarkies, P., Prioleau, M.-N., Balasubramanian, S., Sale, J.E., 2014. Determinants of G quadruplex-induced epigenetic instability in REV1-deficient cells. EMBO J. 33, 2507–2520. https://doi.org/10.15252/embj.201488398

USC UNIVERSIDADE DE SANTIAGO DE COMPOSTELA

Schmidt, K.H., Derry, K.L., Kolodner, R.D., 2002. Saccharomyces cerevisiae RRM3, a 5′ to 3′ DNA Helicase, Physically Interacts with Proliferating Cell Nuclear Antigen *. J. Biol. Chem. 277, 45331–45337. https://doi.org/10.1074/jbc.M207263200

Schulz, V.P., Zakian, V.A., 1994a. The saccharomyces PIF1 DNA helicase inhibits telomere elongation and de novo telomere formation. Cell 76, 145–155. https://doi.org/10.1016/0092-8674(94)90179-1

Schulz, V.P., Zakian, V.A., 1994b. The saccharomyces PIF1 DNA helicase inhibits telomere elongation and de novo telomere formation. Cell 76, 145–155. https://doi.org/10.1016/0092-8674(94)90179-1

Schwab, R.A., Nieminuszczy, J., Shin-ya, K., Niedzwiedz, W., 2013. FANCJ couples replication past natural fork barriers with maintenance of chromatin structure. J. Cell Biol. 201, 33–48. https://doi.org/10.1083/jcb.201208009

Schwartz, E.K., Heyer, W.-D., 2011. Processing of joint molecule intermediates by structure-selective endonucleases during homologous recombination in eukaryotes. Chromosoma 120, 109–127. https://doi.org/10.1007/s00412-010-0304-7

Schwartz, E.K., Wright, W.D., Ehmsen, K.T., Evans, J.E., Stahlberg, H., Heyer, W.-D., 2012. Mus81-Mms4 functions as a single heterodimer to cleave nicked intermediates in recombinational DNA repair. Mol. Cell. Biol. 32, 3065–3080. https://doi.org/10.1128/MCB.00547-12

Sebesta, M., Burkovics, P., Haracska, L., Krejci, L., 2011. Reconstitution of DNA repair synthesis in vitro and the role of polymerase and helicase activities. DNA Repair 10, 567–576. https://doi.org/10.1016/j.dnarep.2011.03.003

Seong, C., Colavito, S., Kwon, Y., Sung, P., Krejci, L., 2009. Regulation of Rad51 recombinase presynaptic filament assembly via interactions with the Rad52 mediator and the Srs2 anti-recombinase. J. Biol. Chem. 284, 24363–24371. https://doi.org/10.1074/jbc.M109.032953

Sfeir, A., Kosiyatrakul, S.T., Hockemeyer, D., MacRae, S.L., Karlseder, J., Schildkraut, C.L., de Lange, T., 2009. Mammalian Telomeres Resemble Fragile Sites and Require TRF1 for Efficient Replication. Cell 138, 90–103. https://doi.org/10.1016/j.cell.2009.06.021

Sfeir, A., Symington, L.S., 2015. Microhomology-Mediated End Joining: A Back-up Survival Mechanism or Dedicated Pathway? Trends Biochem. Sci. 40, 701–714. https://doi.org/10.1016/j.tibs.2015.08.006

Sharma, S., Otterlei, M., Sommers, J.A., Driscoll, H.C., Dianov, G.L., Kao, H.-I., Bambara, R.A., Brosh, R.M., 2004. WRN Helicase and FEN-1 Form a Complex upon Replication Arrest and Together Process Branchmigrating DNA Structures Associated with the Replication Fork. Mol. Biol. Cell 15, 734–750. https://doi.org/10.1091/mbc.e03-08-0567

Sherman, F., 2002. Getting started with yeast, in: Guthrie, C., Fink, G.R. (Eds.), Methods in Enzymology, Guide to Yeast Genetics and Molecular and Cell Biology - Part B. Academic Press, pp. 3–41. https://doi.org/10.1016/S0076-6879(02)50954-X

USC UNIVERSIDADE DE SANTIAGO DE COMPOSTELA

Shi, I., Hallwyl, S.C.L., Seong, C., Mortensen, U., Rothstein, R., Sung, P., 2009. Role of the Rad52 Amino-terminal DNA Binding Activity in DNA Strand Capture in Homologous Recombination. J. Biol. Chem. 284, 33275–33284. https://doi.org/10.1074/jbc.M109.057752

Shibata, A., Moiani, D., Arvai, A.S., Perry, J., Harding, S.M., Genois, M.-M., Maity, R., van Rossum-Fikkert, S., Kertokalio, A., Romoli, F., Ismail, A., Ismalaj, E., Petricci, E., Neale, M.J., Bristow, R.G., Masson, J.-Y., Wyman, C., Jeggo, P.A., Tainer, J.A., 2014. DNA Double-Strand Break Repair Pathway Choice Is Directed by Distinct MRE11 Nuclease Activities. Mol. Cell 53, 7–18. https://doi.org/10.1016/j.molcel.2013.11.003

Shim, E.Y., Hong, S.J., Oum, J.-H., Yanez, Y., Zhang, Y., Lee, S.E., 2007. RSC Mobilizes Nucleosomes To Improve Accessibility of Repair Machinery to the Damaged Chromatin. Mol. Cell. Biol. 27, 1602–1613. https://doi.org/10.1128/MCB.01956-06

Shimada, K., Gasser, S.M., 2012. DNA replication: Pif1 pulls the plug on stalled replication forks. Curr. Biol. CB 22, R404-405. https://doi.org/10.1016/j.cub.2012.04.015

Shimura, T., Ochiai, Y., Noma, N., Oikawa, T., Sano, Y., Fukumoto, M., 2013. Cyclin D1 overexpression perturbs DNA replication and induces replication-associated DNA double-strand breaks in acquired radioresistant cells. Cell Cycle 12, 773–782. https://doi.org/10.4161/cc.23719

Shimura, T., Torres, M.J., Martin, M.M., Rao, V.A., Pommier, Y., Katsura, M., Miyagawa, K., Aladjem, M.I., 2008. Bloom's Syndrome Helicase and Mus81 are Required to Induce Transient Double-strand DNA Breaks in Response to DNA Replication Stress. J. Mol. Biol. 375, 1152–1164. https://doi.org/10.1016/j.jmb.2007.11.006

Shiotani, B., Zou, L., 2009. Single-Stranded DNA Orchestrates an ATM-to-ATR Switch at DNA Breaks. Mol. Cell 33, 547–558. https://doi.org/10.1016/j.molcel.2009.01.024

Siede, W., Friedberg, A.S., Dianova, I., Friedberg, E.C., 1994. Characterization of G1 checkpoint control in the yeast Saccharomyces cerevisiae following exposure to DNA-damaging agents. Genetics 138, 271–281. https://doi.org/10.1093/genetics/138.2.271

Siede, W., Friedberg, A.S., Friedberg, E.C., 1993. RAD9-dependent G1 arrest defines a second checkpoint for damaged DNA in the cell cycle of Saccharomyces cerevisiae. Proc. Natl. Acad. Sci. 90, 7985–7989. https://doi.org/10.1073/pnas.90.17.7985

Singh, T.R., Ali, A.M., Busygina, V., Raynard, S., Fan, Q., Du, C., Andreassen, P.R., Sung, P., Meetei, A.R., 2008. BLAP18/RMI2, a novel OB-fold-containing protein, is an essential component of the Bloom helicase-double Holliday junction dissolvasome. Genes Dev. 22, 2856–2868. https://doi.org/10.1101/gad.1725108

Slusher, L.B., Gillman, E.C., Martin, N.C., Hopper, A.K., 1991. mRNA leader length and initiation codon context determine alternative AUG selection for the yeast gene MOD5. Proc. Natl. Acad. Sci. 88, 9789–9793. https://doi.org/10.1073/pnas.88.21.9789

Smirnov, M.N., Smirnov, V.N., Budowsky, E.I., Inge-Vechtomov, S.G., Serebrjakov, N.G., 1967. Red pigment of adenine-deficient yeast Saccharomyces cerevisiae. Biochem.

USC UNIVERSIDADE DE SANTIAGO DE COMPOSTELA

Biophys. Res. Commun. 27, 299–304. https://doi.org/10.1016/S0006-291X(67)80096-2

Smith, C.E., Lam, A.F., Symington, L.S., 2009. Aberrant Double-Strand Break Repair Resulting in Half Crossovers in Mutants Defective for Rad51 or the DNA Polymerase δ Complex. Mol. Cell. Biol. 29, 1432–1441. https://doi.org/10.1128/MCB.01469-08

Smolka, M.B., Albuquerque, C.P., Chen, S., Zhou, H., 2007. Proteome-wide identification of in vivo targets of DNA damage checkpoint kinases. Proc. Natl. Acad. Sci. 104, 10364–10369. https://doi.org/10.1073/pnas.0701622104

Snow, B.E., Mateyak, M., Paderova, J., Wakeham, A., Iorio, C., Zakian, V., Squire, J., Harrington, L., 2007. Murine Pif1 interacts with telomerase and is dispensable for telomere function in vivo. Mol. Cell. Biol. 27, 1017–1026. https://doi.org/10.1128/MCB.01866-06

Sogo, J.M., Lopes, M., Foiani, M., 2002. Fork Reversal and ssDNA Accumulation at Stalled Replication Forks Owing to Checkpoint Defects. Science 297, 599–602. https://doi.org/10.1126/science.1074023

Solinger, J.A., Kiianitsa, K., Heyer, W.-D., 2002. Rad54, a Swi2/Snf2-like Recombinational Repair Protein, Disassembles Rad51:dsDNA Filaments. Mol. Cell 10, 1175–1188. https://doi.org/10.1016/S1097-2765(02)00743-8

Song, B., Sung, P., 2000. Functional Interactions among Yeast Rad51 Recombinase, Rad52 Mediator, and Replication Protein A in DNA Strand Exchange *. J. Biol. Chem. 275, 15895–15904. https://doi.org/10.1074/jbc.M910244199

Spingola, M., Grate, L., Haussler, D., Ares, M., 1999. Genome-wide bioinformatic and molecular analysis of introns in Saccharomyces cerevisiae. RNA 5, 221–234. https://doi.org/10.1017/S1355838299981682

Sriram, A., Bohlen, J., Teleman, A.A., 2018. Translation acrobatics: how cancer cells exploit alternate modes of translational initiation. EMBO Rep. 19, e45947. https://doi.org/10.15252/embr.201845947

Sriramachandran, A.M., Petrosino, G., Méndez-Lago, M., Schäfer, A.J., Batista-Nascimento, L.S., Zilio, N., Ulrich, H.D., 2020. Genome-wide Nucleotide-Resolution Mapping of DNA Replication Patterns, Single-Strand Breaks, and Lesions by GLOE-Seq. Mol. Cell 78, 975-985.e7. https://doi.org/10.1016/j.molcel.2020.03.027

Srivatsan, A., Bowen, N., Kolodner, R.D., 2014. Mispair-specific Recruitment of the Mlh1-Pms1 Complex Identifies Repair Substrates of the Saccharomyces cerevisiae Msh2-Msh3 Complex *. J. Biol. Chem. 289, 9352–9364. https://doi.org/10.1074/jbc.M114.552190

Stafa, A., Donnianni, R.A., Timashev, L.A., Lam, A.F., Symington, L.S., 2014. Template switching during break-induced replication is promoted by the Mph1 helicase in Saccharomyces cerevisiae. Genetics 196, 1017–1028. https://doi.org/10.1534/genetics.114.162297

USC UNIVERSIDADE DE SANTIAGO DE COMPOSTELA

Staresincic, L., Fagbemi, A.F., Enzlin, J.H., Gourdin, A.M., Wijgers, N., Dunand-Sauthier, I., Giglia-Mari, G., Clarkson, S.G., Vermeulen, W., Schärer, O.D., 2009. Coordination of dual incision and repair synthesis in human nucleotide excision repair. EMBO J. 28, 1111–1120. https://doi.org/10.1038/emboj.2009.49

Stein, I., Peleg, Y., Even-Ram, S., Pines, O., 1994. The single translation product of the FUM1 gene (fumarase) is processed in mitochondria before being distributed between the cytosol and mitochondria in Saccharomyces cerevisiae. Mol. Cell. Biol. 14, 4770–4778. https://doi.org/10.1128/mcb.14.7.4770-4778.1994

Steinacher, R., Osman, F., Dalgaard, J.Z., Lorenz, A., Whitby, M.C., 2012. The DNA helicase Pfh1 promotes fork merging at replication termination sites to ensure genome stability. Genes Dev 26, 594–602. https://doi.org/10.1101/gad.184663.111

Stelter, P., Ulrich, H.D., 2003. Control of spontaneous and damage-induced mutagenesis by SUMO and ubiquitin conjugation. Nature 425, 188–191. https://doi.org/10.1038/nature01965

Storici, F., Resnick, M.A., 2006. The Delitto Perfetto Approach to In Vivo Site-Directed Mutagenesis and Chromosome Rearrangements with Synthetic Oligonucleotides in Yeast, in: Methods in Enzymology. Elsevier, pp. 329–345. https://doi.org/10.1016/S0076-6879(05)09019-1

Stundon, J.L., Zakian, V.A., 2015a. Identification of Saccharomyces cerevisiae Genes Whose Deletion Causes Synthetic Effects in Cells with Reduced Levels of the Nuclear Pif1 DNA Helicase. G3 Bethesda Md 5, 2913–2918. https://doi.org/10.1534/g3.115.021139

Stundon, J.L., Zakian, V.A., 2015b. Identification of Saccharomyces cerevisiae Genes Whose Deletion Causes Synthetic Effects in Cells with Reduced Levels of the Nuclear Pif1 DNA Helicase. G3 Bethesda Md 5, 2913–2918. https://doi.org/10.1534/g3.115.021139

Sturzenegger, A., Burdova, K., Kanagaraj, R., Levikova, M., Pinto, C., Cejka, P., Janscak, P., 2014. DNA2 cooperates with the WRN and BLM RecQ helicases to mediate long-range DNA end resection in human cells. J. Biol. Chem. 289, 27314–27326. https://doi.org/10.1074/jbc.M114.578823

Sugawara, N., Haber, J.E., 1992. Characterization of double-strand break-induced recombination: homology requirements and single-stranded DNA formation. Mol. Cell. Biol. 12, 563–575. https://doi.org/10.1128/mcb.12.2.563-575.1992

Sugiyama, T., Kantake, N., Wu, Y., Kowalczykowski, S.C., 2006. Rad52-mediated DNA annealing after Rad51-mediated DNA strand exchange promotes second ssDNA capture. EMBO J. 25, 5539–5548. https://doi.org/10.1038/sj.emboj.7601412

Sun, T., Yu, Y., Wu, X., Acevedo, A., Luo, J.-D., Wang, J., Schneider, W.M., Hurwitz, B., Rosenberg, B.R., Chung, H., Rice, C.M., 2021. Decoupling expression and editing preferences of ADAR1 p150 and p110 isoforms. Proc. Natl. Acad. Sci. 118, e2021757118. https://doi.org/10.1073/pnas.2021757118

Sun, W., Nandi, S., Osman, F., Ahn, J.S., Jakovleska, J., Lorenz, A., Whitby, M.C., 2008. The FANCM Ortholog Fml1 Promotes Recombination at Stalled Replication Forks and

Limits Crossing Over during DNA Double-Strand Break Repair. Mol. Cell 32, 118–128. https://doi.org/10.1016/j.molcel.2008.08.024

Sung, P., 1997. Yeast Rad55 and Rad57 proteins form a heterodimer that functions with replication protein A to promote DNA strand exchange by Rad51 recombinase. Genes Dev. 11, 1111–1121. https://doi.org/10.1101/gad.11.9.1111

Sung, P., 1994. Catalysis of ATP-Dependent Homologous DNA Pairing and Strand Exchange by Yeast RAD51 Protein. Science 265, 1241–1243. https://doi.org/10.1126/science.8066464

Sung, P., Stratton, S.A., 1996. Yeast Rad51 Recombinase Mediates Polar DNA Strand Exchange in the Absence of ATP Hydrolysis *. J. Biol. Chem. 271, 27983–27986. https://doi.org/10.1074/jbc.271.45.27983

Surova, O., Zhivotovsky, B., 2013. Various modes of cell death induced by DNA damage. Oncogene 32, 3789–3797. https://doi.org/10.1038/onc.2012.556

Suzuki, Y., Holmes, J.B., Cerritelli, S.M., Sakhuja, K., Minczuk, M., Holt, I.J., Crouch, R.J., 2010. An Upstream Open Reading Frame and the Context of the Two AUG Codons Affect the Abundance of Mitochondrial and Nuclear RNase H1. Mol. Cell. Biol. 30, 5123–5134. https://doi.org/10.1128/MCB.00619-10

Svendsen, J.M., Harper, J.W., 2010. GEN1/Yen1 and the SLX4 complex: Solutions to the problem of Holliday junction resolution. Genes Dev. 24, 521–536. https://doi.org/10.1101/gad.1903510

Syed, S., Desler, C., Rasmussen, L.J., Schmidt, K.H., 2016. A Novel Rrm3 Function in Restricting DNA Replication via an Orc5-Binding Domain Is Genetically Separable from Rrm3 Function as an ATPase/Helicase in Facilitating Fork Progression. PLOS Genet. 12, e1006451. https://doi.org/10.1371/journal.pgen.1006451

Symington, L.S., Gautier, J., 2011. Double-Strand Break End Resection and Repair Pathway Choice. Annu. Rev. Genet. 45, 247–271. https://doi.org/10.1146/annurev-genet-110410-132435

Szakal, B., Branzei, D., 2013. Premature Cdk1/Cdc5/Mus81 pathway activation induces aberrant replication and deleterious crossover. EMBO J. 32, 1155–1167. https://doi.org/10.1038/emboj.2013.67

Szostak, J.W., Orr-Weaver, T.L., Rothstein, R.J., Stahl, F.W., 1983. The double-strand-break repair model for recombination. Cell 33, 25–35. https://doi.org/10.1016/0092-8674(83)90331-8

Talhaoui, I., Bernal, M., Mullen, J.R., Dorison, H., Palancade, B., Brill, S.J., Mazon, G., 2018. Slx5-Slx8 ubiquitin ligase targets active pools of the Yen1 nuclease to limit crossover formation. Nat. Commun. 9, 5016. https://doi.org/10.1038/s41467-018-07364-x

Tang, H.-L., Yeh, L.-S., Chen, N.-K., Ripmaster, T., Schimmel, P., Wang, C.-C., 2004. Translation of a Yeast Mitochondrial tRNA Synthetase Initiated at Redundant non-AUG Codons *. J. Biol. Chem. 279, 49656–49663. https://doi.org/10.1074/jbc.M408081200

USC UNIVERSIDADE DE SANTIAGO DE COMPOSTELA

Tay, Y.D., Wu, L., 2010. Overlapping roles for Yen1 and Mus81 in cellular Holliday junction processing. J. Biol. Chem. 285, 11427–11432. https://doi.org/10.1074/jbc.M110.108399

Taylor, S.D., Zhang, H., Eaton, J.S., Rodeheffer, M.S., Lebedeva, M.A., O'rourke, T.W., Siede, W., Shadel, G.S., 2005. The conserved Mec1/Rad53 nuclear checkpoint pathway regulates mitochondrial DNA copy number in Saccharomyces cerevisiae. Mol Biol Cell 16, 3010–8. https://doi.org/10.1091/mbc.e05-01-0053

Thangavel, S., Berti, M., Levikova, M., Pinto, C., Gomathinayagam, S., Vujanovic, M., Zellweger, R., Moore, H., Lee, E.H., Hendrickson, E.A., Cejka, P., Stewart, S., Lopes, M., Vindigni, A., 2015. DNA2 drives processing and restart of reversed replication forks in human cells. J. Cell Biol. 208, 545–562. https://doi.org/10.1083/jcb.201406100

Torres, J.Z., Bessler, J.B., Zakian, V.A., 2004. Local chromatin structure at the ribosomal DNA causes replication fork pausing and genome instability in the absence of the S. cerevisiae DNA helicase Rrm3p. Genes Dev. 18, 498–503. https://doi.org/10.1101/gad.1154704

Touriol, C., Bornes, S., Bonnal, S., Audigier, S., Prats, H., Prats, A.-C., Vagner, S., 2003. Generation of protein isoform diversity by alternative initiation of translation at non-AUG codons. Biol. Cell 95, 169–178. https://doi.org/10.1016/S0248-4900(03)00033-9

Tran, P.L.T., Pohl, T.J., Chen, C.-F., Chan, A., Pott, S., Zakian, V.A., 2017. PIF1 family DNA helicases suppress R-loop mediated genome instability at tRNA genes. Nat. Commun. 8, 15025. https://doi.org/10.1038/ncomms15025

Tran, P.T., Erdeniz, N., Dudley, S., Liskay, R.M., 2002. Characterization of nuclease-dependent functions of Exo1p in Saccharomyces cerevisiae. DNA Repair 1, 895–912. https://doi.org/10.1016/S1568-7864(02)00114-3

Tsaneva, I.R., Müller, B., West, S.C., 1992. ATP-dependent branch migration of holliday junctions promoted by the RuvA and RuvB proteins of E. coli. Cell 69, 1171–1180. https://doi.org/10.1016/0092-8674(92)90638-S

Tseng, H.-M., Tomkinson, A.E., 2004. Processing and Joining of DNA Ends Coordinated by Interactions among Dnl4/Lif1, Pol4, and FEN-1 *. J. Biol. Chem. 279, 47580–47588. https://doi.org/10.1074/jbc.M404492200

Tsukamoto, Y., Mitsuoka, C., Terasawa, M., Ogawa, H., Ogawa, T., 2005. Xrs2p Regulates Mre11p Translocation to the Nucleus and Plays a Role in Telomere Elongation and Meiotic Recombination. Mol. Biol. Cell 16, 597–608. https://doi.org/10.1091/mbc.e04-09-0782

Tubbs, A., Nussenzweig, A., 2017. Endogenous DNA Damage as a Source of Genomic Instability in Cancer. Cell 168, 644–656. https://doi.org/10.1016/j.cell.2017.01.002

Ubersax, J.A., Woodbury, E.L., Quang, P.N., Paraz, M., Blethrow, J.D., Shah, K., Shokat, K.M., Morgan, D.O., 2003. Targets of the cyclin-dependent kinase Cdk1. Nature 425, 859–864. https://doi.org/10.1038/nature02062

Ulrich, H.D., Jentsch, S., 2000. Two RING finger proteins mediate cooperation between ubiquitin-conjugating enzymes in DNA repair 10.

USC

Ulrich, H.D., Walden, H., 2010. Ubiquitin signalling in DNA replication and repair. Nat. Rev. Mol. Cell Biol. 11, 479–489. https://doi.org/10.1038/nrm2921

Umar, A., Buermeyer, A.B., Simon, J.A., Thomas, D.C., Clark, A.B., Liskay, R.M., Kunkel, T.A., 1996. Requirement for PCNA in DNA Mismatch Repair at a Step Preceding DNA Resynthesis. Cell 87, 65–73. https://doi.org/10.1016/S0092-8674(00)81323-9

van den Broek, W.J.A.A., 2002. Somatic expansion behaviour of the (CTG)n repeat in myotonic dystrophy knock-in mice is differentially affected by Msh3 and Msh6 mismatch-repair proteins. Hum. Mol. Genet. 11, 191–198. https://doi.org/10.1093/hmg/11.2.191

van Wietmarschen, N., Sridharan, S., Nathan, W.J., Tubbs, A., Chan, E.M., Callen, E., Wu, W., Belinky, F., Tripathi, V., Wong, N., Foster, K., Noorbakhsh, J., Garimella, K., Cruz-Migoni, A., Sommers, J.A., Huang, Y., Borah, A.A., Smith, J.T., Kalfon, J., Kesten, N., Fugger, K., Walker, R.L., Dolzhenko, E., Eberle, M.A., Hayward, B.E., Usdin, K., Freudenreich, C.H., Brosh, R.M., West, S.C., McHugh, P.J., Meltzer, P.S., Bass, A.J., Nussenzweig, A., 2020. Repeat expansions confer WRN dependence in microsatellite-unstable cancers. Nature 586, 292–298. https://doi.org/10.1038/s41586-020-2769-8

Vannier, J.-B., Pavicic-Kaltenbrunner, V., Petalcorin, M.I.R., Ding, H., Boulton, S.J., 2012. RTEL1 dismantles T loops and counteracts telomeric G4-DNA to maintain telomere integrity. Cell 149, 795–806. https://doi.org/10.1016/j.cell.2012.03.030

Vannier, J.-B., Sandhu, S., Petalcorin, M.IR., Wu, X., Nabi, Z., Ding, H., Boulton, S.J., 2013. RTEL1 Is a Replisome-Associated Helicase That Promotes Telomere and Genome-Wide Replication. Science 342, 239–242. https://doi.org/10.1126/science.1241779

Vasianovich, Y., Harrington, L.A., Makovets, S., 2014. Break-induced replication requires DNA damage-induced phosphorylation of Pif1 and leads to telomere lengthening. PLoS Genet. 10, e1004679. https://doi.org/10.1371/journal.pgen.1004679

Veaute, X., Jeusset, J., Soustelle, C., Kowalczykowski, S.C., Le Cam, E., Fabre, F., 2003. The Srs2 helicase prevents recombination by disrupting Rad51 nucleoprotein filaments. Nature 423, 309–312. https://doi.org/10.1038/nature01585

Vega, L.R., Phillips, J.A., Thornton, B.R., Benanti, J.A., Onigbanjo, M.T., Toczyski, D.P., Zakian, V.A., 2007. Sensitivity of yeast strains with long G-tails to levels of telomere-bound telomerase. PLoS Genet 3, e105. https://doi.org/10.1371/journal.pgen.0030105

Vernekar, D.V., Reginato, G., Adam, C., Ranjha, L., Dingli, F., Marsolier, M.-C., Loew, D., Guérois, R., Llorente, B., Cejka, P., Borde, V., 2021. The Pif1 helicase is actively inhibited during meiotic recombination which restrains gene conversion tract length. Nucleic Acids Res 49, 4522–4533. https://doi.org/10.1093/nar/gkab232

Vilenchik, M.M., Knudson, A.G., 2003. Endogenous DNA double-strand breaks: Production, fidelity of repair, and induction of cancer. Proc. Natl. Acad. Sci. 100, 12871–12876. https://doi.org/10.1073/pnas.2135498100

USC UNIVERSIDADE DE SANTIAGO DE COMPOSTELA

Villarreal, D.D., Lee, K., Deem, A., Shim, E.Y., Malkova, A., Lee, S.E., 2012. Microhomology Directs Diverse DNA Break Repair Pathways and Chromosomal Translocations. PLOS Genet. 8, e1003026. https://doi.org/10.1371/journal.pgen.1003026

Wach, A., Brachat, A., Pöhlmann, R., Philippsen, P., 1994. New heterologous modules for classical or PCR-based gene disruptions in Saccharomyces cerevisiae. Yeast 10, 1793–1808. https://doi.org/10.1002/yea.320101310

Waga, S., Stillman, B., 1994. Anatomy of a DNA replication fork revealed by reconstitution of SV40 DNA replication in vitro. Nature 369, 207–212. https://doi.org/10.1038/369207a0

Wagner, M., Price, G., Rothstein, R., 2006. The absence of Top3 reveals an interaction between the Sgs1 and Pif1 DNA helicases in Saccharomyces cerevisiae. Genetics 174, 555–573. https://doi.org/10.1534/genetics.104.036905

Waizenegger, A., Urulangodi, M., Lehmann, C.P., Reyes, T.A.C., Saugar, I., Tercero, J.A., Szakal, B., Branzei, D., 2020. Mus81-Mms4 endonuclease is an Esc2-STUbL-Cullin8 mitotic substrate impacting on genome integrity. Nat. Commun. 11, 5746. https://doi.org/10.1038/s41467-020-19503-4

Wallgren, M., Mohammad, J.B., Yan, K.-P., Pourbozorgi-Langroudi, P., Ebrahimi, M., Sabouri, N., 2016. G-rich telomeric and ribosomal DNA sequences from the fission yeast genome form stable G-quadruplex DNA structures in vitro and are unwound by the Pfh1 DNA helicase. Nucleic Acids Res 44, 6213–31. https://doi.org/10.1093/nar/gkw349

Wan, B., Yin, J., Horvath, K., Sarkar, J., Chen, Y., Wu, J., Wan, K., Lu, J., Gu, P., Yu, E.Y., Lue, N.F., Chang, S., Liu, Y., Lei, M., 2013. SLX4 assembles a telomere maintenance toolkit by bridging multiple endonucleases with telomeres. Cell Rep. 4, 861–869. https://doi.org/10.1016/j.celrep.2013.08.017

Wang, G., Vasquez, K.M., 2022. Dynamic alternative DNA structures in biology and disease. Nat. Rev. Genet. https://doi.org/10.1038/s41576-022-00539-9

Wang, G., Vasquez, K.M., 2017. Effects of Replication and Transcription on DNA Structure-Related Genetic Instability. Genes 8, 17. https://doi.org/10.3390/genes8010017

Wang, H., Rosidi, B., Perrault, R., Wang, M., Zhang, L., Windhofer, F., Iliakis, G., 2005. DNA Ligase III as a Candidate Component of Backup Pathways of Nonhomologous End Joining. Cancer Res. 65, 4020–4030. https://doi.org/10.1158/0008-5472.CAN-04-3055

Wang, L., Wang, Q.-M., Wang, Y.-R., Xi, X.-G., Hou, X.-M., 2018. DNA-unwinding activity of Saccharomyces cerevisiae Pif1 is modulated by thermal stability, folding conformation, and loop lengths of G-quadruplex DNA. J. Biol. Chem. 293, 18504–18513. https://doi.org/10.1074/jbc.RA118.005071

Wang, R., Brattain, M.G., 2007. The maximal size of protein to diffuse through the nuclear pore is larger than 60kDa. FEBS Lett. 581, 3164–3170. https://doi.org/10.1016/j.febslet.2007.05.082

USC UNIVERSIDADE DE SANTIAGO DE COMPOSTELA

Wang, W., Daley, J.M., Kwon, Y., Krasner, D.S., Sung, P., 2017. Plasticity of the Mre11–Rad50–Xrs2–Sae2 nuclease ensemble in the processing of DNA-bound obstacles. Genes Dev. 31, 2331–2336. https://doi.org/10.1101/gad.307900.117

Wang, W., Daley, J.M., Kwon, Y., Xue, X., Krasner, D.S., Miller, A.S., Nguyen, K.A., Williamson, E.A., Shim, E.Y., Lee, S.E., Hromas, R., Sung, P., 2018. A DNA nick at Ku-blocked double-strand break ends serves as an entry site for exonuclease 1 (Exo1) or Sgs1-Dna2 in long-range DNA end resection. J. Biol. Chem. 293, 17061–17069. https://doi.org/10.1074/jbc.RA118.004769

Wang, Y., Lyu, Y.L., Wang, J.C., 2002. Dual localization of human DNA topoisomerase IIIα to mitochondria and nucleus. Proc. Natl. Acad. Sci. 99, 12114–12119. https://doi.org/10.1073/pnas.192449499

Wanzek, K., Schwindt, E., Capra, J.A., Paeschke, K., 2017. Mms1 binds to G-rich regions in Saccharomyces cerevisiae and influences replication and genome stability. Nucleic Acids Res. 45, 7796–7806. https://doi.org/10.1093/nar/gkx467

Ward, J.J., McGuffin, L.J., Bryson, K., Buxton, B.F., Jones, D.T., 2004. The DISOPRED server for the prediction of protein disorder. Bioinformatics 20, 2138–2139. https://doi.org/10.1093/bioinformatics/bth195

Warner, J.R., 1999. The economics of ribosome biosynthesis in yeast. Trends Biochem. Sci. 24, 437–440. https://doi.org/10.1016/S0968-0004(99)01460-7

Waterman, D.P., Haber, J.E., Smolka, M.B., 2020. Checkpoint Responses to DNA Double-Strand Breaks. Annu. Rev. Biochem. 89, 103–133. https://doi.org/10.1146/annurev-biochem-011520-104722

Waters, L.S., Minesinger, B.K., Wiltrout, M.E., D'Souza, S., Woodruff, R.V., Walker, G.C., 2009. Eukaryotic Translesion Polymerases and Their Roles and Regulation in DNA Damage Tolerance. Microbiol. Mol. Biol. Rev. 73, 134–154. https://doi.org/10.1128/MMBR.00034-08

Watson, J.D., Crick, F.H.C., 1953. Genetical Implications of the Structure of Deoxyribonucleic Acid. Nature 171, 964–967. https://doi.org/10.1038/171964b0

Wechsler, T., Newman, S., West, S.C., 2011. Aberrant chromosome morphology in human cells defective for Holliday junction resolution. Nature 471, 642–646. https://doi.org/10.1038/nature09790

Wein, N., Vulin, A., Falzarano, M.S., Szigyarto, C.A.-K., Maiti, B., Findlay, A., Heller, K.N., Uhlén, M., Bakthavachalu, B., Messina, S., Vita, G., Passarelli, C., Passarelli, S., Bovolenta, M., Neri, M., Gualandi, F., Wilton, S.D., Rodino-Klapac, L.R., Yang, L., Dunn, D.M., Schoenberg, D.R., Weiss, R.B., Howard, M.T., Ferlini, A., Flanigan, K.M., 2014. Translation from a DMD exon 5 IRES results in a functional dystrophin isoform that attenuates dystrophinopathy in humans and mice. Nat. Med. 20, 992–1000. https://doi.org/10.1038/nm.3628

USC UNIVERSIDADE DE SANTIAGO DE COMPOSTELA

Weinert, T.A., Hartwell, L.H., 1988. The RAD9 Gene Controls the Cell Cycle Response to DNA Damage in Saccharomyces cerevisiae. Science 241, 317–322. https://doi.org/10.1126/science.3291120

Wellinger, R.J., Zakian, V.A., 2012. Everything You Ever Wanted to Know About *Saccharomyces cerevisiae* Telomeres: Beginning to End. Genetics 191, 1073–1105. https://doi.org/10.1534/genetics.111.137851

West, S.C., 1997. PROCESSING OF RECOMBINATION INTERMEDIATES BY THE RuvABC PROTEINS. Annu. Rev. Genet. 31, 213–244. https://doi.org/10.1146/annurev.genet.31.1.213

Wickramasinghe, C.M., Arzouk, H., Frey, A., Maiter, A., Sale, J.E., 2015. Contributions of the specialised DNA polymerases to replication of structured DNA. DNA Repair, DNA polymerases 29, 83–90. https://doi.org/10.1016/j.dnarep.2015.01.004

Wiest, N.E., Houghtaling, S., Sanchez, J.C., Tomkinson, A.E., Osley, M.A., 2017. The SWI/SNF ATP-dependent nucleosome remodeler promotes resection initiation at a DNA double-strand break in yeast. Nucleic Acids Res. 45, 5887–5900. https://doi.org/10.1093/nar/gkx221

Wild, P., Matos, J., 2016. Cell cycle control of DNA joint molecule resolution. Curr. Opin. Cell Biol. 40, 74–80. https://doi.org/10.1016/j.ceb.2016.02.018

Wild, P., Susperregui, A., Piazza, I., Dorig, C., Oke, A., Arter, M., Yamaguchi, M., Hilditch, A.T., Vuina, K., Chan, K.C., Gromova, T., Haber, J.E., Fung, J.C., Picotti, P., Matos, J., 2019. Network Rewiring of Homologous Recombination Enzymes during Mitotic Proliferation and Meiosis. Mol. Cell 75, 859-874.e4. https://doi.org/10.1016/j.molcel.2019.06.022

Willer, M., Rainey, M., Pullen, T., Stirling, C.J., 1999. The yeast CDC9 gene encodes both a nuclear and a mitochondrial form of DNA ligase I. Curr. Biol. 9, 1085-S1. https://doi.org/10.1016/S0960-9822(99)80477-1

Wilson, M.A., Kwon, Y., Xu, Y., Chung, W.-H., Chi, P., Niu, H., Mayle, R., Chen, X., Malkova, A., Sung, P., Ira, G., 2013. Pif1 helicase and Poldelta promote recombination-coupled DNA synthesis via bubble migration. Nature 502, 393–396. https://doi.org/10.1038/nature12585

Wilson, T.E., Grawunder, U., Lieber, M.R., 1997. Yeast DNA ligase IV mediates non-homologous DNA end joining. Nature 388, 495–498. https://doi.org/10.1038/41365

Winzeler, E.A., Shoemaker, D.D., Astromoff, A., Liang, H., Anderson, K., Andre, B., Bangham, R., Benito, R., Boeke, J.D., Bussey, H., Chu, A.M., Connelly, C., Davis, K., Dietrich, F., Dow, S.W., El Bakkoury, M., Foury, F., Friend, S.H., Gentalen, E., Giaever, G., Hegemann, J.H., Jones, T., Laub, M., Liao, H., Liebundguth, N., Lockhart, D.J., Lucau-Danila, A., Lussier, M., M'Rabet, N., Menard, P., Mittmann, M., Pai, C., Rebischung, C., Revuelta, J.L., Riles, L., Roberts, C.J., Ross-MacDonald, P., Scherens, B., Snyder, M., Sookhai-Mahadeo, S., Storms, R.K., Véronneau, S., Voet, M., Volckaert, G., Ward, T.R., Wysocki, R., Yen, G.S., Yu, K., Zimmermann, K.,

USC UNIVERSIDADE DE SANTIAGO DE COMPOSTELA

Philippsen, P., Johnston, M., Davis, R.W., 1999. Functional Characterization of the S. cerevisiae Genome by Gene Deletion and Parallel Analysis. Science 285, 901–906. https://doi.org/10.1126/science.285.5429.901

Wu, L., Hickson, I.D., 2003. The Bloom's syndrome helicase suppresses crossing over during homologous recombination. Nature 426, 870–874. https://doi.org/10.1038/nature02253

Wu, Y., Brosh, R.M.J., 2009. FANCJ helicase operates in the Fanconi Anemia DNA repair pathway and the response to replicational stress. Curr. Mol. Med. 9, 470–482. https://doi.org/10.2174/156652409788167159

Wyatt, H.D.M., Laister, R.C., Martin, S.R., Arrowsmith, C.H., West, S.C., 2017. The SMX DNA Repair Tri-nuclease. Mol. Cell 65, 848-860.e11. https://doi.org/10.1016/j.molcel.2017.01.031

Wyatt, H.D.M., Sarbajna, S., Matos, J., West, S.C., 2013. Coordinated actions of SLX1-SLX4 and MUS81-EME1 for Holliday junction resolution in human cells. Mol. Cell 52, 234–247. https://doi.org/10.1016/j.molcel.2013.08.035

Wyatt, H.D.M., West, S.C., 2014. Holliday Junction Resolvases. Cold Spring Harb. Perspect. Biol. 6, a023192–a023192. https://doi.org/10.1101/cshperspect.a023192

Xu, J., Zhao, L., Xu, Y., Zhao, W., Sung, P., Wang, H.-W., 2017. Cryo-EM structures of human RAD51 recombinase filaments during catalysis of DNA-strand exchange. Nat. Struct. Mol. Biol. 24, 40–46. https://doi.org/10.1038/nsmb.3336

Xue, X., Raynard, S., Busygina, V., Singh, A.K., Sung, P., 2013. Role of replication protein A in double holliday junction dissolution mediated by the BLM-Topo IIIalpha-RMI1-RMI2 protein complex. J. Biol. Chem. 288, 14221–14227. https://doi.org/10.1074/jbc.M113.465609

Yan, W.X., Mirzazadeh, R., Garnerone, S., Scott, D., Schneider, M.W., Kallas, T., Custodio, J., Wernersson, E., Li, Y., Gao, L., Federova, Y., Zetsche, B., Zhang, F., Bienko, M., Crosetto, N., 2017. BLISS is a versatile and quantitative method for genome-wide profiling of DNA double-strand breaks. Nat. Commun. 8, 15058. https://doi.org/10.1038/ncomms15058

Yang, H., Zhou, C., Dhar, A., Pavletich, N.P., 2020. Mechanism of strand exchange from RecA–DNA synaptic and D-loop structures. Nature 586, 801–806. https://doi.org/10.1038/s41586-020-2820-9

Ying, S., Minocherhomji, S., Chan, K.L., Palmai-Pallag, T., Chu, W.K., Wass, T., Mankouri, H.W., Liu, Y., Hickson, I.D., 2013. MUS81 promotes common fragile site expression. Nat. Cell Biol. 15, 1001–1007. https://doi.org/10.1038/ncb2773

Yogev, O., Karniely, S., Pines, O., 2007. Translation-coupled Translocation of Yeast Fumarase into Mitochondria in Vivo*. J. Biol. Chem. 282, 29222–29229. https://doi.org/10.1074/jbc.M704201200

Youds, J.L., O'Neil, N.J., Rose, A.M., 2006. Homologous Recombination Is Required for Genome Stability in the Absence of DOG-1 in *Caenorhabditis elegans*. Genetics 173, 697–708. https://doi.org/10.1534/genetics.106.056879

USC UNIVERSIDADE DE SANTIAGO DE COMPOSTELA

Yu, X., Gabriel, A., 2003. Ku-Dependent and Ku-Independent End-Joining Pathways Lead to Chromosomal Rearrangements During Double-Strand Break Repair in Saccharomyces cerevisiae. Genetics 163, 843–856. https://doi.org/10.1093/genetics/163.3.843

Yun, M.H., Hiom, K., 2009. CtIP-BRCA1 modulates the choice of DNA double-strand-break repair pathway throughout the cell cycle. Nature 459, 460–463. https://doi.org/10.1038/nature07955

Zakian, V.A., 1995. Telomeres: Beginning to Understand the End. Science 270, 1601–1607. https://doi.org/10.1126/science.270.5242.1601

Zegerman, P., Diffley, J.F.X., 2010. Checkpoint-dependent inhibition of DNA replication initiation by Sld3 and Dbf4 phosphorylation. Nature 467, 474–478. https://doi.org/10.1038/nature09373

Zeman, M.K., Cimprich, K.A., 2014. Causes and consequences of replication stress. Nat. Cell Biol. 16, 2–9. https://doi.org/10.1038/ncb2897

Zhang, D.-H., Zhou, B., Huang, Y., Xu, L.-X., Zhou, J.-Q., 2006. The human Pif1 helicase, a potential Escherichia coli RecD homologue, inhibits telomerase activity. Nucleic Acids Res. 34, 1393–1404. https://doi.org/10.1093/nar/gkl029

Zhang, H., Freudenreich, C.H., 2007. An AT-Rich Sequence in Human Common Fragile Site FRA16D Causes Fork Stalling and Chromosome Breakage in S. cerevisiae. Mol. Cell 27, 367–379. https://doi.org/10.1016/j.molcel.2007.06.012

Zhang, W., Durocher, D., 2010. De novo telomere formation is suppressed by the Mec1-dependent inhibition of Cdc13 accumulation at DNA breaks. Genes Dev. 24, 502–515. https://doi.org/10.1101/gad.1869110

Zhao, J., Li, Y., Wang, C., Zhang, Haotian, Zhang, Hao, Jiang, B., Guo, X., Song, X., 2020. IRESbase: A Comprehensive Database of Experimentally Validated Internal Ribosome Entry Sites. Genomics Proteomics Bioinformatics, Special Issue:Bioinformatics Commons—2020 18, 129–139. https://doi.org/10.1016/j.gpb.2020.03.001

Zhao, J., Wang, G., del Mundo, I.M., McKinney, J.A., Lu, X., Bacolla, A., Boulware, S.B., Zhang, C., Zhang, H., Ren, P., Freudenreich, C.H., Vasquez, K.M., 2018. Distinct Mechanisms of Nuclease-Directed DNA-Structure-Induced Genetic Instability in Cancer Genomes. Cell Rep. 22, 1200–1210. https://doi.org/10.1016/j.celrep.2018.01.014

Zhao, X., Muller, E.G.D., Rothstein, R., 1998. A Suppressor of Two Essential Checkpoint Genes Identifies a Novel Protein that Negatively Affects dNTP Pools. Mol. Cell 2, 329–340. https://doi.org/10.1016/S1097-2765(00)80277-4

Zhou, C., Pourmal, S., Pavletich, N.P., 2015. Dna2 nuclease-helicase structure, mechanism and regulation by Rpa. eLife 4, e09832. https://doi.org/10.7554/eLife.09832

Zhou, J.-Q., 2000a. Pif1p Helicase, a Catalytic Inhibitor of Telomerase in Yeast. Science 289, 771–774. https://doi.org/10.1126/science.289.5480.771

Zhou, J.-Q., 2000b. Pif1p Helicase, a Catalytic Inhibitor of Telomerase in Yeast. Science 289, 771–774. https://doi.org/10.1126/science.289.5480.771

USC DE SANTIAGO DE COMPOSTELA

Zhou, J.-Q., Qi, H., Schulz, V.P., Mateyak, M.K., Monson, E.K., Zakian, V.A., 2002. Schizosaccharomyces pombe pfh1+ encodes an essential 5' to 3' DNA helicase that is a member of the PIF1 subfamily of DNA helicases. Mol. Biol. Cell 13, 2180–2191. https://doi.org/10.1091/mbc.02-02-0021

Zhou, X., Ren, W., Bharath, S.R., Tang, X., He, Y., Chen, C., Liu, Z., Li, D., Song, H., 2016. Structural and Functional Insights into the Unwinding Mechanism of Bacteroides sp Pif1. Cell Rep. 14, 2030–2039. https://doi.org/10.1016/j.celrep.2016.02.008

Zhu, Y., Biernacka, A., Pardo, B., Dojer, N., Forey, R., Skrzypczak, M., Fongang, B., Nde, J., Yousefi, R., Pasero, P., Ginalski, K., Rowicka, M., 2019. qDSB-Seq is a general method for genome-wide quantification of DNA double-strand breaks using sequencing. Nat. Commun. 10, 2313. https://doi.org/10.1038/s41467-019-10332-8

Zhu, Z., Chung, W.-H., Shim, E.Y., Lee, S.E., Ira, G., 2008. Sgs1 Helicase and Two Nucleases Dna2 and Exo1 Resect DNA Double-Strand Break Ends. Cell 134, 981–994. https://doi.org/10.1016/j.cell.2008.08.037

Ziesel, A., Weng, Q., Ahuja, J.S., Bhattacharya, A., Dutta, R., Cheng, E., Börner, G.V., Lichten, M., Hollingsworth, N.M., 2022. Rad51-mediated interhomolog recombination during budding yeast meiosis is promoted by the meiotic recombination checkpoint and the conserved Pif1 helicase. PLOS Genet. 18, e1010407. https://doi.org/10.1371/journal.pgen.1010407

USC UNIVERSIDADE DE SANTIAGO DE COMPOSTELA

INDEX OF FIGURES

Figure 1. DNA repair overview 30
Figure 2. BER pathway 32
Figure 3. NER pathway 34
Figure 4. MMR pathway. 36
Figure 5. DSB repair by NHEJ 38
Figure 6. DSB repair by HR 40
Figure 7. DSB repair pathways 42
Figure 8. DDT pathways and fork reversal 43
Figure 9. DDT and fork reversal at and behind the fork. 45
Figure 10. Regulation of DDT pathways by post-translational modifications. 47
Figure 11. Possible DNA transactions during fork reversal. 49
Figure 12. Overview of DDC response in budding yeast. 51
Figure 13. Phosphorylation events involved in DDC activation in budding yeast. 53
Figure 14. End-resection at blocked DSB ends. 57
Figure 15. Cell cycle stage dictates DSBR pathway choice. 59
Figure 16. Rad51 nucleofilament catalyses D-loop formation. 61
Figure 17. Regulation of nascent D-loop stability in budding yeast. 64
Figure 18. SDSA pathways. 65
Figure 19. Rad51-dependent BIR pathway. 67
Figure 20. Second-end capture channels HR intermediates to DSBR. 69
Figure 21. Schematic view of dHJ processing pathways during mitosis in *S. cerevisiae*. 71
Figure 22. Domain structures of Slx1-Slx4/SLX1-SLX4 and *in vitro* DNA substrate specificities. (a,b) 73
Figure 23. Domain structure of Mus81-Mms4 and MUS81-EME1/EME2 and *in vitro* DNA substrate specificities. (a,b) 74
Figure 24. Domain structures of Yen1 and GEN1 and *in vitro* DNA substrate specificities. (a,b) 76
Figure 25 Control of HJ processing by the cell cycle. 79
Figure 26. Schematic representation of the sequential activation of HJ processing pathways biases DSBR output towards NCO. 80
Figure 27. Schematic representation of secondary DNA structures that may serve as substrates for SSEs 83
Figure 28. Structural motifs in the Pif1 family helicases. 90
Figure 29. Mutant variants of Yen1 to study the regulation of HJ resolution. 99

USC UNIVERSIDADE DE SANTIAGO DE COMPOSTELA

Figure 30. Overexpression of catalytically active and nuclease-dead versions of deregulated Yen1 causes cell death in a dose-dependent manner. 102
Figure 31. Overexpression of deregulated versions of Yen1 leads to checkpoint activation and disrupts cell cycle progression. 103
Figure 32. Prolonged cell cycle arrest by DDC activation is not the main cause of cell death in strains overexpressing *YEN1*^{ON} variants. 104
Figure 33 Abrogation of HR pathways does not suppress *YEN1*^{ON}-dependent lethality. 106
Figure 34. Premature activation of Yen1 is beneficial in strains with an excess of toxic recombination intermediates. 107
Figure 35. *YEN1*^{ON} does not suppress the synthetic lethality of *sgs1*Δ *slx1*Δ and *sgs1*Δ *slx4*Δ. 108
Figure 36. *YEN1*^{ON} alters the hypersensitivity of mutants for HR-related helicases to DNA-damaging agents. 109
Figure 37. Genetic interaction between *YEN1*^{ON} and absence of *PIF1*-family helicases in the presence of MMS or HU. 110
Figure 38. *PIF1* mitochondrial and nuclear separation-of-function alleles fail to recapitulate the genetic interaction in *pif1*Δ *YEN1*^{ON}. 111
Figure 39. Hypersensitivity of *pif1*Δ *YEN1*^{ON} strains to HU is caused by the loss of Pif1 nuclear function. 113
Figure 40. ATI from AUG^{1} and AUG^{40} produces Pif1 mitochondrial and nuclear isoforms. 118
Figure 41. Schematic representation of *PIF1* separation of function alleles with their predicted molecular weight and subcellular localization. 119
Figure 42. *pif1-m2* recapitulates neither *pif1*Δ telomere lengthening nor its synthetic sickness with *dia2*Δ. 122
Figure 43. *pif1-m2* does not fully recapitulate *pif1*Δ genetic interactions with *dna2*Δ and *rad3-102*. 124
Figure 44. A fast-migrating isoform is enriched in *pif1-m2* mutants. 126
Figure 45. The fast-migrating Pif1 isoform could arise by ATI from downstream AUG codons. 127
Figure 46. Schematic representation of canonical cap-dependent translation initiation. 128
Figure 47. Schematic overview of the main mechanisms of ATI from different AUGs. 131
Figure 48. ATI can initiate translation from a cluster of ATGs downstream ATG40. 132
Figure 49. Optimization of Kozak context surrounding AUG^{40} abrogates the expression of the fast-migrating isoform. 133
Figure 50. *In vivo* characterization of Pif1$^{107-859}$ localization, mitochondrial functionality, and toxicity by overexpression. 134
Figure 51. Functional characterization of purified Pif1$^{107-859}$. 135
Figure 52. *In vivo* characterization of *pif1*$^{107-859}$. 136

Figure 53. Putative NLS in Pif1. 138
Figure 54. Importing of Pif1 nuclear isoform is impaired in Pif1$^{\Delta 775-803}$ 139
Figure 55. Mutation of ^{781}KKRK^{784} basic patch located at position 781-784 suppress *PIF1* overexpression toxicity. 140
Figure 56. ^{781}KKRK^{784} is necessary to mediate import of Pif1 nuclear isoforms. 141
Figure 57. ^{781}KKRK^{784} is sufficient to drive the nuclear accumulation of eGFP. 142
Figure 58.Functional characterization of purified Pif1^{nls}. 143
Figure 59. Disruption of Pif1 NLS does not completely abolish nuclear function. 144
Figure 60. *pif1^{mit}* recapitulates the nuclear phenotypes of *pif1*Δ. 145
Figure 61. *pif1-m1* retains functional mitochondria. 146
Figure 62. In-frame near-cognate start codons surrounding AUG^{1} could produce mitochondrial-targeted isoforms. 148
Figure 63. Translation initiation from near-cognates AUGs can sustain mitochondrial function in the absence of AUG^{1} 149
Figure 64. Mutations of four near-cognates in *pif1-m1* phenocopies *pif1*Δ mitochondrial defects. 150
Figure 65. Improved, mitochondrial-deficient *pif1-m1^{L9L}* and *pif1-m1^{4L}* alleles phenocopy the HU hypersensitivity of *pif1*Δ in *rad3-102* mutants. 151
Figure 66. Integrated model of Pif1 isoforms production mediated by leaky scanning in different *PIF1* alleles. 154
Figure 67. Analysis of the Kozak context in dual-targeted genes in *S. cerevisiae*. 161
Figure 68. Analysis of the Kozak context in dual-targeted genes in *H. sapiens*. 162
Figure 69. Isoform p110 of *ADAR1* is produced by both alternative splicing and leaky scanning. 163
Figure 70. hPIF1α produces two isoforms by ATI with dual-targeted localization. 165
Figure 71. Coomassie staining of all Pif1 variants purified in this study. Pif1, the ATPase-dead version Pif1^{KA}, Pif1^{nls} and the truncated isoform Pif1$^{107-859}$ were purified, analysed by SDS-PAGE and stained with Coomassie. 210

USC
UNIVERSIDADE DE SANTIAGO DE COMPOSTELA





Yen1 resolution activity is restrained by Cdk1 until the onset of anaphase. To understand the biological consequences of this regulation, we analyzed strains harbouring a constitutively active allele of *YEN1* in different genetic backgrounds. Here, we show that deletion of *PIF1* helicase in *YEN1*^{ON} strains results in a dramatic reduction of its viability under genotoxic stress. Further characterization with classical *PIF1* separation-of-function alleles failed to recapitulate such genetic interaction. This prompted us to delve into the translational mechanism of Pif1, leading us to the re inement of the molecular mechanism of alternative translation initiation for *PIF1* mRNA, the discovery of a new nuclear Pif1 isoform and the development of the first bona- ide mitochondrial and nuclear-null Pif1 alleles.